Chemogenomic Investigation of *Burkholderia cenocepacia* K56-2 Reveals the Targets of Antibiotics and Potentiators

by

Andrew Michael Hogan

A Thesis submitted to the Faculty of Graduate Studies of The University of Manitoba in partial fulfilment of the requirements of the degree of

DOCTOR OF PHILOSOPHY

Department of Microbiology
University of Manitoba
Winnipeg, Manitoba, Canada

ABSTRACT

To counter the rise in resistance, new antibiotics are desperately needed. Part of characterizing these compounds involves identifying the target, mechanism of action, and determinants of resistance and susceptibility. Chemogenomic assays coupled to next-generation sequencing (NGS) can rapidly probe genome-wide contributions to antibiotic action. Tools such as transposons have enabled genome-wide studies of species in the *Burkholderia cepacia* complex, a group of Gram-negative opportunistic pathogens noted for high levels of intrinsic antibiotic resistance. Thus, the goal of my thesis was to validate transposon-based methodologies for target and mechanism of action identification of antibiotics in *B. cenocepacia*.

I started my investigation with an uncharacterized compound called C109, which displayed broad-spectrum bactericidal activity. To identify the target of C109, I used a transposon with outward-facing rhamnose-inducible promoters, allowing tunable knockdown of mutants in essential genes. By NGS-based tracking of a pool of mutants in essential genes, I identified that C109 targeted FtsZ, a highly-conserved essential cell division protein. *In vitro*, C109 inhibited the GTPase and polymerization of FtsZ, which are critical for its function.

To improve on our set of genetic tools to manipulate essential genes, I adapted robust CRISPR-interference (CRISPRi) technology for *Burkholderia*. The single guide RNA cassette controlling gene targeting can be easily replaced, enabling rapid mutant creation.

Lastly, I constructed a randomly-barcoded transposon mutant library to probe genome-wide fitness determinants in the presence of a large panel of cell envelope-targeting antibiotics. I validated over a hundred new functional annotations for genes not previously associated with antibiotic activity in *B. cenocepacia*. I made new connections between β-lactam susceptibility and disruptions in undecaprenyl phosphate metabolic pathways, likely due to a weakened peptidoglycan matrix. Dissecting the effect of antibiotic combinations revealed that the PenB carbapenemase was the primary target of avibactam, paving the way for more effective antibiotic combinations active against *Burkholderia*. Overall, my thesis demonstrates how chemogenomics can be used to determine antibiotic targets, and mechanisms of action and resistance. This work has implications for antibiotic development, target prioritization, and using rational combinations to extend the utility of our current clinical arsenal.

ACKNOWLEDGEMENTS

How could I start any other way than to thank my supervisor, Dr. Silvia Cardona? You've taught me so much about the amazing secret world of microbes and shared your passion for *Burkholderia*; it has been truly inspiring. Thank-you for all the times you had to deal with my crazy ideas; some of them turned out to be just crazy enough to work. You gave me the freedom to fail, and in so doing I learned so much more about myself and my science.

To my committee members, Dr. Karen Brassinga, Dr. Sean McKenna and Dr. Ayush Kumar, thank-you for your guidance and advice during my scientific journey. I would also like to thank my collaborators Dr. Silvia Buroni, Dr. Vadim Makarov, Dr. Pavel Nunvar, and Dr. Krisztina Papp-Wallace for expanding my boundaries in new areas.

To all the Cardona Lab members past and present, you really are something special. It was a pleasure to work and learn with each of you. Thank-you to the many young scientists I mentored over the years for contributing to my research: Haben Tesfu, Armando Palacios, Kevin Jeffers, Maya Gusak, Kartik Sachar, Ryan Ha, Zayra Batun, and Aakash Natarajan. When I taught you, it felt like I was really the one learning. To the students in the Cardona lab, April Gislason, Brijesh Kumar, Matt Choy, Tasia Lightly, Haben Tesfu, Zisan Rahman, Dustin Maydaniuk, Zhong Ling Yap, Becca Lohmann, Zayra Batun and Anna Motnenko: I will cherish everything I've learned from you. With all the idea ping pong we played over the years, there's a little bit of each of you here in my thesis.

I would also like to thank the many funding sources that supported my work over the past several years: NSERC, CIHR, Cystic Fibrosis Canada, The Cystic Fibrosis Foundation, the UofM Faculty of Science, the UofM Faculty of Graduate Studies, and the Department of Microbiology.

A big thank you goes out to everyone in the Microbiology Department. There's not one lab from which I didn't borrow equipment or go to for ideas. We had some of the best brainstorming sessions over a pint at The Hub, and I will always fondly remember them. I hope that you keep up the friendly working and learning environment that I enjoyed so much. Your colleagues in the department are one of your greatest assets, and most of them can be payed in beer!

To my family, who endured me practicing my 1 minute "Grandparent talk" so many times… I hope they eventually got better and I convinced you why I spend so much time in the

lab. Even though I was so far away from home, it was always reassuring to know that I had a little cheerleading team rooting for me.

And finally to Brad, my partner to whom I turn for inspiration in life and science. I owe so many things to you, and now my thesis is one of them. Thank-you for your patience for all the times when I said “I’ll just be in for 5 minutes to make an overnight”, but it actually took half an hour. When I got stuck down rabbit holes, you pulled me out and reminded me to think more broadly of my work’s translations. You helped me along every step of the way: from my grad school application to the long nights before deadlines, and you were there for every milestone celebration. Soon, this will be you writing your thesis, and after that I can’t wait to see what the future has in store for us!

TABLE OF CONTENTS

PERMISSIONS

Several tables, figures, and passages of text in this thesis have been taken directly and/or adapted from publications that I have authored.

Chapter 1: Hogan AM and Cardona ST. 2022. Gradients in gene essentiality reshape antibacterial research. *FEMS Microbiol. Rev.* **46**(3): fuac005.

Content associated with this publication is used under license 5346110285964 from Oxford University Press (via RightsLink).

Chapter 3 (and associated methods): Hogan AM, Scoffone VC, Makarov V, Gislason AS, Tesfu H, Stietz MS, Brassinga AKC, Domaratzki M, Li X, Azzalin A, Biggiogera M, Monakhova N, Chiarelli LR, Riccardi G, Buroni S, Cardona ST. 2018. Competitive fitness of essential gene knockdowns reveals a broad-spectrum antibacterial inhibitor of the cell division protein FtsZ. *Antimicrob. Agents Chemother.* **62**(12): e01231-18.

Copyright © 2018 Hogan et al. This is an open access article distributed under the terms of the Creative Commons.

Chapter 4 (and associated methods): Hogan AM, Rahman ASMZ, Lightly TJ, Cardona ST. 2019. A broad-host-range CRISPRi toolkit for silencing gene expression in *Burkholderia*. *ACS Synth. Biol.* **8**(10): 2372-84

Copyright © 2019 American Chemical Society. This is an open access article published under an ACS AuthorChoice License, which permits copying and redistribution of the article or any adaptations for non-commercial purposes

Chapter 5 (and associated methods): Hogan AM, Léon B, Batun Z, Motnenko A, Bosch A, Cardona ST. Chemogenomics reveals susceptibility determinants of cell envelope-targeting antibiotics in *Burkholderia cenocepacia*. *Manuscript in preparation*.

This manuscript has been formatted for submission to fit the requirements of a “sandwich” style thesis as per the Faculty of Graduate Studies but has not yet been submitted to a journal.

AUTHOR CONTRIBUTIONS

Multiple authors have contributed to the work presented in Chapters 3, 4, and 5.

Chapter 3: V Makarov and N Monakhova conceived the structure of and synthesized the compound known as C109. VC Scoffone, A Azzalin, M Biggiogera, LR Chiarelli, G Riccardi, and S Buroni performed the *in vitro* biochemical assays on the ability of C109 to inhibit polymerization and GTPase activity of purified FtsZ. Gislason AS constructed the transposon mutant library and enriched it for mutants in essential genes. Stietz MS performed nematode killing assays and Tesfu H performed *in vitro* interaction assays of C109 with other antibiotics. Brassinga AKC provided access to microscopy facilities. Domaratzki M and Li X worked with us to use computational and statistical resources to process and analyze the data. While these individuals performed select experiments, often under my supervision, I designed and performed the majority of the other experiments, assembled the data and figures, and wrote and edited the manuscript with guidance from Silvia Cardona.

Chapter 4: Rahman ASMZ designed several of the sgRNA expression plasmids and performed experiments related to motility and use of phenylacetic acid as a sole carbon source. Lightly TJ performed RT-qPCR analysis for *paaA* expression in CRISPRi mutants. These individuals performed select experiments under my supervision. I designed and performed the majority of the other experiments and was responsible for data analysis, figure preparation, and writing and editing the manuscript, with guidance from Silvia Cardona.

Chapter 5: Léon B (supported by her graduate supervisor Bosch A) aided in construction of the randomly-barcoded transposon mutant library. Motnenko A analyzed LPS profiles by PAGE and silver staining using extracts I prepared. Batun Z and Natarajan A performed *in vitro* assays of β-lactam/β-lactamase susceptibility. These individuals performed select experiments under my supervision. I designed and performed the majority of the other experiments and was responsible for data analysis, figure preparation, and writing and editing the manuscript, with guidance from Silvia Cardona.

LIST OF TABLES

LIST OF FIGURES

LIST OF ABBREVIATIONS

ABC	ATP-binding cassette
AMP	Ampicillin
ASKA	A complete set of E. coli K-12 ORF archive
asRNA	antisense RNA
AVI/CAZ	Ceftazidime/Avibactam
AVI-H	Avibactam - High concentration
AVI-L	Avibactam - Low concentration
AZT	Aztreonam
BAC	Bacitracin
BAM	β-barrel assembly machinery
BarSeq	Barcode sequencing
Bcc	*Burkholderia cepacia* complex
BCP	Bacterial cytological profiling
Bpc	*Burkholderia pseudomallei* complex
CAA	Casamino acids
CAMHB	Cation-adjusted Mueller-Hinton broth
CAZ-H	Ceftazidime - High concentration
CAZ-L	Ceftazidime - Low concentration
CF	Cystic fibrosis
CFD	Cefiderocol
CFTR	Cystic fibrosis transmembrane conductance regulator
CGD	Chronic granulomatous disease
CHIR	CHIR-090
CHL	Chloramphenicol
CHX	Chlorhexidine
COG	Cluster of orthologous genes
COL	Colistin
CRISPRi	Clustered regularly interspaced short palindromic repeats interference
CTT	Cefotetan

CTX	Cholera toxin
CYC	Cycloserine
DAPI	4′,6-diamidino-2-phenylindole
DIC	Differential interference contrast
DMSO	Dimethyl sulfoxide
DSB	Disulfide bond formation
DTT	Dithiothreitol
EDTA	Ethylenediaminetetraacetic acid
ERY	Erythromycin
ET12	Electrophoretic type 12
FOS	Fosfomycin
FR-9	FR-900098
FRT	Flippase recognition target
GDP	Guanosine diphosphate
GFP	Green fluorescent protein
GTP	Guanosine triphosphate
HDTM	High-density transposon mutant
HEPES	4-(2-hydroxyethyl)-1-piperazineethanesulfonic acid
HITS	High-throughput insertion tracking by deep sequencing
ICP-MS	Inductively coupled plasma mass spectrometry
IC_x	Inhibitory concentration X%
INSeq	Transposon insertion sequencing
IPTG	Isopropyl β-D-1-thiogalactopyranoside
LB	Lysogeny broth
LPS	Lipopolysaccharide
MATE	Multidrug and toxic compound extrusion
MBEC	Minimum biofilm eradication concentration
MBIC	Minimum biofilm inhibitory concentration
MBL	Metallo-β-lactamase
MCR	Mobile colistin resistance
MEM	Meropenem

MFS	Major facilitator superfamily
MIC	Minimum inhibitory concentration
MIC_{50}	Minimum inhibitory concentration (50% of isolates)
Mla	Maintenance of lipid assymetry
NADH	Nicotinamide adenine dinucleotide (reduced)
NADPH	Nicotinamide adenine dinucleotide phosphate (reduced)
NBT/BCIP	Nitro-blue tetrazolium chloride/5-bromo-4-chloro-3'-indolyphosphate p-toluidine salt
NGM	Nematode growth medium
NGS	Next-generation sequencing
NOV	Novobiocin
NPN	1-N-phenylnaphthylamine
NT	Non-template
OD_{600} (OD)	Optical density measured at 600 nm
PA	Phenylacetic acid
PACE	Proteobacterial antimicrobial compound efflux
PAM	Protospace adjacent motif
PBP	Pencillin-binding protein
PBS	Phosphate-buffered saline
PF-04	PF-04753299
PHA	Polyhydroxyalkanoate
PHB	Polyhydroxybutyrate
PMB	Polymyxin B
qPCR	Quantitative polymerase chain reaction
RB-TnSeq	Random bar code transposon-site sequencing
Rha	L-rhamnose
RIF	Rifampicin
RND	Resistance-nodulation-division
ROS	Reactive oxygen species
RT-qPCR	Quantitative reverse transcription polymerase chain reaction
SCFM	Synthetic cystic fibrosis sputum medium

SDS	Sodium dodecyl sulfate
SDS-PAGE	Sodium dodecyl sulfate polyacrylamide gel electrophoresis
sgRNA	single guide RNA
SMR	Small multidrug resistance
SOC	Super optimal broth with catabolite repression
TAZ	Tazobactam
TBDR	TonB-dependent receptor
TBST	Tris-buffered saline with 0.1% Tween
TEM	Transmission electron microscopy
TnSeq	Transposon site sequencing
TraDIS	Transposon-directed insertion site sequencing
TSS	Transcription start site
UDP	Uridine diphosphate
UndP	Undecaprenyl phosphate
UndPP	Undecaprenyl pyrophosphate
WT	Wild type
WTA	Wall teichoic acid

CHAPTER 1: LITERATURE REVIEW

1.0 Overview of the genus Burkholderia

1.0.1 Taxonomy and ecology of Burkholderia and related genera

The taxonomy of *Burkholderia* sensu lato (*Burkholderia* and related genera) is closely tied to the ecology and lifestyles of the bacteria within each genus. *Burkholderia* s.l. are variably known to fix nitrogen, nodulate legumes, degrade pollutants, promote the growth of agricultural crops and protect them from pathogens, and to produce a variety of important secondary metabolites (e.g. antimicrobials, polyhydroxyalkanoate bioplastics, and rhamnolipids) (Eberl and Vandamme, 2016; Elshafie and Camele, 2021). However, some species are noted plant and/or animal pathogens (Elshafie and Camele, 2021; Isles et al., 1984). There have been, and continue to be, many revisions to the taxonomy of *Burkholderia* s.l. species to attempt to separate beneficial from pathogenic species.

The first description of a *Burkholderia* species was in 1950 as a cause of "sour skin" onion rot, by Walter Burkholder who originally named it *Pseudomonas cepacia*, within the phylum Pseudomonadota (Proteobacteria). As part of a larger restructuring of the genus *Pseudomonas* (Palleroni et al., 1972, 1973; Swings et al., 1983; Woese et al., 1984), in 1992 seven related species were moved to create the genus *Burkholderia* on the basis of 16S rRNA sequences, DNA-DNA hybridization, and nutrient assimilation (Yabuuchi et al., 1992). In 1997, isolates presumed to be *B. cepacia* were further divided into five genomovars as new distinct species, and together were termed the *B. cepacia* complex (Bcc). Today, the Bcc comprises over 22 distinct species, all of which are opportunistic human pathogens (Eberl and Vandamme, 2016).

Further changes to the genus *Burkholderia* were proposed in 2014, with the transfer of many species of *Burkholderia* to the new genus *Paraburkholderia* (Sawana et al., 2014). This split was based on rare conserved sequence indels and separates the plant and animal pathogenic species of *Burkholderia* from the generally non-pathogenic species of *Paraburkholderia*. Then in 2016, several species were transferred from *Burkholderia* and *Paraburkholderia* to the new genus *Caballeronia* (Dobritsa and Samadpour, 2016). The monospecific genus *Robbsia* was created in 2017 with the transfer of *B. andropogonis* (Lopes-Santos et al., 2017). In 2018, on the basis of whole genome sequence comparisons, some species of *Burkholderia* were transferred into the new genera *Mycetohabitans* and *Trinickia*, and while most of the species are not pathogenic, at least one (*T. caryophylli*) is a plant pathogen (Estrada-de Los Santos et al., 2018). The last published

transfer of species from the genus *Burkholderia* was in 2020 when *B. alpina* was reclassified as *Pararobbsia alpina* (Lin et al., 2020).

Today, there are at least 140 validly named *Burkholderia* sensu stricto species, and an additional 60 Candidatus *Burkholderia* species (https://lpsn.dsmz.de/). While efforts have been made to taxonomically separate pathogenic species, some plant and animal pathogens remain in genera with non-pathogenic species. It has been suggested that some of the traits required for pathogenesis are also required for plant growth promotion and biocontrol, thus non-pathogenic species may be less biotechnologically useful (Eberl and Vandamme, 2016). However, members the pathogenic *B. pseudomallei* complex (*B. mallei, B. pseudomallei, B. thailandensis,* and *B. oklahomensis*) are taxonomically separate from other *Burkholderia* species. *B. mallei* and *B. pseudomallei,* are both Tier 1 select agent bioterror threats (Centers for Disease Control and Prevention, 2012) and the causative agents of glanders and melioidosis, respectively, diseases endemic to southeast Asia. Species in the *B. pseudomallei* complex are genetically and phenotypically distinct from other *Burkholderia* species (Wiersinga et al., 2018).

1.0.2 Bcc infections in immunocompromised individuals

All species within the Bcc are opportunistic human pathogens. Most frequently, infections occur in immunocompromised individuals, such as those with cystic fibrosis (CF) or chronic granulomatous disease (CGD). However, rare cases of infection have been reported in immunocompetent individuals who were otherwise healthy (Ranjan et al., 2017) or had comorbidities, such as pneumonia and chronic-obstructive pulmonary disease (El Chakhtoura et al., 2017; Matthaiou et al., 2011). Bcc infection may be caused by contact with agricultural products (Ranjan et al., 2017), as Bcc species are ubiquitous in the soil, but infection may also occur through contact with contaminated medical products (De Volder et al., 2021; Tavares et al., 2020) or infected individuals (Blanchard et al., 2020). Bcc species are known to persist in medical disinfectants and detergents (Ahn et al., 2016; Kim et al., 2015) and are thus common sources of nosocomial infections (Häfliger et al., 2020; Singhal et al., 2015; Tavares et al., 2020). In fact, between 1998 and 2006, Bcc species were responsible for 22% of hospital and consumer-grade pharmaceutical product recalls, more than any other microbial contaminant (Jimenez, 2007).

CF is a recessive genetic disorder caused by mutations in the *CFTR* gene, which encodes the cystic fibrosis transmembrane conductance regulator (Riordan et al., 1989). The CFTR protein

is a membrane channel that allows chloride to diffuse out of respiratory epithelium cells, water then follows by osmosis to contribute to mucus volume. In the absence of a functional CFTR channel, thick mucus accumulates in the lungs and cannot be cleared by the mucociliary elevator (Ratjen et al., 2015). The mucus is also rich in amino acids and the proteoglycan mucin, which can be degraded by invading pathogens. Several opportunistic pathogens, such as *Staphylococcus aureus*, *Pseudomonas aeruginosa*, *Aspergillus fumigatus*, and several species of Bcc can colonize the stationary, nutrient-rich mucus, often simultaneously (Blanchard and Waters, 2019). In total, 3.2% of people living with CF in Canada are infected by a Bcc species, and the likelihood of infection increases with patient age (Cystic Fibrosis Canada, 2020). Within the Bcc, *B. cenocepacia* is the most common species (50% of the Bcc), followed by *B. multivorans* (38% of the Bcc) (Cystic Fibrosis Canada, 2020).

After colonizing the mucus, Bcc species can invade and replicate within respiratory epithelial cells and macrophages (Lamothe et al., 2006; Martin and Mohr, 2000). Bcc bacteria are able to persist in these cell types by inhibiting the maturation of the bacteria-containing vacuoles into phagolysosomes (Abdulrahman et al., 2011; Lamothe et al., 2006; Schmerk and Valvano, 2013). Additionally, the disfunction of the CFTR in immune cells further reduces the ability to combat infection by inhibiting phagolysosomal acidification and the respiratory burst. The phagolysosome compartments are usually acidified to pH 4.5, an important contributor to the bactericidal activity. However, in the absence of the CFTR channel, these compartments are only able to reach pH 6-6.5 (Di et al., 2006). Furthermore, the rapid production of reactive oxygen species in neutrophils, termed the respiratory burst, is also important for microbial killing. Superoxide and chloride are used as substrate by myeloperoxidase for the formation of hydrogen peroxide and hypochlorous acid, potent reactive oxygen species (Law and Gray, 2017). However, in the absence of a functional CFTR channel, there is decreased formation of hypochlorous acid (Law and Gray, 2017). Additionally, it has been suggested that there are defects in immune cell recruitment and signaling in individuals with CF, but the magnitude of these deficiencies remains unclear (Cohen and Prince, 2012). In total though, the absence of the CFTR channel greatly reduces the ability of immune cells to kill invading bacteria.

Taking into account the pathology of CF and CGD reveals important clues about why individuals with these diseases may be susceptible to Bcc infection. CGD is caused by mutations in any of six genes encoding subunits of the phagocyte NADPH oxidase, an enzyme that generates

superoxide (Leiding and Holland, 1993). In individuals with either CF or CGD, immune cells are therefore deficient in oxidative mechanisms of bacterial killing. In addition to oxidative mechanisms, immune cells also produce cationic antimicrobial peptides as part of innate immunity (Cole and Nizet, 2016). However, Bcc bacteria were found to be resistant to killing by non-oxidative mechanisms of granulocytes from people with CGD (Speert et al., 1994). Thus, oxidative mechanisms appear to be important for immune cell killing of Bcc bacteria, and fully functional innate immunity may be why otherwise healthy people are only rarely infected by Bcc bacteria.

After initial colonization of the lungs with Bcc bacteria, the course of infection proceeds at variable rates in different individuals (Manno et al., 2004; Nunvar et al., 2017; Somayaji et al., 2017). Despite intensive antibiotic regimens, full clearance is not often achieved, but rather there is a slow decline in lung function (often over several years) that is punctuated by flare-ups, called exacerbations, that require hospitalization (Somayaji et al., 2017). While eradication therapies have been reported for Bcc infection, these are generally case reports with a limited patient sample size (Garcia et al., 2018; Iglesias et al., 2014; Kitt et al., 2016). There are currently no objective guidelines for eradicating Bcc infection based on randomized clinical trials (Regan and Bhatt, 2019). Bcc infection is often fatal through a severe episode of pulmonary exacerbation associated with necrotizing pneumonia and bacteremia, termed "*cepacia* syndrome" (Isles et al., 1984; Tablan et al., 1985).

1.0.3 B. cenocepacia K56-2

Personal contact between Bcc-positive and Bcc-negative people with CF resulted in the spread of several virulent *B. cenocepacia* lineages. In the 1980's and early 1990's, children with CF would travel to attend summer camps set up specially for people with CF. These camps were shut down in the mid 1990's when it was realized that Bcc bacteria were rapidly spreading between the campers (Fung et al., 1998; Pegues et al., 1994). The strain examined in this work, *B. cenocepacia* K56-2, is a CF clinical isolate from Toronto and is representative of an epidemic lineage that spread in both the UK and Canada in the early 1990's (Darling et al., 1998; Govan et al., 1993). This lineage is called ET12, for electrophoretic type 12, based on a molecular typing system that uses relative gel mobility of a panel of diagnostic enzymes (Johnson et al., 1994). ET12 strains are associated with faster lung function decline and higher mortality rates than other Bcc strains, even when compared to non-ET12 strains of *B. cenocepacia* (Somayaji et al., 2017).

K56-2 is a commonly studied strain of *B. cenocepacia* because it is representative of the highly virulent ET12 lineage and is more amenable to genetic manipulation than other ET12 strains (Mahenthiralingam et al., 2000). Susceptibility to trimethoprim, chloramphenicol and tetracycline can be exploited as selectable markers. The recently published closed genome of K56-2 shows a genome size of 7,741,920 bp spread over three chromosomes and a plasmid (3,673,077 bp, 3,211,025 bp, 765,157 bp, and 92,661 bp, respectively) with an overall GC content of 67.0% (García-Romero and Valvano, 2020). In *B. cenocepacia* H111 and other species of *Burkholderia*, the smallest chromosome was demonstrated to be a dispensable virulence plasmid required for a variety of secondary traits such as antifungal activity, protease and exopolysaccharide production, and virulence in multiple infection models (Agnoli et al., 2012). Overall, the large genome size and high number of encoded genes in *Burkholderia* species is thought to confer metabolic plasticity for growth in many environments (Bach et al., 2022a, 2022b; Eberl and Vandamme, 2016; Lee et al., 2017).

K56-2, like other ET12 lineage strains, harbours several genomic islands encoding virulence-associated genes. Genomic islands are discrete segments of a genome that have been acquired horizontally, and may or may not still be mobile (Dobrindt et al., 2004; Hacker et al., 1990). Genomic islands are typically recognized as having different GC-content or codon usage from the surrounding genome and are often flanked by small direct DNA repeats reminiscent of the integration event (Schmidt and Hensel, 2004). However, because of their mobile nature, genomic islands can also be unstable. Therefore, to ensure that the genomic island is maintained in the lineage, the cargo genes often confer fitness advantages to the host cell, such as virulence or antibiotic resistance genes (Juhas et al., 2009). J2315, a closely related clonal strain to K56-2, encodes 14 genomic islands (Holden et al., 2009). One island in particular, the 31.7 kb "*cenocepacia* island" (*cci*), has been associated with highly virulent *B. cenocepacia* strains (Baldwin et al., 2004; Mahenthiralingam et al., 2001; Speert et al., 2002). Indeed, several of the 35 genes encoded on the *cci* were important for virulence in a rat model of chronic respiratory infection (Baldwin et al., 2004). Additionally, the unstable nature of genomic islands suggests that *cci* confers a fitness advantage to the *B. cenocepacia* host during CF lung infection.

1.1 Antibiotic resistance mechanisms within the Bcc

Currently, the only viable therapeutic avenue to eradicate, or even suppress, Bcc infection is with antibiotics. While bacteriophage therapy and vaccination holds great promise to address the multiple shortcomings of antibiotics, there remain important biological and policy/regulatory hurdles (Lauman and Dennis, 2021; Pradenas et al., 2016; Scoffone et al., 2020). However, high levels of antibiotic resistance create challenges for effective management of Bcc infection. In general, Bcc bacteria are near uniformly resistant to aminoglycosides, cationic antimicrobial peptides, and older generations of β-lactams (Aaron et al., 2000; Abbott et al., 2016; Zhou et al., 2007). Below, we explore some of the reported resistance mechanisms in the Bcc and how they each contribute to antibiotic resistance.

1.1.1 β-lactamases

The β-lactams are the most prescribed antibiotic class in the US (Centers for Disease Control and Prevention (CDC), 2021). Current clinically available β-lactams are derived from fungal natural products (Abraham, 1979; Fleming, 1929) and just as β-lactams were isolated from natural sources, enzymes that degrade β-lactams (β-lactamases) can also be readily found in nature. Moreover, the first documented case of a penicillinase was in 1940 (Abraham and Chain, 1940), years before β-lactams were produced commercially. β-lactams are substrate mimics and suicide inhibitors of the transpeptidase domain of penicillin-binding proteins (PBPs), the major enzymes that synthesize cell wall peptidoglycan, resulting in a covalent bond to the active site serine and enzyme inactivation (Yocum et al., 1979, 1980). Consequently, cells cannot efficiently synthesize peptidoglycan and then lyse due to defects in structural integrity. Additionally, cell killing is also achieved by a futile cycling of peptidoglycan building block synthesis and degradation that depletes cellular ATP (Cho et al., 2014).

Mirroring the natural diversity of β-lactams, there are also many types of β-lactamases which reside in the periplasm to protect PBPs. Two different classification schemes exist for β-lactamases: the Ambler classification, based on sequence similarity, and the Bush–Jacoby–Medeiros classification, based on enzymatic mechanism and substrate spectrum (Tooke et al., 2019). For the sake of simplicity, we will refer to all β-lactamases in this study by their Ambler classification. Ambler Class A, C, and D enzymes are all serine β-lactamases in that an active site serine performs the hydrolysis. Conversely, Class B enzymes are metallo-β-lactamases that use an active site zinc for hydrolysis (Ambler, 1980). Much like how β-lactams inhibit PBPs, a covalent

bond between the β-lactam and serine β-lactamases also form during hydrolysis; however, β-lactamases are able to activate an additional water molecule to liberate the enzyme and a degraded β-lactam (Tooke et al., 2019). Several types of β-lactamases with high turnover rates and extended substrate spectra have spread around the world on mobile resistance plasmids and are of primary concern for treatment failure of Gram-negative infections (Bush, 2010). β-lactamases are generally restricted to Gram-negatives, with β-lactam resistance in Gram-positives arising from the use of alternate PBPs (Zapun et al., 2008).

In Bcc species, only two β-lactamases have been biochemically and genetically characterized: PenA/PenB and AmpC. PenA/PenB are homologues of an Ambler Class A serine β-lactamase with broad activity against cephalosporins, carbapenems, monobactams (Papp-Wallace et al., 2013). Due to naming conventions, the homologue in *B. multivorans* is termed PenA, while the homologue in *B. cenocepacia* is termed PenB (Poirel et al., 2009). AmpC is an Ambler Class C serine β-lactamases; however, it has very low hydrolytic activity and is suggested to play a minor role in β-lactam resistance (Becka et al., 2018). The chromosomal genes encoding these β-lactamases (bla_{AmpC} and bla_{PenA}/ bla_{PenB}, respectively) are both regulated by PenR, a LysR-type transcriptional regulator, in a similar manner to AmpR/AmpC of *P. aeruginosa* (Hwang and Kim, 2015; Trépanier et al., 1997). In *P. aeruginosa*, it is thought that exposure to β-lactams which target PBP4 (but not other PBPs) leads to an excess of specific peptidoglycan degradation products (1,6-anhydroMurNAc-pentapeptide) which bind and activate AmpR (the PenR homologue) (Juan et al., 2017; Moya et al., 2009). In this way, the up-regulated β-lactamases are said to be inducible. In *B. multivorans*, it is known that imipenem and tebipenem – but not piperacillin, tazobactam, ceftazidime, and avibactam – induce PenA expression (Becka et al., 2022; Zeiser et al., 2019a). The induction or constitutive expression of β-lactamases can be countered by the addition of appropriate β-lactamase inhibitors. β-lactamase inhibitors form a covalent bond to the enzyme active site, thus inactivating the enzyme (Tooke et al., 2019). PenA from *B. multivorans* is known to be efficiently inactivated by avibactam, relebactam, and vaborbactam (Nukaga et al., 2021). Combinations of β-lactam/β-lactamase inhibitors are devised to preserve β-lactam activity in the face of a wide array of β-lactamases. Commonly available combinations with demonstrated activity against Bcc species are piperacillin/tazobactam (58% susceptible, n = 151) (Zeiser et al., 2019a), ceftolozane/tazobactam (77% susceptible, n = 221) (Mazer et al., 2017), cefepime/zidebactam (100% susceptible, n = 4) (Karlowsky et al., 2020), imipenem/relebactam

(71.3% susceptible, n = 15) (Becka et al., 2021), ceftazidime/avibactam (90% susceptible, n = 150) (Becka et al., 2021), and meropenem/vaborbactam (97% susceptible, n = 150) (Caverly et al., 2019).

1.1.2 The cell envelope and modifications

As a Gram-negative, *Burkholderia* cells are protected by an envelope composed of a thin layer of peptidoglycan between two lipid membranes. The outer membrane is an asymmetric bilayer with lipopolysaccharide (LPS) on the outer leaflet and phospholipids on the inner leaflet. Outer membrane asymmetry is maintained by the Mla pathway, which performs retrograde transport of excess phospholipids from the outer membrane to the inner membrane (Powers et al., 2020). An asymmetric membrane of phospholipid and LPS was found to be ~100-fold less permeable than a simple phospholipid bilayer (Snyder and McIntosh, 2000), likely due to tight packing of LPS molecules. Together, the inner and outer membranes have opposing permeability requirements: small hydrophilic compounds (generally <600 Da; (Decad and Nikaido, 1976) are able to diffuse through water-filled porins in the outer membrane, while hydrophobic compounds are able to more easily diffuse through the inner membrane (Masi et al., 2017). By itself, the permeability barrier imposed by the Gram-negative cell envelope is a substantial contributor to antibiotic resistance, as most antibiotic classes have intracellular targets.

Bacteria possess a variety of LPS modification pathways to change the physical properties of the outer membrane. For example, the PhoPQ two-component system of *Salmonella enterica* subsp. Typhimurium is able to sense changes in extracellular Mg^{2+} concentration (García Véscovi et al., 1996), osmolarity (Yuan et al., 2017), and cationic antimicrobial peptide concentration (Richards et al., 2012), thus activating the PmrAB regulon. Consequences include increased LPS acylation and the addition of phosphoethanolamine or 4-amino-4-deoxy-L-arabinose (Ara4N) to the phosphate groups on the LPS core (Simpson and Trent, 2019). Importantly, bacterial membranes typically bear a net negative charge; thus, cationic antimicrobials such as polymyxins and antimicrobial peptides form strong electrostatic interactions with bacterial membranes as the basis for their membrane-disruptive mechanisms of cell killing (Glukhov et al., 2005). Therefore, reducing the negative charge on the membranes by masking the phosphate groups may render cationic antimicrobial resistance. While most species display inducible LPS modifications, the Ara4N modification in *B. cenocepacia* is essential for cell viability (Ortega et al., 2007). Moreover,

genes necessary for the Ara4N modification are uniquely essential in *Burkholderia* species (Gislason et al., 2017a). It was found that the LPS transport machinery in *B. cenocepacia* recognizes the Ara4N modification as a molecular signature to export LPS to the outer membrane (Hamad et al., 2012). Consequently, MIC values for cationic antimicrobial peptides are approximately 2 orders of magnitude higher for *Burkholderia* species than for *E. coli* or *P. aeruginosa*, for example (Loutet and Valvano, 2011). The Ara4N modification is also thought to contribute to cationic aminoglycoside resistance, by preventing compound entry through the "self-promoted uptake" mechanism of membrane disruption (Moore and Hancock, 1986). Overall, the *Burkholderia* cell envelope is a formidable barrier to antibiotic entry and action.

1.1.3 Efflux pumps

While the Gram-negative cell envelope allows diffusion of compounds with a narrow range of chemical properties, passing this threshold does not guarantee activity for an antibiotic. Bacterial membranes are studded with efflux pumps that actively remove compounds, including antibiotics, from the cell. While many effective inhibitors of efflux pumps have been discovered, they have not been developed as antibiotics due to issues with spectrum of activity and eukaryotic cytotoxicity (Blanco et al., 2018; Spengler et al., 2017; Wang et al., 2016). In bacteria, it was recently determined that an impermeable membrane acts synergistically with active efflux to protect cells from antibiotics (Krishnamoorthy et al., 2017). The genome of *B. cenocepacia* J2315 is annotated to putatively encode members of all six efflux families: 173 major facilitator superfamily (MFS) transporters, 154 ATP-binding cassette (ABC) transporters, 1 multidrug and toxic compound extrusion (MATE) transporter, 1 small multidrug resistance (SMR) transporter, 3 proteobacterial antimicrobial compound efflux (PACE) transporters, and 16 resistance-nodulation-division (RND) pumps (Bazzini et al., 2011; Elbourne et al., 2017; Holden et al., 2009; Kornelsen and Kumar, 2021).

The RND efflux family has a tripartite structure (inner membrane protein, periplasmic adapter, and outer membrane protein) that allows efflux from the periplasm to the extracellular medium using the proton motive force (Du et al., 2018). RND efflux pumps have a wide variety of substrates, including many types of antibiotics, detergents, heavy metals, and quorum sensing compounds (Venter et al., 2015). By exporting quorum sensing compounds, RND pumps play roles in the regulation of virulence. As a consequence of wide substrate specificity, the

overexpression of RND efflux pumps is also a common cause of antibiotic resistance in clinical isolates (Lin et al., 2017; Podnecky et al., 2013; Swick et al., 2011). Specifically in *B. cenocepacia*, studies have linked some of the 16 RND family pumps to antibiotic resistance. The BpeAB-OprB pump confers resistance to aztreonam, tobramycin, chloramphenicol, and fluoroquinolones, the BpeEF-OprC pump confers resistance to chloramphenicol, fluoroquinolones, and trimethoprim, while the AmrAB-OprA pump confers resistance to tobramycin and ciprofloxacin (Bazzini et al., 2011; Buroni et al., 2009; Nair et al., 2004)

1.1.4 Biofilms

Biofilms are physically structured communities of microbes encased in a matrix of exopolysaccharide, protein, lipid, and DNA that can be attached to a surface or free-floating aggregate (Flemming et al., 2016). The dense matrix, abundance of cells, and large size of mature biofilms (up to hundreds of microns in diameter (Rice et al., 2009)) causes oxygen and nutrient gradients within and surrounding the biofilm (Klementiev et al., 2020; Sønderholm et al., 2017). Consequently, the bacterial population is heterogenous with variations in metabolic and growth rates depending on nutrient and oxygen availability. In *B. cenocepacia*, biofilm growth and population heterogeneity is known to contribute to antibiotic tolerance to tobramycin, chlorhexidine, and a variety of β-lactams (Acker et al., 2013; Caraher et al., 2007; Coenye et al., 2011). Tolerance is a phenomenon whereby bacteria are able to survive transient exposure to otherwise lethal concentrations of antibiotics. Importantly, tolerance differs from true resistance in that tolerant bacteria are still susceptible to, and killed by, the antibiotic but at a slow rate (Brauner et al., 2016). While Bcc species readily form biofilms *in vitro* (Acker et al., 2013; Coenye et al., 2011), examination of patient samples has shown that Bcc species do not exist in biofilms during CF respiratory infection, but rather as single cells in the mucus and within macrophages (Schwab et al., 2014). However, it should be pointed out that the lung tissue used by Schwab et al. was obtained from transplanted lungs and autopsies, both of which represent advanced stages of infection (Schwab et al., 2014). Therefore, the localization of Bcc bacteria during earlier stages of infection remains unknown. Despite this, biofilms are important factors in the contamination of water pipes and medical products associated with Bcc infection outbreaks (Collymore et al., 2019; Heo et al., 2008; Lucero et al., 2011; Raddaoui et al., 2022).

1.2 Genetic tools for characterizing essential genes and genomes

The explicit purpose of all antibiotics is to prevent bacterial cell growth or kill bacterial cells. To do this, antibiotics must interfere with a process that is required for bacterial life. The genes encoding processes required for life in a specified set of conditions are called essential genes (D'Elia et al., 2009; Hillenmeyer et al., 2008). Thus, a list of essential genes represents a good starting point for potential targets of synthetic or natural antibiotics.

In efforts to answer the question about which genes are essential in a given microorganism, several targeted and untargeted methods have been employed. For targeted approaches, genes are systematically deleted or interrupted. For untargeted approaches, genes are randomly inactivated by a genetic element, such as a transposon. Hundreds of large-scale essential gene and genome projects have been performed in multiple species and conditions. The major methodologies used to characterize essential genes and genomes are discussed below. An important distinction that will addressed for each method is whether it allows the creation and recovery of essential gene conditional mutants or only generation of a catalog of putative essential genes.

1.2.1 Transposon mutagenesis

Mycoplasma genitalium and *M. pneumoniae* have small genomes of 580 kb and 816 kb, respectively (Fraser et al., 1995; Himmelreich et al., 1996) and thus are logical experimental platforms to develop genome-wide studies. In particular, the Venter group chose these bacteria to apply transposon mutagenesis and identify the first essential genome in laboratory conditions (Hutchison et al., 1999). At their simplest, transposons are "mobile" tracts of DNA, flanked by inverted repeats, that encode a transposase capable of recognizing the inverted repeat and excising the transposon DNA. At a defined or random position, the transposase then integrates the transposon elsewhere in the genome, perhaps disrupting a gene (Babakhani and Oloomi, 2018). The Venter group collected thousands of transposon mutants and sequenced the transposon-genome junction to identify insertion sites. The absence of insertions within the 5'-most 80% of a gene suggested that gene was essential for growth. In total, ~2,200 unique insertion sites were identified, allowing them to approximate the number of essential genes in *M. genitalium* as 265 - 350 of the 482 protein-coding genes (Hutchison et al., 1999).

The density of transposon insertions in a genome can greatly influence which genes are identified as essential. Larger genomes require screening more transposon mutants to maintain

statistical power in essential gene calls (Baym et al., 2016). Furthermore, the Mekalanos group (Cameron et al., 2008) found that the probability of mis-annotating a gene as essential decreased as gene length increased, as longer genes are more likely to be disrupted by a transposon insertion. Currently, next generation sequencing (NGS) techniques allow the creation of high-density transposon mutant libraries comprising hundreds of thousands of unique mutants, thus increasing insertion density and the accuracy of gene essentiality annotations. Several methods of transposon sequencing by NGS now exist such as TnSeq (Opijnen et al., 2009), TnSeq-circle (Gallagher et al., 2011), TraDIS (Barquist et al., 2013; Langridge et al., 2009), HITS (Gawronski et al., 2009), and INSeq (Goodman et al., 2011) (collectively summarized here as TnSeq). By far, transposon mutagenesis is the most common method for identifying essential genes due to the variety of transposon-based genetic tools that exist for different organisms (Liu et al., 2018).

An improvement on TnSeq methods is the introduction of unique, random DNA barcodes to the transposon elements. Once the unique DNA barcodes are delivered with the transposon element to a genomic region, an initial TnSeq analysis is necessary to link insertion sites with DNA barcodes (random barcoded TnSeq, RB-TnSeq). In subsequent experiments using the same mutant library, quantitative tracking of the transposon mutant population in different conditions can be achieved by simple PCR amplification of the DNA barcodes followed by NGS (barcode sequencing, BarSeq) (Price et al., 2018; Simpkins et al., 2019; Wetmore et al., 2015). For experiments with multiple conditions, BarSeq offers increased throughput by substantially reducing the DNA library preparation times.

In principle, transposon-based approaches can only identify essential genes indirectly through the lack of their corresponding mutants. Mutants with disrupted essential genes, or their essential promoters, are not viable. However, transposons can be modified to include an outward-facing constitutive promoter allowing expression of genes downstream of the insertion. Thus transposon mutants with insertions in the promoter region, 5’ end of a gene, or non-essential gene upstream of an essential gene in an operon can be recovered, albeit with altered (non-native) essential gene expression (Coe et al., 2019; Hutchison et al., 1999; Jacobs et al., 2003; Lee et al., 2015; Santiago et al., 2018a; Shaw et al., 2020; Wang et al., 2011). Variable levels of expression can be obtained through a pool of transposons harbouring constitutive promoters with different strengths (Wang et al., 2011). Titratable control of expression can be achieved with inducible promoters, allowing the creation of conditional growth mutants that depend on the inducer for

growth (Bloodworth et al., 2013; Chow and Berg, 1988; Gislason et al., 2017a; Hu et al., 2007; Judson and Mekalanos, 2000; Le Breton et al., 2015; Rappleye and Roth, 1997; Takiff et al., 1992; Yasir et al., 2020). Essential gene mutants can then be isolated from a library of transposon mutants by screening for growth only in the presence of the inducer (Bloodworth et al., 2013; Judson and Mekalanos, 2000).

1.2.2 Gene deletion collections

The availability of the first microbial genome sequences (Blattner et al., 1997; Fleischmann et al., 1995; Fraser et al., 1995; Goffeau et al., 1996) enabled precise mutations to interrogate gene function. Several multinational teams quickly moved on the ability to accurately manipulate genomes and focused on targeted methods for gene-by-gene inactivation, based on homologous recombination. The technical requirements of these endeavours were challenging, but they ultimately resulted in the creation of the first well-defined libraries in yeast (Giaever et al., 2002; Winzeler et al., 1999) and bacteria (Baba et al., 2006; Kobayashi et al., 2003). In particular, the handful of ordered bacterial mutant libraries that now exist have contributed greatly to the understanding of genotype-phenotype relationships (Baba et al., 2006; Berardinis et al., 2008; Kobayashi et al., 2003; Koo et al., 2017; Porwollik et al., 2014; Xu et al., 2011). The utility of gene-by-gene deletion libraries is also demonstrated by their continuing creation in other bacteria of interest (Muir et al., 2020). Additionally, the *E. coli* Keio collection (Baba et al., 2006) has over 3100 citations on PubMed in the 15 years since its creation and continues to yield new insights (Casanova-Hampton et al., 2021; Klobucar et al., 2020; Tong et al., 2020; Wang et al., 2021).

During the construction of gene deletion mutant collections, hundreds of mutants for each bacterial species could not be isolated. The inability to delete a gene is considered a “gold standard” test of essentiality; however, this method does present some limitations. For example, genes could be misannotated as non-essential if suppressor mutations quickly arise after deleting essential genes (Durand et al., 2016; Riber et al., 2006). Solutions are to re-sequence the genomes of mutants of interest or to independently recreate them using inducible genetic tools, such as CRISPR-interference (see below). Another limitation is that mutants of small non-protein coding RNA (ncRNA) genes are missing from deletion collections simply because many ncRNA genes were not identified at the time of library construction. In summary, while gene deletion remains

the gold-standard for creating essential gene lists, this method does not render essential gene mutants for further characterization of gene function.

1.2.3 Antisense RNA

Non-coding RNAs are a broad family of important regulators in both eukaryotes and prokaryotes. Among the members are antisense RNAs (asRNA), that generally cause sequence-specific inhibition of gene expression by interfering with mRNA transcription and translation, or by signaling mRNA degradation (Saberi et al., 2016; Sesto et al., 2013). The first use of asRNA to probe essential genes in bacteria was an untargeted approach (Ji et al., 2001). The Rosenberg group ligated randomly sheared *S. aureus* genomic DNA fragments into a replicative plasmid featuring a promoter under anhydrotetracycline-inducible control. The random ligation allowed gene fragments to be transcribed in the reverse direction, thus generating an asRNA. Reintroduction of the plasmid constructs into *S. aureus* and screening for anhydrotetracycline-induced growth defects allowed identification and isolation of conditional growth mutants or knockdowns; hence, asRNA methods can be used to both identify essential genes and recover conditional mutants for further study of gene function. Since the first report, additional small- (Goh et al., 2015; Nakashima and Tamura, 2009) and large-scale asRNA approaches have been used to identify essential genes and genomes in various bacteria (Forsyth et al., 2002; Knuth et al., 2004; Meng et al., 2012; Rusmini et al., 2014; Wang and Kuramitsu, 2005).

Drawbacks of asRNA knockdown include the possibility of off-target effects and incomplete silencing of gene expression, resulting in a high proportion of false negatives when screening for growth defects. In fact, most reports of essential genes determined by asRNA knockdown identify substantially fewer essential genes than deletion and transposon methods (Ji et al., 2001; Knuth et al., 2004; Meng et al., 2012; Rusmini et al., 2014). Hence, there have been no recent essential genome projects using asRNA.

1.2.4 Protein Degradation Tags

Instead of interfering with transcription or translation of essential genes, fully formed essential proteins can be targeted for destruction by exploiting natural protein degradation pathways. There are many proteases in bacteria (Mahmoud and Chien, 2018), and some have been manipulated for targeted degradation (Butzin and Mather, 2018; Herman et al., 1998; Sekar et al.,

2016). The general approach is to insert a DNA sequence encoding a degradation tag (degron) at the 3' end of the gene of interest within the genome then introduce a plasmid-borne protease or adapter under inducible control. Upon induction, the adapter binds the degron and shuttles the targeted protein to the protease, yielding mutants with titratable essential protein abundance and conditional growth (Davis et al., 2011; Johnson et al., 2019; Kim et al., 2011, 2013). As each mutant must be custom-made, this is a targeted approach to study essential gene function. The Schnappinger group demonstrated that the ssrA degron and SspB adapter can be functionally transferred from *E. coli* to mycobacteria and used to achieve dose-dependent essential gene knockdown and cell death, both *in vitro* (Kim et al., 2011) and in murine models of acute and chronic infection (Kim et al., 2013). On a larger scale, custom-made libraries of essential protein depletion mutants can be used to investigate chemical-genetic interactions and physiological consequences of essential gene depletion (Cameron and Collins, 2014; Johnson et al., 2019).

However, there have been no reports using degrons for *de novo* essential genome identification in bacteria, likely due to the laborious nature of tagging every protein-coding gene. Furthermore, the expression of essential RNAs (e.g. tRNAs) cannot be modulated by degron tagging. Even the libraries that do exist in *E. coli* (Cameron and Collins, 2014) and *Mycobacterium tuberculosis* (Johnson et al., 2019) do not represent more than 80% of a complete essential genome. It has been suggested that the degron tag may interfere with protein localization or function, limiting the ability to examine every essential gene (Johnson et al., 2019).

1.2.5 CRISPR-interference

Another RNA-mediated silencing method that has gained traction with researchers recently is CRISPR-interference, or CRISPRi. The bacterial CRISPR/Cas system provides acquired sequence-specific immunity against phages and foreign DNA (Garneau et al., 2010; Jinek et al., 2012). The Cas9 component of this system is an RNA-guided endonuclease; however, a "dead" Cas9, dCas9, from *Streptococcus pyogenes* has been modified to retain sequence-specific binding of DNA, but without nuclease activity (Bikard et al., 2013; Qi et al., 2013). Synthetic single guide RNAs (sgRNAs) can be introduced to direct dCas9 to bind any DNA sequence of interest downstream of a protospacer-adjacent motif (PAM), a small, but critical, sequence motif. Targeting the promoter region sterically inhibits binding of the RNA polymerase complex and transcription initiation, while targeting the gene body inhibits elongation (Bikard et al., 2013; Qi

et al., 2013), both causing a polar effect in operons. In this way, gene expression can be repressed up to 3,500-fold (Reis et al., 2019). When the exact location of the promoter is unknown, as is the case for most genes in non-model organisms, the 5' end of the gene near the ATG start codon can be targeted (Lee et al., 2019; Liu et al., 2017b; Singh et al., 2016).

Since its inception, there has been rapid adoption of CRISPRi methods to study many aspects of diverse microbes. Typical approaches to CRISPRi use a constitutively expressed sgRNA and place the *dcas9* gene under control of an inducible promoter, both either on a plasmid or in the chromosome (Larson et al., 2013a). Dynamic levels of targeted gene knockdown can be achieved by titrating levels of inducer, changing sgRNA binding location or by introducing mismatches in the sgRNA (Hawkins et al., 2020; Mathis et al., 2021; Qi et al., 2013). There are several distinct features of CRISPRi that address shortcomings of other methods: 1) sgRNA constructs can be made with relative ease; 2) multiple genes can be simultaneously repressed (multiplexing); 3) no genomic modifications are made to the target gene. In order to probe large numbers of genes, many sgRNA-expressing plasmids must be constructed. This can be done quickly in 96-well format using inverse PCR and blunt-end ligation, allowing hundreds of custom mutants to be constructed in a matter of days (Larson et al., 2013a). Furthermore, with multiplexing, several sgRNA cassettes can be introduced into the same plasmid, allowing investigations into high-order knockdown mutants (Ni et al., 2019; Reis et al., 2019). To host range of CRISPRi can also be broadened by using a codon-optimized *dcas9* gene (Choudhary et al., 2015; Farzadfard et al., 2013; Maeder et al., 2013; Peng et al., 2018; Rock et al., 2017; Tong et al., 2015) or different Cas orthologues to avoid potential issues of high dCas9 expression by itself affecting growth (Cho et al., 2018; Depardieu and Bikard, 2019; Rock et al., 2017).

The fact that gene expression can be turned on and off with CRISPRi has been exploited for the isolation and characterization of essential gene mutants. Reports studying essential genes using CRISPRi can be separated on whether they use targeted or untargeted approaches, dictating how the sgRNAs are designed and cloned individually vs. in pools. Targeted CRISPRi validated previously identified essential genomes and has focused on essential genetic networks (Liu et al., 2017b; Peters et al., 2016; Shields et al., 2020; Silvis et al., 2021; de Wet et al., 2020). Untargeted methods use pools of sgRNAs in parallel to target all PAM sites or known genetic elements, enabling genome-wide screens and mutant tracking by sequencing of the gRNA genes, which are unique for each mutant (Cui et al., 2018; Donati et al., 2021; Lee et al., 2019; Liu et al., 2020;

Mathis et al., 2021; Peters et al., 2019; Rousset et al., 2018, 2021; Wang et al., 2018). The logic behind untargeted CRISPRi is similar to transposon mutagenesis: CRISPRi mutants in essential genes are recovered in low abundance, resulting in low sgRNA sequencing read density (termed CRISPRi-Seq). Interestingly, it has been reported that CRISPRi screens are more efficient than transposon mutagenesis in identifying essential genes, requiring at least ten-fold fewer mutants to achieve similar statistical power (Calvo-Villamañán et al., 2020; Rousset et al., 2018, 2021; Wang et al., 2018). To aid in genome-wide screens, new computational tools can automate sgRNA design and selection (Mohr et al., 2016; Spoto et al., 2020) to reduce chances of confounding off-target effects (Cui et al., 2018); however, mismatches are sometimes desired as they can predictably titrate gene repression (Hawkins et al., 2020; Jost et al., 2020; Mathis et al., 2021). Some genes cannot be targeted by CRISPRi as they lack PAM sites, limiting genome-wide approaches (Shields et al., 2020). The requirement of a PAM site is a drawback for all CRISPR/Cas approaches, but can be partially compensated for by using dCas9 enzymes that recognize different (Rock et al., 2017) or synthetically reduced PAM sites (Hu et al., 2018; Walton et al., 2020).

1.3 In vivo screens to identify antibiotic targets and mechanisms of action

Despite the incredible difficulty in finding new antimicrobial scaffolds, many other challenges remain in the process of antibiotic development. One such bottleneck is target and mechanism of action identification. Unless the cellular target is known, initial hit compounds cannot be rationally redesigned to improve activity. Many technologies have emerged to rapidly and accurately link compound to target. Whole-cell target-based assays have the added benefit of intrinsically screening for cell-permeable compounds, a major roadblock noted in previous large-scale screens (Payne et al., 2007; Tommasi et al., 2015). *In vivo* studies consider the target within its natural setting, potentially with specific localization or interaction partners, and can also examine the cellular consequences of target inhibition. Thus, here we will only discuss *in vivo* screens to identify antibiotic targets.

1.3.1 Macromolecular synthesis assays

Synthesis of each of the bacterial macromolecules (DNA, RNA, protein, peptidoglycan, and lipid) is essential for viability. Thus, one step to narrowing down the target of a new antimicrobial is to determine if the antimicrobial inhibits the synthesis of a macromolecule.

Briefly, if a synthesis of a specific macromolecule is inhibited, then radiolabelled precursors will not be incorporated into that macromolecule. Commonly used precursors are [^{3}H]-thymidine (for DNA synthesis), [^{3}H]-uridine (for RNA synthesis), [^{3}H]-glycerol (for lipid synthesis), [^{14}C]-*N*-acetylglucosamine (for peptidoglycan synthesis), and [^{3}H]-leucine (for protein synthesis) (Cotsonas King and Wu, 2009; Mattingly et al., 1976; Roth et al., 1971). Classically, macromolecular synthesis has been used to demonstrate that the penicillins inhibit peptidoglycan synthesis (Higgins et al., 1980) and that the tetracyclines inhibit protein synthesis (Rasmussen et al., 1991). However, this assay continues to be used for characterizing novel compounds, such as teixobactin (Ling et al., 2015) and the bis-indoles (Opperman et al., 2016). However, a limitation to this method is that the five macromolecules commonly assayed may not be targeted by growth-inhibitory compounds (e.g. CCCP, fosmidomycin, and CHIR-090) (Vincent et al., 2016), especially with the push to exploit new cellular targets (Miethke et al., 2021; Watkins and Unnikrishnan, 2020).

1.3.2 Target mutations conferring antibiotic resistance

Antibiotics exert a pressure on bacterial populations that results in the selection of resistant mutants. One pathway to resistance is the acquisition of mutations in the target that reduce binding to the antibiotic. This theory has been used to link novel antibiotics to their target and has a good track record in the literature. For example, mutations in DNA gyrase A (encoded by *gyrA*) result in nalidixic acid resistance in *E. coli* (Higgins et al., 1978), and mutations in the RNA polymerase β subunit result in rifampicin resistance in *M. tuberculosis*. (Telenti et al., 1993). Generation and sequencing of spontaneously resistant mutants is relatively simple, especially with availability of NGS methods, and continues to be used for characterizing new compounds. Resistance to 1,3-benzothiazin-4-ones in *M. tuberculosis* was linked to target mutations in decaprenylphosphoryl-β-D-ribose 2'-epimerase (encoded by *DprE1*) (Makarov et al., 2009), and recently, resistance to the novel arylomycin class Gram-negative antibiotics was caused by target mutations in the type I signal peptidase (encoded by *LepB*) (Smith et al., 2018). However, simply identifying mutations in potential target genes is not conclusive evidence of a valid target. Hits must be followed up with further biochemical or genetic studies (Makarov et al., 2009; Smith et al., 2018; Zampieri et al., 2018). These follow-up experiments may not identify the valid target but rather another resistance

mechanism, such as efflux, as mutations in essential gene targets may be difficult to generate or result in fitness defects (Woodford and Ellington, 2007).

1.3.3 Bacterial cytological profiling

Bacterial cell morphology is remarkably plastic and can be altered by a variety of stimuli (Caccamo and Brun, 2018; Chan et al., 1987; Wainwright et al., 1999). For example, cells with defects in divisome formation or those exposed to β-lactams targeting divisome peptidoglycan synthesis form long filaments (Addinall and Lutkenhaus, 1996; Zimmerman and Stapley, 1976). Taking advantage of antibiotic-induced morphological effects, the Pogliano group developed a method termed bacterial cytological profiling (BCP) to make predictions on antibiotic mechanisms of action in *E. coli* (Nonejuie et al., 2013). The method was benchmarked using 41 antibiotics with known targets and mechanisms of action. Following exposure to these antibiotics, the cells were stained with FM4-64 (to highlight the membrane), DAPI (to highlight the nucleoid), and SYTOX Green (to highlight the nucleoid of cells with damaged envelopes), then imaged by confocal microscopy. Following principal component analysis of cell and nucleoid morphology, there were clear separations between the cellular effects of antibiotics with different classes. As a proof of principle, BCP was used to identify that spirohexenolide A, an uncharacterized antimicrobial, collapsed the proton motive force. The Pogliano group extended their method to *B. subtilis* and further showed that the morphological effects of antibiotic treatment often mirrored the morphology of cells depleted in the cognate essential protein target (Lamsa et al., 2016). More recently, the method has been extended to *Acinetobacter baumannii* (Htoo et al., 2019) and *M. tuberculosis* (under the name MorphEUS) (Smith et al., 2020).

The Pogliano group has suggested that as bacterial cells lack many checkpoints for inter-pathway communication, the inhibition of one pathway has limited effect on other cellular processes (Nonejuie et al. 2013). Thus, uninhibited processes may continue, and result in morphological defects. Which may be why, for example, that β-lactams targeting divisome peptidoglycan synthesis cause cell filamentation: lateral peptidoglycan synthesis and DNA replication carry one, allowing cells to continue growing. However, a limitation to BCP is that the method cannot determine the exact molecular target, only the inhibited pathway. Thus, additional validations are required to complement the findings of BCP. Furthermore, as BCP relies on comparison to antibiotics with known mechanisms of action, determining the mechanism of

compounds representing first-in-class inhibitors with novel mechanisms may prove challenging. It should be pointed out that the mechanisms identified by BCP for novel compounds were all included in the benchmark set of known antibiotics (Nonejuie et al. 2013, Lamsa et al. 2016, Smith et al. 2020).

1.3.4 Modulating gene dosage: chemical genetics and chemogenomics

The susceptibility of cells to antibiotics is a function with multiple variables, including, for example, vulnerability of the target essential gene/process and resistance mechanisms. Antibiotic susceptibility can be altered by genetic manipulation of resistance genes and, importantly, expression of the target gene. Overexpression of a target gene requires more antibiotic to inhibit the target gene's function, reducing antibiotic susceptibility (Li et al., 2004). Indeed, overexpression of the dihydrofolate reductase target gene (Matthews et al., 1985) is the basis for using trimethoprim as a selectable antibiotic marker. On the other hand, target gene knockdown results in enhanced antibiotic susceptibility as there are fewer gene products performing their essential function (Cardona et al., 2015; DeVito et al., 2002). Together, these ideas form the basis of chemical genetic and chemogenomics. In 2001, chemogenomics was first defined as the "discovery and description of all possible drugs to all possible drug targets" (Caron et al. 2001). More accessibly, chemogenomics has become known as the use of small molecules to probe genetic networks on a genome-wide scale; chemical genetics is thus a subset focused, for example, on specific pathways or sets of genes.

The first demonstration that modulating target gene expression could link an antibiotic to its target was from the pharmaceutical company Bristol-Myers-Squibb. The group created mutants with genomic copies of essential genes placed under arabinose-inducible control. Growth in the presence of low concentrations of arabinose made the cells sensitive to specific antibiotics and was used to identify novel inhibitors of MurA (DeVito et al., 2002). Since then, a variety of other groups have adapted different methods to reduce target gene expression to modulate antibiotic susceptibility, including asRNA (Therien et al., 2012; Xu et al., 2010), inducible promoter replacement (Bloodworth et al., 2013; Sass et al., 2018; Wang et al., 2011), protein degradation (Cameron and Collins, 2014; Johnson et al., 2019; Wei et al., 2011), and CRISPRi (Li et al., 2022; Martin et al., 2020; Peters et al., 2016). As a complementary approach, groups have used genomic (shotgun) overexpression libraries (Gingras et al., 2018; Li et al., 2004; Pathania et al., 2009; Xiao

et al., 2012) and transposons bearing outward-facing strong promoters (Coe et al., 2019; Wang et al., 2011). As there is single gene resolution associated with many of these methods, they permit *de novo* identification of novel antibiotic mechanisms of action (Johnson et al., 2019; Peters et al., 2019; Xiao et al., 2012). For example, Johnson et al. recently reported the use of a near essential genome-wide knockdown mutant library in *M. tuberculosis* to link small molecules with their target. Using high-throughput compound screening and NGS fed into a machine-learning model, they identified novel inhibitors of DNA gyrase, the RNA polymerase, folate biosynthesis, and the essential EfpA efflux pump (Johnson et al. 2019). Chemical optimizations of the EfpA inhibitor yielded a molecule with potent and specific bactericidal activity against *M. tuberculosis* and low *in vitro* eukaryotic cell toxicity (Johnson et al. 2019).

A related strategy is to expose transposon mutant libraries (Geisinger et al., 2020; Rajagopal et al., 2016; Santiago et al., 2018a) or gene deletion collections (Nichols et al., 2011; Tamae et al., 2008) to antibiotics and observe changes in mutant fitness. However, transposon and deletion collections can only yield clues about antibiotic targets and mechanisms as these methods cannot directly probe essential functions, with some exceptions for transposons bearing outward-facing promoters. In a recent chemogenomic screen in *A. baumannii*, Geisinger et al. identified dozens of non-essential gene modulators of antibiotic susceptibility, then used these susceptibility profiles to propose functions for new genes and to predict antibiotic synergy (Geisinger et al., 2020). Overall, the use of complementary approaches (overexpression vs. knockdown, and probing essential vs. non-essential genes) shines a light on how all genes affect antibiotic susceptibility.

1.3.5 Metabolomics assays

As a consequence of inhibiting essential processes, antibiotics induce changes to cellular metabolite levels that may be indicative of the inhibitory mechanism (Ortmayr et al., 2022). These changes can be measured directly using metabolomics (Zampieri et al., 2017). As a simple example, inhibition of an enzyme will alter levels of metabolic intermediates in the affected pathway, including perhaps an increase in substrate and decrease in product abundance. Indeed, Vincent et al. have shown that treating *E. coli* with the compound AZ1, an inhibitor of thymidylate kinase, caused large changes in levels of deoxynucleotide precursors, including higher levels of deoxythymidine monophosphate (the substrate) and lower levels of deoxythymidine diphosphate (the product) (Keating et al., 2012; Vincent et al., 2016). Benchmarking can be used to compare

the effect of known perturbations (e.g. genetic manipulations or antibiotic exposure) to make predictions about mechanisms of uncharacterized compounds (Vincent et al. 2016, Zampieri et al. 2017, 2018, Anglada-Girotto et al. 2022). Very recently, the Zampieri group profiled the metabolome of ~300 CRISPRi mutants in essential genes and found good correlation between perturbations caused by CRISPRi and antibiotics of specific classes. Then using similarities between metabolomic profiles from CRISPRi mutants and a panel of growth inhibitory compounds, the group identified then validated the mechanism of action for four uncharacterized compounds (tegaserod, suloctidil, chloroxine, and thiethylperazine). Metabolomics has also been used to identify how cells metabolize antibiotics (Vincent et al., 2016) and to make broad conclusions about the role of reactive oxygen species in antibiotic lethality (Belenky et al., 2015; Lobritz et al., 2022). However, a caveat to using metabolomics is that the method is apparently blind to some compounds, as not all inhibitory compounds induce changes in the metabolome, such as the uncoupler CCCP (Vincent et al., 2016). Overall, the vast amount of data generated by metabolomics approaches has the potential to yield unprecedented insight into antibiotic mechanisms of action.

1.4 Contextualizing essential genes as antibiotic targets

After more than two decades of research identifying and characterizing essential genomes, it has become clear that the biological reality of gene essentiality is not binary (essential vs. non-essential). Instead, gene essentiality is a quantitative trait with each gene placed on a spectrum between classical definitions of essential and non-essential. Gene essentiality depends on growth conditions, genetic context, and how susceptible cells are to depletion of the essential gene product. I refer to these diversities of growth phenotypes as “essentiality gradients”. The individual characteristics of each essential gene has important consequences for antibiotic target prioritization.

1.4.1 Conditional essentiality

Genes which are essential in some, but not all, conditions are called conditionally essential genes. A classic example of conditional essentiality due to environmental constraints is auxotrophy, where organisms are deficient in various nutrient synthesis genes. While said auxotrophic mutants would grow in rich medium containing essential nutrients, they would not

grow in a minimal medium that requires their *de novo* synthesis. For example, screening the Keio *E. coli* gene deletion collection revealed that many amino acid and cofactor biosynthetic pathways (e.g. pyridoxal phosphate, histidine, and leucine) are conditionally essential for growth in glycerol-supplemented minimal medium (Joyce et al., 2006). Large experimental screens using gene deletion collections across hundreds of conditions have confirmed at least minor fitness contributions for 97% of *S. cerevisiae* genes (Hillenmeyer et al., 2008) (compared to 18.7% of genes in rich medium (Giaever et al., 2002)), and less than 50% of *E. coli* genes (Nichols et al., 2011; Tong et al., 2020). Thus, it is clear that with new, larger studies, conditional essentiality will be observed for an increasing number of genes.

Transposon mutagenesis studies also provide multiple examples of conditional essentiality. For example, the Baughn group (Minato et al., 2019) used transposon mutagenesis to compare the essential genome of *M. tuberculosis* H37Rv in minimal and rich media. They identified up to 601 essential genes in rich medium, while an additional 130 genes were conditionally essential when grown on minimal medium. As expected, the majority of the conditionally essential genes encoded biosynthetic functions, such as vitamin/cofactor, amino acid, and nucleotide biosynthesis (Minato et al., 2019). Additionally, with their experimental data, the group was able to suggest important refinements to the metabolic model for *M. tuberculosis* (Ma et al., 2015).

Although *in vitro* growth phenotypes can be used to assign specific functions for uncharacterized genes, these conditions may not reflect real-world scenarios. For example, the nutritional environment or external stresses that bacteria encounter during infection are difficult or impossible to reproduce in a test tube (Bjarnsholt et al., 2021; Grazziotin et al., 2015; Liu et al., 2020; Miller and Scott, 2020; Umland et al., 2012; Zhu et al., 2020). Several studies have shown poor overlap of essential gene sets identified in rich medium and either synthetic medium designed to mimic infection conditions or medium supplemented with *ex vivo* components. Studying which genes are essential in more realistic conditions is therefore very informative. One such condition is the lung environment of people with CF. The desire to simulate the CF lung environment led the Whiteley group to create synthetic CF sputum medium (SCFM and SCFM2) (Palmer et al., 2007; Turner et al., 2015). The group then compared the essential genome of *Pseudomonas aeruginosa* grown in real CF sputum vs. SCFM2. Cofactors such as riboflavin, pyridoxal phosphate, and biotin were not abundant in either media; thus, many cofactor biosynthetic genes were conditionally essential (Turner et al., 2015). By showing an overlapping set of essential genes

in both SCFM2 and CF sputum, these authors demonstrated that SCFM2 can mimic CF sputum conditions for microbiological studies.

1.4.2 Synthetic genetic interactions

Similar to the interactions of environmental conditions with genetic backgrounds, there are also epistatic interactions between genes that can change an observed phenotype. The term epistasis refers to an event where expression of a gene affects the expression of a second gene. Epistatic interactions are also known as synthetic genetic interactions, whereby the effect of combinations of mutations is statistically greater than the expected result if observed independently (Fisher, 1919; Ruiz et al., 2006). In the context of growth, synthetic interactions can either be negative and result in lower fitness – or death – than expected (synthetic lethal/sick) or can be positive and result in greater fitness (synthetic viability). Interestingly, antibiotic drug interactions phenocopy genetic interactions wherein one drug can either antagonize or synergize the activity of another, (Brochado et al., 2018; Tyers and Wright, 2019).

Nutrient transporters and biosynthetic pathways are often functionally redundant and found in synthetic lethal pairs. To characterize the interactions of nutrient acquisition and biosynthesis genes, the Brown group (Côté et al., 2016) examined the interaction of all non-essential genes in *E. coli* with 82 nutrient stress-associated genes, resulting in over 315,000 interaction pairs (double deletion/knockdown mutants). For example, pantothenate is a common component of rich medium and *E. coli* encodes the PanF transporter import it; however, *E. coli* can also synthesize pantothenate *de novo*. Consequently, *panF* and pantothenate biosynthetic genes are not individually essential in rich media (Baba et al., 2006). However, deletion of any of the pantothenate biosynthetic genes formed a synthetic lethal interaction in a Δ*panF* background (Côté et al., 2016).

Synthetic viable interactions occur when the combined mutant is more fit than expected from the phenotype of each single mutation. A good example of synthetic viability can be found in the so-called protective essential genes, whose essential function is to prevent the accumulation of toxic intermediates and waste products. In *Bacillus subtilis*, there are at least 13 protective essential genes (out of 257 identified essential genes) (Commichau et al., 2013; Koo et al., 2017; Michna et al., 2014). The encoded functions are diverse, including prophage repressors, antitoxins, protection from reactive oxygen species, and resistance to endogenous antimicrobial production.

Interestingly, viable mutants can be constructed of some protective essential genes when the toxic product is no longer produced. For example, SunI provides resistance to the glycocin antibiotic sublancin, produced by SunA; *sunI* can only be deleted when *sunA* is also absent (Dubois et al., 2009).

Synthetic genetic interactions display inconsistent patterns species and strains, reflecting differing evolutionary histories and interactions in genetic circuitry. Case in point, *sunI* and *sunA* are encoded by the SPβ prophage, which is generally limited to strains of subspecies *B. subtilis subtilis* (Brito et al., 2017). Recently, in *E. coli* it was found that horizontally acquired genetic elements associated with bacterial immunity could induce the essentiality of endogenous genes needed to control activity of the acquired genes (Rousset et al., 2018). There are also large differences in the conservation of essentiality in genes involved with cellular redox homeostasis. *E. coli* depends on either a functional thioredoxin or glutathione system for viability and robust growth but cannot tolerate mutations in both pathways simultaneously (Prinz et al., 1997; Russel and Holmgren, 1988). However, synthetic interactions among antioxidant-encoding genes demonstrates the overall essentiality of the processes (Carmel-Harel and Storz, 2000; Staerck et al., 2017).

1.4.3 Essential gene vulnerability

Different critical thresholds of essential product abundance exist for each essential function, below which cell viability is compromised. These thresholds are defined by combinations of gene expression, protein activity and degradation, and metabolic and regulatory buffering, among other factors (Donati et al., 2021; Hawkins et al., 2020; Poyatos, 2020). Studying a cell's response to catastrophic blockage in essential functions – say by CRISPRi or protein degradation – yields important insight into the nature of gene essentiality. Over successive generations, the levels of essential gene products are depleted in the daughter cells, eventually crossing a critical functional threshold and halting cell growth (Gallagher et al., 2020; Hart and Silhavy, 2020; Hawkins et al., 2020; Herring and Blattner, 2004). Essential gene vulnerability reflects a cell's susceptibility to essential process inhibition (Bosch et al., 2021; McNeil et al., 2021; Wei et al., 2011).

Large-scale studies also show that essentiality gradients are created due to essential gene depletion. Recently, the Manoil group (Gallagher et al., 2020) made clever use of a coupled

transformation-transposon mutagenesis method (TFNseq) in *Acinetobacter baylyi* to rank processes based on the timing of mutant depletion from a pool. TFNseq was assessed by sequencing the population at many early timepoints immediately after mutagenesis, giving finer temporal resolution as essential processes were inactivated from essential protein depletion. Overall, disruptions to ATP synthesis, dNTP synthesis, and ribosome production more rapidly arrested growth, suggesting these processes may be more attractive antibiotic targets as inhibition rapidly halts cell growth. Highly vulnerable essential genes are more functionally important and thus incur higher fitness costs and are more likely to result in cell death when depleted, at least in *M. tuberculosis* (McNeil et al., 2021). Conversely, genes with moderate or low vulnerability are more likely result in cell stasis when depleted (McNeil et al., 2021)

Alternatively, CRISPRi can be used to deplete essential genes then track mutant abundance using NGS. Recently, the Gross group (Hawkins et al., 2020) tiled the essential genome of *E. coli* and *B. subtilis* with a panel of 10 fully complementary and 90 single mismatched sgRNAs per gene for a wide range of repression. Expectedly, there was a large diversity of vulnerability profiles; however, the responses within functional classes were generally similar. The vulnerability profiles of essential homologues between *E. coli* and *B. subtilis* were also similar, demonstrating the importance and conservation of central processes even in bacteria with ~2 billion years of evolutionary separation (Hawkins et al., 2020). Additionally, a similar study from the Rock group using CRISPRi in *M. tuberculosis* found highly vulnerable essential genes were more likely to have a homologue in other bacterial species than less vulnerable genes (Bosch et al., 2021). Importantly, quantification of vulnerability allowed the Rock group to suggest ranks for essential genes as drug targets in *M. tuberculosis*.

1.4.4 Core and accessory essential genomes

The comparison of multiple genomes enables the identification of core and accessory genomes, and in a similar fashion we can define core and accessory essential genomes. Remarkably, we have come to a point where claiming to have identified a core or accessory essential genome has become ambiguous. Originally, the core and accessory essential genomes referred to the universal prokaryote/eukaryote and individual species/genera gene sets, respectively (Juhas et al., 2012); however, the vast amount of data has forced a change in that the core essential genome usually refers to species, and that the accessory essential genome refers to

strain-specific differences (Coe et al., 2019; Gislason et al., 2017a; Le Breton et al., 2015; Lewin et al., 2019; Lin and Zhang, 2011; Martínez-Carranza et al., 2018; Narayanan et al., 2017; Poulsen et al., 2019). Pangenomes can be very large (Freschi et al., 2019; Mangas et al., 2019), but the Hung group was able to define a reliable core essential genome for *P. aeruginosa* by comparing only four strains; however, they also noted that the methods for mutant generation and analysis substantially affected core essential genome calls (Poulsen et al., 2019). This was recently remedied by the Bikard group (Rousset et al., 2021) via a unified large CRISPRi screen in 18 diverse strains of *E. coli* representing common phylogroups and lifestyles. Similarly, they found diminishing returns in the number of core essential genes as the number of strains increased. There were also striking strain-specific differences: 266 core essential genes were required for growth in LB in all strains, versus 506 pan-essential genes were required for growth in LB in at least one strain (Rousset et al., 2021).

1.4.5 Antibiotic target prioritization based on essentiality gradients

We propose that essentiality gradients may be used to prioritize targets and unveil new avenues for discovery. Preferred antibiotic targets would be encoded by indispensable essential genes within highly connected networks. Ideally, cells would also be highly vulnerable to inhibition of the target to immediately arrest growth or cause cell death. There is a broad range in the rate of killing for bactericidal antibiotics (Baquero and Levin, 2021), with the rapid cell death associated with physical membrane disruption by detergents and biocides being an aspirational target for new antibiotics. However, the factors leading to vulnerability are still largely unknown in bacteria and these areas require further work, such as genome-wide vulnerability profiling. As proof of principle of the link between vulnerability and target prioritization, the Rock group's genome-wide vulnerability profiling in *M. tuberculosis* identified that the targets of the first-line anti-tuberculosis drugs isoniazid (*inhA*) and rifampicin (*rpoB*) are highly vulnerable (Bosch et al., 2021), supporting a previous report (Wei et al., 2011). However, they also point to many other highly vulnerable potential drug targets, such as the aminoacyl-tRNA synthetases, which are under active investigation (Bouz and Zitko, 2021) with one compound (GSK656) entering clinical trials (Li et al., 2017). Separately, the Cook group examined their genome-wide CRISPRi vulnerability screen in *M. tuberculosis* in the context of targeted pathway and cell fate (bacteriostatic vs. bactericidal) (McNeil et al., 2021). They found that knockdown of genes related to transcription,

translation, cell wall synthesis and division were generally bactericidal. Such studies could form guiding frameworks with implications for antibiotic development and target selection.

Alternatively, if target inhibition does not render complete growth arrest, the gene may exist in a synthetic lethal pair which could be exploited by combination therapy, as recently proposed for cancer therapy (Akimov and Aittokallio, 2021; Huang et al., 2020), a theory called collateral vulnerability (Wang et al., 2019). For example, the recently approved antitubercular bedaquiline depletes the ATP pool from *M. tuberculosis*, thereby sensitizing cells to inhibition of glycolysis (Mackenzie et al., 2020) and the essential ATP-intensive process of glutamine synthesis (Wang et al., 2019).

The conservation of bacterial core essential genes and bacterial essential genes overall (Ish-Am et al., 2015; Jordan et al., 2002), presents these genes are favourable targets for broad-spectrum antibiotics. Indeed, this is behind the broad-spectrum activity and recent interest in darobactin (targeting BamA)(Imai et al., 2019), complestatin and corbomycin (interfering with autolysins and peptidoglycan remodeling)(Culp et al., 2020), the arylomycin G0775 (targeting signal peptidase I)(Schimana et al., 2002; Smith et al., 2018), and new β-lactam/β-lactamase inhibitor combinations (targeting peptidoglycan synthesis) (Durand-Reville et al., 2021; Lomovskaya et al., 2021a). Conversely, the investigation of narrow-spectrum antibiotics is driven by the prospect of reduced negative effects on the healthy microbiome (Melander et al., 2017). In theory, activity can be finely tuned to exploit clade-specific conditional essentiality. For example, the Xu group (Stone et al., 2015) took advantage of differences in *meso*-diaminopimelate synthesis in oral commensal streptococci versus pathogenic *Porphyromonas gingivalis*, to design and validate an inhibitor of the essential *P. gingivalis meso*-diaminopimelate dehydrogenase (Stone et al., 2015). Additionally, the Lewis group reported that hygromycin A, a protein synthesis inhibitor first identified almost 70 years ago (Pittenger et al., 1953), was a selective inhibitor of *Borrelia burgdorferi*, the causative agent of Lyme disease, and related spirochaetes such as *Treponema pallidum*, the causative agent of syphilis (Leimer et al., 2021). Hygromycin A likely mimicked the substrate of the essential BmpDEFG nucleoside transporter. *B. burdorferi* is a purine auxotroph and depends on the BmpDEFG transporter as the only mechanism of purine uptake (Cuellar et al., 2020). This selective uptake mechanism explains the very narrow spectrum of activity and consequently mild effect on the gut microbiome in a murine model (Leimer et al., 2021).

Targeting infection setting conditionally essential genes also shows promise to yield potent and narrow-spectrum pathogen-specific antibiotics. For example, human plasma has low levels of biotin, necessitating *de novo* synthesis by invading pathogens (Carfrae et al., 2019). The Brown group exploited this dependence and identified that the biotin synthesis inhibitor MAC13772 inhibits growth of important pathogens such as *A. baumannii* and *M. tuberculosis*, in biotin-deficient medium and human serum but not rich laboratory medium (Carfrae et al., 2019; Zlitni et al., 2013). Similarly, a screen of 11,862 compounds with increased activity in serum-supplemented nutrient-poor medium identified the RNA polymerase inhibitor rifabutin as having 200-fold reduced MIC against an extensively drug-resistant strain of *A. baumannii*. In nutrient-limited conditions only, non-specific uptake by the outer membrane protein FhuE permitted entry of rifabutin, but not the closely related rifampicin (Luna et al., 2020). Of note, these conditional effects would be completely missed by screening in typical laboratory medium. Thus, integrating the concept of essential gradients into antibiotic discovery shows great promise for prioritizing discovery campaigns against attractive targets.

1.5 Non-essential genes as targets of antibiotic potentiators

Non-essential gene products play important roles in antibiotic mechanisms of action and the cellular response to antibiotics. For example, both imipenem and meropenem permeate *P. aeruginosa* cells through the OprD porin, while the MexAB-OprM pump effluxes both compounds (Köhler et al., 1999). Thus, various non-essential genes may either decrease or increase antibiotic susceptibility. A holistic perspective on antibiotic action requires interrogating both essential and non-essential genes (i.e. genome-wide studies). Here we define a non-essential gene as a gene in which transposon disruption or deletion results in a viable mutant but may still have a growth defect. Several studies have identified a multitude of non-essential genes that modulate antibiotic activity, some of which have been targeted with inhibitors that potentiate antibiotic activity.

1.5.1 Non-essential genes that modulate antibiotic susceptibility

As the number of effective antibiotics used to treat infectious disease dwindles, one strategy is to use rationally designed synergistic combinations. Rather, instead of combining two antibiotics that each suppress cell growth, another approach is to combine an antibiotic with a potentiating compound that increases the effect of the antibiotic without suppressing growth by

itself. The motivation behind this is that compounds without explicit inhibitory activity will reduce selection for mutants resistant to the potentiating effect (Otoupal et al., 2021; Rezzoagli et al., 2020). Various groups have undertaken large-scale/genome-wide studies to identify new targets for potentiator development using gene deletion collections, CRISPRi, and transposon mutagenesis.

Otoupal et al. reported on the interaction of 30 non-essential gene deletion mutants with nine diverse antibiotics (Otoupal et al., 2021). In addition to demonstrating the importance of the AcrAB-TolC efflux pump for resistance, the group also showed that deletion of *fur*, *fnr*, *recA*, and *rpoS* greatly increased susceptibility to multiple antibiotics. Additionally, they showed that non-essential gene knockdown with CRISPRi restored antibiotic susceptibility in a HeLa cell model of intracellular *S.* Typhimurium infection (Otoupal et al., 2021). In larger studies profiling the entire genome, the Isberg and van Opijnen groups used transposon mutagenesis in *A. baumannii* with the goal of guiding rational antibiotic combinations (Geisinger et al., 2020). Mutants with disruptions in the Rod system of lateral peptidoglycan synthesis were highly susceptible to β-lactams that targeted divisome peptidoglycan synthesis. Consequently, they observed that combinations of β-lactams that targeted lateral and divisome peptidoglycan synthesis were synergistic (Geisinger et al., 2020). On the other hand, disruption of non-essential genes may also reduce antibiotic susceptibility. In a screen of *S. pneumoniae* transposon mutants, the van Opijnen group found that mutants in many genes related to purine metabolism had reduced susceptibility to multiple antibiotics. Furthermore, clinical isolates often had non-sense mutations in these genes, which they propose as a set of predictable pathways leading to antibiotic resistance.

Transposon and gene deletion screens can only examine non-essential genes, so the relative contributions of essential vs. non-essential genes to antibiotic susceptibility cannot be assessed. A recent genome-wide CRISPRi screen in *M. tuberculosis* for antibiotic susceptibility found approximately the same number of chemical-genetic interactions among knockdown of essential and non-essential genes. However, considering that essential genes usually make up ~10% of the genome, essential genes were thus enriched as determinants of antibiotic susceptibility (Li et al., 2022).

1.5.2 Compounds that potentiate antibiotics

The identification of antibiotic resistance determinants allows targeted searches for inhibitors of specific resistance mechanisms that can restore antibiotic activity. The β-lactamase inhibitors are common examples of antibiotic potentiators: the inhibitors display negligible growth inhibitory activity on their own, while substantially increasing the potency of β-lactam antibiotics. Currently, β-lactamase inhibitors are the only clinically available potentiators, and they have a decorated history in the clinic since their discovery in the 1970's (Reading and Cole, 1977). β-lactamase inhibitors are substrate mimics of β-lactamases and form a covalent bond with an active site serine to inactive the enzyme (Tooke et al., 2019). To combat the large diversity of β-lactamases, many structurally different β-lactamase inhibitors now exist (Drawz and Bonomo, 2010). While some exhibit narrow inhibitory spectra of activity, newer "ultra-broad spectrum" inhibitors now exist that are active against virtually all classes of β-lactamases (Hecker et al., 2020; Lomovskaya et al., 2021b). As opposed to inhibiting an enzyme that inactivates an antibiotic, an alternative approach is to inhibit efflux pumps that remove antibiotics from the cell. The broad substrate range of efflux pumps (Mehla et al., 2021) and their common identification as the cause of clinical resistance makes them attractive targets. While a variety of natural and synthetic efflux pump inhibitors exist that display impressive potentiation, there are no reports yet of efflux inhibitors that have been approved for clinical use (Laws et al., 2019). An additional approach to potentiation could also be to prevent synthesis of the resistance factor itself. B-lactamases and mobile colistin resistance (MCR) enzymes reside in the periplasm and rely on disulfide bonds, formed by the DsbAB pathway, for correct folding and activity. It was recently shown in *E. coli* that chemical inhibition of DsbB and periplasmic disulfide bond formation with "compound 12" potentiated the activity of colistin and a variety of β-lactamases (Furniss et al., 2022; Landeta et al., 2015).

As discussed previously, the Gram-negative cell envelope is a significant barrier for antibiotic entry and activity. Thus, increasing membrane permeability is an attractive approach to sensitizing cells to antibiotics (Klobucar and Brown, 2022). There are many growth-inhibitory compounds that disrupt bacterial membranes and potentiate the activity of antibiotics (e.g. the polymyxins) (Klobucar and Brown, 2022). As part of a drug repurposing screen, the Wright group found that loperamide, an anti-diarrheal, strongly potentiated minocycline by increasing minocycline uptake. Loperamide also substantially increased minocycline activity in a murine model of *S.* Typhimurium infectious colitis (Ejim et al., 2011). While the potentiation of

loperamide is restricted to the aminoglycosides, the recently synthesized dimeric tobramycin series potentiates the activity of multiple antibiotics (Idowu et al., 2019). The mechanism was found to via increasing membrane permeability; however, dimeric tobramycin did not inhibit growth on their own. Furthermore, dimeric tobramycin was highly effective when combined with novobiocin in a *Galleria mellonella* model of *A. baumannii* infection (Idowu et al., 2019). Overall, non-essential genes can be exploited as targets to increase antibiotic activity by a variety of mechanisms.

1.6 Rationale

Bcc respiratory infections are very difficult to eradicate due to intrinsic antibiotic resistance paired with a lack of effective antibiotics. A variety of resistance mechanisms have been characterised, such as cell envelope composition and modifications and target alterations (Loutet et al., 2011; Rhodes and Schweizer, 2016). Consequently, Bcc species display near uniform resistance to multiple whole classes of antibiotics (Aaron et al., 2000; Abbott et al., 2016; Chmiel et al., 2014; Zhou et al., 2007). Thus, new treatment strategies are urgently needed to improve patient care.

Chemical genetic and chemogenomic approaches have an unparalleled ability to profile genetic contributions to antibiotic resistance and susceptibility. Recent advances in NGS can also be leveraged to increase the throughput and the number of genes or conditions under investigation. Understanding how antibiotics work can drive directed attempts at compound optimization or new antibiotic combinations. Furthermore, as discussed above, both essential and non-essential genes have important roles to play in antibiotic mechanisms.

At the start of my program, there were only a few studies using chemical genetics or chemogenomics to profile antibiotic targets and mechanisms of action by modulating gene dosage (DeVito et al., 2002; Gallagher et al., 2011; Ji et al., 2001; Li et al., 2004; Pathania et al., 2009; Xu et al., 2010). The idea that target depletion enhances antibiotic susceptibility, and vice versa, had been established in model organisms, along with the genetic tools to study them (e.g. for *S. aureus* (Ji et al., 2001) and *E. coli* (DeVito et al., 2002)). The Cardona group has developed genetic tools for manipulating and studying both essential and non-essential genes in *Burkholderia* species (Bloodworth et al., 2013; Cardona et al., 2006). Using these tools, the group demonstrated that knockdown of the essential gene *gyrB* specifically increased susceptibility to novobiocin, the cognate inhibitor of GyrB (Bloodworth et al., 2013). Thus, the background theory and genetic tools for my project were established. However, while the Cardona group and others (Gallagher et al., 2011; Xu et al., 2011) primarily used known antibiotics in their studies, there were no reports using NGS-based chemical genetics approaches to profile uncharacterized antimicrobials and identify their target. Additionally, there were also very few reports using chemical genetics and chemogenomics in general in highly antibiotic-resistant non-model organisms.

1.7 Hypothesis

In *B. cenocepacia* K56-2, chemogenomics can be used to i) identify targets and mechanisms of action of novel antimicrobials and ii) identify susceptibility and resistance determinants of antibiotics targeting the cell envelope.

1.8 Objectives

1. To validate a transposon-based method to create knockdown mutants in *B. cenocepacia* K56-2 essential genes and identify the target of an uncharacterized antimicrobial.

2. To develop a CRISPRi system for targeted and robust gene knockdown in *Burkholderia*

3. To construct a high-density randomly-barcoded transposon mutant library in *B. cenocepacia* K56-2

4. To assess genome-wide fitness contributions of *B. cenocepacia* K56-2 in the presence of a large panel of cell envelope-targeting antibiotics

CHAPTER 2: MATERIALS AND METHODS

Materials and methods for Chapter 3 are reproduced from:
Hogan AM, Scoffone VC, Makarov V, Gislason AS, Tesfu H, Stietz MS, Brassinga AKC, Domaratzki M, Li X, Azzalin A, Biggiogera M, Monakhova N, Chiarelli LR, Riccardi G, Buroni S, Cardona ST. 2018. Competitive fitness of essential gene knockdowns reveals a broad-spectrum antibacterial inhibitor of the cell division protein FtsZ. *Antimicrob. Agents Chemother*. **62**(12): e01231-18.

Materials and methods for Chapter 4 are reproduced from:
Hogan AM, Rahman ASMZ, Lightly TJ, Cardona ST. 2019. A broad-host-range CRISPRi toolkit for silencing gene expression in *Burkholderia*. *ACS Synth. Biol.* **8**(10): 2372-84

Materials and methods for Chapter 5 have not yet been published, but are part of a manuscript in preparation:
Hogan AM, Léon B, Batun Z, Motnenko A, Natarajan A, Lohmann R Bosch A, Cardona ST. Chemogenomics reveals susceptibility determinants of cell envelope-targeting antibiotics in *Burkholderia cenocepacia*. *Manuscript in preparation*.

2.0 Materials and methods related to Chapter 3

2.0.1 Bacterial strains and growth conditions

Strains (Table A1) and the HDTM library were grown in LB-Lennox or LB-Miller medium (Difco) at 37°C with shaking *and* supplemented with 100 µg/ml trimethoprim or 20 µg/ml chloramphenicol as required *by plasmid selection (Table A2)*. The HDTM library was grown with 0.2% rhamnose. A Biotek Synergy 2 multimode plate reader was used to provide continuous orbital shaking at 230 rpm and 37°C for growth curves in 96-well format. Cystic fibrosis sputum clinical isolates of M. abscessus were grown and maintained in LB-Lennox medium.

2.0.2 Antibiotic formulations

C109 was synthesized as previously described (Scoffone et al., 2015). Antibiotic working stock solutions were prepared as follows: C109, 10 mg/ml in dimethyl sulfoxide (DMSO); trimethoprim, 50 mg/ml in DMSO (Sigma); doxycycline hyclate, 25 mg/ml in H2O (Sigma); chloramphenicol, 20 mg/ml in ethanol (EtOH; Sigma), meropenem, 10 mg/ml in DMSO (Sigma); tobramycin sulfate, 10 mg/ml in H2O (Alfa Aesar); ceftazidime, 10 mg/ml in 0.1 M NaOH (Sigma); ciprofloxacin, 10 mg/ml in 0.1 M HCl (Sigma); novobiocin sodium, 10 mg/ml in H2O (Sigma); and piperacillin sodium salt, 10 mg/ml in H2O (Sigma). IPTG and L-rhamnose were obtained from Sigma.

2.0.3 Antimicrobial susceptibility testing using MIC, checkerboard assay, MBIC, and MBEC

To assess the MIC of clinical and lab strains, the broth microdilution method was employed using guidelines provided by the Clinical and Laboratory Standards Institute (Clinical and Laboratory Standards Institute CLSI, 2003, 2012), while the MIC values for the *Burkholderia* clinical isolates were detected using the resazurin viability stain (Martin et al., 2006). *Mycobacterium* inocula in cation-adjusted Mueller-Hinton broth (CAMHB, Oxoid) were prepared from growth on LB agar plates. All other inocula were prepared from overnight cultures diluted to turbidity equal to a 0.5 McFarland standard and then further diluted to produce $5x10^5$ CFU/mL in each well. The initial bacterial concentrations were verified by plating for CFU on LB agar plates. Antibiotic interactions were assessed using broth microdilution checkerboard assays with inocula prepared as outlined above.

To assess the activity of C109 against biofilm formation (minimum biofilm inhibitory concentration, MBIC) and bacterial clearance from established biofilms (minimum biofilm eradication concentration, MBEC), a resazurin-based microplate assay was used (Van den Driessche et al., 2014). In brief, an inoculum of *B. cenocepacia* K56-2 in CAMHB was incubated stationary at 37°C for 4 hours in 96-well format to allow substrate attachment. Planktonic cells were then washed away and medium was replaced with either fresh CAMHB (for the MBEC) or a C109 gradient in CAMHB (for the MBIC) and incubated again for 24 hours. To determine the MBIC, C109-treated biofilms were washed and incubated stationary with CellTitre-Blue (Promega) at 37°C for 1 hour. Only viable cells can reduce resazurin to the fluorescent resorufin, which was measured by excitation at 530/25 nm and emission at 590/30 nm. To determine the MBEC, day-old established biofilms were washed and exposed to a C109 gradient for a further 24 hours and treated with CellTitre-Blue as above.

2.0.4 Creation of the redundant and the combined knockdown mutant library

The initial high-density transposon mutant (HDTM) library was obtained by delivering a transposon element with an outward, rhamnose-inducible promoter with selection of transposon mutants in the presence of rhamnose (Gislason et al., 2017a). The HDTM library was grown in LB with 0.2% rhamnose and 100 μg/mL trimethoprim at 37°C until early log phase (OD_{600nm} ~0.13-0.18) and the cells were washed twice by centrifugation and resuspension in LB. The cells were diluted to an OD_{600nm} of 0.01 and grown in LB (without rhamnose) until the culture reached an OD_{600nm} of 0.18. Meropenem was then added to a final concentration of 160 μg/mL (5-fold the MIC for K56-2) and incubated for 3 hours at 37°C to kill actively growing cells (non-essential gene mutants) (Hogan *et al.* manuscript in preparation). The culture was then washed once, resuspended in LB, and grown for 30 minutes at 37°C. To kill remaining non-essential gene mutants the culture was treated a second time with meropenem as before. Intact cells were removed by filtration, washed off with LB, and plated on 500 cm^2 QTrays supplemented with 0.2% rhamnose and 100 μg/mL trimethoprim. QTrays were incubated at 37°C for 48 hours. Colonies were robotically transferred to 96-well plates with LB and 0.2% rhamnose and 100 μg/mL trimethoprim using a Genetix QPix2 XT colony picker (Molecular Devices). These master plates were grown stationary at 37°C for 48 hours.

For primary screening, cultures in the master plates were robotically inoculated into 96-well plates containing LB with 100 μg/mL trimethoprim and with or without 0.2% rhamnose. After 16 hours of incubation without shaking at 37°C, the conditional growth phenotype was assessed as 50% or less growth (by OD_{600nm}) without rhamnose. Putative conditional growth phenotypes were validated by secondary screening for growth with or without rhamnose as before. Mutants that passed both screens (approximately one third of the initial clones) were stocked in LB with 20% glycerol and kept at -80°C. The transposon insertion sites were determined by TnSeq circle (Gallagher et al., 2011; Gislason et al., 2017a). The redundant knockdown mutant library (830 clones) and 134 previously obtained knockdown mutants (Bloodworth et al., 2013) were grown in 96-well format in LB with 0.2% rhamnose and 100 μg/mL trimethoprim at 37°C overnight. The following day, mutants were pooled in equal amounts by OD_{600nm}, forming the combined knockdown mutant library. Pool aliquots were stored in LB with 20% glycerol at -80°C until needed.

2.0.5 Competitive fitness assay and sequencing data analysis

For culturing, all the knockdown mutants were inoculated into 5 mL LB to a final OD_{600nm} of 0.0025 with individual mutants at an approximate OD_{600nm} of 2.5 $X \cdot 10^{-6}$ and with or without C109 or novobiocin, added at a concentration that inhibited 25% of K56-2 growth (IC_{25}, 2.5 and 2 μg/mL, respectively). Rhamnose was added at the sensitizing concentration of 0.05%, which produced 30% to 60% of wild-type growth. The cultures were grown for 20 hours (approximately 20 generations) at 37°C with 230 rpm shaking. Mutants that were recovered after growth without antibiotics are shown in Table S1. Wild-type *B. cenocepacia* K56-2 controls to check for 25% growth inhibition, and single mutant cultures to check for 30-60% wild-type growth were set up alongside the mutant pools and assessed by OD_{600nm} after 20 hours. Cultures were harvested, the genomic DNA was isolated, and the TnSeq circle method were performed as previously described (Gallagher et al., 2011; Gislason et al., 2017a). PCR primers 681, 690, 715, 717, 718, 719, 729 contain the Nextera indices and were used in appropriate pairs (Table A3). Indexed samples were pooled and sequenced at Génome Québec with an Illumina HiSeq 2500. Raw reads were deposited in the NCBI Sequence Read Archive (SRA) repository and will be publicly available after publication under accession SRP148709. All custom scripts used for data processing can be found at https://github.com/mdomarat/CardonaLab. The DNA reads were trimmed (filter_reads.py) and

mapped (map_reads.py) to the contigs of the K56-2 draft genome (Gislason et al., 2017a). Insertion sites were then called and annotated with affected genes (identify.py). To compare the C109- or novobiocin-treated samples to the no antibiotic controls, insertion sites were merged based on position (expression.py). All insertion sites with fewer than 1000 reads in the no antibiotic controls were removed from the analysis. Reads were then normalized by total read count. Significance was assessed by calculating *P*-values as per Pierce et al. (Pierce et al., 2007). Log_2(Depletion) values for each mutant was then calculated as the log_2 ratio of the average normalized reads in the no antibiotic control to those of the antibiotic-treated sample. Log_2(Depletion) values of mutants that passed the significance threshold of *P*-value < 0.05 were fit to a normal distribution (Delignette-Muller and Dutang, 2015) and candidate targets were taken as greater than two standard deviations from the mean.

2.0.6 Overexpression of dcw proteins in the presence of C109

The effect of *dcw*-GFP fusion protein overexpression was determined by comparing growth curves of each of the strains in varying IPTG concentrations to that of the strain harbouring pCA24N-empty, the empty vector control for the ASKA library (Kitagawa et al., 2005). An overnight culture of the appropriate strains was diluted to low OD_{600nm} and grown until the culture reached OD_{600nm} 0.3-0.6. Mild overexpression was then induced with 10 μM IPTG for 1.5 hours. Cells were washed and used to inoculate a C109 gradient containing 0.01 mM IPTG. After 12 hours of exposure at 37^{o}C and 230 rpm shaking, aliquots were plated for counting CFU/mL. To facilitate inter-assay comparison, the CFU/mL for each strain was normalized to the condition without C109. These ratios were then further normalized to the strain carrying pCA24N-empty at each concentration of C109. The results were reported as abundance relative to the strain containing pCA24N-empty. A two-fold change in abundance was taken as significant.

2.0.7 Construction of CGftsZ and CGtopB

Using the K56-2 background, an unmarked insertion of the following sequence was made between K562_RS16895 and K562_RS16900: 5′ – TCTTAATTAATTTAAATCTAGACTAGTG CGGCCGCACTTGTGTATAAGAGTCATAAGAGACAG – 3′. This sequence is not found in the K56-2 genome and can be used to track transposon mutants via TnSeq. These genes encode a putative anti-sigma factor and a hypothetical protein, respectively. Previously determined criteria

for the creation of a stable, genetically barcoded strain were used to select the insertion site (Buckley et al., 2012). Additionally, dRNA-seq data for the region was examined which found it to be transcriptionally inactive, at least in *B. cenocepacia* J2315 grown in biofilms (Sass et al., 2015).

The method of Flannagan et al. was used for mutant construction (Flannagan et al., 2008). Briefly, a 996 bp fragment including the 3' ends of K562_RS16895 and K562_RS16900, the intergenic region, the unique transposon sequence, and *Kpn*I and *Eco*RI restriction sites was synthesized (IDT). The fragment was digested with *Kpn*I and *Eco*RI (NEB), ligated into pGPI-SceI to create pAH3, and then transformed into *E. coli* SY327. Using *E. coli* SY327/pRK2013 as a helper strain, pAH3 was introduced into K56-2 via triparental mating. The origin of pGPI-SceI is non-functional in *Burkholderia*; therefore, exconjugants resistant to 100 µg/mL trimethoprim had pAH3 recombined into the genome. The presence and correct placement of the recombination event was verified with PCR (Qiagen). To facilitate the second recombination, pDAI-SceI, which expresses the I-*Sce*I homing endonuclease, was introduced via triparental mating. Exconjugants sensitive to trimethoprim and resistant to 100 µg/mL tetracycline were selected and the second recombination was verified by PCR. The mutant was cured of the plasmid by serial passaging in tetracycline-free medium and combined with the conditional growth mutant libraries in the competitive enhanced susceptibility assays.

This Tn-tagged mutant of K56-2 was then used as background for insertion of pAH1 by homologous recombination, as described previously (Gislason et al., 2017b), to create CG*ftsZ*. Briefly, the 5' 301 bp of *ftsZ* (K562_RS16765) was PCR amplified from the K56-2 genome with 5' *Nde*I and 3' *Xba*I restriction sites. The fragment was ligated into pSC201 immediately downstream of the rhamnose-inducible promoter, resulting in pAH1. This plasmid was introduced into the Tn-tagged K56-2 by triparental mating as described above. To create CG*topB*, the 5' 406 bp of *topB* (K562_RS02390) was amplified and ligated into pSC201 as above, resulting in pAH5, and introduced into K56-2 as described. Insertional mutants were verified by PCR and by rhamnose-dependent growth. K562_RS02390 was named as the *B. cenocepacia* homologue of *topB* by reciprocal best hit BLAST against the *E. coli*. The same method was applied for *xseB, ispA, dnaN, holC and pepA.*

2.0.8 Light and fluorescence microscopy

For *E. coli* expressing *dcw* protein-GFP fusions, fresh overnight cultures with 20 µg/mL chloramphenicol were subcultured the next morning with 4 µg/mL C109 or 1 µg/mL cefotaxime without chloramphenicol and IPTG and grown until mid-exponential phase (approximately 3 hours). To account for the difference in doubling time, *B. cenocepacia* K56-2 and mutants were incubated for 6 hours with 8 µg/mL C109 or with 100 µg/mL trimethoprim and 0 or 0.2% rhamnose, respectively. Prior to staining, cells were fixed with 4% formaldehyde (Sigma) in PBS at room temperature for 20 minutes. Cells were then washed with PBS and stained with DAPI (ThermoFisher Scientific) and Nile red (Carbosynth). Cells were then immobilized on 1.5% agarose pads (Invitrogen) and visualized on a Zeiss Axio Observer Z1 inverted microscope.

For time-lapse microscopy, overnight cultures were subcultured without IPTG or C109 and grown to mid-exponential phase. Fifteen minutes before cells were harvested, 4 µg/mL C109 was added to the culture. Cells were diluted to an OD_{600nm} of 0.2 and spotted on a 1.5% low-melt agarose pad (Life Technologies) made with LB and impregnated with 4 µg/mL C109. Temperature was maintained with a TempModule S control unit mounted on a Zeiss Axio Observer Z1 inverted microscope. At each timepoint, DIC and GFP filter images were acquired. Exposure time was limited to mitigate cytotoxicity.

2.0.9 Clonal growth assay of susceptibility

The rhamnose dose-growth response and C109 inhibition curves were first determined in K56-2, CG*dcw*, and CG*ftsZ*. In 96-well plate format, the mutants were then grown in concentration of rhamnose required to produce 45% of wild-type K56-2 growth (0.04% for CG*dcw* and 0.05% for CG*ftsZ*) and in the C109 IC_{10} – $IC_{50.}$ OD_{600nm} of technical triplicates was measured after 20 hours. Log_2(Depletion) was calculated as the log_2 of the average OD_{600nm} in the no antibiotic condition divided by the OD_{600nm} in the presence of C109.

2.0.10 Cloning, expression, and purification of B. cenocepacia J2315 FtsZ (BcFtsZ)

Using the primers pet28presFtsZfor (5'- ATGGGTCGCGGATCCCTGGAAGTTC TGTTCCAGGGGCCCATGGAATTCGAAATGCTGGA-3') and pet28ftsZrev (5'- TGCGGCCGCAAGCTTTCAGTCAGCCTGCTTGCGCA-3'), *ftsZ* (BCAL3457) was amplified from *B. cenocepacia* J2315. PCR products were cloned into the pET-28a vector (Novagen) using the In-Fusion HD Cloning (Takara) according to manufacturer's instructions. Heterologous protein

production was achieved in *E. coli* BL21(DE3), inducing the expression with 0.5 mM IPTG overnight at 20°C. Cells were kept frozen at -80°C until needed, then thawed and resuspended in buffer (pH 8, 50 mM TrisHCl, 300 mM KCl, 5 mM imidazole, and 10% glycerol) and sonicated. The lysates were centrifuged (50000 × *g*, for 1 h) and applied on a HisTrapFF Crude (1 mL, GE Healthcare) column. The column was washed with 20 mM imidazole, then BcFtsZ eluted with 250 mM imidazole. Proteins were dialyzed against 50 mM TrisHCl pH 7.5, 150 mM NaCl, 1 mM EDTA, 1 mM DTT and 10% glycerol and then treated with PreScission Protease (GE Healthcare) to remove the N-terminal histidine tag. Finally, BcFtsZ was further purified by gel filtration chromatography (HiLoad 16/60 Superdex-75 column, GE Healthcare) in 20 mM TrisHCl pH 7.9, 50 mM KCl, 1 mM EDTA, 2.5 mM $Mg(CH_3COO)_2$ and 10% glycerol, concentrated to 6 mg/ml and stored at -80 °C until needed.

2.0.11 In vitro assay of BcFtsZ GTPase activity

GTPase activity was assayed at 30°C, using a pyruvate kinase/L-lactic dehydrogenase (PK/LDH) spectrophotometric coupled assay (Ingerman and Nunnari, 2005). The reaction mixture was first set up to contain 50 µM HEPES pH 7.5, 5 mM $MgCl_2$, 5 mM KCl, 10 U PK/LDH, 0.25 mM NADH, 0.25 mM phosphoenolpyruvate, and 5.25 µM BcFtsZ. The assay was initiated by the addition of 0.5 mM GTP. Steady-state kinetic parameters were determined by monitoring the absorbance at 340 nm at variable concentrations of GTP. The experiments were performed in triplicate, and the kinetic constants were determined by fitting the data to the Michaelis-Menten equation using Origin 8. C109 was added in concentrations ranging from 0.5 µM to 100 µM, and the inhibitory concentration that reduced the activity in half (IC_{50}) was determined using Origin 8. $A_{[I]}$ is the enzyme activity at inhibitor concentration [I] and $A_{[0]}$ is the enzyme activity without inhibitor.

$$A_{[I]} = A_{[0]} \times \left(1 - \frac{[I]}{[I]+IC_{50}}\right) \quad \text{equation 1}$$

The activities of PK and LDH individually were assayed with C109, but no effect was detected, thus excluding the possibility that the molecule can exert an effect on them.

2.0.12 In vitro BcFtsZ polymerization: sedimentation and electron microscopy

FtsZ polymerization was performed using a previously described sedimentation protocol (Król and Scheffers, 2013). The reaction mixture was set up to contain 25 mM PIPES pH 6.8, 10

mM $MgCl_2$, 12 µM BcFtsZ and 2 mM GTP or GDP. The reactions were incubated for 10 minutes at 30°C at 300 rpm to allow the polymerization to occur. Subsequently, samples were ultracentrifugated at 350,000 × *g* for 10 minutes at 25°C and the supernatant was immediately separated from the pellet, which contains the protein polymers. The samples were analyzed by SDS-PAGE on 12% polyacrylamide gels. The *in vitro* polymerization of BcFtsZ was tested in the presence of increasing concentrations of the C109 ranging from 10 µM to 100 µM.

BcFtsZ polymers were visualized by negative-stain electron microscopy. The polymerization reactions were carried out in the same conditions described above for the sedimentation assay. After the incubation time, a small aliquot of the reaction mixture was applied onto a glow-discharged 300 mesh carbon-coated nickel grid. Subsequently, the grid was stained with a 2% uranyl-acetate solution. The grid was analysed with a Zeiss (Jena, Germany) EM900 electron microscope operating at 80 kV.

2.0.13 C. elegans infection assay

To assess the *in vivo* antibiotic activity of C109 on K56-2 infection in *C. elegans*, a liquid killing assay was performed as previously described (Kaplan et al., 2011; Selin et al., 2015; Stietz et al., 2017). In brief, *C. elegans* DH26 (from the *Caenorhabditis* Genetics Center) were hatched and grown on nematode growth medium (NGM) agar to the L4 stage over 48 hours at 25ºC by feeding on *E. coli* OP50. For the infection, the nematodes were washed from the plates with M9 buffer and placed onto fresh plates with *B. cenocepacia* K56-2 or *E. coli* OP50 (no infection control) and incubated at 25ºC for 16 hours. The nematodes were then washed from the plate with M9 buffer, allowed to settle, rinsed with M9 and then resuspended in liquid killing medium (80% M9 and 20% NGMII). Approximately 20-30 nematodes in liquid killing medium were deposited into individual wells of a 96-well plate with or without antimicrobials. Wells were assessed every 24 hours for 6 days under a dissecting microscope for live (S-shaped and moving) and dead (straight and not moving) nematodes.

2.0.14 Hemolysis assay

The hemolytic activity of C109 was determined as previously described (Selin et al., 2015; Stietz et al., 2017; Strom et al., 2003) with modifications. Briefly, ovine erythrocytes (Alere) were washed thrice in PBS and resuspended in PBS to give a 20% stock. In 96-well format, a 100 µL

dilution gradient of DMSO and C109 was set up, to which was added 100 µL of the 20% erythrocyte stock. The plate was incubated stationary at 37ºC for 1 hour. Intact erythrocytes were pelleted by centrifugation at 1500 x *g* for 5 minutes and the absorbance of the supernatant at 540 nm was measured. As a positive control, 0.1% Triton X-100 was added to the wells. Hemolysis was calculated as previously described (Sperandio et al., 2010). High, low, and absent hemolytic activity were defined as >40%, between 5-10%, and <5%, respectively (Sperandio et al., 2010).

2.0.15 MTT assay

Human bronchial epithelial cells (both wild type, 16HBE, or homozygous for the ΔF508 mutation in *CFTR*, CFBE41o-) were used to assess the toxicity of C109. Cells were cultured in minimal essential medium (MEM) supplemented with fetal bovine serum (10%), L-glutamine (1%), penicillin (100 U/ml), streptomycin (100 µg/ml) and maintained at 37°C in 5% CO_2 atmosphere. All reagents were purchased from Life Technologies. Cells were seeded at a density of 2.0 x 10^4 cells per well in 96-well plates. After 24-hours, the medium was refreshed and cells were exposed to a C109 concentration gradient (12.5-100 µM) for 3 hours. The wells were then gently washed with PBS and incubated with 200 µL 0.5 mg/mL 3-(4,5 dimethylthiazol-2-yl)-2,5-diphenyltetrazolium bromide (MTT; Sigma-Aldrich) at 37ºC for 3 hours. The solution was removed and the formazan crystals were dissolved by adding DMSO to the wells for 10 minutes, after which, absorbance at 570 nm was measured by plate reader (EZ Read400, Biochrom).

2.1 Methods and materials related to Chapter 4

2.1.1 Strains, selective antibiotics, and growth conditions

All strains and plasmids are found in Table A1 and A2. All strains were grown in LB-Lennox medium (Difco). *B. cenocepacia* K56-2 and strains of *E. coli* were grown at 37ºC, while *B. thailandensis* E264 and *B. multivorans* ATCC 17616 were grown at 30ºC. The following selective antibiotics were used: chloramphenicol (Sigma; 100 µg/mL for *B. cenocepacia,* 20 µg/mL for *E. coli*), trimethoprim (Sigma; 100 µg/mL for strains of *Burkholderia*, 50 µg/mL for *E. coli*), tetracycline (Sigma; 50 µg/mL for all strains of *Burkholderia*, 20 µg/mL for *E. coli*), kanamycin (Fisher Scientific; 250 µg/mL for *B. thailandensis*, 150 µg/mL for *B. multivorans,* 40 µg/mL for *E. coli*), ampicillin (Sigma; 100 µg/mL for *E. coli*), gentamicin (Sigma; 50 µg/mL for all strains of *Burkholderia*).

2.1.2.Construction of pSC-rhadCas9, pAH-CTX1-rhadCas9, pAH-CTX1-rhadCas9-native, and dCas9 insertional mutants

The endogenous *cas9* gene from *S. pyogenes* has low GC content (averaging 34.1%) and subsequently poor codon usage for GC-rich organisms (http://www.kazusa.or.jp/codon/). The nuclease-inactive variant (*dcas9*) was therefore codon optimized for *B. cenocepacia* by purchasing the optimized gene in two fragments from IDT (2462 bp and 1849 bp, Table A4), each with 38 bp overlapping regions. Strong, rho-independent terminators were added following the gene. The full-length gene (with terminal *Nde*I and *Hind*III cut sites) was synthesized by overlap-extension PCR using Q5 polymerase with high GC buffer (NEB) and primers 979 and 987 (Table A2). The first ten rounds of PCR were performed without primers to synthesize the full-length product using the overlap regions; primers were added for the following 25 cycles. The cycle parameters are as follows: 98ºC for 30 sec, (98ºC for 10 sec, 67.5ºC for 20 sec, 72ºC for 2.5 min)x10 cycles, 72ºC for 5 min, 98ºC for 30 sec, (98ºC for 10 sec, 62.5ºC for 20 sec,72 ºC for 2.5 min)x25 cycles, 72ºC for 10 min. The 4267 bp product was gel-purified (Qiagen) and introduced into pSCrhaB2 by restriction cloning using *Nde*I and *Hind*III (NEB). The resulting plasmid, pSC-rhadCas9, was transformed into *E. coli* DH5α, and trimethoprim-resistant colonies were screened by colony PCR with primers 954 and 955. Triparental mating with *E.* coli MM290/pRK2013 as a helper was performed as previously described (Hogan et al., 2018).

To introduce the optimized *dcas9* into the mini-CTX1 insertion plasmid (Hoang et al., 2000) serial restriction cloning was used (Figure A1). Briefly, the rhamnose-inducible promoter from pSC201 (Ortega et al., 2007) was first PCR amplified with Q5 polymerase and primers 976 and 1071, containing *Hind*III and *Spe*I restriction sites, respectively. This fragment was introduced into mini-CTX1, to create pAH-CTX1-rha, and tetracycline-resistant *E. coli* DH5α were screened by colony PCR using primers 957 and 1074. The fragment containing the dCas9 gene was PCR amplified as above, but instead using primers 1072 and 1073, introducing *Spe*I and *Not*I restriction sites, respectively. This fragment was introduced into pAH-CTX1-rha, to create pAH-CTX1-rhadCas9, and tetracycline-resistant *E. coli* DH5α colonies were screened by colony PCR using primers 954 and 955.

The native (non codon-optimized) *dcas9* was also introduced into pAH-CTX1-rha. The native *dcas9* and transcriptional terminators were PCR amplified from pdCas9-bacteria (Addgene

plasmid # 44249) with Q5 polymerase (NEB) using primers 1216 and 1217. The PCR product was cloned into pAH-CTX1-rha (creating pAH-CTX1-rhadcas9-native) using *Not*I and *Spe*I restriction sites then transformed into *E. coli* DH5α. Tetracycline-resistant colonies were screened by PCR using primers 954 and 1218.

pAH-CTX1-rha, pAH-CTX1-rhadCas9, and pAH-CTX1-rhadCas9-native were introduced into *Burkholderia* species by triparental mating using *E. coli* MM290/pRK2013 as a helper as above. Tetracycline-resistant colonies were screened by colony PCR using primer 954 (for pAH-CTX1-rha) or 1075 (for pAH-CTX1-rhadCas9) or 1219 (for pAH-CTX1-rhadcas9-native) and 1008 (for *B. cenocepacia*), 1167 (for *B. multivorans*), or 1168 (for *B. thailandensis*).

To remove the tetracycline resistance and integrase genes from the insertional mutants constructed using pAH-CTX1-rhadCas9 and pAH-CTX1-rha (Figure A1), the Flannagan method (Flannagan et al., 2008) was used for *B. cenocepacia* K56-2, while the pFLPe system (Choi et al., 2008) was used for *B. multivorans* ATCC 17616 and *B. thailandensis* E264. To remove the regions flanking the *FRT* sites in *B. cenocepacia* K56-2, a fragment with 475 bp overlapping the upstream and downstream regions of the *FRT* sites was designed and synthesized (IDT) with *Kpn*I and *Eco*RI restriction sites, respectively. The fragment was ligated into pGPI-*Sce*I (Flannagan et al., 2008) via the *Kpn*I and *Eco*RI restriction sites, creating pAH18, and transformed into *E. coli* SY327. Trimethoprim-resistant colonies were screened for the insertion of the fragment with primer 153 and 154. pAH18 was introduced into the mutant backgrounds via triparental mating, as described above. Trimethoprim-resistant K56-2 were screened by PCR for both possible integration orientations using primers 154 and 1126, or 153 and 1133. To initiate the second recombination, an *Sce*I-expressing plasmid is required; however, the conventional plasmid, pDAI-*Sce*I, confers tetracycline resistance and could not be selected for in the mutant background. Therefore, the tetracycline resistance cassette was removed by digestion with *Age*I and *Xho*I. The chloramphenicol resistance gene *cat* was PCR amplified from pKD3 (Datsenko and Wanner, 2000) using primers 1084 and 1150, then ligated into the *Age*I and *Xho*I-digested pDAI-*Sce*I backbone and transformed into *E. coli* DH5α, creating pAH25-*Sce*I. Chloramphenicol-resistant colonies were screened with primers 1091 and 1150. pAH25-*Sce*I was introduced into the mutant backgrounds by triparental mating as described above. Chloramphenicol-resistant colonies were screened for sensitivity to trimethoprim (indicating excision of pAH18) and tetracycline

(indicating excision of the genes between the *FRT* sites), and then screened by PCR with primers 1126 and 1133, which bridge the excision.

The pFLPe system was used to remove the tetracycline resistance and integrase genes in the dCas9 mutants in *B. multivorans* ATCC 17616 and *B. thailandensis* E264. Triparental mating to introduce pFLPe4 into the strains was performed as for K56-2 above, except 0.2% rhamnose was added to the mating and antibiotic selection plates. Tetracycline-sensitive colonies were screened by PCR using primers 957 and 1194 (for *B. multivorans*) or 1195 (for *B. thailandensis*). pFLPe4 has a temperature-sensitive origin of replication; therefore, mutants were grown overnight in LB without antibiotics at 37^{o}C. Single colonies were then tested for kanamycin sensitivity and then by colony PCR for pFLPe4 using primers 1128 and 1129.

2.1.3 Design and construction of the sgRNA-expressing plasmids

PAM sequences closest to the 5' end of the transcription start site (TSS) were first identified on both the non-template and template strands. We extracted 20-23 nucleotides adjacent to the PAM sequence to design the base-pairing region of the sgRNAs in the following format: 5'-CCN-$N_{(20-23)}$-3' for targeting the non-template strand and 5'-$N_{(20-23)}$-NGG-3' for the template strand. To score the specificity and identify off-target binding sites, the 5' end of the 20-23nt variable base-pairing sequences were trimmed one base at a time and the remaining base-pairing region was searched against the appropriate organism's reference genome. This was repeated until only 10 nt were used as a search query. Potential sgRNAs were discarded if off-target sites were discovered in this manner.

The expression vector pSCrhaB2 (Cardona and Valvano, 2005) was chosen as the method of sgRNA expression due to the broad host range of the pBBR1 origin of replication. The sgRNA cassette from pgRNA-bacteria (Qi et al., 2013) (Addgene plasmid # 44251) was introduced into pSCrhaB2 by restriction cloning with *Eco*RI and *Hind*III (NEB) to create pSCrhaB2-sgRNA. To remove *rhaS* and *rhaR*, inverse PCR was performed using Q5 polymerase (NEB) and primers 847 and 1025. The resulting fragment was ligated by blunt-end ligation using 1 µL of PCR product incubated with 0.5 µL *Dpn*I, 0.5 µL T4 polynucleotide kinase, and 0.5 µL T4 ligase (NEB) with quick ligation buffer (NEB) at 37^{o}C for 30 minutes. The resulting plasmid, pSCB2-sgRNA, was screened using primers 781 and 848, which span the ligated junction. Individual sgRNAs were introduced into pSCB2-sgRNA using inverse PCR as previously described (Qi et al., 2013)

.

2.1.4 Construction of insertional mutants K56-2 fliF::pAH26 and K56-2 phbC::pAH27

Inactivation of *fliF* was performed with the mutagenesis system of Flannagan et al. (Flannagan et al., 2007). Briefly, a 322 bp internal fragment of *fliF* was PCR amplified from the K56-2 genome using primers 1156 and 1157 and Q5 polymerase (NEB). The fragment and pGPΩ-Tp were double digested with *Kpn*I and *Eco*RI (NEB) and ligated with T4 ligase (NEB). The resulting plasmid, pAH26, was electroporated into *E. coli* SY327, and trimethoprim-resistant colonies were screened by colony PCR for the *fliF* fragment. Triparental matings were performed as above.

Inactivation of *phbC* (K562_RS09360) was performed as for *fliF*. Briefly, a 328 bp internal fragment of *phbC* was PCR amplified from the K56-2 genome using primers 1196 and 1197 and Q5 polymerase (NEB). The plasmid, pAH27, created from ligating the fragment into pGPΩ-Tp using *Kpn*I and *Eco*RI (NEB) restriction sites, was electroporated into *E. coli* SY327 and trimethoprim-resistant colonies were screened by colony PCR for the *phbC* fragment. Triparental matings were performed as above.

2.1.5 Assays for integration efficiency and stability of the mini-CTX1-based system

To assess integration efficiency, triparental matings were started as above. However, after the mating on LB agar, the pellicles were serially diluted and plated for CFU/mL on LB agar with 50 μg/mL gentamicin and LB agar with 50 μg/mL tetracycline and 50 μg/mL gentamicin.

To assess stability of the integration, cultures of the dCas9 mutants (containing the tetracycline resistance cassette) were serial passaged over 4 days without antibiotics. Each day, a fresh culture was started with a 1:2500 dilution of the previous day's stationary phase culture. In addition, the cultures were serially diluted and plated for CFU/mL on LB agar without antibiotics and LB agar with 50 μg/mL tetracycline.

2.1.6 Growth assay with phenylacetic acid as the sole carbon source

Overnight cultures, started from isolated colonies, of the appropriate strains were washed at 4000 xg for 4 minutes and resuspended in PBS (2.7 mM KCl, 136.9 mM NaCl, 1.5 mM KH_2PO_4, 8.9 mM Na_2HPO_4, pH 7.4) to remove growth medium. The OD_{600nm} of the cultures was normalized to 0.01 in M9 medium supplemented with 5 mM phenylacetic acid, 100 μg/mL trimethoprim, and

0.2% rhamnose as required. The culture was added to wells of a 96-well plate and incubated with continuous shaking at 37°C (*B. cenocepacia* K56-2) or 30°C for *B. multivorans* ATCC 17616 and *B. thailandensis* E264). The OD_{600nm} of the cultures was measured after 24 hours for *B. cenocepacia* K56-2 and *B. multivorans* ATCC 17616, or 48 hours for *B. thailandensis* E264.

2.1.7 Fluorescent microscopy and polyhydroxyalkanoate granule detection

Overnight cultures of the appropriate strains with or without rhamnose were first washed to remove growth medium and resuspended in PBS. Cells were fixed in 3.7% formaldehyde + 1% methanol at room temperature for 10 minutes (*B. cenocepacia* K56-2) or 20 minutes (*B. multivorans* ATCC 17616 and *B. thailandensis* E264) then quenched by the addition of an equal volume of 0.5 M glycine. The cells were washed and resuspended in PBS with 0.5 μg/mL Nile Red (Carbosynth) and stained at room temperature in the dark for 20 minutes, after which the cells were washed to remove excess stain and resuspended in PBS. The cells were mounted on 1.5% agarose pads and imaged by fluorescence microscopy at 1000x total magnification on an upright AxioImager Z1 (Zeiss). Nile Red was excited at 546/12 nm and detected at 607/33 nm.

2.1.8 Plate-based motility assay

Assays were performed as previously described (Kumar and Cardona, 2016), with some modifications. Briefly, strains were grown on LB agar with the appropriate antibiotics and single colonies were stab-inoculated into motility medium consisting of nutrient broth (Difco) with 0.3% agar. Medium was supplemented with rhamnose (Sigma) as appropriate. Plates were incubated right-side up for 22 hours at 37°C.

2.1.9 Flagellum staining

Staining was performed as previously described (Kumar and Cardona, 2016). Briefly, an overnight culture was rested statically at room temperature for 20 minutes. Gently, a 1 in 10 dilution was prepared in water and rested statically for a further 20 minutes. A small drop of the diluted culture was placed on a clean glass slide and rested for 20 minutes. A coverglass was gently applied and one side was flooded with Ryu flagellum stain (Remel), then allowed to dry for 2 hours at room temperature. Slides were observed by light microscopy at 1000x total magnification on an upright AxioImager Z1 (Zeiss).

2.1.10 SDS-PAGE and immunoblotting

Cells from an overnight culture were subcultured into fresh medium and grown at 37ºC (30ºC for *B. thailandensis*) to an OD_{600nm} of 0.4, then exposed to various concentrations of rhamnose for 3 hours. Soluble protein was isolated first by sonicating the cells in TNG Buffer (100 mM Tris-HCl, 150 mM NaCl, 10% glycerol, pH 7.4) then by centrifugation at 15 000g for 20 minutes. Following boiling denaturation in SDS loading buffer (50 mM Tris-HCl, 2% SDS, 0.2% bromophenol blue, 20% glycerol, 100 mM DTT, pH 6.8), samples were run on an 8% Tris/glycine gel. To ensure equal loading, 20 µg protein was loaded per well (as determined by NanoDrop) and gels were run in duplicate (one for immunoblot, and another for Coomassie staining). Protein was transferred by iBlot to a PVDF membrane, blocked in 5% skim milk-TBST (150 mM NaCl, 10 mM Tris-HCl, 0.5% Tween-20, pH 7.5) at room temperature for 1 hour, then probed with a 1:2 000 dilution of primary α-Cas9 antibody (ThermoFisher 10C11-A12) in 5% skim milk-TBST overnight at 4ºC. Following washes, the blot was probed with a 1:20 000 dilution of secondary antibody linked to alkaline phosphatase (ThermoFisher G-21060) in 5% skim milk-TBST for 1 hour at room temperature. Protein was detected by incubation with a solution of NBT/BCIP (Roche) as per the manufacturer's protocol.

2.1.11 RNA extraction and reverse transcription quantitative PCR (RT-qPCR) analysis

Cells from an overnight culture were subcultured at an OD_{600nm} of 0.01 into fresh medium with antibiotic and rhamnose, as necessary, and grown for 8 hours. Cells were harvested by centrifugation (3 minutes at 4600xg) and pellets were stored at -80°C until RNA extraction. RNA was purified and DNAse treated using the Ribopure bacteria kit (Ambion) with extended DNAse treatement (2 hours). RNA quality was verified by running on a 2% agarose gel. cDNA was synthesized with the iScript Reverse Transcriptase kit (Bio-Rad) and qPCR was performed using iQ SYBR Green mastermix (Bio-rad) on a CFX96 Touch Real-Time PCR Detection System (Bio-Rad). Primer efficiency was determined for each primer set and efficiencies between 95% and 105% were deemed acceptable. Data was analyzed using the comparative C_T method (Livak and Schmittgen, 2001; Schmittgen and Livak, 2008). Genes were normalized to a commonly used reference gene, the RNA polymerase sigma factor *sigE* (BCAM0918) (O'Grady et al., 2009; Wong et al., 2018).

2.1.12 Plasmid availability

The following plasmids have been deposited to Addgene for distribution: pAH-CTX1-rha (#129390), pAH-CTX1-rhadCas9 (#129391), pAH-CTX1-rhadCas9-native (#129392), pAH25-SceI (#129389), pSCB2-sgRNA (#129463), pgRNA-guideless (#129464), and pgRNA-non-target (#129465).

2.2 Materials and methods related to Chapter 5

2.2.1 Strains, medium preparation and growth conditions

All strains used in this study are listed in Table A1. LB-Lennox medium (Difco) was used for routine strain propagation and maintenance, unless otherwise specified. All strains and mutants of *E. coli* and *B. cenocepacia* were grown at 37°C. All clinical isolates of *P. aeruginosa*, *A. xylosoxidans*, *S. maltophilia* and Bcc species were grown at 37°C. All strains and mutants of *R. pickettii* K-288, *B. thailandensis* E264, *B. multivorans* ATCC 17616, *B. contaminans* FFH2055, and *B. cepacia* ATCC 25416 were grown at 30°C. All plasmids used in this study are listed in Table A2. The following selective antibiotics were used: trimethoprim (Sigma; 50 µg/mL for *E. coli* and 100 µg/mL for all species of *Burkholderia*), kanamycin (Fisher Scientific; 40 µg/mL for *E. coli*), gentamicin (Fisher Scientific; 50 µg/mL for all species of *Burkholderia*), and tetracycline (Sigma; 20 µg/mL for *E. coli* and 100 µg/mL for *B. cenocepacia*)

Stock solutions of D-glucose (Fisher Scientific) and L-rhamnose (Sigma) were made to 20% in de-ionized water then filter sterilized. The following antibiotics were stocked in sterile de-ionized water: kanamycin sulphate (25 mg/mL, stored at 4°C), gentamicin sulphate (50 mg/mL, stored at 4°C), ampicillin sodium (Sigma; 100 mg/mL, stored at -20°C), ceftazidime hydrate (10 mg/mL, stored at -20°C), ceftriaxone sodium (10 mg/mL, stored at -20°C), cefotaxime sodium (Sigma; 10 mg/mL, stored at -20°C), cephalexin hydrate (Carbosynth; 10 mg/mL, stored at -20°C), cefmetazole (Sigma; 10 mg/mL, stored at -20°C), cefoperazone sodium (Sigma; 10 mg/mL, stored at -20°C), moxalactam sodium (Sigma; 10 mg/mL, stored at -20°C), polymyxin B sulphate (Sigma; 25 mg/mL, stored at -20°C), colistin sulphate (GoldBio; 25 mg/mL, stored at 4°C), novobiocin sodium (Sigma; 10 mg/mL, stored at -20°C), and FR-900098 sodium (Toronto Research Chemicals; 10 mg/mL, stored at -20°C). The following antibiotics were stocked in 100% DMSO (Fisher): aztreonam (Alfa Aesar; 10 mg/mL, stored at -20°C),

cefiderocol (MedKoo Biosciences; 5 mg/mL, stored at -20°C), trimethoprim (50 mg/mL, stored at 4°C), tazobactam sodium (Alfa Aesar; 10 mg/mL, stored at -20°C), cefotetan sodium (Target Mol; 10 mg/mL, stored at -20°C), meropenem trihydrate (MedKoo Biosciences; 10 mg/mL, stored at -20°C), avibactam sodium (MedKoo Biosciences; 10 mg/mL, stored at -20°C), CHIR-090 (MedKoo Biosciences; 5 mg/mL, stored at -20°C), PF-04753299 (Sigma; 10 mg/mL, stored at -20°C), chlorhexidine hydrochloride (Angene China; 10 mg/mL, stored at -20°C), and rifampicin (Sigma; 10 mg/mL, stored at -20°C). The following antibiotics were stocked in 95% ethanol: chloramphenicol (Sigma; 20 mg/mL, stored at 4°C), tetracycline hydrochloride (Sigma; 10 mg/mL, stored at -20°C), and erythromycin (Sigma; 10 mg/mL, stored at -20°C). D-Cycloserine (Alfa Aesar) and fosfomycin disodium (Sigma) were both stocked in sterile Dulbecco's PBS (Sigma) pH 7.2 at 10 mg/mL and stored at -20°C). Ciprofloxacin hydrochloride (Sigma) and bacitracin zinc (Sigma) were both stocked in sterile 0.1M HCl and stored at -20°C.

2.2.2 Standard molecular biology techniques

2.2.2.1 Extraction of plasmid and genomic DNA

Plasmid DNA was routinely extracted using with the EZNA Plasmid DNA Mini Kit (Omega Bio-tek) and eluted in 10 mM Tris-HCl pH 8.5. Genomic DNA was isolated from *Burkholderia* with the PureLink Genomic DNA Mini Kit (Invitrogen) or by standard isopropanol precipitation. Genomic DNA was also solubilized in 10 mM Tris-HCl pH 8.5.

2.2.2.2 Construction of plasmids by restriction cloning and inverse PCR

The desired inserts were amplified by PCR using Q5 high-fidelity DNA polymerase (NEB) with the high-GC buffer as per the manufacturer's protocols. Plasmid DNA template was used at a final concentration of 0.1-0.5 ng/µL, while genomic DNA template was used at a final concentration of 10 ng/µL. Primers were designed *in silico* in Geneious R8.1 (Biomatters), ordered from IDT, and resuspended in 10 mM Tris-HCl, pH 8.5. See Table A3 for a list of all primers used in this study. The first time a new primer was used, an annealing temperature gradient was performed to identify the conditions with the highest yield. The Monarch PCR and DNA Cleanup Kit (NEB) and Monarch DNA Gel Extraction Kit (NEB) were routinely used to purify the DNA fragments. DNA concentration was assessed either by Nanodrop (ThermoFisher Scientific) or Qubit (ThermoFisher Scientific) with the broad-range or high-sensitivity dsDNA

detection kits (Biotium). For restriction cloning, the appropriate restriction enzymes (NEB) were used according to the manufacturer's recommendations to digest the vector and insert. To prevent self-ligation, the vector was also treated with Antarctic phosphatase (NEB). Ligations with 100 ng total DNA were incubated with T4 DNA ligase overnight at 16°C. For blunt-end ligation cloning, raw PCR product was mixed with T4 DNA ligase (NEB), DpnI (NEB), and T4 polynucleotide kinase (NEB) in a custom ligase buffer (132 mM Tris-HCl pH 7.5, 20 mM $MgCl_2$, 2 mM ATP, 15% PEG6000 in de-ionized water) and incubated for 30 mins at 37°C.

2.2.2.3 Introduction of plasmid DNA into cells by transformation, electroporation, and triparental mating

For plasmids created by ligation (either by restricted or blunt ends), 2 µL of ligation reaction mix was used to transform chemically competent *E. coli* DH5α (for plasmids containing standard broad-range origins of replication) or SY327λpir$^+$ (for plasmids containing the R6Kγ origin) with a standard heat-shock method. After recovery for 1 hour shaking at 230 rpm in SOC medium, cells were diluted and plated on LB agar plates containing the appropriate selective antibiotics and incubated at 37°C.

Electroporation was also used to introduce plasmids into cells. Electro-competent *E. coli* was made by diluting an overnight culture of the appropriate strain 1:50 in 100 mL fresh LB, then incubating at 37°C for 3 hours until the OD_{600nm} reached 0.4-0.5. The culture was then chilled on ice for 5 mins prior to centrifugation at 6 000 x g for 10 mins. The supernatant was removed, and the pellet was resuspended in cold, sterile de-ionized water. The centrifugation and washing were repeated thrice, and the pellet was finally resuspended in cold, sterile 10% glycerol in de-ionized water. Aliquots were made in microcentrifuge tubes and either used immediately or stored at -80°C until needed. Electro-competent *B. cenocepacia* K56-2 was made as per (Choi et al., 2006a) with some modifications. Briefly, 5 mL of overnight culture of the appropriate strain was split into 1 mL aliquots and washed by centrifugation at 6 000 x g for 5 mins followed by resuspension in sterile, room temperature 300 mM sucrose in de-ionized water. This washing was repeated twice more and each of the aliquots were finally resuspended in 300 mM sucrose solution and either used immediately or stored at -80°C until needed.

To electroporate plasmids created by restriction cloning, the ligation reaction was first heat inactivated at 65°C for 15 mins. Then, 2 µL of ligation reaction (or ~50 ng of purified

supercoiled plasmid DNA as a control) was mixed with 50-100 µL of electro-competent cells, pulsed at 1700 V (for *E. coli*) or 2500 V (for *B. cenocepacia*), then recovered for 1 hour shaking at 230 rpm in LB. Cells were then diluted and plated on LB agar plates containing the appropriate selective antibiotics and incubated at 37°C. The PEG6000 in the buffer used for blunt-end ligation interferes with electroporation, thus only restriction cloning ligation products were used for electroporation.

Colonies that appeared within 24 hours (for *E. coli*) or 48 hours (for *B. cenocepacia*) were counted, patched on fresh plates with the selective antibiotic, and incubated overnight at 37°C. Colonies were screened for the presence of the correct plasmid by colony PCR using the appropriate primers (Table A3) with OneTaq DNA polymerase in quick load buffer (NEB) supplemented with Q5 high-GC buffer (NEB). For very long or very high GC-content genes, Q5 DNA polymerase was occasionally used when OneTaq failed. Additionally, the expected size was confirmed by plasmid extraction (Omega Bio-tek) followed by digestion with a single restriction enzyme to linearize the plasmid. Size was confirmed by gel electrophoresis relative to dsDNA size standard ladder (NEB).

More commonly, plasmids were introduced into Bcc species by triparental mating (Hogan et al., 2018, 2019). The *E. coli* donor strain, bearing the plasmid to be mobilized, the *E. coli* MM294/pRK2013 helper strain and the *Burkholderia* recipient were mated on an LB plate and incubated overnight (16-18 hours) at 37°C. Successful exconjugants were selected on LB plates containing the appropriate antibiotics with 50 µg/mL gentamicin to counterselect for the *E. coli* donor and helper. Colonies that appeared within 48 hours at 37°C were screened by colony PCR as above.

2.2.2.4 Construction of sgRNA expression plasmids

sgRNAs were designed using a previously published python script (van Gestel et al., 2021). sgRNAs were selected to bind as close as possible to the gene start, which has been shown to result in strong silencing (van Gestel et al., 2021). To mitigate the effect of off-target gene silencing, sgRNAs with a 12 bp seed region matching any other site in the genome (adjacent to a PAM site) were removed. Additionally, sgRNAs were removed if they contained any of the following features suggested to reduce silencing efficiency: 1) PAM site of ANN or TNN, 2) the sgRNA ended in GG or GA or 3) very high (>80%) GC-content. Each gene was

typically targeted by two different sgRNAs within the 5' most 75 bp, and the results of the mutant that displayed the stronger phenotype were reported.

New sgRNA targeting regions were introduced into pSCB2-sgRNA and pSCB2-sgRNAv2 by inverse PCR as previously described (Hogan et al., 2019; Larson et al., 2013b; Qi et al., 2013). Briefly, the desired targeting sequence was added as a 5' extension to a primer with sequence: 5' – GTTTTAGAGCTAGAAATAGCAAGTTAAAATAAGGC – 3'. That primer was used with primer 1092 for PCR with Q5 DNA polymerase with high-GC buffer (NEB). The raw PCR product was used for blunt end ligation followed by transformation into *E. coli* DH5α. Plasmids were confirmed by colony PCR with primers 848 and 1409 and then introduced into K56-2::dCas9 by triparental mating.

2.2.2.5 Construction of overexpression/complementation plasmids

pSCrhaB2plus was used as a vector for multicopy expression of the desired genes (Hogan et al., 2021). The desired genes were PCR amplified from the K56-2 genome using primers 2615-2632. The products were cloned into pSCrhaB2plus by restriction cloning with *Nde*I and *Xba*I, then introduced into *E. coli* DH5α. Plasmids were confirmed by colony PCR with primer 848 and the forward primer used to originally amplify the gene, and then introduced into K56-2::dCas9 (and various deletion mutants) by triparental mating.

2.2.2.6 Unmarked gene deletion in K56-2

Genes were deleted as per a double homologous recombination method reported previously (Flannagan et al., 2008; Hamad et al., 2010), with some modifications. Briefly, 360 – 450 bp of the upstream and downstream regions flanking the gene(s) to be deleted were fused and ordered as a single gBlock from IDT with *Xma*I and *Xba*I restriction sites (Table A4). The fragments were cloned into pGPI-SceI and transformed into *E. coli* SY327. Plasmids were confirmed by colony PCR with primers 153 and 154 then introduced into K56-2::dCas9 by triparental mating. The first recombination was confirmed by colony PCR of trimethoprim-resistant exconjugants. To promote the second recombination, pDAI-SceI-SacB (Hamad et al., 2010), constitutively expressing the SceI homing endonuclease, was introduced by triparental mating. Trimethoprim-sensitive colonies were screened by colony PCR for successful gene

deletion. To cure pDAI-SceI-SacB, colonies were patched on LB (without NaCl) + 15% sucrose (Fisher). Tetracycline-sensitive colonies were again screened by colony PCR for the deletion.

2.2.3 Construction of the barcoded plasposon and transposon mutant library

We wished to model our approach to barcoding on a previous report from the Deutschbauer lab (Wetmore et al., 2015). They constructed a 20 bp random barcode flanked by unique priming sites (GTCGACCTGCAGCGTACG and GAGACCTCGTGGACATC). These sequences are not found in K56-2 and were thus used for our approach. Primers 964 and 965 were used for inverse PCR of our parental plasposon pRBrhaBout. The product was circularized with In-Fusion HD Cloning (Takara Bio) as per the manufacturer's protocols. The resulting plasmid, pKS1, was sequence-confirmed to contain *Bam*HI and *Nco*I restriction sites between the inverted repeat and *dhfr*. A dsDNA fragment containing 20 random bases flanked by unique priming sites (Wetmore et al., 2015) and *Bam*HI and *Nco*I restriction sites was ordered from IDT with the sequence: 5′-GTTCAA*CCATG***GATGTCCACGAGGTCTCT**NNNNNNNNNNNNNNNNNNNN**CGTAC GCTGCAGGTCGAC***GGATCC*ACTTA - 3′. Italics show the *Nco*I and *Bam*HI restriction sites, while bold shows the unique priming sites; note that the end of the *Nco*I site (CCATGG) overlaps by one base (G) with one of the priming sites. As the fragment is used to generate the barcoded plasposon, pRBrha-Barcode, primers 972 and 973 were designed to amplify the fragment by PCR with Q5 polymerase and high-GC buffer (NEB). The barcode fragment and pKS1 were both digested with *Nco*I and *Bam*HI and ligated with T4 DNA ligase (NEB) at a 5:1 (insert:vector) ratio (100 ng total DNA/20 µL reaction) overnight at 16°C. The ligation mix was heated inactivated at 65°C for 15 mins then 5 µL was electroporated into *E. coli* SY327 and plated on LB plates with 50 µg/mL trimethoprim. Colonies were collected in subpools of 200 000 – 600 000 and frozen in PCR tubes at -80°C until needed. This process was repeated until ~6 million donor colonies were collected. A pilot BarSeq experiment (see *2.2.7* for the method) sequenced on a MiSeq with reagent kit v2 (Génome Québec, Montréal, Canada) using the first collected subpool confirmed it was highly diverse as expected.

Each subpool of *E. coli* was used only once as donor for triparental mating with K56-2. After only 4 hours of mating at 37°C (to reduce library redundancy), the mating pellicle was spread on Bioassay Qtrays (Molecular Devices) with the appropriate selective antibiotics and

0.2% rhamnose. After 2 days of growth, colonies were counted and harvested in subpools of 75 000 – 100 000 and frozen in PCR tubes at OD 2.0 – 4.0 (~100 million CFU/mL, or ~ 100 CFU/mutant) at -80°C. A pilot BarSeq experiment sequenced on a MiSeq with reagent kit v2 (Génome Québec, Montréal, Canada) was also performed on the first collected subpool of barcoded transposon mutants, which showed there were approximately half as many unique barcodes as total collected colonies.

2.2.4 RB-TnSeq DNA library preparation and sequencing

The transposon-genome junctions were amplified by the TnSeq-circle method as previously reported (Gallagher et al., 2011; Gislason et al., 2017a), with some modifications to accommodate the barcoding scheme (RB-TnSeq-circle). Briefly, DNA was extracted from representatives of the entire transposon mutant library (not treated with antibiotics) by isopropanol precipitation. We found that genomic DNA extractions by standard isopropanol precipitation yielded much higher recovery than any kit we tested, which was favourable for TnSeq-circle. The DNA was sheared to fragments averaging 300 bp with a Covaris M220 ultrasonicator, followed by end repair with the NEBNext End Repair Module (NEB). After this and other steps, Sera-Mag Select magnetic beads (Cytiva) were used to perform clean-up and size selection. Additionally, DNA concentrations were exclusively measured on the Qubit (ThermoFisher) with either AccuGreen broad-range or high-sensitivity dsDNA detection kits (Biotium). Adapters, consisting of annealed primers 683 and 684 (Table 3), were annealed with the Quick Ligation Kit (NEB). The DNA was then digested with *Pac*I (NEB) overnight to expose unique transposon ends. Probe 1426 in the presence of Ampligase (Lucigen) was used to selectively circularize and protect fragments containing the transposon sequence, while all other fragments were digested with a mix of T7 *gene 6* exonuclease (ThermoFisher), Lambda exonuclease (NEB), and Exonuclease I (NEB). qPCR with iTaq Universal SYBR Green Supermix (Bio-Rad) was used to determine enrichment of transposon-genome junctions. The number of cycles corresponding to ~50% maximum product by qPCR was used to amplify transposon-genome junctions with iTaq for Illumina sequencing. All primers used for this purpose were constructed to enable 1-step PCR to add the Illumina flow cell adapter, Nextera index, and sequencing primer binding site. After clean-up, the final PCR product was first analyzed on a TapeStation4150 (Agilent Technologies) then sequenced on an Illumina MiSeq

(Donnelly Centre, Toronto, Canada) to assess library quality with a MiSeq reagent kit v2 (2x250 bp reads) and 20% PhiX spike. To increase sequencing depth, an Illumina HiSeq 2500 (The Applied Centre for Genomics, Toronto, Canada) was used on rapid run mode with a 20% PhiX spike (1x150bp reads). In both cases, the sequencing reads covered the transposon-specific sequence, barcode region, and at least 40 bp of the genome adjacent to the insertion site. In total, ~180 million reads were generated.

2.2.5 RB-TnSeq data analysis

To link barcodes to transposon insertion sites, the bioinformatic pipeline and scripts reported by (Wetmore et al., 2015) were used in a Conda 4.10.0 environment. These are available at https://bitbucket.org/berkeleylab/feba/src/master/. Briefly, the scripts identify reads containing the flanking priming sites and a transposon-specific sequence (terminal repeat) then map it to a genome with BLAT (Kent, 2002). The priming sites flanking the barcode were the same as in the original report (Wetmore et al., 2015). The transposon-specific sequence in our construct is CATGGGCACTTGTGTATAAGAGTCAG. The default stringency and base error tolerances were used, resulting in 86.1% of the observed barcodes being considered "usable" (primarily associated with one insertion site and filtered to remove sequencing/PCR errors). The reads were aligned to the closed K56-2 genome (RefSeq accession GCF_014357995.1) (García-Romero and Valvano, 2020).

2.2.6 Transposon mutant pool antibiotic exposure

Wild-type K56-2 was used to determine the dose-response curves of the antibiotics in conditions mimicking the planned mutant pool exposure. Stationary phase cells were diluted to OD_{600} 0.025 in LB medium and grown at 37°C with 230 rpm shaking until early exponential phase (OD_{600} 0.15, about 3 hours). In 2 mL culture in glass tubes, a range of antibiotic concentrations was added (in technical duplicate) and the cells were grown for 8 hours (approximately 10-12 generations), again at 37°C with 230 rpm shaking. Then, the OD_{600} of each tube was measured to compute the dose-response curve for each antibiotic relative to cells grown without antibiotics. This assay was performed in three biological replicates. The IC_{20-30} was confirmed by repeating this assay with a much narrower antibiotic concentration range around the IC_{20-30}.

To prepare the mutant inoculum, aliquots of the transposon mutant library were thawed and mixed in ratios according to the number of colonies contained in each aliquot to obtain approximately equal abundance of each of the ~340 000 unique mutants. This master pool was then inoculated into flasks with 50 mL of LB medium with 0.2% rhamnose at OD_{600} 0.025 (~75 CFU/mutant) and grown at 37°C with 230 rpm shaking until early exponential phase (OD_{600} 0.15, about 5-6 hours from frozen stocks). The culture was then split up into 2 mL volumes in small glass tubes, six for each antibiotic: three replicate tubes at two slightly different concentrations to ensure at least one achieved the $IC_{20\text{-}30}$. A 2 mL aliquot of cells not exposed to antibiotic was taken at the Time 0 sample. The cultures were then exposed to antibiotics (or 1% DMSO solvent control) for 8 hours 37°C with 230 rpm shaking, after which the OD_{600} of the cultures were taken and cells were harvested from the tubes at the $IC_{20\text{-}30}$.

2.2.7 BarSeq DNA library preparation and sequencing

The method to amplify barcodes for sequencing followed a 1-step PCR as per (Wetmore et al., 2015) with some modifications. After antibiotic exposure, genomic DNA was extracted from cells with the PureLink Genomic DNA Mini Kit (Invitrogen). Yield for this and all subsequent steps was quantified with a Qubit (ThermoFisher) with either AccuGreen broad-range or high-sensitivity dsDNA detection kits (Biotium). To preserve mutant abundance ratios and reduce the propagation of PCR errors, semiquantitative PCR was performed. This was done for six randomly selected conditions. In each of a set of 10 µL reaction volumes, we added 40 ng of genomic DNA and 20 µM of each primer with Q5 high-fidelity DNA polymerase, the high-GC buffer, and standard Q5 reaction buffer (NEB). In an Eppendorf Mastercycler EP Gradient S, the cycling conditions were: 98°C for 4 mins, followed by cycling between 98°C for 30 s, 61°C for 30 s, 72°C for 30 s, then followed by a final extension at 72°C for 5 mins. After each cycle between 13 and 21, we quickly removed one tube and added 3 µL of Gel Loading Dye, Purple 6x (NEB) (with 10 mM EDTA) to stop the reaction. Formation of the product at 196 bp was visualized by electrophoresis through a 2.5% agarose gel in standard TAE buffer. By visual inspection of band intensities, a cycle number was chosen that resulted in ~25% of maximum product formation (found to be cycle 17). This cycle number was the same for all six randomly selected conditions and was thus used for all conditions. These cycling conditions were found in

a small pilot experiment, sequenced on a MiSeq with reagent kit v2 and 20% PhiX spike, to result in 96.4% of reads containing known barcodes.

We found that amplification in 10 µL matched that in 50 µL, thus the exact same PCR setup was used when scaled up to four tubes of 50 µL per condition to increase yields. For the template, 200 ng DNA was added to ensure >75 molecules of genome per mutant. We observed a minor secondary product (<10%) at 315 bp on TapeStation 4150 traces (Agilent Technologies). Thus, for each condition, 200 µL of raw BarSeq PCR product was pooled and subjected to two rounds of dual size selection with Sera-Mag Select (Cytiva) magnetic beads to purify the desired product at 196 bp. The primers were designed with Nextera-type tagmentation sequences as for the RB-TnSeq-circle sequencing primers, except that the 8 bp standard Nextera indexes were replaced with 10 bp Unique Dual Indexes (primers 2163 – 2255). Each product was amplified with a unique i5 and i7 index, enabling greater multiplexing flexibility and higher confidence in correcting up to 2 bp errors during indexing read sequencing. Up to 24 samples were indexed together for runs of a NextSeq 550 in high-output mode (Donnelly Centre, Toronto, Canada) with reagent kit v2.5 and 20% PhiX spike, generating 410 – 510 million 30 bp single-end reads each. A custom sequencing recipe was used for dark-cycling during the first 18 bases, covering the flanking primer region, with the read output starting at the beginning of the barcode and extending 10 bp into the other flanking priming region.

2.2.8 BarSeq gene fitness calculations

BarSeq reads were associated with the correct barcode using the pipeline from (Wetmore et al., 2015). Reads, in fastq format, were first trimmed to contain only the 20 bp barcode using the FASTX toolkit (http://hannonlab.cshl.edu/fastx_toolkit/). Reads with any base having a quality score below 20 were also filtered out. Artificial pre- and post-sequences, NNNGTCGACCTGCAGCGTACG and AGAGACC, respectively, were added to all barcodes so the script RunBarSeq.pl would recognize the barcodes as valid.

Following this, the barcodes were processed with scripts from (Morin et al., 2018) which are designed to compare mutant abundance between conditions (https://github.com/DuttonLab/RB-TnSeq-Microbial-interactions). A pseudocount of 0.1 was added to all barcode counts to prevent 0-value errors with log transformations. Barcodes were removed if they 1) had fewer than 3 reads in the Time 0 condition and 2) represented intergenic

insertions, or insertions in the first or last 10% of a gene. Raw counts were normalized against the counts of 10 non-essential "neutral" genes randomly selected from across the genome that also showed no fitness effect in any condition. These were: K562_RS24650 (ABC-type amino acid transporter), K562_22855 (putative glycosyltransferase), K562_05000 (hydrolase family protein), K562_12100 (acyl-CoA dehydrogenase), K562_01045 (Raf kinase inhibitor-like protein), K562_06455 (putative PHA depolymerase protein), K562_13470 (GudD glucarate dehydratase), K562_16220 (DUF3025 domain-containing protein), K562_18550 (hypothetical protein), K562_28510 (hypothetical protein). Strain fitness values were then calculated as the $\log_2$(reads in Condition X / reads in Time 0). Gene fitness values were calculated as the arithmetic mean of strain fitness values for each gene. To account for artificial inflation of read count due to proximity to the replication forks, fitness values were smoothed based on genomic position using a moving window (Wetmore et al., 2015). Across the three replicates, gene fitness was calculated as the inverse-variance weighted mean. Spearman, Pearson, and Lin correlation coefficients across replicates for each condition were between 0.5 and 0.8. Lastly, the gene fitness values in each condition were compared to the DMSO control by an independent two-sided Student's t-test. The data was also curated to remove any genes from downstream analysis that only had one reporting mutant. We used eggNOG-mapper v2 to provide functional annotations and gene names based on orthology (Cantalapiedra et al., 2021; Huerta-Cepas et al., 2017).

As many bacterial genes are organized in operons, disruptions in upstream genes may have polar effects on the downstream gene expression. Consequently, observed effects would be a combination of disrupting two or more genes. We argue that polarity may have a minimal effect on our findings due to 1) high insertion density and 2) the construction of our transposon. The large number of mutants recovered in our screen virtually guarantees insertions in every non-essential gene, thus genomic saturation would rule out polar effects by reporting fitness scores for nearly all non-essential genes. Secondly, our transposon has outward-facing promoters in both directions, the rhamnose-inducible promoter and the promoter controlling *dhfr*. As the transposon mutant antibiotic exposures were performed with added rhamnose, and the transposon terminal repeat after *dhfr* is not predicted to form an intrinsic terminator, insertion in operons may permit downstream gene expression. The parent transposon pTn*Mod*-OTp (Hunt et al., 2004) was suggested to not cause polar effects (Ortega et al., 2005). However, any

expression, either upstream or downstream of the insertion, would be altered/non-native and was not directly assessed.

2.2.9 Microscopy

To observe the effect of β-lactam exposure on K56-2, cells were inoculated at OD 0.025 in 2 mL glass tubes and incubated at 37°C with 230 rpm shaking until early exponential phase OD 0.15, about 3 hours. Antibiotics were added and the incubation continued for 4 hours. To observe the effect of deletion or overexpression of O-antigen-related genes, the appropriate mutants were inoculated in 2 mL glass tubes at OD 0.025 with or without 0.05% rhamnose and grown at 37°C with 230 rpm shaking for 3 hours. Cells were then diluted to OD ~0.05, fixed in 3.7% formaldehyde + 1% methanol (Sigma) at room temperature for 20 minutes. The formaldehyde was quenched by addition of an equal volume of 0.5 M glycine, and the cells were washed by centrifugation and resuspended in Dulbecco's PBS (Sigma). Cells were spotted on 1.5% agarose pads with PBS to maintain turgor and imaged by DIC microscopy on an Axio Imager upright microscope (Carl Zeiss Microscopy GmbH).

2.2.10 LPS analysis

The general structure of the O-antigen LPS and lipid A core were analyzed qualitatively by silver staining polyacrylamide gels as per (Marolda et al., 2006), with some modifications. For LPS extractions, CRISPRi mutants were grown overnight in liquid LB with 100 µg/mL trimethoprim and 0.5% rhamnose at 37°C. The mutants were subcultured at OD 0.025 and grown with 0.5% rhamnose for an additional 8 hours. For complementation, cells were subcultured to OD 0.025 and grown for 3 hours, then induced with 0.05% rhamnose for an additional 4 hours. For both types of mutants, an equivalent amount of 500 µL of OD 1.5 was harvested, washed by centrifugation, and resuspended in 150 µL lysis buffer (2% w/v SDS, 4% β-mercaptoethanol, 0.5 M Tris, pH 6.8). Cells were lysed by incubation at 95°C for 10 mins. DNase I (Worthington Biochemical) was added to 100 µg/mL and incubated at 37°C for 30 mins. Proteinase K (ThermoFisher) was added to 1.25 mg/mL and incubated at 60°C for 2 hr. An equal volume of 90% phenol (ThermoFisher) (supplemented with 0.1% β-mercaptoethanol and 0.2% 8-hydroxyquinoline) was added the tubes were incubated at 70°C for 15 mins, with vortexing every 5 mins. The extractions were chilled on ice for 10 mins then centrifuged at 16 000 x g for

10 mins. The aqueous phase was washed with 10x volumes of ethyl ether (saturated with 10 mM Tris and 1 mM EDTA, pH 8.0) and centrifuged briefly. The top organic phase was removed by aspiration, then the aqueous phase was gently heated to 55°C for 10 mins to boil off any remaining ethyl ether. An equivalent volume of 2x loading dye (120 mM Tris-HCl pH 6.8, 4% m/v SDS, 20% glycerol, 0.04% bromophenol blue, and 10% β-mercaptoethanol) was added and the samples were stored at -20°C until needed.

The LPS banding patterns were resolved by Tricine-SDS-PAGE as per (Marolda et al., 2006), with some modifications. The gels were cast using 30% acrylamide/bis 29:1 solution (Bio-Rad) at final concentrations of 14% for the resolving gel and 4% for the stacking gel. 10 uL of each sample, diluted with an equal volume of loading buffer, was run in each lane. Gels were run at 50 V for 1 hr, then at 130 V for 3 hrs and 15 mins, then stained with the Pierce Silver Stain Kit (ThermoFisher) and imaged immediately afterwards on a Bio-Rad ChemiDoc.

2.2.11 Rhamnose dose-response curves

After construction, the first objective with the CRISPRi and overexpression mutants was to characterize how varying gene knockdown or overexpression affects growth. Each of the mutants were diluted to OD_{600} 0.01 in 96-well format and inoculated into a rhamnose gradient (with 100 µg/mL trimethoprim). Growth was monitored in a BioTek Synergy 2 plate reader with constant linear shaking and temperature maintained at 37°C.

2.2.12 Antimicrobial susceptibility testing and interaction assays

Broth microdilution susceptibility tests were used to assess and interpret MIC values as per CLSI guidelines (Clinical and Laboratory Standards Institute CLSI, 2012, 2014). Overnight cultures grown in liquid LB were used to prepare inocula for standard microdilution tests and checkerboard interactions assays. Growth was visually assessed in the antibiotic gradients after 20 hrs of static incubation. When interpretive standards for *Burkholderia* did not exist (as for cefiderocol and aztreonam), standards for *Pseudomonas aeruginosa* were used. M9+CAA medium consisted of the following: 1x M9 salts (Difco), 25 mg/L $CaCl_2$, 12.5 mg/L $MgCl_2$, 0.3% low-iron casamino acids (Fisher), and 25 mM glucose.

A very similar format was used to assess changes in antibiotic susceptibility of the CRISPRi mutants. A final concentration of 0.5% rhamnose was added to the wells to induce

dCas9 expression. For fitness-associated/essential genes (e.g. *uppS*), a concentration of rhamnose to achieve 80% WT growth was used. For assays done in M9+CAA medium, 25 mM glycerol was used instead of glucose, as glucose catabolism represses the rhamnose-inducible promoter (Egan and Schleif, 1993) controlling dCas9 expression. Trimethoprim was not included in the assay plates to remove the possibility of chemical interactions. Growth was assessed after 20 hrs of static incubation by reading OD_{600} values with a BioTek Synergy 2 plate reader to record subinhibitory dose effects.

Checkerboard assays were prepared in mini 4x4 well format using antibiotic concentrations of 1/8 – 1/2 the MIC for each compound. Checkerboard data was processed with SynergyFinder2 (http://www.synergyfinder.org/#!/) (Ianevski et al., 2020; Zheng et al., 2022) as this easily handles biological replicates and gives mathematical interpretations of interactions even when compounds do not fully inhibit. When both the Loewe Additivity and Bliss Independence scores were below -10 (as determined from the 95% confidence intervals), the interaction was regarded as strongly antagonistic; synergy was interpreted when both scores were above +10 (as determined from the 95% confidence intervals). A weak interaction was interpreted when one score was above +10 or below -10 and the other was between -10 and +10.

2.2.13 NPN uptake assay

Outer membrane permeability was assessed with the NPN uptake assay as per (Loh et al., 1984; Malott et al., 2012), with some modifications. For CRISPRi mutants, overnight cultures were grown with or without 0.5% rhamnose (or 0.04% for the *uppS* mutants) then diluted to OD 0.025 and grown for an additional 8 hours (with or without the same concentration of rhamnose) until OD ~1.0. For gene deletion mutants, overnight cultures were diluted to OD 0.2 and grown for 3 hours until OD ~1.0. Cells were washed by centrifugation at 5 000 x g for 5 minutes then resuspended in 5 mM HEPES pH 7.2 with 10 mM NaN_3 (Sigma) and rested at room temperature for 30 minutes. An equal volume of cells was mixed with HEPES buffer containing 80 µM NPN (Sigma). The fluorescence signal was measured in a BioTek Synergy 2 plate reader with filter sets: Ex 360/40 nm and Em 420/40 nm. Wild-type K56-2 treated with 32 µg/mL CHX was used as a positive permeabilized control. The blank-corrected fluorescence values were normalized to the OD_{600} of each well. To easily compare between replicates, the fluorescence ratios of the mutants to K56-2 controls (with non-targeting sgRNA as appropriate) were calculated.

2.2.14 Inductively coupled plasma mass spectrometry (ICP-MS) analysis of trace metals in growth media

Samples of growth medium were prepared and autoclaved as per manufacturer's recommendations. The samples were clarified by passing through a 0.22 µm polyvinylidene difluoride filter (Fisher Scientific). Bound ions were liberated by room temperature digestion 1:1 with aqua regia. The solution was then diluted 20-fold with 18.2 MΩ/cm water. ICP-MS analysis was carried out at the Ultra Clean Trace Elements Laboratory at the University of Manitoba with an Agilent 8900 ICP-QQQ-MS. The instrument plasma mode was set to general purpose with -140V omega bias and 6.6 V omega lens settings. H2 gas flow was set to 4.5 mL/min; He gas flow was set to 4.3 mL/min; O2 gas was set at 30%. Before the run, certified reference materials NIST-SRM 1640a and 1643e were used as a measure of quality control.

2.2.15 Statistical analysis

For RB-TnSeq and BarSeq data, the statistical analysis and normalizations built into the scripts were used (Morin et al., 2018; Wetmore et al., 2015). Only the independent Student's t-test was applied to the BarSeq data comparisons, not the false-discovery rate multiple-testing correction as it was found to be too stringent; however, samples were only compared by t-test if they passed Fisher's F-test of equal variances ($\alpha = 0.002$). As this was expected to produce false positive, only genes with fitness effects greater than 0.5 or less than -0.5 were considered for further analysis. Additionally, we performed extensive follow-up validations using CRISPRi mutants many of the effects we observed in the BarSeq data. Pearson's correlation with two-tailed p-values was used to assess the relationship between gene fitness values in AVI/CAZ and the single conditions in the combination. The NPN outer membrane permeability assay was analysed by 1-way ANOVA with a Dunnett's multiple comparison test, with K56-2::dCas9 bearing the non-targeting sgRNA (or without for the deletion mutants) set as the reference.

2.2.16 Data availability

Raw sequencing data is available from the NCBI Sequencing Read Archive (SRA) under the BioProject ID PRJNA859150. All gene fitness scores are available in Supplementary Data 1 (https://doi.org/10.34990/FK2/UIQTSR). Publicly available databases and servers were used for

gene annotations: BioCyc (https://biocyc.org/), EggNOG-mapper v2 (http://eggnog-mapper.embl.de/), GO (http://geneontology.org/), and UniProt (https://www.uniprot.org/).

CHAPTER 3: COMPETITIVE FITNESS OF ESSENTIAL GENE KNOCKDOWNS REVEALS A BROAD-SPECTRUM ANTIBACTERIAL INHIBITOR OF THE CELL DIVISION PROTEIN FTSZ

Reproduced from:
Hogan AM, Scoffone VC, Makarov V, Gislason AS, Tesfu H, Stietz MS, Brassinga AKC, Domaratzki M, Li X, Azzalin A, Biggiogera M, Monakhova N, Chiarelli LR, Riccardi G, Buroni S, Cardona ST. 2018. Competitive fitness of essential gene knockdowns reveals a broad-spectrum antibacterial inhibitor of the cell division protein FtsZ. *Antimicrob. Agents Chemother*. **62**(12): e01231-18.

Silvia Cardona and Silvia Buroni conceived the idea, designed the research, and edited the final version of the paper. Andrew Hogan designed and performed the fitness assays and microscopy experiments and wrote the paper. Viola Scoffone. performed cloning, protein expression, and purification and enzymatic assays. Vadim Makarov, Olag Ryabova, and Natalia Monakhova synthesized C109. April Gislason performed preliminary experiments and edited the final version of the manuscript. Habehn Tesfu and Silvia Buroni performed MIC experiments and checkerboard assays. M. Silvina Stietz performed the C. elegans assays and edited the final version of the manuscript. A. Karen Brassinga. contributed microscopy support. Michael Domaratzki and Xuan Li were involved in processing and analyzing the data. Alberto Azzalin performed cytotoxicity experiments on human cells. Marco Biggiogera performed electron microscopy experiments. Laurent Chiarelli performed enzymatic assays and analyzed data. Giovanna Riccardi, Silvia Buroni, and Silvia Cardona supervised the work and contributed financially.

3.0 Introduction

Imperative to the fight against antibiotic resistance, new antibiotic discovery strategies and platforms must be employed. These platforms must provide rapid target and mechanism of action identification as these are recognized as challenging aspects of antimicrobial screens (Farha and Brown, 2016). Many versions of target-based assays now exist, which examine the effect of antimicrobials on specific targets (Farha and Brown, 2016). To vastly increase throughput and the number of simultaneous targets examined, next-generation sequencing (NGS) can be coupled to target-based assays in whole cells (Gingras et al., 2018; Gislason et al., 2017b; Smith et al., 2010). The power of these NGS hybrid assays lies in the ability to profile the specific abundances of mutants within genomic libraries with high sensitivity and multiplexing potential (Smith et al., 2010). While the development of these platforms in yeast has been fruitful (Giaever et al., 2004; Lum et al., 2004; Smith et al., 2012), the potential of NGS to match new antimicrobials to their targets in bacteria is still emerging.

Burkholderia cenocepacia is a member of the *Burkholderia cepacia* complex (Bcc), a group of at least 20 opportunistic human pathogens (Eberl and Vandamme, 2016). Immunocompromised hosts, such as those with cystic fibrosis, are particularly susceptible to *B. cenocepacia* infections. For cystic fibrosis patients, respiratory infection is the leading cause of mortality. Members of the Bcc are almost completely resistant to aminoglycosides, cationic peptides, and β-lactams (Abbott et al., 2016). Furthermore, the resistance of Bcc isolates can increase over time during successive pulmonary exacerbations (Denis et al., 2007). As a consequence of the lack of effective antibiotics, Bcc infections are difficult to eradicate and can result in *cepacia* syndrome, a lethal form of pneumonia (Isles et al., 1984). We have shown that the novel synthetic compound methyl [(4-nitro-2,1,3-benzothiadiazol-5-yl)thio]acetate 10126109 (called here C109) is a bactericidal antimicrobial against Bcc species (Scoffone et al., 2015). However, the mechanism of action and target of C109 are unknown, warranting further investigations. Here, we employed a combination of an NGS-based fitness assay, fluorescence and electron microscopy, and biochemical assays to show that C109 is a broad-spectrum antibacterial that inhibits the cell division protein FtsZ, an attractive target for antibiotic discovery (Hurley et al., 2016). Opposite to most FtsZ inhibitors, C109 is active against Gram-negative bacteria, and shows properties that merit its development as a new antibacterial drug.

3.1 Results

3.1.1 An Illumina-based fitness assay reveals mutants hypersusceptible to C109

Previously, we developed a high-density transposon mutant (HDTM) library in *B. cenocepacia* K56-2 by delivering a transposon element containing an outward rhamnose-inducible promoter (P_{rhaB}) into the genome (Gislason et al., 2017a). Using an enrichment process to isolate mutants in which P_{rhaB} is driving expression of essential genes, we built a redundant knockdown library of 830 clones. This library was combined with another 134 previously constructed knockdown mutants (Bloodworth et al., 2013), in total representing 83 essential operons. The combined knockdown mutant library showed good representation of Cluster of Orthologous Groups (COG) categories compared to the essential genome of *B. cenocepacia* K56-2 (Figure A1).

To investigate the mechanism of action of C109, we developed the experimental approach shown in Figure 1. Briefly, when the combined knockdown mutant library is pooled and grown in sensitizing conditions (low rhamnose) in the presence of an antibacterial molecule, hypersusceptible mutants become depleted. The relative abundance of the mutants after antibiotic treatment is detected by Illumina sequencing of the transposon-genome junctions (Tn-seq) (Gallagher et al., 2011; Opijnen et al., 2009). As previously observed (Bloodworth et al., 2013; Gislason et al., 2017b), when mutant pools were exposed to the IC_{25} of novobiocin, a mutant with a knockdown in the target coding gene *gyrB* (K562_RS02180) was highly depleted (Figure 2A and 2C). In addition, knockdown mutants in four transcriptional units were hypersusceptible to both novobiocin and C109 (*dnaN*, *xseB-ispA-dxs*, *ispA-dxs*, and *topB*) (Figure 2A, 2B and 2C). A fifth hypersusceptible knockdown mutant of *lolB* (K562_RS04105) was removed from further analysis as only one of several mutants in this gene (Table A5) was hypersusceptible to novobiocin and C109. Closer inspection revealed that the transposon insertion in the only hypersusceptible mutant truncated the first 15 residues from LolB, which is likely the secretory signal peptide (Matsuyama et al., 1997), resulting in reduced viability. Knockdown mutants of two essential operons containing cytosol aminopeptidase (*pepA*, K562_RS05790) and DNA polymerase III subunit chi (*holC*, K562_RS05795), and another containing the *division and cell wall* cluster (*dcw*, K562_RS16835 - K562_RS16765), which includes *ftsZ*, were hypersusceptible to C109 but not to novobiocin (Figure 2A, 2B, and 2C).

Chemical and genetic depletion of essential gene function affects cell morphology (Peters et al., 2016). As such, we reasoned that knockdown of the target of C109 might phenocopy the effect of C109 treatment, further narrowing the list of putative targets. When grown without rhamnose, the mutants hypersusceptible to C109 displayed a variety of morphologies (Figure 2D). To facilitate comparison, we developed a qualitative characteristic matrix based on filamentation, enlargement, shortening, and bending (Table A6). Compared to the wild-type morphology, C109 treatment caused a marked filamentous phenotype that was also observed upon knockdown of the isoprenoid synthesis genes *ispA* and *dxs*, and *dcw* cluster genes, including knockdown of *ftsZ* (Figure 2D). However, filaments formed by *ispA* and *dxs* knockdown were septated and severely bent, a phenotype not observed in C109-treated cells. Additionally, the knockdowns of the other candidate targets caused enlargement on both the lateral and longitudinal cell axes, or cell shortening, but not filamentation (Figure 2D and Table S2). Together, the hypersusceptibility of the *dcw* knockdown to C109 and the similar morphologies of the C109-treated cells and the *dcw* knockdowns, suggest that C109 inhibits a function encoded by the *dcw* cluster.

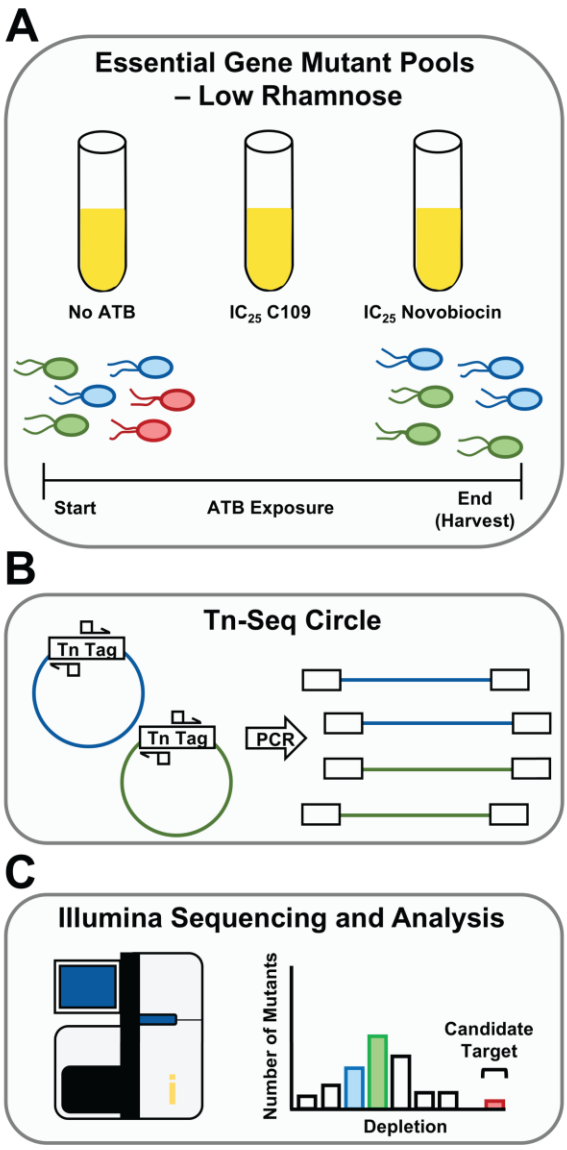

Figure 1. Workflow of competitive fitness assay. A) The sensitized mutant library is grown competitively without antibiotics (control), or with the IC_{25} of C109 or novobiocin. Growth with antibiotics selectively depletes certain mutants. B) To track mutant abundance, transposon-genome junctions are enriched using Tn-Seq Circle. C) Samples are sequenced on a HiSeq and reads are then mapped to the *B. cenocepacia* K56-2 genome to call insertion sites. The reads from the antimicrobial-treated conditions are compared to the no antibiotic controls to determine highly depleted mutants, which are used to call candidate antibacterial-target matches.

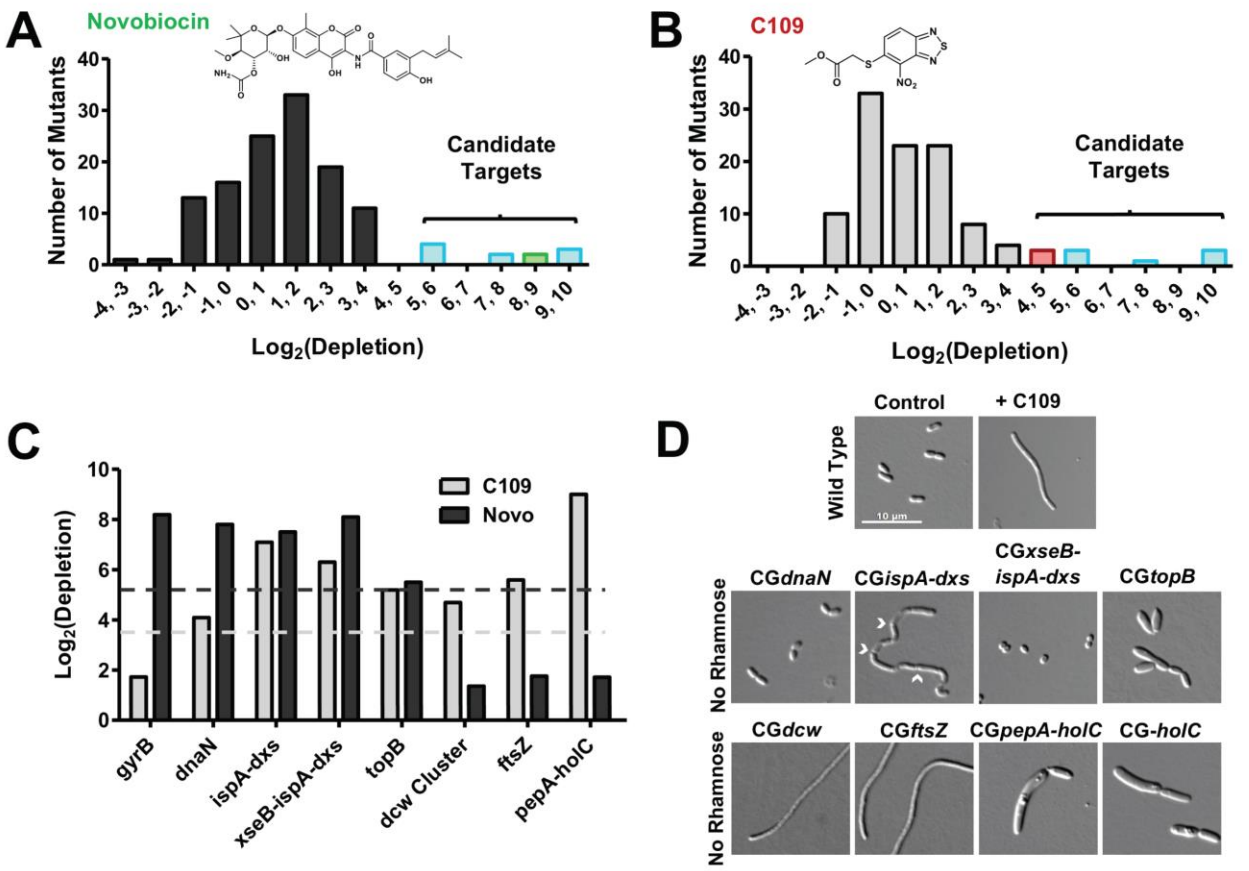

Figure 2. A Tn-seq based fitness assay and morphological phenotype screening links C109 to the *dcw* operon. A) and B) Hypersusceptibility of knockdown mutants to novobiocin (A) and C109 (B). Only mutants with depletion ratios of P-value < 0.05 are shown. The region highlighted as "Candidate Targets" corresponds to knockdown mutants with Log_2 (depletion) greater than two standard deviations from the mean. C) Comparison of hypersusceptible mutants to C109 and novobiocin. Light gray and charcoal dashes represent 2SD thresholds for novobiocin and C109, respectively. D) Morphology of *B. cenocepacia* and knockdown mutants treated with 2xMIC (16 µg/mL) C109 or incubated without rhamnose, respectively, for 6 hours. Chevrons indicate septa in CG*ispA-dxs*. All micrographs are to the same scale.

3.1.2 C109 inhibits divisome formation and induces filamentation

The *dcw* cluster is a well-conserved group of genes encoding functions centered on cell wall synthesis and cell division (Mingorance et al., 2004). Included are proteins required to form the divisome, a structure whose orderly assembly, beginning with FtsA and FtsZ, is critical for cell division (Lutkenhaus and Du, 2017). Perturbation of the recruitment timing or localization of divisome proteins prevents cell division and causes filamentation (Chen and Beckwith, 2001).

To systematically assess if C109 prevents the proper localization of divisome components, we used a subset of the ASKA collection of *Escherichia coli* strains expressing C-terminal GFP fusions of all *dcw* cluster genes (Kitagawa et al., 2005). *E. coli* is a valid tool for use with C109 as its growth is also inhibited by C109 (Table 1), and the organization of the *dcw* clusters of *E. coli* and *B. cenocepacia* are nearly identical (Holden et al., 2009; Mingorance et al., 2004). In the absence of C109, FtsZ-GFP, FtsA-GFP, and FtsW-GFP localized to the midcell, as expected (Figure 3A). MraZ-GFP also appeared to localize correctly, in the nucleoid region (Figure A2). Upon treatment with C109, the localization of the transcription factor MraZ-GFP did not markedly change; however, the fluorescence corresponding to the central divisome components FtsZ-GFP and FtsA-GFP appeared as dispersed puncta, or as in the case of FtsW-GFP, became diffuse (Figure 3A). The localization of cytoplasmic *dcw*-encoded proteins (e.g. MurC, MurD, and DdlB) was not altered by C109 (Figure A2A). FtsI-GFP, FtsL-GFP, MraY-GFP, and FtsQ-GFP did not properly localize to the midcell under control conditions (Figure A2B) and were excluded from further testing.

Table 1. Antibacterial activity of C109 against select Gram-negative and -positive bacteria**.** MIC values are given as the median of three biological replicates

Strain	MIC (μg/ml)
Acinetobacter baumannii ATCC19606	16
Burkholderia cenocepacia K56-2	8
Burkholderia cenocepacia J2315	8
Enterobacter aerogenes ENT001	32
E. aerogenes ATCC 13048	8
Escherichia coli ATCC25922	8
E. coli 117782	4
E. coli 120955	8
Klebsiella pneumoniae 119178	32
Mycobacterium abscessus 13NC740779	4
M. abscessus 14NF251095	4
M. abscessus 14NJ168168	4
M. abscessus 16NH386647	8
Pseudomonas aeruginosa PAO1	256
P. aeruginosa PA7	128
P. aeruginosa PA14	>128
Salmonella enterica Typhimurium	64
Serratia marcescens Db11	16
Staphylococcus aureus ATCC25923	4

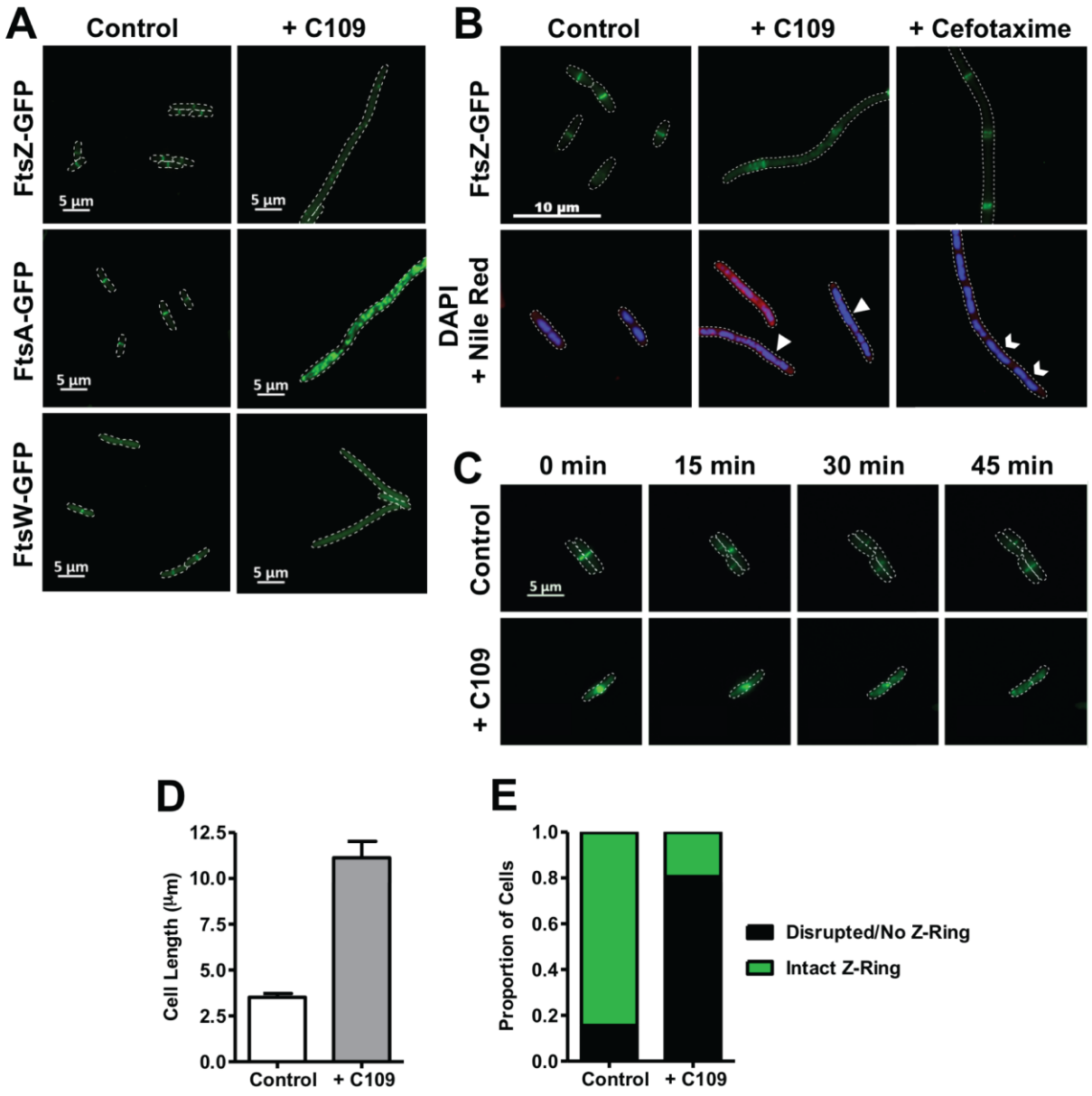

Figure 3. C109 causes cell filamentation and disrupts divisome formation. A) and B) Localization of FtsZ, FtsA and FtsW upon 3-hour treatment of exponentially-growing ASKA strains with C109 (A and B) or cefotaxime (B). Arrowheads show areas with deficient nucleoid segregation. Chevrons show proper nucleoid segregation. C) Time-lapse fluorescence microscopy of FtsZ-GFP cells, spotted onto an agarose pad with or without 4 μg/mL C109. Dashes denote cell boundaries. D, E Cell length (D) and proportion of cells with Z-ring (E) after 3 hours of exposure to C109 (n =200 cells).

Filamentation is a consequence of cell division inhibition (Chen and Beckwith, 2001), yet other cellular processes not related to cell division can cause filamentation, which in turn can prevent divisome formation (Justice et al., 2000, 2008; Wortinger et al., 1998). We therefore assessed the possibility that the observed filamentation caused by C109 is not directly associated with inhibiting divisome formation. We first examined the localization of FtsZ-GFP as a marker for early divisome formation in response to cefotaxime, a β-lactam cell-wall synthesis inhibitor known to cause filamentation (Kjeldsen et al., 2015). In the presence of cefotaxime, the *E. coli* cells had filamentous morphology, yet FtsZ-GFP was regularly localized in bands along the filament (Figure 3B), showing that cell filamentation can be uncoupled from Z-ring formation. Conversely, the filamentous cells formed due to C109 treatment showed mislocalization of FtsZ-GFP, reinforcing the view that C109 specifically targets divisome formation. Moreover, treatment with C109 appeared to cause nucleoid segregation deficiency, which can be a consequence of inhibited divisome assembly (Huls et al., 1999; Wang et al., 2005). As opposed to cells treated with C109, those treated with cefotaxime showed defined nucleoids along the filament (Figure 3B). To further demonstrate that C109 inhibits divisome assembly, we examined how C109 affects the distribution of FtsZ-GFP in live cells using fluorescence time-lapse microscopy. FtsZ-GFP rapidly localized to the mid-cell site in untreated cells (Figure 3C), while in cells treated with C109, FtsZ-GFP did not localize properly, but instead formed puncta throughout the cell. Importantly, we observed that inhibition of FtsZ-GFP localization occurred before filamentation, further suggesting that C109-induced divisome inhibition causes filamentation. After only 3 hours of exposure to 1xMIC of C109, we observed a three-fold increase in length on average (Figure 3D), and 80% of cells had an absent or disrupted Z-ring, compared to 20% in the control (Figure 3E). Together, these findings support the notion that C109 blocks cell division by inhibiting divisome formation, which in turn causes a filamentous morphology.

3.1.3 Genetic evidence suggests that FtsZ is the target of C109

Target overexpression is known to decrease susceptibility to certain antibiotics (Palmer and Kishony, 2014). To seek additional evidence that the target of C109 is encoded by the *dcw* cluster, we mildly overexpressed MraZ-GFP, MurG-GFP, FtsW-GFP, FtsA-GFP, and FtsZ-GFP, and SecA-GFP from an IPTG-inducible promoter in *E. coli*. These fusions were chosen because

they localized correctly without C109. SecA-GFP was used as a control as it is not encoded by the *dcw* cluster. The concentration of IPTG was first titrated to not cause a growth defect in any of the strains (Figure A3); hence 10 μM IPTG was selected. As shown in Figure 4A, the strains expressing SecA-GFP, FtsW-GFP, and MurG-GFP had a similar susceptibility to C109 as the control. On the contrary, the strains expressing MraZ-GFP, FtsA-GFP and FtsZ-GFP displayed higher susceptibility to C109 (Figure 4B). The higher susceptibility of the strain expressing MraZ-GFP was expected since overexpression of MraZ is known to perturb cell division causing a lethal effect (Eraso et al., 2014). As the proper localization of FtsZ and FtsA were affected by C109, we were expecting that increased expression of these proteins might permit continued cell division, reducing susceptibility to C109. However, the increased susceptibility suggests toxic interactions between C109, FtsA and FtsZ. Toxic antibacterial-target interactions have been reported previously (Palmer and Kishony, 2014). These results, together with the sequential assembly of the divisome as a logic model means that the most upstream protein with C109-inhibited localization could be the target. Therefore, our results thus far suggest the target of C109 is FtsZ.

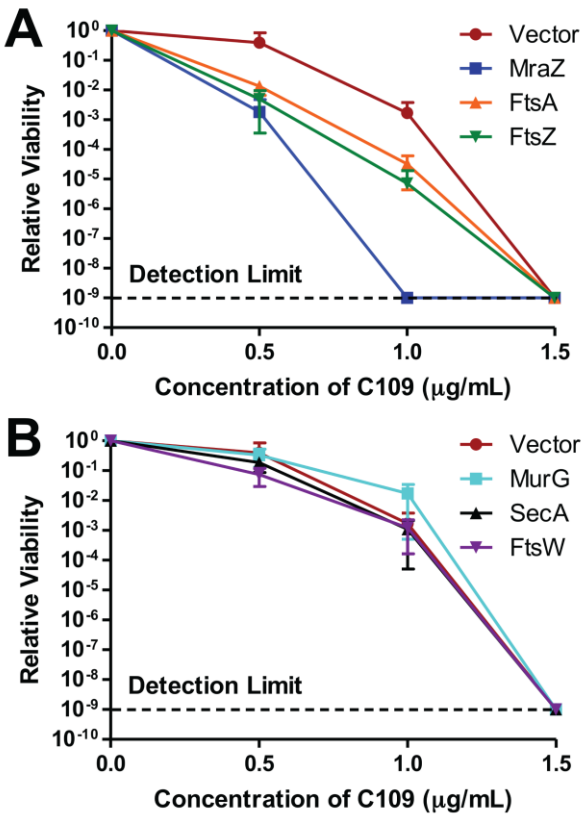

Figure 4. Mild overexpression of MraZ-GFP, FtsA-GFP, and FtsZ-GFP, but not FtsW-GFP, MurG-GFP, or SecA-GFP sensitizes cells to C109. Cells were induced with 10 μM IPTG then exposed to C109 for 12 hours. Spot plate was used to count CFU/mL. Counts are relative to each strain without C109 treatment. A) Growth of strains expressing MurG-GFP, SecA-GFP, and FtsW-GFP. B) Growth of strains expressing MraZ-GFP, FtsA-GFP, and FtsZ-GFP. Vector refers to the strains harbouring pCA24N-empty. Error bars show mean ± SD, n = 3 biological replicates.

To further support the idea that FtsZ is the *in vivo* target of C109, we used homologous recombination to create a *B. cenocepacia* mutant with rhamnose-inducible control of *ftsZ* expression (CG*ftsZ*) (Figure 5A). If FtsZ is targeted by C109, one would expect that knockdown of *ftsZ* expression would cause increased susceptibility to C109. When grown in low rhamnose conditions, we observed that CG*ftsZ* and CG*dcw* were both hypersusceptible to C109 compared to the wild-type control (Figure 5B). Importantly, CG*ftsZ* and CG*dcw* were susceptible to very similar levels, suggesting that the entire susceptibility phenotype of the CG*dcw* mutant can be reproduced by knocking down *ftsZ* alone. These results are further corroborated by the specific depletion of CG*ftsZ* during competitive growth in the presence of C109 (Figure 2C) and by a filamentous morphology that resembles that of wild-type cells treated with C109 (Figure 2D). Further, the filamentous phenotype of CG*ftsZ* was exacerbated in the presence of C109 (Figure 5C and S4). We found that CG*ftsZ* was not susceptible to novobiocin, but displayed comparable susceptibility to C109 as mutants with knockdown of the *dcw* cluster (Figure 2C). Examination of the filaments showed the presence of multiple nucleoids (Figure S4B), and we propose this is why CG*dcw* and CG*ftsZ* were not the most highly depleted mutants in our fitness assay. Tn-seq detects copies of transposon-genome junctions, and we suggest that the multinucleoid phenotype may have partially masked the susceptibility of these cells to C109, reducing the specificity of our assay.

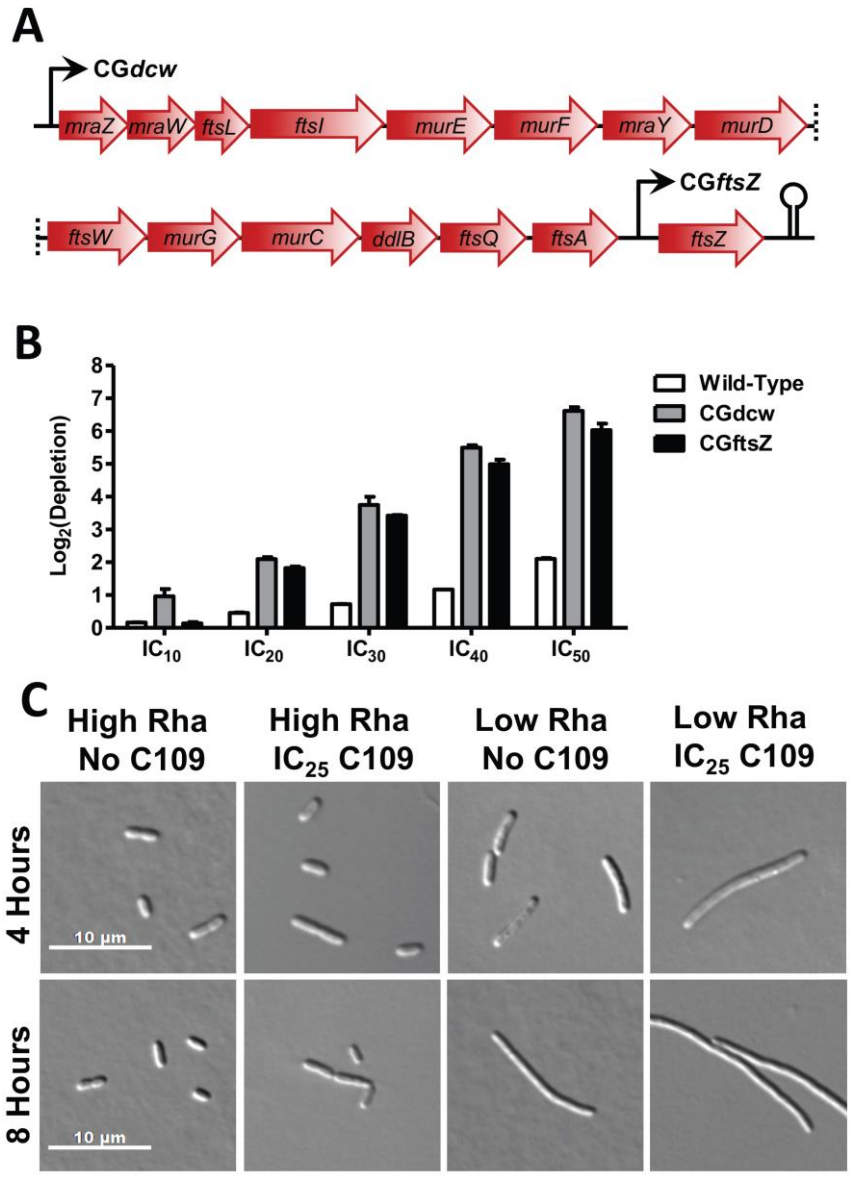

Figure 5. Knockdown of *ftsZ* sensitizes cells to C109. A) Organization of the *B. cenocepacia dcw* cluster and positions of the rhamnose-inducible promoters in CG*dcw* and CG*ftsZ*. B) Hypersusceptibility of sensitized *B. cenocepacia* knockdown mutants grown clonally in response to increasing concentrations of C109. Error bars show mean ± SD, n = 3 biological replicates. C) Morphology of CG*ftsZ* with high (0.20%) or low (0.04%) rhamnose, with or without C109.

3.1.4 C109 targets critical functions of FtsZ

The biochemical functions of FtsZ are to hydrolyze GTP and polymerize, thereby directing septal peptidoglycan synthesis (Yang et al., 2017b). Therefore, disrupting these activities could be the mechanism of action of C109. To definitively validate the target of C109, we first assessed the effect of C109 on the *in vitro* GTPase activity of *B. cenocepacia* FtsZ. Recombinant FtsZ was purified to homogeneity, in a soluble monomeric, catalytically active form (Figure A5). By a coupled spectrophotometric assay, we demonstrated that the protein catalyzed the hydrolysis of GTP (K_m = 6.4 ± 0.8 μM). Moreover, using a previously described sedimentation protocol (Król and Scheffers, 2013) as well as negative stain transmission electron microscopy (TEM), we found that the recombinant FtsZ could form polymers. The enzymatic assay revealed that C109 inhibits the FtsZ GTPase activity with an IC_{50} of 8.2 ± 1.3 μM (Figure 6A). Kinetic analyses in the presence of increasing concentrations of C109 showed that C109 behaves as a non-competitive inhibitor (Figure 6B) as the V_{max}, but not the K_m, values for GTP are reduced by the presence of C109. These data are consistent with the hypothesis that C109 binds to a different site from the GTP binding site, inhibiting the polymerization and, consequently, the formation of the full GTPase active site pocket. To support this hypothesis, the polymerization assay performed in the presence of C109 demonstrated concentration-dependent inhibition of polymerization (Figure 6C and D). Additionally, we observed that C109 acts additively with the FtsZ filament-stabilizing antimicrobial PC190723 (Tan et al., 2012) in both MRSA (CF 225) and MSSA (ATCC 29213) (FIC index of 0.625 and 0.75, respectively; data not shown). While this additive interaction suggests that C109 could bind to the interdomain cleft like PC190723 does, it is not clear why PC190723, but not C109, stabilizes FtsZ polymerization.

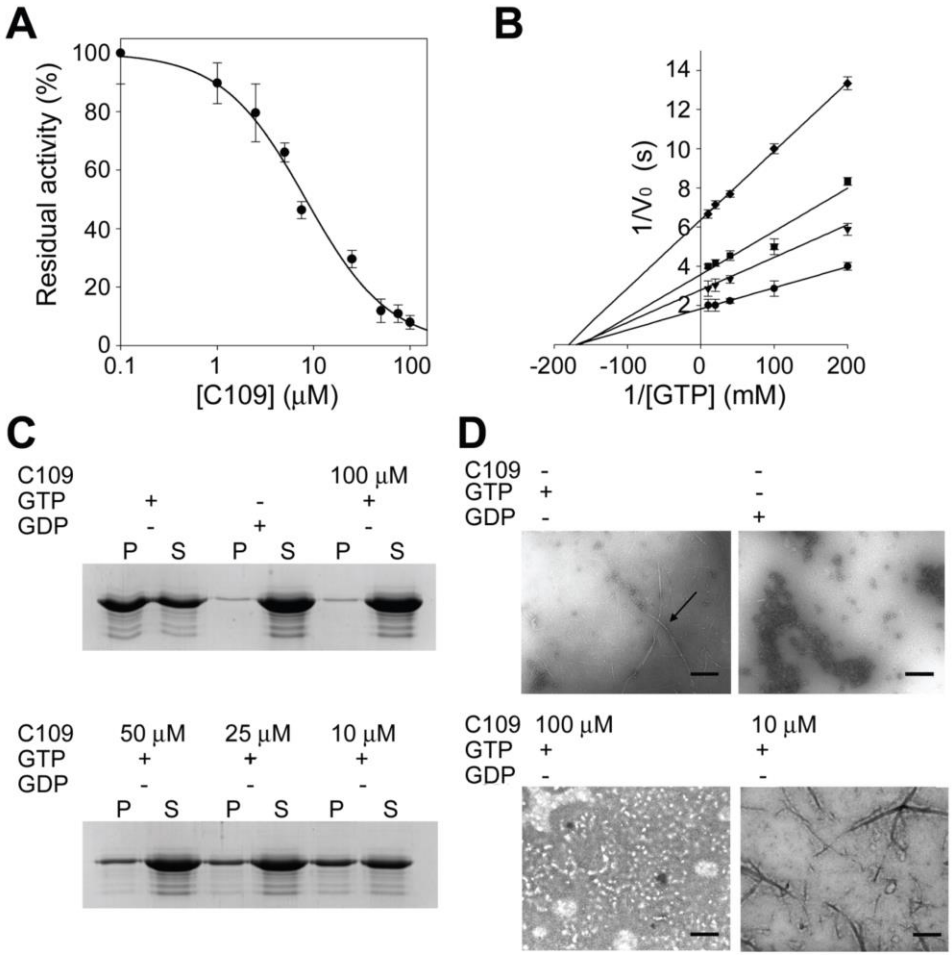

Figure 6. GTPase activity and polymerization assays demonstrate that C109 is a non-competitive inhibitor of FtsZ. A) IC_{50} determination of C109 against BcFtsZ. B) Kinetic analyses of BcFtsZ in the presence of different C109 concentrations ranging from 0 to 50 μM. C) SDS-PAGE of the sedimentation assay, in the presence of different C109 concentrations. D) Structure of FtsZ polymers in the presence of C109 (indicated by the arrow) visualized by TEM. Bar = 0.6 μm. Data are mean ± SD of three different replicates; images are representative of at least three different experiments.

3.1.5 Therapeutic potential of C109

To expand upon the utility of C109 as a prospective antibiotic, we explored the spectrum of its activity against a variety of Gram-positive and Gram-negative pathogens (Table 1). C109 inhibits the growth of extended-spectrum beta-lactamase (ESBL)-producing strains of *Escherichia coli*, methicillin-sensitive *Staphylococcus aureus*, *Serratia marcescens*, *Acinetobacter baumannii*, *Enterobacter aerogenes*, and *Mycobacterium abscessus*. However, C109 was not active against *Pseudomonas aeruginosa* and *Klebsiella pneumoniae*. When further tested against a panel of cystic fibrosis Bcc isolates, a range of MICs were observed from 4 – 64 μg/mL (Table 2). C109 was also effective at inhibiting biofilm formation of *B. cenocepacia* K56-2, with an MBIC of 4 μg/mL, which was lower than the MIC for the same strain. C109 was less capable of eradicating K56-2 residing in established biofilms (MBEC 32 μg/mL; data not shown).

With the increasing prevalence of antibiotic resistance, combination therapies are emerging as one possible method to improve pharmacological efficacy against recalcitrant infections (Imamovic and Sommer, 2013; Micek et al., 2010). With this in mind, we tested the *in vitro* interaction of antibiotics used to treat Bcc infection in cystic fibrosis patients (Scoffone et al., 2017). C109 acted additively in K56-2 with all eight antibiotics tested from many chemical classes (tobramycin, trimethoprim, meropenem, ceftazidime, ciprofloxacin, chloramphenicol, doxycycline, and novobiocin) (Table 3). Similar activity was observed in strain J2315 (Table 3), a clonal isolate of K56-2. Therefore, C109 may be able to decrease the effective dose of many different classes of antibiotics used to treat Bcc infections.

To investigate applications for C109, we next determined if C109 is effective at clearing *B. cenocepacia* K56-2 infection. We used the *C. elegans* liquid killing assay (Kaplan et al., 2011; Selin et al., 2015) in which *B. cenocepacia* produces an intestinal infection. After 2 days, the survival of *B. cenocepacia*-infected nematodes treated with C109 was similar to nematodes fed with the non-pathogenic *E. coli* OP50 or nematodes treated with trimethoprim (Figure A6). Furthermore, we exposed uninfected *C. elegans* to high concentrations of C109 to assess toxicity. Even at 128 μg/mL of C109, 100% of the nematodes survived after 24 hours ($SURV_{100}$ (Selin et al., 2015)) and 79% survived after 6 days (Table A7). We therefore calculated that the nematodes were able to survive at least 16-fold the concentration required to eradicate *B. cenocepacia in vitro* ($Surv_{100}$/MIC) (Table A7). In addition, we investigated if at higher

concentrations C109 induces hemolysis. Up to128 μg/mL we observed only negligible hemolysis levels of approximately 3% (Table A7). We also evaluated the toxicity of C109 on 16HBE (wild-type bronchiolar epithelial) and CFBE41o- (CF bronchiolar epithelial cells, homozygous for the ΔF508 deletion in *CFTR*) cell lines. Only at 75 μM (21.4 μg/mL) the viability of both cell lines was reduced to 50% (TC_{50}) (Table A7). To rule out possible inhibitory effects of C109 on mammalian tubulin, which is homologous to FtsZ, we performed a tubulin polymerization assay with a range of C109 concentrations (Figure A7). This assay is based on the principle that light is scattered by microtubules proportionally to the concentration of microtubule polymers (Lee and Timasheff, 1977; Shelanski et al., 1973). The resulting polymerization curve is representative of the three phases of microtubule polymerization, namely nucleation, growth and steady state equilibrium. Compounds that interact with tubulin will alter one or more of the characteristic phases of polymerization. As an example, the anti-mitotic drug paclitaxel was used as control: at 10 μM it eliminates the nucleation phase and enhances the V_{max} of the growth phase. Up to 100 μM, C109 was did not interfere with tubulin polymerization (Figure A7).

Table 2. Antibacterial activity of C109 against Bcc clinical isolates. MIC values are given as the median of three biological replicates.

Strain	MIC (μg/ml)
B. ambifaria BCC0478	8
B. anthina BCC0485	4
B. cenocepacia FCF 28	32
B. cenocepacia FCF 29	8
B. cenocepacia FCF 30	32
B. cenocepacia FCF 31	32
B. cenocepacia C5424	8
B. cenocepacia CEP511	16
B. cenocepacia BCC1202	32
B. cenocepacia BCC0076	8
B. cenocepacia BCC1119	32
B. cepacia BCC1381	16
B. contaminans 2221	16
B. contaminans 4278	16
B. dolosa BCC0305	32
B. gladioli BCC1710	4
B. gladioli BCC1623	2
B. gladioli BCC1620	4
B. multivorans BCC1379	8
B. multivorans BCC0710	64
B. multivorans FCF 5	32
B. multivorans FCF 6	32
B. multivorans FCF 7	64
B. multivorans FCF 8	64
B. multivorans FCF 9	64

B. multivorans FCF 10	32
B. multivorans FCF 11	8
B. multivorans 454	64
B. multivorans 6094	64
B. pyrrocinia BCC0735	16
B. stabilis BCC0608	8
B. stabilis 3819	16
B. stabilis 9693	16
B. stabilis 10870	32
B. vietnamiensis BCC0296	16

Table 3. C109 has additive effects with common antibiotic used against *B. cenocepacia*. Reported is the median FIC index from three biological replicates.

Antibiotic	K56-2			J2315		
	MIC alone (μg/ml)	**FIC Index with C109**	**Interpretation**	**MIC alone (μg/ml)**	**FIC Index with C109**	**Interpretation**
Meropenem	32	0.625	Additive	32	0.508	Additive
Piperacillin	8	0.625	Additive	256	0.560	Additive
Tobramycin	512	0.625	Additive	512	2	Additive
Ciprofloxacin	2	1	Additive	8	2	Additive
Ceftazidime	64	0.625	Additive	ND	ND	-
Doxycycline	4	0.625	Additive	ND	ND	-
Novobiocin	8	0.75	Additive	ND	ND	-
Trimethoprim	8	0.75	Additive	512	2	Additive
Chloramphenicol	32	1	Additive	ND	ND	-

*Not determined

3.2 Discussion

To combat the emergence of antibiotic resistance, one key approach is to develop classes of antibiotics against new targets. High-throughput assays show promise in addressing the bottleneck of target identification (Farha and Brown, 2016). Here, we outline the development and application of a novel competitive fitness screen for antimicrobial-target pairing in the antibiotic-resistant pathogen *B. cenocepacia*. Importantly, we identified that C109, a broad-spectrum antibacterial, inhibits the critical activities of FtsZ, thereby preventing cell division. Others have used gene knockdowns to identify antimicrobial targets (Giaever et al., 2004; Wang et al., 2011; Xu et al., 2010), but this is the first report to combine this approach with next-generation sequencing and a library enriched in essential gene mutants, which represent many putative antibacterial targets. Furthermore, the competitive growth conditions provide an additional edge: magnified sensitivity versus clonal growth (Gislason et al., 2017b). However, our assay would unlikely be able to specifically match an antimicrobial that inhibits a non-protein target. This is a known limitation of genetic screens, but careful interpretation of the data may reveal the overall mechanism of action from disrupted genetic networks (Giaever et al., 2004). During submission of this work, a study using Tn-seq with gene upregulation and machine learning was published (Santiago et al., 2018b). These authors demonstrated that lipid II is the target of the lysocins in *S. aureus*, therefore demonstrating that improvements in computational analysis can solve many of the challenges of chemogenomics.

Currently, there are no approved antibiotics that target FtsZ. We argue that FtsZ is an attractive drug target because FtsZ is: 1) essential for bacterial life, 2) widely conserved across bacterial pathogens 3) notably absent in mitochondria of higher eukaryotes, and 4) evolutionarily distant of its eukaryotic counterpart, tubulin (Lock and Harry, 2008). Despite the broad conservation of FtsZ, there are few reported inhibitors with antimicrobial activity against Gram-negatives (Chan et al., 2013; Sun et al., 2017a, 2017b) likely owing to the intrinsically lower permeability of the Gram-negative cell envelope (Keffer et al., 2013). C109 is active against Gram-positives, Gram-negatives, and *M. abscessus*, suggesting that it is generally membrane permeable, perhaps due to its small size and cLogP value of 2.5. Notably, no spontaneous, target-related mutations could be isolated upon exposure of *B. cenocepacia* to C109, suggesting that target-related resistance may not develop during therapeutic use of this drug.

A potential limitation of C109 for further development as an antibiotic could be its poor aqueous solubility. None of the C109 derivatives synthesized so far have shown improved solubility in water (data not shown), which may limit its utility for systemic administration. However, C109 is still an attractive drug for the development of an inhaled therapy to treat bacterial infections of the respiratory airways, where systemically-administered antimicrobials observe poor penetration (Rodvold et al., 2011). On the contrary, lipophilic antimicrobials directly deposited into the lungs by inhaled therapy absorb slowly into the circulation thus remain in the lungs at higher concentrations (Wenzler et al., 2016). In people with cystic fibrosis, where infections of the lower respiratory tract are particularly difficult to treat with systemically-delivered antimicrobials, aerosolized antibacterial therapies are becoming more common and the development of novel formulations for pulmonary delivery of more active drugs is an area of intense research (Dalhoff, 2014).

FtsZ inhibitors could be applied in combination with approved antibiotics to improve potency. Alone, the inhibitor PC190723 is highly active *in vitro* against MRSA, linezolid-resistant and vancomycin-resistant *S. aureus* (Tan et al., 2012). PC190723 was found to synergize with seven diverse β-lactams and restore the sensitivity of MRSA strains to β-lactams (Tan et al., 2012). This synergy is based on the observation that PC190723 also inhibits the localization of PBP2 (as it depends on FtsZ), which is responsible for septal peptidoglycan synthesis. It is suggested that the β-lactams then inactivate any residual PBP2 at the divisome (Tan et al., 2012). *In vitro* synergy was validated using a mouse model of MRSA infection, wherein PC190723 synergized with imipenem to strongly reduce bacterial load (Tan et al., 2012). Furthermore, in a screen against several β-lactams, those that inhibited PBP2 displayed the strongest synergy with TXA707, a prodrug form of PC190723 (Ferrer-González et al., 2017). We found that C109 did not synergize with any antibiotics currently prescribed for the treatment of Bcc infection (Table 3); however, the additive interaction with several such as meropenem and ceftazidime would likely lower the effective dose required to clear Bcc infection. *B. cenocepacia* encodes the PenB broad-spectrum carbapenemase, which are shown to give broad-spectrum resistance to many β-lactams, including imipenem and ceftazidime (Hwang and Kim, 2015; Jacoby, 2009; Papp-Wallace et al., 2013). We therefore suggest that the high levels of intrinsic resistance to β-lactams by *B. cenocepacia* could have masked synergistic interactions of C109 with β-lactams.

In summary, we outline the application and validation of a novel fitness screen to identify antimicrobial-target pairs in the cystic fibrosis pathogen *B. cenocepacia*. We propose that this method will allow the screening of many compounds in rapid succession against *B. cenocepacia*. Of further importance, the small size and hydrophobic characteristics of C109, in addition to additive interactions with other antibiotics, make this compound appropriate for inhaled therapy, which are used to treat lung infections in cystic fibrosis patients.

CHAPTER 4: A BROAD-HOST-RANGE CRISPRI TOOLKIT FOR SILENCING GENE EXPRESSION IN BURKHOLDERIA

Reproduced from:
Hogan AM, Rahman ASMZ, Lightly TJ, Cardona ST. 2019. A broad-host-range CRISPRi toolkit for silencing gene expression in *Burkholderia*. *ACS Synth. Biol.* **8**(10): 2372-84

Silvia Cardona conceived the idea and design of the research; Andrew Hogan designed and cloned the dCas9 constructs; Andrew Hogan and Zisanur Rahman designed the gRNAs, assessed knockdown phenotypes, processed data, and wrote and edited the manuscript; Tasia Lightly performed RT-qPCR analysis and edited the manuscript; Silvia Cardona supervised the work and provided financial support.

4.0 Introduction

The genus *Burkholderia* comprises a diverse group of Gram-negative bacteria characterized by remarkable biotechnological potential. Various species can be exploited for bioremediation purposes, production of bioactive compounds, and agricultural growth promotion. Perhaps due to the phylogenetic diversity of the genus, some species of *Burkholderia* can also pose a threat to human health(Eberl and Vandamme, 2016). Within the multiple deep-branching groups of the *Burkholderia* phylogenetic tree (Depoorter et al., 2016), one branch contains the clades known as the *Burkholderia cepacia* complex (Bcc) and the *B. pseudomallei* complex. The Bcc group comprises species that cause severe infections in people with the genetic disease cystic fibrosis and other people with a compromised immune system (Mahenthiralingam et al., 2005). *B. cenocepacia* and *B. multivorans* are two relevant species of this group, which are prevalent in cystic fibrosis patients (Kenna et al., 2017). The *B. pseudomallei* complex contains the risk group 3 members *B. mallei, B. pseudomallei,* and its close relative *B. thailandensis,* the last one being a frequent surrogate used in *B. pseudomallei* and *B. mallei* research (Howe et al., 1971). Other branches, such as the *B. xenovorans* group comprise species isolated from diverse environmental sources, like polluted soils, and plant rhizospheres (Depoorter et al., 2016).

The genetic characteristics that define the pathogenic potential of *Burkholderia* are poorly understood. Environmental species can cause serious infections in human (Nally et al., 2018), calling for caution in the use of *Burkholderia* strains for biotechnological applications. The incomplete understanding of *Burkholderia* pathogenic potential may be related to the limited tools available to link gene to function. Due to high resistance to the antibiotics typically used as genetic markers (Rhodes and Schweizer, 2016), and the high GC content of their large genomes, most genome editing methods designed for Gram-negative bacteria are inefficient and need to be adapted for use in *Burkholderia*.

Tools that facilitate controlled gene expression are necessary for interrogation of gene function. Programmable control of gene expression by promoter replacement is a valuable tool to link gene to phenotype (Judson and Mekalanos, 2000). Yet, promoter replacement implies that the natural regulatory circuitry of the target gene is interrupted. Instead, clustered regularly interspaced short palindromic repeats interference (CRISPRi) (Qi et al., 2013) is a method of silencing native gene expression, which is based on a dead Cas9 (dCas9) and a nuclease-inactive version of the

RNA-guided endonuclease Cas9 (Cho et al., 2013). In CRISPRi, a single guide RNA (sgRNA) designed towards the 5' end of the target gene and the dCas9 protein form an RNA-protein complex that recognizes the target region by base-pairing, and sterically blocks transcription initiation, if targeting the promoter, or elongation if targeting downstream of the promoter, by the RNA polymerase (Qi et al., 2013). Initially developed in *Escherichia coli*, CRISPRi technology has been adapted to a wide range of bacterial strains to address focused efforts such as metabolic rewiring and antimicrobial characterization (Croteau et al., 2018; Kim et al., 2016; Tan et al., 2018; Yao et al., 2016; Zhang et al., 2016), and broader efforts to functionally characterize genomes (Lee et al., 2019; Liu et al., 2017b; Peters et al., 2016). To achieve fine control of gene expression, a wide range of dCas9 expression levels are necessary, which can be provided by expressing *dcas9* with strong inducible promoters (Peters et al., 2016) or by providing multiple copies of *dcas9* engineered in a plasmid (Lee et al., 2019). Limitations to the success of these efforts are the proteotoxicity of dCas9 when expressed at high levels (Cui et al., 2018) and the necessity of customizing CRISPRi delivery tools across bacteria. Recently, the use of Tn*7* transposon mutagenesis, which specifically delivers genetic constructs close to a single *glmS* site (Choi and Schweizer, 2006; Choi et al., 2005) was applied to deliver a mobile CRISPRi system across bacteria (Peters et al., 2019). However, the Tn*7* system is less suitable for *Burkholderia* species as their genomes contain multiple copies of *glmS*, requiring additional steps to confirm the site of chromosomal integration (Choi et al., 2006b).

In this work, we employ a mini-CTX-derived mutagenesis system (Hoang et al., 2000) to achieve specific chromosomal delivery of *dcas9* in three species of *Burkholderia*, *B. cenocepacia*, *B. thailandensis* and *B. multivorans*. By placing the chromosomal copy of *dcas9* under the control of the *E. coli* rhamnose-inducible promoter (Cardona and Valvano, 2005), we demonstrate durable and tunable control of endogenous gene expression in *Burkholderia* species, producing observable phenotypes. We extend the usability of our CRISPRi tool kit by exploring other bacterial genomes for putative mini-CTX insertion sites.

4.1 Results

4.1.1 Construction of the CRISPRi system

The dCas9 from *Streptococcus pyogenes* has been shown to provide robust gene repression in diverse bacteria (Peters et al., 2016, 2019; Qi et al., 2013); we therefore selected it as our first approach. To function, the dCas9 binds a sgRNA and, by complementary base pairing, is guided to target and silences a gene of interest by sterically blocking the RNA polymerase (Qi et al., 2013). However, the genome of *S. pyogenes* has low GC-content (~40%), and from inspection of the *dcas9* gene, we expected poor codon usage in high GC-content organisms such as *Burkholderia* (67%) and subsequently low levels of expression. We first attempted to express the native gene from *S. pyogenes* in single copy in the chromosome under control of the rhamnose-inducible promoter, which is known to yield robust and tightly-regulated expression in *Burkholderia* (Cardona and Valvano, 2005); however, we did not observe detectable levels of dCas9 protein expression by immunoblot (Figure A8). Upon codon optimization for *B. cenocepacia*, we first introduced the gene into a multicopy plasmid under the control of the rhamnose-inducible promoter (Cardona and Valvano, 2005); however, we observed a severe growth defect upon induction, except at minute concentrations of rhamnose (Figure A9A). Growth inhibition was not observed in the vector control (Figure A9B) and it remains unclear if the inhibitory effect of dCas9 expression on growth was caused by metabolic load from expression of a large protein in multicopy, or from proteotoxicity (Rock et al., 2017).

A single chromosomal copy of *dcas9* may provide sufficient levels of expression as observed previously (Choudhary et al., 2015; Peters et al., 2016, 2019). Using the mini-CTX system, we introduced a single copy of *dcas9* under control of the rhamnose-inducible promoter into *B. cenocepacia* K56-2 (Figure A10). We observed titratable dCas9 expression at various levels of rhamnose by immunoblot (Figure 7A and Figure A11). At rhamnose concentrations up to 1% there was no growth defect in K56-2::dCas9 (Figure 7B) or K56-2::dCas9 with non-genome targeting sgRNA (pgRNA-non-target) (Figure 7C) compared to the vector control mutant (Figure 7D).

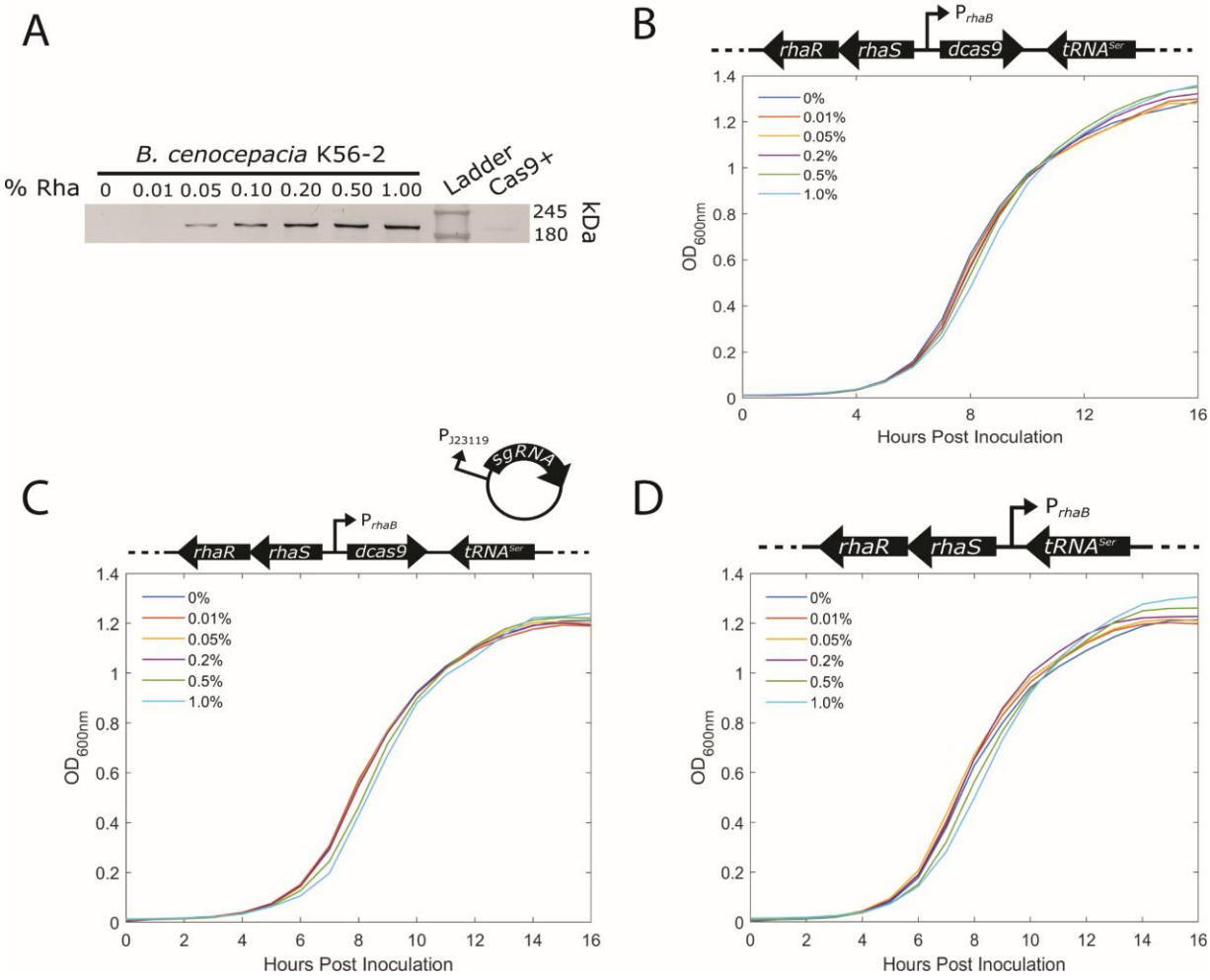

Figure 7. Development of CRISPRi in *B. cenocepacia* K56-2. A) dCas9 was expressed from the chromosome of K56-2 by induction with variable concentrations of rhamnose and detected by immunoblot. The lane labelled Cas9+ was loaded with 5 ng of purified Cas9. Growth curves of B) B. cenocepacia K56-2::dCas9 without a sgRNA plasmid, C) with a non-genome targeting sgRNA plasmid (dCas9/pgRNA-non target) and D) K56-2::CTX1-rha, the vector control plasmid for the integration, in LB with variable concentrations of rhamnose.

4.1.2 Tunable and durable CRISPRi silencing of paaA suppresses growth on phenylacetic acid

To evaluate the utility of the CRISPRi system for gene repression in *B. cenocepacia* K56-2, we first chose to target the *paaA* gene, which encodes phenylacetate-CoA oxygenase subunit PaaA (Teufel et al., 2010). The *paaABCDE* operon enables growth with phenylacetic acid (PA) as a sole carbon source in *B. cenocepacia* K56-2 (Pribytkova et al., 2014), with the lack of growth being a clearly observable phenotype when this operon is silenced. In addition, as this is the first characterization of CRISPRi in *Burkholderia*, we also wished to assess the effect on repression efficiency when targeting the non-template (NT) and template (T) strands, as previous studies have demonstrated profound differences (Bikard et al., 2013; Qi et al., 2013). We therefore designed five sgRNAs: three sgRNAs targeting the promoter elements and adjacent to the transcription start site (TSS) on the NT strand (sgRNA 1, 2 and 3), one sgRNA targeting near the start codon of *paaA* on the NT strand (sgRNA 4), and one sgRNA targeted near the start codon of *paaA* on the T strand (sgRNA 5) (Figure 8A).

For phenotypic characterization of the *paaA* mutants harbouring the codon-optimized *dcas9*, we used M9 minimal medium with PA (M9+PA) as the sole carbon source. Upon induction of dCas9, the growth of all mutants (except the controls) was suppressed approximately 30-fold (Figure 8B) to the same level of a Δ*paaABCDE* mutant, which is unable to utilize PA as a sole carbon source (Pribytkova et al., 2014). We observed only moderate repression (up to ~6-fold) when using the native *dcas9* (Figure A12). Furthermore, in the absence of rhamnose all of the mutants grew at or near wild-type levels, suggesting that *dcas9* expression is tightly repressed in non-inducing conditions. Phenotypically, we did not observe a differential effect of placement of the sgRNA-binding site, as the growth of all mutants was suppressed equally. We also found there were no differences in control strains; mutants expressing dCas9 and either a guideless or non-targeting sgRNA displayed the same levels of growth. However, RT-qPCR demonstrated that while growth was suppressed equally in the mutants, there were sgRNA-dependent differences in gene expression levels (Figure 8C). At 0.2% rhamnose, sgRNA4, targeting near the start codon of *paaA* on the NT strand, was the most effective in repressing *paaA* mRNA expression (at least 114-fold repression), whereas sgRNA1 and sgRNA5 only had ~63-fold and ~51-fold repression, respectively (Figure 8C). In the absence of rhamnose there was no difference in gene expression levels between the mutants and wild type confirming that the *dcas9* is tightly regulated in non-inducing conditions.

Next, we sought to determine the tunability of our CRISPRi system in *Burkholderia*. Tuning is useful to control the level of transcriptional inhibition when precision is required, such as in the study of essential genes. To that end, we examined the growth of K56-2::dCas9 with the sgRNA1 (targeting *paaA*), using PA as a sole carbon source in the presence of various concentrations of rhamnose. The results showed that our CRISPRi system is tunable, exhibiting growth reduction in a dose-dependent manner with variable repression across sub-saturating rhamnose concentrations (between 0.005% and 0.05% rhamnose) (Figure 8D). This trend was confirmed by RT-qPCR (Supplemental Figure A13). We observed a nearly 30-fold repression in OD_{600nm} at concentrations well below maximum induction as identified by immunoblot, suggesting our system produces more dCas9 than is required for maximum repression as observed by this phenotype. Contrary to what had been observed in rich medium (Figure 7B and C), all dCas9 mutants (with or without the sgRNA) showed a growth defect in M9+PA above 0.2% rhamnose (Figure 8D). A similar phenomenon was also seen in M9+glycerol (data not shown). Intermediate levels of growth were observed in concentrations of rhamnose between 0.005% and 0.05%. For consistency, we therefore used 0.2% rhamnose for dCas9 induction in all experiments.

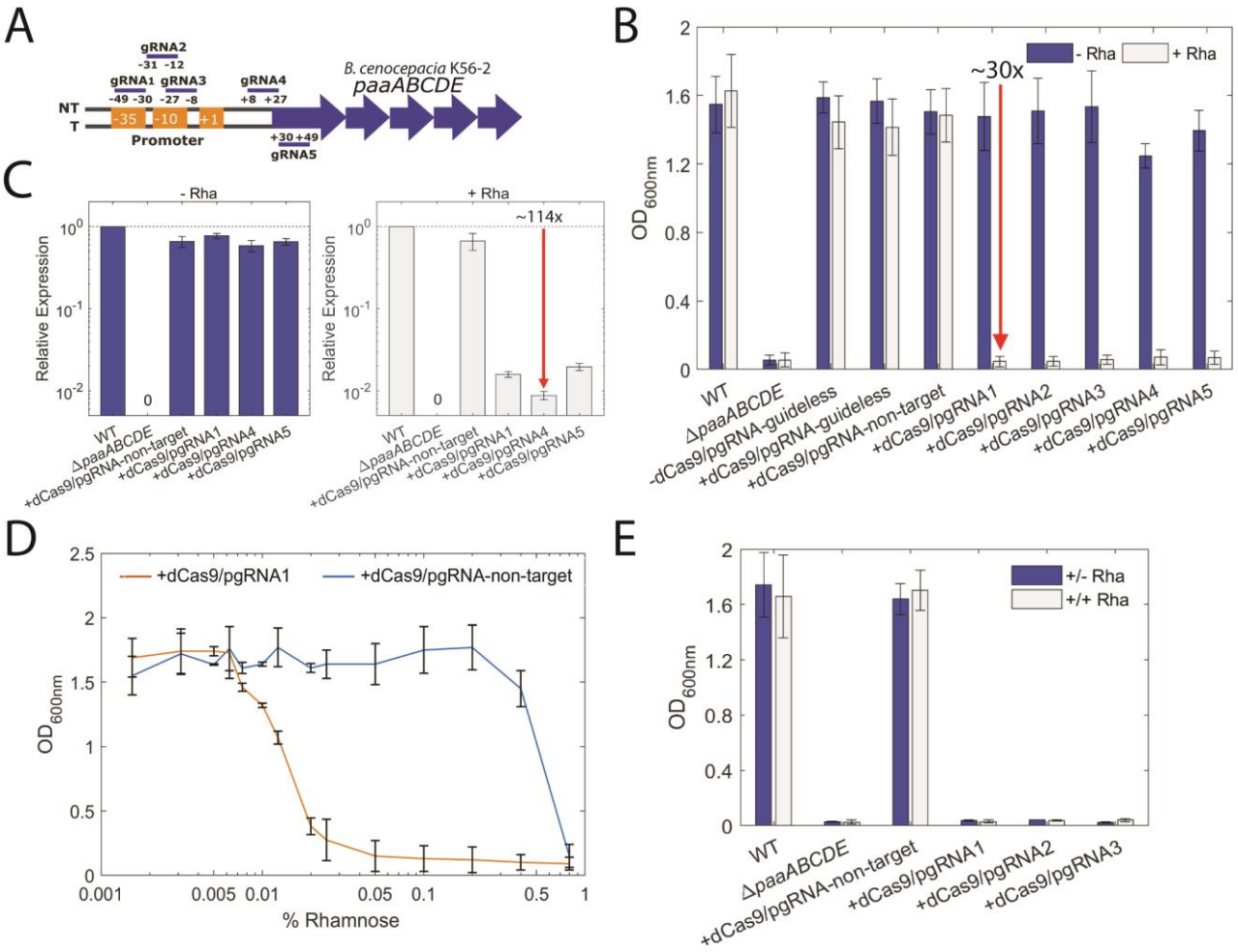

Figure 8. Targeting *paaA* with CRISPRi effectively suppresses growth in phenylacetic acid as the sole carbon source in *B. cenocepacia* K56-2. A) Positions of the sgRNAs targeting different regions upstream of and on paaA. sgRNAs 1, 2, and 3 were designed to target the promoter elements (-35 and -10 boxes) on the non-template (NT) strand. gRNA4 targeted the start codon on the NT strand and gRNA5 targeted the downstream region adjacent to the start codon on the T strand. B) CRISPRi blocks transcription in a strand non-specific manner. WT, a mutant of the *paaABCDE* operon (Δ*paaABCDE*), K56-2::CTX1-rha (-dCas9) and K56-2::dCas9 (+dCas9) harboring pgRNA with or without specific gRNAs were grown for 24 hours in minimal medium with PA (M9+PA) without (-Rha) or with 0.2% rhamnose (+Rha). C) RT-qPCR revealed a ~114-fold reduction in *paaA* mRNA, demonstrating a robust knockdown of *paaA* expression in K56-2. D) Expression of the dCas9 can be controlled by varying the amount of inducer added to the medium, providing tunability to the CRISPRi system. However, high level induction of dCas9 with rhamnose (beyond 0.4%) was lethal for the non-genome targeting mutant (dCas9/pgRNA-non-target) expressing dCas9. E) Cells were grown overnight in LB medium with 0.2% rhamnose to induce expression of dCas9. Then cells were transferred to M9+PA and grown for 24 hours with (+/+ Rha) and without (+/- Rha) 0.2% rhamnose. All the values are the average of three independent biological replicates; error bars represent arithmetic mean ± SD.

Although once rhamnose is removed from the culture expression of dCas9 is no longer induced, it remained possible that the dCas9 already synthesized may persist and cause long-term, or durable, silencing. To address this, the mutant strains harbouring sgRNAs targeting *paaA*, were grown overnight in rich medium with 0.2% rhamnose, effectively priming the cells with dCas9. Strikingly, when grown in M9+PA either with or without rhamnose, we again observed strong repression of growth (~30-fold) regardless of the presence of rhamnose in the M9+PA (Figure 2E). This suggests that after the inducer is removed, dCas9 is either slowly degraded in K56-2 or is present at high enough levels in the cells for durable repression in growth inhibiting conditions. Moreover, the lack of growth is not simply due to a loss in cell viability, as CFU/mL of the cultures did not decrease over time (Figure A14). We likely observed a durable knockdown in this scenario due to the conditional essentiality of *paaA*. Due to the strong interaction of the dCas9:sgRNA complex with its target, repression cannot be easily relieved except by the DNA polymerase machinery (Jones et al. 2017). When transferred to medium with PA as the sole carbon source, cell growth would halt from lack of a carbon source, therefore ensuring *paaA* remained repressed.

4.1.3 Single-cell analysis reveals an 'all or none' effect in B. cenocepacia K56-2

While at the culture level the effect of CRISPRi is tunable, we further explored the effect of maximum dCas9 induction at the single-cell level. We therefore targeted *fliF*, a gene encoding a transmembrane protein that forms both the S and M rings (MS ring) of the basal body complex of the flagellum (Francis et al., 1992). Silencing *fliF* should result in non-flagellated cells as FliF is required for flagellum formation (Yang et al., 2017a). We targeted *fliF* by introducing four sgRNAs designed to bind near the putative promoter and start codon on the NT strand (Figure A15A). Our goal was to assess individual cell flagellation and compare it with swimming motility at the population level. While we observed an approximately 5-fold reduction in swimming motility compared to controls in a plate-based assay (Figure A15B and C), we were unable to observe flagella in any of the mutants harbouring gRNAs targeting *fliF* (Figure A15D). It is possible that interfering with *fliF* expression rendered fragile flagella that could not remained attached to the cell during the staining process, while still being functional when grown in culture (Komatsu et al., 2016). In contrast to the swimming motility of the CRISPRi mutants we confirmed that insertional inactivation of *fliF* (*fliF*::pAH26) completely ablates swimming motility, as seen previously (Figure A15) (Tomich et al., 2002).

To further elucidate the effect of CRISPRi at the single cell level, we targeted *phbC*, a gene encoding poly-β-hydroxybutyrate polymerase, an enzyme required for PHB synthesis. To repress *phbC* expression, we designed three sgRNAs to target the region up to 50 bp before the start codon on the NT strand, at the putative promoter site (Figure 9A). Polyhydroxyalkanoate (PHA) granule accumulation was assessed by fluorescence microscopy with Nile Red staining. For comparison to a null phenotype, we created a *phbC* insertional mutant (*phbC*::pAH27) which was unable to produce PHA granules (Figure 9B and D). Compared to the wild-type and non-target controls, markedly few cells harbouring sgRNAs targeting *phbC* contained PHA granules, ranging from 17-70% depending on the sgRNA (Figure 9B). sgRNA6 rendered the strongest level of repression, with only 17.1% of cells containing PHA granules in contrast to 86.9% for the wild-type (Figure 9B). Interestingly, although few cells possessed PHA granules, the granules were of identical size to those in wild-type cells, averaging 0.65μm in diameter (Figure 9C and 9D). As shown by the insertional mutant, inactivation of *phbC* ablates PHA granule accumulation; therefore, the presence of granules of the same size in the dCas9 mutants as in the wild-type suggests an 'all-or-none' effect in *B. cenocepacia* K56-2, where most cells display the silenced phenotype, but some manage to at least temporarily escape the effect of CRISPRi.

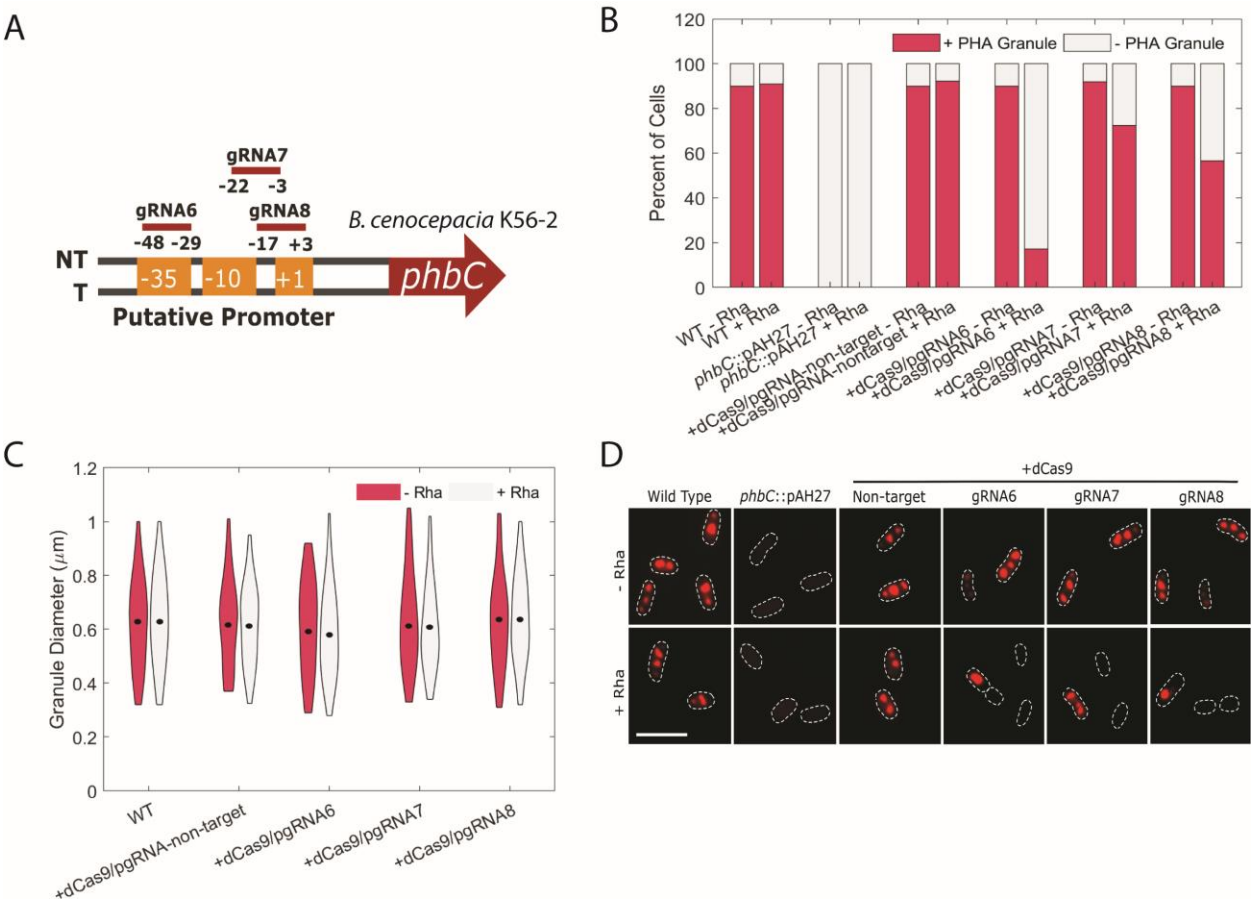

Figure 9. Targeting *phbC* with CRISPRi reduces polyhydroxyalkanoate (PHA) granule accumulation in K56-2. A) Positions of the sgRNAs targeting different regions upstream of *phbC*. sgRNAs 6, 7, and 8 were designed to target the promoter elements (-35 and -10 boxes) on the non-template (NT) strand. B) CRISPRi reduces but does not completely abrogate the number of cells with PHA granules. WT, an insertional mutant of the *phbC* gene (*phbC*::pAH27), K56-2::CTX1-rha (-dCas9) and K56-2::dCas9 (+dCas9) harboring pgRNA with or without specific gRNAs were grown overnight without (-Rha) or with 0.2% rhamnose (+Rha). Cells were washed and stained with Nile Red, and observed by fluorescence microscopy. One to two-hundred cells were counted and the % of cells with PHA granules was calculated. C) PHA granules that remain are identical to those in the WT. Strains were grown and processed as for B and the diameter of the PHA granules was measured. Thicker areas of the violin bars represent more granules with that diameter. The mean in each condition is shown by a black dot. D) The strains were grown and processed as for B). Dashes indicate cell boundaries and the scale bar is 5 μm.

4.1.4 Broad host range of the mini-CTX system extends applicability to other species

Having shown that the *S. pyogenes* dCas9 renders strong gene repression in *B. cenocepacia* K56-2, we next turned our attention to other important species of *Burkholderia.* We introduced the codon-optimized *dcas9* gene into the chromosome of *B. multivorans* ATCC 17616 and targeted the *paaA* and *phbC* genes by designing three sgRNAs for each centered around the putative promoter (Figures 10A and C). Targeted repression of *paaA* by each of the three sgRNAs strongly suppressed growth in M9+PA by approximately 25-fold (Figure 10B), very similar to the activity observed in *B. cenocepacia* K56-2. However, we were unable to detect robust expression of dCas9 by immunoblot in *B. multivorans* ATCC17616 (Figure A16A) despite the observed phenotype being indicative of expression of dCas9 and effective gene silencing. Expression of dCas9 in the presence of the non-targeting sgRNA did not affect growth in *B. multivorans* ATCC 17616 (Figure A16B). Following this, targeting *phbC* rendered relatively poor inhibition of PHA granule accumulation with between 35-50% of cells containing PHA granules, depending on the sgRNA (Figure 10C and D). In contrast to what was seen in *B. cenocepacia* K56-2, we observed granules of reduced size (Figure 10E and F).

Members of the *B. pseudomallei* complex are phylogenetically distinct from the Bcc (Eberl and Vandamme, 2016), but remain of interest due to the ability to cause infection (such as melioidosis and glanders) and for their remarkable capacity for secondary metabolite production (Mao et al., 2017). *B. thailandensis* is a commonly used model for the pathogenic members of the *B. pseudomallei* group, we therefore also introduced the codon-optimized *dcas9* gene into the chromosome of *B. thailandensis* strain E264. When induced with rhamnose, dCas9 was highly expressed (Figure A16A) and did not impair growth in the presence of a non-targeting sgRNA (Figure A16B). Similarly, as for *B. cenocepacia* K56-2 and *B. multivorans* ATCC 17616, we designed three sgRNAs targeting the putative promoters of the *paaA* and *phbC* genes (Figure 11A and C). Upon induction of dCas9 with 0.2% rhamnose, growth of the mutants harbouring the *paaA*-targeting sgRNAs was suppressed in M9+PA to varying levels ranging from 3-fold (sgRNA19) to 25-fold (sgRNA20) (Figure 11B). Lastly, for the sgRNAs targeting *phbC*, depending on the sgRNA there was variation in the percent of cells with PHA granules (10-40%) and the diameter of the granules (overall decrease in size) (Figure 11C- F). Though the exact genetic contributions to PHA synthesis in E264 remain unclear, it has been previously suggested that PhbC is not the only polyhydroxyalkanoate polymerase in E264 (Funston et al., 2017).

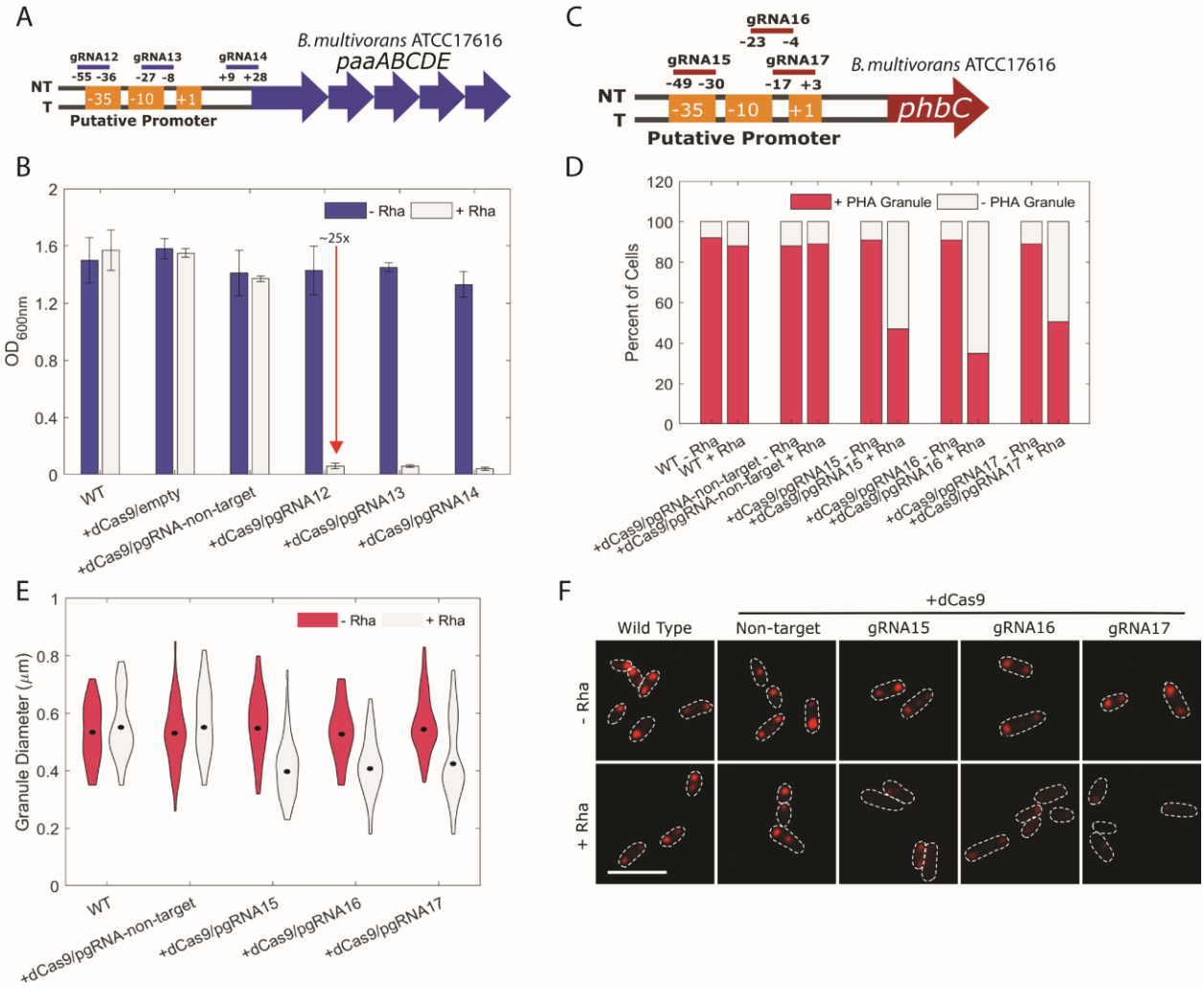

Figure 10. CRISPRi in *B. multivorans* ATCC17616 effectively represses *paaA* and *phbC*. A) Positions of the sgRNAs targeting upstream regions of *paaA*. sgRNAs12 and 13 were designed to target the -35 and -10 boxes of the promoter, while sgRNA14 targeted the 5' region of the ORF. All sgRNAs targeted the NT strand. B) Targeting *paaA* suppressed growth on PA as a sole carbon source. WT, ATCC 17616::dCas9 (+dCas9) with or without sgRNAs in A) were grown for 24 hours in M9+PA without (-Rha) or with 0.2% rhamnose (+Rha). C) Positions of the sgRNAs targeting upstream regions of *phbC*. All sgRNAs were designed to target the -35 or -10 elements of the promoter on the NT strand. D) Targeting *phbC* reduces the overall number of cells with PHA granules. Strains were grown overnight without (-Rha) or with 0.2% rhamnose (+Rha). Cells were washed and stained with Nile Red, and observed by fluorescence microscopy. One to two-hundred cells were counted and the % of cells with PHA granules was calculated. E) PHA granules that remain are smaller than those in the WT. Strains were grown and processed as for D); however, the diameter of the PHA granules was measured, with thicker areas representing more granules with that diameter. The mean in each condition is shown by a black dot. F) The strains were grown and processed as for D). Dashes indicate cell boundaries and the scale bar is 5 μm.

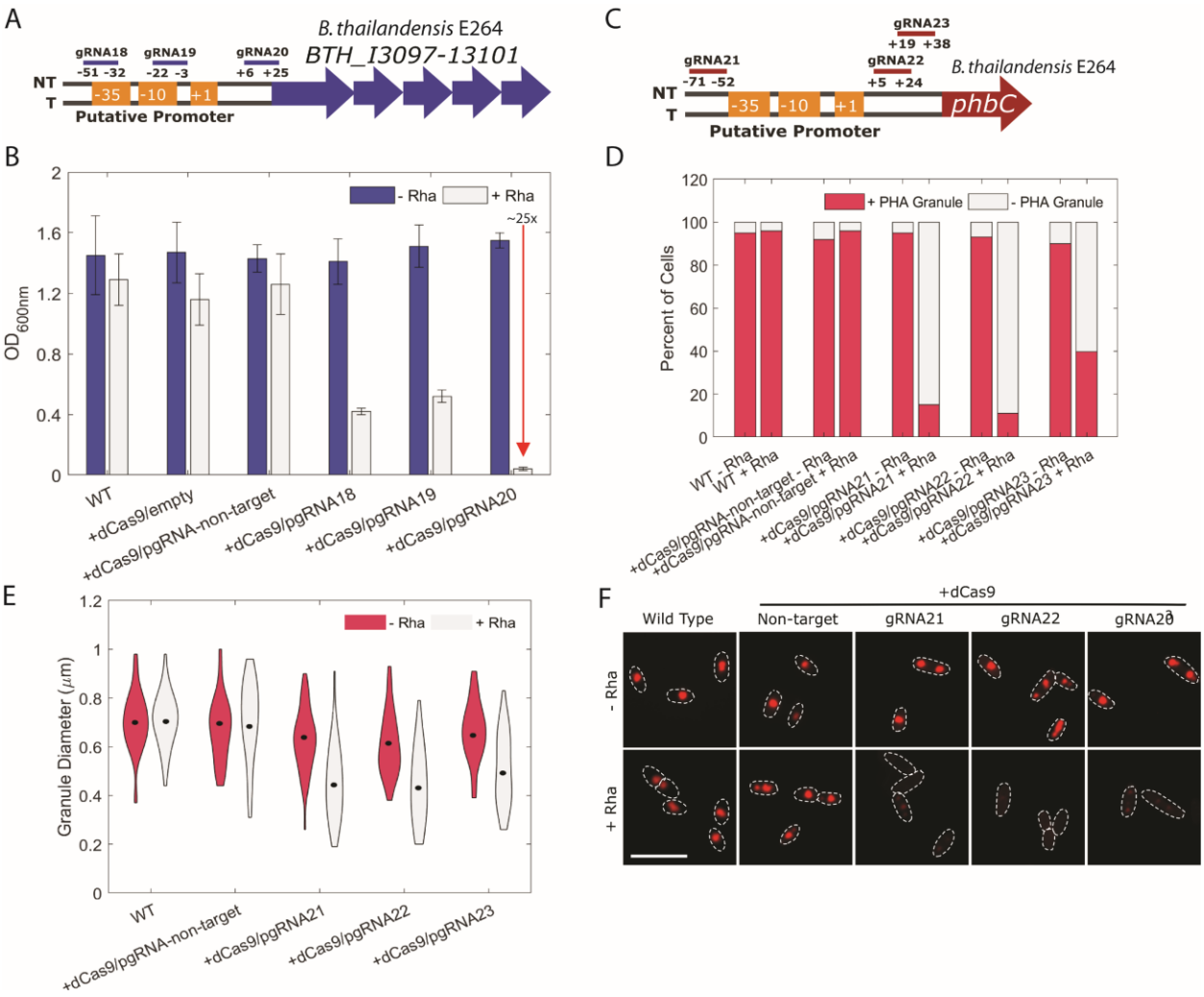

Figure 11. CRISPRi in *B. thailandensis* E264 effectively represses *paaA* (BTH_I3097) and *phbC*. Positions of the sgRNAs targeting upstream regions of *paaA*. sgRNAs 18 and 19 were designed to target the -35 and -10 boxes of the promoter, while sgRNA 20 targeted the 5' region of the ORF. All sgRNAs targeted the NT strand. B) Targeting *paaA* suppressed growth on PA as a sole carbon source. WT, E264::dCas9 (+dCas9) with or without sgRNAs in A) were grown for 48 hours in M9+PA without (-Rha) or with 0.2% rhamnose (+Rha). C) Positions of the sgRNAs targeting regions of *phbC*. sgRNA 21 targeted just upstream of the -35 box, sgRNA22 and 23 targeted just downstream of the -10 box, all on the NT strand. D) Targeting *phbC* reduces the overall number of cells with PHA granules. Strains were grown overnight without (-Rha) or with 0.2% rhamnose (+Rha). Cells were washed and stained with Nile red, and observed by fluorescence microscopy. One to two-hundred cells were counted and the % of cells with PHA granules was calculated. E) PHA granules that remain are smaller than those in the WT. Strains were grown and processed as for D); however, the diameter of the PHA granules was measured, with thicker areas representing more granules with that diameter. The mean in each condition is shown by a black dot. F) The strains were grown and processed as for D). Dashes indicate cell boundaries and the scale bar is 5 μm.

The integration vector we implemented to deliver *dcas9* to the chromosome of various species of *Burkholderia* relies on the expression of the φCTX integrase and recombination using the plasmid-borne *attP* site with the chromosomal *attB* site (Hoang et al., 2000). φCTX is a *Pseudomonas*-infecting phage, and the mini-CTX integration system was originally designed for use in *P. aeruginosa* (Hoang et al., 2000). The mini-CTX integration system has been used successfully in other species; however, this has been mostly limited to members of *Burkholderia* (Chapalain et al., 2017; Le Guillouzer et al., 2017). In the species used in this study, we observed the integration efficiencies to be $6x10^{-7}$ in K56-2, $6x10^{-8}$ in E264, and $5x10^{-9}$ in ATCC 17616 (Figure A17A), which is similar to 10^{-7} to 10^{-8} observed previously in *P. aeruginosa* (Hoang et al., 2000). To further broaden the scope of the applicability of our CRISPRi system, we used NCBI BLAST to search all published genomes for putative *attB* sites. While the full-length *attB* site is 30 nt, integration is known to occur if only the 5' 19 nt are completely complementary, such as for many species of *Burkholderia*. This shorter *attB* site was therefore used as a BLAST query, resulting in 1760 hits with 100% alignment (Table A8). Enterobacteria were excluded from the search as the pMB1 *oriR* in the mini-CTX system is functional is these species; therefore, integrants cannot be easily isolated. Furthermore, the search parameters were modified to only include species of Proteobacteria, as there were few hits of non-Proteobacterial species with 100% alignment (data not shown). Overall, we found hits in 168 unique species from 67 genera. As expected, the most abundant hit corresponded to species and strains of *Pseudomonas* (480 hits), then followed by *Acinetobacter* (443 hits), *Burkholderia* (276 hits), *Neisseria* (170 hits), and *Ralstonia* (146 hits), with members of the other 62 genera comprising the remaining 245 hits. A summary of the major hits and species of interest (pathogenic, environmental, biotechnological, etc.) can be found along with the genomic context in Table 4. We note that the hit table comprises species with both high and low GC-content genomes. While the GC-rich codon-optimized *dcas9* (in pAH-CTX1-rhadCas9) may be better suited for species with high GC-content genomes, such as those in the families *Pseudomonadaceae* and *Alcaligenaceae*, the native *dcas9* (in pAH-CTX1-rhadCas9-native) may have better functionality in species with low GC-content genomes, such as those in the families *Moraxellaceae* and *Neisseriaceae*.

A further consideration for use of our CRISPRi system is that the pFLPe recombinase-expressing plasmids might not be functional in all species. In which case, the *int* gene along with the *oriT*, pBM1 *oriR,* and the *tet* gene would not be excised. Continued expression of the integrase

could cause instability of the integrated DNA and loss of the dCas9 gene over time. To explore this possibility, we assessed the stability of the mini-CTX integration in K56-2, ATCC 17616, and E264 in serial passages over four days without tetracycline selection. For all species over the entire experiment we determined CFU counts on agar with and without tetracycline selection and found equal recovery of tetracycline-resistant colonies as total colonies (Figure A17B-D), suggesting the integration containing the dCas9 is stable.

Table 4. Putative host range of the mini-CTX system and genomic context of selected hit sites

Class	Order	Family	Genus and Species	Strain	%GC	$tRNA^{Ser}$ ( ) Genomic Context
Gammaproteobacteria	Pseudomonadales	Pseudomonadaceae	*Pseudomonas aeruginosa*	PAO1	66.6	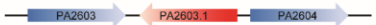
			Pseudomonas fluorescens	NCTC 10783	65.9	
			Pseudomonas mendocina	NK-01	64.7	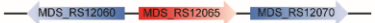
		Moraxellaceae	*Acinetobacter baumannii*	ATCC 17978	39	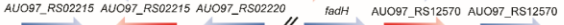
			Acinetobacter nosocomialis	NCTC 8102	38.7	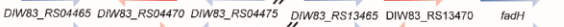
	Xanthomonadales	Xanthomonadaceae	*Xylella fastidiosa*	M12	51.9	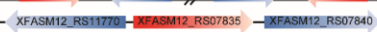
Betaproteobacteria	Burkholderiales	Alcaligenaceae	*Achromobacter xylosoxidans*	NCTC 10808	67.4	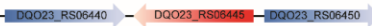
			Bordatella bronchiseptica	D448	68.1	
			Alcaligenes faecalis	DSM 30030	56.6	
		Burkholderiaceae	*Ralstonia pickettii*	DTP0602	65.9	
			Burkholderia cenocepacia	K56-2	67	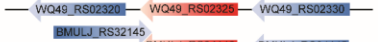
			Burkholderia multivorans	ATCC 17616	66.7	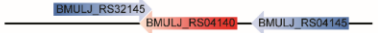
			Burkholderia thailandensis	E264	67.7	
			Burkholderia mallei	NCTC 10229	68.5	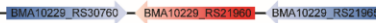
			Burkholderia pseudomallei	NCTC 13178	67.9	
			Burkholderia oklahomensis	EO147	66.9	
			Cupriavidus necator	NH9	65.5	
			Pandoraea apista	AU2161	62.6	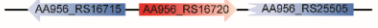
			Lautropia mirabilis	NCTC 12852	65.5	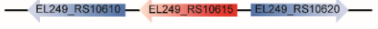
		Oxalobactericeae	*Collimonas fungivorans*	Ter6	59	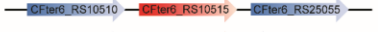
		Commamonadaceae	*Rhodoferax antarcticus*	DSM 24876	58.9	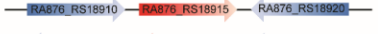
			Polaromonas naphthalenivorans	CJ2	61.7	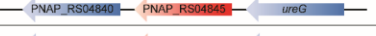
	Neisseriales	Neisseriaceae	*Neisseria meningitidis*	NCTC 10026	51.4	
			Neisseria gonorrheae	NCTC 13484	52.5	
			Neisseria sicca	FDAARGOS_260	50.9	
			Chromobacterium violaceum	CV1197	65.6	
	Nitrosomonadales	Nitrosomonadaceae	*Nitrosomonas communis*	Nm2	44.7	
Hydrogenophilalia	Hydrogenophilales	Hydrogenophilaceae	*Hydrogenophilus thermoluteolus*	TH-1	61.7	
Alphaproteobacteria	Rhodospirillales	Rhodospirillaceae	*Haematospirillum jordaniae*	H5569	55.6	

4.2 Discussion

Genetic tools are necessary to dissect the molecular mechanisms governing cellular processes. Here, we report the development of a CRISPRi system for efficient repression of gene expression in *Burkholderia*. By mobilizing the *dcas9* gene that was codon-optimized for the GC-rich *Burkholderia* on a broad host range mini-CTX1 integration vector, we demonstrate robust, tunable, and durable repression of endogenous genes. While others have shown effective repression using the native *dcas9* gene in *E. coli* (Qi et al., 2013), *B. subtilis* (Peters et al., 2016), *Staphylococcus aureus*, and *Acinetobacter baumannii* (Peters et al., 2019), codon-optimization was a necessary step for K56-2, as expression of the native *dcas9* gene was not detectable in K56-2. Indeed, for expression in species with high GC-content, codon optimization appears to be necessary. In *P. aeruginosa* (66.3% GC) both the *S. pyogenes* dCas9 (Peters et al., 2019) and the *S. pasteurianus* dCas9 (Tan et al., 2018) were not expressed unless first codon-optimized, albeit for *Homo sapiens* (optimized at 50.2% GC) or *Mycobacterium* (~67% GC), respectively. Additionally, the *S. thermophilus* dCas9 needed to be codon-optimized for *Mycobacterium* for efficient expression in *M. tuberculosis* and *M. smegmatis* (Rock et al., 2017).

Upon codon-optimizing the *dcas9* gene, we observed a severe growth defect when expressed from a multicopy pBBR1-origin plasmid. At this time, we are unsure if this was caused by a metabolic burden of expressing a large protein from a multicopy plasmid or from direct proteotoxicity. Previous studies have demonstrated that expression of the canonical *S. pyogenes* dCas9 causes toxicity in *M. smegmatis*, *M. tuberculosis* (Rock et al., 2017), and *E. coli* (Cho et al., 2018), which provides rationale for developing a system with low-enough levels of dCas9 expression to maintain cell viability without sacrificing repression activity. While this effort has spurred the exploration of alternative dCas9 orthologues (Rock et al., 2017), we found that introducing *dcas9* in single copy in the chromosome provided a balance of repression activity without affecting growth. Furthermore, while other systems display up to 3-fold repression in the absence of inducer (Peters et al., 2016; Tan et al., 2018), our application of the tightly regulated rhamnose-inducible promoter from *E. coli* did not display a leaky phenotype in any of the three species tested. While we did observe increased dCas9 expression at rhamnose concentrations of 0.5% and 1.0% with no inhibitory effect on growth in LB (Figure 7C and D), the increased level of dCas9 expression was accompanied by a substantial growth defect in M9 minimal media with PA (Figure 8D) or glycerol (data not shown) as the sole carbon source. As the growth rate is

decreased in minimal media, it is possible that growth inhibitory, off-target effects that are alleviated in fast growing cells by dilution of dCas9 bound DNA sites with newly replicated ones, are more evident in slowly growing cells. While the RNA polymerase is largely incapable of displacing the dCas9:sgRNA complex, the DNA replication machinery is not blocked by dCas9. In fact, it has been observed that the dissociation of the dCas9:sgRNA complex correlates well with the generation time in *E. coli* (Jones et al., 2017). This is an important consideration for understanding the durability of growth suppression we observed when using PA as a sole carbon source. Cells primed by pre-incubation with rhamnose are unable to grow in M9+PA, creating a condition where *paaA* is an essential gene and its absence would arrest cell division and replication. Hence, the DNA replication machinery would not displace the dCas9:sgRNA from the *paaA* gene, resulting in long-term growth suppression. By extension, we predict that strong knockdown of any (conditionally) essential gene that causes a halt in DNA replication would be durable in this manner. This is a useful aspect of CRISPRi that we are investigating further.

Although it has been reported that the CRISPRi system is less effective in silencing gene expression when the template strand (T) is targeted compared to the non-template (NT) strand, our results demonstrated nearly 30-fold suppression of growth irrespective of the *paaA* target strand (Figure 8B). This suggests that the efficiency of the CRISPRi system might not be strand specific at all loci, supporting the findings from Guo et al. (Guo et al., 2018). However, this effect might have been masked by the strong repression we observed, as it is difficult to compare across null phenotypes. Our findings are also supported by the RT-qPCR that demonstrated differential repression of gene expression based on the targeted location. Interestingly, our data suggests that, for *paaA*, targeting near the start codon of the NT strand (gRNA4) was more effective than targeting near the start codon of the T strand (gRNA5). Additionally, sgRNAs targeting different regions of the 5' region of *paaA* produced a strong 25 to 30-fold repression in the three species studied here. Therefore, the observed knockdown efficiency appears to be largely unaffected by sgRNA placement on targeting regions overlapping or adjacent to the −35 and −10 promoter elements, at least for phenotypes where complete repression of gene expression is not required. The cause of this is likely due to the large dCas9:sgRNA complex that when bound to the promoter sterically interferes with RNA polymerase binding. Indeed, the ~160 kDa dCas9 enzyme has an average DNA footprint of 78.1 bp, much larger than most promoter regions (Josephs et al., 2015). This could explain why Cui et al. (Cui et al., 2018), and our results for *paaA*, demonstrate strong

repression when the template strand is targeted a short distance downstream of the transcription start site.

Single cell level analysis of our system suggested an 'all or none' effect in K56-2 with ~17% cells escaping the silenced phenotype when targeting *phbC* compared to an insertion mutant, which did not possess any PHA granules. The PHA granules in these cells were of identical diameter to wild type. The 'all or none' effect might be attributed to an uneven distribution of sugar transporters after cell division as observed previously for arabinose-inducible expression (Siegele and Hu, 1997). If a similar mechanism involved transporting rhamnose into the cell, some cells could escape the rhamnose-mediated *dcas9* induction to silence the target gene. We hypothesize any escape would be temporary as the transporter would be expressed in growing cells, allowing rhamnose uptake. However, a rhamnose transporter in *Burkholderia* has so far not been described. Interestingly, targeting *phbC* in *B. multivorans* ATCC17616 and *B. thailandensis* E264 resulted in a mixed phenotype with a reduced number of cells with granules as well as an overall decrease in granule size. Even though some of the cells appeared to have escaped the repression (up to 35% in ATCC17616 and 6% in E264), more than 90% of the cells contained granules of reduced size. This suggests that there is an unelucidated secondary PHA synthesis pathway in *B. thailandensis* E264 and *B. multivorans* ATCC17616. Funston et al. have observed similar results in *B. thailandensis* E264 where transposon mutants in *phb* genes (*phbA*, *phbB* and *phbC*) retained the ability to synthesize PHA, albeit at lower levels (Funston et al., 2017).

One of the hallmarks of CRISPRi is the broad-range amenability in diverse bacteria, enabling synthetic biology and mechanistic investigations into many dozens of species in innovative ways. We wished to apply our CRISPRi system in this manner and therefore mobilized both the native *dcas9* gene, suitable for low/medium GC-content organisms, and the *dcas9* gene, codon-optimized for GC-rich *Burkholderia*, on the mini-CTX1 integration vector. Our analysis of putative hosts (with *attB* sites near the 3' end of the serine tRNA) identified 168 unique species in 67 genera, mostly from the β- and γ-Proteobacteria. Previous works have mobilized *dcas9* on broad host-range integrative plasmids (Peters et al., 2019; Tan et al., 2018); however, both systems use the mini-Tn*7* system, which has multiple insertion locations in certain genomes, such as many species of *Burkholderia*. Together, our work contributes to the available genetic toolkit for rapid functional analysis of bacteria.

CHAPTER 5: CHEMOGENOMICS REVEALS SUSCEPTIBILITY DETERMINANTS OF CELL ENVELOPE-TARGETING ANTIBIOTICS IN BURKHOLDERIA CENOCEPACIA

Taken from the manuscript in preparation:
Hogan AM, Léon B, Batun Z, Motnenko A, Bosch A, Cardona ST. Chemogenomics reveals susceptibility determinants of cell envelope-targeting antibiotics in *Burkholderia cenocepacia*. *Manuscript in preparation.*

Silvia Cardona and Andrew Hogan conceived the research question and design; Beltina Léon aided with transposon library construction; Zayra Batun and Anna Motnenko performed select follow-up genetic and phenotypic studies; Andrew Hogan performed all experiments, processed data, wrote, and edited the manuscript; Silvia Cardona edited the manuscript; Silvia Cardona and Alejandra Bosch supervised the project and provided financial support.

5.0 Introduction

Antimicrobial resistance is a major threat to global public health. In 2019, an estimated 4.95 million deaths were associated with drug-resistant infections (Murray et al., 2022), and this number is expected to rise in the future (O'Neill, 2014). Gram-negative bacteria consistently top the list as priorities for antibiotic development (CDC, 2019; Tacconelli et al., 2018). Among Gram-negatives are members of the *Burkholderia cepacia* complex (Bcc), opportunistic pathogens that primarily infect immunocompromised individuals. Some species, such as *B. cenocepacia*, may cause a form of pneumonia and bacteremia known as cepacia syndrome (Isles et al., 1984). Near uniform resistance to several antibiotic classes severely limits treatment options (Aaron et al., 2000; Abbott et al., 2016), and eradication protocols often require weeks to months of antibiotic cocktails (Garcia et al., 2018; Kitt et al., 2016). Furthermore, although new therapies (e.g. the CFTR modulator Ivacaftor) are available to treat the symptoms of cystic fibrosis, there may be limited benefit in pathogen clearance (Durfey et al., 2021), but this has not yet been assessed for Bcc infection. Thus, developing new antibiotic therapies for Bcc infections remains a high priority.

Low permeability of the Gram-negative cell envelope is a significant driver of intrinsic antibiotic resistance, as the majority of antibiotics have intracellular targets. The outer membrane is an asymmetric bilayer composed of phospholipids on the inner leaflet and lipopolysaccharide (LPS) on the outer leaflet. LPS, decorated with O-antigen units, is synthesized on the inner membrane then extracted and trafficked to the outer membrane by the Lpt protein complex (Okuda et al., 2016). Asymmetry is maintained by the action of the Mla pathway, which transports excess phospholipids from the outer membrane back to the inner membrane (Powers et al., 2020). Together, the inner and outer membranes have orthogonal permeability requirements: small hydrophilic compounds (generally <600 Da; (Decad and Nikaido, 1976) are able to diffuse through water-filled porins in the outer membrane, while hydrophobic compounds are able to diffuse through the inner membrane (Masi et al., 2017). The peptidoglycan sacculus is not involved in envelope permeability *per se*, but rather performs the essential function of maintaining cell shape and structural integrity (van Teeseling et al., 2017). Many components of the bacterial cell envelope have no human homologue and are thus attractive targets for a variety antibiotics (Sarkar et al., 2017). Indeed, the use of small-molecule potentiators has gained

traction as a route to increase membrane permeability and the activity of other antibiotics (Klobucar and Brown, 2022).

The majority of our knowledge of cell envelope biogenesis comes from model organisms. However, there are noted structural differences in the Bcc cell envelope that alter its function and confer high levels of antibiotic resistance, such as LPS modifications (Hamad et al., 2012; Isshiki et al., 1998), highly restrictive porins (Parr et al., 1987), and an array of efflux pumps (Podnecky et al., 2015; Scoffone et al., 2021). The demonstrated differences between the Bcc cell envelope and common models limits the utility of broad inferences from homology and highlights the need for specific studies of the Bcc.

Here, we performed an extensive transposon mutant screen in *B. cenocepacia* K56-2 against a wide array of cell envelope-targeting antibiotics. We hypothesized that transposon insertions would create specific deficiencies in the cell envelope, thus revealing mechanisms of cell envelope-related antibiotic resistance and susceptibility in K56-2. Using next-generation sequencing (NGS) to quantify mutant fitness in 22 conditions, we generated chemical-genetic interaction profiles that link genotype to phenotype and then validated over a hundred new functional annotations. We uncovered new modulators of antibiotic susceptibility in cell envelope biogenesis pathways in *Burkholderia*, such as parts of the RpoE regulon, peptidoglycan precursor synthesis and recycling, and then dissected the vulnerable connectivity between undecaprenyl phosphate utilization pathways. Analysis of the synergistic ceftazidime/avibactam combination also revealed that the potentiation is primarily through inhibition of the PenB β-lactamase. Additionally, we provide the first detailed characterization of the activity of cefiderocol, a siderophore-cephalosporin conjugate, against the Bcc by identifying the receptor and interactions with iron availability. Overall, we have identified a large number of susceptibility and resistance determinants in *B. cenocepacia* that may be exploited to bolster current antibiotic therapies.

5.1 Results

5.1.1 Identifying the genome-wide response of B. cenocepacia K56-2 to antibiotics and investigational drugs targeting cell envelope processes

5.1.1.1 Rationale and mechanisms of action of the selected antibiotics

The Gram-negative cell envelope presents both a major permeability barrier to antibiotics and a potential source of antibiotic targets. In particular, Bcc species are known for their impermeable cell envelope (~10 fold less permeable compared to *E. coli* (Parr et al., 1987)), which contributes to extreme resistance to membrane-disrupting detergents and multiple classes of antibiotics (Ahn et al., 2016; Everaert and Coenye, 2016; Loutet and Valvano, 2011; Zhou et al., 2007). Our goal was to probe important envelope biogenesis pathways to gain insight into the mechanisms governing cell envelope-related resistance in *B. cenocepacia* K56-2.

We therefore assembled a diverse panel of clinical and pre-clinical antibiotics targeting many aspects of cell envelope biogenesis (Figures A18 and A19). Fosfomycin (FOS) and cycloserine (CYC) inhibit early cytoplasmic steps of peptidoglycan synthesis (Kahan et al., 1974; Walsh, 1989). Eight β-lactams and β-lactamase inhibitors (plus one combination) were selected to target the septal and lateral peptidoglycan synthesis machineries in addition to important β-lactamases (Asli et al., 2016; Davies et al., 2008; Papp-Wallace et al., 2012, 2017; Sanders et al., 1997; Sutaria et al., 2018). FR-900098 (FR-9), and analogue of fosmidomycin, inhibits 1-deoxy-D-xylulose 5-phosphate reductoisomerase, the second enzyme in the isoprenoid biosynthetic pathway (Kuzuyama et al., 1998), while bacitracin (BAC) binds to undecaprenyl pyrophosphate (UndPP) and inhibits a dephosphorylation step that is critical for UndPP recycling (Siewert and Strominger, 1967). CHIR-090 (CHIR) and the related compound PF-04753299 (PF-04) both inhibit lipid A biosynthesis (Barb et al., 2007). The cationic agents chlorhexidine (CHX) and polymyxin B (PMB) disrupt the outer membrane, and inner and outer membranes, respectively (Barrett-Bee et al., 1994; Sabnis et al., 2021). We also included three hydrophobic large scaffold antibiotics in this panel (rifampicin [RIF], erythromycin [ERY], and novobiocin [NOV]; molecular weight > 600 Da) that are generally excluded by the Gram-negative cell envelope (Decad and Nikaido, 1976; Klobucar and Brown, 2022). We expected the large scaffold antibiotics, along with BAC as it is >600 Da, to highlight chemical-genetic interactions caused by cell envelope permeability and disruptions in major cell envelope biogenesis mechanisms. In summary, we aimed to study cell envelope biogenesis and resistance mechanisms and how they may be exploited to inform novel antibiotic combinations.

5.1.1.2 Constructing and validating a randomly-barcoded transposon mutant library

To profile genome-wide contributions to antibiotic susceptibility and resistance, we turned to transposon mutagenesis and TnSeq to measure mutant abundance during antibiotic challenge. While antibiotics target essential processes, encoded by genes that cannot be interrupted by transposons, non-essential genes are known to modify antibiotic susceptibility (Bailey et al., 2022; Geisinger et al., 2020; Leshchiner et al., 2022). Previously, our lab has constructed transposon mutant libraries in strain K56-2, a multidrug-resistant ET12 epidemic lineage clinical isolate (Darling et al., 1998), to identify the essential genome (Gislason et al., 2017a) and characterize targets and mechanisms of action for antimicrobials (Gislason et al., 2017b; Hogan et al., 2018; Nunvar et al., 2019). To leverage advances in sequencing and bioinformatic capabilities, we modified our Tn*5* transposon to contain a random 20 bp barcode, greatly facilitating tracking mutant abundance in many conditions (Wetmore et al., 2015). By sequencing the transposon insertion site, unique barcodes and genomic junctions can be linked (RB-TnSeq). Following growth in experimental conditions, barcodes may then be simply amplified by PCR and sequenced (BarSeq) (Figure 12). We therefore generated a library of ~340,000 uniquely barcoded transposon mutants in K56-2 (approximately equally divided into 10 subpools). Library statistics can be found in Table A9. The library had a median of 12 insertions per protein-coding gene and an average spacing between insertions of 18.7 bp. We found that insertion sites were more likely in low GC-content regions and genes (Figure A20) as we observed previously (Gislason et al., 2017a), which may be due to transposon insertion and DNA sequencing biases.

To ensure we could use BarSeq to accurately quantify mutant abundance, we performed a pilot experiment with known levels of mutant depletion. Quantification of mutant abundance demonstrated high replicate reproducibility (Pearson's r = 0.96, P-value 2.4×10^{-15}) (Figure 13A) and close agreement with expected levels of depletion (two mutants at each of 10-fold and 50-fold depletion vs. an equal abundance pool) (Figure 13B). However, we observed a ~10-fold range in barcode recovery in the equal abundance pool (Figure 13A) that was not due barcode high GC-content (Figure 13C). While the exact cause of this effect is unknown, it has been observed previously by other groups using NGS to detect barcoded mutant abundance (Johnson et al., 2019). Despite this, we were able to successfully and accurately quantify barcoded mutant depletion at small scale.

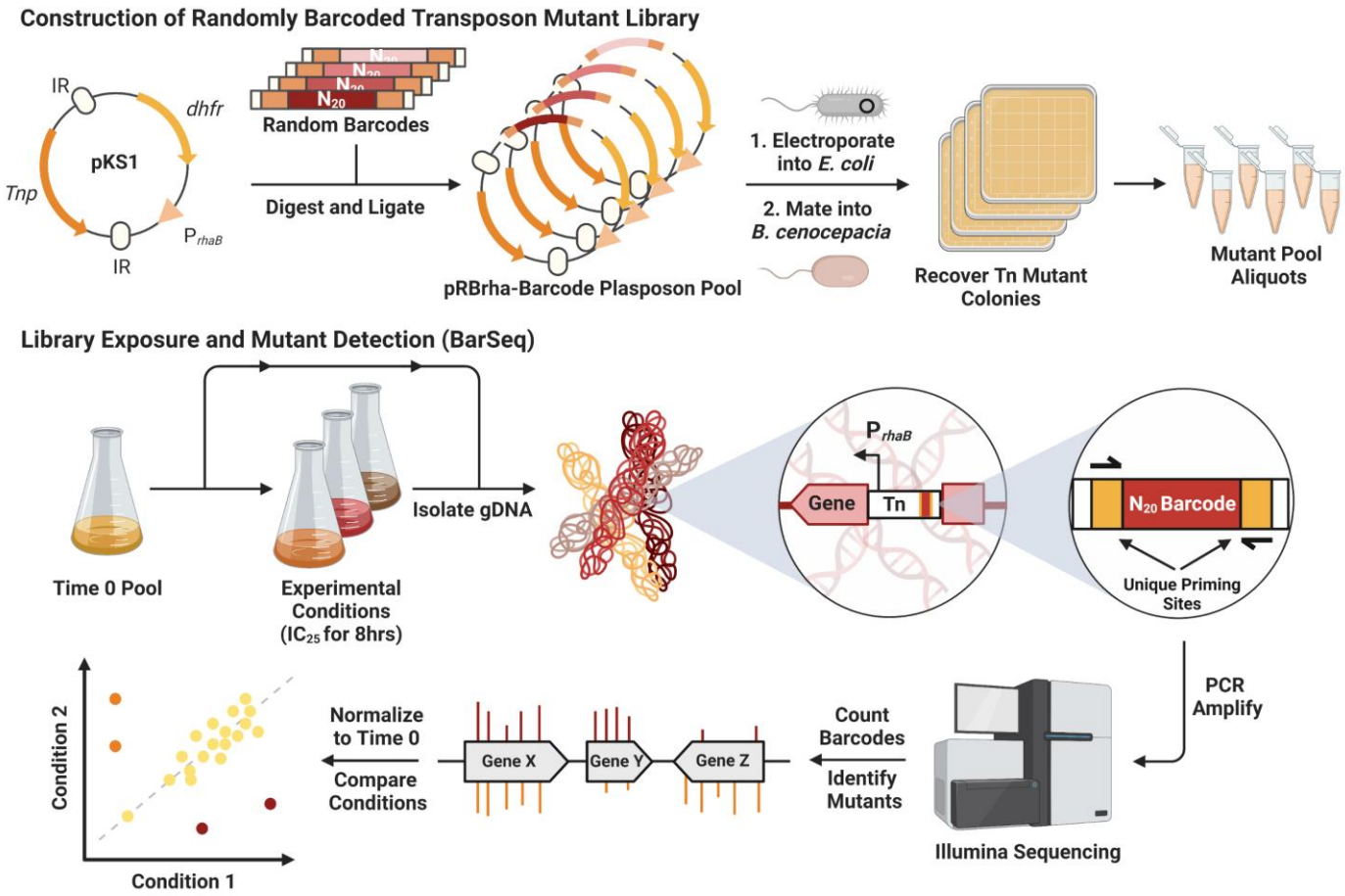

Figure 12. Overview schematic of creating a randomly barcoded transposon mutant library. DNA fragments containing random 20 bp barcodes flanked by priming and restriction sites are ligated into the parent plasposon pKS1. The resultant plasposon pool is electroporated into *E. coli* and then introduced into K56-2 by triparental mating. Mutant colonies are recovered and stored until needed. After growth in a desired condition, genomic DNA is isolated and used as template for one-step PCR to amplify barcodes and add flow cell adapters and sequencing indices. Prepared DNA libraries are then sequenced on an Illumina platform. Barcode abundance is counted and compared between conditions by a bioinformatic pipeline.

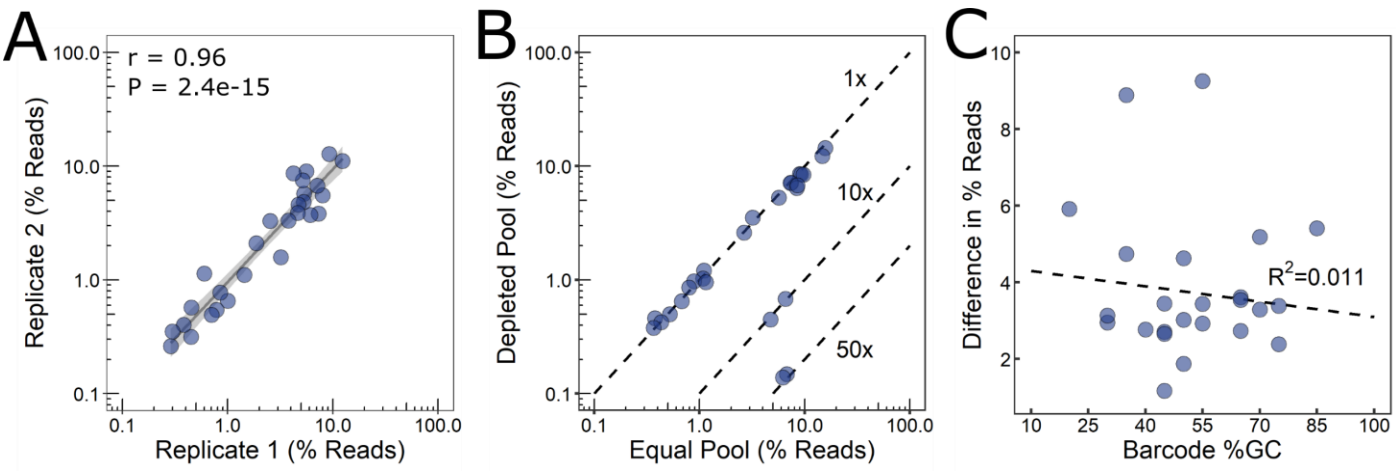

Figure 13. Validation of BarSeq to reproducibly and accurately determine barcoded transposon mutant abundance. A) Reproducibility of BarSeq shown between two replicates from the equal pool of the artificial depletion experiment of 30 pooled mutants. The grey line shows a linear regression with 95% confidence interval in lighter grey. The r and P-values are from Pearson's correlation test. B) Detection of changes in barcode abundance from the artificial depletion experiment. Each point is an average of two replicates. Dashed lines indicate expected differences between the two pools: 1x, 10x, or 50x. C) Absolute difference between the observed and expected barcode abundance (in percent of reads) for the equal pool replicates as a function of individual barcode GC-content. If truly equal, all barcodes would be represent at ~3%. The dashed line shows a linear regression.

5.1.1.3 Antibiotic exposure and detection of broad interactions on whole pathways and processes

The choice of antibiotic exposure conditions has important implications for the sensitivity of high-throughput experiments. Higher antibiotic concentrations generally result in a greater number of interactions, including non-specific/unrelated hits, while lower concentrations detect a smaller number of more specific interactions (Bailey et al., 2022; Geisinger et al., 2020). Thus, antibiotic doses were selected to inhibit 20 – 30% of growth relative to growth without antibiotics, as measured by OD_{600} (Figure A21 and Table 5), to enable detection of specific mechanism-related interactions (Geisinger et al., 2019, 2020; Hogan et al., 2018). As controls for the synergistic combination of ceftazidime/avibactam (AVI/CAZ), each component was also used at the lower concentration present in the combination as well as higher concentrations that individually inhibited 20 – 30% of growth. Ampicillin (AMP), FOS, and CHIR did not attain 20% growth inhibition so were each used at the highest concentration tested (256 μg/mL).

The entire pool of ~340,000 unique mutants was inoculated in LB medium at OD_{600} 0.025 (~75 CFU/mutant) and allowed to reach early exponential phase (OD_{600} 0.15). The cultures were then exposed to antibiotics (or 1% DMSO solvent control) for 8 hours (~10 generations), after which genomic DNA was harvested and used as template for BarSeq. Accommodating three biological replicates of antibiotic exposures, Time 0 (before antibiotic) and DMSO controls, we used three high-output NextSeq runs, resulting in ~500 reads/gene for each condition and replicate. The barcodes were counted and matched to insertion site, then normalized to Time 0 controls and aggregated across replicates to calculate average per-gene fitness scores (Morin et al., 2018; Wetmore et al., 2015).

Table 5. Antibiotics used for genome-wide fitness profiling

Antibiotic	IC_{20-30} Concentration (µg/mL)	Target (Process)
Ampicillin (**AMP**) †	256†	PBP3/Divisome (Cell wall synthesis)
Aztreonam (**AZT**)	40	PBP3/Divisome (Cell wall synthesis)
Cefiderocol (**CFD**)	0.04	PBP3/Divisome (Cell wall synthesis)
Ceftazidime - High (**CAZ-H**)*	4	PBP3/Divisome (Cell wall synthesis)
Ceftazidime - Low (**CAZ-L**)*	1.5	PBP3/Divisome (Cell wall synthesis)
Tazobactam (**TAZ**)	50	PBP3/Divisome (Cell wall synthesis)
Cefotetan (**CTT**)	45	PBP3/Divisome (Cell wall synthesis) + PBP2/Rod complex (Cell wall synthesis)
Meropenem (**MEM**)	3.5	PBP2/Rod complex (Cell wall synthesis)
Avibactam - High (**AVI-H**)*	115	PBP2/Rod complex (Cell wall synthesis) + Diverse β-lactamases
Avibactam - Low (**AVI-L**)*	8	PBP2/Rod complex (Cell wall synthesis) + Diverse β-lactamases
Ceftazidime/Avibactam (**AVI/CAZ**)	1.5/8	PBP2/Rod complex (Cell wall synthesis) + Diverse β-lactamases + PBP3/Divisome (Cell wall synthesis)
Cycloserine (**CYC**)	150	Alr and Ddl (Cell wall precursor synthesis)
Fosfomycin (**FOS**) †	256†	MurA (Cell wall precursor synthesis)
Bacitracin (**BAC**)	375	Und-PP (Undecaprenol metabolism)
FR-900098 (**FR-9**)	85	Dxr (Undecaprenol metabolism)
CHIR-090 (**CHIR**) †	256†	LpxC (Lipid A synthesis)
PF-04753299 (**PF-04**)	0.18	LpxC (Lipid A synthesis)
Chlorhexidine (**CHX**)	1.8	Lipid membranes
Polymyxin B (**PMB**)	550	LPS and lipid membranes
Erythromycin (**ERY**)	100	Peptide exit tunnel/23S rRNA (Protein Synthesis)
Novobiocin (**NOV**)	1.1	GyrB (DNA gyrase)
Rifampicin (**RIF**)	5.5	RpoB (Transcription)

* Two concentrations of AVI and CAZ were used. A higher concentration that independently reached the IC_{20-30}, and a lower concentration the same as that used in the synergistic AVI/CAZ combination.
† IC_{20-30} could not be reached for AMP, FOS, and CHIR, so highest concentration tested was used (256µg/mL).
Shading groups antibiotics by broad target processes.

Given that our panel was designed to specifically target the cell envelope, we expected to identify interactions with structural and functional components of the cell envelope. Comparison between the DMSO control and each condition revealed hundreds of broad and specific factors that contribute to antibiotic susceptibility, many of which are novel in K56-2 (Figure A22). As a first look to reveal effects on whole pathways and processes, the genes significantly affecting fitness in each condition were analyzed for enrichment in BioCyc pathways and GO terms (Figures A23-A25) (Ashburner et al., 2000; Castillo-Davis and Hartl, 2003; Gene Ontology Consortium, 2021; Karp et al., 2019). For negative fitness effects, we observed an enrichment in genes in (phospho)lipid metabolism pathways (e.g. *pgpA, plsC1, plsC2, shc* and K562_RS10290 lipid N-methyltransferase) (Figures A23 and A25). Additionally, we found enrichment in many GO terms related to the cell envelope (Figures A24 and A25). These are, for example, "peptidoglycan metabolic process" (e.g. *mltD*), "integral component of the membrane" (e.g. *mlaD*, K562_RS05020 PhoQ-type sensor, *dbcA, ftsK* and *hpnN*), and "periplasmic space" (e.g. *slt*, *lolA*, K562_RS01705 S1C-family endopeptidase). Broadly, these findings are in line with expectations that cell envelope-targeting antibiotics will report on susceptibility determinants in the cell envelope.

Although antibiotics act by distinct mechanisms based on their class, many also exert common physiological effects, such as metabolic perturbations and the induction of reactive oxygen species (ROS) (Dwyer et al., 2014; Kohanski et al., 2007). Identifying similar hallmarks as other large studies would therefore serve as additional validation of our results. We found that disruptions in genes related to purine and pyrimidine metabolism (e.g. *pyrC, pyrR, carAB, surE, purM, purQ*) and amino acid metabolism (e.g. *aspA, metK, hutGH, glyA*) pathways often showed reduced susceptibility to antibiotics, especially the β-lactams (Figures A23 and A25). Inactivating these genes may slightly reduce metabolic rate and nucleotide pools, both known to affect antibiotic susceptibility (Lopatkin et al., 2019; Yang et al., 2019). Similarly, disruptions in NADH dehydrogenase components *nuoC* and *nuoJ*, and the ATP synthase epsilon subunit *atpC* also reduced susceptibility to many antibiotics (Figure A22), likely by depleting ATP pools and slowing metabolism. Conversely, we found that disruptions in several genes related to ROS mitigation increased antibiotic susceptibility. Indeed, we found that when genes related to polyamine (e.g. *speH*, K562_RS22770 ornithine decarboxylase and K562_RS19285 agmatinase) and reductant (e.g. *grxC* and *gshA*) metabolism pathways were disrupted, susceptibility often

increased (Figure A23). This was also detected by GO term enrichment of "response to oxidative stress" (e.g. *msrB*, *katG*, and *soxR*), "glutathione metabolic process" (e.g. K562_RS31890 and K562_RS10025 glutathione S-transferases), and "peroxiredoxin activity" (e.g. K562_RS21700 Ohr/OsmC family peroxiredoxin, K562_RS15530 alkylhydroperoxidase, and K562_RS08590 *ahpC*-type peroxiredoxin) (Figure A24). Glutathione and polyamines, such as putrescine, are both known to be important in *B. cenocepacia* for protection against ROS (El-Halfawy and Valvano, 2014; Van Acker et al., 2016). Together, the corroboration of several previous works and expected findings confirms the validity of our BarSeq approach to uncover detailed chemical-genetic interactions at the foundations of antibiotic action.

5.1.2 Chemical-genetic interactions with outer membrane components

5.1.2.1 The Mla, BAM, and Lol pathways are important for membrane integrity and resistance to multiple antibiotics

The Mla pathway functions in retrograde transport of excess phospholipids from the outer membrane to the inner membrane, thereby maintaining an asymmetric, and more impermeable, outer membrane enriched in LPS (Figure 14A) (Malinverni and Silhavy, 2009; Powers et al., 2020). However, defects in the Mla pathway in *E. coli* K-12 and *P. aeruginosa* PA14 were found to not alter susceptibility to a variety of antibiotics (Bernier et al., 2018). In K56-2, the Mla pathway is encoded by six genes organized in two operons, and two accessory genes (K562_RS01610 and K562_RS01615, homologous to *E. coli yadG* and *yadH*) of unclear function in an adjacent operon (Bernier et al., 2018) (Figure 14B).

In our BarSeq experiment, genes encoding components of the Mla pathway had negative fitness scores for nearly all tested antibiotic conditions (20/22 conditions) (Figures A22 and Figure 14C). Disruptions in *mlaFED*, the first three genes of the cluster, generally resulted in greater susceptibility increases, especially for the large scaffold antibiotics (ERY, NOV, and RIF) than did disruption in *vacJ* and *mlaCB* (Figure 14C). Additionally, susceptibility to three of the smallest antibiotics in the panel, FOS, CYC, and FR-9, was generally not affected by disruptions in any of the Mla pathway genes. Our findings of broad susceptibility profiles for mutants in the Mla pathway support a unique importance of this pathway in maintaining the permeability barrier of the outer membrane in *Burkholderia*, similar to a previous report (Bernier et al., 2018). Furthermore, our unique finding of moderately increased β-lactam susceptibility may stem from

the competitive growth conditions that are known to highlight even subtle fitness differences (Bailey et al., 2022; Gislason et al., 2017b).

Other major cell envelope biogenesis machineries, the BAM complex (β-barrel insertion into the outer membrane) (Voulhoux et al., 2003; Wu et al., 2005), Lol pathway (lipoprotein trafficking to the outer membrane) (Okuda and Tokuda, 2011) and Lpt system (lipopolysaccharide transport) (Ruiz et al., 2009), are encoded by a greater number of essential genes (Gislason et al., 2017a), thus are not well-represented in our transposon mutant library. All three pathways are known to be important for maintaining membrane integrity in *E. coli* (Falchi et al., 2017; Grabowicz and Silhavy, 2017; Muheim et al., 2017; Ruiz et al., 2005). From our BarSeq experiment, we were able to link disruptions in the *lolA* lipoprotein shuttle with susceptibility to many antibiotics (e.g. AVI, AZT, MEM, CHX, and PMB) and disruptions in *bamD* to susceptibility to PMB and CHX (Figure A22). Given the transport and folding functions of the Lol and BAM pathways, it is likely that these changes in susceptibility are a consequence of improper localization of important outer membrane factors (e.g. Lpt and Mla proteins and porins).

We next reasoned that chemical permeabilization of the membrane may also increase antibiotic susceptibility of K56-2. Using an *N*-phenyl-1-naphthylamine (NPN) uptake assay (Loh et al., 1984; Malott et al., 2012), we found CHX to greatly increase outer membrane permeability (Figure A26). Consequently, in checkerboard interaction assays, CHX synergized strongly with large scaffold antibiotics and the β-lactams (Figure 14D). Overall, our findings show that cell envelope impermeability severely limits antibiotic entry into K56-2.

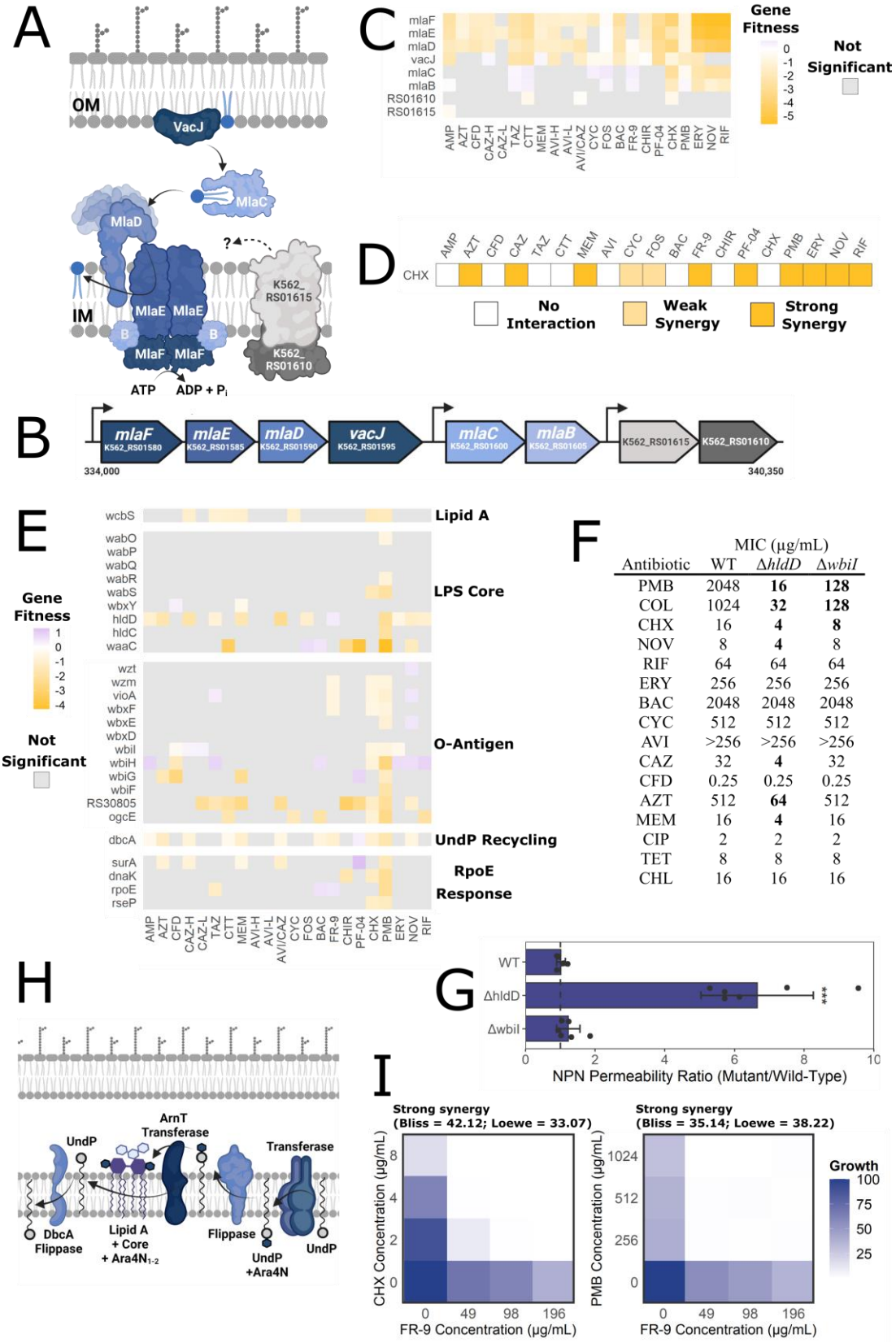
A
OM
VacJ
MlaC
MlaD
?
K562_
RS01615
IM
MlaE MlaE
B
B
MlaF MlaF
K562_
RS01610
ATP
ADP + Pi
C
mlaF
mlaE
mlaD
vacJ
mlaC
mlaB
RS01610
RS01615
AMP AZT CFD CAZ-L TAZ CTT MEM AVI-H AVI-L AVI/CAZ CYC FOS BAC FR-9 CHIR PF-04 CHX PMB ERY NOV RIF
Gene Fitness
0 -1 -2 -3 -4 -5
Not Significant
D
AMP AZT CFD CAZ TAZ CTT MEM AVI CYC FOS BAC FR-9 CHIR PF-04 CHX PMB ERY NOV RIF
CHX
No Interaction
Weak Synergy
Strong Synergy
B
mlaF K562_RS01580
mlaE K562_RS01585
mlaD K562_RS01590
vacJ K562_RS01595
mlaC K562_RS01600
mlaB K562_RS01605
K562_RS01615
K562_RS01610
334,000
340,350
E
wcbS
Lipid A
wabO
wabP
wabQ
wabR
wabS
wbxY
hldD
hldC
waaC
LPS Core
wzt
wzm
vioA
wbxF
wbxE
wbxD
wbiI
wbiH
wbiG
wbiF
RS30805
ogcE
O-Antigen
dbcA
UndP Recycling
surA
dnaK
rpoE
rseP
RpoE Response
AMP AZT CFD CAZ-H CAZ-L TAZ CTT MEM AVI-H AVI-L AVI/CAZ CYC FOS BAC FR-9 CHIR PF-04 CHX PMB ERY NOV RIF
Gene Fitness
1 0 -1 -2 -3 -4
Not Significant
F
MIC (μg/mL)
Antibiotic | WT | ΔhldD | ΔwbiI
PMB | 2048 | 16 | 128
COL | 1024 | 32 | 128
CHX | 16 | 4 | 8
NOV | 8 | 4 | 8
RIF | 64 | 64 | 64
ERY | 256 | 256 | 256
BAC | 2048 | 2048 | 2048
CYC | 512 | 512 | 512
AVI | >256 | >256 | >256
CAZ | 32 | 4 | 32
CFD | 0.25 | 0.25 | 0.25
AZT | 512 | 64 | 512
MEM | 16 | 4 | 16
CIP | 2 | 2 | 2
TET | 8 | 8 | 8
CHL | 16 | 16 | 16
G
WT
ΔhldD
ΔwbiI
***
0 2 4 6 8 10
NPN Permeability Ratio (Mutant/Wild-Type)
H
ArnT Transferase
UndP
Transferase
DbcA Flippase
Lipid A + Core + Ara4N1-2
Flippase
UndP +Ara4N
UndP
I
Strong synergy
(Bliss = 42.12; Loewe = 33.07)
Strong synergy
(Bliss = 35.14; Loewe = 38.22)
CHX Concentration (μg/mL)
0 2 4 8
PMB Concentration (μg/mL)
0 256 512 1024
0 49 98 196
FR-9 Concentration (μg/mL)
Growth
100 75 50 25

Figure 14. Structural defects in the outer membrane increase susceptibility to multiple antibiotics. A) Retrograde phospholipid trafficking from the outer (OM) to inner (IM) membranes by the Mla pathway, inferred by homology (Bernier et al. 2018; Powers et al. 2020). The roles of K562_RS01610 and K562_RS01615 are unclear. B) Genetic organization of the Mla pathway gene cluster in K56-2. Nucleotide position on K56-2 chromosome 1 is indicated at the beginning and end of the cluster. C) Gene fitness scores relative to DMSO control of the genes in the Mla pathway. Grey squares indicate the value was not significant ($P > 0.05$). D) Summary of antibiotic checkerboard interaction assay with CHX. Interactions were assessed and interpreted with SynergyFinder as per the Materials and Methods. E) Gene fitness scores relative to DMSO control of the genes associated with LPS, lipid A modifications, and the rpoE regulon. F) MIC values of K56-2 and the Δ*hldD* and Δ*wbiI* mutants. The K56-2 and deletion backgrounds have dCas9 integrated in the chromosome. Values are medians of three biological replicates, with bold indicating at least 2-fold change from WT. G) Ratios of NPN fluorescence of the deletion mutants to the fluorescence of the wild-type control. Errorbar represents means ± SD of six replicates. Significance was determined by 1-way ANOVA with Dunnett's *post hoc* test to the wild-type control. *** $P < 0.001$. The dashed lines indicate a NPN fluorescence ratio of 1. H) Diagram of the membrane-associated steps of the Ara4N LPS modification, inferred from homology and experimental evidence in *Burkholderia* (Panta et al. 2019; Wang et al. 2015). I) Mini checkboard assays of FR-9 interaction with CHX and PMB. Values are normalized to the OD_{600} of growth without antibiotic.

5.1.2.2 LPS, lipid A modifications, and RpoE regulon confer resistance to cationic antibiotics

As part of their mechanisms of action, the cationic antibiotics CHX and PMB bind to and disrupt bacterial membranes. In *E. coli,* PMB binds the lipid A moiety of LPS (Pristovsek and Kidric, 1999), both in the inner and outer membranes, resulting in cell lysis (Sabnis et al., 2021). CHX is reported to collapse the membrane potential (Kuyyakanond and Quesnel, 1992) and disrupt only the outer membrane (Barrett-Bee et al., 1994). In Gram-negatives, such as *Salmonella enterica* and *P. aeruginosa*, cationic antibiotic resistance is inducible (Simpson and Trent, 2019); however, *Burkholderia* species are intrinsically resistant to these agents, mediated both by physical protection of the membrane and by adaptive responses (Loutet et al., 2011). The *Burkholderia* O-antigen, LPS core, and RpoE envelope stress regulon are known to be important for PMB resistance (Loutet et al., 2011; Ortega et al., 2009).

We thus leveraged our BarSeq experiment for a deeper look into cationic antibiotic resistance in *Burkholderia*. When the mutant library was exposed to these compounds, we identified genes important for PMB and CHX fitness associated with lipid A synthesis (*wcbS*), LPS core synthesis (*hldC, hldD, waaC, wabO,* and *wabSR*), lipid A modification (*dbcA*), and polymeric O-antigen synthesis (*wbiFGHI, ogcE, vioA, wbxFE,* and *wzm*) (Figure 14E). To further dissect the function of LPS synthesis genes, we created unmarked deletion mutants in *wbiI* and *hldD*. These genes encode the putative epimerase-dehydratase that synthesizes the UDP-GalNAc sugar for O-antigen chain formation (Ortega et al., 2005; Valvano, 2015) and a heptose epimerase required for LPS core synthesis (Loutet et al., 2006), respectively. The Δ*hldD* mutant was expected to be devoid of O-antigen, as the LPS core is incomplete (Loutet et al., 2006), while the Δ*wbiI* mutant was expected to present a heavily truncated O-antigen with only N-acetyl-D-quinovosamine and L-rhamnose (Ortega et al., 2005). Both mutants lacked polymeric O-antigen as detected by silver staining LPS extracts; however, we could not resolve the subtleties of lower molecular weight species (e.g. LPS core with two sugars) (Figure A27). Polymeric O-antigen expression could be complemented *in trans* for both mutants (Figure A27). Both the Δ*wbiI* and Δ*hldD* mutants were markedly more susceptible than WT to PMB, colistin (COL) and CHX (Figure 14F); however, the Δ*wbiI* mutant was generally less susceptible than the Δ*hldD* mutant, and the increase in CHX susceptibility was only modest for both mutants. The Δ*hldD* mutant was also more susceptible to AZT, CAZ, and MEM (Figure 14F).

The Δ*hldD* and Δ*wbiI* mutants have outer membrane compositional defects; therefore, it is possible that increased antibiotic susceptibility is due to increased outer membrane permeability. As measured by NPN uptake, the Δ*wbiI* mutant showed no change in outer membrane permeability, while the Δ*hldD* mutant showed a large increase in permeability (Figure 14G), demonstrating a complete LPS core, but not O-antigen, is required for outer membrane integrity. Taken together, we suggest that only part of the antibiotic susceptibility caused by defects in the LPS core are due to increased permeability, as the Δ*hldD* mutant was not more susceptible to large scaffold antibiotics (ERY, NOV, RIF; Figure 14F). Additionally, in the competitive conditions of the BarSeq experiment, disruption of *hldD* caused only moderate susceptibility to ERY, NOV, and RIF (Figure 14E). These findings support independent roles of the O-antigen and LPS core in physically protecting the cell from cationic antibiotics.

Lipid A modification with 4-deoxy-4-aminoarabinose (Ara4N) is known to provide cationic antibiotic resistance by reducing the net negative charge of LPS (Gunn et al., 1998; Wang et al., 2015). UndP is the lipid carrier for Ara4N before it is linked to the LPS core (Trent et al., 2001a, 2001b) (Figure 14H). Supporting the connection between UndP and the Ara4N modification, we found that disruption of *dbcA* increased susceptibility to PMB and CHX (Figure 14E). *dbcA* is a homologue of *E. coli uptA*, encoding a DedA-family UndP flippase critical for UndP recycling (Figure 14H) (Panta et al., 2019; Roney and Rudner, 2022; Sit et al., 2022); thus, disruption of *dbcA* likely reduces the abundance of free UndP available for linkage to Ara4N. We also found that inhibition of UndP synthesis with FR-9 strongly synergized with both PMB and CHX (Figure 14I). These findings are in line with a previous report that *dbcA* is required for polymyxin resistance in *B. thailandensis* (Panta et al., 2019).

Cell envelope stress responses monitor the presence of unfolded outer membrane proteins in the periplasm and upregulate various adaptive responses (Hews et al., 2019). The Rcs and Cpx response genes lack strong homologues in K56-2, thus only the extracytoplasmic sigma factor (RpoE) response has been characterized in *B. cenocepacia* (Flannagan and Valvano, 2008). We thus examined our BarSeq data for components of the RpoE regulon. We found that RpoE itself, RseP (a protease necessary for RpoE activation), and the RpoE-regulated protein chaperones SurA and DnaK were important for fitness in the presence of PMB and/or CHX (Figure 14E). SurA has been linked to the maintenance of membrane integrity in *P. aeruginosa* (Klein et al., 2019), and disruption of these chaperones likely impairs outer membrane protein folding and the

cell envelope stress response (Hews et al., 2019). Together, our findings demonstrate that both physical protective and adaptive responses are important for cationic antibiotic resistance in K56-2.

5.1.2.3 Changes in susceptibility reveal new substrates for the BpeAB-OprB efflux pump and specific porins

Bacteria possess a variety of efflux pumps that are associated with a diverse range of functions, including the removal of toxic compounds such as antibiotics. However, many of the antibiotics used in the current study are not known to be substrates for *Burkholderia* efflux pumps. We hypothesized that transposon insertions in genes encoding efflux pumps would decrease fitness in the presence of each pump's range of substrates. From our BarSeq experiment, we observed that disruption of K562_RS30055 PACE family efflux pump was important for fitness in the presence of multiple antibiotics, while disruption of the K562_RS10630 EmrE pump homologue was specifically important for fitness with CHX (Figure 15A).

B. cenocepacia K56-2 encodes 16 tripartite RND efflux pumps, of which several are important for antibiotic resistance (Bazzini et al., 2011). From our BarSeq experiment, we found that disruptions in components of the BpeAB-OprB efflux pump (also called RND-4, a homologue of the MexAB-OprM pump in *P. aeruginosa* (Chan et al., 2004)) increased susceptibility to NOV, AVI, AVI/CAZ, PF-04 and CHIR (Figure 15A). Enhanced susceptibility was only seen for disruptions in *bpeA* and *bpeB*, but not for *oprB*, suggesting that the *bpeAB* complex may also form functional associations with other outer membrane factors. Before this study NOV, AVI, PF-04, and CHIR were not known to be effluxed by BpeAB-OprB in *B. cenocepacia*. To verify these findings, we used CRISPRi (Hogan et al., 2019) to knock down the *bpeABoprB* operon. Silencing of the operon by CRISPRi was validated by a 2-fold reduction in MIC of the known substrate chloramphenicol (CHL) (Figure 15B). Knockdown of this pump did not cause a growth defect without antibiotics (Fig A28). Upon dCas9 induction, susceptibility to NOV, PF-04, AVI, and AVI/CAZ moderately increased, but not to CAZ only (Figure 15B). We thus conclude that NOV, AVI, PF-04, and CHIR are new substrates for the BpeAB-oprB efflux pump in *B. cenocepacia*.

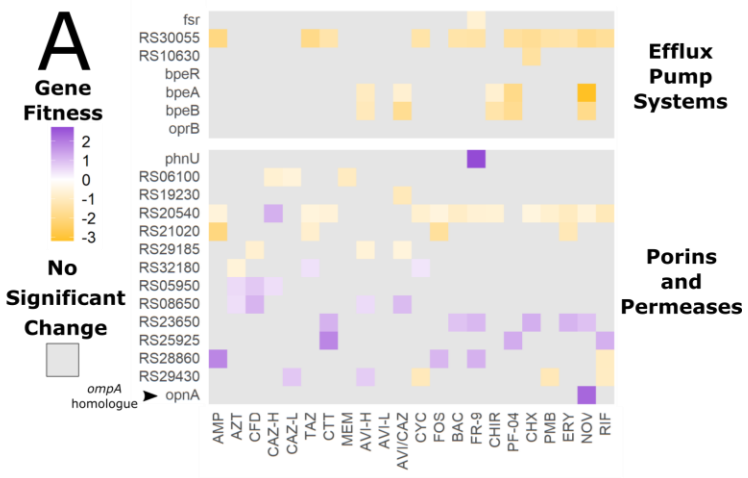

B

CRISPRi Target	MIC (µg/mL) CHL	PF-04	NOV	AVI	CAZ	AVI/CAZ
NTC	16	1	8	>256	32	8/4
bpeAB-oprB	**8**	**0.5**	**4**	**128**	32	**8/2**

C

CRISPRi Target	NOV MIC (µg/mL) *B. cenocepacia* K56-2	*B. multivorans* ATCC17616	*B. thailandensis* E264
NTC	8	8	8
opnA	**16**	**16**	**16**

Figure 15. Disruptions in efflux pumps, porins, and permeases alter antibiotic susceptibility. A) Gene fitness scores relative to DMSO control of the genes associated with efflux pumps, porins, and permeases. For genes not assigned names, the K562_# locus tags are given. B) MIC values of K56-2::dCas9 harbouring plasmids expressing a non-targeting sgRNA control (NTC) or an sgRNA targeting the *bpeAB-oprB* operon. AVI was kept constant at 8 µg/mL. C) MIC values of CRISPRi mutants of *Burkholderia* species targeting *opnA*. For B and C, values shown are with rhamnose induction of CRISPRi. MIC values are medians of three biological replicates, with bold indicating at least 2-fold change with the addition of rhamnose.

As porins and permeases have opposing functions of efflux pumps, we hypothesized that disruption of membrane permeases and porins allowing antibiotic entry would increase fitness in specific conditions. K56-2 encodes at least 130 putative porins and permeases, and few have been characterized in terms of their physiological importance. We observed that disruption of K562_RS29850, encoding the PhnU putative 2-aminoethylphosphonate ABC-type permease (Manav et al., 2018), resulted in markedly reduced susceptibility exclusively in the presence of FR-9 (Figure 15A). The structural similarity between 2-aminoethylphosphonate and FR-9 leaves open the possibility that FR-9 may also be taken into K56-2 via this transporter. We found that other porins were important for fitness in multiple conditions (e.g. K562_RS21020 and K562_RS20540) (Figure 15A and Supplemental Data 1). Some porins, such as OmpA and OmpC in *E. coli*, are known to be important for maintaining membrane integrity (Choi and Lee, 2019), which may explain why the lack of porins may reduce fitness in the presence of antibiotics. On the other hand, we observed several porins that when disrupted resulted in increased fitness in at least one condition (e.g. K562_RS23650 and K562_RS25925) (Figure 15A and Supplemental Data 1). There were no porins associated with fitness in all conditions, not even for all β-lactams, which is suggestive of an intricate network of minor variations in porin specificity and partial functional redundancy.

Of note, we observed that disruption of K562_RS14130, a homologue of *E. coli* K-12 *ompA* (53.4% identity; top hit by reciprocal best-hit BLAST), specifically increased fitness in the presence of NOV (Figure 4A). In *E. coli*, deletion of *ompA* does not affect susceptibility to NOV (Choi and Lee, 2019). Phylogenetics revealed that the porin encoded by K562_RS14130 is conserved with greater than 60% amino acid identity among many Burkholderiaceae genera (Figure A29A). The presence of this porin appears to correlate with low MIC values of NOV compared to *E. coli* and *P. aeruginosa* (Figure A29B). In K56-2, *B. multivorans* ATCC 17616 and *B. thailandensis* E264, CRISPRi repression of the K562_RS14130 homologue modestly reduced susceptibility to NOV (2-fold increase in MIC) (Figure 15C), but not other antibiotics (Figure A29C). Of note, repressing K562_RS14130 did not increase the MIC of NOV to the level of non-susceptible Gram-negatives (e.g. *E. coli* and *P. aeruginosa*), indicating that other factors play a role in the observed differences in NOV susceptibility between *Burkholderia* species and other Gram-negatives. Together, our findings support a different role of

K562_RS14130 in K56-2 and we propose it to be annotated as *opnA* for Outer membrane Protein, Novobiocin entry A.

5.1.3 Chemical-genetic interactions with periplasmic components

5.1.3.1 Peptidoglycan biosynthesis factors modify susceptibility to β-lactams and cycloserine

β-lactams remain one of the few options to treat Bcc infections. We thus decided to examine the genome-wide β-lactam susceptibility profiles with a focus on their target: peptidoglycan metabolism. We also considered CYC and FOS as these two molecules target peptidoglycan precursor assembly in the cytoplasm. Although both display poor inhibitory activity in K56-2 (Figure A21C), FOS and CYC are still useful for treating *E. coli* infection (Zhanel et al., 2020) and tuberculosis (Alghamdi et al., 2019), respectively. FOS is an inhibitor of MurA, a UDP-*N*-acetylglucosamine 1-carboxyvinyltransferase, which catalyzes the first committed step in peptidoglycan precursor synthesis (Kahan et al., 1974). CYC is a dual inhibitor of alanine racemases (Alr and DadX), which synthesize D-alanine from L-alanine, and D-alanine-D-alanine ligase (Ddl), which synthesizes D-Ala-D-Ala (Walsh, 1989). In *E. coli* and most Gram-negatives, peptidoglycan precursors contain a pentapeptide stem of L-Ala-D-Glu-*meso*-diaminopimelate-D-Ala-D-Ala. Glutamate racemase is needed to convert L-Glu to D-Glu (Barreteau et al., 2008).

The targets of CYC are encoded by the *ddl*, *alr*, and *dadX* genes. While *ddl* is essential in K56-2 and not represented in our screen, we found that disruptions in *alr* and *dadX* caused susceptibility to CYC (Figure 16A). In *P. aeruginosa,* DadX is known to be more important for growth in nutrient poor medium (He et al., 2011); accordingly, we observed that the fitness defect due to *dadX* disruption was less than that of *alr*. Conversely, a disruption in *dadA*, encoding a catabolic D-amino acid dehydrogenase resulted in moderately reduced susceptibility to CYC (Figure 16A). Cells lacking DadA may have elevated pools of D-amino acids, including D-alanine, thus reducing dependence on the Alr and DadX alanine racemases.

Intriguingly, disruption of *murI*, encoding glutamate racemase, and K562_RS27665, encoding a putative fusion GntR-type transcriptional regulator and pyridoxal phosphate (PLP)-dependent aminotransferase, also rendered the cells highly susceptible to CYC (Figure 16A). K562_RS27665 bears homology with *E. coli* K-12 *ydcR, yjiR, patA, selA*, and *ybdL*. The interactions of CYC with D-glutamate biosynthesis have not been reported before. MurI is the only glutamate racemase in *E. coli* that synthesizes D-Glu for incorporation into peptidoglycan

precursors (Doublet et al., 1993). Species of *Staphylococcus* and *Bacillus* encode glutamate racemase and a PLP-dependent D-amino acid transaminase, also capable of synthesizing D-glutamate using D-alanine and α-ketoglutarate as substrates (Fotheringham et al., 1998; Pucci et al., 1995). ProteInfer confidently predicts (score >0.95) K562_RS27665 is associated with amino acid metabolic GO terms such as L-aspartate: α-ketoglutarate aminotransferase activity (GO:0004069) and alanine catabolic process (GO:0006524) (Sanderson et al., 2021). We therefore suggest that both MurI and K562_RS27665 are each able to synthesize enough D-glutamate for peptidoglycan synthesis, as both were found to be non-essential in K56-2 (Gislason et al., 2017a). It is possible that inhibition of Alr/DadX/Ddl by CYC renders the peptidoglycan biosynthesis pathway highly susceptible to further disruption, or that MurI and K562_RS27665 are themselves inhibited by CYC. Together, these results hint at the fine balance of D-amino acid metabolism required for peptidoglycan synthesis.

As the primary target of the β-lactams are penicillin-binding proteins (PBPs), we also expected that disruption of specific PBPs may expose weaknesses in peptidoglycan matrix biosynthetic processes. The PBP targets of the β-lactams used here have not been determined for *Burkholderia* species; thus, we drew on similarities to other Gram-negative pathogens (Asli et al., 2016; Davies et al., 2008; Ito et al., 2017; Papp-Wallace et al., 2012; Sanders et al., 1997; Sutaria et al., 2018) (Figure 1). We observed that disruption of only two PBP-encoding genes altered β-lactam susceptibility: K562_RS05010 (encoding a homologue of the DacB DD-carboxypeptidase, also called PBP4) and K562_RS01445 (encoding a high-identity homologue of *E. coli mrcA/pbp1a* we are referring to as *mrcA2*) (Figure 16A). Only a disruption in *dacB* resulted in very low fitness in the presence of AVI-H and MEM. Only a disruption in *mrcA2* impaired fitness in the presence of AZT, TAZ, CYC, FOS, and CFD. Transposon disruptions in either *mrcA2* and *dacB* increased susceptibility to CTT, CAZ-H, and AVI/CAZ (Figure 16A). Upon CRISPRi knockdown of *dacB*, we found that susceptibility only increased to MEM, AVI, and AVI/CAZ. These were the conditions in the BarSeq experiment that resulted in the greatest fitness defect when *dacB* was disrupted.

Notably, the findings from our BarSeq experiment contrast results obtained in *P. aeruginosa* (Moya et al., 2009), *Yersinia enterocolitica* (Liu et al., 2017a), and *Aeromonas hydrophila* (Tayler et al., 2010), which show that inactivation of DacB causes β-lactam resistance. In *P. aeruginosa*, the disruption of DacB leads to activation of AmpR and the CreBC/BlrAB two-

component system, resulting in AmpC overexpression (Moya et al., 2009). Disruption of the K56-2 CreBC/BlrAB homologues (K562_RS27235-40) did not affect fitness in any condition tested here (Supplemental Data 1). Overall, we suggest that DacB, and the consequences of its inactivation, may play a different physiological role in *B. cenocepacia*.

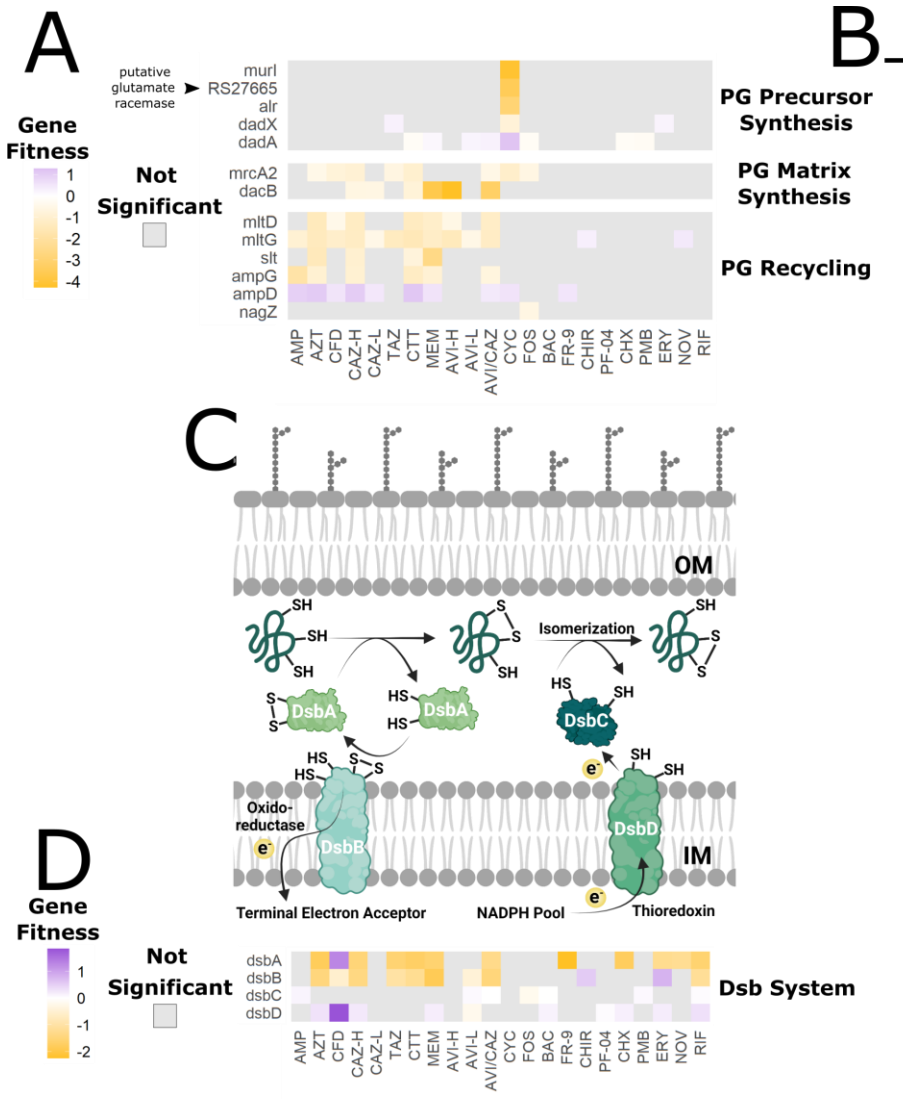

B

Antibiotic	Gene	MIC (µg/mL) -Rha	MIC (µg/mL) +Rha
AMP	NTC	>512	>512
	dacB	>512	>512
	ampD	>512	>512
	slt	>512	>512
AZT	NTC	512	512
	dacB	512	512
	ampD	512	512
	slt	512	**32**
CFD	NTC	0.25	0.25
	dacB	0.25	0.25
	ampD	0.25	**0.5**
	slt	0.25	0.25
CAZ	NTC	32	32
	dacB	32	32
	ampD	32	**64**
	slt	32	**8**
TAZ	NTC	128	128
	dacB	128	128
	ampD	128	128
	slt	128	**32**
CTT	NTC	64	64
	dacB	64	64
	ampD	64	64
	slt	64	**16**
MEM	NTC	16	16
	dacB	16	**4**
	ampD	16	**32**
	slt	16	**8**
AVI	NTC	>256	>256
	dacB	>256	**64**
	ampD	>256	>256
	slt	>256	**128**
AVI/CAZ*	NTC	4	4
	dacB	4	**2**
	ampD	4	**8**
	slt	4	**2**

Figure 16. Chemical genetic interactions with periplasmic processes (peptidoglycan synthesis and the DSB system). A) Gene fitness scores relative to DMSO control of the genes encoding peptidoglycan precursor and matrix synthesis, and peptidoglycan recycling. B) MIC values of K56-2::dCas9 harbouring plasmids expressing a non-targeting sgRNA control (NTC) or an sgRNA targeting the indicated genes. Rhamnose induces dCas9 expression. MIC values are medians of three biological replicates, with bold indicating at least 2-fold change with the addition of rhamnose. * AVI was kept constant at 8 µg/mL. C) Periplasmic disulfide bond formation by DsbAB and isomerization by DsbCD (Landeta et al. 2018). D) Gene fitness scores relative to the DMSO control of the genes in the DSB system.

5.1.3.2 Deficiencies in peptidoglycan recycling cause susceptibility to β-lactams

Peptidoglycan recycling and trimming occur simultaneously with peptidoglycan synthesis, and has substantial implications for β-lactam resistance. In *E. coli*, a variety of endopeptidases, lytic transglycosylases, and transporters are required for peptidoglycan recycling (Dik et al., 2018). Lytic transglycosylases and endopeptidases cleave (muro)peptides from peptidoglycan chains, which are then transported into the cell for recycling (Dik et al., 2018). Peptidoglycan lytic enzymes are thought to mediate protection from β-lactams in *E. coli* by removing aberrant peptidoglycan crosslinks formed by β-lactam-poisoned PBP complexes (Cho et al., 2014) and in *Vibrio cholerae* by site-specific trimming activity that prevents cell lysis (Dörr et al., 2015). While very little is known about peptidoglycan recycling in *Burkholderia*, analysis of the BarSeq data for homologues of genes putatively associated with peptidoglycan recycling revealed several as important for fitness in the presence of β-lactams. Disruptions in *slt* (encoding a soluble lytic transglycosylase), and in *mltD* and *mltG* (each encoding a membrane-bound lytic transglycosylase) all resulted in susceptibility to many β-lactams, but not the early peptidoglycan synthesis inhibitors CYC and FOS (Figure 16A). To validate our findings from the BarSeq experiment, we silenced *slt* with CRISPRi, which increased susceptibility to AZT, CAZ, CTT, MEM, TAZ, AVI/CAZ, and AVI (Figure 16B). Silencing *slt* expression did not cause a growth defect in the absence of antibiotics (Figure A28). While other endopeptidases and transglycosylases are encoded in K56-2 in addition to *slt*, *mltD*, and *mltG*, they did not contribute to fitness in the conditions used for the BarSeq experiment, perhaps due to partial functional redundancy, as recently demonstrated in *V. cholerae* (Weaver et al., 2022).

The balance of various peptidoglycan degradation products has important implications for β-lactamase expression. In the model *Citrobacteri freundii*, β-lactam exposure causes lytic enzymes to liberate GlcNAc-anhydroMurNAc-pentapeptide fragments, which enter the cytoplasm through the AmpG permease (Jacobs et al., 1994) then are processed by NagZ into anhydroMurNAc-pentapeptide, then into anhydroMurNAc by AmpD (Jacobs et al., 1995). The AmpR transcriptional activator of β-lactamase genes binds both the substrate and product of NagZ, but not the product of AmpD (Balcewich et al., 2010; Bartowsky and Normark, 1991); thus, AmpD activity reduces β-lactamase expression. In *B. cenocepacia*, while mutations in *ampD* are known to confer β-lactamase resistance (Hwang and Kim, 2015), the contributions of AmpG have not been experimentally characterized. Here, we observed that disruption of *ampG* increased

susceptibility to many β-lactams, while disruption of *ampD* reduced susceptibility to many β-lactams and no effect was observed with disruption of *nagZ* (Figure 16A). Upon silencing of *ampD* with CRISPRi, susceptibility was reduced to AZT, AVI/CAZ, CAZ, CFD, and MEM, (Figure 16B). Knocking down *ampD* did not produce a growth defect in the absence of antibiotics (Figure A28). Our findings support the role of AmpG as a permease for peptidoglycan degradation products, and of AmpD as reducing the accumulation of anhydroMurNAc-pentapeptides in K56-2. Moreover, as disruption of NagZ did not alter susceptibility, PenR (the *Burkholderia* homologue of AmpR discussed further in *Section 5.1.4.2*) is likely activated by both GlcNAc-anhydroMurNAc-pentapeptide and anhydroMurNAc-pentapeptide.

5.1.3.3 The DSB system of periplasmic disulfide bond formation

The folding and stability of secreted proteins is aided by disulfide bond (DSB) formation via the periplasmic DSB system. In *E. coli*, this system is encoded by four genes organized in two pathways, the DsbAB pathway and the DsbCD pathway, required for efficient disulfide bond formation and isomerization, respectively, in periplasmic proteins (Figure 16C) (Landeta et al., 2018). Reports from the pre-genomic era have associated DsbAB in *Burkholderia* with pleiotropic effects on protease activity, motility, and resistance to multiple antibiotics (Abe and Nakazawa, 1996; Hayashi et al., 2000). We confirmed that disruptions in *dsbA* and *dsbB* resulted in large changes in susceptibility to many β-lactams and large scaffold antibiotics, while disruptions in *dsbC* and *dsbD* did little to alter the susceptibility profile (Figure 16D). B-lactamases have previously been implicated as substrates of DsbA in *P. aeruginosa* (Furniss et al., 2022), and we suggest this as the cause of susceptibility to most β-lactams used here. Consequently, the susceptibility to avibactam was not affected by disruptions in the Dsb system (Figure 16D), likely because avibactam is not effectively degraded by *Burkholderia* β-lactamases (Papp-Wallace et al., 2017). Additionally, given the susceptibility to non-β-lactam antibiotics (e.g. ERY, CHX, NOV), the Dsb system may be important for the function of other resistance mechanisms, such as efflux pumps (Hayashi et al., 2000; Vezina et al., 2020).

5.1.4 The interconnection of cell envelope processes opens avenues for overcoming β-lactam resistance

5.1.4.1 Antagonizing undecaprenyl phosphate recycling causes β-lactam susceptibility, hinders growth, and affects cell morphology

Polysaccharides are important structural and functional components of bacterial cell envelopes, including exopolysaccharides, the O-antigen, peptidoglycan, and protein *O*-glycosylation. From the BarSeq data, we observed that mutants with disruptions in LPS/O-antigen synthesis (e.g. *hldD*, *wbiGH*, and K562_RS30805) and protein glycosylation (e.g. *ogcABE* and *pglL*) had altered susceptibility to several β-lactam antibiotics (Figure 14E, 17A, and A22). To examine if defects in outer membrane permeability were the source of increased antibiotic susceptibility, we again turned to the NPN uptake assay. Genes/operons highlighted by the BarSeq experiment were targeted for silencing by CRISPRi. We found that knockdown of genes related to LPS core and O-antigen synthesis and protein glycosylation did not significantly impair outer membrane integrity (Figure 17B), except for *hldD* which was in line with the effect observed for *hldD* deletion (Figure 14G). Thus, increased antibiotic susceptibility is not simply due to increased antibiotic influx alone.

Closer examination revealed that cell envelope glycan pathways are linked by the shared lipid carrier UndP (Figure 17C) (Manat et al., 2014). In *E. coli*, both *de novo* UndP synthesis and UndP recycling are essential for viability (Baba et al., 2006; El Ghachi et al., 2005). As a carrier, UndP is recycled after a cleavage step removes the linked glycans. UndP intermediates are present at low levels in Gram-negative membranes (<1% of total membrane lipids) (Barreteau et al., 2009; Trent et al., 2001a; Wang et al., 2009). Previous reports in *E. coli* and *Shigella flexneri* have found that disruptions in O-antigen and enterobacterial common antigen pathways cause morphological defects (Jorgenson and Young, 2016; Jorgenson et al., 2016; Maczuga et al., 2022). It was suggested that disruptions cause pathway intermediate accumulation and prevent UndP recycling, thus sequestering UndP away from the essential process of peptidoglycan synthesis.

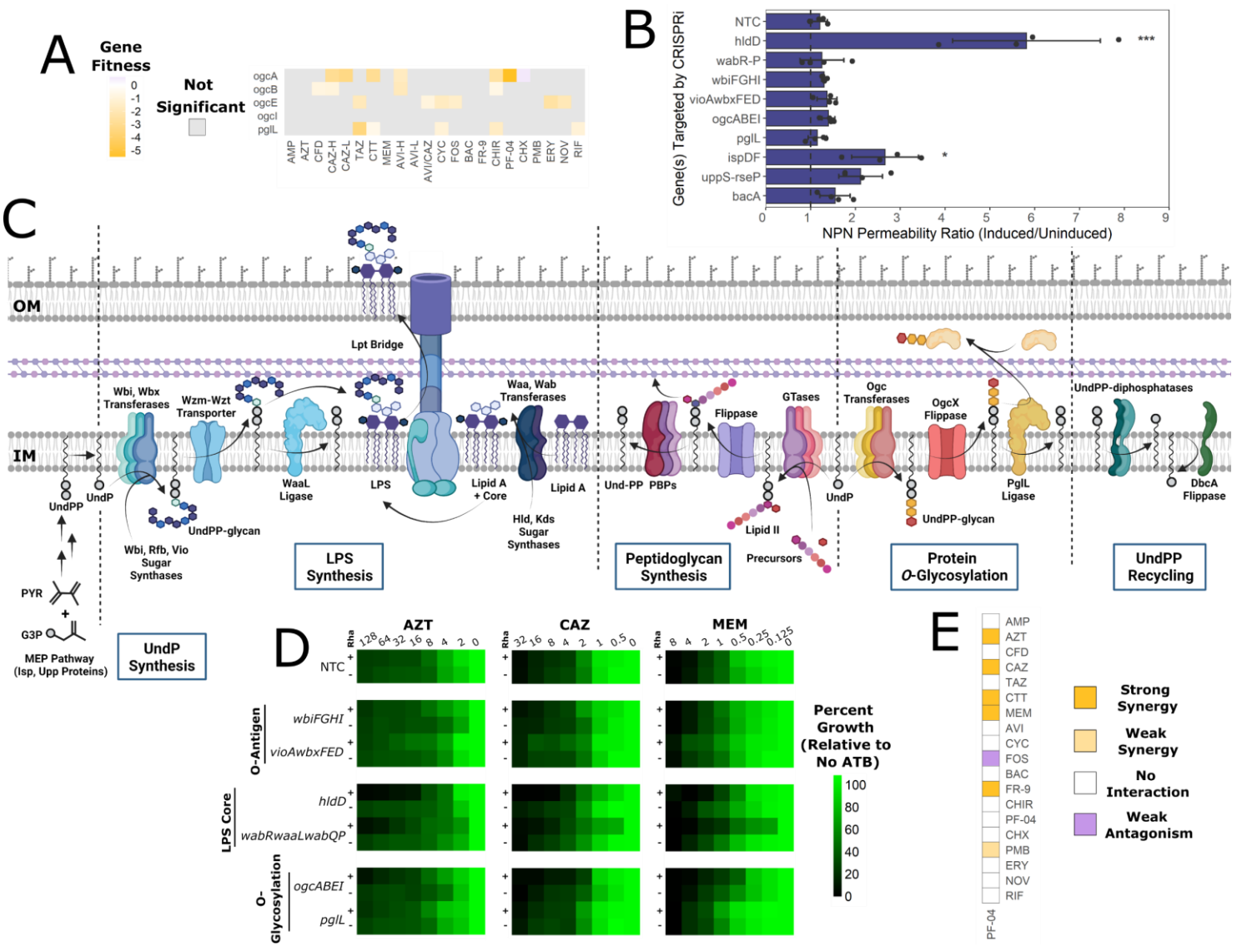

Figure 17. Defects in UndP utilization pathways sensitize cells to β-lactams. A) Gene fitness scores relative to the DMSO control of the genes in the protein *O*-glycosylation (Ogc) pathway. B) Ratios of NPN fluorescence of the CRISPRi mutants in inducing vs uninducing conditions. Error bars represent means ± SD of four replicates. Significance was determined by 1-way ANOVA with Dunnett's *post hoc* test to the wild-type control. * $P < 0.05$; *** $P < 0.001$. The dashed lines indicate a NPN fluorescence ratio of 1. C) Summary of the major UndP metabolic pathways in *B. cenocepacia* (from experimental evidence and inferred by homology), annotated with proteins names if they are known (Egan 2020; Manat et al. 2014; Mohamed et al. 2019; Ortega et al. 2005, 2009; Roney and Rudner 2022; Valvano 2015). The Ara4N modification is shown in Figure 14H. UndPP is synthesized in the cytoplasm by the methylerythritol phosphate (MEP) pathway then dephosphorylated to UndP. UndP is a lipid carrier for construction of the O-antigen, peptidoglycan building blocks (in the form of lipid I and II), and the protein *O*-glycan. After use as a carrier, UndPP is liberated and recycled into UndP on the cytoplasmic leaflet. IM = inner membrane, OM = outer membrane. D) Antibiotic dose responses (μg/mL) of growth of CRISPRi mutants with or without induction with 0.5% rhamnose. Values are normalized to the OD600 of growth without antibiotic. NTC = non-targeting control sgRNA. E) Summary of antibiotic checkerboard interaction assay with PF-04. Interactions were assessed and interpreted with SynergyFinder as per the Materials and Methods.

While inhibition of *de novo* UndP synthesis renders *B. cenocepacia* and *E. coli* cells more susceptible to β-lactams (Jorgenson et al., 2019; Sass et al., 2018), the link between UndP utilization pathways and β-lactam susceptibility has not been examined. We reasoned that due to the connection with peptidoglycan synthesis, disruptions preventing or reducing the efficiency of UndP recycling would increase susceptibility to the β-lactams, FR-9, and BAC. Supporting this hypothesis, in the competitive conditions of the BarSeq experiment, disruption of *dbcA*, encoding a UndP flippase important for UndP recycling, resulted in susceptibility to β-lactams, FR-9, and BAC (Figure 14E and A22). To validate the findings of the BarSeq experiment, we assessed susceptibility of CRISPRi mutants in genes related to LPS core and O-antigen synthesis and protein glycosylation to AZT, CAZ, and MEM, as representatives of the β-lactams. Susceptibility to subinhibitory concentrations of AZT, CAZ, and MEM increased upon knockdown of cytoplasmic steps in the protein *O*-glycosylation pathway (encoded by *ogcABEI*) and LPS core synthesis (encoded by *hldD* and *wabRwaaLwabQP*) (Figure 17D). Knockdown of LPS core synthesis genes may cause an accumulation of UndP-O-antigen intermediates in the periplasm as the O-antigen cannot be ligated to a heavily truncated core, thus possibly reducing UndP recycling. To support our genetic evidence for the interactions among UndP utilization pathways, we leveraged antibiotics as inhibitors of specific processes in checkerboard assays. We used the LpxC inhibitor PF-04, which prevents lipid A formation. We reasoned that exposing cells to PF-04 may cause accumulation of UndP-O-antigen intermediates in the periplasm, similar to knockdown of core biosynthetic genes *hldD* and *wabRwaaLwabQP*. Indeed, PF-04 strongly synergized with MEM, CTT, CAZ, AZT, and the isoprenoid synthesis inhibitor FR-9 (Figure 17E). Interaction with FR-9 suggests PF-04 may cause sequestration of UndP-linked intermediates, while the resulting stress on peptidoglycan synthesis is supported by synergism of PF-04 with the β-lactams. We argue that the observed synergy was not likely due to increased outer membrane permeability as PF-04 did not synergize with the large scaffold antibiotics ERY, NOV, or RIF.

When we silenced LPS core and *O*-glycosylation genes, we noticed that the antibiotic susceptibility profiles were very similar, regardless of the β-lactam used (Figure 17D). This may indicate an independence from which peptidoglycan synthesis complex is targeted and instead points to an interaction with UndP levels itself. If UndP sequestration causes β-lactam susceptibility by reducing flux through peptidoglycan synthesis, we also expect that reducing the

total amount of UndP would produce a similar effect. To achieve this, we targeted *ispDF* (encoding early genes in isoprenoid/UndP synthesis) and *uppS* (also called *ispU*, encoding UndPP synthase) with CRISPRi. As *uppS* is an essential gene and repression strongly suppresses growth (Figure A28), we carefully titrated the concentration of rhamnose to suppress growth by 20-30% for further assays. Indeed, knockdown of *ispDF* and *uppS* increased susceptibility to AZT, CAZ, and MEM (Figure 18A). However, knockdown of *ispDF* moderately increased membrane permeability (Figure 17B), suggesting that the β-lactam susceptibility of that mutant may be partly due to increased antibiotic influx. In addition to genetically depleting levels of UndP, we also investigated antibiotic interactions with FR-9 and BAC. FR-9 is an inhibitor of Dxr, which catalyzes an early step in isoprenoid biosynthesis (Kuzuyama et al., 1998), while BAC binds UndPP and prevents its recycling (Siewert and Strominger, 1967) (Figure A18). FR-9 strongly synergized with many β-lactams and BAC (Figure 18B), demonstrating that double targeting at different points within UndP metabolic pathways greatly increases the inhibitory effect. BAC strongly antagonized the activity of most β-lactams (Figure 18B). However, we found the antagonism not due to BAC itself, but by two components of the solution: 1) the acidic pH required to solubilize high concentrations of BAC, and 2) the 1:1 formulation with Zn^{2+} that is required for BAC to bind UndPP (Economou et al., 2013) (Table A2). Acidic pH has been found in *E. coli* to reduce β-lactam susceptibility (Goodell et al., 1976; Mueller et al., 2019), and we suggest that high levels of Zn^{2+} may activate metallo-β-lactamases (Karsisiotis et al., 2014) in K56-2. Overall however, both chemical and genetic evidence supports our assertion that depletion of free UndP pools causes β-lactam susceptibility.

A

Antibiotic	Gene	MIC (μg/mL) -Rha	+Rha
AZT	NTC	256	256
	ispDF	256	**32**
	uppS	256	**64**
CAZ	NTC	32	32
	ispDF	32	**8**
	uppS	32	**16**
MEM	NTC	16	16
	ispDF	16	**8**
	uppS	16	**8**

B

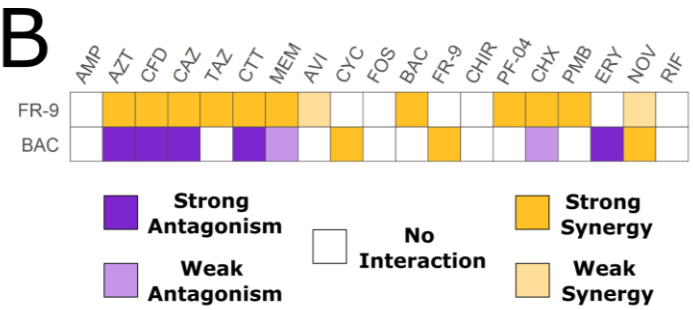

Figure 18. Inhibiting isoprenoid and UndP synthesis sensitizes cells to β-lactams. A) MIC values of K56-2::dCas9 harbouring plasmids expressing a non-targeting sgRNA control (NTC) or an sgRNA targeting the indicated genes. Rhamnose induces dCas9 expression. MIC values are medians of three biological replicates, with bold indicating at least 2-fold change with the addition of rhamnose. B) Summary of antibiotic checkerboard interaction assay with FR-9 and BAC. Interactions were assessed and interpreted with SynergyFinder as per the Materials and Methods.

Following the BarSeq experiment, we expected that mutants in the O-antigen synthesis operons *wbiFGHI* and *vioAwbxFED* would be more susceptible to β-lactams; however, the CRISPRi mutants we constructed displayed no change in susceptibility. As CRISPRi silencing is polar, we decided to create unmarked deletion mutants in six genes (*bacA, bceB, wzm-wzt, waaL, hldD* and *wbiI*) to link phenotype to individual genes.The K56-2::dCas9 background was used to permit additional perturbation with CRISPRi. BacA has a role in UndP recycling as the major UndPP phosphatase responsible for 75% of that activity in *E. coli* (El Ghachi et al., 2004). BceB is the initiating enzyme for cepacian synthesis, an exopolysaccharide also built on the UndP carrier (Ferreira et al., 2011). Wzm and Wzt are components of the ABC-type transporter that translocates the UndPP-linked O-antigen to the periplasmic leaflet. The encoding genes *wzm* and *wzt* are adjacent and were both deleted. WaaL cleaves the O-antigen from UndPP and ligates the glycan chain to the LPS core (Ortega et al., 2009). In *E. coli*, cells with blockages in UndP utilization pathways develop severe morphological defects and frequently lyse (Jorgenson and Bryant, 2021; Jorgenson and Young, 2016). However, we found in K56-2 that either individual deletion or overexpression of *bacA, bceB, wzm-wzt, waaL, hldD* and *wbiI* resulted in only minor growth reductions and no major cell morphology defects, except for overexpression of *wbiI* (Figure A31).

We thus hypothesized that the physiology of K56-2 may be more robust to UndP metabolism disruptions than that of *E. coli*, which has been used previously as a model. To enhance stress on UndP metabolism and peptidoglycan synthesis we constructed double mutants to trigger synthetic genetic interactions. In deletion mutant backgrounds, we selected genes for silencing with CRISPRi or overexpression from a plasmid and then assessed growth. As UndP is an essential molecule for peptidoglycan synthesis, perturbations that further reduce UndP availability would be expected to inhibit growth (synthetic lethality/sickness). Supporting a block in UndP metabolism, the Δ*hldD* and Δ*waaL* mutants were more susceptible to knockdown of *ispDF* and *uppS*, and to overexpression of *wbiI* (Figure 19A and B). Despite overexpression of *wzm-wzt* causing only moderate growth defects in the Δ*waaL* mutant, we observed morphological changes such as bulging that are indicative of defects in the peptidoglycan matrix (Figure 19C). Overall, we have shown by complementary chemical, genetic, and physiological methods that disruption of UndP synthesis and utilisation pathways increases susceptibility to β-lactams. We propose a tentative model to fit our results within the literature (Figure 19D)

(Jorgenson et al. 2016, 2019; Jorgenson and Young 2016). In wild-type cells, recycling is important to replenish the UndP pools available for the essential process of peptidoglycan synthesis (Figure 19D). However, blockages in UndP utilisation cause sequestration of UndP-glycan intermediates, reducing the efficiency of recycling and the levels of free UndP available. We then reason that impaired peptidoglycan synthesis results in a weaker matrix and increases susceptibility to β-lactams.

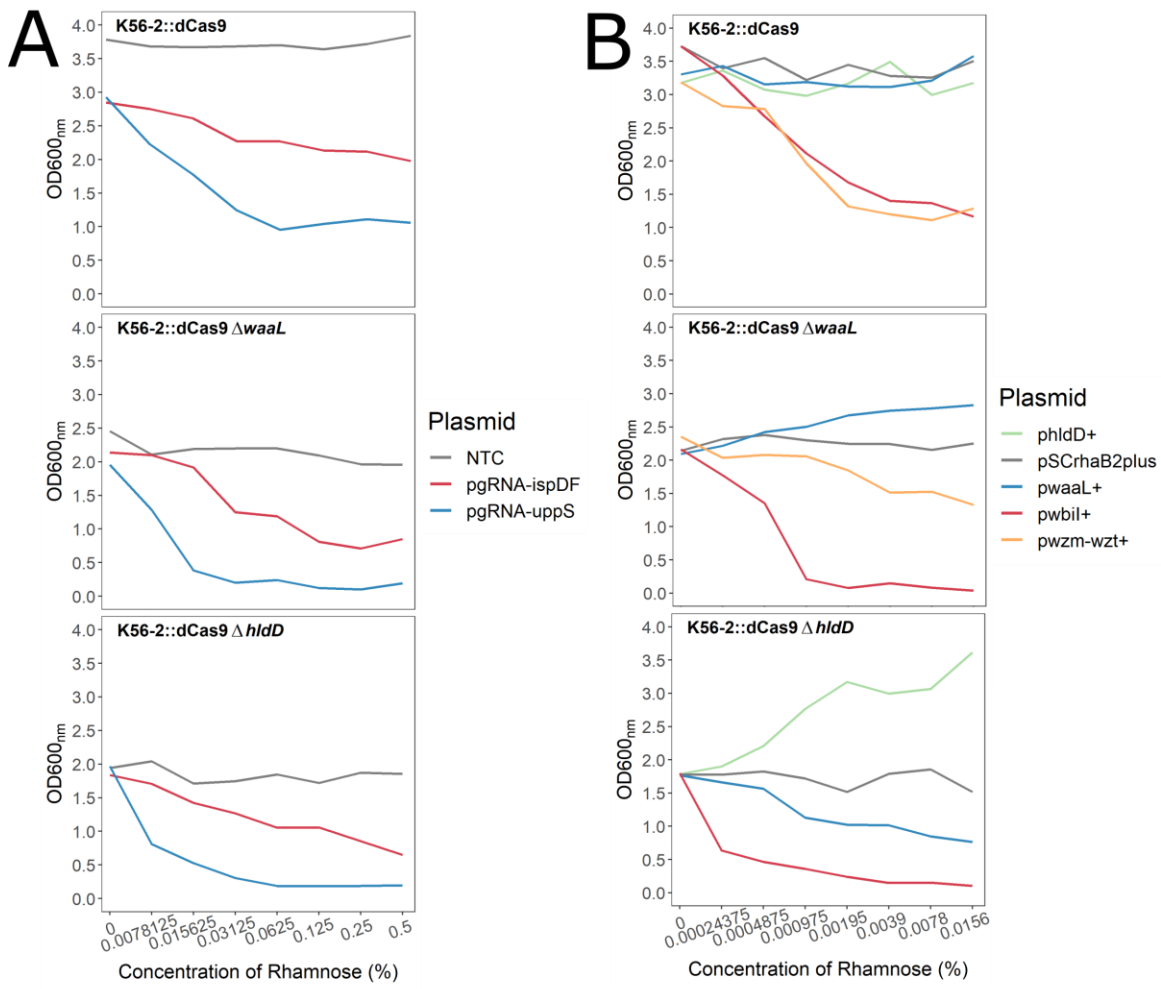
A
K56-2::dCas9
K56-2::dCas9 ΔwaaL
K56-2::dCas9 Δ hldD
OD600nm
Concentration of Rhamnose (%)
0
0.0078125
0.015625
0.03125
0.0625
0.125
0.25
0.5
Plasmid
NTC
pgRNA-ispDF
pgRNA-uppS
B
K56-2::dCas9
K56-2::dCas9 ΔwaaL
K56-2::dCas9 Δ hldD
OD600nm
Concentration of Rhamnose (%)
0
0.00024375
0.0004875
0.000975
0.00195
0.0039
0.0078
0.0156
Plasmid
phldD+
pSCrhaB2plus
pwaaL+
pwbil+
pwzm-wzt+

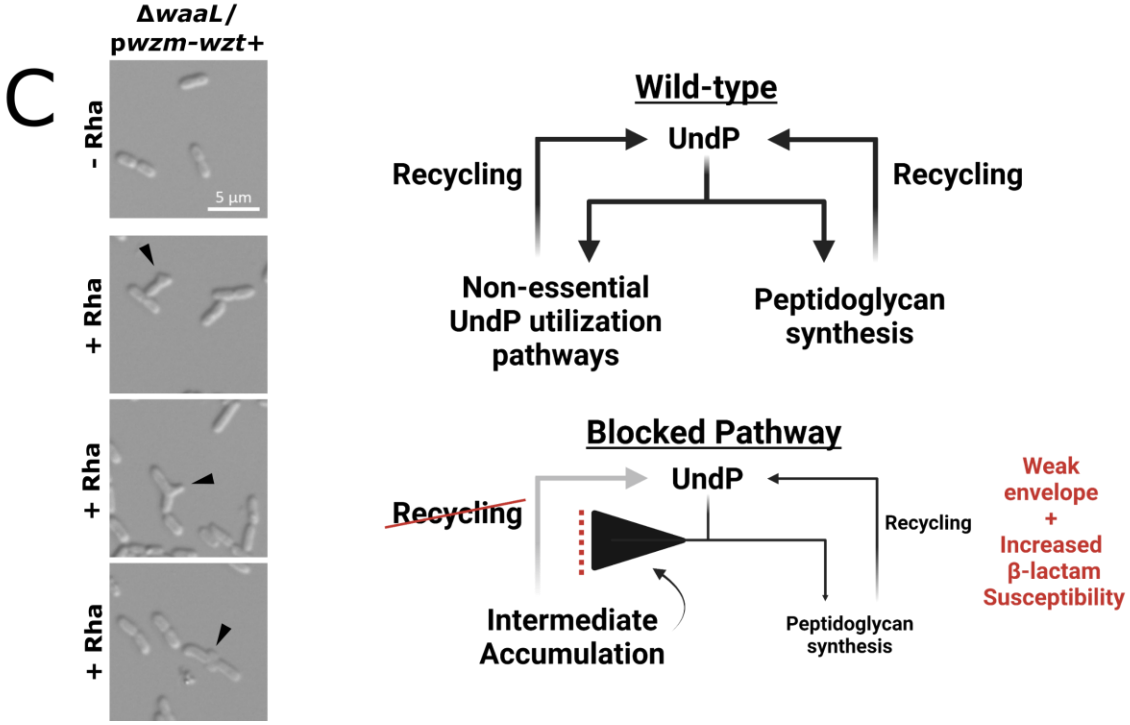
C
ΔwaaL/
pwzm-wzt+
- Rha
+ Rha
+ Rha
+ Rha
5 µm
Wild-type
UndP
Recycling
Recycling
Non-essential
UndP utilization
pathways
Peptidoglycan
synthesis
Blocked Pathway
UndP
Recycling
Recycling
Intermediate
Accumulation
Peptidoglycan
synthesis
Weak
envelope
+
Increased
β-lactam
Susceptibility

Figure 19. Growth and morphology of double mutants support a model that UndP sequestration causes defects in peptidoglycan synthesis. Cultures of deletion mutants with A) CRISPRi plasmids or B) overexpression plasmids were grown with the indicated concentrations of rhamnose for 18 hours, the time at which the control strains reached the maximum OD_{600}. Panels are organized by mutant background: Values shown are averages of three biological replicates. C) Mid exponential phase cells of the Δ*waaL*/p*wzm-wzt+* mutant were induced with 0.05% rhamnose for 3 hours then immobilized on 1% agarose pads and imaged by DIC at 100x magnification. The black arrowheads mark morphological abnormalities such as bulging. D) Framework for how disruptions in UndP metabolism reduce UndP recycling and flux into peptidoglycan synthesis, weakening the peptidoglycan matrix and increasing β-lactam susceptibility.

5.1.4.2 TnSeq reveals the basis for β-lactam/avibactam synergy and rationalizes new effective combinations

AVI/CAZ is a current front-line treatment for many infections caused by multidrug-resistant Gram-negative bacteria. The synergy of the combination is due to avibactam inhibiting a broad spectrum of β-lactamases that degrade ceftazidime (Ehmann et al., 2012; Lahiri et al., 2014). Studies on *Burkholderia* β-lactamases have focused on the Ambler class C AmpC β-lactamase and the Ambler class A PenB carbapenemase, of which only PenB is inhibited by AVI (Becka et al., 2018; Poirel et al., 2009). However, K56-2 encodes a further 19 putative β-lactamases, and it is unknown how each contributes to β-lactam resistance and if they are inhibited by AVI.

If the targets of AVI are the β-lactamases that degrade CAZ, transposon mutants of said β-lactamases would have a fitness defect in the presence of CAZ because CAZ cannot be degraded. The same mutants would also have no fitness differences between AVI/CAZ and the DMSO control because in either case the β-lactamase target is chemically inhibited or genetically disrupted (Figure 20A). Using the data from our BarSeq experiment, we compared pairs of conditions involved in the AVI/CAZ combination to identify genes important for fitness in one or both of the constituent conditions. For all comparisons, there were more genes unique to each condition than shared between any two, highlighting strong concentration-dependent physiological effects, even for the same antibiotic (Figure A32). Pair-wise comparison also revealed that bla_{PenB} and K562_RS32470 (encoding a putative metallo-β-lactamase (MBL); Pfam 00753) were only important for fitness with CAZ-H, and not once AVI is added (Figure A32). Importantly, neither disruption of bla_{PenB} nor K562_RS32470 affected fitness in AVI or AVI/CAZ (Figure 20B). K56-2 encodes up to 19 other β-lactamases, including the PenR-regulated *ampC*; however, only *penB* and K562_R S32470 were important for fitness in any condition tested here (Supplementary Data 1). Together, our findings suggest that PenB and K562_RS32470 are the only targets of AVI in K56-2.

We next asked whether bla_{PenB}, K562_RS32470, and *penR* (the regulator of bla_{penB}) contribute to resistance against other β-lactam antibiotics. Disruptions in *penR*, bla_{PenB}, and K562_RS32470 increased susceptibility to AZT, AMP, CAZ-H, and MEM (Figure 20B). Notably, neither disruption increased susceptibility to CFD, and only a disruption in *penR* increased susceptibility to CTT. Although K562_RS32470 is annotated as an MBL, the

interactions with AVI and AZT make us question this assignment. AZT is a poor substrate for most MBLs (Felici et al., 1993; Lohans et al., 2017), and MBL activity is not generally inhibited by AVI (Abboud et al., 2016), both of which seem to contradict our findings. However, we did not conduct further experiments to investigate this.

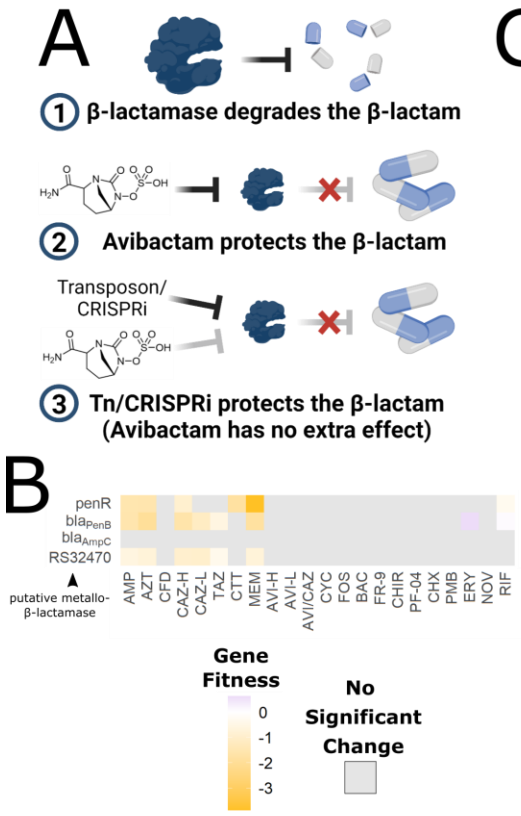

C

Antibiotic	Gene	MIC (μg/mL) -Rha	MIC (μg/mL) +Rha	Fold MIC†
AVI	NTC	>128	>128	-
	penR	>128	>128	-
	bla_{AmpC}	>128	>128	-
	bla_{PenB}	>128	>128	-
AZT	NTC	256	256	1
	penR	256	64	**4**
	bla_{AmpC}	256	256	1
	bla_{PenB}	256	**8**	**32**
AVI/AZT*	NTC	8	8	1
	penR	8	**4**	**2**
	bla_{AmpC}	8	8	1
	bla_{PenB}	8	**4**	**2**
CAZ	NTC	32	32	1
	penR	32	**8**	**4**
	bla_{AmpC}	32	32	1
	bla_{PenB}	32	**8**	**4**
AVI/CAZ*	NTC	4	4	1
	penR	4	4	1
	bla_{AmpC}	4	4	1
	bla_{PenB}	4	4	1
MEM	NTC	16	16	1
	penR	16	**4**	**4**
	bla_{AmpC}	16	16	1
	bla_{PenB}	16	**2**	**8**
AVI/MEM*	NTC	2	2	1
	penR	2	2	1
	bla_{AmpC}	2	2	1
	bla_{PenB}	2	2	1

Figure 20. PenB is the predominant β-lactamase in K56-2 and is inhibited by AVI. A) Rationale for identifying targets of AVI. If a target is disrupted with a transposon or repressed with CRISPRi there will be no change in β lactam MIC when AVI is added B) Gene fitness scores relative to the DMSO control of β-lactamase and regulatory genes. C) MIC values of K56-2::dCas9 harbouring plasmids expressing a non-targeting sgRNA control (NTC) or an sgRNA targeting the indicated genes. Rhamnose induces dCas9 expression. MIC values are medians of three biological replicates, with bold indicating at least 2-fold change with the addition of rhamnose. † Fold MIC is the ratio of the MIC -Rha to the MIC +Rha. * AVI kept constant at 8 μg/mL

To validate our BarSeq findings, we first examined the contributions of previously characterized AmpR-regulated genes *bla*$_{\text{AmpC}}$ and *bla*$_{\text{PenB}}$ (Hwang and Kim, 2015; Trépanier et al., 1997) to β-lactam susceptibility using CRISPRi. In the absence of antibiotics, neither were important for growth (Figure A28). Knockdown of *bla*$_{\text{AmpC}}$ did not increase susceptibility to any of the tested β-lactams (Figure 20C). On the other hand, knockdown of *bla*$_{\text{PenB}}$ resulted in marked susceptibility to AMP, TAZ, CAZ, AZT, and MEM (up to 32-fold reduction in MIC) (Figure 20C and Table A11). We reasoned that if PenB is the major β-lactamase responsible for the degradation of CAZ, AZT, and MEM, then knockdown of *bla*$_{\text{PenB}}$ would result in the same MIC as adding AVI. In other words, the cells would be "blind" to the addition of AVI as the primary target is already knocked down. Indeed, in the presence of AVI, there was no change in MIC upon *bla*$_{\text{PenB}}$ knockdown for CAZ and MEM (Figure 20C). For the AVI/AZT combination, knockdown of *penB* still reduced the MIC by 2-fold, suggesting that in the absence of PenB, K562_RS32470 may have a minor contribution to AZT resistance. Taken together, these results demonstrate that in K56-2, PenB is the predominant β-lactamase responsible for degrading clinically relevant β-lactams. Our findings also demonstrate that BarSeq can be used to elucidate the mechanisms and targets of antibiotic potentiation.

The marked β-lactam susceptibility of knockdown mutants in *bla*$_{\text{PenB}}$, together with the ability of avibactam to inhibit PenA-family β-lactamases in *Burkholderia* species (Zeiser et al., 2019b), suggested a broader applicability of AVI/AZT and AVI/MEM combinations. AVI/AZT and AVI/MEM are not commonly used to treat Bcc respiratory infection. We assembled a panel of 20 clinical Bcc isolates (including *B. gladioli*) spanning the last two decades and representing the most commonly recovered species across three Canadian provinces (British Columbia, Manitoba, and Ontario). We also included isolates of other CF pathogens: *P. aeruginosa*, *Achromobacter xylosoxidans*, and *Stenotrophomonas maltophilia*. Susceptibility to AZT, MEM and CAZ was assessed with and without 8 μg/mL AVI (Table A12). For the three non-Bcc species, there was minimal potentiation by AVI, except with AZT against *S. maltophilia*. Among Bcc species, MIC values of the β-lactams alone varied widely: 4 – >128 μg/mL for AZT; 1 – 32 μg/mL for MEM; 2 – 32 μg/mL for CAZ. Potentiation by AVI was strongest for AZT and MEM (up to 16-fold MIC reduction) (Figure 21). These trends are in line with the changes in susceptibility upon *bla*$_{\text{PenB}}$ and *penR* knockdown (Figure 20C). Consequently, and in the context of clinical breakpoints, without AVI 12/20 Bcc isolates were resistant to AZT, which was

reduced to 3/20 with AVI. For MEM and CAZ, 8/20 and 4/20 of the Bcc isolates were resistant without AVI, respectively, and all Bcc isolates were sensitive with AVI (Figure 21). For CFD, 3/20 were resistant regardless of AVI addition.

The activity of AZT, CAZ, and MEM was not uniformly potentiated by AVI in all Bcc isolates. Even for K56-2, in which we have demonstrated the importance of PenB, AVI does not potentiate the activity of all β-lactams or even all cephalosporins (Table A13). Moreover, even if AVI potentiated the activity of one β-lactam, it did not guarantee potentiation for the others (Table A12). Thus, although alternative β-lactamases that are not inhibited by AVI may contribute to β-lactam resistance, they likely only play minor roles in most isolates. Overall, our findings suggest that, in addition to AVI/CAZ, combinations of AVI/AZT and AVI/MEM may be valuable therapeutic options for treating Bcc infection. Additionally, as AVI did not strongly potentiate the activity of AZT, CAZ, and MEM in other common CF pathogens (except for AZT against *S. maltophilia*), this highlights the differences in β-lactamase arsenals and demonstrates the need to perform genome-wide investigations in each species to uncover novel resistance mechanisms. Consequently, we suggest that among CF pathogens, combinations of AVI/AZT, AVI/CAZ, and AVI/MEM may be more tailored for use against Bcc infections.

A

	AZT		MEM		CAZ		CFD	
	-AVI	+AVI	-AVI	+AVI	-AVI	+AVI	-AVI	+AVI
Resistant/Total Isolates	12/20	3/20	8/20	0/20	4/20	0/20	3/20	3/20
(% Resistant)	(60%)	(15%)	(40%)	(0%)	(20%)	(0%)	(15%)	(15%)

B

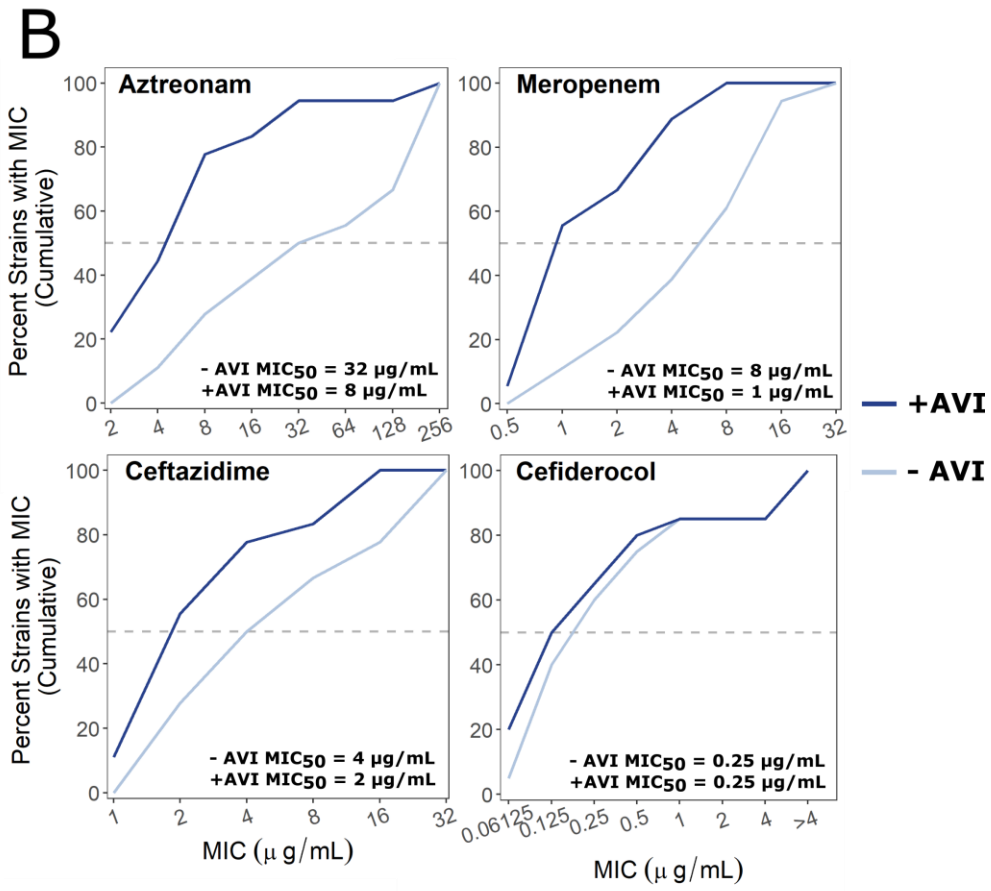

Figure 21. AVI strongly potentiates AZT and MEM in 20 Bcc clinical isolates. A) Percent resistant isolates to AZT, MEM, and CAZ with or without 8 µg/mL AVI. CLSI resistant breakpoints for Bcc: MEM ≥ 16 µg/mL; CAZ ≥ 32 µg/mL. CLSI resistant breakpoint for *Pseudomonas aeruginosa*: AZT ≥ 32 µg/mL; CFD > 4 µg/mL. B) Percent cumulative growth inhibition of 20 Bcc clinical isolates with or without AVI. Data is summarized from Table A12. The dashed line indicates the MIC_{50}, the concentration at which 50% of the isolates were inhibited.

5.1.4.3 Cefiderocol enters K56-2 through a PiuA receptor homologue and requires physiological levels of iron for activity

Cefiderocol is a novel antibiotic with a catechol siderophore conjugated to a cephalosporin structurally similar to ceftazidime. The siderophore chelates ferric iron and enables active transport into cells, resulting in substantially increased potency against a variety of Gram-negative pathogens (Kohira et al. 2016). However, except for a few cases of compassionate care (Shionogi Inc., 2019) and general Gram-negative panels (Hackel et al., 2017, 2018), there are no other reports on the activity of CFD in *Burkholderia* species. We thus tested the susceptibility of the Bcc clinical panel we assembled to CFD. Of the 20 isolates, the MIC_{50} was 0.25 µg/mL and only three (15%) were resistant to CFD (Figure 22 and Table A12), demonstrating very potent activity. Susceptibility of the Bcc isolates was generally not affected by the addition of AVI (Table A12).

To explore the antibiotic mechanism of CFD, we analyzed our BarSeq data for chemical-genetic interactions specific to CFD activity. Broadly, interactions were enriched in pathways related to iron and heme metabolism, which was not observed for other β-lactams (Figures A23-A25). Additionally, disruptions of β-lactamase genes bla_{PenB} and K563_RS32470 did not affect fitness in CFD (Figure 20B). Thus, while the active warhead of CFD is a β-lactam closely related to CAZ, the conjugation with siderophore changes important chemical-genetic interaction signatures.

In *P. aeruginosa*, CFD gains entry into cells by active transport through a variety of TBDRs (Ito et al., 2017; Luscher et al., 2018). Our BarSeq data showed that disruptions in K562_RS04910 (encoding a TonB-related protein) and K562_RS23150 (encoding a homologue of the *P.aeruginosa* PAO1 *piuA* TBDR) reduced susceptibility to CFD (Figure 22A). Of 24 putative TBDRs encoded by K56-2, *piuA* was the only TBDR identified by the screen with significantly enhanced fitness (Supplemental Data 1). We confirmed the link of CFD to *piuA* with a CRISPRi knockdown, which showed reduced susceptibility to CFD (but not the structurally related CAZ) (Figure 22B and C). We then suggest that this TBDR is a receptor for CFD in K56-2. Even with *piuA* knocked down the cells remain much more susceptible to CFD than to the related β-lactam CAZ (MIC of 4 µg/mL vs 32 µg/mL); therefore, we suggest that mutations in *piuA* alone will not result in CFD resistance.

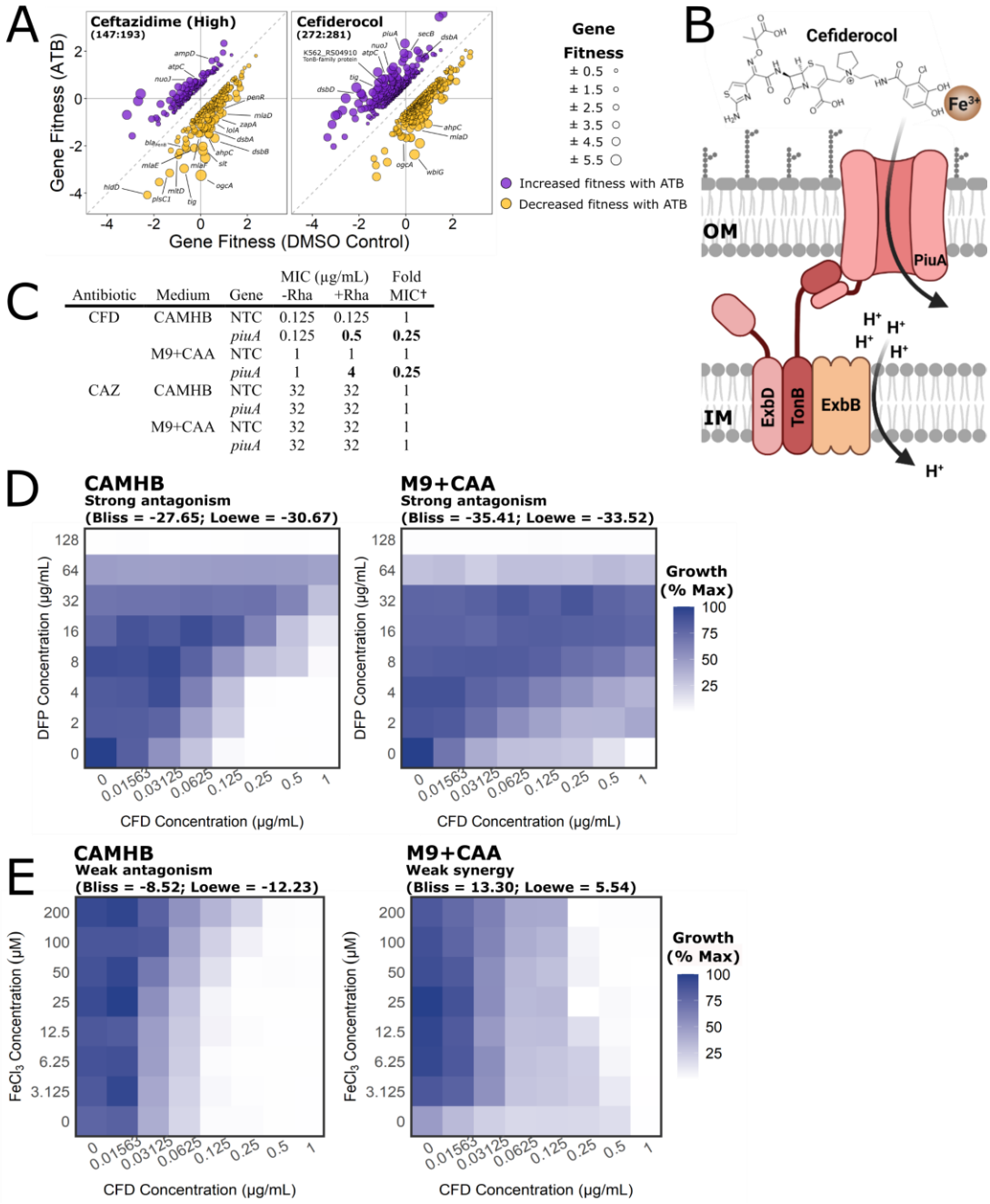

Antibiotic	Medium	Gene	MIC (µg/mL) -Rha	MIC (µg/mL) +Rha	Fold MIC†
CFD	CAMHB	NTC	0.125	0.125	1
		piuA	0.125	**0.5**	**0.25**
	M9+CAA	NTC	1	1	1
		piuA	1	**4**	**0.25**
CAZ	CAMHB	NTC	32	32	1
		piuA	32	32	1
	M9+CAA	NTC	32	32	1
		piuA	32	32	1

Figure 22. CFD uptake in K56-2 is *via* the PiuA siderophore receptor and is strongly dependent on iron concentration. A) Gene fitness profiles of CAZ and CFD from Figure A22. The points are coloured based on positive (increased fitness; purple) or negative (decreased fitness; gold) interactions. B) The catechol group of CFD binds ferric iron (Fe^{3+}) and is recognized by the PiuA siderophore receptor. TonB, in complex with ExbBD, transduces energy from the proton motive force to PiuA for siderophore uptake into the cell. C) MIC values of CRISPRi mutants in *piuA* for CFD and CAZ in CAMHB and M9+CAA medium. NTC = non-targeting control sgRNA.. Rhamnose induces dCas9 expression. MIC values are medians of three biological replicates, with bold indicating at least 2-fold change with the addition of rhamnose. † Fold MIC is the ratio of the MIC -Rha to the MIC +Rha. D) Checkerboard assays of CFD crossed with deferiprone in K56-2 in CAMHB and M9+CAA. E) Checkerboard assays of CFD crossed with $FeCl_3$ in K56-2 in CAMHB and M9+CAA. Values are normalized to the OD_{600} of the well with the most growth. Interactions were assessed and interpreted with SynergyFinder as per the Materials and Methods

Iron is an essential micronutrient for microbial growth and is often growth-limiting in infection settings. In low iron conditions, iron acquisition mechanisms, such as TBDRs, are upregulated (Butt and Thomas, 2017). We thus reasoned susceptibility to CFD in K56-2 inversely correlates with the concentration of iron in the medium, as in *P. aeruginosa* (Luscher et al., 2018). For low-iron medium, we used a minimal medium without added iron (M9 salts + 0.3% low-iron casamino acids; M9+CAA). The concentration of total iron in our batches of M9+CAA and CAMHB was 0.61 µM (± 0.07 µM) and 6.75 µM (± 0.71 µM), respectively, as determined by ICP-MS. Contrary to what was expected, the MIC of CFD in K56-2 was 8-fold higher in M9+CAA than in CAMHB (Figure 22C). Furthermore, the FDA-approved iron chelator deferiprone strongly antagonized CFD in both CAMHB and M9+CAA (Figure 22D). Reduced susceptibility was not due to *piuA* receptor repression, as we observed an additional 4-fold increase in MIC when *piuA* was knocked down in M9+CAA (Figure 22C). These findings suggest that the involvement of *piuA* in CFD activity is independent of iron concentration. As our BarSeq experiment was performed in high iron conditions (rich medium), disruption of other low iron-induced TBDRs important for CFD uptake may not have displayed a fitness change.

The concentration of iron in the sputum of individuals with severe CF is several fold higher than normal lung sputum (18 µM vs. on average 62 µM, but can go up to 125 µM) (Hunter et al., 2013). To address if CFD would be active at these higher iron concentrations, we performed checkerboard assays with CFD and $FeCl_3$. For K56-2, supplementing CAMHB with iron antagonized CFD and raised the MIC by 4-fold at 100 µM $FeCl_3$ (Figure 22E). Conversely, supplementing M9+CAA with iron lowered the MIC to the level observed in CAMHB (Figure 22E). Overall, in K56-2, CFD susceptibility is reduced in both low (< ~5 µM) and high (> ~50 µM) iron conditions, suggesting critical iron concentration thresholds exist for CFD activity. Additionally, despite iron concentration-dependent activity, we note that CFD MIC values are generally well below those of other β-lactams (Table A12), even at the elevated iron concentrations present in CF infection settings.

5.2 Discussion

The alarming rate of antibiotic resistance among Gram-negative organisms requires immediate attention. NGS-based assays provide scalable high-throughput approaches that can be applied to virtually any organism. Chemical-genetic interaction profiles can be created and examined to inform on antibiotic resistance and susceptibility determinants to guide rational antibiotic combinations. Here, using *B. cenocepacia* K56-2 as a model, we measured genome-wide fitness contributions with BarSeq in the presence of 22 antibiotic conditions primarily targeting the cell envelope. Generation of thousands of chemical-genetic interactions allowed confident assignment and validation of over a hundred new functional annotations for many genes not previously associated with antibiotic susceptibility in K56-2. By screening with compounds that target the cell envelope, the majority of the identified factors play roles in cell envelope biogenesis and represent approaches to overcome antibiotic resistance.

High levels of cationic antibiotic resistance in *B. cenocepacia* are suggested to stem from a "two-tier" model involving contributions from LPS and adaptive responses to cell envelope damage (Loutet et al., 2011). We confirmed previous findings that disruptions in many genes along the O-antigen, LPS core, and lipid A modification pathways caused susceptibility to PMB (Hamad et al., 2012; Ortega et al., 2009), and extend this to CHX as well (Figure 6). Together, this demonstrates that the O-antigen, LPS core, and Ara4N modification work together to electrostatically and sterically hinder cationic antimicrobials from accessing their binding sites on lipid A. Furthermore, we extended on the importance of the RpoE cell envelope stress response for PMB and CHX resistance by showing contributions of key components sensing the damage stimulus (*rpoE* and *rseP*) and responding to it (*dnaK* and *surA*) (Figure 6). The RpoE regulon has not been fully characterized in *B. cenocepacia*, but is known in *E. coli* to include protein chaperones, such as DnaK and SurA, that enhance outer membrane integrity (Calloni et al., 2012; Dartigalongue et al., 2001; Hews et al., 2019). Overall, the extent of resistance factors to cationic antibiotics, including the integration of the Ara4N modification into an essential network, suggests strong and long-term environmental selection for antimicrobial peptide resistance. Breaking this resistance could therefore pave new therapeutic avenues.

The centrality and essentiality of UndP for cell envelope biogenesis hints at a weakness that may be exploited for antibiotic development. In *B. cenocepacia*, at least four pathways use UndP intermediates (Figure 11A), and two are essential for growth (peptidoglycan synthesis and

the Ara4N modification). Our BarSeq experiment pointed to disruptions in O-antigen synthesis and protein *O*-glycosylation causing susceptibility to β-lactams, FR-9, and/or BAC. Targeted genetic and chemical validations indicated midpoint disruptions in these pathways caused a buildup of UndP intermediates, thus reducing the free UndP available for peptidoglycan synthesis. Mutations causing accumulation of UndP-O-antigen and UndP-enterobacterial common antigen intermediates in *E. coli* (Jorgenson and Young, 2016; Jorgenson et al., 2016) and *Shigella flexneri* (Maczuga et al., 2022) are known to cause substantial morphological defects from insufficient peptidoglycan synthesis. While, β-lactam susceptibility has been observed in other large-scale screens for disruptions in UndP utilization pathways in *A. baylyi* (Bailey et al., 2022), *Vibrio cholerae* (Weaver et al., 2018), and *P. aeruginosa* (Dötsch et al., 2009; Sonnabend et al., 2020), we are the first to validate these interactions with targeted genetic and chemical investigations.

An important question that remains is if targeting UndP utilization pathways is a viable strategy for antibiotic development. Indeed, there are two documented successes: targocil and BTZ043 (Lee et al., 2010; Makarov et al., 2009; Swoboda et al., 2009). Targocil is an inhibitor of the TarG transporter for wall teichoic acid (WTA), a surface-linked glycan constructed on UndP, in *Staphylococcus aureus.* However, as the WTA pathway is non-essential, spontaneous resistance occurs relatively frequently *in vitro* (~1 in 10^6 cells) (Swoboda et al., 2009). BTZ043 is an antimycobacterial that targets DprE1 in the essential cell wall arabinan biosynthesis (Makarov et al., 2009). In the related species *Corynebacterium glutamicum* (Alderwick et al., 2005), BTZ043 was found to inhibit growth via sequestering decaprenyl phosphate intermediates required for peptidoglycan synthesis (Grover et al., 2014). Overall however, the outlook is not favourable for targeting UndP utilization pathways, as suppressor mutants are commonly identified when attempting to manipulate these non-essential pathways (Burrows and Lam, 1999; Jorgenson and Young, 2016; Xayarath and Yother, 2007). Furthermore, while single genetic mutations in UndP utilization pathways in *E. coli* substantially affect cell morphology (Jorgenson and Young, 2016; Jorgenson et al., 2016), we did not see this in K56-2 (Figure A14). It was only upon deleting the *waaL* O-antigen ligase and overexpressing the *wzm-wzt* O-antigen transporter that cell morphology displayed evidence of peptidoglycan defects (Figure 8). We suggest that *Burkholderia* may be more robust to alterations in UndP levels perhaps due to higher initial abundance of UndP, as the essential Ara4N LPS modification may otherwise place

a very high burden on UndP pools. Additionally, O-antigen synthesis in *Burkholderia* may require less UndP than in *E. coli*. The Wzy-dependent pathway predominant in *E. coli* strains uses one UndP carrier for each O-antigen subunit, while the ABC transporter-dependent pathway in *Burkholderia* (and many other species (Greenfield and Whitfield 2012)) uses a single UndP carrier to assemble the entire polymeric O-antigen. Thus, species that use the ABC transporter-dependent O-antigen pathway may be less susceptible to antibiotic inhibition of UndP utilization pathways.

In addition to developing new antibiotics, there is also a great deal of interest in discovering potentiators (also called adjuvants) that synergize with antibiotics to substantially increase potency and spare doses of the paired antibiotic. The presented transposon-based screen is well-suited to identify attractive targets for new potentiators, as gene disruption/silencing can mimic the effect of gene product inhibition with a small molecule (Anglada-Girotto et al., 2022). We found that disruption of the DsbAB, but not the DsbCD, pathway substantially increased susceptibility to many antibiotics, including β-lactams and large-scaffold antibiotics (Figure 5D). Another transposon screen by the Manoil group also found that DsbA and DsbB were important for resistance to meropenem in *A. baumannii* (Bailey et al., 2022). Recently in *E. coli*, the disulfide bonds introduced by the DsbAB pathway were found to be important for stability of periplasmic proteins such as β-lactamases and MCR enzymes (mobile colistin resistance) (Furniss et al., 2022). DsbAB has been previously linked to multiple traits in *B. pseudomallei* and *B. cepacia*, including extracellular protease activity, motility, and virulence in a murine model (McMahon et al. 2018; Hayashi et al. 2000). The pleiotropic effect of the DsbAB system on virulence and antibiotic resistance makes it an attractive target for further investigation.

In the context of antibiotic potentiation, the fitness profile of the mutant in *dbcA* deserves further attention. Disruption of *dbcA* increased susceptibility to β-lactams, BAC, FR-9, CHX, and PMB (Figure 3E). DbcA, a DedA-family UndP flippase and homologue of UptA in *E. coli* (Roney and Rudner, 2022), was found to be important for the Ara4N lipid A modification in *B. thailandensis* E264 (Panta et al., 2019), and a Δ*dbcA* mutant had a colistin MIC of 4 μg/mL (compared to > 256 μg/mL in WT E264). The peak sputum concentration of some inhaled colistin therapies is above 300 μg/mL sputum (Yapa et al., 2014), well above the inhibitory concentration for a mutant lacking DbcA. We suggest that DbcA, and UndP recycling more broadly, may be a linchpin in both β-lactam and cationic antibiotic resistance in *Burkholderia.*

Thus, inhibiting UndP recycling with a small molecule may potentiate the activity of multiple clinically available antibiotics.

B-lactamase inhibitors, such as AVI and TAZ, potentiate the activity of β-lactams by protecting them from hydrolysis by β-lactamases. AVI/CAZ shows promise as a treatment for Bcc respiratory infection (Spoletini et al., 2019); however, resistance has been identified to this combination (Everaert and Coenye, 2016; Papp-Wallace et al., 2017). By comparing fitness profiles of CAZ treatment in the presence or absence of AVI, we identified that the PenB serine β-lactamase and the K562_RS32470 putative metallo-β-lactamase are targets of AVI. Targeted validations then demonstrated that PenB is the predominant β-lactamase in K56-2. A similar transposon-based approach was recently used by the Manoil group in *A. baylyi* to show that AVI potentiates CAZ by inhibiting the GES-14 β-lactamase, while MEM is potentiated by inhibiting GES-14 and OXA-23 (Bailey et al., 2022).

We then exploited the dependence on PenB to demonstrate that AVI strongly potentiates AZT and MEM in a panel of Bcc clinical isolates (Figure 10 and Table A4). These combinations are not commonly reported for treatment of Bcc infection and may represent alternative therapeutic approaches. AVI/AZT is reported to be most potent against species of enterobacteria that express a serine β-lactamase (which is inhibited by AVI) and a metallo-β-lactamase (which generally cannot degrade AZT) (Biedenbach et al., 2015). However, for treatment of CF respiratory infections, inhaled formulations of aztreonam are available that can achieve concentrations over 725 µg/g sputum with new inhaler technology (Gilead Sciences Inc., 2012), which is nearly 100-fold the MIC_{50} we determined for the AVI/AZT combination. AZT is also generally-well tolerated by people with allergies to other β-lactams (Romano et al. 2011). Although inhaled MEM has been used in some cases (Hewer 2012), no other β-lactams are currently licensed as inhaled formulations. Additionally, as we found that the BpeAB-OprB pump effluxes AVI in K56-2, it may be possible that pump overexpression in clinical isolates may break AVI/β-lactam synergy; however, this remains to be determined.

Our genome-wide view into the mechanism of action of CFD may have an impact in moving CFD forward for therapeutic uses as it is not yet indicated to treat CF infections. In K56-2, we found that CFD activity was not affected by disruptions in the major β-lactamases (Figure 9). Additionally, in the largest screen of CFD activity in Bcc isolates to date, 85% were susceptible to CFD alone and there was little benefit of combination with AVI (Figure 11).

Indeed, CFD is generally stable to β-lactamase hydrolysis; however, the NDM-1 and NDM-5 metallo-β-lactamases are linked to resistance in *Enterobacter cloacae* and *Klebsiella pneumoniae*, respectively (Lan et al., 2022; Nurjadi et al., 2021). An additional consideration for CFD activity is also the concentration of iron in the growth conditions. We observed that physiological iron concentrations, even elevated levels associated with chronic CF (Hunter et al., 2013), are adequate for CFD activity. Furthermore, CFD activity was reduced by iron limitation from growth in a low-iron medium and from chelation. We therefore suggest that critical iron concentration thresholds exist that reflect the interplay between the availability of free iron for CFD to bind and the cellular responses to iron levels. In summary, we demonstrate how chemogenomics can be used to functionally annotate uncharacterized genes and prioritize targets for rational antibiotic combinations to increase effectiveness of current antibiotic therapies.

CHAPTER 6: DISCUSSION AND CONCLUSION

Remarkable strides in the care of Canadian CF patients have been made over recent decades. As an indicator, the average age at death of people with CF has increased from 25.2 years in 2001 to 42.0 years in 2020 (Cystic Fibrosis Canada, 2020). Additionally, CFTR modulators, a new class of drug that improves production of functional CFTR protein, have been approved for use in Canada. These drugs are projected to substantially improve lung function, reduce the incidence of severe infection, and increase life expectancy of most people with CF (Stanojevic et al., 2021, Zaher et al., 2021).

Respiratory infections remain prevalent and are the leading cause of mortality in people with CF. The specific environment of the CF lung, with stationary nutrient-rich mucus, leads to polymicrobial infection by several bacterial species, including members of the Bcc (Rabin and Surette, 2012). Antibiotics must be administered to eradicate, or at least suppress, the infecting organism (Bossche et al., 2021, Chmiel et al., 2014). Specifically for members of the Bcc, the lack of randomized clinical trials means that there are no recommended eradication protocols for Bcc respiratory infection (Regan and Bhatt, 2019). However, some case studies exist on a few patients (Garcia et al., 2018, Kitt et al., 2016). Such protocols involve long term therapy (often months) with antibiotic cocktails. Other options, such as bacteriophage therapy and vaccination targeting the Bcc, are not yet ready to be deployed in the clinic (Lauman and Dennis, 2021; Pradenas et al., 2016; Scoffone et al., 2020). Thus, developing antibiotic therapies to clear Bcc infection remains an important goal.

Approaches to new antibiotic therapies can focus on developing new antibiotics and on devising ways to increase activity of the currently available antibiotics. Both approaches require investigation of how antibiotics interact with and inactivate bacterial cells, that is, what are their targets and mechanisms of action. The field of chemical genetics provides useful tools to address these questions. Chemical genetics is the use of small molecules to probe biological systems and genetic networks. When done on a large scale, this becomes chemogenomics (Cacace et al., 2017; Warrier et al., 2022). Other groups have used chemogenomics to find the target for new antibiotics and develop rational antibiotic combinations (Geisinger et al., 2020; Martin et al., 2020; Santiago et al., 2018). I reasoned that chemogenomics could also be used in *Burkholderia* to tailor antibiotic development against this pathogen. The focus of my thesis was therefore to

develop and utilize genetic tools for genome-wide and precision investigation of antibiotic susceptibility in the *Burkholderia*.

The first objective of my thesis was to validate a transposon-based method to create knockdown mutants in *B. cenocepacia* K56-2 essential genes and identify the target of the uncharacterized antimicrobial C109. Our Tn*5* transposon contained an outward-facing rhamnose-inducible promoter, allowing selective recovery and study of mutants with knockdowns in essential genes (Bloodworth et al., 2013), which are the targets of antibiotics. As determined by next-generation sequencing, 83 of 358 (23.2%) essential operons in K56-2 were placed under rhamnose-inducible control. Leveraging the theory that knockdown of target essential genes sensitizes cells to cognate antibiotics (Cardona et al., 2015), a competitive growth assay with low rhamnose concentrations identified a short-list of putative C109 targets. Follow-up studies found that FtsZ was the *in vivo* target and that C109 inhibited critical GTPase and polymerization activities of FtsZ. FtsZ drives assembly of the divisome through a series of steps involving GTP binding, polymerization, GTP hydrolysis and polymer disassembly (Yang et al., 2017b). Our findings are important for two reasons: 1) this was the first study to use a transposon library enriched in mutants of essential genes to identify the target of an uncharacterized antimicrobial, and 2) FtsZ is a highly-conserved and underexploited target for antibiotic development. Our demonstrated proof of principle on this method enabled us to pursue further studies using chemogenomics. Additionally, our collaborators for this study have continued to investigate C109 as a potential inhaled antibiotic, as C109 is active against several CF pathogens (e.g. *S. aureus*, *M. abscessus*, and Bcc species) (Costabile et al., 2020).

During investigation of my first objective, I realized that improvements can be made to the current set of genetic tools for *Burkholderia*, specifically to the tools used to manipulate essential genes. Motivated by reports on the ability of CRISPRi to rapidly knock down virtually any genetic element (Peters et al., 2016; Qi et al., 2013), the second objective of my thesis was to adapt a CRISPRi system for *Burkholderia*. To balance high dCas9 expression with low toxicity, I placed a codon-optimized *dcas9* gene in single copy in the chromosome under control of the rhamnose-inducible promoter. Upon induction with rhamnose, I demonstrated expression of dCas9 protein by immunoblot and subsequent gene silencing with RT-qPCR and phenotypic assays. To bring this technology to other species, the CRISPRi system was mobilized on a vector that may be able to integrate into many species within the family Burkholderiales and genus

Pseudomonas. Indeed, I have shown that the CRISPRi system is functional in *B. thailandensis* and *B. multivorans*.

Realizing the potential of CRISPRi technology, several other groups have used CRISPRi for chemogenomics (Li et al., 2022; Peters et al., 2016) and profiling essential genomes (Rousset et al., 2018; Silvis et al., 2021). CRISPRi has several biological and technical advantages over other approaches used to control essential gene expression. When CRISPRi is not uninduced, the genetic locus being targeted is effectively wild-type, thus preserving endogenous regulatory architecture. To fine tune the desired levels of repression, there are a variety of modifications that can be made to the system (e.g. using other dCas9 orthologues, introducing mismatches into the sgRNA, and multiplexing) (Hawkins et al., 2020; Ni et al., 2019; Rock et al., 2017). Additionally, the sgRNA expression plasmids can be rapidly constructed individually or in pools (Peters et al., 2019; Rousset et al., 2018). Overall, I expect that my adaptation of CRISPRi for *Burkholderia* will greatly facilitate precision genetics to link genotype to phenotype in our lab and many others. Indeed, our lab has constructed over 1000 individual CRISPRi mutants thus far.

As mentioned above, in addition to developing new antibiotics, the challenge of antibiotic resistance can also be confronted by finding new ways to increase the activity of currently available antibiotics. The Gram-negative cell envelope is a major barrier to antibiotic entry, and is thus an attractive target for small molecule permeabilizers (Klobucar and Brown, 2022). Specifically, the cell envelope of Bcc species has noted differences in porin content and lipid modifications that substantially reduce permeability (Loutet and Valvano, 2011). I therefore reasoned that interrupting key aspects of cell envelope structure or biogenesis may increase antibiotic activity in *B. cenocepacia*. My third and fourth thesis objectives were designed to address this goal: 3) to construct a randomly-barcoded transposon mutant library in K56-2 and then 4) to use this library to assess genome-wide fitness contributions in the presence of a large panel of cell envelope-targeting antibiotics. For my third objective, I modified the original transposon I used above to contain a random 20 bp DNA barcode, based on a report that this enables rapid detection of mutant abundance in pools by BarSeq (Wetmore et al., 2015). Fast sample processing was required so that I might include a large number of antibiotics in the fourth objective.

The design of the competitive growth experiment for my fourth objective focused primarily on non-essential genes. Interrogating the contributions of non-essential genes to antibiotic activity is complementary to the approach I used to address my first objective. In this way, the screen mainly informs on the mechanistic details of how antibiotic and/or potentiator combinations may work together for greater effect. By performing the largest transposon-based screen of cell envelope targeting antibiotics in a Gram-negative, I uncovered and validated over a hundred new functional annotations for genes not previously associated with antibiotic susceptibility in *B. cenocepacia*. The sheer number of interactions highlights the connectivity between cell envelope processes. For example, susceptibility to β-lactams was affected by disrupting steps within the synthesis and recycling of UndP, the synthesis of peptidoglycan precursors and the peptidoglycan matrix itself, the synthesis of the LPS core, and the formation of periplasmic disulfide bonds. Each of these may represent an avenue for development of chemical inhibitors that potentiate the activity of β-lactams. Furthermore, the screen shed light on the mechanistic basis for the potentiation of β-lactams by AVI and suggested new rational combinations with increased potency.

Overall, this work shows how comprehensive and complementary sets of genetic tools can be used to dissect how small inhibitory molecules interact with bacterial cells. Genome-wide perspectives intrinsically reduce bias in the study direction and reveal the true complexity of chemical-genetic interactions. Hits from genome-wide screens can be used to prioritize targets for investigation and development of novel inhibitors, either as direct antibiotics or potentiators.

My study has opened new possibilities to address some unanswered questions. Following up on the promising activity and novel target of C109, more recent work by our collaborators has expanded upon the antibacterial activity of C109 to new strains of methicillin-resistant *S. aureus* (Trespidi et al., 2021) and multidrug-resistant *A. baumannii* (Scoffone et al., 2022). Derivatives of C109 embedded in polyethylene glycol nanocrystals have also been developed for inhaled therapy (Costabile et al., 2020). Future work on C109 should focus on the pharmacokinetic and pharmacodynamic properties of C109 in healthy and disease-state murine models.

CRISPRi tools enable rapid construction of targeted gene knockdown mutants. After I adapted these tools for *Burkholderia*, I made over 100 CRISPRi mutants to follow up on select hits identified by the BarSeq experiment. A future direction could be to create an (essential) genome-wide CRISPRi library in K56-2 to study antibiotic mechanisms, as we were unable to

obtain essential genome-wide representation with our transposon-based approach. This CRISPRi library could also be used to identify conditionally essential genes or genes regulating cell morphology (Silvis et al., 2021; de Wet et al., 2020). Select mutants from this library could also be used to further investigate all of the hit genes/pathways identified by the BarSeq experiment as important for fitness in the presence of antibiotics. Changes in antibiotic susceptibility upon gene knockdown could then be quantified and ranked to prioritize new targets for inhibitor development. It is expected that these inhibitors would act as antibiotic potentiators and greatly increase antibiotic susceptibility, such as for DsbA inhibitors (Furniss et al., 2021) or β-lactamase inhibitors (Drawz and Bonomo, 2010). Additionally, questions remain on the physiological significance of *B. cenocepacia* encoding apparently parallel pathways for D-glutamate synthesis, contrary to other Gram-negatives, and on the mechanism that reduces CFD susceptibility in low-iron conditions, contrary to *P. aeruginosa*.

CHAPTER 7: APPENDIX

Supplementary Data 1. Fitness scores for every gene in all conditions assessed in Chapter 5.

The datafile is available at: https://doi.org/10.34990/FK2/UIQTSR

Table A1. Strains used in Chapters 3, 4 and 5 of this study

Strain	Features	Source
Achromobacter xylosoxidans ACH02	Canadian cystic fibrosis isolate; multidrug resistant	H. Adam (Shared Health MB)
A. xylosoxidans ACH03	Canadian cystic fibrosis isolate; multidrug resistant	H. Adam (Shared Health MB)
A. xylosoxidans ACH09	Canadian cystic fibrosis isolate; multidrug resistant	H. Adam (Shared Health MB)
Acinetobacter baumannii ATCC 19606	Clinical isolate reference strain	ATCC
Burkholderia ambifaria BCC0478	Cystic fibrosis clinical isolate	E. Mahenthiralingam
B. ambifaria BCC0485	Cystic fibrosis clinical isolate	E. Mahenthiralingam
B. cenocepacia 110041	Canadian cystic fibrosis isolate	National Microbiology Lab, MB
B. cenocepacia BC7	Canadian cystic fibrosis isolate; epidemic lineage	CBCCRRR
B. cenocepacia BCC0076	Cystic fibrosis clinical isolate	E. Mahenthiralingam
B. cenocepacia BCC1119	Cystic fibrosis clinical isolate	E. Mahenthiralingam
B. cenocepacia BCC1202	Cystic fibrosis clinical isolate	E. Mahenthiralingam
B. cenocepacia C5424	Cystic fibrosis clinical isolate	D. Speert
B. cenocepacia CEP511	Cystic fibrosis clinical isolate	D. Speert
B. cenocepacia CG*dcw*	*mraZ*::pRBrhaBoutgfp in K56-2 background	(Bloodworth et al., 2013)
B. cenocepacia CG*dnaN*	*dnaN*:: pRBrhaBoutgfp in K56-2 background	(Bloodworth et al., 2013)

B. cenocepacia CG*ftsZ*	K562_RS16895-K562_RS16900::Tn-Tag and ftsZ::pAH1 in K56-2 background	This study
B. cenocepacia CG*holC*	*holC*:: pRBrhaBoutgfp in K56-2 background	(Bloodworth et al., 2013)
B. cenocepacia CG*ispAdxs*	*ispA*:: pRBrhaBoutgfp in K56-2 background	(Bloodworth et al., 2013)
B. cenocepacia CG*pepAholC*	pepA:: pRBrhaBoutgfp in K56-2 background	(Bloodworth et al., 2013)
B. cenocepacia CG*topB*	*topB*::pAH5 in K56-2 background	This study
B. cenocepacia CG*xseBispA-dxs*	*xseB*:: pRBrhaBoutgfp in K56-2 background	(Bloodworth et al., 2013)
B. cenocepacia FCF 28	Cystic fibrosis clinical isolate	(Papaleo et al., 2010)
B. cenocepacia FCF 29	Cystic fibrosis clinical isolate	(Papaleo et al., 2010)
B. cenocepacia FCF 30	Cystic fibrosis clinical isolate	(Papaleo et al., 2010)
B. cenocepacia FCF 31	Cystic fibrosis clinical isolate	(Papaleo et al., 2010)
B. cenocepacia J2315	ET12 lineage cystic fibrosis clinical isolate from the UK	(Govan et al., 1993)
B. cenocepacia K56-2	ET12 lineage cystic fibrosis clinical isolate from Toronto	(Darling et al., 1998)
B. cenocepacia K56-2 *fliF*::pAH26	Derived from K56-2; pAH26 integrated into *fliF*; Tp^r	This study
B. cenocepacia K56-2 *phbC::*pAH27	Derived from K56-2; pAH27 integrated into *fliF*; Tp^r	This study
B. cenocepacia K56-2 Δ*paaABCDE*	Derived from K56-2; clean deletion of the *paaABCDE* operon	(Pribytkova et al., 2014)

B. cenocepacia K56-2::CTX1-rha	Derived from K56-2; pAH-CTX1rha integrated at *attB* site; clean deletion of plasmid accessory genes	This study
B. cenocepacia K56-2::dCas9	Derived from K56-2; pAH-CTX1rhadCas9 integrated at *attB* site; clean deletion of plasmid accessory genes	This study
B. cenocepacia K56-2::dCas9-native	Derived from K56-2; pAH-CTX1rhadCas9-native integrated at *attB* site; clean deletion of plasmid accessory genes	This study
B. cenocepacia VC10414	Canadian cystic fibrosis isolate	CBCCRRR
B. cenocepacia VC14488	Canadian cystic fibrosis isolate	CBCCRRR
B. cenocepacia VC14543	Canadian cystic fibrosis isolate	CBCCRRR
B. cenocepacia VC14761	Canadian cystic fibrosis isolate	CBCCRRR
B. cepacia ATCC 25416	Onion pathogen, reference strain	ATCC
B. cepacia BCC1381	Cystic fibrosis clinical isolate	E. Mahenthiralingam
B. contaminans 21NG595759	Canadian cystic fibrosis isolate	H. Adam (Shared Health MB)
B. contaminans 21NG609698	Canadian cystic fibrosis isolate	H. Adam (Shared Health MB)
B. contaminans 2221	Cystic fibrosis clinical isolate	P. Drevinek
B. contaminans 4278	Cystic fibrosis clinical isolate	P. Drevinek
B. contaminans FFH2055	Cystic fibrosis clinical isolate from Argentina	(Bloodworth et al., 2015)
B. contaminans LMG23361	Veterinary isolate	BCCM
B. dolosa BCC0305	Cystic fibrosis clinical isolate	E. Mahenthiralingam
B. dolosa CEP021	Cystic fibrosis isolate	D. Speert

B. gladioli BCC1620	Cystic fibrosis clinical isolate	E. Mahenthiralingam
B. gladioli BCC1623	Cystic fibrosis clinical isolate	E. Mahenthiralingam
B. gladioli BCC1710	Cystic fibrosis clinical isolate	E. Mahenthiralingam
B. gladioli VC14812	Canadian cystic fibrosis isolate	CBCCRRR
B. gladioli VC19233	Canadian cystic fibrosis isolate	CBCCRRR
B. multivorans 130034	Canadian cystic fibrosis isolate	National Microbiology Lab, MB
B. multivorans 21NH942533	Canadian cystic fibrosis isolate	H. Adam (Shared Health MB)
B. multivorans 21NJ503211	Canadian cystic fibrosis isolate	H. Adam (Shared Health MB)
B. multivorans 454	Cystic fibrosis clinical isolate	P. Drevinek
B. multivorans 6094	Cystic fibrosis clinical isolate	P. Drevinek
B. multivorans ATCC 17616::dCas9	Derived from ATCC 17616; pAH-CTX1-rhadCas9 integrated at attB site; clean deletion of plasmid accessory genes	This study
B. multivorans BCC0710	Cystic fibrosis clinical isolate	E. Mahenthiralingam
B. multivorans BCC1379	Cystic fibrosis clinical isolate	E. Mahenthiralingam
B. multivorans C5393	Canadian cystic fibrosis isolate	D. Speert
B. multivorans FCF 10	Cystic fibrosis clinical isolate	(Papaleo et al., 2010)
B. multivorans FCF 11	Cystic fibrosis clinical isolate	(Papaleo et al., 2010)

B. multivorans FCF 5	Cystic fibrosis clinical isolate	(Papaleo et al., 2010)
B. multivorans FCF 6	Cystic fibrosis clinical isolate	(Papaleo et al., 2010)
B. multivorans FCF 7	Cystic fibrosis clinical isolate	(Papaleo et al., 2010)
B. multivorans FCF 8	Cystic fibrosis clinical isolate	(Papaleo et al., 2010)
B. multivorans FCF 9	Cystic fibrosis clinical isolate	(Papaleo et al., 2010)
B. multivorans VC15535	Canadian cystic fibrosis isolate	CBCCRRR
B. multivorans VC15555	Canadian cystic fibrosis isolate	CBCCRRR
B. multivorans VC19694	Canadian cystic fibrosis isolate	CBCCRRR
B. multivorans VC9825	Canadian cystic fibrosis isolate	CBCCRRR
B. mutlivorans ATCC 17616	Soil sample	ATCC
B. pyrrocinia BCC0735	Cystic fibrosis clinical isolate	E. Mahenthiralingam
B. stabilis 10870	Cystic fibrosis clinical isolate	P. Drevinek
B. stabilis 3819	Cystic fibrosis clinical isolate	P. Drevinek
B. stabilis 9693	Cystic fibrosis clinical isolate	P. Drevinek
B. stabilis BCC0608	Cystic fibrosis clinical isolate	E. Mahenthiralingam
B. thailandensis E264	Rice-field soil sample in Thailand	DSMZ
B. thailandensis E264::dCas9	Derived from ATCC E264; pAH-CTX1-rhadCas9 integrated at attB site; clean deletion of plasmid accessory genes	This study

B. vietnamiensis BCC0296	Cystic fibrosis clinical isolate	E. Mahenthiralingam
B. vietnamiensis CEP40	American cystic fibrosis isolate	(Mahenthiralingam et al., 2000)
B. vietnamiensis VC11431	Canadian cystic fibrosis isolate	CBCCRRR
B. vietnamiensis VC18984	Canadian cystic fibrosis isolate	CBCCRRR
Escherichia coli 117782	Canadian clinical isolate; ESBL-positive	G. Zhanel
E. coli 120955	Canadian clinical isolate; ESBL-positive	G. Zhanel
E. coli AG1	*recA1 endA1 gyrA96 thi-1 hsdR17(rK-, mK+) supE44 relA1*	E. Brown
E. coli ATCC 25922	Reference strain	ATCC
E. coli BL21(DE3)	F- *ompT gal dcm lon hsdS*$_B$($r_B^- m_B^-$) λ(DE3 [*lacI lacUV5-T7p07 ind1 sam7 nin5*]) [*malB*$^+$]$_{K-12}$(λ^S)	Invitrogen
E. coli DH5α	F- Φ80*lac*ZΔM15 Δ(*lac*ZYA*arg*F) U169 *rec*A1 *end*A1 *hsd*R17 (rK-, mK$^+$) *pho*A *sup*E44 λ- *thi*-1 *gyr*A96 *rel*A1	Invitrogen
E. coli MM294	F− *φ*80 *lacZ*ΔM15 *endA1 recA1 hsdR17* (rH− mK+) *supE44 thi-1* Δ*gyrA96* (*ΔlacZYA-argF*)U169 *relA1*	(Meselson and Yuan, 1968)
E. coli SY327	F- *araD* Δ(*lac-proAB*) *argE*(Am) *recA56* Rifr *nalA* λ*pir*	(Miller and Mekalanos, 1988)
Klebsiella aerogenes ATCC 13048	Reference strain	ATCC
K. aerogenes ENT001	Urine culture isolate; meropenem-resistant	A. Kumar
K. pneumoniae 119178	Canadian clinical isolate; ESBL-positive	G. Zhanel

Mycobacterium abscessus 14NF251095	Ciprofloxacin-resistant clinical isolate	H. Adam (Shared Health MB)
M. abscessus 14NJ168168	Ciprofloxacin-resistant clinical isolate	H. Adam (Shared Health MB)
M. abscessus 16NH386647	Ciprofloxacin-resistant clinical isolate	H. Adam (Shared Health MB)
M. abscessus 13NC740779	Ciprofloxacin-resistant clinical isolate	H. Adam (Shared Health MB)
Pseudomonas. aeruginosa 20NB681421	Canadian cystic fibrosis isolate	H. Adam (Shared Health MB)
P. aeruginosa 21NE72623	Canadian cystic fibrosis isolate	H. Adam (Shared Health MB)
P. aeruginosa PA14	Highly virulent burn wound isolate	(Schroth et al., 2018)
P. aeruginosa PA7	Non-respiratory clinical isolate	(Roy et al., 2010)
P. aeruginosa PAO1	Lab strain from burn wound	A. Kumar
Salmonella enterica serovar Typhimurium DT104	SGI1 genomic island; multidrug resistant	(Threlfall et al., 1994)
Serratia marcescens Db11	Streptomycin-resistant strain	(Flyg et al., 1980)
Staphylococcus aureus ATCC 25923	Methicillin-resistant reference strain	ATCC
S. aureus ATCC 29213	Methicillin-sensitive reference strain	ATCC
S. aureus CF 225	Methicillin-resistant strain (SCC*mec* IV)	(Pena Amaya et al., 2018)
Stenotrophomonas maltophilia 20NC580771	Canadian cystic fibrosis isolate	H. Adam (Shared Health MB)
S. maltophilia 21NE928511	Canadian cystic fibrosis isolate	H. Adam (Shared Health MB)
S. maltophilia D457	Non-CF respiratory isolate from Spain	ATCC

S. maltophilia K279a	Bloodstream isolate from UK; multidrug resistant	ATCC

Table A2. Plasmids use in Chapter 3,4 and 5 of this work.

Plasmid	Features	Source
pAH1	Derivative of pSC201 with 5' region of *ftsZ* (K562_RS16765) downstream of the rhamnoseinducible promoter	This study
pAH3	Derivative of pGPI-SceI with a cloned region of the Tn Tag flanked by 300 bp each of the 3' and intergenic regions of K562_RS16895 and K562_RS16900	This study
pAH5	Derivative of pSC201 with 5' region of *topB* (K562_RS02390) downstream of the rhamnoseinducible promoter	This study
pCA24N-*gfp*	ori_{colE1} Chl^r $lacI^q$ PT5-lac *gfp*	(Kitagawa et al., 2005)
pDAI-*Sce*I	ori_{pBBR1} Tet^r mob^+ P*dhfr I-SceI*	(Flannagan et al., 2008)
pDAI-SceI-*sacB*	pDAI-SceI expressing *sacB*	(Aubert et al., 2014; Hamad et al., 2010)
pGPI-SceI	ori_{R6K} Tmp^r mob^+ carries I-SceI cut site	(Flannagan et al., 2008)
pET-28a	ori_{pBR322} ; Kan^r; *lacI*	Novagen
pSCrhaBoutgfp	pTnMod-OTp′, *rhaR rhaS* P_{rhaB} *e-gfp*	(Cardona et al., 2006)
pRBrhaBout	pSCrhaboutgfp derivative ori_{R6K} *dhfr rhaR rhaS* P*rhaB* (also called pRB-rham)	(Bloodworth et al., 2013)
pKS1	pRBrhaBout with *Nco*I and *Bam*HI restriction sites inserted after *dhfr*	This study

pRBrha-Barcode	Pool of pKS1 with the random barcode ligated in the *Nco*I and *Bam*HI sites	This study
pRK2013	ori_{colE1} RK2 derivative Kan^r mob^+ tra^+	(Figurski and Helinski, 1979)
pSC201	ori_{R6K} *rhaR rhaS* P*rhaB dhfr*	(Ortega et al., 2007)
pTnMod-STp	$orip_{SC101}$, Tn*5* inverted repeats, Tn*5* transposase, Tp^r	(Dennis and Zylstra, 1998)
mini-CTX1	Tet^r , Ω-FRT-*attP* MCS ori_{pMB1} $int_{\varphi CTX}$ and oriT	(Hoang et al., 2000)
pKD3	Cm^r *rgnB* ori_{R6K}	(Datsenko and Wanner, 2000)
pAH18	Derived from pGPI-*Sce*I; ori_{R6K} Tp^r mob^+ carries I-SceI gene; 475 bp from both upstream and downstream flanking regions between the *FRT* sites on pAH-CTX1-rhadCas9 cloned between *Kpn*I and *Eco*RI sites	This study
pHA25-SceI	Derived from pDAI-*Sce*I; ori_{pBBR1} Cm^r mob^+ P*dhfr I-SceI*; *cat* gene from pKD3 cloned into *Age*I and *Xho*I sites	This study
pFLPe4	Ap^r Km^r *oriT* ori_{RO1600}-*rep*(Ts_{Bt}) *rhaR rhaS* P_{rhaB}	(Choi et al., 2008)
pGPΩ-Tp	ori_{R6K}, ΩTp^r, mob^+	(Flannagan et al., 2007)
pAH26	pGPΩ-TP with 330 bp 5’	This study

	fragment of *B. cenocepacia* K56-2 *fliF* cloned between *Kpn*I and *Eco*RI sites	
pAH27	pGPΩ-TP with 335 bp 5' fragment of *B. cenocepacia* K56-2 *phbC* cloned between *Kpn*I and *Eco*RI sites	This study
pAH-CTX1-rha	Derived from mini-CTX1; *rhaS rhaR* P_{rhaB} from pSC201 cloned into *Spe*I and *Hind*III sites	This study
pAH-CTX1-rhadCas9	Derived from pAH-CTX1-rha; codon-optimized *dcas9* cloned into *Spe*I and *Not*I sites	This study
pAH-CTX1-rhadCas9-native	Derived from pAH-CTX1-rha; native *dcas9* cloned into *Spe*I and *Not*I sites	This study
pSCrhaB2	*ori*pBBR1 *rhaR, rhaS, PrhaB* TpR mob^+	(Cardona and Valvano, 2005)
pSCrhaB2plus	pSCrhaB2 with $rhaI_1$-$rhaI_1$ permutation of *rhaS* binding sites upstream of P_{rhaBAD} and bacteriophage T7 *gene 10* stem loop inserted upstream of native *rhaBAD* 5′ UTR	(Hogan et al., 2021)
pSCrhaB2-sgRNA	Derived from pSCrhaB2; gRNA cassette from pgRNA-bacteria cloned into *Kpn*I and *Eco*RI sites	This study
pSCB2-sgRNA	Template for pgRNA created by inverse PCR; derived from pSCrhaB2-sgRNA by inverse PCR to remove *rhaS, rhaR,* and P*rhaB*	This study
pSCB2-sgRNAv2	Derived from pSCB2-sgRNA. A *Bam*HI site was introduced to facilitate CRISPRi multiplexing	Rahman et al. , Unpublished
pgRNA-guideless	Derived from pSCB2-sgRNA; 20 nt binding region of gRNA removed by inverse PCR	This study

pgRNA-non-target	Derived from pSCB2-sgRNA; random 20 nt sequence added as gRNA binding region by inverse PCR	This study
pgRNA1-23	Derived from pSCB2-sgRNA by inverse PCR to add new 20 nt gRNA binding region	This study
pSC-rhadCas9	Derived from pSCrhaB2; codonoptimized *dcas9* was cloned into *Nde*I and *Hind*III cites	This study
p*bacA*+	pSCrhaB2plus with K56-2 *bacA* gene (K562_RS148950) cloned between *Nde*I and *Xba*I sites	This study
p*bceB*+	pSCrhaB2plus with K56-2 *bceB* gene (K562_RS21495) cloned between *Nde*I and *Xba*I sites	This study
p*hldD*+	pSCrhaB2plus with K56-2 *hldD* gene (K562_RS14060) cloned between *Nde*I and *Xba*I sites	This study
p*murA*+	pSCrhaB2plus with K56-2 *murA* gene (K562_RS01625) cloned between *Nde*I and *Xba*I sites	This study
p*ogcA*+	pSCrhaB2plus with K56-2 *ogcA* gene (K562_RS15015) cloned between *Nde*I and *Xba*I sites	This study
p*uppS*+	pSCrhaB2plus with K56-2 *uppS* gene (K562_RS08220) cloned between *Nde*I and *Xba*I sites	This study
p*waaL*+	pSCrhaB2plus with K56-2 *waaL* gene (K562_RS06530) cloned between *Nde*I and *Xba*I sites	This study

p*wbiI*+	pSCrhaB2plus with K56-2 *wbiI* gene (K562_RS15035) cloned between *Nde*I and *Xba*I sites	This study
p*wzm-wzt*+	pSCrhaB2plus with K56-2 *wzm* and *wzt* genes (K562_RS15080 and K562_RS15085) cloned between *Nde*I and *Xba*I sites	This study
pGPI-SceI-*bacA*	pGPI-SceI with a fusion of 360 bp regions immediately upstream and downstream of *bacA* cloned into *Xba*I and *Xma*I sites. Enables deletion of entire *bacA* gene.	This study
pGPI-SceI-*bceB*	pGPI-SceI with a fusion of 450 bp regions immediately upstream and downstream of *bceB* cloned into *Xba*I and *Xma*I sites. Enables deletion of entire *bceB* gene.	This study
pGPI-SceI-*hldD*	pGPI-SceI with a fusion of 360 bp regions immediately upstream and downstream of *hldD* cloned into *Xba*I and *Xma*I sites. Enables deletion of the 3' 796/993 bp of *hldD*.	This study
pGPI-SceI-*waaL*	pGPI-SceI with a fusion of 360 bp regions immediately upstream and downstream of *waaL* cloned into *Xba*I and *Xma*I sites. Enables deletion of the 5' 785/1230 bp of *waaL*.	This study
pGPI-SceI-*wbiI*	pGPI-SceI with a fusion of 450 bp regions immediately upstream and downstream of *wbiI* cloned into *Xba*I and *Xma*I sites. Enables deletion of entire *wbiI* gene.	This study
pGPI-SceI-*wzm-wzt*	pGPI-SceI with a fusion of 450 bp regions immediately upstream and downstream of *wzm-wzt* cloned into *Xba*I and *Xma*I sites. Enables deletion of entire *wzm* and *wzt* genes.	This study

pgRNA-*ampC*1	pSCB2-sgRNAv2 expressing sgRNA targeting *ampC*	This study
pgRNA-*ampC*2	pSCB2-sgRNAv2 expressing sgRNA targeting *ampC*	This study
pgRNA-*ampD*1	pSCB2-sgRNAv2 expressing sgRNA targeting *ampD*	This study
pgRNA-*ampD*2	pSCB2-sgRNAv2 expressing sgRNA targeting *ampD*	This study
pgRNA-*bacA*1	pSCB2-sgRNAv2 expressing sgRNA targeting *bacA*	This study
pgRNA-*bacA*2	pSCB2-sgRNAv2 expressing sgRNA targeting *bacA*	This study
pgRNA-*bceB*1	pSCB2-sgRNAv2 expressing sgRNA targeting *bceB*	This study
pgRNA-*bceB*2	pSCB2-sgRNAv2 expressing sgRNA targeting *bceB*	This study
pgRNA-*bceQ*1	pSCB2-sgRNAv2 expressing sgRNA targeting *bceQ*	This study
pgRNA-*bceQ*2	pSCB2-sgRNAv2 expressing sgRNA targeting *bceQ*	This study
pgRNA-*bpeABoprB*1	pSCB2-sgRNAv2 expressing sgRNA targeting *bpeABoprB* operon	This study
pgRNA-*bpeABoprB*2	pSCB2-sgRNAv2 expressing sgRNA targeting *bpeABoprB* operon	This study
pgRNA-*dacB*1	pSCB2-sgRNAv2 expressing sgRNA targeting *dacB*	This study
pgRNA-*dacB*2	pSCB2-sgRNAv2 expressing sgRNA targeting *dacB*	This study
pgRNA-*hldD*1	pSCB2-sgRNAv2 expressing sgRNA targeting *hldD*	This study

pgRNA-*hldD*2	pSCB2-sgRNAv2 expressing sgRNA targeting *hldD*	This study
pgRNA-*ispDF*1	pSCB2-sgRNAv2 expressing sgRNA targeting *ispDF* operon	This study
pgRNA-*ispDF*2	pSCB2-sgRNAv2 expressing sgRNA targeting *ispDF* operon	This study
pgRNA-*ogcABEI*1	pSCB2-sgRNAv2 expressing sgRNA targeting *ogcABEI* operon	This study
pgRNA-*ogcABEI*2	pSCB2-sgRNAv2 expressing sgRNA targeting *ogcABEI* operon	This study
pgRNA-*penB*1	pSCB2-sgRNAv2 expressing sgRNA targeting *penB*	This study
pgRNA-*penB*2	pSCB2-sgRNAv2 expressing sgRNA targeting *penB*	This study
pgRNA-*penR*1	pSCB2-sgRNAv2 expressing sgRNA targeting *penR*	This study
pgRNA-*penR*2	pSCB2-sgRNAv2 expressing sgRNA targeting *penR*	This study
pgRNA-*pglL*1	pSCB2-sgRNAv2 expressing sgRNA targeting *pglL*	This study
pgRNA-*pglL*2	pSCB2-sgRNAv2 expressing sgRNA targeting *pglL*	This study
pgRNA-*piuA*1	pSCB2-sgRNAv2 expressing sgRNA targeting *piuA*	This study
pgRNA-*piuA*2	pSCB2-sgRNAv2 expressing sgRNA targeting *piuA*	This study
pgRNA-*opnA1*	pSCB2-sgRNAv2 expressing sgRNA targeting *opnA*	This study
pgRNA-*opnA2*	pSCB2-sgRNAv2 expressing sgRNA targeting *opnA*	This study
pgRNA-*slt*1	pSCB2-sgRNAv2 expressing sgRNA targeting *slt*	This study

pgRNA-*slt*2	pSCB2-sgRNAv2 expressing sgRNA targeting *slt*	This study
pgRNA-*uppS*1	pSCB2-sgRNAv2 expressing sgRNA targeting *uppS*	This study
pgRNA-*uppS*2	pSCB2-sgRNAv2 expressing sgRNA targeting *uppS*	This study
pgRNA-*vio-wbx*1	pSCB2-sgRNAv2 expressing sgRNA targeting *vio-wbx* operon	This study
pgRNA-*vio-wbx*2	pSCB2-sgRNAv2 expressing sgRNA targeting *vio-wbx* operon	This study
pgRNA-*waaL*1	pSCB2-sgRNAv2 expressing sgRNA targeting *waaL*	This study
pgRNA-*waaL*2	pSCB2-sgRNAv2 expressing sgRNA targeting *waaL*	This study
pgRNA-*wabR-P*1	pSCB2-sgRNAv2 expressing sgRNA targeting *wabR-P* operon	This study
pgRNA-*wabR-P*2	pSCB2-sgRNAv2 expressing sgRNA targeting *wabR-P* operon	This study
pgRNA-*wbiFGHI*1	pSCB2-sgRNAv2 expressing sgRNA targeting *wbiFGHI* operon	This study
pgRNA-*wbiFGHI*2	pSCB2-sgRNAv2 expressing sgRNA targeting *wbiFGHI* operon	This study
pgRNA-*wzm-wzt*1	pSCB2-sgRNAv2 expressing sgRNA targeting *wzm-wzt* operon	This study
pgRNA-*wzm-wzt*2	pSCB2-sgRNAv2 expressing sgRNA targeting *wzm-wzt* operon	This study
pgRNA-*zapA*1	pSCB2-sgRNAv2 expressing sgRNA targeting *zapA*	This study
pgRNA-*zapA*2	pSCB2-sgRNAv2 expressing sgRNA targeting *zapA*	This study

Table A3. Primers and oligonucleotides used in Chapter 3, 4, and 5 of this work.

Primer	Sequence (restriction sites in lowercase)	Notes
153	GTGGATGACCTTTTGAATGACCTTT	Colony PCR for pGPΩ-Tp
154	ACAGGAACACTTAACGGCTGACATG	Colony PCR for pGPΩ-Tp
681	CAAGCAGAAGACGGCATACGAGATTCGCCTTAGTCTCG TGG GCTCGGAGATGTGTATAAGAGACAG	Used for TnSeq circle
682	CACAAGTGCGGCCGCACTAGTCTAGATTTAAATTACCG TAGTGAGTTCTTCGTCCGAGCCAC	Collector probe for TnSeq-circle
683	P – CCGTAGTGAGTTCTTCGTCCGAGCCACTCGGAGATGTG TAT AAGAGACAGT	Half of adapter for TnSeq-circle
684	P – CTGTCTCTTATACACATCTCCGAGTGGCTCGGACGAAG AAC TCACTACGG	Half of adapter for TnSeq-circle
690	AATGATACGGCGACCACCGAGATCTACACTAGATCGCT CGTCGGCAGCGTCAGATGTGTATAAGAGACAGNNNNA ATCTAGACTAGTGCGGCC	Used for TnSeq circle
715	CAAGCAGAAGACGGCATACGAGATCTAGTACGGTCTCG TGG GCTCGGAGATGTGTATAAGAGACAG	Used for TnSeq circle
717	CAAGCAGAAGACGGCATACGAGATGCTCAGGAGTCTC GTGG GCTCGGAGATGTGTATAAGAGACAG	Used for TnSeq circle
718	CAAGCAGAAGACGGCATACGAGATAGGAGTCCGTCTC GTGG GCTCGGAGATGTGTATAAGAGACAG	Used for TnSeq circle
719	AATGATACGGCGACCACCGAGATCTACACCTCTCTATT CGTCGGCAGCGTCAGATGTGTATAAGAGACAGNNNNA ATCTAGACTAGTGCGGCC	Used for TnSeq circle
729	CAAGCAGAAGACGGCATACGAGATCATGCCTAGTCTCG TGG GCTCGGAGATGTGTATAAGAGACAG	Used for TnSeq circle
781	TAAGATggatccTCAGTTGGCTTCATCGCTAC	Colony PCR for pSCB2-sgRNA
847	TTCCTGTCAGTAACGAGAAGG	Colony PCR for plasmids based on pSCrhaB2; used with 1025 to create pSCB2-sgRNA

848	CCGCCAGGCAAATTCTGTTT	Reverse primer for colony PCR, all gRNAs
954	GGGTTCTATCGCCACGGAC	Colony PCR for pSC-rhadCas9
955	ATTTTTGCGGCGCGTGTAG	Colony PCR for pSC-rhadCas9
957	GTCAGCAATTTCGCCAGCAG	Colony PCR for pAH-CTX1-rha
964	CACTTGTGTATAAGAGTCAG	Reverse primer for In-fusion construction of pKS1
965	CTTATACACAAGTGCccatggGTCTTCAACGAGGCAggatcc GGCCGCACTAGTCTAGA	Forward primer for In-fusion construction of pKS1
972	ATAATACCATGGATGTCCACGAGGTCTCT	Used to amplify the barcode during pRBrha-Barcode construction
973	AATTAAGGATCCGTCGACCTGCAGCGTACG	Used to amplify the barcode during pRBrha-Barcode construction
976	TATAATAaagcttATGTCAACTGGGTTCGTGC	Amplifies rhamnose system from pSC201 to clone into mini-CTX
979	TATATAaagcttACGCAGAAAGGCCCACCCGAAG	Amplifies K56-2 codon optimized dCas9 for insertion into pSCrhaB2
987	AAATTAcatatgGACAAGAAGTACTCGATCGGCC	Amplifies K56-2 codon optimized dCas9 for insertion into pSCrhaB2

1008	GTTTCCTCAACGACCTGCAG	Colony PCR for insertion of mini-CTX1 into K56-2 genome
1025	ATAATAggtaccCGCACGAACCCAGTTGAC	Used with 847 to create pSCB2-sgRNA
1071	ATAATAactagtTCCTGCTGAATTTCATTACGACC	Amplifies rhamnose system from pSC201 to clone into mini-CTX
1072	ATAATAactagtTATGGACAAGAAGTACTCGATCGG	Amplifies K56-2 codon optimized dCas9 for insertion into mini-CTX1
1073	ATAATAgcggccgcACGCAGAAAGGCCCACCCGAAG	Amplifies K56-2 codon optimized dCas9 for insertion into mini-CTX1
1074	AAGTGGATCAGCAAGGACGG	Colony PCR for pAH-CTX1-rha
1075	AAGTCCTGAGCGCCTACAAC	Colony PCR for insertion of mini-CTX1 into K56-2 genome
1077	CCGTGCCATGTTCGACAATC	Colony PCR for insertion of mini-CTX1 into K56-2 genome
1084	ATAATActcgagCGCCTACCTGTGACGGAAGA	To amplify *cat* gene from pKD3
1091	ACTGCCTACCCCACAACAAC	Colony PCR for pAH25-SceI
1092	ACTAGTATTATACCTAGGACTGAGCTAGC	Reverse primer, all gRNAs
1093	GTTTTAGAGCTAGAAATAGCAAGTTAAAATAAGGC	Forward primer, control gRNA
1095	GCGGGACGACTGAGCTCGCTGTTTTAGAGCTAGAAATAGCAAGTTAAAATAAGGC	Forward primer, gRNA 9 for targeting *fliF* in K56-2

1096	CACGATGCGATTATCGTGACGTTTTAGAGCTAGAAATAGCAAGTTAAAATAAGGC	Forward primer, gRNA 10 for targeting *fliF* in K56-2
1097	CTCCGATCGACCGAAAAGAGGTTTTAGAGCTAGAAATAGCAAGTTAAAATAAGGC	Forward primer, gRNA 11 for targeting *fliF* in K56-2
1098	GTATAATACTAGTGTTTTAGAGCTAGAAATAG	Forward primer for colony PCR, control gRNA
1100	TAGGTATAATACTAGTGCGGGAC	Forward primer for colony PCR, gRNA 9
1101	TAGGTATAATACTAGTCACGATGCG	Forward primer for colony PCR, gRNA 10
1102	CCTAGGTATAATACTAGTCTCCGATC	Forward primer for colony PCR, gRNA 11
1126	TCGTTGCGCAGATAGGTCAC	Colony PCR for integration of pAH18 into K56-2::dCas9
1128	GATCGATCCTACCCCTTGCG	Colony PCR to screen for pFLPe4
1129	GCCTAAGGTGCTTGTTCGTC	Colony PCR to screen for pFLPe4
1150	AATTAAaccggtACTCATCGCAGTACTGTTGTATTC	To amplify cat gene from pKD3
1156	TAAGATggtaccTTCCCTACAAGTTCGCCGATG	To amplify internal fragment of *fliF* for insertion into pGPΩ-Tp
1157	TAAGATgaattcGGGTAGAGGTCGACGAACAC	To amplify internal fragment of *fliF* for insertion into pGPΩ-Tp
1161	GTCGGTTAATAAATTTGTTGGTTTTAGAGCTAGAAATAGCAAGTTAAAATAAGGC	Forward primer, gRNA 1 for targeting *paaA* in K56-2

1162	GTATAAACCAACCGACCGGTGTTTTAGAGCTAGAAATAGCAAGTTAAAATAAGGC	Forward primer, K56-2 gRNA 2 for targeting *paaA* in K56-2
1163	CGAAGTATAAACCAACCGACGTTTTAGAGCTAGAAATAGCAAGTTAAAATAAGGC	Forward primer, K56-2 gRNA 3 for targeting *paaA* in K56-2
1164	TCCTAGGTATAATACTAGTGTCGGTT	Forward primer for colony PCR, gRNA 1
1165	GTGTATAAACCAACCGACCGG	Forward primer for colony PCR, gRNA 2
1166	CGAAGTATAAACCAACCGAC	Forward primer for colony PCR, gRNA 3
1167	CTGCCGTTCGAGTTCATGC	Colony PCR for integration of pAH-CTX1-rhadCas9 into *B. multivorans*
1168	CGGTTACAATGCTCGACCTTG	Colony PCR for integration of pAH-CTX1-rhadCas9 into *B. thailandensis*
1171	CTCCAGATTCTGCCGCAGTGGTTTTAGAGCTAGAAATAGCAAGTTAAAATAAGGC	Forward primer,gRNA 6 and 15 for targeting *phbC* in K56-2 and ATCC17616, respectively
1172	CGGGCCGTCATGCTCTGGAGGTTTTAGAGCTAGAAATAGCAAGTTAAAATAAGGC	Forward primer, gRNA 7 for targeting *phbC* in K56-2
1173	CGAGCCGGGCCGTCATGCTCGTTTTAGAGCTAGAAATAGCAAGTTAAAATAAGGC	Forward primer, gRNA 8 for targeting *phbC* in K56-2
1174	CCGTTCAGCCGGGCGTGTTCGTTTTAGAGCTAGAAATAGCAAGTTAAAATAAGGC	Forward primer, gRNA 21 for targeting *phbC* in E264

1175	TTTCCTCGGTGTTGCCTGCGGTTTTAGAGCTAGAAATAG CAAGTTAAAATAAGGC	Forward primer, gRNA 22 for targeting *phbC* in E264
1176	GTGGTTCCTCGGTGTTTCCTGTTTTAGAGCTAGAAATAG CAAGTTAAAATAAGGC	Forward primer, gRNA 23 for targeting *phbC* in E264
1177	CGGGCCGTCATGCCCTGGAGGTTTTAGAGCTAGAAATA GCAAGTTAAAATAAGGC	Forward primer, gRNA 16 for targeting *phbC* in ATCC17616
1178	CGAGCCGGGCCGTCATGCCCGTTTTAGAGCTAGAAATA GCAAGTTAAAATAAGGC	Forward primer, gRNA 17 for targeting phbC in ATCC17616
1179	GTCCTAGGTATAATACTAGTCTCCAG	Forward primer for colony PCR, gRNA 6
1180	CCTAGGTATAATACTAGTCGGGC	Forward primer for colony PCR, gRNA 7 and 16
1181	CCTAGGTATAATACTAGTCGAGCC	Forward primer for colony PCR, gRNA 8 and 17
1182	GGTATAATACTAGTCCGTTCAGCC	Forward primer for colony PCR, gRNA 21
1183	AGTCCTAGGTATAATACTAGTTTTCC	Forward primer for colony PCR, gRNA 22
1184	GGTATAATACTAGTGTGGTTCCTC	Forward primer for colony PCR, gRNA 23
1194	AGGGCTTCATGACGGGTTTC	Colony PCR tetracycline cassette removal from *B. multivorans*::dCas9
1195	TCGGTATCTCTGGCTGTTCG	Colony PCR tetracycline cassette removal from *B. thailandensis*::dCas9
1196	ATAATAggtaccCGTTCCAGATGCCGTCGATG	To amplify internal fragment of *phbC* for insertion into pGPΩ-Tp

1197	ATAATAgaattcGTGAAACGGATGCGCTCAC	To amplify internal fragment of *phbC* for insertion into pGPΩ-Tp
1198	CGACGAATGCCAAGCAGATAGTTTTAGAGCTAGAAATAGCAAGTTAAAATAAGGC	Forward primer, non-target gRNA in all three species
1199	CTAGGTATAATACTAGTCGACGAATGC	Forward primer for colony PCR, non-target gRNA
1200	TTAATAAATTTGTTGCGGAATTTGTTTTAGAGCTAGAAATAGCAAGTTAAAATAAGGC	Forward primer, gRNA 12 for targeting *paaA* in ATCC17616
1201	CGCAGTATAAACCAACCGACGTTTTAGAGCTAGAAATAGCAAGTTAAAATAAGGC	Forward primer, gRNA 13 for targeting *paaA* in ATCC17616
1202	ACATGGCGAGCGCTCTCGTCGTTTTAGAGCTAGAAATAGCAAGTTAAAATAAGGC	Forward primer, gRNA 14 for targeting *paaA* in ATCC17616
1203	GTCCTAGGTATAATACTAGTTTAATAAATTTG	Forward primer for colony PCR, gRNA 12
1204	GGTATAATACTAGTCGCAGTATAAAC	Forward primer for colony PCR, gRNA 13
1205	GGTATAATACTAGTACATGGCGAG	Forward primer for colony PCR, gRNA 14
1206	CGGTTAATAAATGATTTTAGGTTTTAGAGCTAGAAATAGCAAGTTAAAATAAGGC	Forward primer, gRNA 18 for targeting *paaA* in E264
1207	GTTCACGCAGTATAAACCAAGTTTTAGAGCTAGAAATAGCAAGTTAAAATAAGGC	Forward primer, E264 gRNA 19 for targeting *paaA* in E264
1208	TGGCGATGTTCTCGTCCAGGGTTTTAGAGCTAGAAATAGCAAGTTAAAATAAGGC	Forward primer, E264 gRNA 20 for targeting *paaA* in E264

1209	GGTATAATACTAGTCGGTTAATAAATGAT	Forward primer for colony PCR, gRNA 18
1210	GGTATAATACTAGTGTTCACGCAG	Forward primer for colony PCR, gRNA 19
1211	GTATAATACTAGTTGGCGATGTTC	Forward primer for colony PCR, gRNA 20
1212	ACATGGCGAAGGCTCTCGTCGTTTTAGAGCTAGAAATAGCAAGTTAAAATAAGGC	Forward primer, gRNA 4 for targeting *paaA* in K56-2
1213	ACGCAATCCCTCGACATCCCGTTTTAGAGCTAGAAATAGCAAGTTAAAATAAGGC	Forward primer, gRNA 5 for targeting *paaA* in K56-2
1214	GGTATAATACTAGTACATGGCGAAG	Forward primer for colony PCR, gRNA 4
1215	GGTATAATACTAGTACGCAATCCC	Forward primer for colony PCR, gRNA 5
1216	ATAATAactagtTATGGATAAGAAATACTCAATAGGCTT	Used to amplify the native dCas9
1217	ATAATAgcggccgcACGCAGAAAGGCCCAC	Used to amplify the native dCas9
1218	CTTCCGCTGTCTCTCCACTG	Colony PCR for pAH-CTX1-rhadcas9-native
1219	GTAAACGGATGCTGGCTAGTG	Colony PCR for pAH-CTX1-rhadcas9-native integration into K56-2
1409	GGCTTATGTCAACTGGGTTCG	Forward primer for general colony PCR of sgRNA plasmids
1429	GGATCCGGCCGCACTAGTCTAGATTTAAATTACCGTAGTGAGTTCTTCGTCCGAGCCAC	Collector probe for RB-TnSeq-circle

2163	CAAGCAGAAGACGGCATACGAGATGCTTACGGACGTCT CGTGGGCTCGGAGATGTGTATAAGAGACAGGTCGACCT GCAGCGTACG	BarSeq primer with i7 index; UDP0089
2164	CAAGCAGAAGACGGCATACGAGATCGCTTGAAGTGTCT CGTGGGCTCGGAGATGTGTATAAGAGACAGGTCGACCT GCAGCGTACG	BarSeq primer with i7 index; UDP0090
2165	CAAGCAGAAGACGGCATACGAGATCGCCTTCTGAGTCT CGTGGGCTCGGAGATGTGTATAAGAGACAGGTCGACCT GCAGCGTACG	BarSeq primer with i7 index; UDP0091
2166	CAAGCAGAAGACGGCATACGAGATCTGGATATGTGTCT CGTGGGCTCGGAGATGTGTATAAGAGACAGGTCGACCT GCAGCGTACG	BarSeq primer with i7 index; UDP0092
2167	CAAGCAGAAGACGGCATACGAGATATACCAACGCGTC TCGTGGGCTCGGAGATGTGTATAAGAGACAGGTCGACC TGCAGCGTACG	BarSeq primer with i7 index; UDP0093
2168	CAAGCAGAAGACGGCATACGAGATCAATCTATGAGTCT CGTGGGCTCGGAGATGTGTATAAGAGACAGGTCGACCT GCAGCGTACG	BarSeq primer with i7 index; UDP0094
2169	CAAGCAGAAGACGGCATACGAGATGGTGGAATACGTC TCGTGGGCTCGGAGATGTGTATAAGAGACAGGTCGACC TGCAGCGTACG	BarSeq primer with i7 index; UDP0095
2170	CAAGCAGAAGACGGCATACGAGATTGGACGGAGGGTC TCGTGGGCTCGGAGATGTGTATAAGAGACAGGTCGACC TGCAGCGTACG	BarSeq primer with i7 index; UDP0096
2171	AATGATACGGCGACCACCGAGATCTACACCGTGTATCT TTCGTCGGCAGCGTCAGATGTGTATAAGAGACAGGATG TCCACGAGGTCTCT	BarSeq primer with i5 index; UDP0089
2172	AATGATACGGCGACCACCGAGATCTACACGAACCATGA ATCGTCGGCAGCGTCAGATGTGTATAAGAGACAGGATG TCCACGAGGTCTCT	BarSeq primer with i5 index; UDP0090
2173	AATGATACGGCGACCACCGAGATCTACACGGCCATCAT ATCGTCGGCAGCGTCAGATGTGTATAAGAGACAGGATG TCCACGAGGTCTCT	BarSeq primer with i5 index; UDP0091
2174	AATGATACGGCGACCACCGAGATCTACACACATACTTC CTCGTCGGCAGCGTCAGATGTGTATAAGAGACAGGATG TCCACGAGGTCTCT	BarSeq primer with i5 index; UDP0092

2175	AATGATACGGCGACCACCGAGATCTACACTATGTGCAATTCGTCGGCAGCGTCAGATGTGTATAAGAGACAGGATGTCCACGAGGTCTCT	BarSeq primer with i5 index; UDP0093
2176	AATGATACGGCGACCACCGAGATCTACACGATTAAGGTGTCGTCGGCAGCGTCAGATGTGTATAAGAGACAGGATGTCCACGAGGTCTCT	BarSeq primer with i5 index; UDP0094
2177	AATGATACGGCGACCACCGAGATCTACACATGTAGACAATCGTCGGCAGCGTCAGATGTGTATAAGAGACAGGATGTCCACGAGGTCTCT	BarSeq primer with i5 index; UDP0095
2178	AATGATACGGCGACCACCGAGATCTACACCACATCGGTGTCGTCGGCAGCGTCAGATGTGTATAAGAGACAGGATGTCCACGAGGTCTCT	BarSeq primer with i5 index; UDP0096
2208	CAAGCAGAAGACGGCATACGAGATAGACACATTAGTCTCGTGGGCTCGGAGATGTGTATAAGAGACAGGTCGACCTGCAGCGTACG	BarSeq primer with i7 index; UDP0065
2209	AATGATACGGCGACCACCGAGATCTACACGTAAGGCATATCGTCGGCAGCGTCAGATGTGTATAAGAGACAGGATGTCCACGAGGTCTCT	BarSeq primer with i5 index; UDP0065
2210	CAAGCAGAAGACGGCATACGAGATGCGTTGGTATGTCTCGTGGGCTCGGAGATGTGTATAAGAGACAGGTCGACCTGCAGCGTACG	BarSeq primer with i7 index; UDP0066
2211	AATGATACGGCGACCACCGAGATCTACACAATTGCTGCGTCGTCGGCAGCGTCAGATGTGTATAAGAGACAGGATGTCCACGAGGTCTCT	BarSeq primer with i5 index; UDP0066
2212	CAAGCAGAAGACGGCATACGAGATAGCACATCCTGTCTCGTGGGCTCGGAGATGTGTATAAGAGACAGGTCGACCTGCAGCGTACG	BarSeq primer with i7 index; UDP0067
2213	AATGATACGGCGACCACCGAGATCTACACTTACAATTCCTCGTCGGCAGCGTCAGATGTGTATAAGAGACAGGATGTCCACGAGGTCTCT	BarSeq primer with i5 index; UDP0067
2214	CAAGCAGAAGACGGCATACGAGATTTGTTCCGTGGTCTCGTGGGCTCGGAGATGTGTATAAGAGACAGGTCGACCTGCAGCGTACG	BarSeq primer with i7 index; UDP0068
2215	AATGATACGGCGACCACCGAGATCTACACAACCTAGCACTCGTCGGCAGCGTCAGATGTGTATAAGAGACAGGATGTCCACGAGGTCTCT	BarSeq primer with i5 index; UDP0068

2216	CAAGCAGAAGACGGCATACGAGATAAGTACTCCAGTCT CGTGGGCTCGGAGATGTGTATAAGAGACAGGTCGACCT GCAGCGTACG	BarSeq primer with i7 index; UDP0069
2217	AATGATACGGCGACCACCGAGATCTACACTCTGTGTGG ATCGTCGGCAGCGTCAGATGTGTATAAGAGACAGGATG TCCACGAGGTCTCT	BarSeq primer with i5 index; UDP0069
2218	CAAGCAGAAGACGGCATACGAGATACGTCAATACGTCT CGTGGGCTCGGAGATGTGTATAAGAGACAGGTCGACCT GCAGCGTACG	BarSeq primer with i7 index; UDP0070
2219	AATGATACGGCGACCACCGAGATCTACACGGAATTCCA ATCGTCGGCAGCGTCAGATGTGTATAAGAGACAGGATG TCCACGAGGTCTCT	BarSeq primer with i5 index; UDP0070
2220	CAAGCAGAAGACGGCATACGAGATGGTGTACAAGGTC TCGTGGGCTCGGAGATGTGTATAAGAGACAGGTCGACC TGCAGCGTACG	BarSeq primer with i7 index; UDP0071
2221	AATGATACGGCGACCACCGAGATCTACACAAGCGCGCT TTCGTCGGCAGCGTCAGATGTGTATAAGAGACAGGATG TCCACGAGGTCTCT	BarSeq primer with i5 index; UDP0071
2222	CAAGCAGAAGACGGCATACGAGATCCACCTGTGTGTCT CGTGGGCTCGGAGATGTGTATAAGAGACAGGTCGACCT GCAGCGTACG	BarSeq primer with i7 index; UDP0072
2223	AATGATACGGCGACCACCGAGATCTACACTGAGCGTTG TTCGTCGGCAGCGTCAGATGTGTATAAGAGACAGGATG TCCACGAGGTCTCT	BarSeq primer with i5 index; UDP0072
2224	CAAGCAGAAGACGGCATACGAGATGTTCCGCAGGGTCT CGTGGGCTCGGAGATGTGTATAAGAGACAGGTCGACCT GCAGCGTACG	BarSeq primer with i7 index; UDP0073
2225	AATGATACGGCGACCACCGAGATCTACACATCATAGGC TTCGTCGGCAGCGTCAGATGTGTATAAGAGACAGGATG TCCACGAGGTCTCT	BarSeq primer with i5 index; UDP0073
2226	CAAGCAGAAGACGGCATACGAGATACCTTATGAAGTCT CGTGGGCTCGGAGATGTGTATAAGAGACAGGTCGACCT GCAGCGTACG	BarSeq primer with i7 index; UDP0074
2227	AATGATACGGCGACCACCGAGATCTACACTGTTAGAAG GTCGTCGGCAGCGTCAGATGTGTATAAGAGACAGGATG TCCACGAGGTCTCT	BarSeq primer with i5 index; UDP0074

2228	CAAGCAGAAGACGGCATACGAGATCGCTGCAGAGGTC TCGTGGGCTCGGAGATGTGTATAAGAGACAGGTCGACC TGCAGCGTACG	BarSeq primer with i7 index; UDP0075
2229	AATGATACGGCGACCACCGAGATCTACACGATGGATGT ATCGTCGGCAGCGTCAGATGTGTATAAGAGACAGGATG TCCACGAGGTCTCT	BarSeq primer with i5 index; UDP0075
2230	CAAGCAGAAGACGGCATACGAGATGTAGAGTCAGGTC TCGTGGGCTCGGAGATGTGTATAAGAGACAGGTCGACC TGCAGCGTACG	BarSeq primer with i7 index; UDP0076
2231	AATGATACGGCGACCACCGAGATCTACACACGGCCGTC ATCGTCGGCAGCGTCAGATGTGTATAAGAGACAGGATG TCCACGAGGTCTCT	BarSeq primer with i5 index; UDP0076
2232	CAAGCAGAAGACGGCATACGAGATGGATACCAGAGTC TCGTGGGCTCGGAGATGTGTATAAGAGACAGGTCGACC TGCAGCGTACG	BarSeq primer with i7 index; UDP0077
2233	AATGATACGGCGACCACCGAGATCTACACCGTTGCTTA CTCGTCGGCAGCGTCAGATGTGTATAAGAGACAGGATG TCCACGAGGTCTCT	BarSeq primer with i5 index; UDP0077
2234	CAAGCAGAAGACGGCATACGAGATCGCACTAATGGTCT CGTGGGCTCGGAGATGTGTATAAGAGACAGGTCGACCT GCAGCGTACG	BarSeq primer with i7 index; UDP0078
2235	AATGATACGGCGACCACCGAGATCTACACTGACTACAT ATCGTCGGCAGCGTCAGATGTGTATAAGAGACAGGATG TCCACGAGGTCTCT	BarSeq primer with i5 index; UDP0078
2236	CAAGCAGAAGACGGCATACGAGATTCCTGACCGTGTCT CGTGGGCTCGGAGATGTGTATAAGAGACAGGTCGACCT GCAGCGTACG	BarSeq primer with i7 index; UDP0079
2237	AATGATACGGCGACCACCGAGATCTACACCGGCCTCGT TTCGTCGGCAGCGTCAGATGTGTATAAGAGACAGGATG TCCACGAGGTCTCT	BarSeq primer with i5 index; UDP0079
2238	CAAGCAGAAGACGGCATACGAGATCTGGCTTGCCGTCT CGTGGGCTCGGAGATGTGTATAAGAGACAGGTCGACCT GCAGCGTACG	BarSeq primer with i7 index; UDP0080
2239	AATGATACGGCGACCACCGAGATCTACACCAAGCATCC GTCGTCGGCAGCGTCAGATGTGTATAAGAGACAGGATG TCCACGAGGTCTCT	BarSeq primer with i5 index; UDP0080

2240	CAAGCAGAAGACGGCATACGAGATACCAGCGACAGTC TCGTGGGCTCGGAGATGTGTATAAGAGACAGGTCGACC TGCAGCGTACG	BarSeq primer with i7 index; UDP0081
2241	AATGATACGGCGACCACCGAGATCTACACTCGTCTGAC TTCGTCGGCAGCGTCAGATGTGTATAAGAGACAGGATG TCCACGAGGTCTCT	BarSeq primer with i5 index; UDP0081
2242	CAAGCAGAAGACGGCATACGAGATTTGTAACGGTGTCT CGTGGGCTCGGAGATGTGTATAAGAGACAGGTCGACCT GCAGCGTACG	BarSeq primer with i7 index; UDP0082
2243	AATGATACGGCGACCACCGAGATCTACACCTCATAGCG ATCGTCGGCAGCGTCAGATGTGTATAAGAGACAGGATG TCCACGAGGTCTCT	BarSeq primer with i5 index; UDP0082
2244	CAAGCAGAAGACGGCATACGAGATGTAAGGCATAGTC TCGTGGGCTCGGAGATGTGTATAAGAGACAGGTCGACC TGCAGCGTACG	BarSeq primer with i7 index; UDP0083
2245	AATGATACGGCGACCACCGAGATCTACACAGACACATT ATCGTCGGCAGCGTCAGATGTGTATAAGAGACAGGATG TCCACGAGGTCTCT	BarSeq primer with i5 index; UDP0083
2246	CAAGCAGAAGACGGCATACGAGATGTCCACTTGTGTCT CGTGGGCTCGGAGATGTGTATAAGAGACAGGTCGACCT GCAGCGTACG	BarSeq primer with i7 index; UDP0084
2247	AATGATACGGCGACCACCGAGATCTACACGCGCGATGT TTCGTCGGCAGCGTCAGATGTGTATAAGAGACAGGATG TCCACGAGGTCTCT	BarSeq primer with i5 index; UDP0084
2248	CAAGCAGAAGACGGCATACGAGATTTAGGTACCAGTCT CGTGGGCTCGGAGATGTGTATAAGAGACAGGTCGACCT GCAGCGTACG	BarSeq primer with i7 index; UDP0085
2249	AATGATACGGCGACCACCGAGATCTACACCATGAGTAC TTCGTCGGCAGCGTCAGATGTGTATAAGAGACAGGATG TCCACGAGGTCTCT	BarSeq primer with i5 index; UDP0085
2250	CAAGCAGAAGACGGCATACGAGATGGAATTCCAAGTC TCGTGGGCTCGGAGATGTGTATAAGAGACAGGTCGACC TGCAGCGTACG	BarSeq primer with i7 index; UDP0086
2251	AATGATACGGCGACCACCGAGATCTACACACGTCAATA CTCGTCGGCAGCGTCAGATGTGTATAAGAGACAGGATG TCCACGAGGTCTCT	BarSeq primer with i5 index; UDP0086

2252	CAAGCAGAAGACGGCATACGAGATCATGTAGAGGGTC TCGTGGGCTCGGAGATGTGTATAAGAGACAGGTCGACC TGCAGCGTACG	BarSeq primer with i7 index; UDP0087
2253	AATGATACGGCGACCACCGAGATCTACACGATACCTCC TTCGTCGGCAGCGTCAGATGTGTATAAGAGACAGGATG TCCACGAGGTCTCT	BarSeq primer with i5 index; UDP0087
2254	CAAGCAGAAGACGGCATACGAGATTACACGCTCCGTCT CGTGGGCTCGGAGATGTGTATAAGAGACAGGTCGACCT GCAGCGTACG	BarSeq primer with i7 index; UDP0088
2255	AATGATACGGCGACCACCGAGATCTACACATCCGTAAG TTCGTCGGCAGCGTCAGATGTGTATAAGAGACAGGATG TCCACGAGGTCTCT	BarSeq primer with i5 index; UDP0088
2421	GAGCGGGGTCGGGCAAGCAGGTTTTAGAGCTAGAAAT AGCAAGTTAAAATAAGGC	Primer containing sgRNA to target *ogcABEI* operon
2422	TCGTCGTGCCCGTTGTAGGCGTTTTAGAGCTAGAAATA GCAAGTTAAAATAAGGC	Primer containing sgRNA to target *ogcABEI* operon
2431	CCGTCGCGACAGTGATTAAGGTTTTAGAGCTAGAAATA GCAAGTTAAAATAAGGC	Primer containing sgRNA to target *bpeABoprB* operon
2432	GTGAAGACCGGTACGGATTGGTTTTAGAGCTAGAAATA GCAAGTTAAAATAAGGC	Primer containing sgRNA to target *bpeABoprB* operon
2437	GCCGAACAGGCGAGCCGATAGTTTTAGAGCTAGAAATA GCAAGTTAAAATAAGGC	Primer containing sgRNA to target *zapA*
2438	CGAGCGGATTTTCGACATTTGTTTTAGAGCTAGAAATA GCAAGTTAAAATAAGGC	Primer containing sgRNA to target *zapA*
2443	TTCGCGTCGACCGACAACGCGTTTTAGAGCTAGAAATA GCAAGTTAAAATAAGGC	Primer containing sgRNA to target *ampD*
2444	GCGGGCCGCATCTCGAAGTTGTTTTAGAGCTAGAAATA GCAAGTTAAAATAAGGC	Primer containing sgRNA to target *ampD*
2445	TGCGGCGACCAGCAGGGTCGGTTTTAGAGCTAGAAATA GCAAGTTAAAATAAGGC	Primer containing sgRNA to target *ampC*

2446	TCTGGCGCGTGACGGTGTCGGTTTTAGAGCTAGAAATA GCAAGTTAAAATAAGGC	Primer containing sgRNA to target *ampC*
2453	GGCCTCGTCTTGAACTGGGCGTTTTAGAGCTAGAAATA GCAAGTTAAAATAAGGC	Primer containing sgRNA to target *piuA*
2454	GTTTCGGCGGAGGCGAGCAGGTTTTAGAGCTAGAAATA GCAAGTTAAAATAAGGC	Primer containing sgRNA to target *piuA*
2457	CGTCGCGGCGGCCAGCAACAGTTTTAGAGCTAGAAATA GCAAGTTAAAATAAGGC	Primer containing sgRNA to target *penB*
2458	GCGGTGGCGGTGAGAACGAGGTTTTAGAGCTAGAAAT AGCAAGTTAAAATAAGGC	Primer containing sgRNA to target *penB*
2459	CGTCACGCTCAGCTCGAGGCGTTTTAGAGCTAGAAATA GCAAGTTAAAATAAGGC	Primer containing sgRNA to target *penR*
2460	CTGAACGCGTCGCTCAGCACGTTTTAGAGCTAGAAATA GCAAGTTAAAATAAGGC	Primer containing sgRNA to target *penR*
2461	GGAATCAGGGCGAAAAGTCGGTTTTAGAGCTAGAAAT AGCAAGTTAAAATAAGGC	Primer containing sgRNA to target *ispDF* operon
2462	CGTGCCGGCACAGGGAATCAGTTTTAGAGCTAGAAATA GCAAGTTAAAATAAGGC	Primer containing sgRNA to target *ispDF* operon
2467	GCCGACGTCAGGCACGCGAAGTTTTAGAGCTAGAAATA GCAAGTTAAAATAAGGC	Primer containing sgRNA to target *uppS* operon
2468	ATGATGATCGCGATGTGACGGTTTTAGAGCTAGAAATA GCAAGTTAAAATAAGGC	Primer containing sgRNA to target *uppS* operon
2469	GATGTTCGCGCCGATAAAACGTTTTAGAGCTAGAAATA GCAAGTTAAAATAAGGC	Primer containing sgRNA to target *hldD*
2470	ATTGCGAAACTTGTCTGCGCGTTTTAGAGCTAGAAATA GCAAGTTAAAATAAGGC	Primer containing sgRNA to target *hldD*
2471	CGGGCGGAAAGATCGGAAATGTTTTAGAGCTAGAAAT AGCAAGTTAAAATAAGGC	Primer containing sgRNA to target *dacB*
2472	GGCGAACCGGGCGGAAAGATGTTTTAGAGCTAGAAAT AGCAAGTTAAAATAAGGC	Primer containing sgRNA to target *dacB*

2475	GCGCGACCGCGCGATATACTGTTTTAGAGCTAGAAATAGCAAGTTAAAATAAGGC	Primer containing sgRNA to target *slt*
2476	GAGCGTGTCGTCGTTCGGTGGTTTTAGAGCTAGAAATAGCAAGTTAAAATAAGGC	Primer containing sgRNA to target *slt*
2477	TGTTTCGTCGACGGAATGCGGTTTTAGAGCTAGAAATAGCAAGTTAAAATAAGGC	Primer containing sgRNA to target *wbiFGHI*
2478	GCGGAGACTGGAGAGCGTCCGTTTTAGAGCTAGAAATAGCAAGTTAAAATAAGGC	Primer containing sgRNA to target *wbiFGHI* operon
2479	ATCGGCTTGTCGAATACGTCGTTTTAGAGCTAGAAATAGCAAGTTAAAATAAGGC	Primer containing sgRNA to target *vio-wbx* operon
2480	ATTGGCTTGGTCACATAGATGTTTTAGAGCTAGAAATAGCAAGTTAAAATAAGGC	Primer containing sgRNA to target *vio-wbx* operon
2481	TGTGGATACGTCCGGGGAAGGTTTTAGAGCTAGAAATAGCAAGTTAAAATAAGGC	Primer containing sgRNA to target *wabR-P* operon
2482	AGCGGCTTGAACAGCAATCTGTTTTAGAGCTAGAAATAGCAAGTTAAAATAAGGC	Primer containing sgRNA to target *wabR-P* operon
2483	CGCAACGAGCGACAACGAACGTTTTAGAGCTAGAAATAGCAAGTTAAAATAAGGC	Primer containing sgRNA to target *pglL*
2484	GTGTGATTCGTGATCGCGTAGTTTTAGAGCTAGAAATAGCAAGTTAAAATAAGGC	Primer containing sgRNA to target *pglL*
2485	AGGTGACCGGTGCTCGACACGTTTTAGAGCTAGAAATAGCAAGTTAAAATAAGGC	Primer containing sgRNA to target *bacA*
2486	GCCCGCGACGATCAGGTGACGTTTTAGAGCTAGAAATAGCAAGTTAAAATAAGGC	Primer containing sgRNA to target *bacA*
2615	ATTAcatatgGACTGGATCCTGATCTGCAAG	Used to amplify *bacA* (K562_RS14895)
2616	ATTAtctagaGCATCACGCCCAGTTCAG	Used to amplify *bacA* (K562_RS14895)
2617	ATTAcatatgTTGAGCGTGCTGGCGA	Used to amplify *bceB* (K562_RS21495)

2618	ATTAtctagaGTCGGTGTCAGTACGCGTTG	Used to amplify *bceB* (K562_RS21495)
2619	ATTAcatatgACCCTCATCGTCACCGG	Used to amplify *hldD* (K562_RS14060)
2620	ATTAtctagaGACCCAGTCTATCGATGCAACG	Used to amplify *hldD* (K562_RS14060)
2621	ATTAcatatgCAAGTCACCGTCAACGAGC	Used to amplify *murA* (K562_RS01625)
2622	ATTAtctagaCGCGGTCATGCTTGGCTC	Used to amplify *murA* (K562_RS01625)
2623	ATTAcatatgACGTCCCCTGCTTGC	Used to amplify *ogcA* (K562_RS15015)
2624	ATTAtctagaCCGGATGCACGTCAGGC	Used to amplify *ogcA* (K562_RS15015)
2625	ATTAcatatgACCTATACCAGCTCTACCG	Used to amplify *uppS* (K562_RS08220)
2626	ATTAtctagaTCACACGGGTTTTCAGCATG	Used to amplify *uppS* (K562_RS08220)
2627	ATTAcatatgTTCGCCATCATGTTCGG	Used to amplify *waaL* (K562_RS06530)
2628	ATTAtctagaTTCACGATCCGCTCCCC	Used to amplify *waaL* (K562_RS06530)
2629	ATTAcatatgTTGCAATCCAGAGCATCTTGG	Used to amplify *wbiI* (K562_RS15035)
2630	ATTAtctagaCCTGGAGCCACGTCACCC	Used to amplify *wbiI* (K562_RS15035)
2631	ATTAcatatgCGGGATAACATTCAAAGTTCC	Used to amplify *wzm-wzt* (K562_RS15085-80)
2632	ATTAtctagaCGTCGACGCTAAACTCATCATC	Used to amplify *wzm-wzt* (K562_RS15085-80)

2668	CGTTGCTGGTCCATTTTTCGAC	Colony PCR for *wzm-wzt* deletion
2669	TTCCGCCGAATTAAACAACTTCG	Colony PCR for *wzm-wzt* deletion
2670	TGCGTTTTTCTGCACACTTG	Colony PCR for *wbiI* deletion
2671	GCTCGGCTTCTTCCTGTGG	Colony PCR for *wbiI* deletion
2672	AGGCGGCGATGCCGCCAGAGGTTTTAGAGCTAGAAATAGCAAGTTAAAATAAGGC	Primer containing sgRNA to target *wzm-wzt* operon
2673	ATACGGCCAGCAGGAGCAACGTTTTAGAGCTAGAAATAGCAAGTTAAAATAAGGC	Primer containing sgRNA to target *wzm-wzt* operon
2674	AACGGCCACCGGAACACCGCGTTTTAGAGCTAGAAATAGCAAGTTAAAATAAGGC	Primer containing sgRNA to target *waaL*
2675	TCGGGACGAACAACGGCCACGTTTTAGAGCTAGAAATAGCAAGTTAAAATAAGGC	Primer containing sgRNA to target *waaL*
2679	GATGCTGCCGTCGTGCAACGGTTTTAGAGCTAGAAATAGCAAGTTAAAATAAGGC	Primer containing sgRNA to target *bceB*
2680	CCACGACTGGTAGATGCCGAGTTTTAGAGCTAGAAATAGCAAGTTAAAATAAGGC	Primer containing sgRNA to target *bceB*
2681	CCGAGCGCGTGGATGTACGCGTTTTAGAGCTAGAAATAGCAAGTTAAAATAAGGC	Primer containing sgRNA to target *bceQ*
2682	CTTCGAGATGTGGTTCTGCGGTTTTAGAGCTAGAAATAGCAAGTTAAAATAAGGC	Primer containing sgRNA to target *bceQ*
2689	CGGTTTCGGGATGGGCG	Colony PCR for *bacA* deletion
2690	GAGAGGGTTCAGCATGACCG	Colony PCR for *bacA* deletion
2691	GGCAAGAATCACGGGCTG	Colony PCR for *bceB* deletion

2692	CTTGAAGCCGGTCATGTAGC	Colony PCR for *bceB* deletion
2693	GCTTTGTCGGTTGCGTGA	Colony PCR for *hldD* deletion
2694	CACTGTTGCTCACCCGTTC	Colony PCR for *hldD* deletion
2695	CGCCGATCTTTGGCATCTCTA	Colony PCR for *waaL* deletion
2696	GTCGGTCGGGAAGGCAAC	Colony PCR for *waaL* deletion
2863	AGCGGATGCAGCCATAACTGGTTTTAGAGCTAGAAATAGCAAGTTAAAATAAGGC	Primer containing sgRNA to target *opnA* in K56-2, ATCC 17616, and E264
2864	CGGCACCGACTGTGCCGAAGGTTTTAGAGCTAGAAATAGCAAGTTAAAATAAGGC	Primer containing sgRNA to target *opnA* in K56-2, ATCC 17616, and E264

Table A4. gBlocks and gene fragments used in Chapters 3,4 and 5 of this study

Name	Sequence (restriction sites in lowercase)	Description
TnTag	AATTAAggtaccGGCCCGCGGAATCGGAACATCGGCTGC TAACCGCTGGACAACGCGTGGATGGCGCGCTGCTGGCGCGGTAT GGATCCGTGAACGGGCTCAACTATGCGGTGGTCGGGCCGGCCGG GAGTCTCGGGGAAAAGGCGGTCGTGCAGGCGCTCGATCAGCAGA CTTGAAGCGGCAGGATGCGCGTCCGGCTGGCGGTCGGTAATGGC CGCCAGCGCCTTTTTTGGCGCGGCTTGGCCGGCTTGCACCGGTGC GTGCTCACCACTCGAATGCACAGCGTTTCGACTGACTTGCTCGCA CTGTTATTCACACCGAAACCTCGCTGGCACCCTCACCTTTAAAATC ACAGGGTTTCGAGTCGCCGCGGAACGGGATATCCACACCTCTCCT GATGGTGCTGCGTGCTGACTTCGATGGGTTCGCTCACCGTTGACAT GCACAGCGTTTCTCGTTGTTTTGGGCATCGCTCTTAATTAATTTAAA TCTAGACTAGTGCGGCCGCACTTGTGTATAAGAGTCAATATCCACA ACCCGGGTAATTGACCGATCGTCTTCGCCGGGTTCGACTACGCTCA CCCATTGAATGCAGCCGGTTTCGAGTGGCTTCGAGTCAACGATATC CACACGGCATTCGACATCCGGACGTCGCCGGCGATTCGTTCGCTG CCCTCTTTCATGGTCGGCAAAGCCTTGCCGGGCAATGCATTCAGGC CGACGAGCCCATCGAAACCGGGACGCTCACCGCTCGGATGCACAG GGTTTCAACTGGATCGTGCGCCGGTTATCCACACACCGCCGCTCGC GCGTCGGGTCACTTCGTCCCGACTCTCCCGAGAATCTCGCCGGTTTCCGGC GCGATGACGTAGTGGATCGACTTCCCGAGCCGATTTGCATTGCCCAGTCCG CGCATACCCGGAATCAGCTTTGCCACGAACGTGATGGTGACGACATCGTCA TCTGGCACGGGGTCCACCGTGGATgaattcAATTAA	Used to introduce the unique Tn tag between K562_RS16895 and K562_RS16900
5’ *dcas9* fragment	AAAAGATCTAAAGAGGAGAAAGGATCTATGGACAAGAAGTACTCG ATCGGCCTCGCGATCGGCACGAATTCCGTGGGCTGGGCGGTCATCC GGACGAATACAAGGTCCCGAGTAAGAAATTCAAAGTGCTCGGCAATACGG ACCGCCACTCCATTAAGAAAAATCTGATTGGCGCGCTGCTGT TCGATTCGGGCGAAACGGCCGAAGCGACCCGCCTCAAGCGTACGG CGCGTCGGCGCTACACGCGCCGCAAAAATCGCATTTGCTACCTGCA GGAAATCTTCAGCAACGAAATGGCCAAGGTGGACGATAGCTTCTTC CACCGTCTGGAGGAGAGCTTCCTGGTCGAGGAGGACAAGAAGCACG AGCGCCATCCGATTTTCGGTAACATCGTCGACGAAGTTGCGTACCAT GAGAAGTATCCCACGATCTATCACCTCCGCAAGAAACTGGTTGACTC CACCGATAAAGCGGACCTGCGCCTCATCTACCTCGCCCTGGCCCACA TGATTAAGTTCCGCGGTCACTTCCTGATCGAGGGCGACCTGAACCCC GATAATTCGGACGTCGATAAGCTCTTCATTCAGCTGGTGCAGACGTA CAATCAGCTGTTCGAAGAAAACCCCATTAATGCGTCCGGCGTCGAC GCGAAGGCGATCCTCAGCGCGCGCCTCAGTAAGTCGCGCCGCCTGG AAAACCTCATCGCCCAACTCCCGGGCGAGAAGAAGAACGGTCTCTT CGGCAACCTCATCGCCCTGTCCCTGGGCCTCACGCCCAACTTCAAGA GCAACTTTGACCTGGCCGAAGACGCGAAGCTGCAACTGAGCAAGGA TACCTACGACGACGACCTGGACAACCTGCTGGCCCAGATCGGCGA TCAGTACGCCGATCTCTTCCTCGCCGCCAAGAACCTGTCCGACGCG ATTCTGCTCTCCGACATTCTCCGCGTCAACACGGAGATTACGAAGG CGCCGCTGTCGGCCAGCATGATTAAGCGCTACGACGAACACCACC AGGATCTGACCCTGCTGAAGGCCCTCGTTCGCCAGCAACTCCCGG AGAAGTACAAGGAAATTTTCTTCGACCAGTCGAAAAACGGCTATG CCGGCTATATCGACGGTGGCGCGTCCCAAGAAGAGTTCTACAAGT TCATTAAACCGATTCTGGAGAAGATGGACGGCACGGAGGAGCTGC TGGTCAAGCTGAACCGCGAAGATCTGCTGCGCAAACAACGCACCT TCGACAACGGCAGCATCCCCCACCAGATTCACCTGGGCGAACTCC ATGCCATCCTGCGGCGCCAGGAGGACTTCTATCCGTTCCTGAAAG ACAATCGGGAAAAAATCGAAAAAATTCTCACCTTCCGCATTCCGT ACTATGTCGGCCCGCTGGCGCGCGGCAACAGCCGGTTCGCCTGGA TGACGCGCAAGAGTGAAGAGACCATCACGCCCTGGAACTTCGAAG AAGTGGTTGATAAGGGTGCCAGCGCCCAGAGCTTCATTGAACGCA	Used to clone 5’ segment of dCas9 gene codon-optimized for *B. cenocepacia*

	TGACGAATTTCGACAAGAACCTGCCGAACGAGAAGGTGCTCCCCA AGCACTCGCTCCTCTATGAATACTTCACCGTGTACAACGAGCTCAC CAAGGTCAAGTATGTCACCGAGGGCATGCGCAAGCCGGCCTTCCT CTCGGGCGAGCAGAAGAAGGCCATTGTCGACCTGCTCTTCAAGAC GAACCGTAAAGTCACCGTGAAGCAGCTGAAGGAGGACTACTTCAA AAAAATCGAATGCTTCGACAGCGTGGAGATTTCGGGCGTGGAGGA CCGCTTCAACGCCAGCCTCGGTACCTACCACGATCTGCTCAAAATC ATCAAGGATAAGGACTTCCTGG	
3’ *dcas9* fragment	CGATCTGCTCAAAATCATCAAGGATAAGGACTTCCTGGACAACGA GGAGAATGAGGATATTCTGGAAGATATCGTCCTGACGCTGACGCT CTTTGAAGACCGGGAAATGATCGAGGAGCGCCTGAAGACGTACGC CCACCTCTTCGACGACAAGGTGATGAAACAACTCAAACGCCGCCGC TATACGGGCTGGGGCCGCCTGAGTCGCAAGCTGATCAACGGCATCC GGGACAAACAGAGCGGCAAGACCATTCTCGACTTCCTGAAATCCGA CGGCTTCGCCAACCGCAACTTCATGCAGCTCATCCATGACGATAGCC TGACGTTCAAGGAGGACATCCAGAAGGCGCAGGTGTCGGGCCAGG GTGACTCGCTCCACGAACATATTGCCAACCTGGCAGGCTCCCCGGC AATCAAGAAGGGCATTCTGCAGACCGTCAAAGTTGTGGACGAACT CGTCAAAGTGATGGGTCGCCATAAGCCCGAGAACATCGTGATCGAA ATGGCCCGCGAGAACCAGACGACCCAGAAGGGTCAGAAGAACTCC CGCGAGCGCATGAAGCGCATTGAAGAAGGCATCAAAGAACTGGGC AGCCAAATCCTCAAGGAGCACCCGGTTGAGAATACCCAGCTGCAGA ACGAAAAGCTCTACCTGTACTACCTGCAGAACGGCCGCGACATGTA TGTTGACCAGGAGCTGGACATTAATCGTCTCTCGGATTACGACGTCG ATGCCATCGTGCCCCAGTCCTTCCTCAAAGACGACTCGATTGACAAC AAAGTGCTCACCCGCTCCGACAAAAACCGCGGCAAGAGCGACAACG TGCCGAGTGAGGAAGTGGTCAAAAAGATGAAGAATTACTGGCGCCA GCTGCTGAACGCGAAGCTCATTACGCAGCGCAAGTTTGACAACCTGA CCAAAGCCGAACGCGGCGGCCTCAGCGAGCTGGACAAGGCAGGCTT CATTAAGCGCCAGCTCGTGGAAACGCGCCAGATCACCAAGCACGTC GCGCAGATCCTCGACAGCCGGATGAATACGAAGTACGACGAAAAT GATAAGCTGATCCGCGAAGTGAAGGTCATTACCCTCAAGTCGAAGC TCGTCTCGGATTTCCGCAAAGACTTCCAGTTTTACAAGGTTCGCGA AATTAACAACTATCACCACGCACACGACGCATATCTCAACGCGGTC GTCGGCACCGCGCTGATTAAGAAATATCCCAAGCTGGAATCGGAAT TCGTCTACGGCGACTATAAGGTGTATGACGTGCGGAAGATGATTGC GAAAAGCGAACAGGAAATCGGCAAGGCCACGGCCAAGTACTTCTT CTACTCGAATATCATGAATTTCTTTAAAACCGAGATTACGCTCGC CAACGGCGAGATCCGCAAACGCCCGCTCATCGAGACGAACGGCG AAACGGGTGAAATCGTGTGGGATAAGGGCCGCGATTTCGCGACCG TGCGCAAGGTGCTCTCGATGCCGCAAGTCAATATCGTCAAGAAGA CCGAAGTCCAGACGGGCGGTTTCTCCAAGGAAAGCATCCTGCCG AAGCGCAACTCGGACAAACTCATCGCCCGCAAGAAAGATTGGGA TCCCAAGAAGTATGGCGGCTTCGACTCGCCCACGGTGGCGTATTC GGTGCTCGTGGTCGCGAAGGTGGAAAAGGGCAAGTCCAAAAAAC TCAAATCGGTTAAAGAGCTGCTCGGCATCACCATTATGGAGCGCT CCAGCTTCGAGAAAAACCCGATCGACTTCCTCGAAGCCAAGGGCT ACAAAGAGGTGAAAAAGGATCTGATTATCAAGCTGCCGAAATATT CGCTGTTCGAACTCGAAAATGGCCGCAAGCGCATGCTGGCGTCG GCGGGTGAGCTCCAAAAAGGTAACGAACTGGCGCTGCCGAGCAA ATACGTCAACTTTCTGTACCTCGCCAGCCACTACGAAAAGCTCAA GGGTTCGCCGGAGGATAACGAGCAAAAGCAACTCTTTGTTGAAC AGCATAAACACTACCTGGATGAGATCATTGAACAGATCTCGGAG TTCTCCAAGCGCGTCATTCTCGCGGACGCAAACCTGGATAAAGT CCTGAGCGCCTACAACAAACACCGCGATAAGCCGATCCGCGAA CAGGCGGAGAACATCATCCACCTGTTCACCCTGACCAACCTGGG CGCCCCCGCGGCCTTCAAGTATTTCGACACGACCATCGACCGCA AGCGCTATACCAGCACCAAGGAGGTTCTCGACGCCACGCTGATC CACCAGAGCATTACCGGCCTCTACGAAACGCGTATCGACCTCTC GCAGCTGGGTGGTGACTGACTCGAGTGAGGATCTCCAGGCATCA AATGAAACGAAAGGCTCAGTCGAAAGACTGGGCCTTTCGTTTTA	Used to clone 3’ segment of dCas9 gene codon-optimized for *B. cenocepacia*

	TCTGTTGTTTGTCGGTGAACGCTCTCTACTAGAGTCACACTGGCT CACCTTCGGGTGGGCCTTTCTGCGT	
bacA frag	ATTAcccgggCAAGCCTCGACGGCGTGCACATCTTCTTCCCGGAT CCGTGGCACAAGGCGCGTCACCACAAGCGCCGGCTGATCCAGCC GCCGCTCGTCGCGCATCTCGCATCGCGCCTGAAACCCGGCGCGTA CCTGCACTGCGCGACCGACTGGCAGAACTACGCGGAGCAGATGC TTGAAGTACTCGGCGCGGAACCGACGCTCGAAAACACCGCCGCC GATTACGCACCGCGCCCCGACTACCGTCCGGTGACGAAATTCGAA CGGCGCGGGCTGCGGCTCGGCCACGGCGTGTGGGACTTGGTGTTC CGCAAGCGCGCAAGCTGAGCGGCTTCGCCCCACGCAAAATGAAA AAGCCCGACCGTCACTTTTCGACGATCGCCACGCGTATGCCGTTT GTAAGAATCGTAATTGTACCGGGTTCGTAGTTCACCCCGGCAAAT TGGAGCTGTTCGGGCTTGAACGTGTAGATCGGATAGTTGGTCAGC AACTGCGTCGCCAGCAGGCCGGCGGCCGCGCCGACCTGCTGCGC GTACATCTGCGCATCGCCGTCGAGCATGAGGCTGTCGACGGCCGG CGCCTTCAGCACGACCGAGCGGCTCGGCGCGTCGTACGCGAGCTG GCCCGACACGGTGAACTTGCCGCTGACGGGCCCGCGCAGGAACGG GCTCGCGAAATGGGCGTCGAGCTGCACGGCGACGCGGTTCTGGTC GGGCAGCAGGTtctagaTTAA	Enables deletion of entire *bacA* gene
bceB frag	ATTAcccgggCGGTTGCGGCGGAAGAAGAATGGCGCGTTTCGGCGG CCACTGCCGGAGCATTCATGATGACACTCTCCACGGTTGAAGTCA GTGCCTGTCGTTGTAGCATGAAGTAAATCGACAATAAAACCGGAC CCAATGCCGAATATCCGCCACGCATTCATCCGGAAGAATTTTCCTC GATGGCATCGGCTGGAAATAAAAAAATAAAAAATAATTCCGGTCG CCGGCCGGACGTGCCCGCCCGCAAAGGGTGCACGGCAAGCGTAAC GACTCTGAAAAAATCCCTGTTTCCGCCCGATTCGGGAAAACCTGCC GATTTAATTAAAAAAGATCGCGGCAAGAATTTCCGATTATTTTTCG AAATACTTGTGCGCTTGAGGGGGAATTTTCTTGTCGCTTCAATAGCG TCATGCAACGTTTGAATCGAAGGTGCGGCACGGGTCGCACGAGGAG CTGGACCAGATCGAGAAGATGATGGGCCGCGTGAAGCTCGACCTGT ACTACATGCAGAACTGGTCGTTCTGGCTCGACATCAAGATCGTCGT GCTGATGCTGTGGAAAGGGTTCACCGGCAGCAACGCGTACTGACAC CGACGCGCTGCGTCACGCAGGCATTCCGGTTTTACGAATTTCGAATC ATTGGTCAAGGGGTCCGACACATCATGAATCTGACTATCATCGGCA GCGGTTACGTAGGGCTTGTCACCGGCGCCTGTCTCGCCGACATCGGG CACGACGTGTTCTGTCTCGACGTCGACCAGGCGAAGATCGACATCC TGAACGACGGCGGCGTGCCGATCCACGAGCCGGGCCTGAAGGAAGT CATCGCGCGCAACCGTTCGGCCGGCCGCCTGCGCTTCTCGACCGACA TCGAGGCCGCGGTTGCGCACGGCGACGTGCAGTTCAtctagaTTA	Enables deletion of entire *bceB* gene
hldD frag	ATTAcccgggATCGTCAAGCCTTCCTGCTGAAGCCGCTCGACGGTGTG CCCGCCCATGCCCTTCACACGCTTGGCGAGATCGTCCGCATTCCTG AACGGACCGCGTGCGCCGCGCTCGTCGAGAATCGCCTTCGCGCGTG CCGGGCCGATGCCCTTGATGCCGACGAGCGCATCCTCGTTCGCGGTG TTGACGTCGACGGCCGCCCAGGCCGACGCTACTGCGCCGAGCATGA CCGCTGCGGCAAACCATTCCCTGAACATGTGCTGGATCTCCGAAGAA AACGGCCGGCGGCTGCCGACCGTGAGACCCAGTCTATCGATGCAAC GCGCCGGTTTAAACCTGGCCGGATAGCCAACGCACGTAACGATCTTG TCGAGATAGTCGTCGATCTCGCAATCGACGAGATTGCGAAACTTGTC TGCGCGGGTCAGGTTGTCGACCGCGATGATGCGCGTCTCGCCGCGC TCGTTGAGCGCCTTGACGATGTTCGCGCCGATAAAACCGGCTGCGCC GGTGACGATGAGGGTCATGATCGTCCTGCCTGAAAAGTGCGAGCCC ACTCGGGCGACGCGCTCGTCGCGCCGCCGAATGCGCTCAGTGAAACA GTTCGTCGTAATCCACCGTGGCCGTGCCGAGCTTGCCGACCACGATG CCTGCCGCGCGATTCGCGAGCACCACCGCGTCGACGAGCGGCACCCC GGCGCCGAGCATCGTCGCGACCGTCGCGATCAtctagaTTA	Enables deletion of the 3' 796bp (of total 993 bp) of *hldD*
waaL frag	ATTATcccgggTGCCGGACGTTACTGGCGCGACGTTCCGTTCGTCGCC GTAACGATCGCGGACATGCCATGCCGCGATCAACCGTATATTTTCC GGCGTCACGTCCAGTGGGTCAGGCGATGCGATCGCGACGCCACGAC	Enables deletion of

	ATGCGTCGCGTGGCACGACGGCTCCGCGGGCTGCATGAGCGGGCT GTCGGTGGACGCGGTACGTGGCGCACTGAAACACGTTCTGGTGCAA GTTCGATGACGGCTATTGCGGCGCGTATGGAGCGTCTTCTGTGGATT GGCTGCCCCGTTCTGATGTTCGCCATCATGTTCGGGCACATGGCGGC GTTCGTGAATTGCAGCATGGTGCTGGTCGGGATTGCGCTGATCGAA ACCGGTGCCGGGAATGGCCTACCGCAGCGAGATGCCGCCCGAATTGC TGGCACTCGAGCCGCAGGCGCTGACGCACGCGCACAATCTTTTCCTG AATACGTGGCTACAGACCGGGCGCATCGGCCTGGCAATGCAGGCACT GTTGCTGGCGGCGCTCGTATTCGCGTTCTGGCGACTGCGGAAGGCTG ACCCGTGGATTGCGGCGGGCGGCATCGCGCTCGTGGTCGGGATGGTC ACGAAGAACCTGGTGGACGATTTCATGTGGCAGACGACGATCCTGGC ATTCTGGGCATTTGCCGGGCTGGTGCTCGGGCATGGCGAGCGACGCG CACGCGTGCGTCGCGCGCAACCGGGGAGCGGATCGTGAAtctagaTTAT	the 5' 785 bp (of total 1230 bp) of *waaL*
wbiI frag	AATTAAcccgggTGCTGCTGTTCATGTATCCGATCTTCGAGACCTGCT TCTCGATCTACCGGAAGAAGTTCATTCGCGGGATGTCGCCAGGGAT TCCGGACGGCGTGCACCTGCACATGCTCGTGTACAAGCGGCTGAT GCGCTGGGCCGTCGGTACGAAGCATGCGCACGACCTGACGCGGCGG AATTCGCTGACTTCACCTTATCTGTGGTTGCTGTGCCTCGTCGCGGT GATACCGGCGACGCTGTTCTGGCGGCATACGGTGCACCTGTTCGCG TTCGTCGTGCTGTTCGCGGTGACTTATGTGTGGCTTTATCTCAGCAT CGTGCGGTTCAAGGCGCCGAGGTGGATGGTGGTGAGGAAGCATCG ACAGAGCCGTTGAGCGATACGCTCGCTTCCGAACAAAAAAGCGCC CAGCCGGGCGCTTTTTTTACCACTCGGGTTCCGGCCTGGAGCCAGC GGGAAACCTCAAGAATTGTTTTCGGCAGCCACTTGAACCCGGCGCC AACGCATGTCGATCAACCATCCGAACCATGCCAGGACGCCATACCA CGCGAGGAACGACAGCCATTGCTGCAGTTCAGGGCGGCCCTTTGC CCACACGGCGACAATTATGCCGGCGAGCATGATGAGGTACCAATAA AGAGCGGTCCGACCGTGGCTGACGCCCGATCGAACCATCCTTTGAT AATAATGCTCGCGATGCGCCTGCCAGAACTTTTCTCCGCGTAACAAG CGTCTCAGAAGTGTTACAGATGCATCGAGAATAAAGGGCGAGAAC ACCATGGCCGGAAACCAGATCGGCCAGACATTGGTACGCCAGCCCC AGTAGCCCAGCGCACCGGCCAGGAAGCCGAGCGGAATCGAGCCGGC GTCGCCAAGGAATAGTCTCGCCGGGTGGAAATTGAtctagaATTAA	Enables deletion of entire *wbiI* gene
wzm-wzt frag	AATTAAcccgggCCGGTGGTACGCGAGGTAATCAATGCCTCAGCGG CCACCGGATCGAGCGTGAGCGTTTCCTCGTCGATATCGCAGAACAC CGGCGTCACGTTGTTCCAATGAAGCACATGGGGTGTCGCCGGAAA CGTAAACGGTGTCGTGATAACCTCGCCCGCAAGCCGCAACGCCTGG CATGCGACCAGCAAAGCGCTCGTCCCGTTATTGAAGAGCGAAAAA TGCGGTGCGCCGAGCCTATCCGCCAGCGCGGCCTCGAGCGCCGCAT GCTTCTGCCCACCATTCGTCAACCACGCGCTACCCCATATGTCCGCC AACTGCGCCGAATATTCGTCGAGCGGCGGCAACATTGGCTTGGTCA CATAGATCGGCTTGTCGAATACGTCCGGCTTCTGATTCATCCTGCTC TCCACTCCATCCCGTCAGGTTTGCCCGTCGACGCTAAACTCATCATC ACTAAACAAGATACCCAAGCGACGCGCCGCACCTTGCGCCATCATC CCGAACAACGTCAGGTGCCGTAATACTCATCGAGAACGAGCGCCAG CGCGTCCACCCATTGCGGGCGATACAGTCCGAAACGTTCATCAAAA CGCATATTATCCAGCACCGAATACGTTGGACGTGGCGTCTTGGTCGG ATACTCTGCAGCGGGGATAGGGGTTACCTCCCGGATCGCGAGATCG CACTGCGGGGACACACGTCTCGCGCCGGTGAAGATAGCTTCGGCAA ACTCGTGCCATGTCGTCGTACCGCGCGCCGTCATATGGTAGACGCCA CTCTCAAAAGTACCGGCACGCCGTTCCGCGAGGGACTTCGCGATCGC GTGCACCGTCAGATCCGCGATCGTCCGCGCACTTGTCGGCGCACCAT ATTGATCGTTGACGACGGACAACGCCTCACGGCtctagaATTAA	Enables deletion of entire *wzm* and *wzt* genes

Table A5. Mutants recovered in two replicates of the no antibiotic control. See the spreadsheet for additional details on data composition. See below link for the data: https://doi.org/10.34990/FK2/XV3L79

Table A6. Morphological characteristics of the mutants hypersusceptible to C109. The five categories here were chosen to highlight differences between the mutants

	Morphology Characteristic (% of total cells)				
Mutant or Treatment	Filamentation	Enlargement*	Shortening	Bending	Lysis (earliest occurrence)
C109	+ (91)	-	-	-	+ (3 hr)
CG*dcw*	+ (100)	-	-	-	+ (24 hr)
CG*ftsZ*	+ (100)	-	-	-	+ (24 hr)
CG*pepA-holC*	-	+ (87)	-	-	+ (6 hr)
CG*holC*	-	+ (82)	-	-	+ (6 hr)
CG*topB*	-	+ (78)	-	-	+ (6 hr)
CG*xseB-ispA-dxs*	-	-	+ (95)	-	-
CG*ispA-dxs*	+ (100)	-	-	+ (88)	+ (6 hr)
CG*dnaN*	-	-	-	-	+ (6 hr)

*Enlargement is defined as an increase in cell length and width

Table A7. Cytotoxic properties of C109 reported in uninfected *C. elegans*, human cells, and for ovine erythrocytes.

C. elegans	
$SURV_{100}$	128 μg/mL
$SURV_{100}$/MIC	16
6-Day Tolerance at 128 μg/mL C109	79%
Mammalian Cells	
Erythrocyte Lysis at 128 μg/mL	3.1%
TC_{50} (16HBE)	75 μM (21.4 μg/mL)
TC_{50} (CFBE41o-)	75 μM

Table A8. Published genomes within the NCBI GenBank that contain the *φ*CTX *attB* site. See the spreadsheet for additional details on data composition. See below link for the data: https://doi.org/10.34990/FK2/ZS89DI

Table A9. Summary statistics of the randomly barcoded transposon mutant library

Category	K56-2 Library
Number of mutant colonies recovered	~815, 000
Number of unique barcodes	338,116
Number of unique insertion positions	145,585
Protein-coding genes with (or without) central insertions (10-90% of gene)	6412 (561)
Mean/median strains per interrupted protein-coding gene	31.9 / 12
Gene and transposon on same strand	49.9%
Average distance between insertions	18.7 bp

Table A10. Antagonism of AZT, CAZ, and MEM by BAC is due to an acidic pH and high levels of zinc. MIC values are the median of three replicates and are reported in µg/mL.

	Medium Supplement			
	CAMHB Only	+ $ZnCl_2$ (4 mM)	pH 5.7	+ BAC (512 µg/mL)*
AZT	256	256	**>512**	**>512**
CAZ	16	**32**	**128**	**128**
MEM	8	**16**	**64**	**64**

*Due to the formulation, at 512 µg/mL BAC, the medium is at pH 5.7 and contains 4 mM Zn^{2+}.

Table A11. Effect of CRISPRi knockdown of β-lactamase genes on susceptibility to AMP, CFD, TAZ, and CTT. MIC values are the median of three replicates and are reported in μg/mL. Bolded values indicate at least 2-fold change.

		MIC (μg/mL)		Fold
Antibiotic	Gene	-Rha	+Rha	MIC*
AMP	NTC	>512	>512	-
	penR	>512	>512	-
	bla$_{AmpC}$	>512	>512	-
	bla$_{PenB}$	>512	**256**	**>2**
CFD	NTC	0.125	0.125	1
	penR	0.125	0.125	1
	bla$_{AmpC}$	0.125	0.125	1
	bla$_{PenB}$	0.125	0.125	1
TAZ	NTC	128	128	1
	penR	128	**64**	**2**
	bla$_{AmpC}$	128	128	**1**
	bla$_{PenB}$	128	**32**	**4**
CTT	NTC	64	64	1
	penR	64	**16**	**4**
	bla$_{AmpC}$	64	64	1
	bla$_{PenB}$	64	64	1

*Fold MIC is the ratio of the MIC -Rha to the MIC +Rha

Table A12. Susceptibility of Gram-negative panel to AVI combinations (± 8 µg/mL AVI). MICs are the median of three replicates and are reported in µg/mL. Ratios are calculated as the MIC of the β-lactam alone by the MIC of the β-lactam with AVI. Bold indicate ≥2-fold change.

Species	Strain	AZT	AVI/AZT	Ratio	Mero	AVI/MEM	Ratio	CAZ	AVI/CAZ	Ratio	CFD	AVI/CFD	Ratio
A. xylosoxidans	ACH02	64	64	1	1	1	1	2	2	1	0.25	0.25	1
	ACH03	32	32	1	0.25	0.25	1	1	1	1	0.125	0.125	1
	ACH09	16	16	1	0.125	0.125	1	1	1	1	0.25	0.25	1
S. maltophilia	D457	16	2	**8**	32	32	1	1	1	1	0.125	0.125	1
	K279a	128	1	**128**	2	2	1	2	1	**2**	0.125	0.125	1
P. aeruginosa	PAO1	4	4	1	0.5	0.5	1	1	1	1	1	1	1
	PA14	8	8	1	0.5	0.25	**2**	2	2	1	1	1	1
B. cenocepacia	110041	64	16	**4**	32	4	**8**	4	4	1	0.0625	0.0625	1
	BC7	>128	>128	1	16	1	**16**	16	16	1	>4	>4	1
	K56-2	256	8	**32**	16	2	**8**	32	4	**8**	0.125	0.125	1
	VC10414	16	8	**2**	32	2	**16**	8	4	**2**	0.125	0.125	1
	VC14488	16	2	**8**	4	1	**4**	4	2	**2**	0.25	0.25	1
	VC14543	256	32	**8**	16	4	**4**	8	8	1	0.125	0.0625	**2**
	VC14761	8	2	**4**	4	1	**4**	2	2	1	0.125	0.0625	**2**
B. contaminans	LMG23361	32	2	**16**	4	0.5	**8**	2	2	1	0.125	0.125	1
B. dolosa	CEP021	8	8	1	2	1	**2**	2	1	**2**	0.5	0.5	1
B. gladioli	VC14812	128	32	**4**	8	8	1	32	16	**2**	0.5	0.5	1
	VC19233	32	8	**4**	1	1	1	4	2	**2**	0.25	0.25	1
B. multivorans	130034	16	8	**2**	8	4	**2**	8	8	1	0.125	0.125	1
	C5393	64	8	**8**	16	1	**16**	8	4	**2**	0.25	0.25	1
	VC15535	256	16	**16**	16	8	**2**	32	16	**2**	0.5	0.5	1
	VC15555	4	4	1	8	4	**2**	2	2	1	>4	>4	1
	VC19694	128	4	**32**	8	4	**2**	4	1	**4**	1	1	1
	VC9825	8	4	**2**	2	1	**2**	2	2	1	0.25	0.125	**2**
B. vietnamiensis	CEP40	4	2	**2**	1	1	1	4	2	**2**	0.125	0.0625	**2**
	VC11431	256	4	**64**	16	1	**16**	32	2	**16**	1	0.125	**8**
	VC18984	256	8	**32**	8	4	**2**	16	4	**4**	>4	>4	1

Table A13. MIC values of other β-lactams in K56-2 with AVI and TAZ. MIC values are the median of three replicates and are reported in μg/mL. Bolded values indicate changes upon β-lactamase addition.

	β-Lactam Alone	**+ 8 μg/mL AVI**	**+ 8 μg/mL TAZ**
Ceftazidime	32	**4**	32
Cefotaxime	>128	**16**	>128
Cephalexin	>128	**128**	>128
Cefmetazole	128	128	128
Cefoperazone	>128	**64**	>128
Ceftriaxone	>128	**4**	>128
Moxalactam	128	128	128

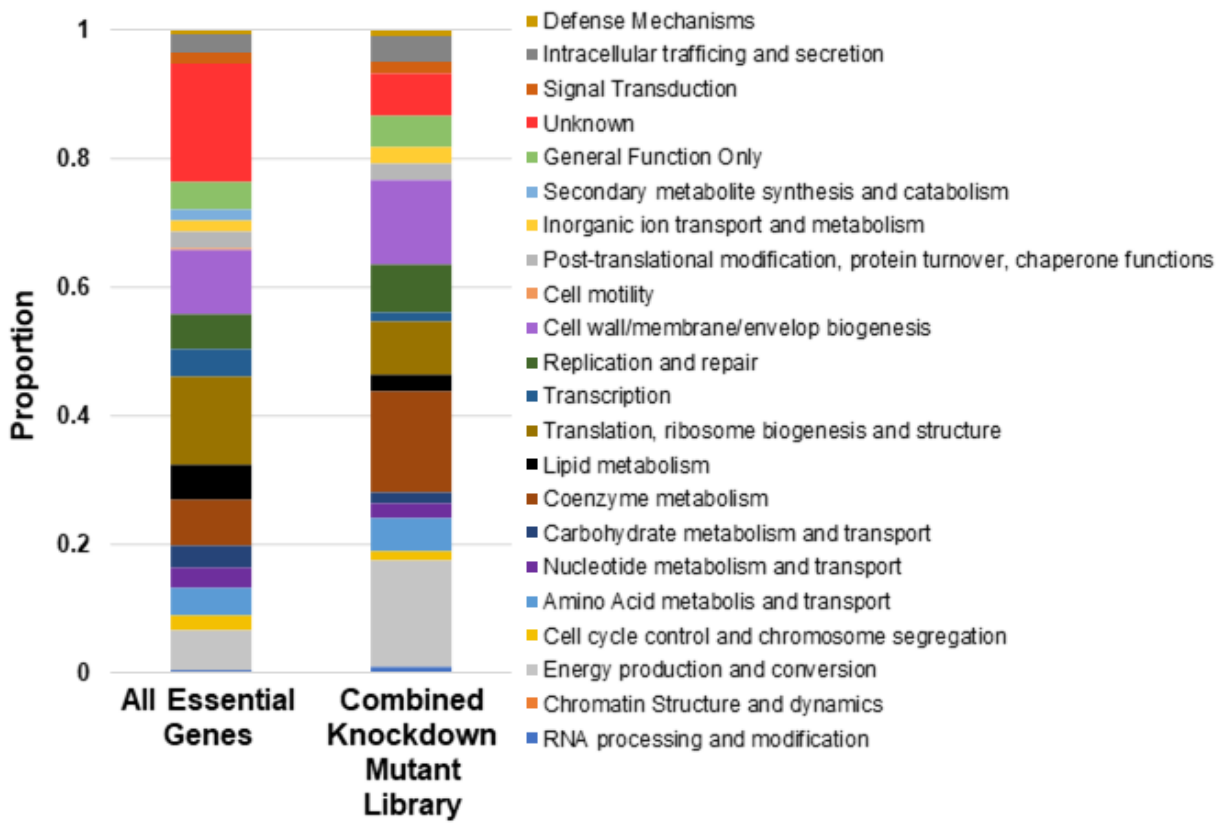

Figure A1. Essential genes in *B. cenocepacia* K56-2 and in the combined knockdown mutant library. Bars are colour-coded based on COG category. Essential genes in K56-2 are from Gislason et al. (2017a).

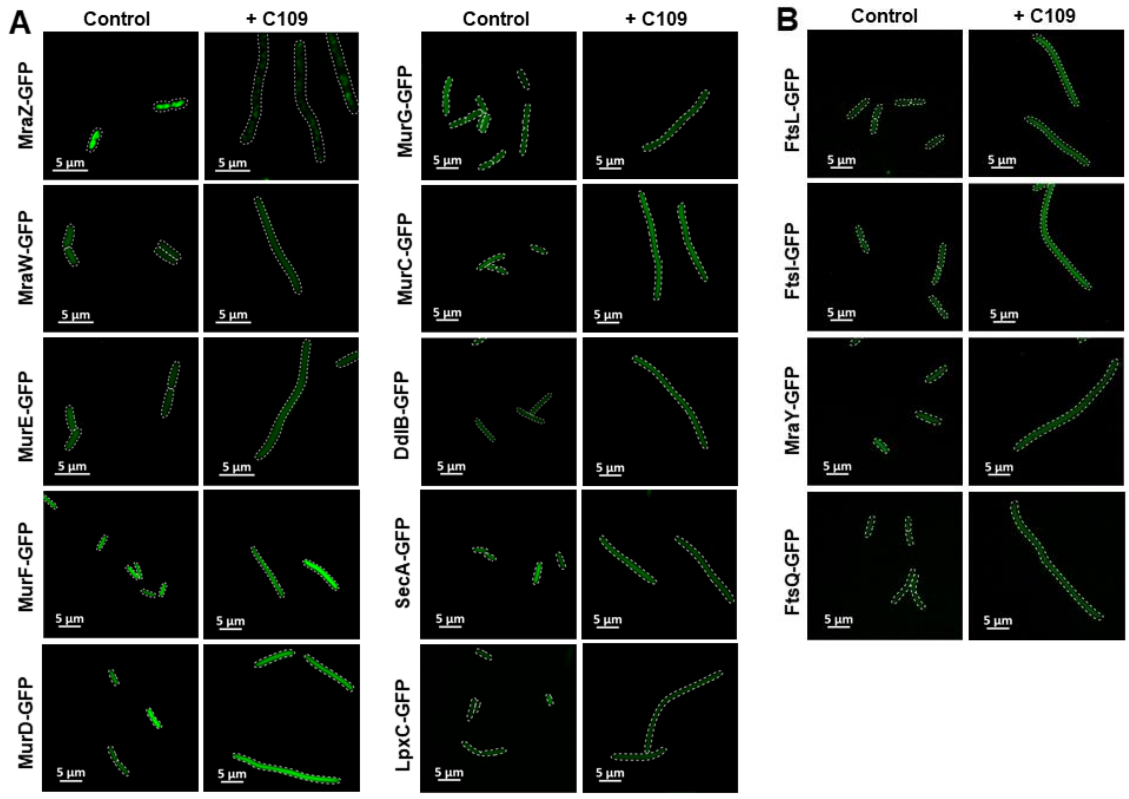

Figure A2. Treatment of the *dcw*-GFP fusion ASKA stains. The noted ASKA strains were subcultured to reach exponential phase then treated with 4 µg/mL C109 for 3 hours. Dashes denote cell boundaries. A) Fusions that localized properly despite addition of C109. MraW, MurE, MurF, MurD, MurC, DdlB, SecA, and LpxC are primarily cytoplasmic. B) Fusions that did not localize properly in the control condition.

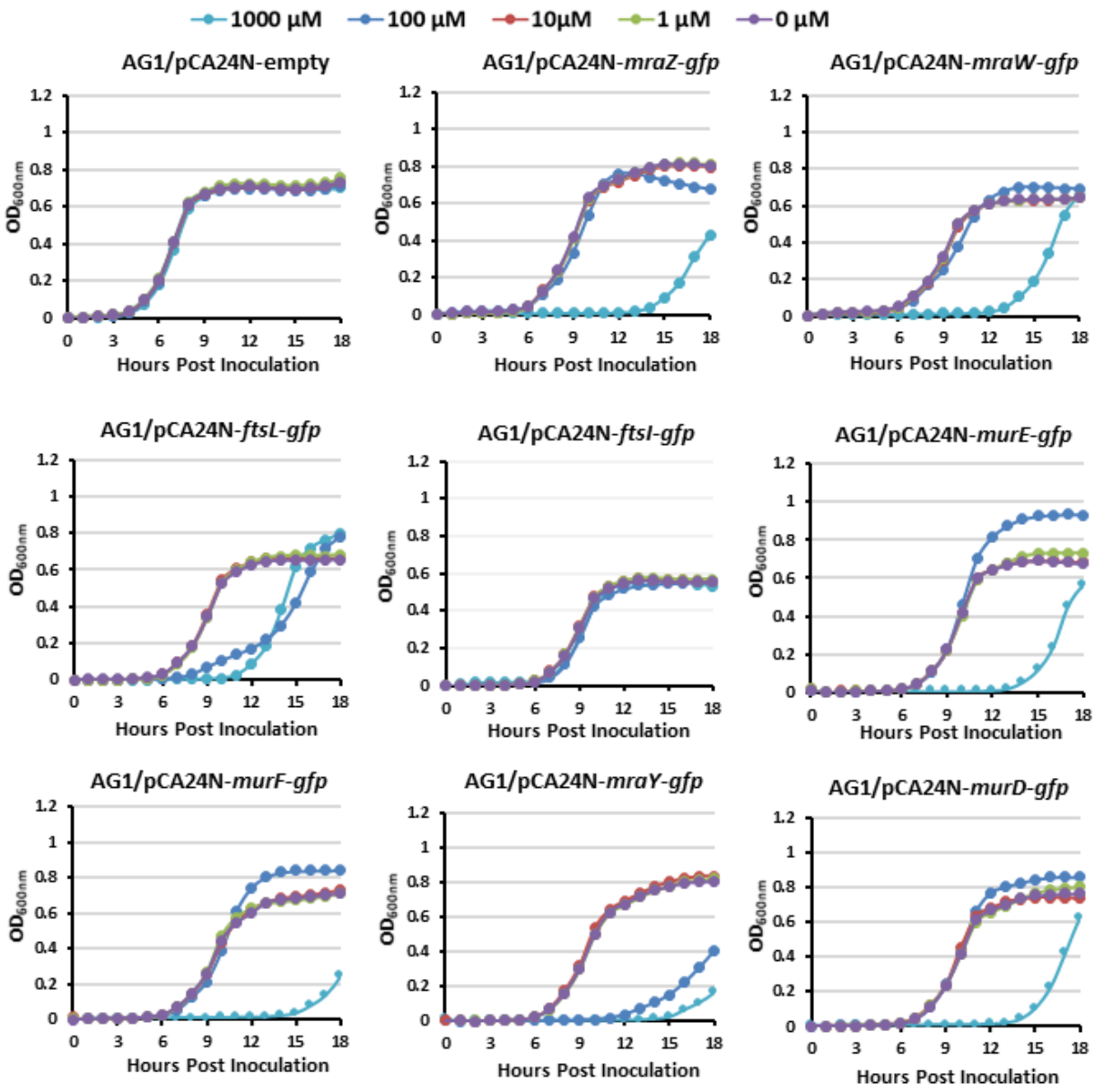
1000 µM
100 µM
10µM
1 µM
0 µM
AG1/pCA24N-empty
AG1/pCA24N-mraZ-gfp
AG1/pCA24N-mraW-gfp
AG1/pCA24N-ftsL-gfp
AG1/pCA24N-ftsI-gfp
AG1/pCA24N-murE-gfp
AG1/pCA24N-murF-gfp
AG1/pCA24N-mraY-gfp
AG1/pCA24N-murD-gfp
OD600nm
Hours Post Inoculation

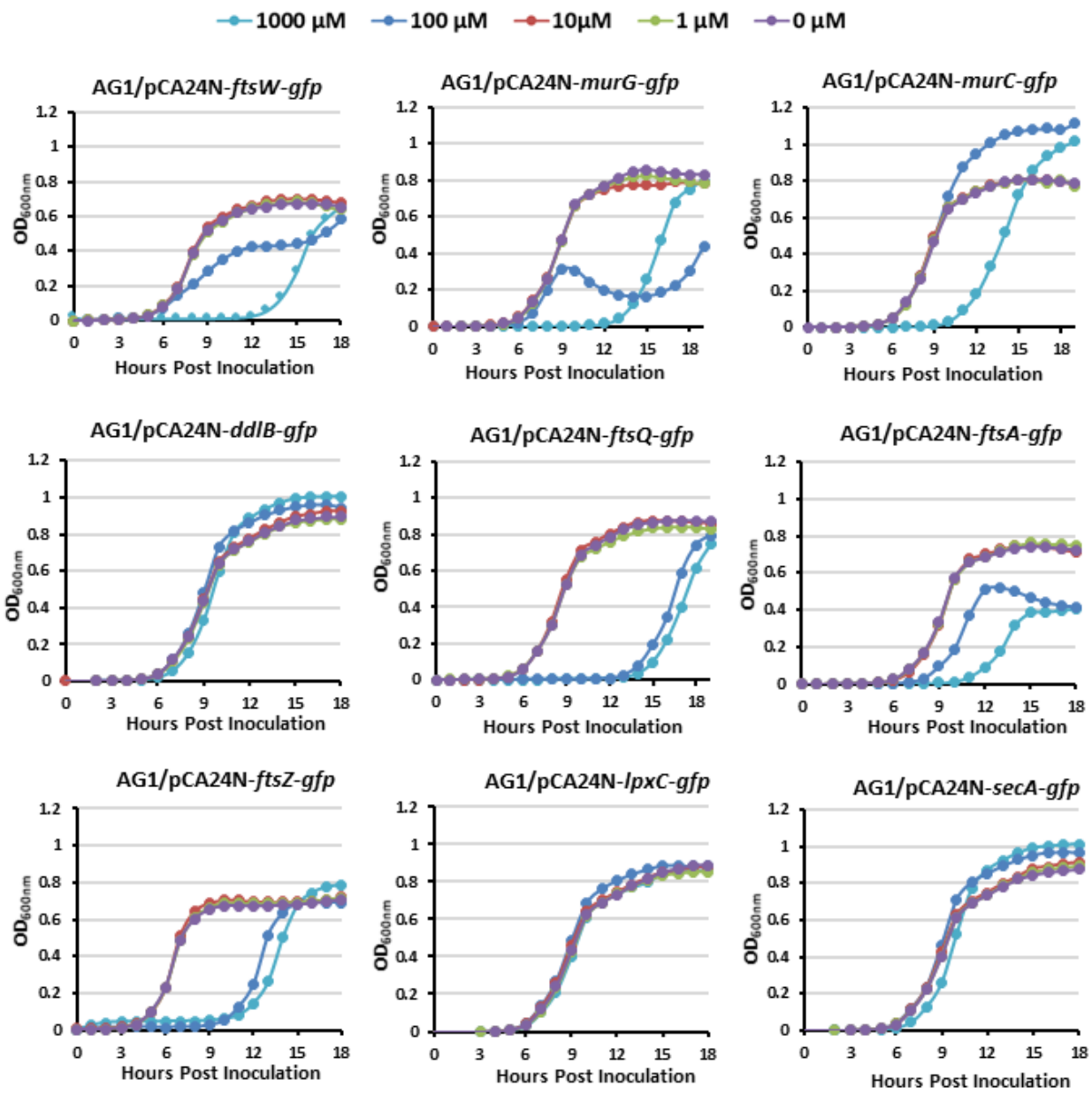

Figure A3. ASKA strains expressing *dcw* protein-GFP fusions grown in varying IPTG concentrations. Strains of *E. coli* AG1 bearing the indicated plasmids were grown in microtiter plates shaking at 37ºC with the indicated concentrations of IPTG to induce overexpression of various *dcw* proteins. Values are expressed as the means of two biological replicates

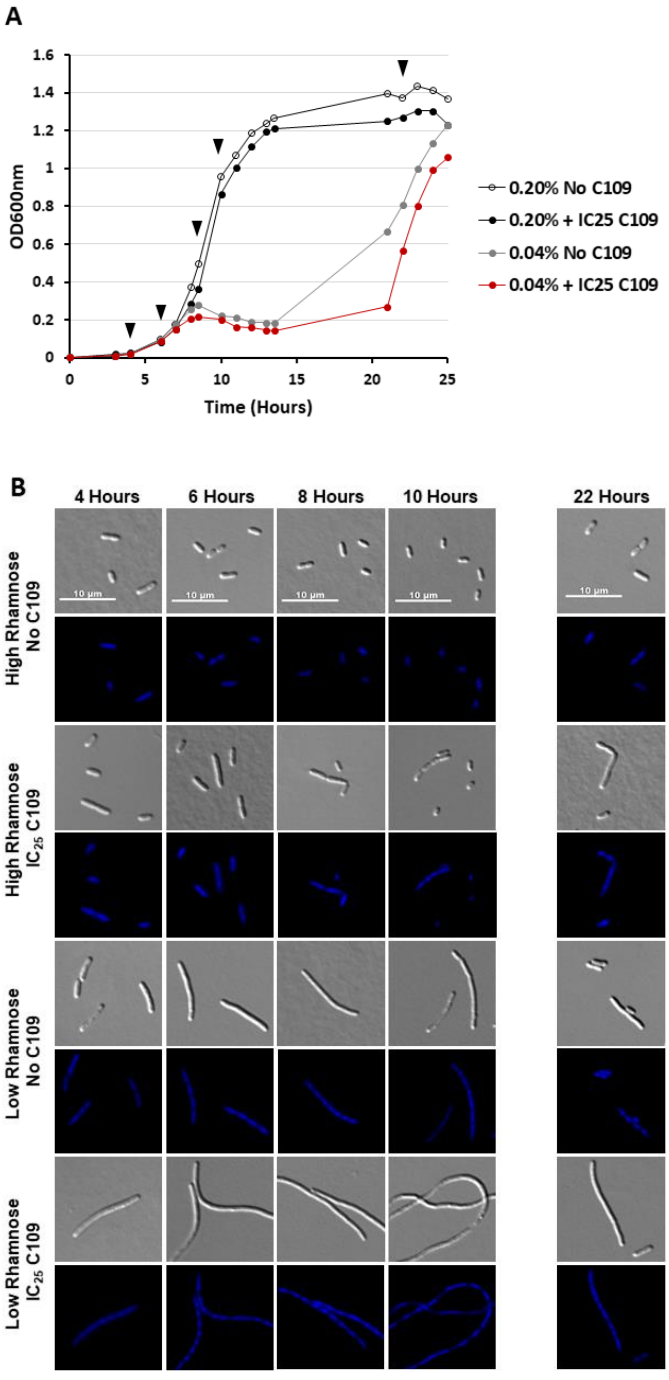

Figure A4. Knockdown of *ftsZ* enhances the filamentous phenotype in response to C109. Cells were inoculated in medium with high (0.20%) or low (0.04%) rhamnose with or without the IC_{25} of C109. At each timepoint, the A) OD_{600nm} was recorded and samples were processed for B) DIC and DAPI fluorescence microscopy. Wedges in A) indicate when samples were processed for microscopy.

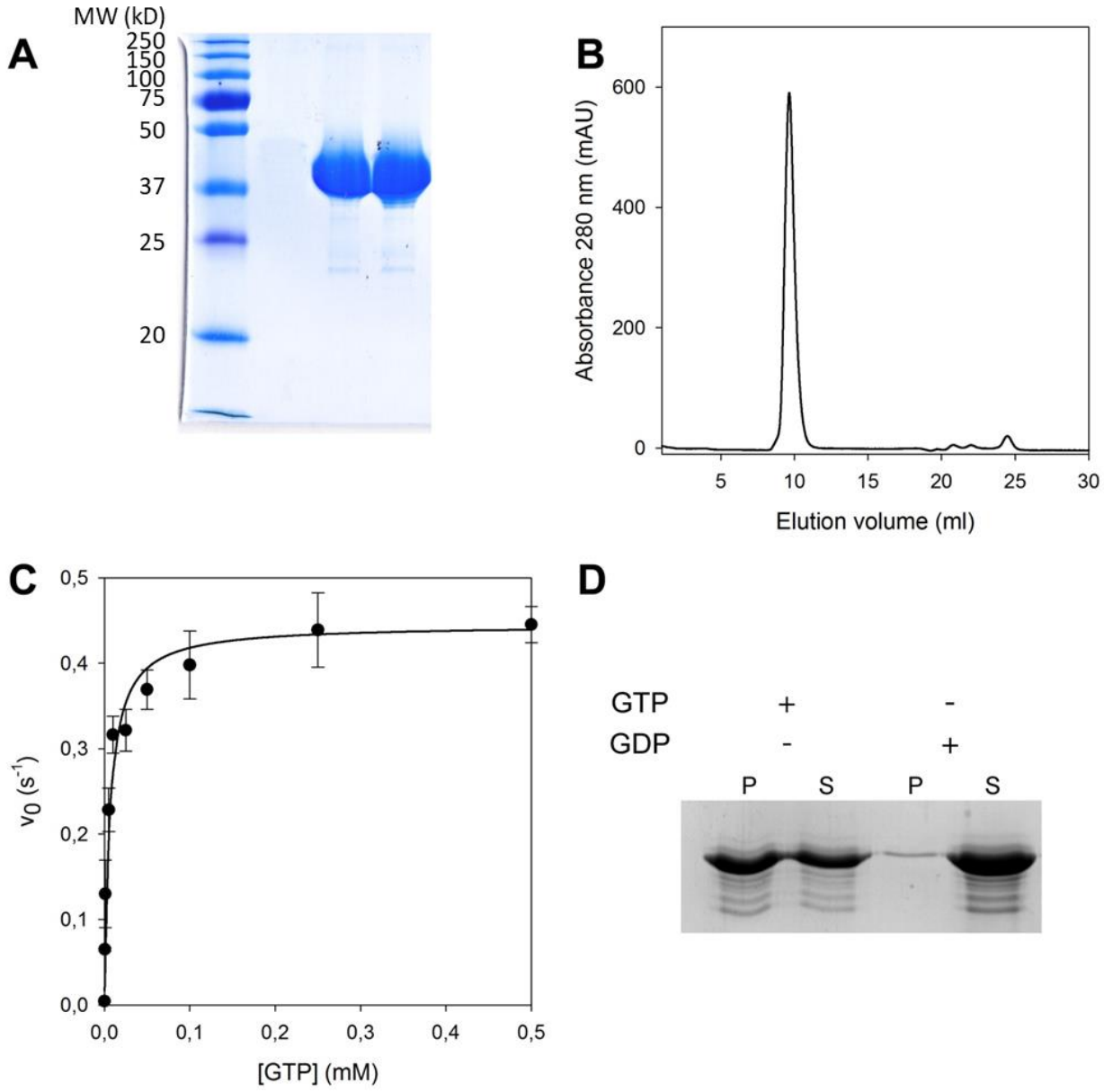

Figure A5. Biochemical characterization of the recombinant B. cenocepacia FtsZ. The recombinant *B. cenocepacia* FtsZ was purified to homogeneity in a soluble and monomeric protein, catalytically active and able to form polymers. A) SDS-PAGE of the purified FtsZ. B) Analytical gel filtration profile of the protein on a Superdex 75 column. C) Steady state kinetic analysis of FtsZ activity as a function of GTP concentration. D) SDS-PAGE of the sedimentation of FtsZ tubules, P: pellet fraction, S: sedimentation fraction.

A

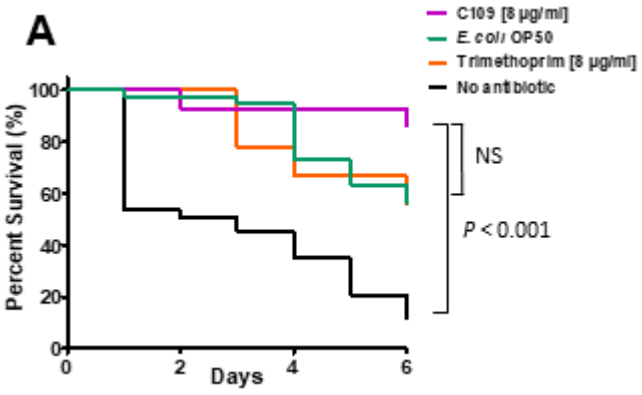

B

2-Day Survival from Panel A	
Fed with *E. coli* OP50	98% (NS)
No Antibiotic	51% ($P < 0.001$)
Trimethoprim (8 µg/mL)	100% (NS)
C109 (8 µg/mL)	93%

Figure A6. C109 rescues *C. elegans* from *B. cenocepacia* infection and is not toxic to the nematodes. A) *C. elegans* nematodes were infected with strain K56-2 and treated with 8 µg/mL of C109 or trimethoprim and observed over 6 days. B) Survival of *C. elegans* at 2-days post-infection. Significance from the C109-treated sample was determined by Mantel-Cox log-rank test. Values are means from three biological replicates. NS, not significant.

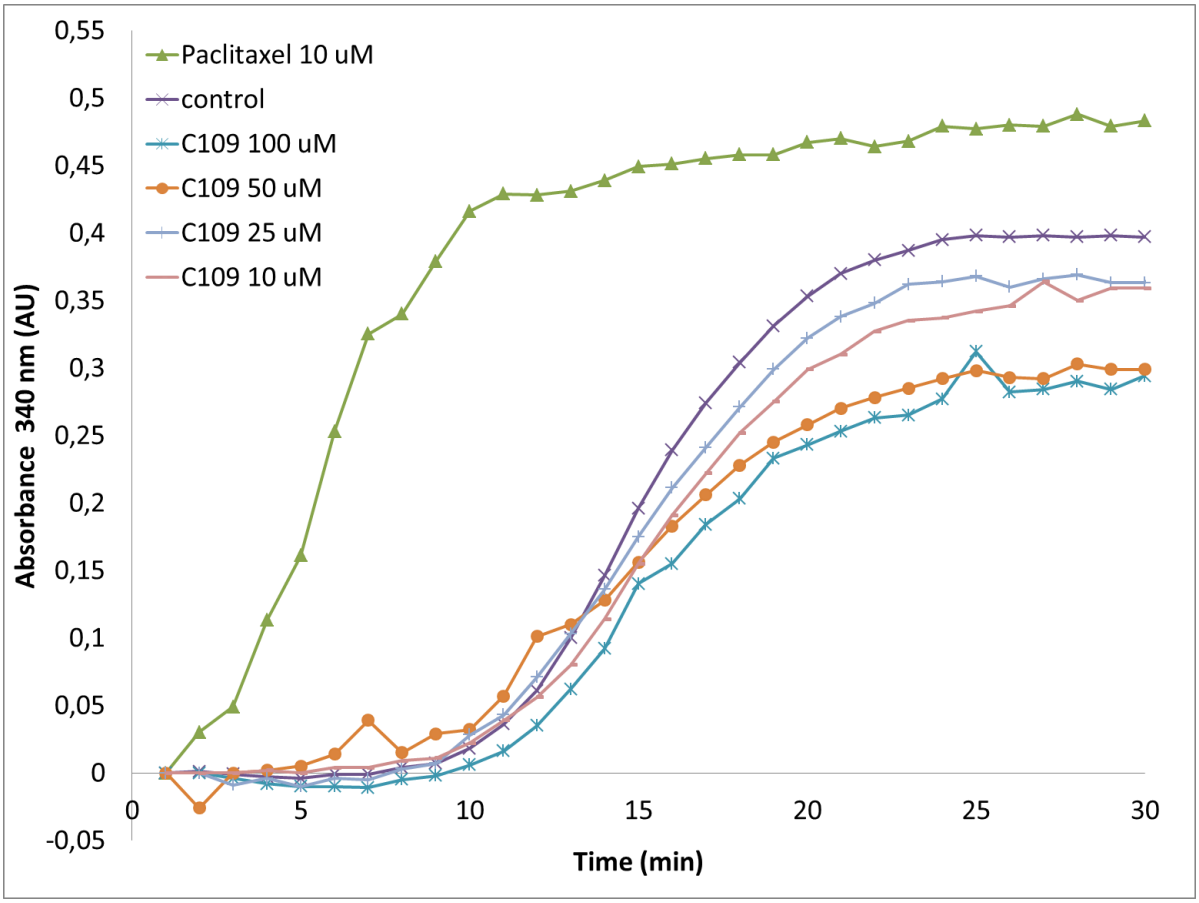

Figure A7. C109 does not affect tubulin polymerization. Set amounts of bovine tubulin and GTP were incubated with paclitaxel or increasing concentrations of C109. Light scattering at 340 nm was measured every minute.

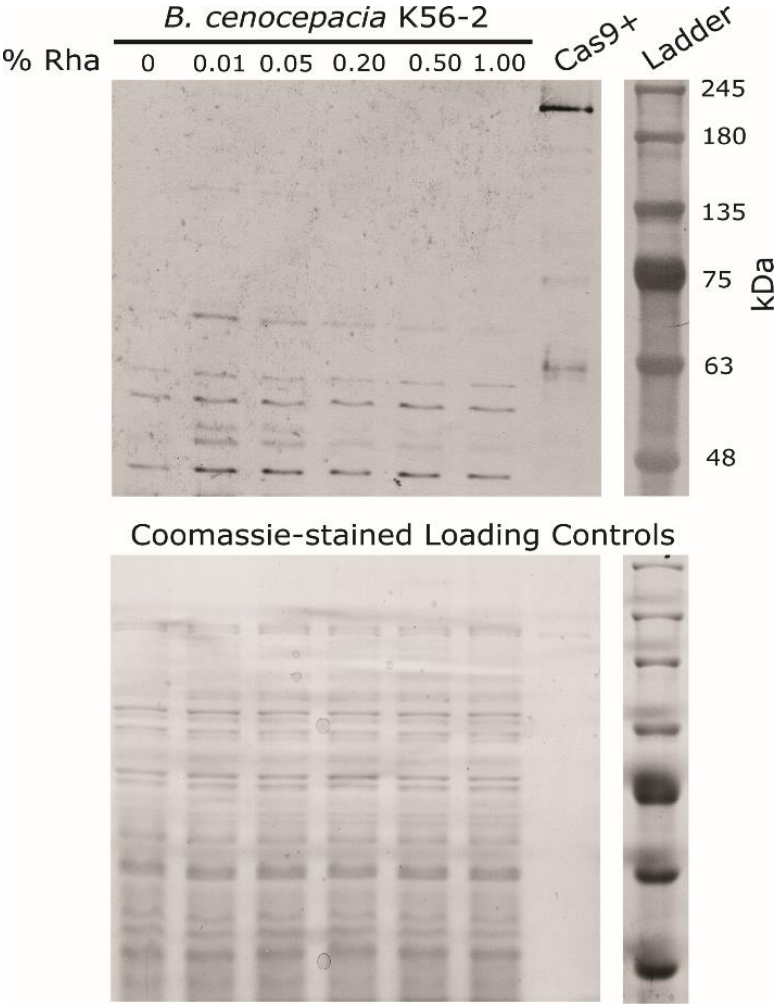

Figure A8. The native *dcas9* is not expressed in *B. cenocepacia* K56-2. *B. cenocepacia* K56-2::dCas9-native was grown to OD_{600nm} 0.6 then induced fore three hours with the indicated concentrations of rhamnose and the soluble protein fraction was extracted. dCas9 was detected with α-Cas9 antibodies. The lane labelled Cas9+ was loaded with 15 ng of purified Cas9. The Coomassie-stained gel run was in parallel to that used for immunoblotting to ensure equal loading.

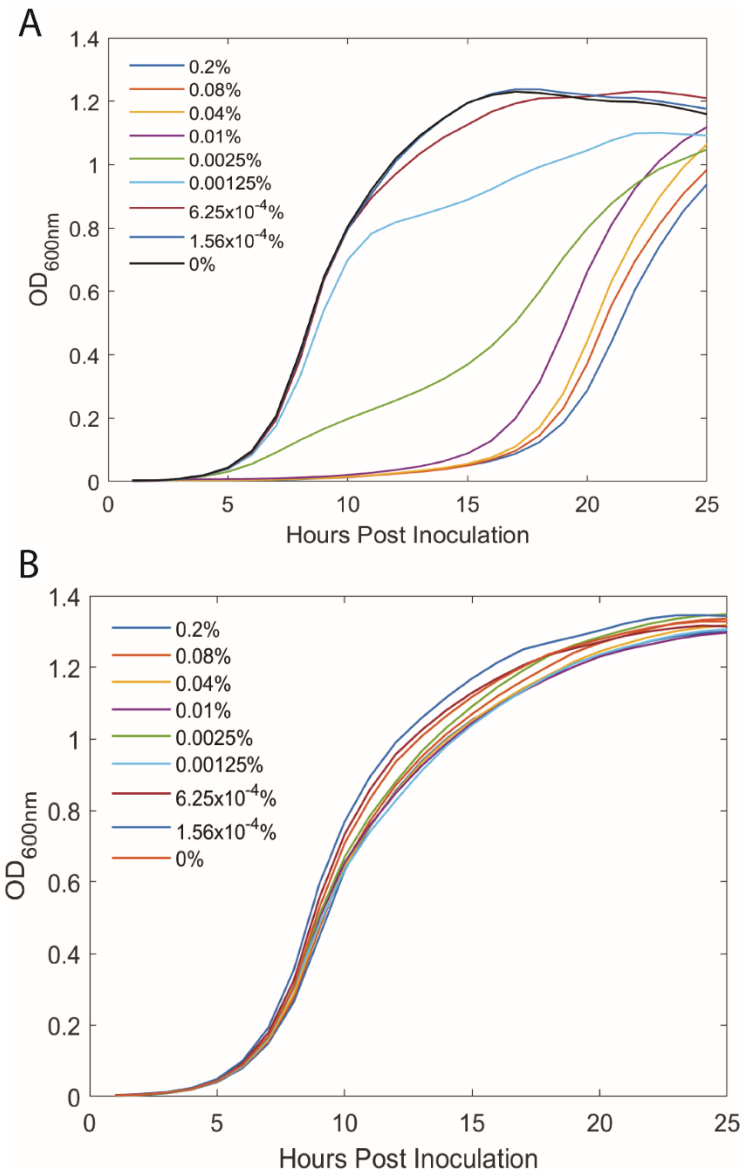

Figure A9. dCas9 expressed from a multicopy plasmid causes a growth defect in *B. cenocepacia* K56-2. *B. cenocepacia* K56-2 harboring the plasmid pSC-rhadCas9 (A) or the vector control, pSCrhaB2 (B) was cultured with the indicated concentrations of rhamnose.

A

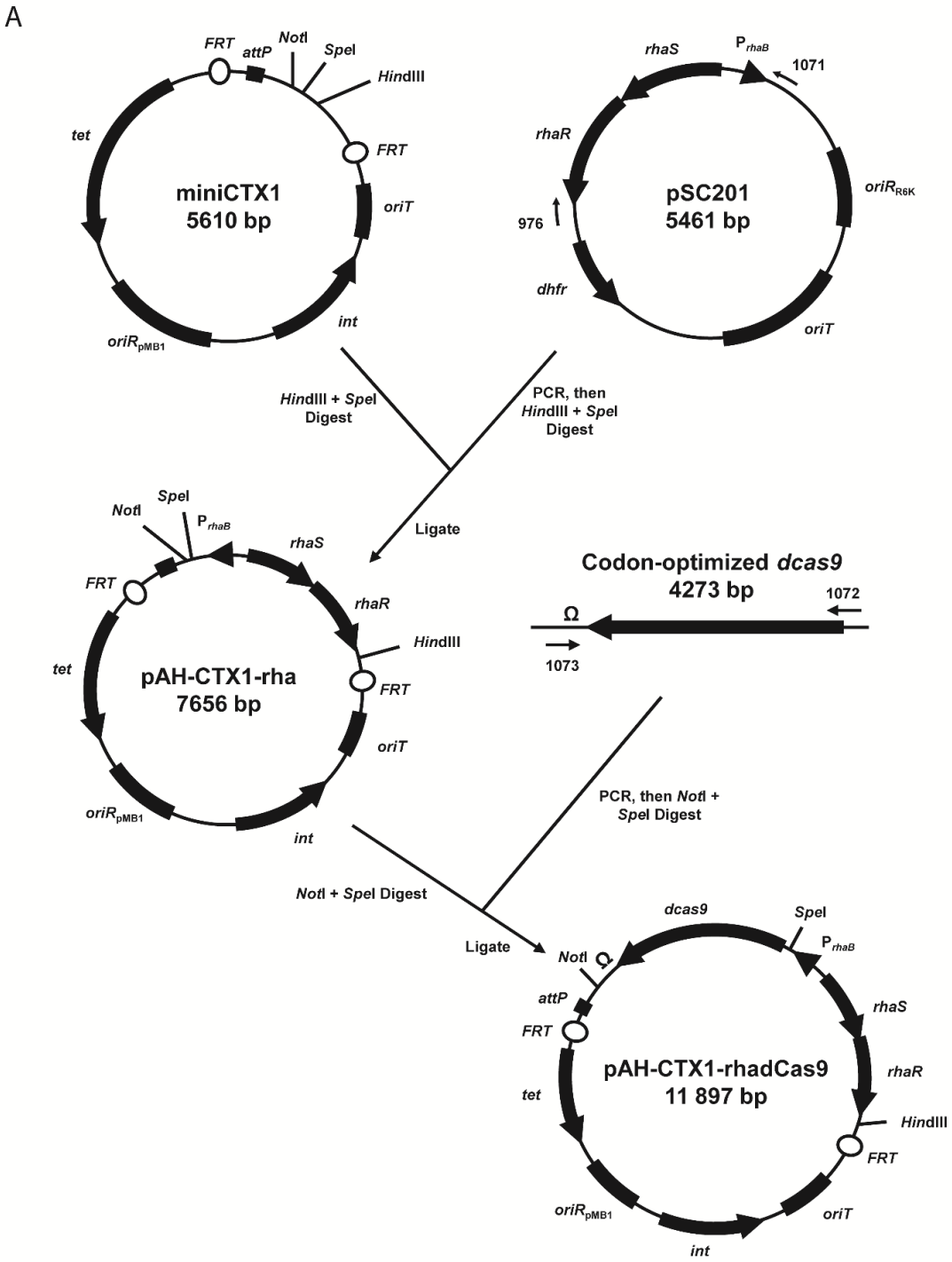
FRT
attP
NotI
SpeI
HindIII
FRT
oriT
int
oriR pMB1
tet
miniCTX1
5610 bp
rhaS
P rhaB
1071
rhaR
oriR R6K
976
dhfr
oriT
pSC201
5461 bp
HindIII + SpeI
Digest
PCR, then
HindIII + SpeI
Digest
Ligate
NotI
SpeI
P rhaB
rhaS
FRT
rhaR
HindIII
tet
pAH-CTX1-rha
7656 bp
FRT
oriT
oriR pMB1
int
Codon-optimized dcas9
4273 bp
1072
Ω
1073
PCR, then NotI +
SpeI Digest
NotI + SpeI Digest
Ligate
dcas9
SpeI
P rhaB
NotI
Ω
attP
FRT
rhaS
rhaR
tet
pAH-CTX1-rhadCas9
11 897 bp
HindIII
FRT
oriR pMB1
oriT
int

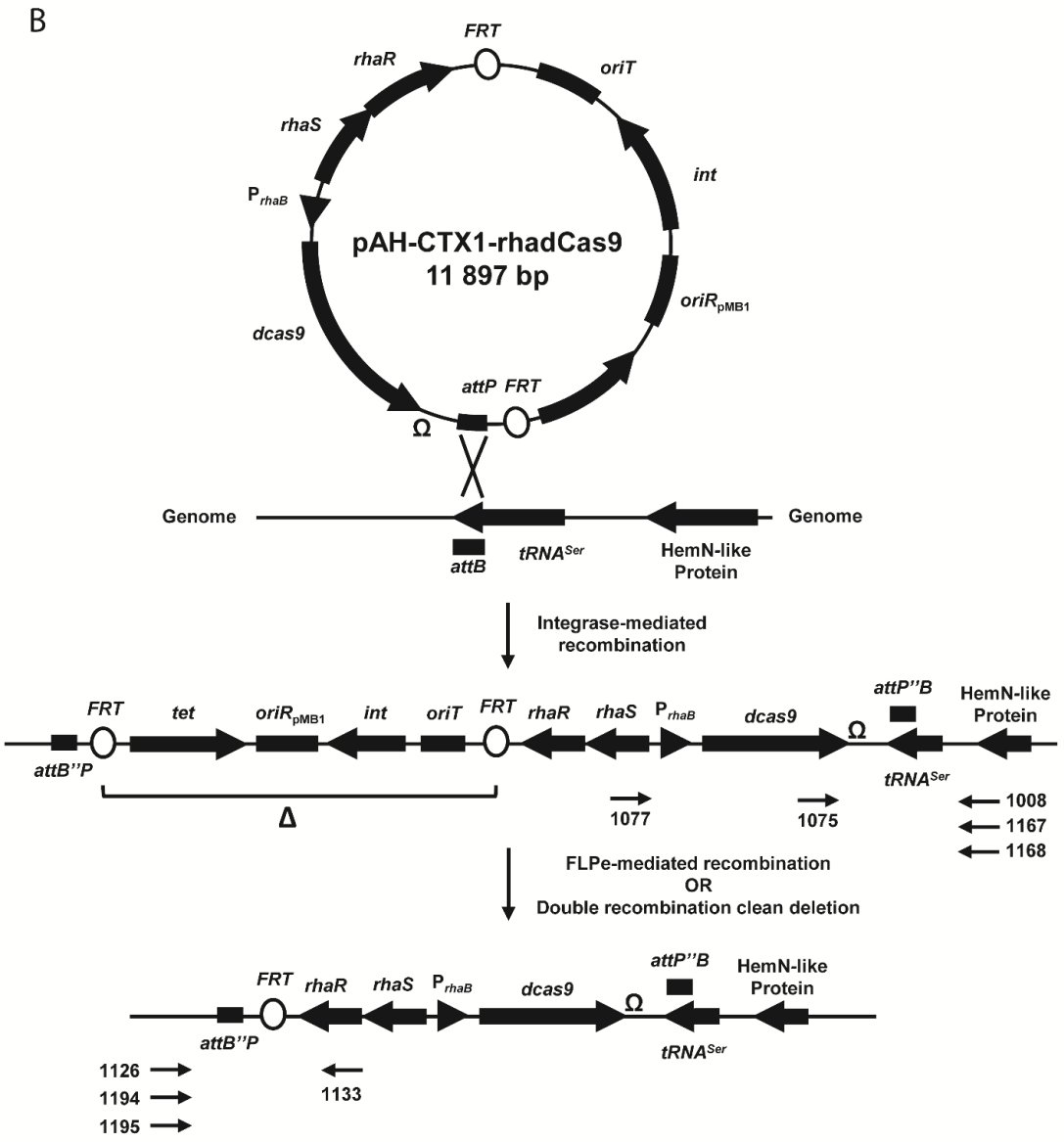

Figure A10. Construction and insertion scheme for the integrative plasmids pAH-CTX1-rha and pAH-CTX1-rhadCas9. A) The rhamnose-inducible promoter was amplified from pSC201 with *Spe*I and *Hind*III restriction sites and introduced into mini-CTX1, creating pAH-CTX1-rha. The codon-optimized *dcas9* was constructed with flanking *Not*I and *Spe*I restriction sites as per Materials and Methods, and introduced into pAH-CTX1-rha, creating pAH-CTX1-rhadCas9. B) pAH-CTX1-rha and pAH-CTX1-rhadcas9 integrate into the genome of a host organism at the *attB* site, usually located at the 3' end of the serine tRNA. Either FLPe of double homologous recombination can be used to remove the accessory genes, such as *tet*, creating an antibiotic-sensitive clean insertion mutant. Primer numbers refer to those found in Table A3.

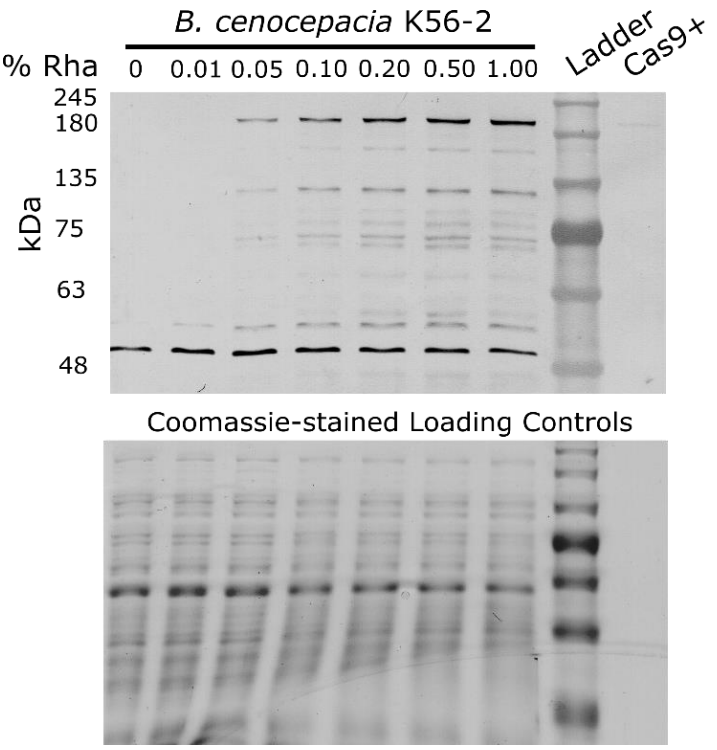

Figure A11. Entire immunoblot from Figure 7 and corresponding SDS-PAGE gel stained with Coomassie to demonstrate equal loading. The lane labelled Cas9+ was loaded with 15 ng of purified Cas9.

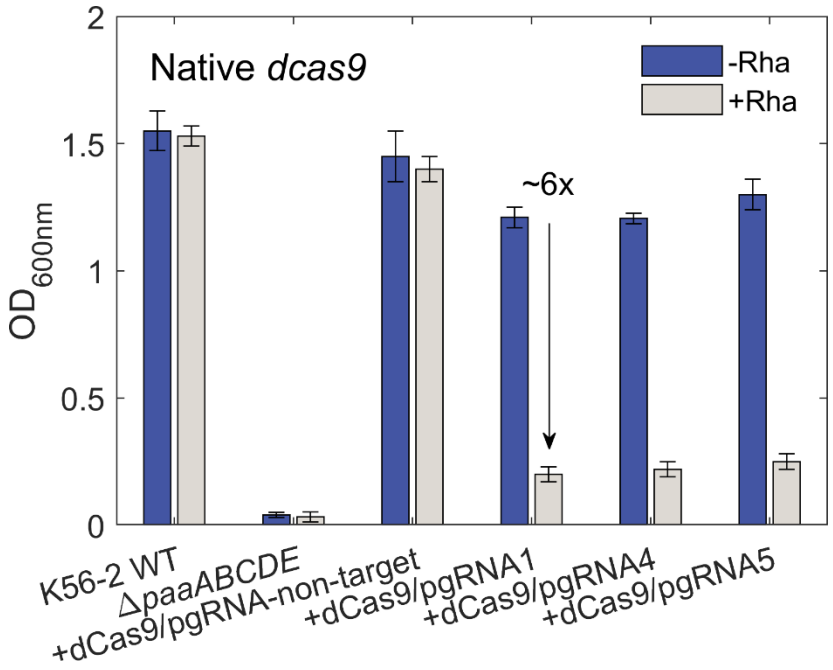

Figure A12. Targeting *paaA* with CRISPRi using the native *dcas9* yields moderate growth suppression in phenylacetic acid as the sole carbon source in *B. cenocepacia* K56-2.. K56-2 WT, a mutant of the *paaABCDE* operon (Δ*paaABCDE*), and K56-2::dCas9 (+dCas9) harboring pgRNAs (as per Figure 2) were grown for 24 hours in minimal medium with PA (M9+PA) without (-Rha) or with 0.2% rhamnose (+Rha). All the values are the average of three independent biological replicates; error bars represent arithmetic mean ± SD.

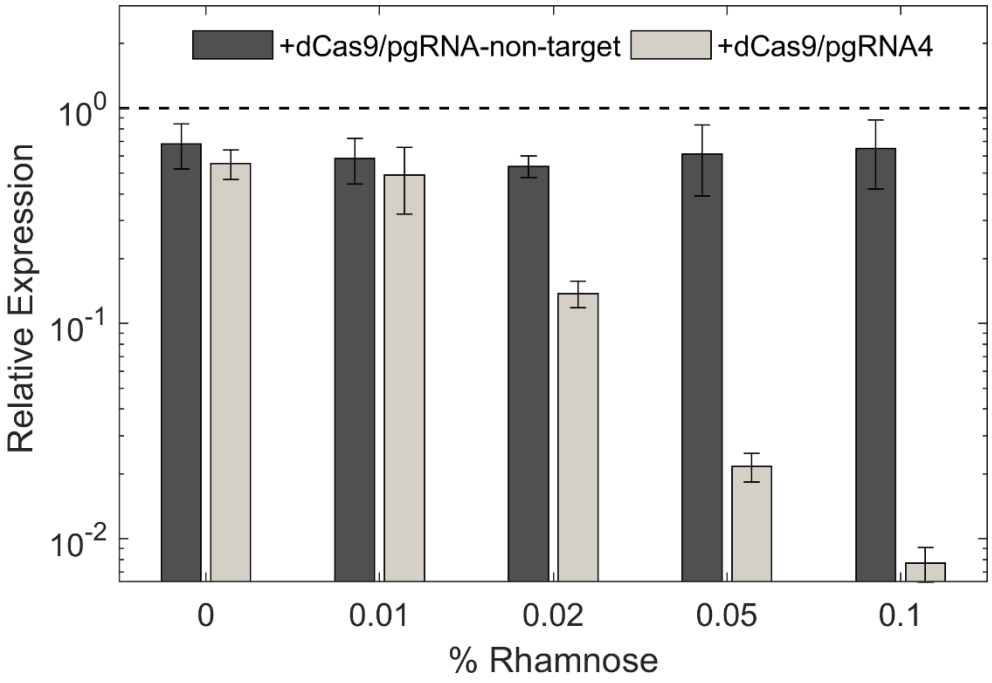

Figure A13. CRISPRi repression of *paaA* mRNA expression is tunable. K56-2 WT, and K56-2::dCas9 (+dCas9) harboring pgRNAs (as per Figure 2) were grown overnight in LB with the specified concentration of rhamnose. Cells were subcultured also in rhamnose for 8 hours in LB, after which RNA was extracted and prepared for RT-qPCR. Expression of *paaA* is shown relative to WT (dashed line). Values are shown as mean ± SD of three independent biological replicates.

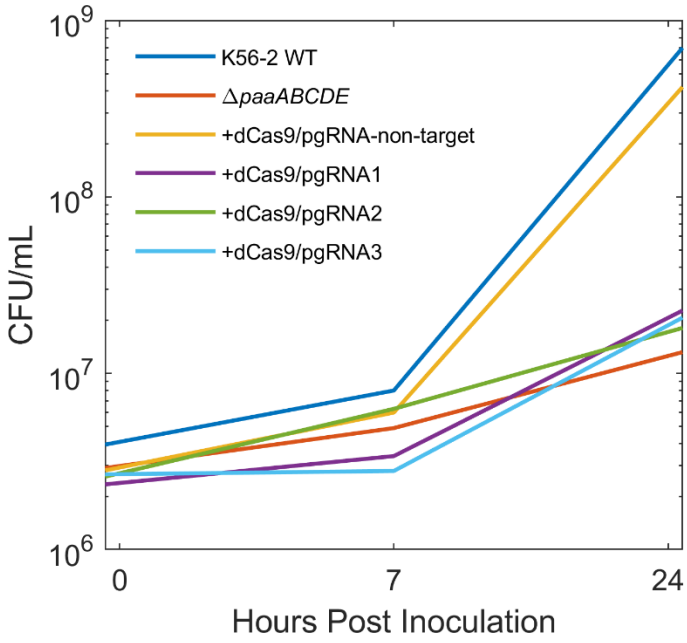

Figure A14. .Incubation in M9 with PA as the sole carbon source (M9+PA) does not reduce cell viability. K56-2 WT, a mutant of the paaABCDE operon (ΔpaaABCDE), and K56-2::dCas9 (+dCas9) harboring pgRNAs (as per Figure 2) were grown overnight in LB with 0.2% rhamnose, washed, and transferred to M9+PA. At the specified time points, cells were harvested and plated for CFU/mL on rich medium. All values presented are the means of two independent biological replicates.

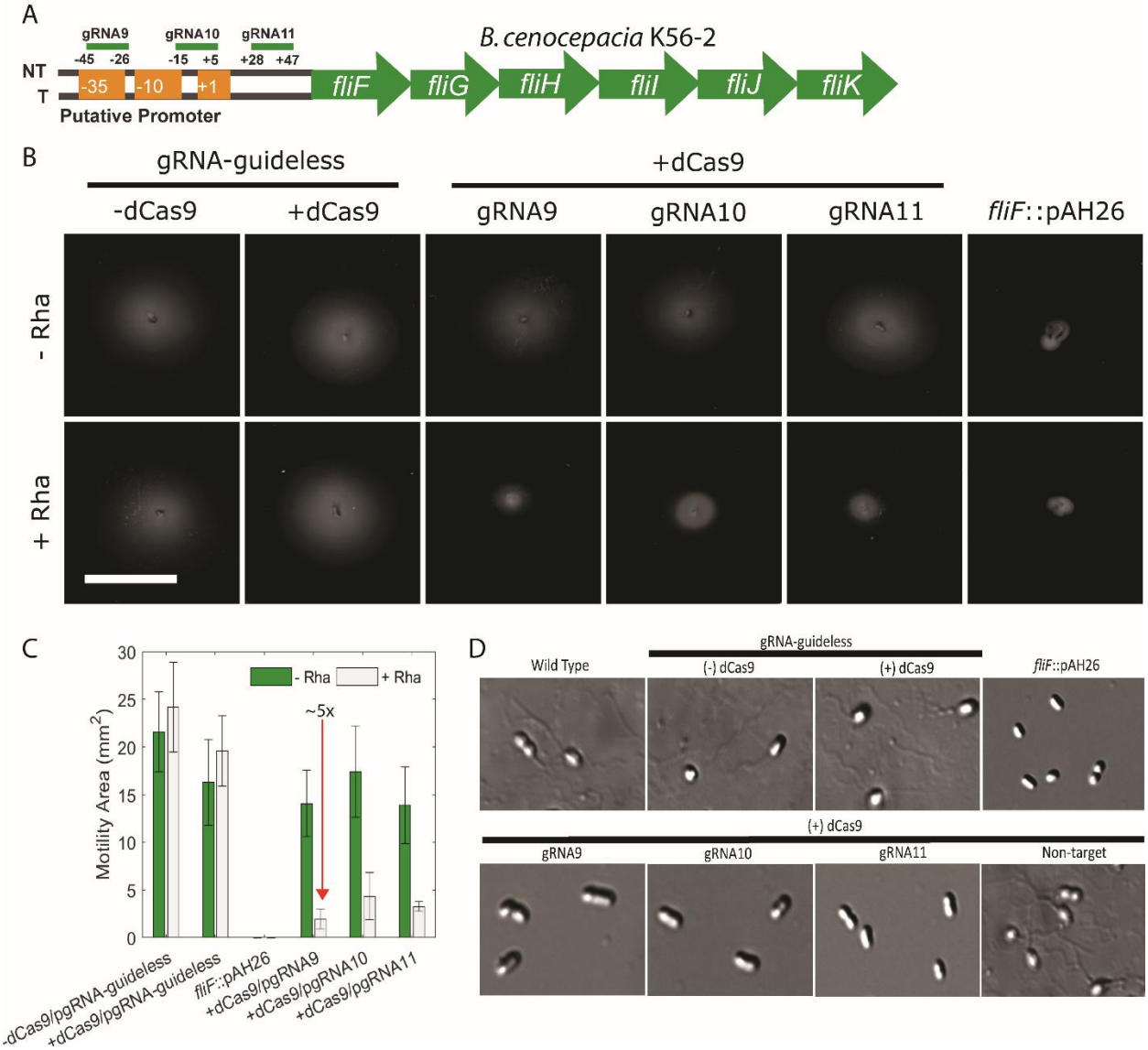

Figure A15. Targeting *fliF* by CRISPRi in *B. cenocepacia* K56-2 reduces swimming motility. A) Positions of the sgRNAs targeting regions upstream of the *fliFGHIJK* operon. sgRNA9 and 10 were designed to target the promoter elements (-35 and -10 boxes), while sgRNA11 targeted just upstream of the *fliF* ORF on the non-template (NT) strand. B) Motility was reduced, but not ablated by CRISPRi targeting of *fliF*. K56-2::CTX1-rha (-dCas9), K56-2::CTX1-rhadCas9 (+dCas9) (both harbouring pgRNA-guideless), and +dCas9 mutants harbouring sgRNAs targeting *fliF* were stab inoculated into 0.3% agar nutrient broth medium containing 100 µg/mL trimethoprim and with or without 0.2% rhamnose. The scale bar is 2 cm. C) Area of the swimming motility halos in B). D) The indicated strains were grown overnight with 0.2% rhamnose and 100 µg/mL trimethoprim, as required, and used for flagellum staining. Cells were imaged by DIC as we found better contrast versus brightfield microscopy.

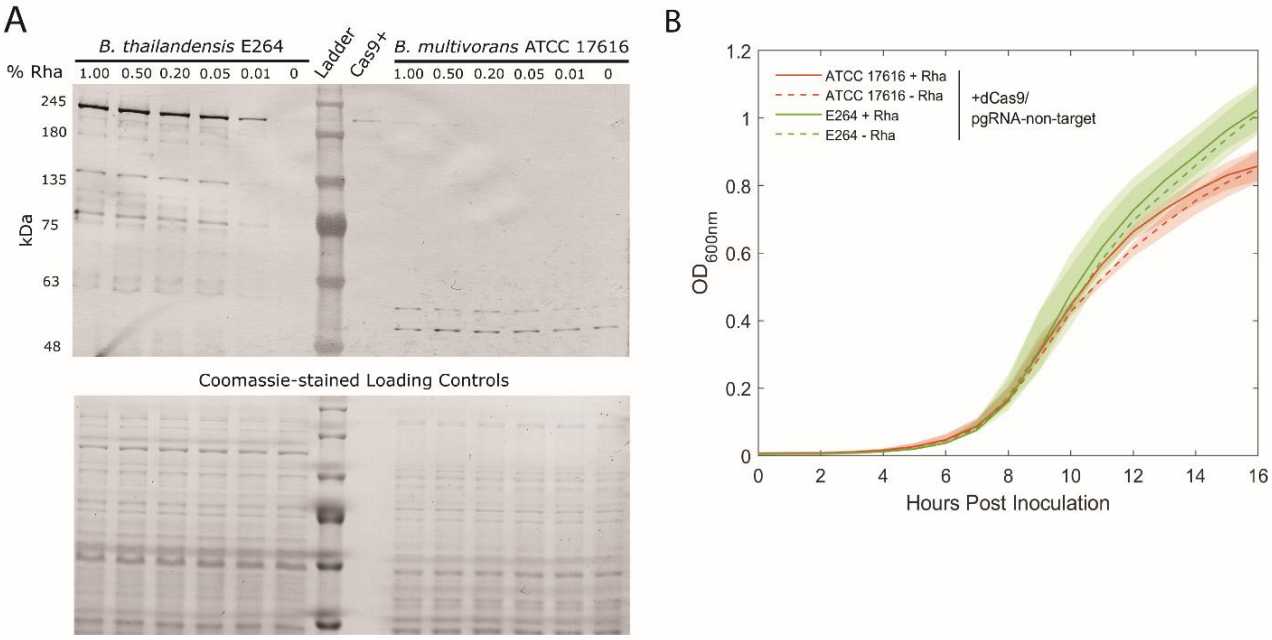

Figure A16. dCas9 expression is detected from chromosomal expression in B. *thailandensis* E264, but poorly from *B. multivorans* ATCC 17616. A) Strains harbouring the codon-optimized dcas9 in the chromosome were grown at OD600nm 0.6 then induced for three hours with the indicated concentrations of rhamnose and soluble protein was harvested. dCas9 expression was detected by probing with an α-dCas9 antibody. The lane labelled Cas9+ was loaded with 5 ng of purified Cas9 (Genscript). Below, the protein was run in parallel on SDS-PAGE and stained with Coomassie to ensure equal protein loading. B) Growth curves of *B. multivorans* ATCC17616 and *B. thailandensis* E264 species harbouring a chromosomal copy of the codon-optimized dcas9 and the non-genome targeting guide plasmid, pgRNA-non-target. Shading represents SD of three biological replicates.

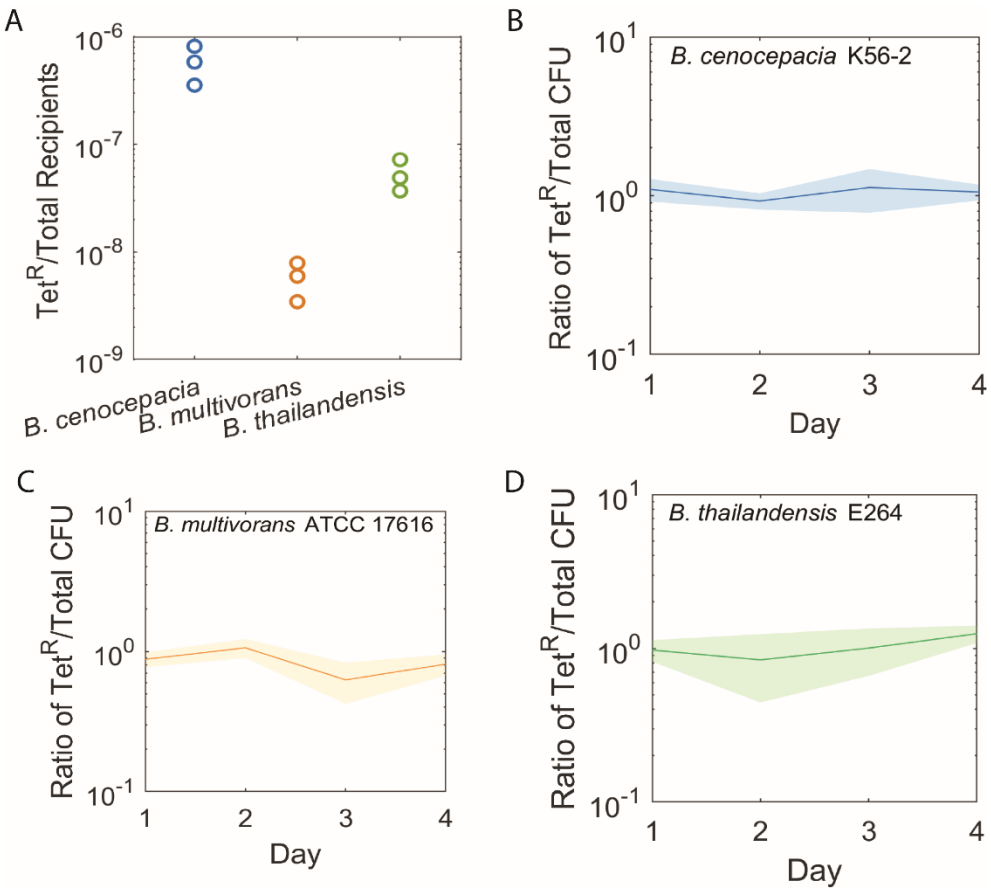

Figure A17. pAH-CTX1-rhadCas9 integrates with variable efficiency but is maintained without antibiotic selection. A) Strains were subjected to triparental mating with pAH-CTX1-rhadCas9. After mating, CFU counts were done on LB agar with 50 µg/mL gentamicin supplemented with and without 50 µg/mL tetracycline (Tet50). Ratios of CFU on the Tet50 to non-selective medium are reported. For B), C), and D) strains harbouring pAH-CTX1-rhadCas9 (without the accessory genes, such as *tetR*, deleted) were passaged over four days in LB without tetracycline. For each day, the CFU counts on Tet50 and non-selective medium were determined and the ratios are reported. Shading represents SD of three biological replicates.

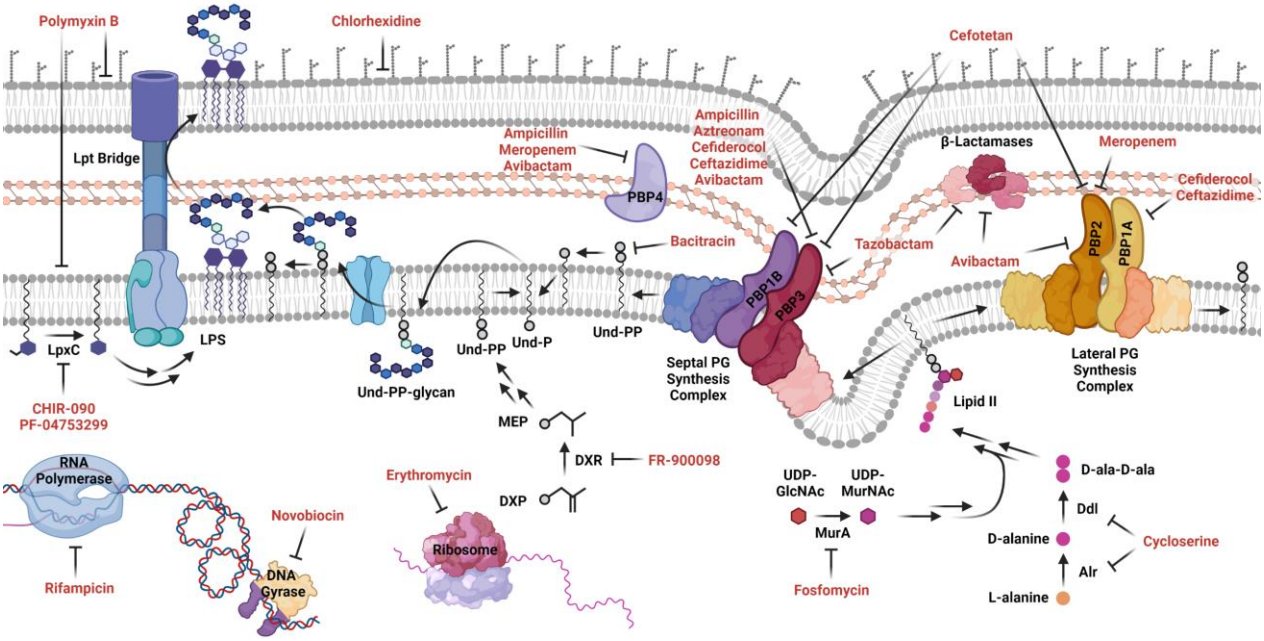

Figure A18. Targets of cell envelope-active antibiotics in the panel. Schematic of the Gram-negative cell envelope and steps inhibited by the antibiotic panel. Rifampicin, novobiocin, and erythromycin are controls that do not target the envelope. Targets are shown based on previous experimental evidence from *E. coli* (see in text references), and only if a Bcc homologue exists. High molecular weight PBPs 5, 6, 7 are omitted for clarity.

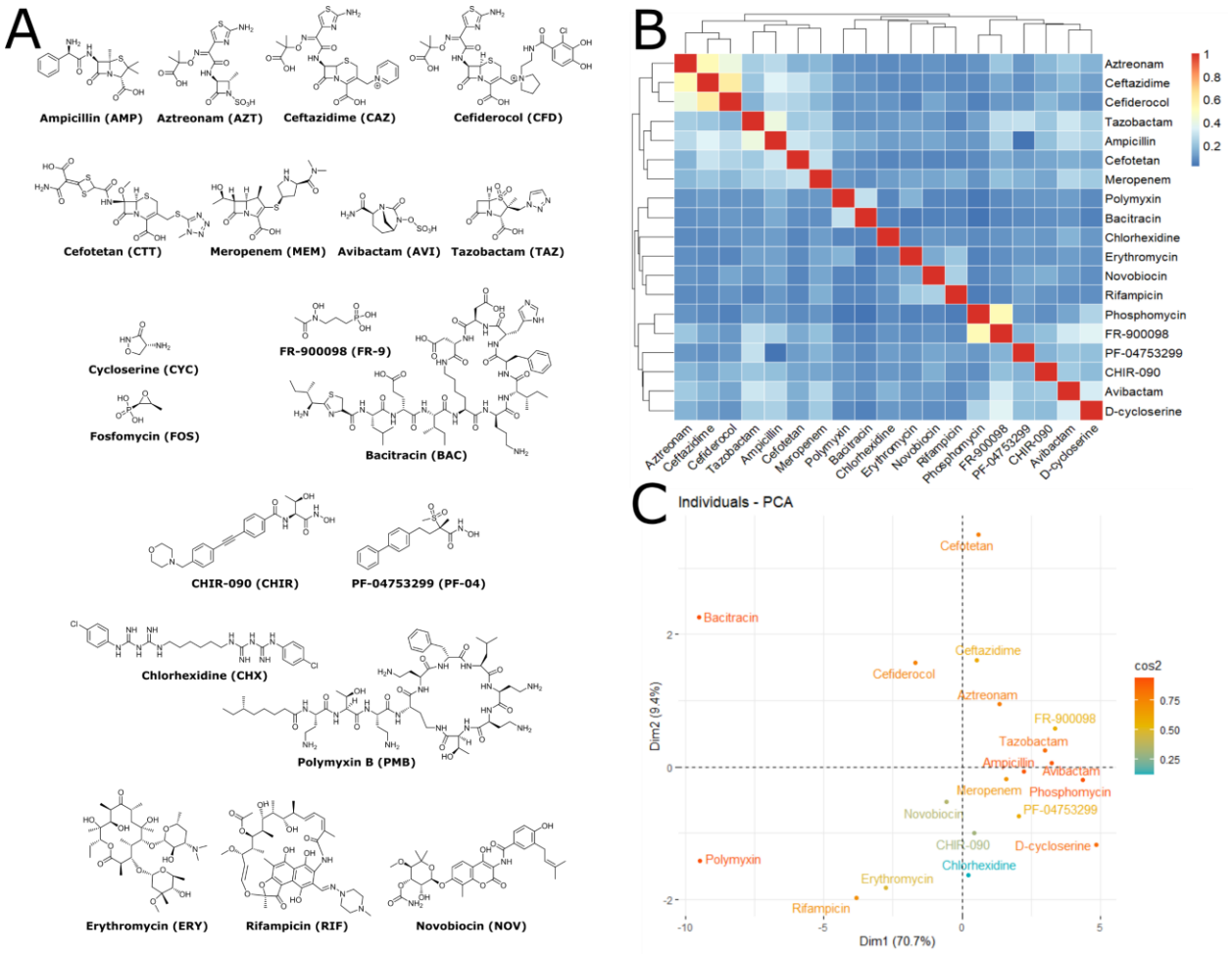

Figure A19. Structures and similarities among compounds in the antibiotic panel. A) The structure of each of the antibiotics used in the BarSeq experiment. B) 2-D hierarchical clustering of atom pair Tanimoto similarity scoring from the ChemMine Tools package *(Backman et al., 2011)*. C) Principal component analysis based on chemical properties from the ChemMine Tools package. Warmer colours indicate better representation by the principal components.

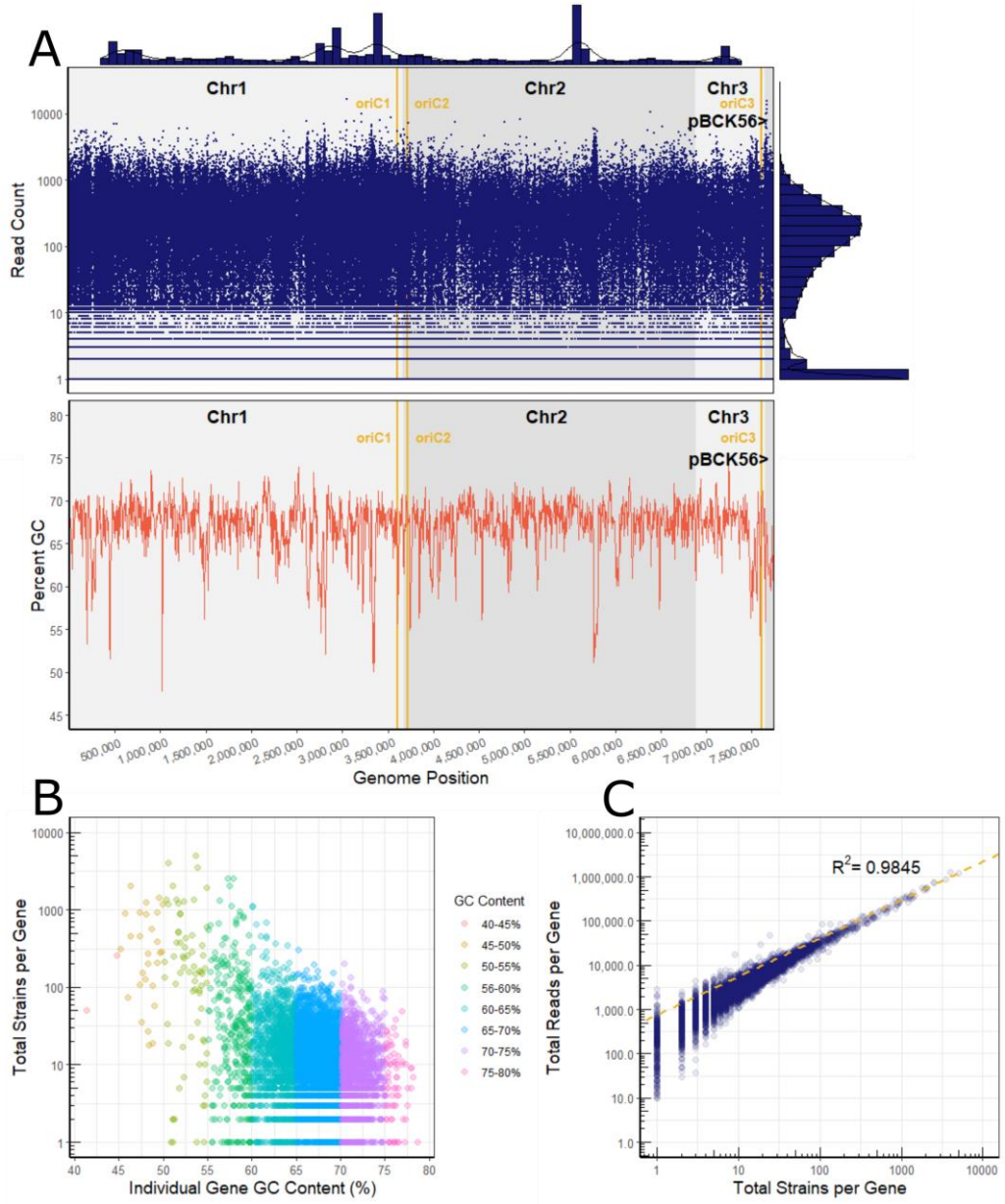

Figure A20. Transposon insertion density across the K56-2 genome. A). Each insertion in the library was mapped along with the read count. The marginal histograms represent 1D point density in the x and y dimensions of the plot. The x-marginal histogram has a bin width of 100,000 bp and shows insertion density. The y-marginal histogram splits each $\log_{10}$ into 5 bins and shows read count density. The chromosomal origins (OriC) were identified by homology from *B. cenocepacia* J2315 using DoriC 10.0 (Luo and Gao 2019). The GC_content perl script (https://github.com/DamienFr/GC_content_in_sliding_window) was used to calculate GC content with a 5,000 bp window and 5,000 bp step size. B) Gene-level breakdown of the number of strains per gene versus GC content. Each point is coloured by binned GC-content of the gene. C) The number of reads per gene versus the number of strains the gene is represented by in the library. The dashed yellow line is a linear regression showing the relationship between the number of reads and number of strains for each gene.

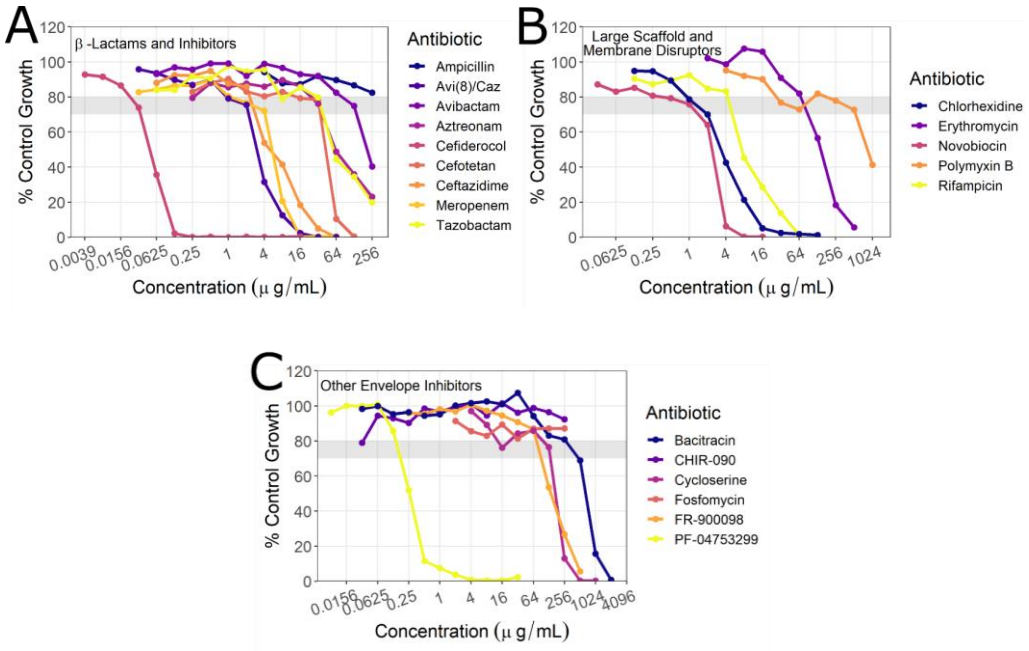

Figure A21. Growth dose-response curves of wild-type K56-2 to antibiotics in the panel. Cells were grown stationary in microtiter plates with concentration gradients of the indicated antibiotics. The grey box indicates the region of 20 – 30% growth inhibition relative to the no-antibiotic control (by OD_{600}) . Points are averages of three replicates. Cells were grown in LB to more closely represent conditions of the mutant library exposure.

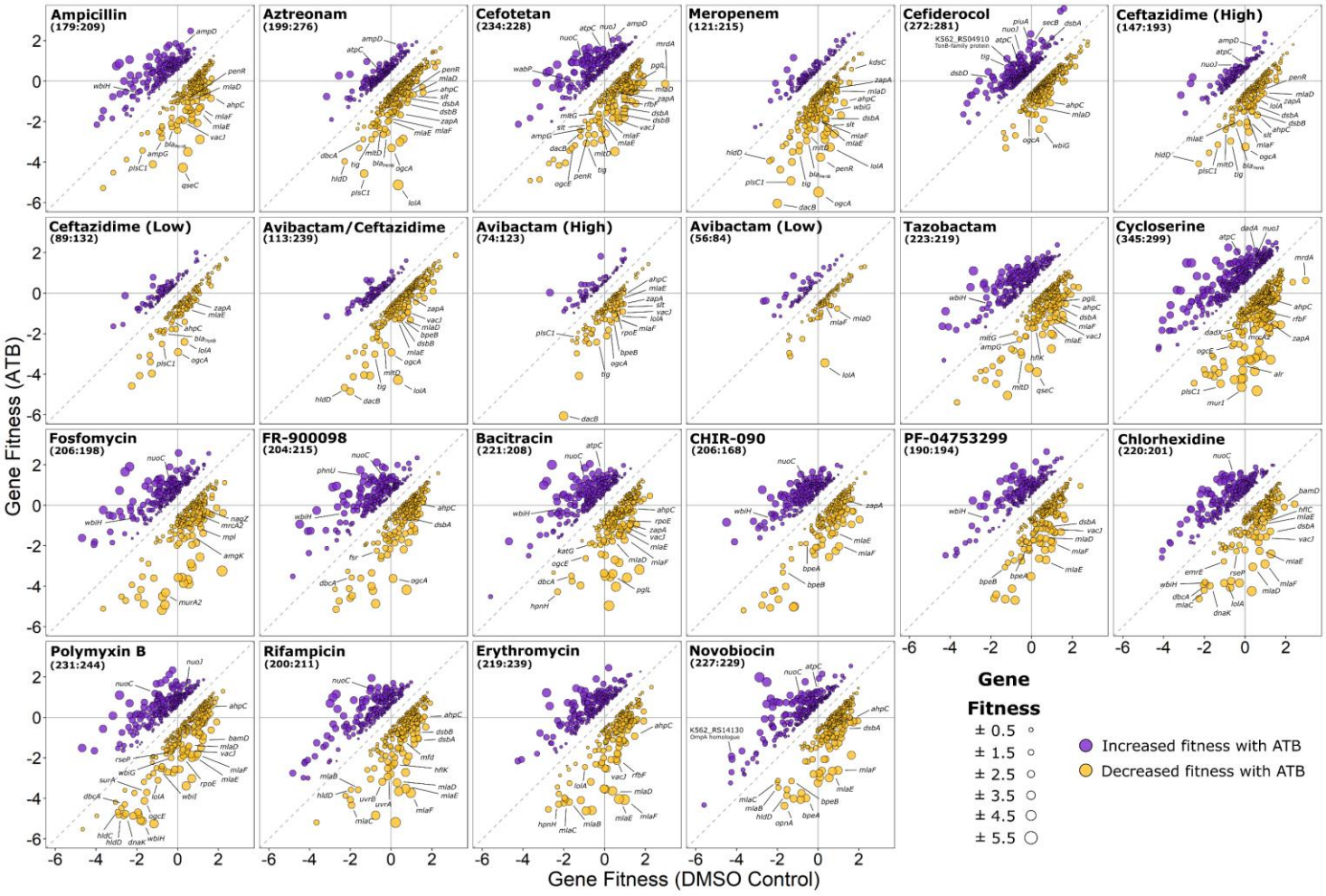

Figure A22. Gene fitness profiles of K56-2 transposon mutant library exposed to cell envelope-targeting antibiotic panel. Each point represents a gene that when disrupted by a transposon, affected fitness of the mutant in the presence of an antibiotic versus the DMSO control (two-sided t-test; $P < 0.05$; only genes with fitness effects greater than 0.5 or less than -0.5 were considered). The points are coloured based on positive (increased fitness; purple) or negative (decreased fitness; gold) interactions between the genes and tested antibiotics. The absolute difference in fitness score for a gene in each condition versus the DMSO control is given by the size of the point. Select genes of interest are indicated and named. The total number of genes in each condition with altered fitness (increased:decreased) is shown.

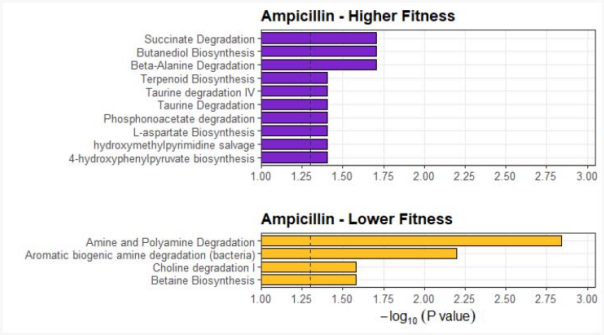
Ampicillin - Higher Fitness
Succinate Degradation
Butanediol Biosynthesis
Beta-Alanine Degradation
Terpenoid Biosynthesis
Taurine degradation IV
Taurine Degradation
Phosphonoacetate degradation
L-aspartate Biosynthesis
hydroxymethylpyrimidine salvage
4-hydroxyphenylpyruvate biosynthesis
1.00 1.25 1.50 1.75 2.00 2.25 2.50 2.75 3.00
Ampicillin - Lower Fitness
Amine and Polyamine Degradation
Aromatic biogenic amine degradation (bacteria)
Choline degradation I
Betaine Biosynthesis
1.00 1.25 1.50 1.75 2.00 2.25 2.50 2.75 3.00
−log10 (P value)

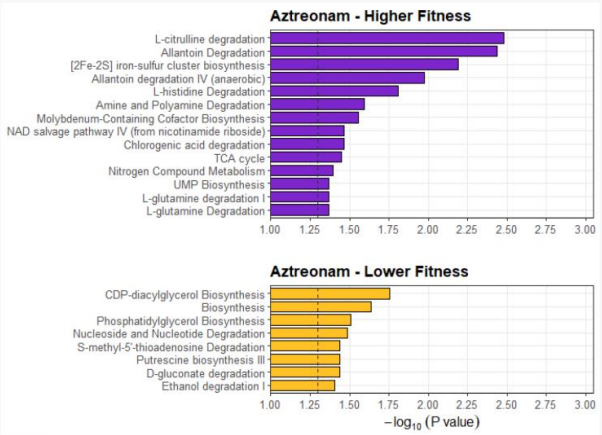
Aztreonam - Higher Fitness
L-citrulline degradation
Allantoin Degradation
[2Fe-2S] iron-sulfur cluster biosynthesis
Allantoin degradation IV (anaerobic)
L-histidine Degradation
Amine and Polyamine Degradation
Molybdenum-Containing Cofactor Biosynthesis
NAD salvage pathway IV (from nicotinamide riboside)
Chlorogenic acid degradation
TCA cycle
Nitrogen Compound Metabolism
UMP Biosynthesis
L-glutamine degradation I
L-glutamine Degradation
1.00 1.25 1.50 1.75 2.00 2.25 2.50 2.75 3.00
Aztreonam - Lower Fitness
CDP-diacylglycerol Biosynthesis
Biosynthesis
Phosphatidylglycerol Biosynthesis
Nucleoside and Nucleotide Degradation
S-methyl-5'-thioadenosine Degradation
Putrescine biosynthesis III
D-gluconate degradation
Ethanol degradation I
1.00 1.25 1.50 1.75 2.00 2.25 2.50 2.75 3.00
−log10 (P value)

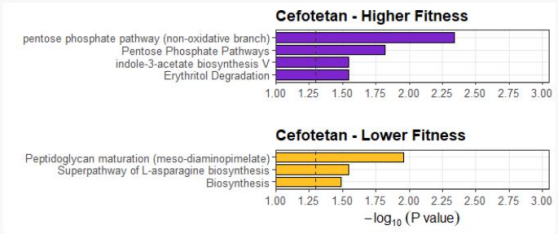
Cefotetan - Higher Fitness
pentose phosphate pathway (non-oxidative branch)
Pentose Phosphate Pathways
indole-3-acetate biosynthesis V
Erythritol Degradation
1.00 1.25 1.50 1.75 2.00 2.25 2.50 2.75 3.00
Cefotetan - Lower Fitness
Peptidoglycan maturation (meso-diaminopimelate)
Superpathway of L-asparagine biosynthesis
Biosynthesis
1.00 1.25 1.50 1.75 2.00 2.25 2.50 2.75 3.00
−log10 (P value)

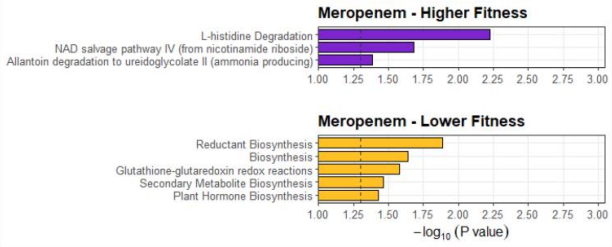
Meropenem - Higher Fitness
L-histidine Degradation
NAD salvage pathway IV (from nicotinamide riboside)
Allantoin degradation to ureidoglycolate II (ammonia producing)
1.00 1.25 1.50 1.75 2.00 2.25 2.50 2.75 3.00
Meropenem - Lower Fitness
Reductant Biosynthesis
Biosynthesis
Glutathione-glutaredoxin redox reactions
Secondary Metabolite Biosynthesis
Plant Hormone Biosynthesis
1.00 1.25 1.50 1.75 2.00 2.25 2.50 2.75 3.00
−log10 (P value)

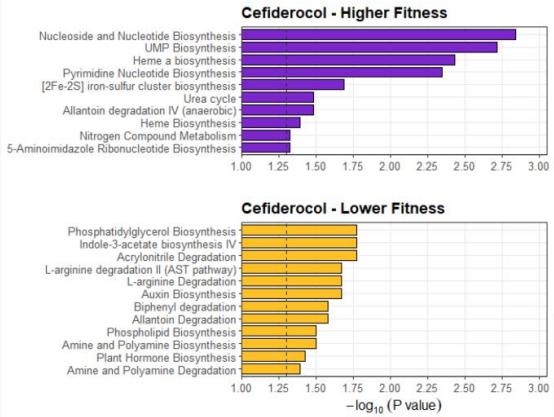
Cefiderocol - Higher Fitness
Nucleoside and Nucleotide Biosynthesis
UMP Biosynthesis
Heme a biosynthesis
Pyrimidine Nucleotide Biosynthesis
[2Fe-2S] iron-sulfur cluster biosynthesis
Urea cycle
Allantoin degradation IV (anaerobic)
Heme Biosynthesis
Nitrogen Compound Metabolism
5-Aminoimidazole Ribonucleotide Biosynthesis
1.00 1.25 1.50 1.75 2.00 2.25 2.50 2.75 3.00
Cefiderocol - Lower Fitness
Phosphatidylglycerol Biosynthesis
Indole-3-acetate biosynthesis IV
Acrylonitrile Degradation
L-arginine degradation II (AST pathway)
L-arginine Degradation
Auxin Biosynthesis
Biphenyl degradation
Allantoin Degradation
Phospholipid Biosynthesis
Amine and Polyamine Biosynthesis
Plant Hormone Biosynthesis
Amine and Polyamine Degradation
1.00 1.25 1.50 1.75 2.00 2.25 2.50 2.75 3.00
−log10 (P value)

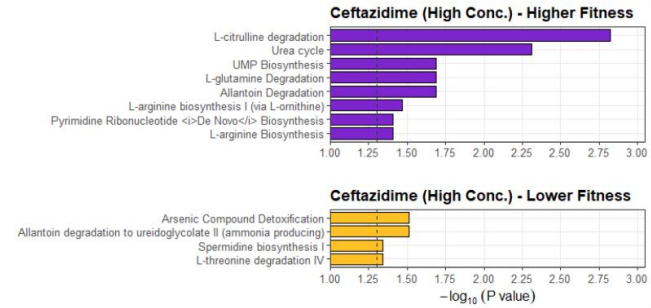
Ceftazidime (High Conc.) - Higher Fitness
L-citrulline degradation
Urea cycle
UMP Biosynthesis
L-glutamine Degradation
Allantoin Degradation
L-arginine biosynthesis I (via L-ornithine)
Pyrimidine Ribonucleotide De Novo Biosynthesis
L-arginine Biosynthesis
1.00 1.25 1.50 1.75 2.00 2.25 2.50 2.75 3.00
Ceftazidime (High Conc.) - Lower Fitness
Arsenic Compound Detoxification
Allantoin degradation to ureidoglycolate II (ammonia producing)
Spermidine biosynthesis I
L-threonine degradation IV
1.00 1.25 1.50 1.75 2.00 2.25 2.50 2.75 3.00
−log10 (P value)

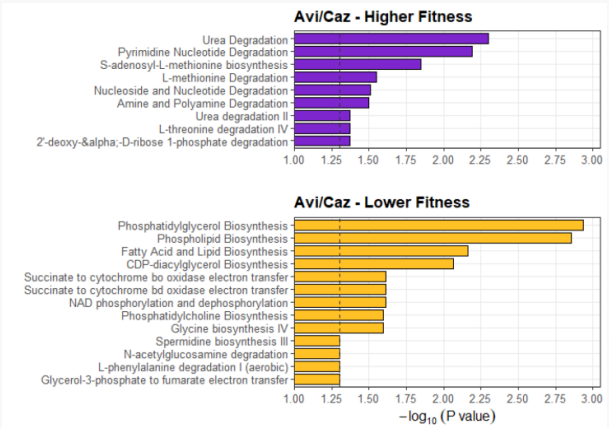
Avi/Caz - Higher Fitness
Urea Degradation
Pyrimidine Nucleotide Degradation
S-adenosyl-L-methionine biosynthesis
L-methionine Degradation
Nucleoside and Nucleotide Degradation
Amine and Polyamine Degradation
Urea degradation II
L-threonine degradation IV
2'-deoxy-α-D-ribose 1-phosphate degradation
1.00 1.25 1.50 1.75 2.00 2.25 2.50 2.75 3.00
Avi/Caz - Lower Fitness
Phosphatidylglycerol Biosynthesis
Phospholipid Biosynthesis
Fatty Acid and Lipid Biosynthesis
CDP-diacylglycerol Biosynthesis
Succinate to cytochrome bo oxidase electron transfer
Succinate to cytochrome bd oxidase electron transfer
NAD phosphorylation and dephosphorylation
Phosphatidylcholine Biosynthesis
Glycine biosynthesis IV
Spermidine biosynthesis III
N-acetylglucosamine degradation
L-phenylalanine degradation I (aerobic)
Glycerol-3-phosphate to fumarate electron transfer
1.00 1.25 1.50 1.75 2.00 2.25 2.50 2.75 3.00
−log10 (P value)

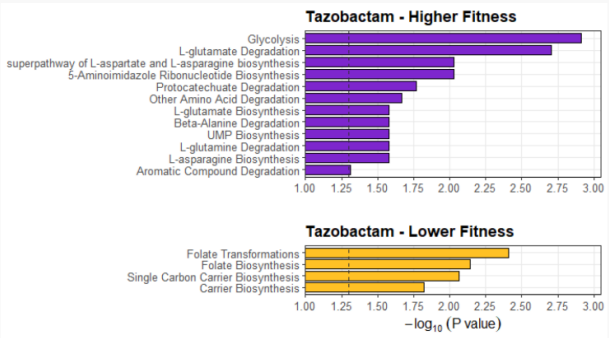
Tazobactam - Higher Fitness
Glycolysis
L-glutamate Degradation
superpathway of L-aspartate and L-asparagine biosynthesis
5-Aminoimidazole Ribonucleotide Biosynthesis
Protocatechuate Degradation
Other Amino Acid Degradation
L-glutamate Biosynthesis
Beta-Alanine Degradation
UMP Biosynthesis
L-glutamine Degradation
L-asparagine Biosynthesis
Aromatic Compound Degradation
1.00 1.25 1.50 1.75 2.00 2.25 2.50 2.75 3.00
Tazobactam - Lower Fitness
Folate Transformations
Folate Biosynthesis
Single Carbon Carrier Biosynthesis
Carrier Biosynthesis
1.00 1.25 1.50 1.75 2.00 2.25 2.50 2.75 3.00
−log10 (P value)

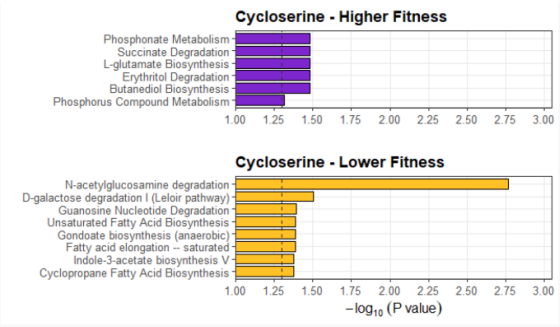
Cycloserine - Higher Fitness
Phosphonate Metabolism
Succinate Degradation
L-glutamate Biosynthesis
Erythritol Degradation
Butanediol Biosynthesis
Phosphorus Compound Metabolism
1.00 1.25 1.50 1.75 2.00 2.25 2.50 2.75 3.00
Cycloserine - Lower Fitness
N-acetylglucosamine degradation
D-galactose degradation I (Leloir pathway)
Guanosine Nucleotide Degradation
Unsaturated Fatty Acid Biosynthesis
Gondoate biosynthesis (anaerobic)
Fatty acid elongation -- saturated
Indole-3-acetate biosynthesis V
Cyclopropane Fatty Acid Biosynthesis
1.00 1.25 1.50 1.75 2.00 2.25 2.50 2.75 3.00
−log10 (P value)

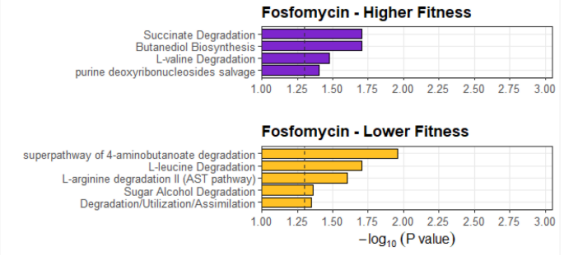
Fosfomycin - Higher Fitness
Succinate Degradation
Butanediol Biosynthesis
L-valine Degradation
purine deoxyribonucleosides salvage
1.00 1.25 1.50 1.75 2.00 2.25 2.50 2.75 3.00
Fosfomycin - Lower Fitness
superpathway of 4-aminobutanoate degradation
L-leucine Degradation
L-arginine degradation II (AST pathway)
Sugar Alcohol Degradation
Degradation/Utilization/Assimilation
1.00 1.25 1.50 1.75 2.00 2.25 2.50 2.75 3.00
−log10 (P value)

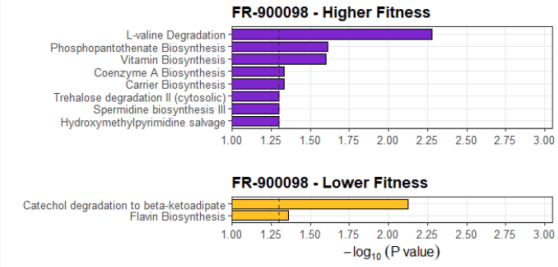
FR-900098 - Higher Fitness
L-valine Degradation
Phosphopantothenate Biosynthesis
Vitamin Biosynthesis
Coenzyme A Biosynthesis
Carrier Biosynthesis
Trehalose degradation II (cytosolic)
Spermidine biosynthesis III
Hydroxymethylpyrimidine salvage
1.00 1.25 1.50 1.75 2.00 2.25 2.50 2.75 3.00
FR-900098 - Lower Fitness
Catechol degradation to beta-ketoadipate
Flavin Biosynthesis
1.00 1.25 1.50 1.75 2.00 2.25 2.50 2.75 3.00
−log10 (P value)

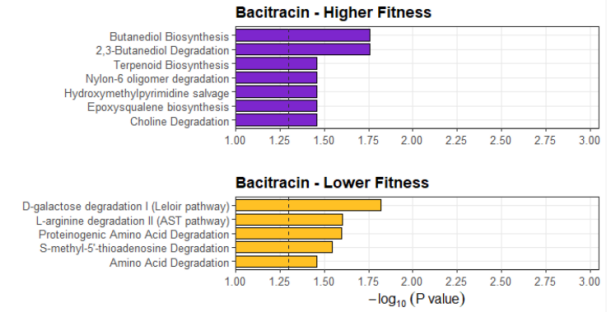
Bacitracin - Higher Fitness
Butanediol Biosynthesis
2,3-Butanediol Degradation
Terpenoid Biosynthesis
Nylon-6 oligomer degradation
Hydroxymethylpyrimidine salvage
Epoxysqualene biosynthesis
Choline Degradation
1.00 1.25 1.50 1.75 2.00 2.25 2.50 2.75 3.00
Bacitracin - Lower Fitness
D-galactose degradation I (Leloir pathway)
L-arginine degradation II (AST pathway)
Proteinogenic Amino Acid Degradation
S-methyl-5'-thioadenosine Degradation
Amino Acid Degradation
1.00 1.25 1.50 1.75 2.00 2.25 2.50 2.75 3.00
−log10 (P value)

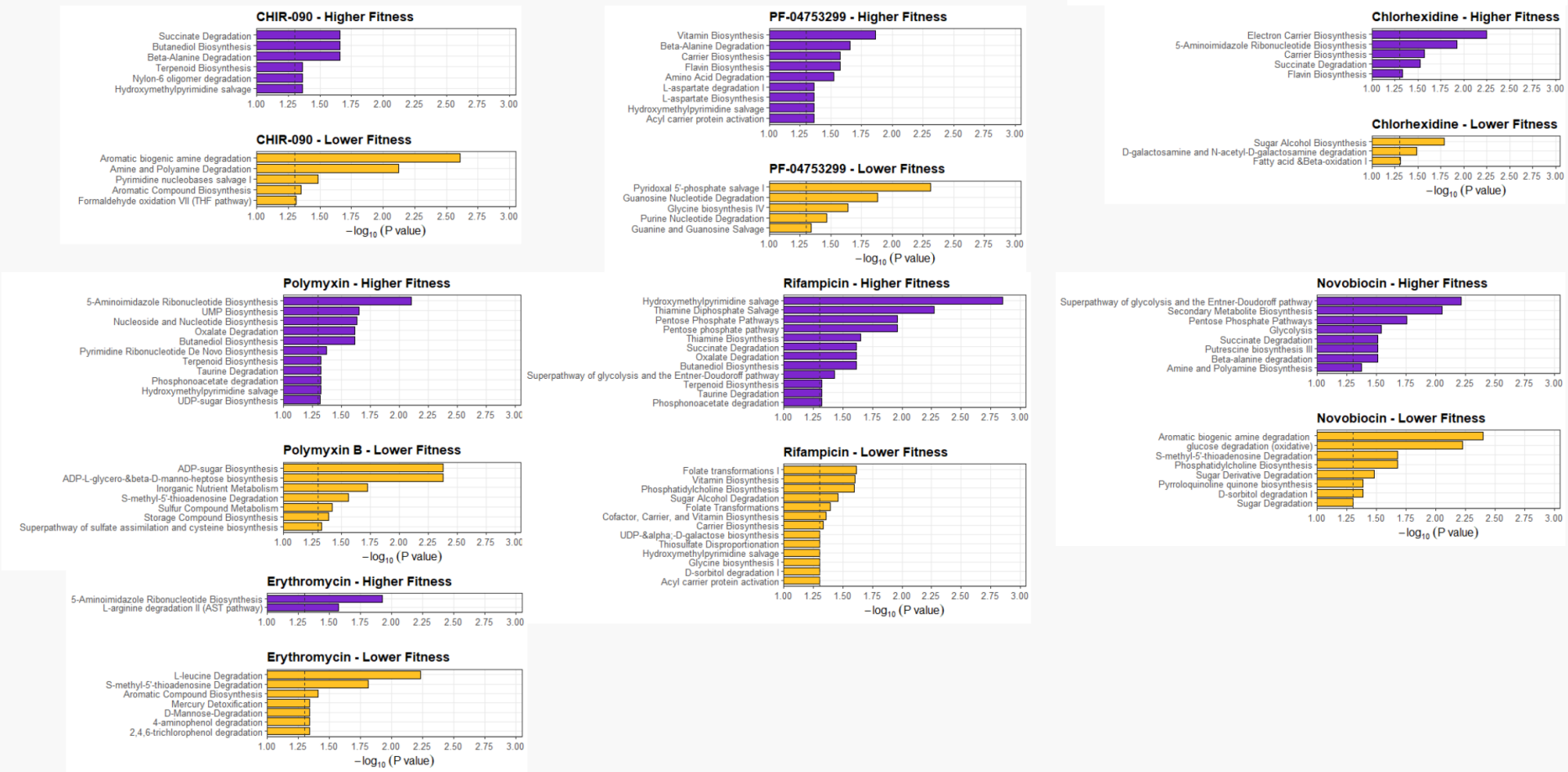

Figure A23. BioCyc pathway enrichment of genes affecting fitness in the presence of the antibiotic panel. Genes with fitness scores either above 0.5 or below -0.5 were submitted to BioCyc for enrichment analysis (Fisher exact test without multiple testing correction) (against K56-2 genome from GenBank accession GCA_000333155.2). Enrichments from genes with positive and negative fitness scores are given in purple and gold, respectively. The dashed line indicates P = 0.05. The high resolution figure can be found at : https://doi.org/10.34990/FK2/C8X5EU

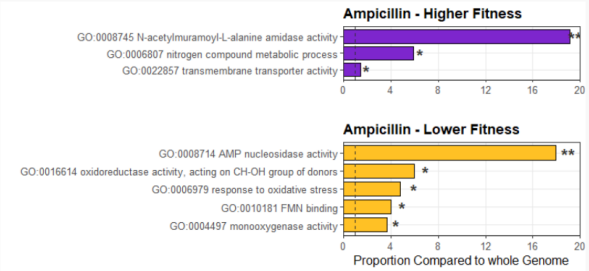
Ampicillin - Higher Fitness
GO:0008745 N-acetylmuramoyl-L-alanine amidase activity
GO:0006807 nitrogen compound metabolic process
GO:0022857 transmembrane transporter activity
0
4
8
12
16
20

Ampicillin - Lower Fitness
GO:0008714 AMP nucleosidase activity
GO:0016614 oxidoreductase activity, acting on CH-OH group of donors
GO:0006979 response to oxidative stress
GO:0010181 FMN binding
GO:0004497 monooxygenase activity
0
4
8
12
16
20
Proportion Compared to whole Genome

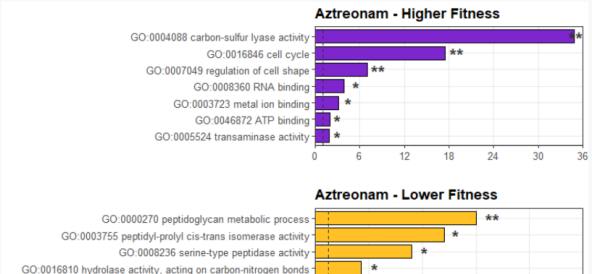
Aztreonam - Higher Fitness
GO:0004088 carbon-sulfur lyase activity
GO:0016846 cell cycle
GO:0007049 regulation of cell shape
GO:0008360 RNA binding
GO:0003723 metal ion binding
GO:0046872 ATP binding
GO:0005524 transaminase activity
0
6
12
18
24
30
36

Aztreonam - Lower Fitness
GO:0000270 peptidoglycan metabolic process
GO:0003755 peptidyl-prolyl cis-trans isomerase activity
GO:0008236 serine-type peptidase activity
GO:0016810 hydrolase activity, acting on carbon-nitrogen bonds
GO:0016020 membrane
GO:0005975 carbohydrate metabolic process
GO:0042597 periplasmic space
GO:0016021 integral component of membrane
0
4
8
12
16
20
Proportion Compared to whole Genome

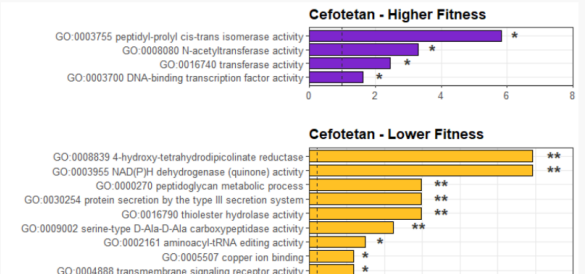
Cefotetan - Higher Fitness
GO:0003755 peptidyl-prolyl cis-trans isomerase activity
GO:0008080 N-acetyltransferase activity
GO:0016740 transferase activity
GO:0003700 DNA-binding transcription factor activity
0
2
4
6
8

Cefotetan - Lower Fitness
GO:0008839 4-hydroxy-tetrahydrodipicolinate reductase
GO:0003955 NAD(P)H dehydrogenase (quinone) activity
GO:0000270 peptidoglycan metabolic process
GO:0030254 protein secretion by the type III secretion system
GO:0016790 thiolester hydrolase activity
GO:0009002 serine-type D-Ala-D-Ala carboxypeptidase activity
GO:0002161 aminoacyl-tRNA editing activity
GO:0005507 copper ion binding
GO:0004888 transmembrane signaling receptor activity
GO:0006935 chemotaxis
GO:0016020 membrane
GO:0042597 periplasmic space
GO:0005887 integral component of plasma membrane
0
5
10
15
20
25
30
35
Proportion Compared to whole Genome

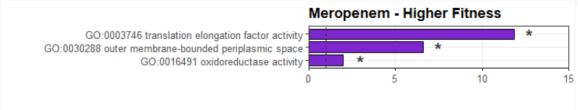
Meropenem - Higher Fitness
GO:0003746 translation elongation factor activity
GO:0030288 outer membrane-bounded periplasmic space
GO:0016491 oxidoreductase activity
0
5
10
15

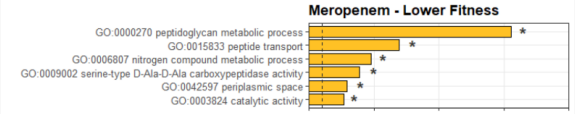
Meropenem - Lower Fitness
GO:0000270 peptidoglycan metabolic process
GO:0015833 peptide transport
GO:0006807 nitrogen compound metabolic process
GO:0009002 serine-type D-Ala-D-Ala carboxypeptidase activity
GO:0042597 periplasmic space
GO:0003824 catalytic activity
0
5
10
15
20
Proportion Compared to whole Genome

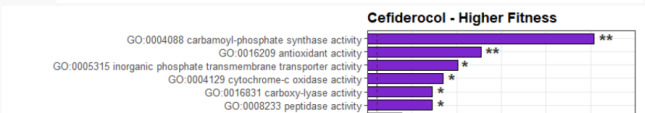
Cefiderocol - Higher Fitness
GO:0004088 carbamoyl-phosphate synthase activity
GO:0016209 antioxidant activity
GO:0005315 inorganic phosphate transmembrane transporter activity
GO:0004129 cytochrome-c oxidase activity
GO:0016831 carboxy-lyase activity
GO:0008233 peptidase activity
GO:0007049 cell cycle
GO:0003723 RNA binding
GO:0000287 magnesium ion binding
GO:0009055 electron transfer activity
GO:0046872 metal ion binding
GO:0005524 ATP binding
0
5
10
15
20
25

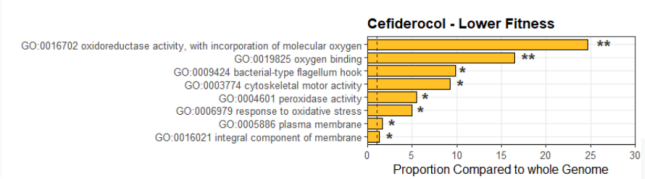
Cefiderocol - Lower Fitness
GO:0016702 oxidoreductase activity, with incorporation of molecular oxygen
GO:0019825 oxygen binding
GO:0009424 bacterial-type flagellum hook
GO:0003774 cytoskeletal motor activity
GO:0004601 peroxidase activity
GO:0006979 response to oxidative stress
GO:0005886 plasma membrane
GO:0016021 integral component of membrane
0
5
10
15
20
25
30
Proportion Compared to whole Genome

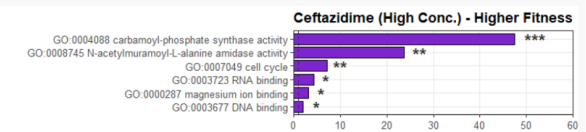
Ceftazidime (High Conc.) - Higher Fitness
GO:0004088 carbamoyl-phosphate synthase activity
GO:0008745 N-acetylmuramoyl-L-alanine amidase activity
GO:0007049 cell cycle
GO:0003723 RNA binding
GO:0000287 magnesium ion binding
GO:0003677 DNA binding
0
10
20
30
40
50
60

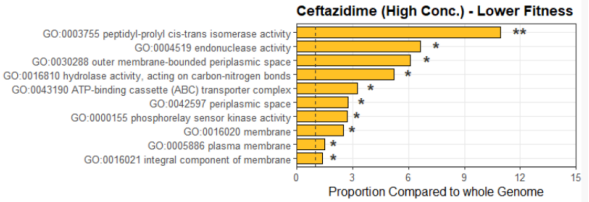
Ceftazidime (High Conc.) - Lower Fitness
GO:0003755 peptidyl-prolyl cis-trans isomerase activity
GO:0004519 endonuclease activity
GO:0030288 outer membrane-bounded periplasmic space
GO:0016810 hydrolase activity, acting on carbon-nitrogen bonds
GO:0043190 ATP-binding cassette (ABC) transporter complex
GO:0042597 periplasmic space
GO:0000155 phosphorelay sensor kinase activity
GO:0016020 membrane
GO:0005886 plasma membrane
GO:0016021 integral component of membrane
0
3
6
9
12
15
Proportion Compared to whole Genome

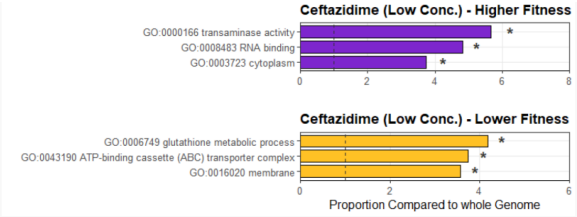
Ceftazidime (Low Conc.) - Higher Fitness
GO:0000166 transaminase activity
GO:0008483 RNA binding
GO:0003723 cytoplasm
0
2
4
6
8

Ceftazidime (Low Conc.) - Lower Fitness
GO:0006749 glutathione metabolic process
GO:0043190 ATP-binding cassette (ABC) transporter complex
GO:0016020 membrane
0
2
4
6
Proportion Compared to whole Genome

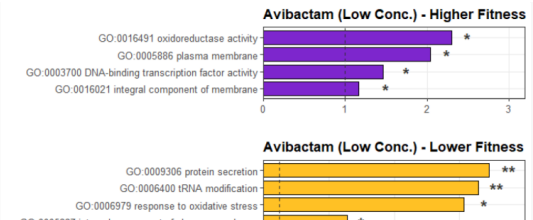
Avibactam (Low Conc.) - Higher Fitness
GO:0016491 oxidoreductase activity
GO:0005886 plasma membrane
GO:0003700 DNA-binding transcription factor activity
GO:0016021 integral component of membrane
0
1
2
3

Avibactam (Low Conc.) - Lower Fitness
GO:0009306 protein secretion
GO:0006400 tRNA modification
GO:0006979 response to oxidative stress
GO:0005887 integral component of plasma membrane
0
4
8
12
16
Proportion Compared to whole Genome

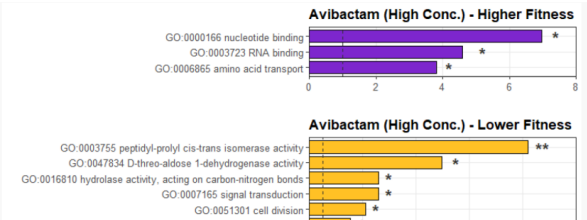
Avibactam (High Conc.) - Higher Fitness
GO:0000166 nucleotide binding
GO:0003723 RNA binding
GO:0006865 amino acid transport
0
2
4
6
8

Avibactam (High Conc.) - Lower Fitness
GO:0003755 peptidyl-prolyl cis-trans isomerase activity
GO:0047834 D-threo-aldose 1-dehydrogenase activity
GO:0016810 hydrolase activity, acting on carbon-nitrogen bonds
GO:0007165 signal transduction
GO:0051301 cell division
GO:0042597 periplasmic space
GO:0016021 integral component of membrane
0
4
8
12
16
20
Proportion Compared to whole Genome

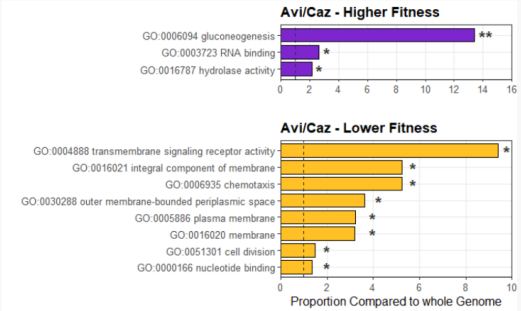
Avi/Caz - Higher Fitness
GO:0006094 gluconeogenesis
GO:0003723 RNA binding
GO:0016787 hydrolase activity
0
2
4
6
8
10
12
14
16

Avi/Caz - Lower Fitness
GO:0004888 transmembrane signaling receptor activity
GO:0016021 integral component of membrane
GO:0006935 chemotaxis
GO:0030288 outer membrane-bounded periplasmic space
GO:0005886 plasma membrane
GO:0016020 membrane
GO:0051301 cell division
GO:0000166 nucleotide binding
0
2
4
6
8
10
Proportion Compared to whole Genome

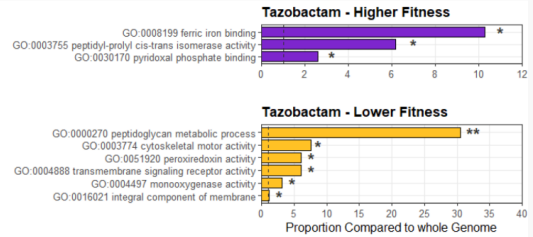
Tazobactam - Higher Fitness
GO:0008199 ferric iron binding
GO:0003755 peptidyl-prolyl cis-trans isomerase activity
GO:0030170 pyridoxal phosphate binding
0
2
4
6
8
10
12

Tazobactam - Lower Fitness
GO:0000270 peptidoglycan metabolic process
GO:0003774 cytoskeletal motor activity
GO:0051920 peroxiredoxin activity
GO:0004888 transmembrane signaling receptor activity
GO:0004497 monooxygenase activity
GO:0016021 integral component of membrane
0
5
10
15
20
25
30
35
40
Proportion Compared to whole Genome

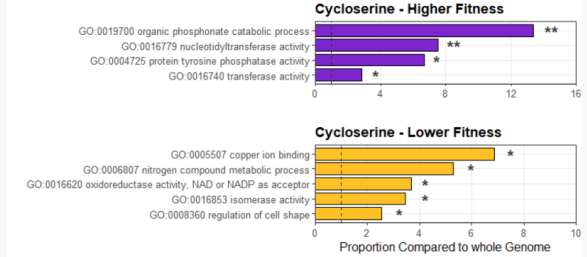
Cycloserine - Higher Fitness
GO:0019700 organic phosphonate catabolic process
GO:0016779 nucleotidyltransferase activity
GO:0004725 protein tyrosine phosphatase activity
GO:0016740 transferase activity
0
4
8
12
16

Cycloserine - Lower Fitness
GO:0005507 copper ion binding
GO:0006807 nitrogen compound metabolic process
GO:0016620 oxidoreductase activity, NAD or NADP as acceptor
GO:0016853 isomerase activity
GO:0008360 regulation of cell shape
0
2
4
6
8
10
Proportion Compared to whole Genome

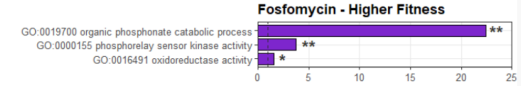
Fosfomycin - Higher Fitness
GO:0019700 organic phosphonate catabolic process
GO:0000155 phosphorelay sensor kinase activity
GO:0016491 oxidoreductase activity
0
5
10
15
20
25

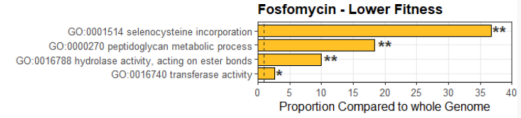
Fosfomycin - Lower Fitness
GO:0001514 selenocysteine incorporation
GO:0000270 peptidoglycan metabolic process
GO:0016788 hydrolase activity, acting on ester bonds
GO:0016740 transferase activity
0
5
10
15
20
25
30
35
40
Proportion Compared to whole Genome

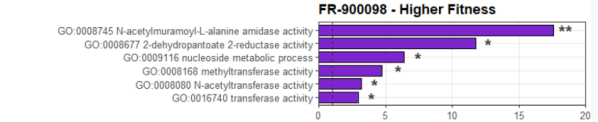
FR-900098 - Higher Fitness
GO:0008745 N-acetylmuramoyl-L-alanine amidase activity
GO:0008677 2-dehydropantoate 2-reductase activity
GO:0009116 nucleoside metabolic process
GO:0008168 methyltransferase activity
GO:0008080 N-acetyltransferase activity
GO:0016740 transferase activity
0
5
10
15
20

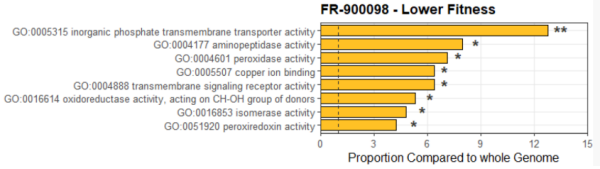
FR-900098 - Lower Fitness
GO:0005315 inorganic phosphate transmembrane transporter activity
GO:0004177 aminopeptidase activity
GO:0004601 peroxidase activity
GO:0005507 copper ion binding
GO:0004888 transmembrane signaling receptor activity
GO:0016614 oxidoreductase activity, acting on CH-OH group of donors
GO:0016853 isomerase activity
GO:0051920 peroxiredoxin activity
0
3
6
9
12
15
Proportion Compared to whole Genome

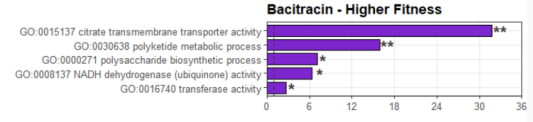
Bacitracin - Higher Fitness
GO:0015137 citrate transmembrane transporter activity
GO:0030638 polyketide metabolic process
GO:0000271 polysaccharide biosynthetic process
GO:0008137 NADH dehydrogenase (ubiquinone) activity
GO:0016740 transferase activity
0
6
12
18
24
30
36

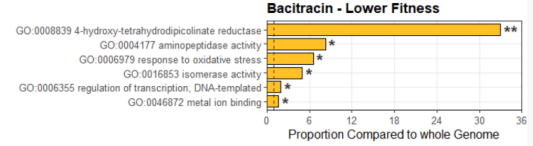
Bacitracin - Lower Fitness
GO:0008839 4-hydroxy-tetrahydrodipicolinate reductase
GO:0004177 aminopeptidase activity
GO:0006979 response to oxidative stress
GO:0016853 isomerase activity
GO:0006355 regulation of transcription, DNA-templated
GO:0046872 metal ion binding
0
6
12
18
24
30
36
Proportion Compared to whole Genome

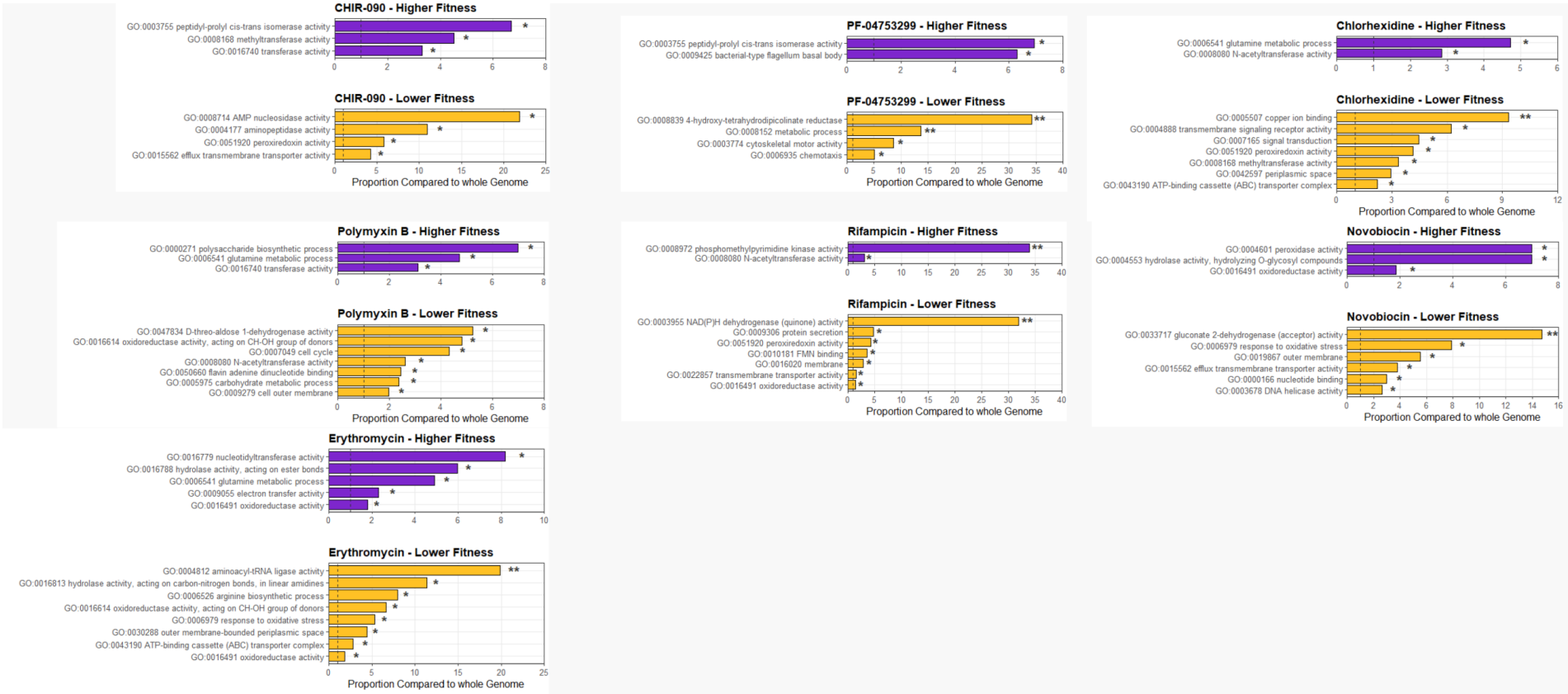

Figure A24. GO term enrichment of genes affecting fitness in the presence of the antibiotic panel. Genes with fitness scores either above 0.5 or below -0.5 were used for GO term enrichment relative to the whole K56-2 genome (Hypergeometric test without multiple testing correction) with GeneMerge 1.5 (Castillo-Davis et al. 2003). Enrichments from genes with positive and negative fitness scores are given in purple and gold, respectively. The dashed line indicates equal proportions in the genome and antibiotic condition. * P < 0.05, ** P < 0.01, *** P < 0.001. The high resolution figure can be found at : https://doi.org/10.34990/FK2/C8X5EU

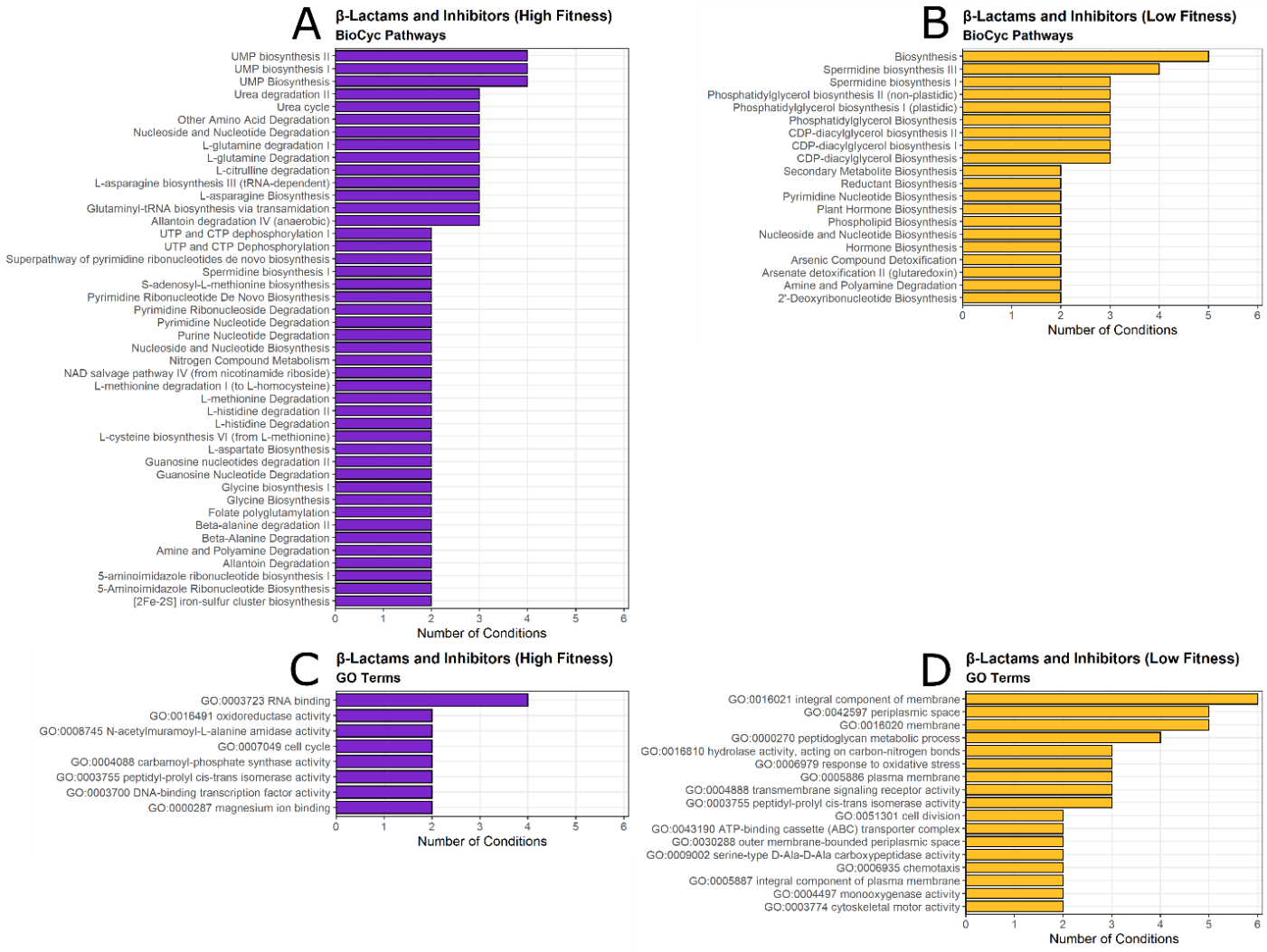

Figure A25. Summary of BioCyc pathway and GO term enrichments from gene scores among the β-lactam and β-lactamase inhibitor conditions. Significant enrichments ($P < 0.05$) from BioCyc pathways and GO terms were pooled from Figures A4 and A5. Only those pathways and terms present in at least two antibiotic conditions are shown.

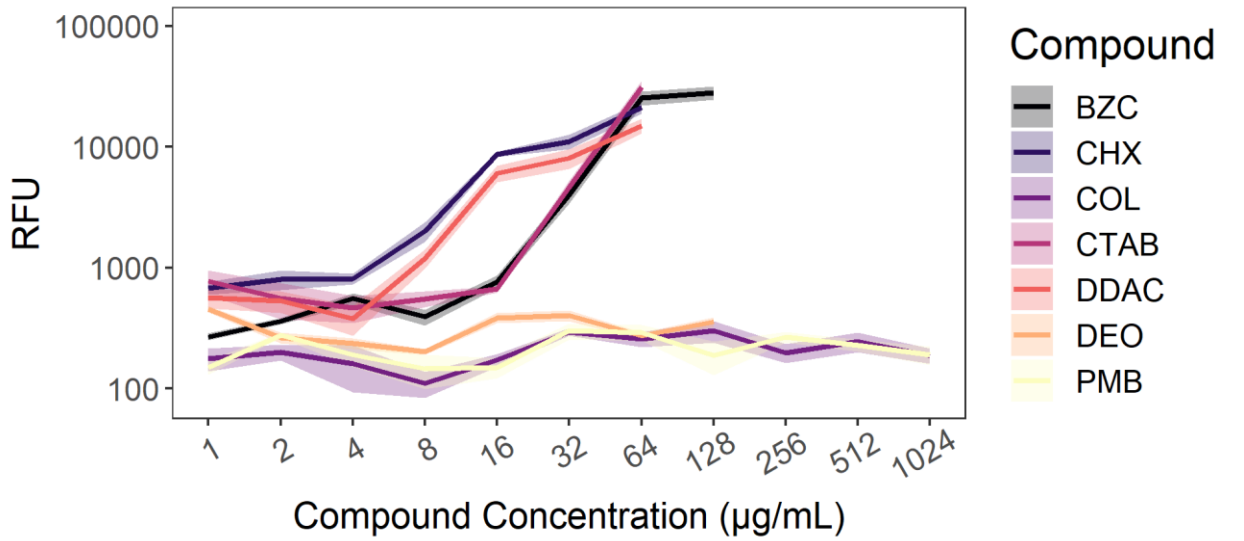

Figure A26. Outer membrane permeability is increased by exposure to membrane disruptors. Exponential phase K56-2 was incubated with NPN and a concentration gradient of the indicated compounds. BZC = benzethonium chloride; CHX = chlorhexidine; COL = colistin; CTAB = cetrimonium bromide; DDAC = dodecyl dimethylammonium bromide; DEO = sodium deoxycholate; PMB = polymyxin B. Raw fluorescence values were blank corrected. The shading represents means ± SD of three replicates.

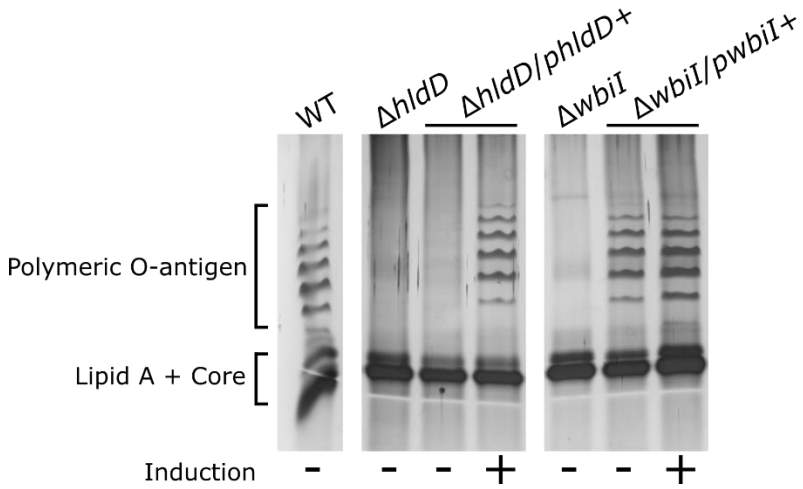

Figure A27 Effect of deletion and complementation of *hldD* and *wbiI* on O-antigen expression. Silver-stained SDS polyacrylamide gels of LPS extracts from mid-exponential phase deletion and complementation mutants grown for 4 hours with or without 0.05% rhamnose (0.002% for Δ*wbiI*/p*wbiI*).

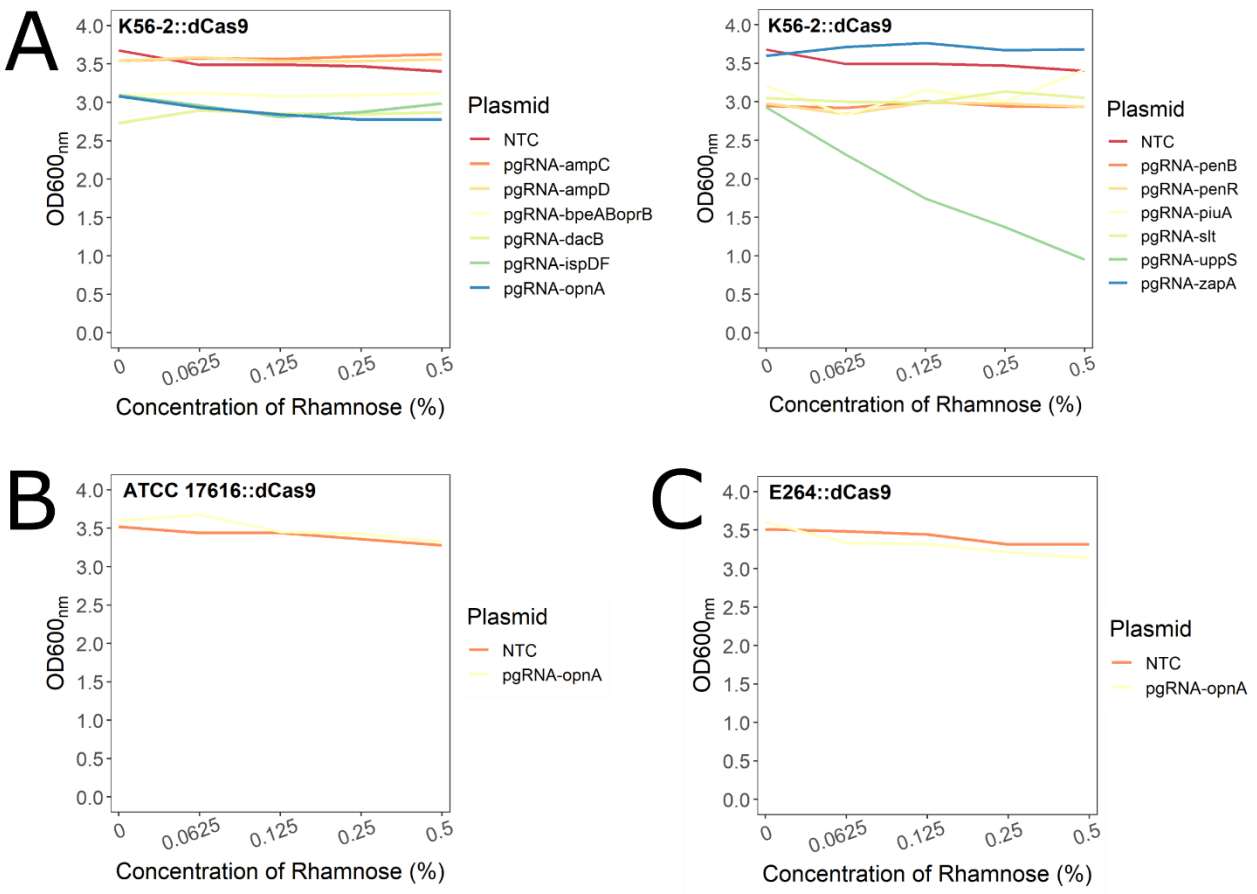

Figure A28. Rhamnose dose-responses of select CRISPRi mutants constructed in this study. Cultures were grown with the indicated concentrations of rhamnose in LB for 18 hours, the time at which the control strains reached the maximum OD_{600}, and then OD_{600} values were recorded Mutant backgrounds are A) *B. cenocepacia* K56-2::dCas9 (top two panels, separated to improve clarity) B) *B. multivorans* ATCC 17616::dCas9, and C) *B. thailandensis* E264::dCas9. Each gene was targeted with two sgRNA, and one representative is shown here. Values shown are averages of at least three biological replicates; SD values are omitted for clarity.

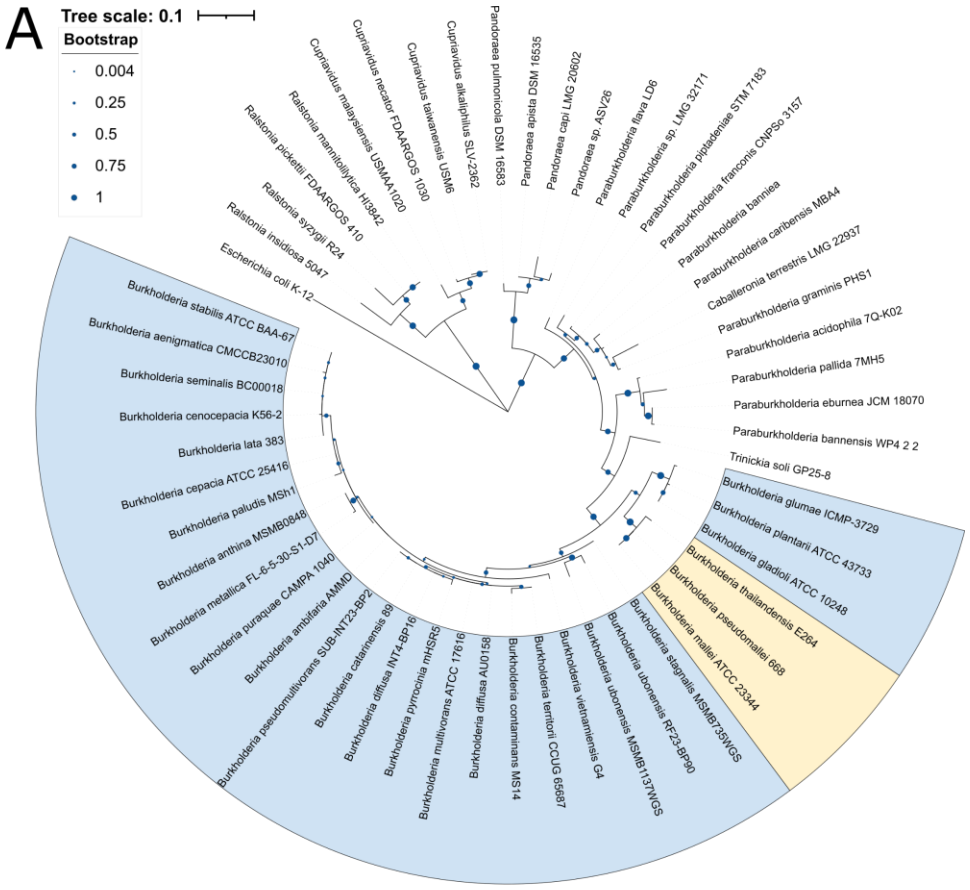

Figure A29. Susceptibility to novobiocin, and phylogenetic distribution of *opnA*, within Burkholderiaceae. A) The amino acid sequence of OpnA (K562_RS14130) was submitted to BLASTP with default settings against the Proteobacteria/Pseudomonadota. The hits from representative strains were aligned with default settings in Clustal W (Larkin et al. 2007). Bootstrapping was performed 500 times with MEGA11 (Tamura et al. 2021), and the values are shown on the branches with size-scaled circles (values scaled from 0-1). The tree was drawn with the Interactive Tree of Life (Letunic and Bork 2021) and rooted to *E. coli* K-12 OmpA. Species in the Bcc are shaded in light blue. Species in the *B. pseudomallei* complex are shaded in yellow. The branch length scale corresponds to the average substitutions per site. B) MIC of novobiocin against selected Gram-negative organisms and *Burkholderia* species. C) MICs of CAZ and RIF against K56-2::dCas9, ATCC 17616::dCas9, and E264::dCas9 harbouring plasmids expressing non-targeting sgRNA control (NTC) and targeting *opnA*. Values are medians of three biological replicates.

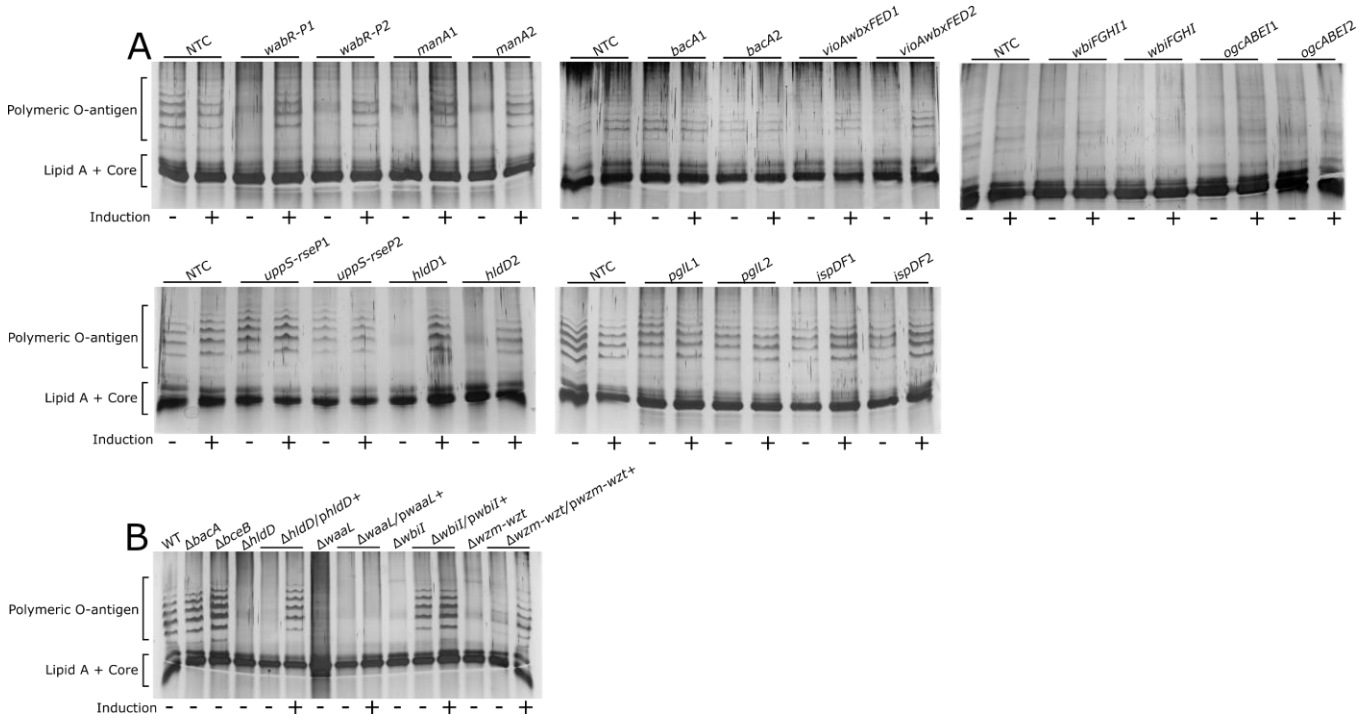

Figure A30. **Full SDS gels of LPS extracts of CRISPRi and unmarked deletion mutants.** Descriptions for sample preparation can be found in the caption of Figure A27.

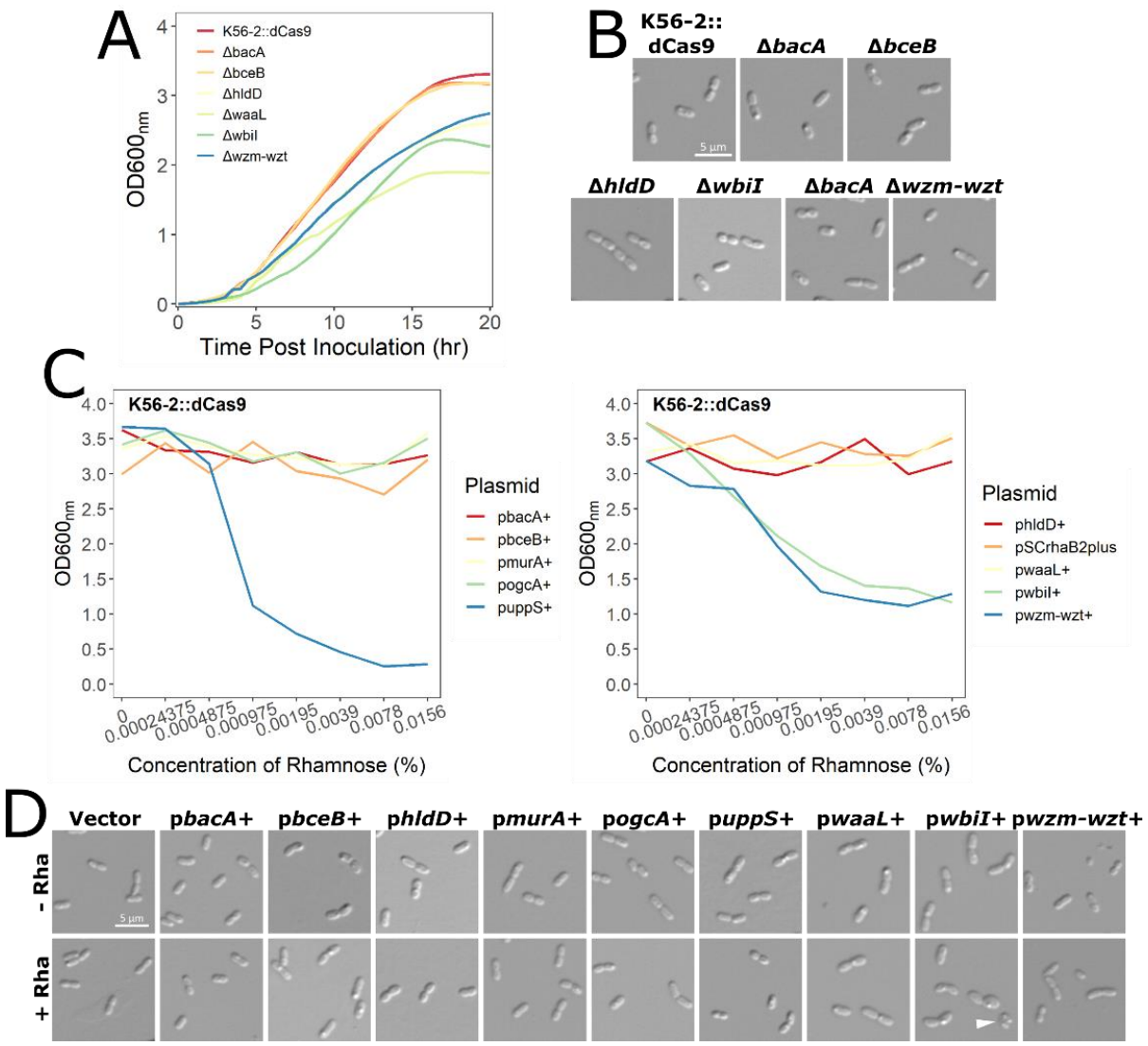

Figure A31. K56-2 is growth and morphology is robust to single genetic defects in UndP utilization pathways. A) Growth curves of the dCas9 background control and single deletion mutants. B) Mid exponential phase cells were immobilized on 1% agarose pads and imaged by DIC at 100x magnification. C) Cultures bearing overexpression plasmids were grown with the indicated concentrations of rhamnose for 18 hours, the time at which the control strains reached the maximum OD_{600}: Values shown are averages of three biological replicates. D) Unmarked deletion mutants in the K56-2::dCas9 background. D) K56-2::dCas9 bearing pSCrhaB2plus with indicated genes cloned under rhamnose-inducible control. The white arrowhead marks a lysing cell.

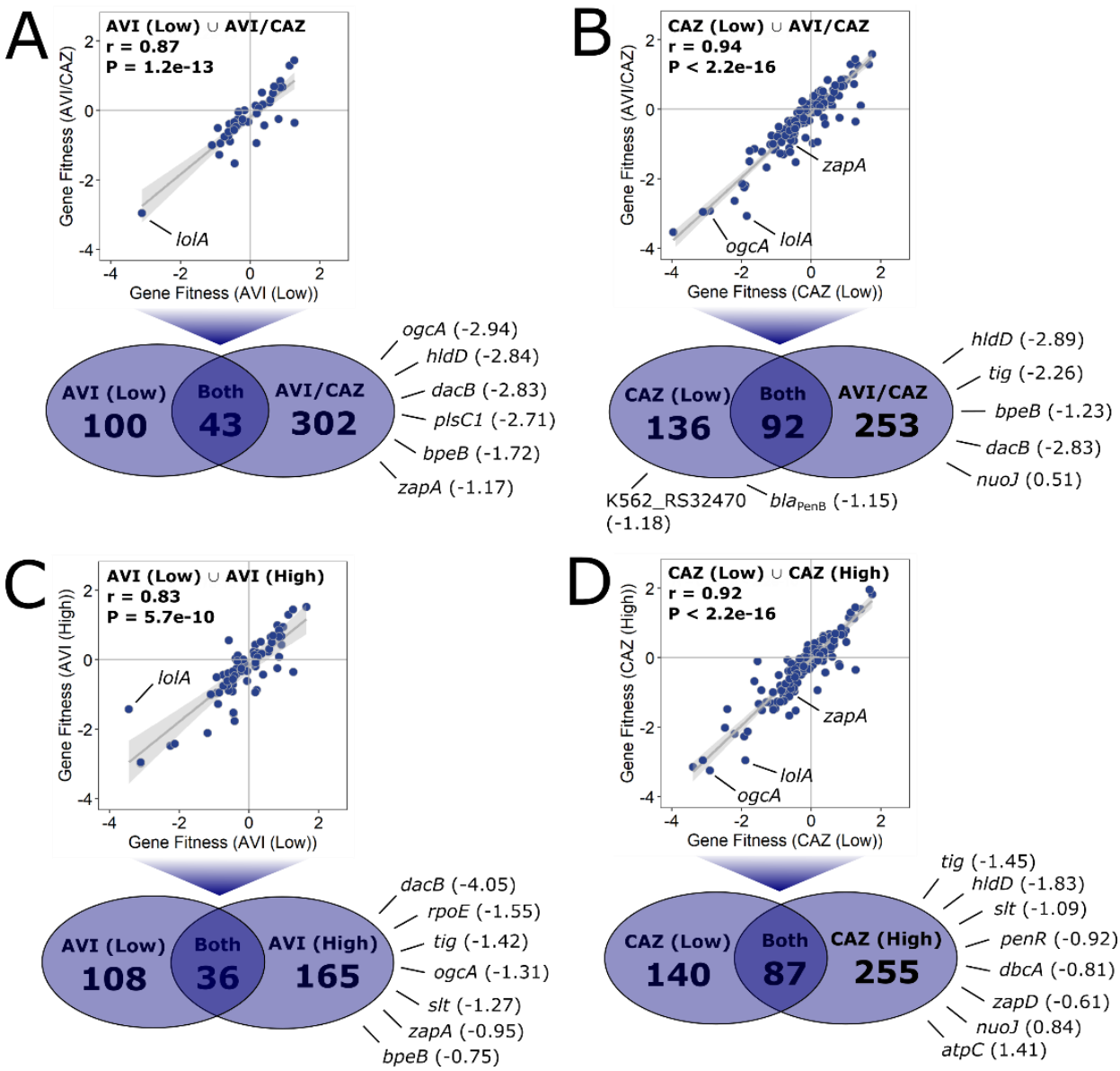

Figure A32. Concentration- and combination-dependent chemical-genetic interactions with AVI/CAZ. Comparison gene fitness scores between A) AVI/CAZ to AVI-L, B) AVI/CAZ to CAZ-L, C) AVI-H to AVI-L, and D) CAZ-H to CAZ-L. All genes with significantly different fitness scores greater than 0.5 or less than -0.5 relative to the DMSO control ($P < 0.05$) were used for comparison. For the genes that were common to both conditions, the scatter plots show a Pearson's correlation test (with 95% confidence interval in light grey) and associated r and P-values. Fitness scores next to genes are relative to the DMSO control.

CHAPTER 8: REFERENCES

Aaron, S.D., Ferris, W., Henry, D.A., Speert, D.P., and Macdonald, N.E. (2000). Multiple combination bactericidal antibiotic testing for patients with cystic fibrosis infected with *Burkholderia cepacia*. Am. J. Respir. Crit. Care Med. *161*, 1206–1212. https://doi.org/10.1164/ajrccm.161.4.9907147.

Abbott, F.K., Milne, K.E.N., Stead, D.A., and Gould, I.M. (2016). Combination antimicrobial susceptibility testing of *Burkholderia cepacia* complex: significance of species. Int J Antimicrob Agents *48*, 521–527. https://doi.org/10.1016/j.ijantimicag.2016.07.020.

Abboud, M.I., Damblon, C., Brem, J., Smargiasso, N., Mercuri, P., Gilbert, B., Rydzik, A.M., Claridge, T.D.W., Schofield, C.J., and Frère, J.-M. (2016). Interaction of avibactam with class B metallo-β-lactamases. Antimicrob Agents Chemother. *60*, 5655–5662. https://doi.org/10.1128/AAC.00897-16.

Abdulrahman, B.A., Khweek, A.A., Akhter, A., Caution, K., Kotrange, S., Abdelaziz, D.H., Newland, C., Rosales-Reyes, R., Kopp, B., McCoy, K., et al. (2011). Autophagy stimulation by rapamycin suppresses lung inflammation and infection by *Burkholderia cenocepacia* in a model of cystic fibrosis. Autophagy *7*, 1359–1370. https://doi.org/10.4161/auto.7.11.17660 [doi].

Abe, M., and Nakazawa, T. (1996). The *dsbB* gene product is required for protease production by *Burkholderia cepacia*. Infect Immun *64*, 4378–4380. https://doi.org/10.1128/iai.64.10.4378-4380.1996.

Abraham, E.P. (1979). A glimpse of the early history of the cephalosporins. Rev Infect Dis *1*, 99–105. https://doi.org/10.1093/clinids/1.1.99.

Abraham, E.P., and Chain, E. (1940). An enzyme from bacteria able to destroy penicillin. Nature *146*, 837–837. https://doi.org/10.1038/146837a0.

Acker, H.V., Sass, A., Bazzini, S., Roy, K.D., Udine, C., Messiaen, T., Riccardi, G., Boon, N., Nelis, H.J., Mahenthiralingam, E., et al. (2013). Biofilm-grown *Burkholderia cepacia* complex cells survive antibiotic treatment by avoiding production of reactive oxygen species. PloS One *8*, e58943. https://doi.org/10.1371/journal.pone.0058943; 10.1371/journal.pone.0058943.

Addinall, S.G., and Lutkenhaus, J. (1996). FtsA is localized to the septum in an FtsZ-dependent manner. J. Bacteriol. *178*, 7167–7172. https://doi.org/10.1128/jb.178.24.7167-7172.1996.

Agnoli, K., Schwager, S., Uehlinger, S., Vergunst, A., Viteri, D.F., Nguyen, D.T., Sokol, P.A., Carlier, A., and Eberl, L. (2012). Exposing the third chromosome of *Burkholderia cepacia* complex strains as a virulence plasmid. Mol Microbiol *83*, 362–378. https://doi.org/10.1111/j.1365-2958.2011.07937.x.

Ahn, Y., Kim, J.M., Kweon, O., Kim, S.-J., Jones, R.C., Woodling, K., Gamboa da Costa, G., LiPuma, J.J., Hussong, D., Marasa, B.S., et al. (2016). Intrinsic resistance of *Burkholderia cepacia* complex to benzalkonium chloride. MBio *7*. https://doi.org/10.1128/mBio.01716-16.

Akimov, Y., and Aittokallio, T. (2021). Re-defining synthetic lethality by phenotypic profiling for precision oncology. Cell Chem Biol. *28*, 246–256. https://doi.org/10.1016/j.chembiol.2021.01.026.

Alderwick, L.J., Radmacher, E., Seidel, M., Gande, R., Hitchen, P.G., Morris, H.R., Dell, A., Sahm, H., Eggeling, L., and Besra, G.S. (2005). Deletion of Cg-*emb* in *Corynebacterianeae* leads to a novel truncated cell wall arabinogalactan, whereas inactivation of Cg-*ubiA* results in an arabinan-deficient mutant with a cell wall galactan core. J Biol Chem *280*, 32362–32371. https://doi.org/10.1074/jbc.M506339200.

Alghamdi, W.A., Alsultan, A., Al-Shaer, M.H., An, G., Ahmed, S., Alkabab, Y., Banu, S., Barbakadze, K., Houpt, E., Kipiani, M., et al. (2019). Cycloserine population pharmacokinetics and pharmacodynamics in patients with tuberculosis. Antimicrob Agents Chemother https://doi.org/10.1128/AAC.00055-19.

Ambler, R.P. (1980). The structure of beta-lactamases. Philos Trans R Soc Lond B Biol Sci *289*, 321–331. https://doi.org/10.1098/rstb.1980.0049.

Anglada-Girotto, M., Handschin, G., Ortmayr, K., Campos, A.I., Gillet, L., Manfredi, P., Mulholland, C.V., Berney, M., Jenal, U., Picotti, P., et al. (2022). Combining CRISPRi and metabolomics for functional annotation of compound libraries. Nat Chem Biol *18*, 482–491. https://doi.org/10.1038/s41589-022-00970-3.

Ashburner, M., Ball, C.A., Blake, J.A., Botstein, D., Butler, H., Cherry, J.M., Davis, A.P., Dolinski, K., Dwight, S.S., Eppig, J.T., et al. (2000). Gene Ontology: tool for the unification of biology. Nat Genet *25*, 25–29. https://doi.org/10.1038/75556.

Asli, A., Brouillette, E., Krause, K.M., Nichols, W.W., and Malouin, F. (2016). Distinctive binding of avibactam to penicillin-binding proteins of Gram-negative and Gram-positive bacteria. Antimicrob Agents Chemother. *60*, 752–756. https://doi.org/10.1128/AAC.02102-15.

Aubert, D.F., Hamad, M.A., and Valvano, M.A. (2014). A markerless deletion method for genetic manipulation of *Burkholderia cenocepacia* and other multidrug-resistant gram-negative bacteria. Methods Mol Biol *1197*, 311–327. https://doi.org/10.1007/978-1-4939-1261-2_18.

Baba, T., Ara, T., Hasegawa, M., Takai, Y., Okumura, Y., Baba, M., Datsenko, K.A., Tomita, M., Wanner, B.L., and Mori, H. (2006). Construction of *Escherichia coli* K-12 in-frame, single-gene knockout mutants: the Keio collection. Mol Syst Biol *2*, 2006.0008. https://doi.org/10.1038/msb4100050.

Babakhani, S., and Oloomi, M. (2018). Transposons: the agents of antibiotic resistance in bacteria. Journal of Basic Microbiology *58*, 905–917. https://doi.org/10.1002/jobm.201800204.

Bach, E., Passaglia, L.M.P., Jiao, J., and Gross, H. (2022a). *Burkholderia* in the genomic era: from taxonomy to the discovery of new antimicrobial secondary metabolites. Crit Rev Microbiol *48*, 121–160. https://doi.org/10.1080/1040841X.2021.1946009.

Bach, E., Sant'Anna, F.H., Seger, G.D. dos S., and Passaglia, L.M.P. (2022b). Pangenome inventory of *Burkholderia sensu lato, Burkholderia sensu stricto*, and the *Burkholderia cepacia* complex reveals the uniqueness of *Burkholderia catarinensis*. Genomics *114*, 398–408. https://doi.org/10.1016/j.ygeno.2021.11.011.

Backman, T.W.H., Cao, Y., and Girke, T. (2011). ChemMine tools: an online service for analyzing and clustering small molecules. Nucleic Acid Res *39*, W486–W491. https://doi.org/10.1093/nar/gkr320.

Bailey, J., Gallagher, L., Barker, W.T., Hubble, V.B., Gasper, J., Melander, C., and Manoil, C. (2022). Genetic dissection of antibiotic adjuvant activity. MBio e0308421. https://doi.org/10.1128/mbio.03084-21.

Balcewich, M.D., Reeve, T.M., Orlikow, E.A., Donald, L.J., Vocadlo, D.J., and Mark, B.L. (2010). Crystal structure of the AmpR effector binding domain provides insight into the molecular regulation of inducible Ampc beta-lactamase. J Mol Biol *400*, 998–1010. https://doi.org/10.1016/j.jmb.2010.05.040.

Baldwin, A., Sokol, P.A., Parkhill, J., and Mahenthiralingam, E. (2004). The *Burkholderia cepacia* epidemic strain marker is part of a novel genomic island encoding both virulence and metabolism-associated genes in *Burkholderia cenocepacia*. Infect.Immun. *72*, 1537–1547. .

Baquero, F., and Levin, B.R. (2021). Proximate and ultimate causes of the bactericidal action of antibiotics. Nat Rev Microbiol *19*, 123–132. https://doi.org/10.1038/s41579-020-00443-1.

Barb, A.W., McClerren, A.L., Snehelatha, K., Reynolds, C.M., Zhou, P., and Raetz, C.R.H. (2007). Inhibition of lipid A biosynthesis as the primary mechanism of CHIR-090 antibiotic activity in *Escherichia coli*. Biochemistry *46*, 3793–3802. https://doi.org/10.1021/bi6025165.

Barquist, L., Boinett, C.J., and Cain, A.K. (2013). Approaches to querying bacterial genomes with transposon-insertion sequencing. RNA Biol *10*, 1161–1169. https://doi.org/10.4161/rna.24765.

Barreteau, H., Kovač, A., Boniface, A., Sova, M., Gobec, S., and Blanot, D. (2008). Cytoplasmic steps of peptidoglycan biosynthesis. FEMS Microbiol Rev *32*, 168–207. https://doi.org/10.1111/j.1574-6976.2008.00104.x.

Barreteau, H., Magnet, S., El Ghachi, M., Touzé, T., Arthur, M., Mengin-Lecreulx, D., and Blanot, D. (2009). Quantitative high-performance liquid chromatography analysis of the pool levels of undecaprenyl phosphate and its derivatives in bacterial membranes. J Chromatogr B Analyt Technol Biomed Life Sci *877*, 213–220. https://doi.org/10.1016/j.jchromb.2008.12.010.

Barrett-Bee, K., Newboult, L., and Edwards, S. (1994). The membrane destabilising action of the antibacterial agent chlorhexidine. FEMS Microbiol Lett *119*, 249–253. https://doi.org/10.1111/j.1574-6968.1994.tb06896.x.

Bartowsky, E., and Normark, S. (1991). Purification and mutant analysis of *Citrobacter freundii* AmpR, the regulator for chromosomal AmpC beta-lactamase. Mol Microbiol *5*, 1715–1725. https://doi.org/10.1111/j.1365-2958.1991.tb01920.x.

Baym, M., Shaket, L., Anzai, I.A., Adesina, O., and Barstow, B. (2016). Rapid construction of a whole-genome transposon insertion collection for *Shewanella oneidensis* by Knockout Sudoku. Nat Commun *7*, 1–13. https://doi.org/10.1038/ncomms13270.

Bazzini, S., Udine, C., Sass, A., Pasca, M.R., Longo, F., Emiliani, G., Fondi, M., Perrin, E., Decorosi, F., Viti, C., et al. (2011). Deciphering the role of RND efflux transporters in *Burkholderia cenocepacia*. PLoS ONE *6*, e18902. https://doi.org/10.1371/journal.pone.0018902.

Becka, S.A., Zeiser, E.T., Barnes, M.D., Taracila, M.A., Nguyen, K., Singh, I., Sutton, G.G., LiPuma, J.J., Fouts, D.E., and Papp-Wallace, K.M. (2018). Characterization of the AmpC β-Lactamase from *Burkholderia multivorans*. Antimicrob Agents Chemother *62*, e01140-18. https://doi.org/10.1128/AAC.01140-18.

Becka, S.A., Zeiser, E.T., LiPuma, J.J., and Papp-Wallace, K.M. (2021). Activity of imipenem-relebactam against multidrug- and extensively drug-resistant *Burkholderia cepacia* complex and *Burkholderia gladioli*. Antimicrob Agents Chemother *65*, e01332-21. https://doi.org/10.1128/AAC.01332-21.

Becka, S.A., Zeiser, E.T., LiPuma, J.J., and Papp-Wallace, K.M. (2022). The class A β-lactamase produced by *Burkholderia* species compromises the potency of tebipenem against a panel of isolates from the United States. Antibiotics (Basel) *11*, 674. https://doi.org/10.3390/antibiotics11050674.

Belenky, P., Ye, J.D., Porter, C.B.M., Cohen, N.R., Lobritz, M.A., Ferrante, T., Jain, S., Korry, B.J., Schwarz, E.G., Walker, G.C., et al. (2015). Bactericidal antibiotics induce toxic metabolic perturbations that lead to cellular damage. Cell Rep *13*, 968–980. https://doi.org/10.1016/j.celrep.2015.09.059.

Berardinis, V. de, Vallenet, D., Castelli, V., Besnard, M., Pinet, A., Cruaud, C., Samair, S., Lechaplais, C., Gyapay, G., Richez, C., et al. (2008). A complete collection of single-gene deletion mutants of *Acinetobacter baylyi* ADP1. Mol Syst Biol *4*, 174–189. https://doi.org/10.1038/msb.2008.10.

Bernier, S.P., Son, S., and Surette, M.G. (2018). The Mla pathway plays an essential role in the intrinsic resistance of *Burkholderia cepacia* complex species to antimicrobials and host innate components. J Bacteriol *200*, e00156-18, /jb/200/18/e00156-18.atom. https://doi.org/10.1128/JB.00156-18.

Biedenbach, D.J., Kazmierczak, K., Bouchillon, S.K., Sahm, D.F., and Bradford, P.A. (2015). *In vitro* activity of aztreonam-avibactam against a global collection of gram-negative pathogens from 2012 and 2013. Antimicrob Agents Chemother *59*, 4239–4248. https://doi.org/10.1128/AAC.00206-15.

Bikard, D., Jiang, W., Samai, P., Hochschild, A., Zhang, F., and Marraffini, L.A. (2013). Programmable repression and activation of bacterial gene expression using an engineered CRISPR-Cas system. Nucleic Acids Res. *41*, 7429–7437. https://doi.org/10.1093/nar/gkt520.

Bjarnsholt, T., Whiteley, M., Rumbaugh, K.P., Stewart, P.S., Jensen, P.Ø., and Frimodt-Møller, N. (2021). The importance of understanding the infectious microenvironment. Lancet Infect Dis S1473-3099(21)00122-5. https://doi.org/10.1016/S1473-3099(21)00122-5.

Blanchard, A.C., and Waters, V.J. (2019). Microbiology of cystic fibrosis airway disease. Semin Respir Crit Care Med *40*, 727–736. https://doi.org/10.1055/s-0039-1698464.

Blanchard, A.C., Tang, L., Tadros, M., Muller, M., Spilker, T., Waters, V.J., LiPuma, J.J., and Tullis, E. (2020). *Burkholderia cenocepacia* ET12 transmission in adults with cystic fibrosis. Thorax *75*, 88–90. https://doi.org/10.1136/thoraxjnl-2019-214098.

Blanco, P., Sanz-García, F., Hernando-Amado, S., Martínez, J.L., and Alcalde-Rico, M. (2018). The development of efflux pump inhibitors to treat Gram-negative infections. Expert Opin Drug Disc *13*, 919–931. https://doi.org/10.1080/17460441.2018.1514386.

Blattner, F.R., Plunkett, G., Bloch, C.A., Perna, N.T., Burland, V., Riley, M., Collado-Vides, J., Glasner, J.D., Rode, C.K., Mayhew, G.F., et al. (1997). The complete genome sequence of *Escherichia coli* K-12. Science *277*, 1453–1462. .

Bloodworth, R.A., Gislason, A.S., and Cardona, S.T. (2013). *Burkholderia cenocepacia* conditional growth mutant library created by random promoter replacement of essential genes. MicrobiologyOpen *2*, 243–258. https://doi.org/10.1002/mbo3.71.

Bloodworth, R.A., Selin, C., Volder, M.A.L.D., Drevinek, P., Galanternik, L., Degrossi, J., and Cardona, S.T. (2015). Draft genome sequences of *Burkholderia contaminans*, a *Burkholderia cepacia* complex species that is increasingly recovered from cystic fibrosis patients. Genome Announ *3*, 10.1128/genomeA.00766-15. https://doi.org/10.1128/genomeA.00766-15 [doi].

Bosch, B., DeJesus, M.A., Poulton, N.C., Zhang, W., Engelhart, C.A., Zaveri, A., Lavalette, S., Ruecker, N., Trujillo, C., Wallach, J.B., et al. (2021). Genome-wide gene expression tuning reveals diverse vulnerabilities of *M. tuberculosis*. Cell *184*, 4579-4592.e24. https://doi.org/10.1016/j.cell.2021.06.033.

Bossche, S., Broe, E., Coenye, T., Braeckel, E., Crabbé, A. (2021). The cystic fibrosis lung microenvironment alters antibiotic activity: causes and effects. Eur Resp Rev *30*, 210055

Bouz, G., and Zitko, J. (2021). Inhibitors of aminoacyl-tRNA synthetases as antimycobacterial compounds: An up-to-date review. Bioorg Chemi *110*, 104806. https://doi.org/10.1016/j.bioorg.2021.104806.

Brauner, A., Fridman, O., Gefen, O., and Balaban, N.Q. (2016). Distinguishing between resistance, tolerance and persistence to antibiotic treatment. Nat Rev Microbiol *14*, 320–330. https://doi.org/10.1038/nrmicro.2016.34.

Brito, P.H., Chevreux, B., Serra, C.R., Schyns, G., Henriques, A.O., and Pereira-Leal, J.B. (2017). Genetic competence drives genome diversity in *Bacillus subtilis*. Genome Biol Evol *10*, 108–124. https://doi.org/10.1093/gbe/evx270.

Brochado, A.R., Telzerow, A., Bobonis, J., Banzhaf, M., Mateus, A., Selkrig, J., Huth, E., Bassler, S., Beas, J.Z., Zietek, M., et al. (2018). Species-specific activity of antibacterial drug combinations. Nature *559*, 259–263. https://doi.org/10.1038/s41586-018-0278-9.

Buckley, P., Rivers, B., Katoski, S., Kim, M.H., Kragl, F.J., Broomall, S., Krepps, M., Skowronski, E.W., Rosenzweig, C.N., Paikoff, S., et al. (2012). Genetic barcodes for improved environmental tracking of an anthrax simulant. Appl Environ Microbiol *78*, 8272–8280. https://doi.org/10.1128/AEM.01827-12; 10.1128/AEM.01827-12.

Buroni, S., Pasca, M.R., Flannagan, R.S., Bazzini, S., Milano, A., Bertani, I., Venturi, V., Valvano, M.A., and Riccardi, G. (2009). Assessment of three Resistance-Nodulation-Cell Division drug efflux transporters of *Burkholderia cenocepacia* in intrinsic antibiotic resistance. BMC Microbiol. *9*, 200. https://doi.org/10.1186/1471-2180-9-200.

Burrows, L.L., and Lam, J.S. (1999). Effect of *wzx (rfbX)* mutations on A-band and B-band lipopolysaccharide biosynthesis in *Pseudomonas aeruginosa* O5. J Bacteriol *181*, 973–980. .

Bush, K. (2010). Bench-to-bedside review: The role of β-lactamases in antibiotic-resistant Gram-negative infections. Crit Care *14*, 224. https://doi.org/10.1186/cc8892.

Butt, A.T., and Thomas, M.S. (2017). Iron acquisition mechanisms and their role in the virulence of *Burkholderia* Species. Front Cell Infect Microbiol *7*, 460. https://doi.org/10.3389/fcimb.2017.00460.

Butzin, N.C., and Mather, W.H. (2018). Crosstalk between diverse synthetic protein degradation tags in *Escherichia coli*. ACS Synth. Biol. *7*, 54–62. https://doi.org/10.1021/acssynbio.7b00122.

Cacace, E., Kritikos, G., Typas, A. (2017). Chemical genetics in drug discovery. Curr Op Syst Biol *4*, 35

Caccamo, P.D., and Brun, Y.V. (2018). The molecular basis of noncanonical bacterial morphology. Trends Microbiol *26*, 191–208. https://doi.org/10.1016/j.tim.2017.09.012.

Calloni, G., Chen, T., Schermann, S.M., Chang, H., Genevaux, P., Agostini, F., Tartaglia, G.G., Hayer-Hartl, M., and Hartl, F.U. (2012). DnaK functions as a central hub in the *E. coli* chaperone network. Cell Rep *1*, 251–264. https://doi.org/10.1016/j.celrep.2011.12.007.

Calvo-Villamañán, A., Ng, J.W., Planel, R., Ménager, H., Chen, A., Cui, L., and Bikard, D. (2020). On-target activity predictions enable improved CRISPR–dCas9 screens in bacteria. Nucleic Acids Res *48*, e64–e64. https://doi.org/10.1093/nar/gkaa294.

Cameron, D.E., and Collins, J.J. (2014). Tunable protein degradation in bacteria. Nat Biotechnol *32*, 1276–1281. https://doi.org/10.1038/nbt.3053 [doi].

Cameron, D.E., Urbach, J.M., and Mekalanos, J.J. (2008). A defined transposon mutant library and its use in identifying motility genes in *Vibrio cholerae*. Proc Natl Acad Sci *105*, 8736–8741. https://doi.org/10.1073/pnas.0803281105.

Cantalapiedra, C.P., Hernández-Plaza, A., Letunic, I., Bork, P., and Huerta-Cepas, J. (2021). eggNOG-mapper v2: Functional annotation, orthology assignments, and domain prediction at the metagenomic scale. BioRxiv 2021.06.03.446934. https://doi.org/10.1101/2021.06.03.446934.

Caraher, E., Reynolds, G., Murphy, P., McClean, S., and Callaghan, M. (2007). Comparison of antibiotic susceptibility of *Burkholderia cepacia* complex organisms when grown planktonically or as biofilm in vitro. Euro J Clin Microbiol Infect Dis *26*, 213–216. https://doi.org/10.1007/s10096-007-0256-x.

Cardona, S.T., and Valvano, M.A. (2005). An expression vector containing a rhamnose-inducible promoter provides tightly regulated gene expression in *Burkholderia cenocepacia*. Plasmid *54*, 219–228. https://doi.org/10.1016/j.plasmid.2005.03.004.

Cardona, S.T., Mueller, C., and Valvano, M.A. (2006). Identification of essential operons in *Burkholderia cenocepacia* with a rhamnose inducible promoter. Appl Environ Microbiol. *72*, 2547–2555. .

Cardona, S.T., Selin, C., and Gislason, A.S. (2015). Genomic tools to profile antibiotic mode of action. Crit Rev Microbiol *4*, 465–472. https://doi.org/10.3109/1040841X.2013.866073.

Carfrae, L.A., MacNair, C.R., Brown, C.M., Tsai, C.N., Weber, B.S., Zlitni, S., Rao, V.N., Chun, J., Junop, M.S., Coombes, B.K., et al. (2019). Mimicking the human environment in mice reveals that inhibiting biotin biosynthesis is effective against antibiotic-resistant pathogens. Nat Microbiol 1–9. https://doi.org/10.1038/s41564-019-0595-2.

Carmel-Harel, O., and Storz, G. (2000). Roles of the glutathione- and thioredoxin-dependent reduction systems in the Escherichia coli and saccharomyces cerevisiae responses to oxidative stress. Annu. Rev. Microbiol. *54*, 439–461. https://doi.org/10.1146/annurev.micro.54.1.439.

Caron, P.R., Mullican M.D., Mashal R.D., Wilson K.P., Su, M. S., Murcko, M.A. (2001). Chemogenomic approaches to drug discovery. Curr. Opin. Chem. Biol *5*, 464-470.

Casanova-Hampton, K., Carey, A., Kassam, S., Garner, A., Donati, G.L., Thangamani, S., and Subashchandrabose, S. (2021). A genome-wide screen reveals the involvement of enterobactin-mediated iron acquisition in *Escherichia coli* survival during copper stress. Metallomics *13*, mfab052. https://doi.org/10.1093/mtomcs/mfab052.

Castillo-Davis, C.I., and Hartl, D.L. (2003). GeneMerge--post-genomic analysis, data mining, and hypothesis testing. Bioinformatics *19*, 891–892. https://doi.org/10.1093/bioinformatics/btg114.

Caverly, L.J., Spilker, T., Kalikin, L.M., Stillwell, T., Young, C., Huang, D.B., and LiPuma, J.J. (2019). In vitro activities of β-lactam–β-lactamase inhibitor antimicrobial agents against cystic

fibrosis respiratory pathogens. Antimicrob Agents Chemother *64*, e01595-19. https://doi.org/10.1128/AAC.01595-19.

CDC (2019). Antibiotic resistance threats in the United States.

Centers for Disease Control and Prevention (2012). Possession, use, and transfer of select agents and toxins; biennial review. Final rule. Fed Regist *77*, 61083–61115. .

Centers for Disease Control and Prevention (CDC) (2021). Outpatient Antibiotic Prescriptions — United States, 2020 | Antibiotic Use | CDC.

Chan, E.L., Harris, R.C., and Dalton, H.P. (1987). The effect of antibiotics on the cell morphology of *Legionella pneumophila*. J Med Microbiol *23*, 149–154. https://doi.org/10.1099/00222615-23-2-149.

Chan, F.-Y., Sun, N., Neves, M.A.C., Lam, P.C.-H., Chung, W.-H., Wong, L.-K., Chow, H.-Y., Ma, D.-L., Chan, P.-H., Leung, Y.-C., et al. (2013). Identification of a new class of FtsZ inhibitors by structure-based design and *in vitro* screening. J Chem Inf Model *53*, 2131–2140. https://doi.org/10.1021/ci400203f.

Chan, Y.Y., Tan, T.M.C., Ong, Y.M., and Chua, K.L. (2004). BpeAB-OprB, a multidrug efflux ump in *Burkholderia pseudomallei*. Antimicrob Agents Chemother *48*, 1128–1135. https://doi.org/10.1128/AAC.48.4.1128-1135.2004.

Chapalain, A., Groleau, M.-C., Le Guillouzer, S., Miomandre, A., Vial, L., Milot, S., and Déziel, E. (2017). Interplay between 4-hydroxy-3-methyl-2-alkylquinoline and N-acyl-homoserine lactone signaling in a *Burkholderia cepacia* complex clinical strain. Front Microbiol *8*, 1021. https://doi.org/10.3389/fmicb.2017.01021.

Chen, J.C., and Beckwith, J. (2001). FtsQ, FtsL and FtsI require FtsK, but not FtsN, for co-localization with FtsZ during *Escherichia coli* cell division. Mol Microbiol *42*, 395–413. https://doi.org/10.1046/j.1365-2958.2001.02640.x.

Chmiel, J.F., Aksamit, T.R., Chotirmall, S.H., Dasenbrook, E.C., Elborn, J.S., LiPuma, J.J., Ranganathan, S.C., Water, V.J., Ratjen, F.A. (2014). Antibiotic management of lung infections in cystic fibrosis. I. The microbiome, methicillin-resistant *Staphylococcus aureus*, Gram-negative bacteria, and multiple infections. Annal Am Thor Soc *11*, 1120

Cho, H., Uehara, T., and Bernhardt, T.G. (2014). Beta-lactam antibiotics induce a lethal malfunctioning of the bacterial cell wall synthesis machinery. Cell *159*, 1300–1311. https://doi.org/10.1016/j.cell.2014.11.017.

Cho, S., Choe, D., Lee, E., Kim, S.C., Palsson, B., and Cho, B.-K. (2018). High-level dCas9 expression induces abnormal cell morphology in *Escherichia coli*. ACS Synth Biol https://doi.org/10.1021/acssynbio.7b00462.

Cho, S.W., Kim, S., Kim, J.M., and Kim, J.-S. (2013). Targeted genome engineering in human cells with the Cas9 RNA-guided endonuclease. Nat. Biotechnol. *31*, 230–232. https://doi.org/10.1038/nbt.2507.

Choi, K.-H., and Schweizer, H.P. (2006). mini-Tn7 insertion in bacteria with single attTn7 sites: example *Pseudomonas aeruginosa*. Nat Protoc *1*, 153–161. https://doi.org/10.1038/nprot.2006.24.

Choi, U., and Lee, C.-R. (2019). Distinct roles of outer membrane porins in antibiotic resistance and membrane integrity in *Escherichia coli*. Front Microbiol *10*.

Choi, K.H., Gaynor, J.B., White, K.G., Lopez, C., Bosio, C.M., Karkhoff-Schweizer, R.R., and Schweizer, H.P. (2005). A Tn7-based broad-range bacterial cloning and expression system. Nat.Methods *2*, 443–448. .

Choi, K.-H., Kumar, A., and Schweizer, H.P. (2006a). A 10-min method for preparation of highly electrocompetent *Pseudomonas aeruginosa* cells: application for DNA fragment transfer between chromosomes and plasmid transformation. J. Microbiol. Methods *64*, 391–397. https://doi.org/10.1016/j.mimet.2005.06.001.

Choi, K.H., DeShazer, D., and Schweizer, H.P. (2006b). mini-Tn7 insertion in bacteria with multiple glmS-linked attTn7 sites: example *Burkholderia mallei* ATCC 23344. Nat Prot *1*, 162–169. https://doi.org/10.1038/nprot.2006.25.

Choi, K.H., Mima, T., Casart, Y., Rholl, D., Kumar, A., Beacham, I.R., and Schweizer, H.P. (2008). Genetic tools for select-agent-compliant manipulation of *Burkholderia pseudomallei*. Appl Environ Microbiol *74*, 1064–1075. https://doi.org/10.1128/AEM.02430-07.

Choudhary, E., Thakur, P., Pareek, M., and Agarwal, N. (2015). Gene silencing by CRISPR interference in mycobacteria. Nat Commun *6*, ncomms7267. https://doi.org/10.1038/ncomms7267.

Chow, W.Y., and Berg, D.E. (1988). Tn*5*tac1, a derivative of transposon Tn*5* that generates conditional mutations. Proc Natl Acad Sci U S A *85*, 6468–6472. .

Clinical and Laboratory Standards Institute CLSI (2003). Susceptibility testing of mycobacteria, nocardiae, and other aerobic actinomycetes; approved standard (Pennsylvania, USA: CLSI).

Clinical and Laboratory Standards Institute CLSI (2012). Methods for dilution antimicrobial susceptibility tests for bacteria that grow aerobically; approved standard—ninth edition (Pennsylvania, USA: CLSI).

Clinical and Laboratory Standards Institute CLSI (2014). Performance standards for antimicrobial disk susceptibility testing; twenty-fourth informational supplement M100-S24 (Wayne, PA: Clinical and Laboratory Standards Institute).

Coe, K.A., Lee, W., Stone, M.C., Komazin-Meredith, G., Meredith, T.C., Grad, Y.H., and Walker, S. (2019). Multi-strain Tn-Seq reveals common daptomycin resistance determinants in *Staphylococcus aureus*. PLOS Path *15*, e1007862. https://doi.org/10.1371/journal.ppat.1007862.

Coenye, T., Van Acker, H., Peeters, E., Sass, A., Buroni, S., Riccardi, G., and Mahenthiralingam, E. (2011). Molecular mechanisms of chlorhexidine tolerance in *Burkholderia cenocepacia* biofilms. Antimicrob Agents Chemother *55*, 1912–1919. https://doi.org/10.1128/AAC.01571-10.

Cohen, T.S., and Prince, A. (2012). Cystic fibrosis: a mucosal immunodeficiency syndrome. Nat Med *18*, 509–519. https://doi.org/10.1038/nm.2715; 10.1038/nm.2715.

Cole, J.N., and Nizet, V. (2016). Bacterial evasion of host antimicrobial peptide defenses. Microbiol Spectr *4*, 10.1128/microbiolspec.VMBF-0006–2015. https://doi.org/10.1128/microbiolspec.VMBF-0006-2015.

Collymore, C., Giuliano, F., and Banks, E.K. (2019). Head tilt in immunodeficient mice due to contamination of drinking water by *Burkholderia gladioli*. J Am Assoc Lab Anim Sci *58*, 246–250. https://doi.org/10.30802/AALAS-JAALAS-18-000106.

Commichau, F.M., Pietack, N., and Stulke, J. (2013). Essential genes in *Bacillus subtilis*: a re-evaluation after ten years. Mol BioSyst *9*, 1068–1075. https://doi.org/10.1039/c3mb25595f; 10.1039/c3mb25595f.

Costabile, G., Provenzano, R., Azzalin, A., Scoffone, V.C., Chiarelli, L.R., Rondelli, V., Grillo, I., Zinn, T., Lepioshkin, A., Savina, S., Miro, A., Quaglia, F., Makarov, V., Coenye, T., Brocca, P., Riccardi, G., Buroni, S., Ungaro, F. (2020). PEGylated mucus-penetrating nanocrystals for lung delivery of a new FtsZ inhibitor against *Burkholderia cenocepacia* infection. Nanomed: Nanotech, Biol, Med *23*, 102113.

Côté, J.-P., French, S., Gehrke, S.S., MacNair, C.R., Mangat, C.S., Bharat, A., and Brown, E.D. (2016). The genome-wide interaction network of nutrient stress genes in *Escherichia coli*. MBio *7*. https://doi.org/10.1128/mBio.01714-16.

Cotsonas King, A., and Wu, L. (2009). Macromolecular synthesis and membrane perturbation assays for mechanisms of action studies of antimicrobial agents. Curr Protoc Pharmacol *Chapter 13*, Unit 13A.7. https://doi.org/10.1002/0471141755.ph13a07s47.

Croteau, F.R., Rousseau, G.M., and Moineau, S. (2018). [The CRISPR-Cas system: beyond genome editing]. Med Sci (Paris) *34*, 813–819. https://doi.org/10.1051/medsci/2018215.

Cuellar, J., Åstrand, M., Elovaara, H., Pietikäinen, A., Sirén, S., Liljeblad, A., Guédez, G., Salminen, T.A., and Hytönen, J. (2020). Structural and biomolecular analyses of *Borrelia burgdorferi* BmpD reveal a substrate-binding protein of an ABC-type nucleoside transporter family. Infection and Immunity *88*, e00962-19. https://doi.org/10.1128/IAI.00962-19.

Cui, L., Vigouroux, A., Rousset, F., Varet, H., Khanna, V., and Bikard, D. (2018). A CRISPRi screen in *E. coli* reveals sequence-specific toxicity of dCas9. Nat Commun *9*, 1912. https://doi.org/10.1038/s41467-018-04209-5.

Culp, E.J., Waglechner, N., Wang, W., Fiebig-Comyn, A.A., Hsu, Y.-P., Koteva, K., Sychantha, D., Coombes, B.K., Van Nieuwenhze, M.S., Brun, Y.V., et al. (2020). Evolution-guided discovery of antibiotics that inhibit peptidoglycan remodelling. Nature 1–6. https://doi.org/10.1038/s41586-020-1990-9.

Cystic Fibrosis Canada (2020). The Canadian cystic fibrosis registry (Cystic Fibrosis Canada).

Dalhoff, A. (2014). Pharmacokinetics and pharmacodynamics of aerosolized antibacterial agents in chronically infected cystic fibrosis patients. Clin. Microbiol. Rev. *27*, 753–782. https://doi.org/10.1128/CMR.00022-14.

Darling, P., Chan, M., Cox, A.D., and Sokol, P.A. (1998). Siderophore production by cystic fibrosis isolates of *Burkholderia cepacia*. Infect Immun *66*, 874–877. .

Dartigalongue, C., Missiakas, D., and Raina, S. (2001). Characterization of the *Escherichia coli* sigma E regulon. J Biol Chem *276*, 20866–20875. https://doi.org/10.1074/jbc.M100464200.

Datsenko, K.A., and Wanner, B.L. (2000). One-step inactivation of chromosomal genes in *Escherichia coli* K-12 using PCR products. Proc. Natl. Acad. Sci. U S A *97*, 6640–6645. .

Davies, T.A., Shang, W., Bush, K., and Flamm, R.K. (2008). Affinity of doripenem and comparators to penicillin-binding proteins in *Escherichia coli* and *Pseudomonas aeruginosa*. Antimicrob Agents Chemother *52*, 1510–1512. https://doi.org/10.1128/AAC.01529-07.

Davis, J.H., Baker, T.A., and Sauer, R.T. (2011). Small-molecule control of protein degradation using split adaptors. ACS Chem Biol *6*, 1205–1213. https://doi.org/10.1021/cb2001389.

De Volder, A.L., Teves, S., Isasmendi, A., Pinheiro, J.L., Ibarra, L., Breglia, N., Herrera, T., Vazquez, M., Hernandez, C., and Degrossi, J. (2021). Distribution of Burkholderia cepacia complex species isolated from industrial processes and contaminated products in Argentina. Int Microbiol *24*, 157–167. https://doi.org/10.1007/s10123-020-00151-z.

Decad, G.M., and Nikaido, H. (1976). Outer membrane of gram-negative bacteria. XII. Molecular-sieving function of cell wall. J Bacteriol *128*, 325–336. https://doi.org/10.1128/jb.128.1.325-336.1976.

D'Elia, M.A., Pereira, M.P., and Brown, E.D. (2009). Are essential genes really essential? Trends Microbiol. *17*, 433–438. https://doi.org/10.1016/j.tim.2009.08.005.

Delignette-Muller, M., and Dutang, C. (2015). fitdistrplus: an R package for fitting distributions. J. Stat. Soft. *64*. https://doi.org/10.18637/jss.v064.i04.

Denis, M.S., Ramotar, K., Vandemheen, K., Tullis, E., Ferris, W., Chan, F., Lee, C., Slinger, R., and Aaron, S.D. (2007). Infection with *Burkholderia cepacia* complex bacteria and pulmonary exacerbations of cystic fibrosis. Chest *131*, 1188–1196. https://doi.org/10.1378/chest.06-2611.

Dennis, J.J., and Zylstra, G.J. (1998). Plasposons: modular self-cloning minitransposon derivatives for rapid genetic analysis of gram-negative bacterial genomes. Appl Environ Microbiol *64*, 2710–2715. .

Depardieu, F., and Bikard, D. (2019). Gene silencing with CRISPRi in bacteria and optimization of dCas9 expression levels. Methods https://doi.org/10.1016/j.ymeth.2019.07.024.

Depoorter, E., Bull, M.J., Peeters, C., Coenye, T., Vandamme, P., and Mahenthiralingam, E. (2016). *Burkholderia*: an update on taxonomy and biotechnological potential as antibiotic producers. Appl. Microbiol. Biotechnol. *100*, 5215–5229. https://doi.org/10.1007/s00253-016-7520-x.

DeVito, J.A., Mills, J.A., Liu, V.G., Agarwal, A., Sizemore, C.F., Yao, Z., Stoughton, D.M., Cappiello, M.G., Barbosa, M.D., Foster, L.A., et al. (2002). An array of target-specific screening strains for antibacterial discovery. Nat.Biotechnol. *20*, 478–483. https://doi.org/10.1038/nbt0502-478.

De Wet, T., Winkler, K.R., Mhlanga, M., Mizrahi, V., Warner, D.F. (2020). Arrayed CRISPRi and quantitative imaging describe the morphotypic landscape of essential mycobacterial genes. eLife. *9*, e60083

Di, A., Brown, M.E., Deriy, L.V., Li, C., Szeto, F.L., Chen, Y., Huang, P., Tong, J., Naren, A.P., Bindokas, V., et al. (2006). CFTR regulates phagosome acidification in macrophages and alters bactericidal activity. Nat Cell Biol *8*, 933. https://doi.org/10.1038/ncb1456.

Dik, D.A., Fisher, J.F., and Mobashery, S. (2018). Cell-wall recycling of the Gram-negative bacteria and the nexus to antibiotic resistance. Chem Rev *118*, 5952–5984. https://doi.org/10.1021/acs.chemrev.8b00277.

Dobrindt, U., Hochhut, B., Hentschel, U., and Hacker, J. (2004). Genomic islands in pathogenic and environmental microorganisms. Nat Rev Microbiol *2*, 414–424. https://doi.org/10.1038/nrmicro884.

Dobritsa, A.P., and Samadpour, M. 2016 (2016). Transfer of eleven species of the genus *Burkholderia* to the genus *Paraburkholderia* and proposal of *Caballeronia gen. nov.* to accommodate twelve species of the genera *Burkholderia* and *Paraburkholderia*. Int J Syst Evol Microbiol *66*, 2836–2846. https://doi.org/10.1099/ijsem.0.001065.

Donati, S., Kuntz, M., Pahl, V., Farke, N., Beuter, D., Glatter, T., Gomes-Filho, J.V., Randau, L., Wang, C.-Y., and Link, H. (2021). Multi-omics analysis of CRISPRi-knockdowns identifies mechanisms that buffer decreases of enzymes in *E. coli* metabolism. Cels *12*, 56-67.e6. https://doi.org/10.1016/j.cels.2020.10.011.

Dörr, T., Davis, B.M., and Waldor, M.K. (2015). Endopeptidase-mediated beta lactam tolerance. PLoS Pathog *11*, e1004850. https://doi.org/10.1371/journal.ppat.1004850.

Dötsch, A., Becker, T., Pommerenke, C., Magnowska, Z., Jänsch, L., and Häussler, S. (2009). Genomewide identification of genetic determinants of antimicrobial drug resistance in *Pseudomonas aeruginosa*. Antimicrob Agents Chemother *53*, 2522–2531. https://doi.org/10.1128/AAC.00035-09.

Doublet, P., van Heijenoort, J., Bohin, J.P., and Mengin-Lecreulx, D. (1993). The *murI* gene of *Escherichia coli* is an essential gene that encodes a glutamate racemase activity. J Bacteriol *175*, 2970–2979. https://doi.org/10.1128/jb.175.10.2970-2979.1993.

Drawz, S.M., and Bonomo, R.A. (2010). Three decades of β-lactamase inhibitors. Clin Microbiol Rev *23*, 160. https://doi.org/10.1128/CMR.00037-09.

Du, D., Wang-Kan, X., Neuberger, A., van Veen, H.W., Pos, K.M., Piddock, L.J.V., and Luisi, B.F. (2018). Multidrug efflux pumps: structure, function and regulation. Nat Rev Microbiol *16*, 523–539. https://doi.org/10.1038/s41579-018-0048-6.

Dubois, J.-Y.F., Kouwen, T.R.H.M., Schurich, A.K.C., Reis, C.R., Ensing, H.T., Trip, E.N., Zweers, J.C., and van Dijl, J.M. (2009). Immunity to the bacteriocin sublancin 168 Is determined by the SunI (YolF) protein of *Bacillus subtilis*. Antimicrob. Agents Chemother. *53*, 651–661. https://doi.org/10.1128/AAC.01189-08.

Durand, A., Sinha, A.K., Dard-Dascot, C., and Michel, B. (2016). Mutations affecting potassium import restore the viability of the *Escherichia coli* DNA polymerase III *holD* mutant. PLoS Genet. *12*, e1006114. https://doi.org/10.1371/journal.pgen.1006114.

Durand-Reville, T.F., Miller, A.A., O'Donnell, J.P., Wu, X., Sylvester, M.A., Guler, S., Iyer, R., Shapiro, A.B., Carter, N.M., Velez-Vega, C., et al. (2021). Rational design of a new antibiotic class for drug-resistant infections. Nature *597*, 698–702. https://doi.org/10.1038/s41586-021-03899-0.

Durfey, S.L., Pipavath, S., Li, A., Vo, A.T., Ratjen, A., Carter, S., Morgan, S.J., Radey, M.C., Grogan, B., Salipante, S.J., et al. (2021). Combining ivacaftor and intensive antibiotics achieves limited clearance of cystic fibrosis infections. MBio e0314821. https://doi.org/10.1128/mbio.03148-21.

Dwyer, D.J., Belenky, P.A., Yang, J.H., MacDonald, I.C., Martell, J.D., Takahashi, N., Chan, C.T.Y., Lobritz, M.A., Braff, D., Schwarz, E.G., et al. (2014). Antibiotics induce redox-related physiological alterations as part of their lethality. Proc Natl Acad Sci *111*, E2100–E2109. https://doi.org/10.1073/pnas.1401876111.

Eberl, L., and Vandamme, P. (2016). Members of the genus *Burkholderia*: good and bad guys. F1000Res *5*, 1007. https://doi.org/10.12688/f1000research.8221.1.

Economou, N.J., Cocklin, S., and Loll, P.J. (2013). High-resolution crystal structure reveals molecular details of target recognition by bacitracin. Proc Natl Acad Sci *110*, 14207–14212. https://doi.org/10.1073/pnas.1308268110.

Egan, S.M., and Schleif, R.F. (1993). A regulatory cascade in the induction of rhaBAD. J Mol Biol *234*, 87–98. https://doi.org/10.1006/jmbi.1993.1565.

Ehmann, D.E., Jahić, H., Ross, P.L., Gu, R.-F., Hu, J., Kern, G., Walkup, G.K., and Fisher, S.L. (2012). Avibactam is a covalent, reversible, non–β-lactam β-lactamase inhibitor. Proc Natl Acad Sci *109*, 11663–11668. https://doi.org/10.1073/pnas.1205073109.

Ejim, L., Farha, M.A., Falconer, S.B., Wildenhain, J., Coombes, B.K., Tyers, M., Brown, E.D., and Wright, G.D. (2011). Combinations of antibiotics and nonantibiotic drugs enhance antimicrobial efficacy. Nat Chem Biol. *7*, 348–350. https://doi.org/10.1038/nchembio.559.

El Chakhtoura, N.G., Saade, E., Wilson, B.M., Perez, F., Papp-Wallace, K.M., and Bonomo, R.A. (2017). A 17-year nationwide study of *Burkholderia cepacia* complex bloodstream infections among patients in the United States Veterans Health Administration. Clin Infect Dis *65*, 1327–1334. https://doi.org/10.1093/cid/cix559.

El Ghachi, M., Bouhss, A., Blanot, D., and Mengin-Lecreulx, D. (2004). The *bacA* gene of *Escherichia coli* encodes an undecaprenyl pyrophosphate phosphatase activity. J Biol Chem *279*, 30106–30113. https://doi.org/10.1074/jbc.M401701200.

El Ghachi, M., Derbise, A., Bouhss, A., and Mengin-Lecreulx, D. (2005). Identification of multiple genes encoding membrane proteins with undecaprenyl pyrophosphate phosphatase (UppP) activity in Escherichia coli. J Biol Chem *280*, 18689–18695. https://doi.org/10.1074/jbc.M412277200.

Elbourne, L.D.H., Tetu, S.G., Hassan, K.A., and Paulsen, I.T. (2017). TransportDB 2.0: a database for exploring membrane transporters in sequenced genomes from all domains of life. Nucleic Acids Res *45*, D320–D324. https://doi.org/10.1093/nar/gkw1068.

El-Halfawy, O.M., and Valvano, M.A. (2014). Putrescine reduces antibiotic-induced oxidative stress as a mechanism of modulation of antibiotic resistance in *Burkholderia cenocepacia*. Antimicrob. Agents Chemother. *58*, 4162–4171. https://doi.org/10.1128/AAC.02649-14.

Elshafie, H.S., and Camele, I. (2021). An overview of metabolic activity, beneficial and pathogenic aspects of *Burkholderia* spp. Metabolites *11*, 321. https://doi.org/10.3390/metabo11050321.

Eraso, J.M., Markillie, L.M., Mitchell, H.D., Taylor, R.C., Orr, G., and Margolin, W. (2014). The highly conserved MraZ protein is a transcriptional regulator in *Escherichia coli*. J Bacteriol *196*, 2053–2066. https://doi.org/10.1128/JB.01370-13 [doi].

Estrada-de Los Santos, P., Palmer, M., Chávez-Ramírez, B., Beukes, C., Steenkamp, E.T., Briscoe, L., Khan, N., Maluk, M., Lafos, M., Humm, E., et al. (2018). Whole genome analyses suggests that *Burkholderia sensu lato* contains two additional novel genera (*Mycetohabitans gen.*

nov., and *Trinickia gen. nov.*): implications for the evolution of diazotrophy and nodulation in the *Burkholderiaceae*. Genes (Basel) *9*, E389. https://doi.org/10.3390/genes9080389.

Everaert, A., and Coenye, T. (2016). Effect of β-lactamase inhibitors on in vitro activity of β-lactam antibiotics against *Burkholderia cepacia* complex species. Antimicrob Resist Infect Control *5*, 44. https://doi.org/10.1186/s13756-016-0142-3.

Falchi, F.A., Maccagni, E.A., Puccio, S., Peano, C., De Castro, C., Palmigiano, A., Garozzo, D., Martorana, A.M., Polissi, A., Dehò, G., et al. (2017). Mutation and suppressor analysis of the essential lipopolysaccharide transport protein LptA reveals strategies to overcome severe outer membrane permeability defects in *Escherichia coli*. J Bacteriol *200*, e00487-17. https://doi.org/10.1128/JB.00487-17.

Farha, M.A., and Brown, E.D. (2016). Strategies for target identification of antimicrobial natural products. Nat.Prod.Rep. *33*, 668–680. https://doi.org/10.1039/c5np00127g.

Farzadfard, F., Perli, S.D., and Lu, T.K. (2013). Tunable and multifunctional eukaryotic transcription factors based on CRISPR/Cas. ACS Synth Biol *2*, 604–613. https://doi.org/10.1021/sb400081r.

Felici, A., Amicosante, G., Oratore, A., Strom, R., Ledent, P., Joris, B., Fanuel, L., and Frère, J.M. (1993). An overview of the kinetic parameters of class B beta-lactamases. Biochem J *291*, 151–155. .

Ferreira, A.S., Silva, I.N., Oliveira, V.H., Cunha, R., and Moreira, L.M. (2011). Insights into the role of extracellular polysaccharides in *Burkholderia* adaptation to different environments. Front Cell Infect Microbiol *1*, 16. https://doi.org/10.3389/fcimb.2011.00016.

Ferrer-González, E., Kaul, M., Parhi, A.K., LaVoie, E.J., and Pilch, D.S. (2017). β-Lactam Antibiotics with a High Affinity for PBP2 Act Synergistically with the FtsZ-Targeting Agent TXA707 against Methicillin-Resistant Staphylococcus aureus. Antimicrob. Agents Chemother. AAC.00863-17. https://doi.org/10.1128/AAC.00863-17.

Figurski, D.H., and Helinski, D.R. (1979). Replication of an origin-containing derivative of plasmid RK2 dependent on a plasmid function provided in trans. Proceedings of the National Academy of Sciences of the United States of America *76*, 1648–1652. .

Fisher, R.A. (1919). XV.—The correlation between relatives on the supposition of Mendelian inheritance. Earth Environ Sci Trans RSC Edinburgh *52*, 399–433. https://doi.org/10.1017/S0080456800012163.

Flannagan, R.S., and Valvano, M.A. (2008). *Burkholderia cenocepacia* requires RpoE for growth under stress conditions and delay of phagolysosomal fusion in macrophages. Microbiology (Reading, England) *154*, 643–653. https://doi.org/10.1099/mic.0.2007/013714-0.

Flannagan, R.S., Aubert, D., Kooi, C., Sokol, P.A., and Valvano, M.A. (2007). *Burkholderia cenocepacia* requires a periplasmic HtrA protease for growth under thermal and osmotic stress and for survival *in vivo*. Infect Immun *75*, 1679–1689. https://doi.org/10.1128/IAI.01581-06.

Flannagan, R.S., Linn, T., and Valvano, M.A. (2008). A system for the construction of targeted unmarked gene deletions in the genus *Burkholderia*. Environ Microbiol *10*, 1652–1660. https://doi.org/10.1111/j.1462-2920.2008.01576.x.

Fleischmann, R.D., Adams, M.D., White, O., Clayton, R.A., Kirkness, E.F., Kerlavage, A.R., Bult, C.J., Tomb, J.F., Dougherty, B.A., and Merrick, J.M. (1995). Whole-genome random sequencing and assembly of *Haemophilus influenzae* Rd. Science *269*, 496–512. .

Fleming, A. (1929). On the antibacterial action of cultures of a *Penicillium*, with special reference to their use in the isolation of *B. influenzæ*. Br J Exp Pathol. *10*, 226–236. .

Flemming, H.-C., Wingender, J., Szewzyk, U., Steinberg, P., Rice, S.A., and Kjelleberg, S. (2016). Biofilms: an emergent form of bacterial life. Nat Rev Microbiol *14*, 563–575. https://doi.org/10.1038/nrmicro.2016.94.

Flyg, C., Kenne, K., and Boman, H.G. (1980). Insect pathogenic properties of *Serratia marcescens* : phage-resistant mutants with a decreased resistance to *Cecropia* immunity and a decreased virulence to *Drosophila*. J. Gen. Microbiol. *120*, 173–181. https://doi.org/10.1099/00221287-120-1-173.

Forsyth, R.A., Haselbeck, R.J., Ohlsen, K.L., Yamamoto, R.T., Xu, H., Trawick, J.D., Wall, D., Wang, L., V, B.-D., Froelich, J.M., et al. (2002). A genome-wide strategy for the identification of essential genes in *Staphylococcus aureus*. Mol. Microbiol. *43*, 1387–1400. .

Fotheringham, I.G., Bledig, S.A., and Taylor, P.P. (1998). Characterization of the genes encoding d-amino acid transaminase and glutamate racemase, two d-glutamate biosynthetic enzymes of *Bacillus sphaericus* ATCC 10208. J Bacteriol *180*, 4319–4323. .

Francis, N.R., Irikura, V.M., Yamaguchi, S., DeRosier, D.J., and Macnab, R.M. (1992). Localization of the *Salmonella typhimurium* flagellar switch protein FliG to the cytoplasmic M-ring face of the basal body. Proc Natl Acad Sci *89*, 6304–6308. https://doi.org/10.1073/pnas.89.14.6304.

Fraser, C.M., Gocayne, J.D., White, O., Adams, M.D., Clayton, R.A., Fleischmann, R.D., Bult, C.J., Kerlavage, A.R., Sutton, G., Kelley, J.M., et al. (1995). The minimal gene complement of *Mycoplasma genitalium*. Science *270*, 397–404. https://doi.org/10.1126/science.270.5235.397.

Freschi, L., Vincent, A.T., Jeukens, J., Emond-Rheault, J.-G., Kukavica-Ibrulj, I., Dupont, M.-J., Charette, S.J., Boyle, B., and Levesque, R.C. (2019). The *Pseudomonas aeruginosa* pan-genome provides new insights on its population structure, horizontal gene transfer, and pathogenicity. Genome Biol Evol *11*, 109–120. https://doi.org/10.1093/gbe/evy259.

Fung, S.K., Dick, H., Devlin, H., and Tullis, E. (1998). Transmissibility and infection control implications of *Burkholderia cepacia* in cystic fibrosis. Can J Infect Dis *9*, 177–182. .

Funston, S.J., Tsaousi, K., Smyth, T.J., Twigg, M.S., Marchant, R., and Banat, I.M. (2017). Enhanced rhamnolipid production in *Burkholderia thailandensis* transposon knockout strains

deficient in polyhydroxyalkanoate (PHA) synthesis. Appl Microbiol Biotechnol *101*, 8443–8454. https://doi.org/10.1007/s00253-017-8540-x.

Furniss, R.C.D., Kaderabkova, N., Barker, D., Bernal, P., Maslova, E., Antwi, A.A., McNeil, H.E., Pugh, H.L., Dortet, L., Blair, J.M., et al. (2022). Breaking antimicrobial resistance by disrupting extracytoplasmic protein folding. ELife *11*, e57974. https://doi.org/10.7554/eLife.57974.

Gallagher, L.A., Shendure, J., and Manoil, C. (2011). Genome-scale identification of resistance functions in *Pseudomonas aeruginosa* using Tn-seq. MBio *2*, e00315-10. https://doi.org/10.1128/mBio.00315-10.

Gallagher, L.A., Bailey, J., and Manoil, C. (2020). Ranking essential bacterial processes by speed of mutant death. Proc Natl Acad Sci *117*, 18010–18017. https://doi.org/10.1073/pnas.2001507117.

Garcia, B.A., Carden, J.L., Goodwin, D.L., Smith, T.A., Gaggar, A., Leon, K., Antony, V.B., Rowe, S.M., and Solomon, G.M. (2018). Implementation of a successful eradication protocol for *Burkholderia cepacia* complex in cystic fibrosis patients. BMC Pulm Med *18*. https://doi.org/10.1186/s12890-018-0594-8.

García Véscovi, E., Soncini, F.C., and Groisman, E.A. (1996). Mg2+ as an extracellular signal: environmental regulation of *Salmonella* virulence. Cell *84*, 165–174. https://doi.org/10.1016/s0092-8674(00)81003-x.

García-Romero, I., and Valvano, M.A. (2020). Complete genome sequence of *Burkholderia cenocepacia* K56-2, an opportunistic pathogen. Microbiol Resour Announc *9*. https://doi.org/10.1128/MRA.01015-20.

Garneau, J.E., Dupuis, M.-È., Villion, M., Romero, D.A., Barrangou, R., Boyaval, P., Fremaux, C., Horvath, P., Magadán, A.H., and Moineau, S. (2010). The CRISPR/Cas bacterial immune system cleaves bacteriophage and plasmid DNA. Nature *468*, 67–71. https://doi.org/10.1038/nature09523.

Gawronski, J.D., Wong, S.M.S., Giannoukos, G., Ward, D.V., and Akerley, B.J. (2009). Tracking insertion mutants within libraries by deep sequencing and a genome-wide screen for *Haemophilus* genes required in the lung. Proc Natl Acad Sci *106*, 16422–16427. https://doi.org/10.1073/pnas.0906627106.

Geisinger, E., Vargas-Cuebas, G., Mortman, N.J., Syal, S., Dai, Y., Wainwright, E.L., Lazinski, D., Wood, S., Zhu, Z., Anthony, J., et al. (2019). The landscape of phenotypic and transcriptional responses to ciprofloxacin in *Acinetobacter baumannii*: acquired resistance alleles modulate drug-induced SOS response and prophage replication. MBio *10*, e01127-19. https://doi.org/10.1128/mBio.01127-19.

Geisinger, E., Mortman, N.J., Dai, Y., Cokol, M., Syal, S., Farinha, A., Fisher, D.G., Tang, A.Y., Lazinski, D.W., Wood, S., et al. (2020). Antibiotic susceptibility signatures identify potential

antimicrobial targets in the *Acinetobacter baumannii* cell envelope. Nat Commun *11*, 4522. https://doi.org/10.1038/s41467-020-18301-2.

Gene Ontology Consortium (2021). The Gene Ontology resource: enriching a GOld mine. Nucleic Acids Res *49*, D325–D334. https://doi.org/10.1093/nar/gkaa1113.

van Gestel, J., Hawkins, J.S., Todor, H., and Gross, C.A. (2021). Computational pipeline for designing guide RNAs for mismatch-CRISPRi. STAR Protocols *2*, 100521. https://doi.org/10.1016/j.xpro.2021.100521.

Giaever, G., Chu, A.M., Ni, L., Connelly, C., Riles, L., Véronneau, S., Dow, S., Lucau-Danila, A., Anderson, K., André, B., et al. (2002). Functional profiling of the *Saccharomyces cerevisiae* genome. Nature *418*, 387–391. https://doi.org/10.1038/nature00935.

Giaever, G., Flaherty, P., Kumm, J., Proctor, M., Nislow, C., Jaramillo, D.F., Chu, A.M., Jordan, M.I., Arkin, A.P., and Davis, R.W. (2004). Chemogenomic profiling: identifying the functional interactions of small molecules in yeast. Proc. Natl. Acad. Sci. U.S.A. *101*, 793–798. https://doi.org/10.1073/pnas.0307490100.

Gilead Sciences Inc. (2012). Cayston [package insert] (Foster City, California).

Gingras, H., Dridi, B., Leprohon, P., and Ouellette, M. (2018). Coupling next-generation sequencing to dominant positive screens for finding antibiotic cellular targets and resistance mechanisms in *Escherichia coli*. Microb Genom https://doi.org/10.1099/mgen.0.000148.

Gislason, A.S., Turner, K., Domaratzki, M., and Cardona, S.T. (2017a). Comparative analysis of the *Burkholderia cenocepacia* K56-2 essential genome reveals cell envelope functions that are uniquely required for survival in species of the genus *Burkholderia*. Microb Genom *3*, e000140. https://doi.org/10.1099/mgen.0.000140.

Gislason, A.S., Choy, M., Bloodworth, R.A.M., Qu, W., Stietz, M.S., Li, X., Zhang, C., and Cardona, S.T. (2017b). Competitive growth enhances conditional growth mutant sensitivity to antibiotics and exposes a two-component system as an emerging antibacterial target in *Burkholderia cenocepacia*. Antimicrob. Agents Chemother. *61*, e00790-16. https://doi.org/10.1128/AAC.00790-16.

Glukhov, E., Stark, M., Burrows, L.L., and Deber, C.M. (2005). Basis for selectivity of cationic antimicrobial peptides for bacterial versus mammalian membranes. J Biol Chem *280*, 33960–33967. https://doi.org/10.1074/jbc.M507042200.

Goffeau, A., Barrell, B.G., Bussey, H., Davis, R.W., Dujon, B., Feldmann, H., Galibert, F., Hoheisel, J.D., Jacq, C., Johnston, M., et al. (1996). Life with 6000 genes. Science *274*, 546, 563–567. https://doi.org/10.1126/science.274.5287.546.

Goh, S., Hohmeier, A., Stone, T.C., Offord, V., Sarabia, F., Garcia-Ruiz, C., and Good, L. (2015). Silencing of essential genes within a highly coordinated operon in *Escherichia coli*. Appl Environ Microbiol *81*, 5650–5659. https://doi.org/10.1128/AEM.01444-15.

Goodell, E.W., Lopez, R., and Tomasz, A. (1976). Suppression of lytic effect of beta lactams on *Escherichia coli* and other bacteria. Proc Natl Acad Sci *73*, 3293–3297. https://doi.org/10.1073/pnas.73.9.3293.

Goodman, A.L., Wu, M., and Gordon, J.I. (2011). Identifying microbial fitness determinants by Insertion Sequencing (INSeq) using genome-wide transposon mutant libraries. Nat Protoc *6*, 1969–1980. https://doi.org/10.1038/nprot.2011.417.

Govan, J.R., Brown, P.H., Maddison, J., Doherty, C.J., Nelson, J.W., Dodd, M., Greening, A.P., and Webb, A.K. (1993). Evidence for transmission of *Pseudomonas cepacia* by social contact in cystic fibrosis. Lancet *342*, 15–19. .

Grabowicz, M., and Silhavy, T.J. (2017). Redefining the essential trafficking pathway for outer membrane lipoproteins. Proc Natl Acad Sci *114*, 4769–4774. https://doi.org/10.1073/pnas.1702248114.

Grazziotin, A.L., Vidal, N.M., and Venancio, T.M. (2015). Uncovering major genomic features of essential genes in Bacteria and a methanogenic Archaea. The FEBS Journal *282*, 3395–3411. https://doi.org/10.1111/febs.13350.

Grover, S., Alderwick, L.J., Mishra, A.K., Krumbach, K., Marienhagen, J., Eggeling, L., Bhatt, A., and Besra, G.S. (2014). Benzothiazinones mediate killing of Corynebacterineae by blocking decaprenyl phosphate recycling involved in cell wall biosynthesis. J Biol Chem *289*, 6177–6187. https://doi.org/10.1074/jbc.M113.522623.

Gunn, J.S., Lim, K.B., Krueger, J., Kim, K., Guo, L., Hackett, M., and Miller, S.I. (1998). PmrA–PmrB-regulated genes necessary for 4-aminoarabinose lipid A modification and polymyxin resistance. Mol Microbiol *27*, 1171–1182. https://doi.org/10.1046/j.1365-2958.1998.00757.x.

Guo, J., Wang, T., Guan, C., Liu, B., Luo, C., Xie, Z., Zhang, C., and Xing, X.-H. (2018). Improved sgRNA design in bacteria via genome-wide activity profiling. Nucleic Acids Res *46*, 7052–7069. https://doi.org/10.1093/nar/gky572.

Hackel, M.A., Tsuji, M., Yamano, Y., Echols, R., Karlowsky, J.A., and Sahm, D.F. (2017). In vitro activity of the siderophore cephalosporin, cefiderocol, against a recent collection of clinically relevant Gram-negative bacilli from North America and Europe, including carbapenem-nonsusceptible isolates (SIDERO-WT-2014 Study). Antimicrob Agents Chemother *61*, e00093-17. https://doi.org/10.1128/AAC.00093-17.

Hackel, M.A., Tsuji, M., Yamano, Y., Echols, R., Karlowsky, J.A., and Sahm, D.F. (2018). In Vitro Activity of the Siderophore Cephalosporin, Cefiderocol, against Carbapenem-Nonsusceptible and Multidrug-Resistant Isolates of Gram-Negative Bacilli Collected Worldwide in 2014 to 2016. Antimicrob. Agents Chemother. *62*. https://doi.org/10.1128/AAC.01968-17.

Hacker, J., Bender, L., Ott, M., Wingender, J., Lund, B., Marre, R., and Goebel, W. (1990). Deletions of chromosomal regions coding for fimbriae and hemolysins occur in vitro and in vivo

in various extraintestinal *Escherichia coli* isolates. Microb Pathog *8*, 213–225. https://doi.org/10.1016/0882-4010(90)90048-u.

Häfliger, E., Atkinson, A., and Marschall, J. (2020). Systematic review of healthcare-associated *Burkholderia cepacia* complex outbreaks: presentation, causes and outbreak control. Infect Prev Practice *2*, 100082. https://doi.org/10.1016/j.infpip.2020.100082.

Hamad, M.A., Skeldon, A.M., and Valvano, M.A. (2010). Construction of aminoglycoside-sensitive *Burkholderia cenocepacia* strains for use in studies of intracellular bacteria with the gentamicin protection assay. Appl Environ Microbiol *76*, 3170–3176. https://doi.org/10.1128/AEM.03024-09.

Hamad, M.A., Di Lorenzo, F., Molinaro, A., and Valvano, M.A. (2012). Aminoarabinose is essential for lipopolysaccharide export and intrinsic antimicrobial peptide resistance in *Burkholderia cenocepacia*. Mol Microbiol *85*, 962–974. https://doi.org/10.1111/j.1365-2958.2012.08154.x.

Hart, E.M., and Silhavy, T.J. (2020). Functions of the BamBCDE lipoproteins revealed by bypass mutations in BamA. J Bacteriol *202*. https://doi.org/10.1128/JB.00401-20.

Hawkins, J.S., Silvis, M.R., Koo, B.-M., Peters, J.M., Osadnik, H., Jost, M., Hearne, C.C., Weissman, J.S., Todor, H., and Gross, C.A. (2020). Mismatch-CRISPRi reveals the co-varying expression-fitness relationships of essential genes in *Escherichia coli* and *Bacillus subtilis*. Cell Syst *11*, 523-535.e9. https://doi.org/10.1016/j.cels.2020.09.009.

Hayashi, S., Abe, M., Kimoto, M., Furukawa, S., and Nakazawa, T. (2000). The DsbA-DsbB disulfide bond formation system of *Burkholderia cepacia* is involved in the production of protease and alkaline phosphatase, motility, metal resistance, and multi-drug resistance. Microbiol and Immun *44*, 41–50. https://doi.org/10.1111/j.1348-0421.2000.tb01244.x.

He, W., Li, C., and Lu, C.-D. (2011). Regulation and characterization of the *dadRAX* locus for d-amino acid catabolism in *Pseudomonas aeruginosa* PAO1. J Bacteriol *193*, 2107–2115. https://doi.org/10.1128/JB.00036-11.

Hecker, S.J., Reddy, K.R., Lomovskaya, O., Griffith, D.C., Rubio-Aparicio, D., Nelson, K., Tsivkovski, R., Sun, D., Sabet, M., Tarazi, Z., et al. (2020). Discovery of cyclic boronic acid QPX7728, an ultrabroad-spectrum inhibitor of serine and metallo-β-lactamases. J. Med. Chem. *63*, 7491–7507. https://doi.org/10.1021/acs.jmedchem.9b01976.

Heo, S.T., Kim, S.J., Jeong, Y.G., Bae, I.G., Jin, J.S., and Lee, J.C. (2008). Hospital outbreak of *Burkholderia stabilis* bacteraemia related to contaminated chlorhexidine in haematological malignancy patients with indwelling catheters. J. Hosp. Infect. *70*, 241–245. https://doi.org/10.1016/j.jhin.2008.07.019.

Herman, C., Thévenet, D., Bouloc, P., Walker, G.C., and D'Ari, R. (1998). Degradation of carboxy-terminal-tagged cytoplasmic proteins by the *Escherichia coli* protease HflB (FtsH). Genes Dev *12*, 1348–1355. .

Herring, C.D., and Blattner, F.R. (2004). Conditional lethal amber mutations in essential *Escherichia coli* genes. J Bacteriol *186*, 2673–2681. .

Hews, C.L., Cho, T., Rowley, G., and Raivio, T.L. (2019). Maintaining integrity under stress: Envelope stress response regulation of pathogenesis in Gram-negative bacteria. Front Cell Infect Microbiol *9*. .

Higgins, M.L., McDowell, T.D., Sleytr, U.B., Mychajlonka, M., and Shockman, G.D. (1980). Effects of penicillin on macromolecular synthesis and surface growth of a tolerant streptococcus as studied by computer reconstruction methods. J Bacteriol *144*, 1168–1173. .

Higgins, N.P., Peebles, C.L., Sugino, A., and Cozzarelli, N.R. (1978). Purification of subunits of *Escherichia coli* DNA gyrase and reconstitution of enzymatic activity. Proc Natl Acad Sci U S A *75*, 1773–1777. https://doi.org/10.1073/pnas.75.4.1773.

Hillenmeyer, M.E., Fung, E., Wildenhain, J., Pierce, S.E., Hoon, S., Lee, W., Proctor, M., St Onge, R.P., Tyers, M., Koller, D., et al. (2008). The chemical genomic portrait of yeast: uncovering a phenotype for all genes. Science *320*, 362–365. https://doi.org/10.1126/science.1150021.

Himmelreich, R., Hilbert, H., Plagens, H., Pirkl, E., Li, B.-C., and Herrmann, R. (1996). Complete sequence analysis of the genome of the bacterium *Mycoplasma pneumoniae*. Nucleic Acids Res *24*, 4420–4449. https://doi.org/10.1093/nar/24.22.4420.

Hoang, T.T., Kutchma, A.J., Becher, A., and Schweizer, H.P. (2000). Integration-proficient plasmids for Pseudomonas aeruginosa: site-specific integration and use for engineering of reporter and expression strains. Plasmid *43*, 59–72. https://doi.org/10.1006/plas.1999.1441.

Hogan, A.M., Scoffone, V.C., Makarov, V., Gislason, A.S., Tesfu, H., Stietz, M.S., Brassinga, A.K.C., Domaratzki, M., Li, X., Azzalin, A., et al. (2018). Competitive fitness of essential gene knockdowns reveals a broad-spectrum antibacterial inhibitor of the cell division protein FtsZ. Antimicrob Agents Chemother *62*, e01231-18. https://doi.org/10.1128/AAC.01231-18.

Hogan, A.M., Rahman, A.S.M.Z., Lightly, T.J., and Cardona, S.T. (2019). A broad-host-range CRISPRi toolkit for silencing gene expression in *Burkholderia*. ACS Synth. Biol. *8*, 2372–2384. https://doi.org/10.1021/acssynbio.9b00232.

Hogan, A.M., Jeffers, K.R., Palacios, A., and Cardona, S.T. (2021). Improved dynamic range of a rhamnose-inducible promoter for gene expression in *Burkholderia* spp. Appl Environ Microbiol *87*, e0064721. https://doi.org/10.1128/AEM.00647-21.

Holden, M.T., Seth-Smith, H.M., Crossman, L.C., Sebaihia, M., Bentley, S.D., Cerdeno-Tarraga, A.M., Thomson, N.R., Bason, N., Quail, M.A., Sharp, S., et al. (2009). The genome of *Burkholderia cenocepacia* J2315, an epidemic pathogen of cystic fibrosis patients. J Bacteriol *191*, 261–277. https://doi.org/10.1128/JB.01230-08.

Howe, C., Sampath, A., and Spotnitz, M. (1971). The *pseudomallei* group: a review. J. Infect. Dis. *124*, 598–606. .

Htoo, H.H., Brumage, L., Chaikeeratisak, V., Tsunemoto, H., Sugie, J., Tribuddharat, C., Pogliano, J., and Nonejuie, P. (2019). Bacterial cytological profiling as a tool to study mechanisms of action of antibiotics that are active against *Acinetobacter baumannii*. Antimicrob Agents Chemother *63*, e02310-18. https://doi.org/10.1128/AAC.02310-18.

Hu, J.H., Miller, S.M., Geurts, M.H., Tang, W., Chen, L., Sun, N., Zeina, C.M., Gao, X., Rees, H.A., Lin, Z., et al. (2018). Evolved Cas9 variants with broad PAM compatibility and high DNA specificity. Nature *556*, 57–63. https://doi.org/10.1038/nature26155.

Hu, W., Sillaots, S., Lemieux, S., Davison, J., Kauffman, S., Breton, A., Linteau, A., Xin, C., Bowman, J., Becker, J., et al. (2007). Essential gene identification and drug target prioritization in *Aspergillus fumigatus*. PLOS Pathogens *3*, e24. https://doi.org/10.1371/journal.ppat.0030024.

Huang, A., Garraway, L.A., Ashworth, A., and Weber, B. (2020). Synthetic lethality as an engine for cancer drug target discovery. Nat Rev Drug Discov *19*, 23–38. https://doi.org/10.1038/s41573-019-0046-z.

Huerta-Cepas, J., Forslund, K., Coelho, L.P., Szklarczyk, D., Jensen, L.J., von Mering, C., and Bork, P. (2017). Fast genome-wide functional annotation through orthology assignment by eggNOG-Mapper. Mol Biol Evol *34*, 2115–2122. https://doi.org/10.1093/molbev/msx148.

Huls, P.G., Vischer, N.O.E., and Woldringh, C.L. (1999). Delayed nucleoid segregation in *Escherichia coli*. Mol Microbiol *33*, 959–970. https://doi.org/10.1046/j.1365-2958.1999.01535.x.

Hunt, T.A., Kooi, C., Sokol, P.A., and Valvano, M.A. (2004). Identification of *Burkholderia cenocepacia* genes required for bacterial survival *in vivo*. Infect Immun *72*, 4010–4022. .

Hunter, R.C., Asfour, F., Dingemans, J., Osuna, B.L., Samad, T., Malfroot, A., Cornelis, P., and Newman, D.K. (2013). Ferrous iron Is a significant component of bioavailable iron in cystic fibrosis airways. MBio *4*, e00557-13. https://doi.org/10.1128/mBio.00557-13.

Hurley, K.A., Santos, T.M., Nepomuceno, G.M., Huynh, V., Shaw, J.T., and Weibel, D.B. (2016). Targeting the bacterial division protein FtsZ. J.Med.Chem. *59*, 6975–6998. https://doi.org/10.1021/acs.jmedchem.5b01098.

Hutchison, C.A., Peterson, S.N., Gill, S.R., Cline, R.T., White, O., Fraser, C.M., Smith, H.O., and Venter, J.C. (1999). Global transposon mutagenesis and a minimal *Mycoplasma* genome. Science *286*, 2165–2169. .

Hwang, J., and Kim, H.S. (2015). Cell wall recycling-linked coregulation of AmpC and PenB β-lactamases through *ampD* mutations in *Burkholderia cenocepacia*. Antimicrob. Agents Chemother. *59*, 7602–7610. https://doi.org/10.1128/AAC.01068-15.

Ianevski, A., Giri, A.K., and Aittokallio, T. (2020). SynergyFinder 2.0: visual analytics of multi-drug combination synergies. Nucleic Acids Res *48*, W488–W493. https://doi.org/10.1093/nar/gkaa216.

Idowu, T., Ammeter, D., Rossong, H., Zhanel, G.G., and Schweizer, F. (2019). Homodimeric tobramycin adjuvant repurposes novobiocin as an effective antibacterial agent against Gram-negative bacteria. J. Med. Chem. *62*, 9103–9115. https://doi.org/10.1021/acs.jmedchem.9b00876.

Iglesias, A., Artiles, I., Cabanillas, J.J., Alvarez-Sala, R., and Prados, C. (2014). Eradication of *Burkholderia cepacia* using inhaled aztreonam lysine in two patients with bronchiectasis. Case Rep Pulmonol *2014*, 192146. https://doi.org/10.1155/2014/192146.

Imai, Y., Meyer, K.J., Iinishi, A., Favre-Godal, Q., Green, R., Manuse, S., Caboni, M., Mori, M., Niles, S., Ghiglieri, M., et al. (2019). A new antibiotic selectively kills Gram-negative pathogens. Nature *576*, 459–464. https://doi.org/10.1038/s41586-019-1791-1.

Imamovic, L., and Sommer, M.O.A. (2013). Use of collateral sensitivity networks to design drug cycling protocols that avoid resistance development. Sci Trans Med *5*, 204ra132-204ra132. https://doi.org/10.1126/scitranslmed.3006609.

Ingerman, E., and Nunnari, J. (2005). A continuous, regenerative coupled GTPase assay for dynamin-related proteins. Meth. Enzymol. *404*, 611–619. https://doi.org/10.1016/S0076-6879(05)04053-X.

Ish-Am, O., Kristensen, D.M., and Ruppin, E. (2015). Evolutionary conservation of bacterial essential metabolic genes across all bacterial culture media. PLoS One *10*. https://doi.org/10.1371/journal.pone.0123785.

Isles, A., Maclusky, I., Corey, M., Gold, R., Prober, C., Fleming, P., and Levison, H. (1984). *Pseudomonas cepacia* infection in cystic fibrosis: an emerging problem. J. Pediatr. *104*, 206–210. .

Isshiki, Y., Kawahara, K., and Zähringer, U. (1998). Isolation and characterisation of disodium (4-amino-4-deoxy-β-l-arabinopyranosyl)-(1-8)-(d-glycero-α-d-talo-oct-2-ulopyranosylonate)-(2-4)-(methyl 3-deoxy-d-manno-oct-2-ulopyranosid)onate from the lipopolysaccharide of *Burkholderia cepacia*. Carbohydrate Res *313*, 21–27. https://doi.org/10.1016/S0008-6215(98)00179-7.

Ito, A., Sato, T., Ota, M., Takemura, M., Nishikawa, T., Toba, S., Kohira, N., Miyagawa, S., Ishibashi, N., Matsumoto, S., et al. (2017). In vitro antibacterial properties of cefiderocol, a novel siderophore cephalosporin, against Gram-negative bacteria. Antimicrob Agents Chemother *62*. https://doi.org/10.1128/AAC.01454-17.

Jacobs, C., Huang, L.J., Bartowsky, E., Normark, S., and Park, J.T. (1994). Bacterial cell wall recycling provides cytosolic muropeptides as effectors for beta-lactamase induction. EMBO J *13*, 4684–4694. https://doi.org/10.1002/j.1460-2075.1994.tb06792.x.

Jacobs, C., Joris, B., Jamin, M., Klarsov, K., van Beeumen, J., Mengin-Lecreulx, D., van Heijenoort, J., Park, J.T., Normark, S., and Frère, J.-M. (1995). AmpD, essential for both β-lactamase regulation and cell wall recycling, is a novel cytosolic N-acetylmuramyl-L-alanine amidase. Mol Microbiol *15*, 553–559. https://doi.org/10.1111/j.1365-2958.1995.tb02268.x.

Jacobs, M.A., Alwood, A., Thaipisuttikul, I., Spencer, D., Haugen, E., Ernst, S., Will, O., Kaul, R., Raymond, C., Levy, R., et al. (2003). Comprehensive transposon mutant library of *Pseudomonas aeruginosa*. Proc. Natl. Acad. Sci. U S A *100*, 14339–14344. .

Jacoby, G.A. (2009). AmpC beta-lactamases. Clin. Microbiol. Rev. *22*, 161–182. https://doi.org/10.1128/CMR.00036-08.

Ji, Y., Zhang, B., Van, S.F., Horn, Warren, P., Woodnutt, G., Burnham, M.K., and Rosenberg, M. (2001). Identification of critical staphylococcal genes using conditional phenotypes generated by antisense RNA. Science (New York, N.Y.) *293*, 2266–2269. https://doi.org/10.1126/science.1063566.

Jimenez, L. (2007). Microbial diversity in pharmaceutical product recalls and environments. PDA J Pharma Sci Technol / PDA *61*, 383–399. .

Jinek, M., Chylinski, K., Fonfara, I., Hauer, M., Doudna, J.A., and Charpentier, E. (2012). A programmable dual-RNA-guided DNA endonuclease in adaptive bacterial immunity. Science *337*, 816–821. https://doi.org/10.1126/science.1225829.

Johnson, E.O., LaVerriere, E., Office, E., Stanley, M., Meyer, E., Kawate, T., Gomez, J.E., Audette, R.E., Bandyopadhyay, N., Betancourt, N., et al. (2019). Large-scale chemical–genetics yields new *M. tuberculosis* inhibitor classes. Nature *571*, 72–78. https://doi.org/10.1038/s41586-019-1315-z.

Johnson, W.M., Tyler, S.D., and Rozee, K.R. (1994). Linkage analysis of geographic and clinical clusters in *Pseudomonas cepacia* infections by multilocus enzyme electrophoresis and ribotyping. J Clin Microbiol *32*, 924–930. https://doi.org/10.1128/jcm.32.4.924-930.1994.

Jones, D.L., Leroy, P., Unoson, C., Fange, D., Ćurić, V., Lawson, M.J., and Elf, J. (2017). Kinetics of dCas9 target search in *Escherichia coli*. Science *357*, 1420–1424. https://doi.org/10.1126/science.aah7084.

Jordan, I.K., Rogozin, I.B., Wolf, Y.I., and Koonin, E.V. (2002). Essential genes are more evolutionarily conserved than are nonessential genes in bacteria. Genome Res. *12*, 962–968. .

Jorgenson, M.A., and Bryant, J.C. (2021). A genetic screen to identify factors affected by undecaprenyl phosphate recycling uncovers novel connections to morphogenesis in *Escherichia coli*. Mol Microbiol *115*, 191–207. https://doi.org/10.1111/mmi.14609.

Jorgenson, M.A., and Young, K.D. (2016). Interrupting biosynthesis of o-antigen or the lipopolysaccharide core produces morphological defects in *Escherichia coli* by sequestering undecaprenyl phosphate. J Bacteriol *198*, 3070–3079. https://doi.org/10.1128/JB.00550-16.

Jorgenson, M.A., Kannan, S., Laubacher, M.E., and Young, K.D. (2016). Dead-end intermediates in the enterobacterial common antigen pathway induce morphological defects in *Escherichia coli* by competing for undecaprenyl phosphate. Mol Microbiol *100*, mmi.13284. https://doi.org/10.1111/mmi.13284.

Jorgenson, M.A., MacCain, W.J., Meberg, B.M., Kannan, S., Bryant, J.C., and Young, K.D. (2019). Simultaneously inhibiting undecaprenyl phosphate production and peptidoglycan synthases promotes rapid lysis in *Escherichia coli*. Mol Microbiol *112*, 233–248. https://doi.org/10.1111/mmi.14265.

Josephs, E.A., Kocak, D.D., Fitzgibbon, C.J., McMenemy, J., Gersbach, C.A., and Marszalek, P.E. (2015). Structure and specificity of the RNA-guided endonuclease Cas9 during DNA interrogation, target binding and cleavage. Nucleic Acids Res *43*, 8924–8941. https://doi.org/10.1093/nar/gkv892.

Jost, M., Santos, D.A., Saunders, R.A., Horlbeck, M.A., Hawkins, J.S., Scaria, S.M., Norman, T.M., Hussmann, J.A., Liem, C.R., Gross, C.A., et al. (2020). Titrating gene expression using libraries of systematically attenuated CRISPR guide RNAs. Nat. Biotechnol. https://doi.org/10.1038/s41587-019-0387-5.

Joyce, A.R., Reed, J.L., White, A., Edwards, R., Osterman, A., Baba, T., Mori, H., Lesely, S.A., Palsson, B.Ø., and Agarwalla, S. (2006). Experimental and computational assessment of conditionally essential genes in *Escherichia coli*. J Bacteriol *188*, 8259–8271. https://doi.org/10.1128/JB.00740-06.

Juan, C., Torrens, G., González-Nicolau, M., and Oliver, A. (2017). Diversity and regulation of intrinsic β-lactamases from non-fermenting and other Gram-negative opportunistic pathogens. FEMS Microbiol Rev *41*, 781–815. https://doi.org/10.1093/femsre/fux043.

Judson, N., and Mekalanos, J.J. (2000). TnAraOut, a transposon-based approach to identify and characterize essential bacterial genes. Nat. Biotechnol. *18*, 740–745. .

Juhas, M., van der Meer, J.R., Gaillard, M., Harding, R.M., Hood, D.W., and Crook, D.W. (2009). Genomic islands: tools of bacterial horizontal gene transfer and evolution. FEMS Microbiol. Rev. *33*, 376–393. https://doi.org/10.1111/j.1574-6976.2008.00136.x.

Juhas, M., Eberl, L., and Church, G.M. (2012). Essential genes as antimicrobial targets and cornerstones of synthetic biology. Trends in Biotechnology *30*, 601–607. https://doi.org/10.1016/j.tibtech.2012.08.002; 10.1016/j.tibtech.2012.08.002.

Justice, S.S., García-Lara, J., and Rothfield, L.I. (2000). Cell division inhibitors SulA and MinC/MinD block septum formation at different steps in the assembly of the *Escherichia coli* division machinery. Mol. Microbiol. *37*, 410–423. .

Justice, S.S., Hunstad, D.A., Cegelski, L., and Hultgren, S.J. (2008). Morphological plasticity as a bacterial survival strategy. Nat Rev Micro *6*, 162–168. https://doi.org/10.1038/nrmicro1820.

Kahan, F.M., Kahan, J.S., Cassidy, P.J., and Kropp, H. (1974). The mechanism of action of fosfomycin (phosphonomycin). Ann N Y Acad Sci *235*, 364–386. https://doi.org/10.1111/j.1749-6632.1974.tb43277.x.

Kaplan, J.B., Lovetri, K., Cardona, S.T., Madhyastha, S., Sadovskaya, I., Jabbouri, S., and Izano, E.A. (2011). Recombinant human DNase I decreases biofilm and increases antimicrobial

susceptibility in staphylococci. J Antibiot *65*, 73–77. https://doi.org/10.1038/ja.2011.113; 10.1038/ja.2011.113.

Karlowsky, J.A., Hackel, M.A., Bouchillon, S.K., and Sahm, D.F. (2020). In vitro activity of WCK 5222 (cefepime-zidebactam) against worldwide collected Gram-negative bacilli not susceptible to carbapenems. Antimicrob Agents Chemother *64*. https://doi.org/10.1128/AAC.01432-20.

Karp, P.D., Billington, R., Caspi, R., Fulcher, C.A., Latendresse, M., Kothari, A., Keseler, I.M., Krummenacker, M., Midford, P.E., Ong, Q., et al. (2019). The BioCyc collection of microbial genomes and metabolic pathways. Brief Bioinform *20*, 1085–1093. https://doi.org/10.1093/bib/bbx085.

Karsisiotis, A.I., Damblon, C.F., and Roberts, G.C.K. (2014). A variety of roles for versatile zinc in metallo-β-lactamases. Metallomics *6*, 1181–1197. https://doi.org/10.1039/c4mt00066h.

Keating, T.A., Newman, J.V., Olivier, N.B., Otterson, L.G., Andrews, B., Boriack-Sjodin, P.A., Breen, J.N., Doig, P., Dumas, J., Gangl, E., et al. (2012). In vivo validation of thymidylate inase (TMK) with a rationally designed, selective antibacterial compound. ACS Chem. Biol. *7*, 1866–1872. https://doi.org/10.1021/cb300316n.

Keffer, J.L., Huecas, S., Hammill, J.T., Wipf, P., Andreu, J.M., and Bewley, C.A. (2013). Chrysophaentins are competitive inhibitors of FtsZ and inhibit Z-ring formation in live bacteria. Bioorg. Med. Chem. *21*, 5673–5678. https://doi.org/10.1016/j.bmc.2013.07.033.

Kenna, D.T.D., Lilley, D., Coward, A., Martin, K., Perry, C., Pike, R., Hill, R., and Turton, J.F. (2017). Prevalence of *Burkholderia species*, including members of *Burkholderia cepacia* complex, among UK cystic and non-cystic fibrosis patients. J. Med. Microbiol. *66*, 490–501. https://doi.org/10.1099/jmm.0.000458.

Kent, W.J. (2002). BLAT--the BLAST-like alignment tool. Genome Res *12*, 656–664. https://doi.org/10.1101/gr.229202.

Kim, J.-H., Wei, J.-R., Wallach, J.B., Robbins, R.S., Rubin, E.J., and Schnappinger, D. (2011). Protein inactivation in mycobacteria by controlled proteolysis and its application to deplete the beta subunit of RNA polymerase. Nucleic Acids Res *39*, 2210–2220. https://doi.org/10.1093/nar/gkq1149.

Kim, J.H., O'Brien, K.M., Sharma, R., Boshoff, H.I., Rehren, G., Chakraborty, S., Wallach, J.B., Monteleone, M., Wilson, D.J., Aldrich, C.C., et al. (2013). A genetic strategy to identify targets for the development of drugs that prevent bacterial persistence. Proc.Natl.Acad.Sci.U.S.A. *110*, 19095–19100. https://doi.org/10.1073/pnas.1315860110;

Kim, J.M., Ahn, Y., LiPuma, J.J., Hussong, D., and Cerniglia, C.E. (2015). Survival and susceptibility of *Burkholderia cepacia* complex in chlorhexidine gluconate and benzalkonium chloride. J. Ind. Microbiol. Biotechnol. *42*, 905–913. https://doi.org/10.1007/s10295-015-1605-x.

Kim, S.K., Han, G.H., Seong, W., Kim, H., Kim, S.-W., Lee, D.-H., and Lee, S.-G. (2016). CRISPR interference-guided balancing of a biosynthetic mevalonate pathway increases terpenoid production. Metabol Engin *38*, 228–240. https://doi.org/10.1016/j.ymben.2016.08.006.

Kitagawa, M., Ara, T., Arifuzzaman, M., Ioka-Nakamichi, T., Inamoto, E., Toyonaga, H., and Mori, H. (2005). Complete set of ORF clones of *Escherichia coli* ASKA library (a complete set of *E. coli* K-12 ORF archive): unique resources for biological research. DNA Research : An International Journal for Rapid Publication of Reports on Genes and Genomes *12*, 291–299. https://doi.org/10.1093/dnares/dsi012.

Kitt, H., Lenney, W., and Gilchrist, F.J. (2016). Two case reports of the successful eradication of new isolates of *Burkholderia cepacia* complex in children with cystic fibrosis. BMC Pharmacol Toxicol *17*, 14-016-0054–0. https://doi.org/10.1186/s40360-016-0054-0 [doi].

Kjeldsen, T.S.B., Sommer, M.O.A., and Olsen, J.E. (2015). Extended spectrum β-lactamase-producing *Escherichia coli* forms filaments as an initial response to cefotaxime treatment. BMC Microbiol. *15*, 63. https://doi.org/10.1186/s12866-015-0399-3.

Klein, K., Sonnabend, M.S., Frank, L., Leibiger, K., Franz-Wachtel, M., Macek, B., Trunk, T., Leo, J.C., Autenrieth, I.B., Schütz, M., et al. (2019). Deprivation of the periplasmic chaperone SurA reduces virulence and restores antibiotic susceptibility of multidrug-resistant *Pseudomonas aeruginosa*. Front Microbiol *10*. .

Klementiev, A.D., Jin, Z., and Whiteley, M. (2020). Micron scale spatial measurement of the O2 gradient surrounding a bacterial biofilm in real time. MBio *11*, e02536-20. https://doi.org/10.1128/mBio.02536-20.

Klobucar, K., and Brown, E.D. (2022). New potentiators of ineffective antibiotics: Targeting the Gram-negative outer membrane to overcome intrinsic resistance. Curr Opin Chem Biol *66*, 102099. https://doi.org/10.1016/j.cbpa.2021.102099.

Klobucar, K., French, S., Côté, J.-P., Howes, J.R., and Brown, E.D. (2020). Genetic and chemical-genetic interactions map biogenesis and permeability determinants of the outer membrane of *Escherichia coli*. MBio *11*. https://doi.org/10.1128/mBio.00161-20.

Knuth, K., Niesalla, H., Hueck, C.J., and Fuchs, T.M. (2004). Large-scale identification of essential *Salmonella* genes by trapping lethal insertions. Mol Microbiol *51*, 1729–1744. .

Kobayashi, K., Ehrlich, S.D., Albertini, A., Amati, G., Andersen, K.K., Arnaud, M., Asai, K., Ashikaga, S., Aymerich, S., Bessieres, P., et al. (2003). Essential *Bacillus subtilis* genes. Proc. Natl. Acad. Sci. U S A *100*, 4678–4683. .

Kohanski, M.A., Dwyer, D.J., Hayete, B., Lawrence, C.A., and Collins, J.J. (2007). A common mechanism of cellular death induced by bactericidal antibiotics. Cell *130*, 797–810. https://doi.org/10.1016/j.cell.2007.06.049.

Köhler, T., Michea-Hamzehpour, M., Epp, S.F., and Pechere, J.-C. (1999). Carbapenem activities against *Pseudomonas aeruginosa*: respective contributions of OprD and efflux systems. Antimicrob Agents Chemother https://doi.org/10.1128/AAC.43.2.424.

Kohira, N., West, J., Ito, A., Ito-Horiyama, T., Nakamura, R., Sato, T., Rittenhouse, S., Tsuji, M., Yamano, Y. (2016). *In vitro* antimicrobial activity of a siderophore cephalosporin, S-649266, against Enterobacteriaceae clinical isolates, including carbapenem-resistant strains. Antimicrob Agents Chemother. *60*, 729-734.

Komatsu, H., Hayashi, F., Sasa, M., Shikata, K., Yamaguchi, S., Namba, K., and Oosawa, K. (2016). Genetic analysis of revertants isolated from the rod-fragile *fliF* mutant of *Salmonella*. Biophys Physicobiol *13*, 13–25. https://doi.org/10.2142/biophysico.13.0_13.

Koo, B.-M., Kritikos, G., Farelli, J.D., Todor, H., Tong, K., Kimsey, H., Wapinski, I., Galardini, M., Cabal, A., Peters, J.M., et al. (2017). Construction and analysis of two genome-scale deletion libraries for *Bacillus subtilis*. Cell Syst *4*, 291–303. https://doi.org/10.1016/j.cels.2016.12.013.

Kornelsen, V., and Kumar, A. (2021). Update on multidrug resistance efflux pumps in *Acinetobacter* spp. Antimicrob Agents Chemother *65*, e0051421. https://doi.org/10.1128/AAC.00514-21.

Krishnamoorthy, G., Leus, I.V., Weeks, J.W., Wolloscheck, D., Rybenkov, V.V., and Zgurskaya, H.I. (2017). Synergy between active efflux and outer membrane diffusion defines rules of antibiotic permeation into Gram-negative bacteria. MBio *8*. https://doi.org/10.1128/mBio.01172-17.

Król, E., and Scheffers, D.-J. (2013). FtsZ polymerization assays: simple protocols and considerations. J Vis Exp https://doi.org/10.3791/50844.

Kumar, B., and Cardona, S.T. (2016). Synthetic Cystic Fibrosis Sputum Medium Regulates Flagellar Biosynthesis through the flhF Gene in *Burkholderia* cenocepacia. Front Cell Infect Microbiol *6*, 65. https://doi.org/10.3389/fcimb.2016.00065.

Kuyyakanond, T., and Quesnel, L.B. (1992). The mechanism of action of chlorhexidine. FEMS Microbiol Lett *100*, 211–215. https://doi.org/10.1111/j.1574-6968.1992.tb14042.x.

Kuzuyama, T., Shimizu, T., Takahashi, S., and Seto, H. (1998). Fosmidomycin, a specific inhibitor of 1-deoxy-d-xylulose 5-phosphate reductoisomerase in the nonmevalonate pathway for terpenoid biosynthesis. Tetrahedron Letters *39*, 7913–7916. https://doi.org/10.1016/S0040-4039(98)01755-9.

Lahiri, S.D., Johnstone, M.R., Ross, P.L., McLaughlin, R.E., Olivier, N.B., and Alm, R.A. (2014). Avibactam and class C β-lactamases: Mechanism of inhibition, conservation of the binding pocket, and implications for resistance. Antimicrob Agents Chemother *58*, 5704–5713. https://doi.org/10.1128/AAC.03057-14.

Lamothe, J., Huynh, K.K., Grinstein, S., and Valvano, M.A. (2006). Intracellular survival of *Burkholderia cenocepacia* in macrophages is associated with a delay in the maturation of

bacteria-containing vacuoles. Cell Microbiol *9*, 40–53. https://doi.org/CMI766 [pii]; 10.1111/j.1462-5822.2006.00766.x [doi].

Lamsa, A., Lopez-Garrido, J., Quach, D., Riley, E.P., Pogliano, J., and Pogliano, K. (2016). Rapid inhibition profiling in *Bacillus subtilis* to identify the mechanism of action of new antimicrobials. ACS Chem. Biol. *11*, 2222–2231. https://doi.org/10.1021/acschembio.5b01050.

Lan, P., Lu, Y., Chen, Z., Wu, X., Hua, X., Jiang, Y., Zhou, J., and Yu, Y. (2022). Emergence of high-level cefiderocol resistance in carbapenem-resistant *Klebsiella pneumoniae* from bloodstream infections in patients with hematologic malignancies in China. Microbiol Spectr *10*, e00084-22. https://doi.org/10.1128/spectrum.00084-22.

Landeta, C., Blazyk, J.L., Hatahet, F., Meehan, B.M., Eser, M., Myrick, A., Bronstain, L., Minami, S., Arnold, H., Ke, N., et al. (2015). Compounds targeting disulfide bond forming enzyme DsbB of Gram-negative bacteria. Nat Chem Biol *11*, 292–298. https://doi.org/10.1038/nchembio.1752.

Landeta, C., Boyd, D., and Beckwith, J. (2018). Disulfide bond formation in prokaryotes. Nat Microbiol *3*, 270–280. https://doi.org/10.1038/s41564-017-0106-2.

Langridge, G.C., Phan, M.D., Turner, D.J., Perkins, T.T., Parts, L., Haase, J., Charles, I., Maskell, D.J., Peters, S.E., Dougan, G., et al. (2009). Simultaneous assay of every *Salmonella Typhi* gene using one million transposon mutants. Genome Res. *19*, 2308–2316. https://doi.org/10.1101/gr.097097.109.

Larson, M.H., Gilbert, L.A., Wang, X., Lim, W.A., Weissman, J.S., and Qi, L.S. (2013a). CRISPR interference (CRISPRi) for sequence-specific control of gene expression. Nat.Protoc. *8*, 2180–2196. https://doi.org/10.1038/nprot.2013.132.

Larson, M.H., Gilbert, L.A., Wang, X., Lim, W.A., Weissman, J.S., and Qi, L.S. (2013b). CRISPR interference (CRISPRi) for sequence-specific control of gene expression. Nat Protoc *8*, 2180–2196. https://doi.org/10.1038/nprot.2013.132.

Lauman, P., and Dennis, J.J. (2021). Advances in phage therapy: Targeting the *Burkholderia cepacia* complex. Viruses *13*, 1331. https://doi.org/10.3390/v13071331.

Law, S.M., and Gray, R.D. (2017). Neutrophil extracellular traps and the dysfunctional innate immune response of cystic fibrosis lung disease: a review. J Inflamm *14*, 29. https://doi.org/10.1186/s12950-017-0176-1.

Laws, M., Shaaban, A., and Rahman, K.M. (2019). Antibiotic resistance breakers: current approaches and future directions. FEMS Microbiol Rev *43*, 490–516. https://doi.org/10.1093/femsre/fuz014.

Le Breton, Y., Belew, A.T., Valdes, K.M., Islam, E., Curry, P., Tettelin, H., Shirtliff, M.E., El-Sayed, N.M., and McIver, K.S. (2015). Essential genes in the core genome of the human pathogen *Streptococcus pyogenes*. Sci Rep *5*, 9838. https://doi.org/10.1038/srep09838.

Le Guillouzer, S., Groleau, M.-C., and Déziel, E. (2017). The complex quorum sensing circuitry of *Burkholderia thailandensis* is both hierarchically and homeostatically organized. MBio *8*. https://doi.org/10.1128/mBio.01861-17.

Lee, J.C., and Timasheff, S.N. (1977). *In vitro* reconstitution of calf brain microtubules: effects of solution variables. Biochemistry *16*, 1754–1764. .

Lee, A.H.-Y., Flibotte, S., Sinha, S., Paiero, A., Ehrlich, R.L., Balashov, S., Ehrlich, G.D., Zlosnik, J.E.A., Mell, J.C., and Nislow, C. (2017). Phenotypic diversity and genotypic flexibility of *Burkholderia cenocepacia* during long-term chronic infection of cystic fibrosis lungs. Genome Res. *27*, 650–662. https://doi.org/10.1101/gr.213363.116.

Lee, H.H., Ostrov, N., Wong, B.G., Gold, M.A., Khalil, A.S., and Church, G.M. (2019). Functional genomics of the rapidly replicating bacterium *Vibrio natriegens* by CRISPRi. Nat Microbiol https://doi.org/10.1038/s41564-019-0423-8.

Lee, K., Campbell, J., Swoboda, J.G., Cuny, G.D., and Walker, S. (2010). Development of improved inhibitors of wall teichoic acid biosynthesis with potent activity against *Staphylococcus aureus*. Bioorg Med Chem Lett *20*, 1767–1770. https://doi.org/10.1016/j.bmcl.2010.01.036.

Lee, S.A., Gallagher, L.A., Thongdee, M., Staudinger, B.J., Lippman, S., Singh, P.K., and Manoil, C. (2015). General and condition-specific essential functions of *Pseudomonas aeruginosa*. Proc Natl Acad Sci U S A *112*, 5189–5194. https://doi.org/10.1073/pnas.1422186112 [doi].

Leiding, J.W., and Holland, S.M. (1993). Chronic granulomatous disease. In GeneReviews, M.P. Adam, G.M. Mirzaa, R.A. Pagon, S.E. Wallace, L.J. Bean, K.W. Gripp, and A. Amemiya, eds. (Seattle (WA): University of Washington, Seattle), p.

Leimer, N., Wu, X., Imai, Y., Morrissette, M., Pitt, N., Favre-Godal, Q., Iinishi, A., Jain, S., Caboni, M., Leus, I.V., et al. (2021). A selective antibiotic for Lyme disease. Cell *184*, 5405-5418.e16. https://doi.org/10.1016/j.cell.2021.09.011.

Leshchiner, D., Rosconi, F., Sundaresh, B., Rudmann, E., Ramirez, L.M.N., Nishimoto, A.T., Wood, S.J., Jana, B., Buján, N., Li, K., et al. (2022). A genome-wide atlas of antibiotic susceptibility targets and pathways to tolerance. Nat Commun *13*, 3165. https://doi.org/10.1038/s41467-022-30967-4.

Lewin, G.R., Stacy, A., Michie, K.L., Lamont, R.J., and Whiteley, M. (2019). Large-scale identification of pathogen essential genes during coinfection with sympatric and allopatric microbes. Proc Natl Acad Sci *116*, 19685–19694. https://doi.org/10.1073/pnas.1907619116.

Li, S., Poulton, N.C., Chang, J.S., Azadian, Z.A., DeJesus, M.A., Ruecker, N., Zimmerman, M.D., Eckartt, K.A., Bosch, B., Engelhart, C.A., et al. (2022). CRISPRi chemical genetics and comparative genomics identify genes mediating drug potency in Mycobacterium tuberculosis. Nat Microbiol *7*, 766–779. https://doi.org/10.1038/s41564-022-01130-y.

Li, X., Zolli-Juran, M., Cechetto, J.D., Daigle, D.M., Wright, G.D., and Brown, E.D. (2004). Multicopy suppressors for novel antibacterial compounds reveal targets and drug efflux susceptibility. Chem.Biol. *11*, 1423–1430. https://doi.org/10.1016/j.chembiol.2004.08.014.

Li, X., Hernandez, V., Rock, F.L., Choi, W., Mak, Y.S.L., Mohan, M., Mao, W., Zhou, Y., Easom, E.E., Plattner, J.J., et al. (2017). Discovery of a potent and specific *M. tuberculosis* leucyl-tRNA synthetase inhibitor: (S)-3-(aminomethyl)-4-chloro-7-(2-hydroxyethoxy)benzo[c][1,2]oxaborol-1(3H)-ol (GSK656). J Med Chem *60*, 8011–8026. https://doi.org/10.1021/acs.jmedchem.7b00631.

Lin, Y., and Zhang, R.R. (2011). Putative essential and core-essential genes in *Mycoplasma* genomes. Sci Rep *1*, 53. https://doi.org/10.1038/srep00053.

Lin, M.-F., Lin, Y.-Y., Tu, C.-C., and Lan, C.-Y. (2017). Distribution of different efflux pump genes in clinical isolates of multidrug-resistant *Acinetobacter baumannii* and their correlation with antimicrobial resistance. J Microbiol Immunol Infect *50*, 224–231. https://doi.org/10.1016/j.jmii.2015.04.004.

Lin, Q.-H., Lv, Y.-Y., Gao, Z.-H., and Qiu, L.-H. (2020). *Pararobbsia silviterrae gen. nov., sp. nov.*, isolated from forest soil and reclassification of *Burkholderia alpina* as *Pararobbsia alpina comb. nov*. Int J Syst Evol Microbiol *70*, 1412–1420. https://doi.org/10.1099/ijsem.0.003932.

Ling, L.L., Schneider, T., Peoples, A.J., Spoering, A.L., Engels, I., Conlon, B.P., Mueller, A., Schaberle, T.F., Hughes, D.E., Epstein, S., et al. (2015). A new antibiotic kills pathogens without detectable resistance. Nature *517*, 455–459. https://doi.org/10.1038/nature14098.

Liu, C., Li, C., Chen, Y., Hao, H., Liang, J., Duan, R., Guo, Z., Zhang, J., Zhao, Z., Jing, H., et al. (2017a). Role of low-molecular-mass penicillin-binding proteins, NagZ and AmpR in AmpC β-lactamase regulation of *Yersinia enterocolitica*. Front. Cell. Infect. Microbiol. *7*. .

Liu, H., Price, M.N., Waters, R.J., Ray, J., Carlson, H.K., Lamson, J.S., Chakraborty, R., Arkin, A.P., and Deutschbauer, A.M. (2018). Magic pools: Parallel assessment of transposon delivery vectors in bacteria. MSystems *3*. https://doi.org/10.1128/mSystems.00143-17.

Liu, X., Gallay, C., Kjos, M., Domenech, A., Slager, J., van Kessel, S.P., Knoops, K., Sorg, R.A., Zhang, J.-R., and Veening, J.-W. (2017b). High-throughput CRISPRi phenotyping identifies new essential genes in *Streptococcus pneumoniae*. Mol. Syst. Biol. *13*, 931. .

Liu, X., Kimmey, J.M., Matarazzo, L., Bakker, V. de, Maele, L.V., Sirard, J.-C., Nizet, V., and Veening, J.-W. (2020). Exploration of bacterial bottlenecks and *Streptococcus pneumoniae* pathogenesis by CRISPRi-Seq. Cell Host & Microbe *0*. https://doi.org/10.1016/j.chom.2020.10.001.

Livak, K.J., and Schmittgen, T.D. (2001). Analysis of relative gene expression data using real-time quantitative PCR and the 2(-Delta Delta C(T)) Method. Methods *25*, 402–408. https://doi.org/10.1006/meth.2001.1262.

Lobritz, M.A., Andrews, I.W., Braff, D., Porter, C.B.M., Gutierrez, A., Furuta, Y., Cortes, L.B.G., Ferrante, T., Bening, S.C., Wong, F., et al. (2022). Increased energy demand from anabolic-catabolic processes drives β-lactam antibiotic lethality. Cell Chem Biol *29*, 276-286.e4. https://doi.org/10.1016/j.chembiol.2021.12.010.

Lock, R.L., and Harry, E.J. (2008). Cell-division inhibitors: new insights for future antibiotics. Nat.Rev.Drug Discov. *7*, 324–338. https://doi.org/10.1038/nrd2510.

Loh, B., Grant, C., and Hancock, R.E. (1984). Use of the fluorescent probe 1-N-phenylnaphthylamine to study the interactions of aminoglycoside antibiotics with the outer membrane of Pseudomonas aeruginosa. Antimicrob. Agents Chemother. *26*, 546–551. .

Lohans, C.T., Brem, J., and Schofield, C.J. (2017). New Delhi metallo-β-lactamase 1 catalyzes avibactam and aztreonam hydrolysis. Antimicrobial Agents and Chemotherapy *61*, e01224-17. https://doi.org/10.1128/AAC.01224-17.

Lomovskaya, O., Rubio-Aparicio, D., Nelson, K., Sun, D., Tsivkovski, R., Castanheira, M., Lindley, J., Loutit, J., and Dudley, M. (2021a). *In vitro* activity of the ultra-broad-spectrum beta-lactamase inhibitor QPX7728 in combination with multiple beta-lactam antibiotics against *Pseudomonas aeruginosa*. Antimicrob Agents Chemother https://doi.org/10.1128/AAC.00210-21.

Lomovskaya, O., Tsivkovski, R., Sun, D., Reddy, R., Totrov, M., Hecker, S., Griffith, D., Loutit, J., and Dudley, M. (2021b). QPX7728, an ultra-broad-ppectrum B-lactamase inhibitor for intravenous and oral therapy: overview of biochemical and microbiological characteristics. Frontiers in Microbiology *12*. .

Lopatkin, A.J., Stokes, J.M., Zheng, E.J., Yang, J.H., Takahashi, M.K., You, L., and Collins, J.J. (2019). Bacterial metabolic state more accurately predicts antibiotic lethality than growth rate. Nat Microbiol 1–9. https://doi.org/10.1038/s41564-019-0536-0.

Lopes-Santos, L., Castro, D.B.A., Ferreira-Tonin, M., Corrêa, D.B.A., Weir, B.S., Park, D., Ottoboni, L.M.M., Neto, J.R., and Destéfano, S.A.L. (2017). Reassessment of the taxonomic position of *Burkholderia andropogonis* and description of *Robbsia andropogonis gen. nov., comb. nov.* Antonie Van Leeuwenhoek *110*, 727–736. https://doi.org/10.1007/s10482-017-0842-6.

Loutet, S.A., and Valvano, M.A. (2011). Extreme antimicrobial peptide and polymyxin B resistance in the genus *Burkholderia*. Front Microbiol *2*, fmicb.2011.00159. https://doi.org/10.3389/fmicb.2011.00159.

Loutet, S.A., Flannagan, R.S., Kooi, C., Sokol, P.A., and Valvano, M.A. (2006). A complete lipopolysaccharide inner core oligosaccharide is required for resistance of *Burkholderia cenocepacia* to antimicrobial peptides and bacterial survival *in vivo*. Journal of Bacteriology *188*, 2073–2080. https://doi.org/188/6/2073 [pii]; 10.1128/JB.188.6.2073-2080.2006 [doi].

Loutet, S.A., Mussen, L.E., Flannagan, R.S., and Valvano, M.A. (2011). A two-tier model of polymyxin B resistance in *Burkholderia cenocepacia*. Environ Microbiol Rep *3*, 278–285. https://doi.org/10.1111/j.1758-2229.2010.00222.x.

Lucero, C.A., Cohen, A.L., Trevino, I., Rupp, A.H., Harris, M., Forkan-Kelly, S., Noble-Wang, J., Jensen, B., Shams, A., Arduino, M.J., et al. (2011). Outbreak of *Burkholderia cepacia* complex among ventilated pediatric patients linked to hospital sinks. Am J Infect Cont *39*, 775–778. https://doi.org/10.1016/j.ajic.2010.12.005.

Lum, P.Y., Armour, C.D., Stepaniants, S.B., Cavet, G., Wolf, M.K., Butler, J.S., Hinshaw, J.C., Garnier, P., Prestwich, G.D., Leonardson, A., et al. (2004). Discovering modes of action for therapeutic compounds using a genome-wide screen of yeast heterozygotes. Cell *116*, 121–137. .

Luna, B., Trebosc, V., Lee, B., Bakowski, M., Ulhaq, A., Yan, J., Lu, P., Cheng, J., Nielsen, T., Lim, J., et al. (2020). A nutrient-limited screen unmasks rifabutin hyperactivity for extensively drug-resistant *Acinetobacter baumannii*. Nat Microbiol *5*, 1134–1143. https://doi.org/10.1038/s41564-020-0737-6.

Luscher, A., Moynié, L., Auguste, P.S., Bumann, D., Mazza, L., Pletzer, D., Naismith, J.H., and Köhler, T. (2018). TonB-dependent receptor repertoire of *Pseudomonas aeruginosa* for uptake of siderophore-drug conjugates. Antimicrob Agents Chemother https://doi.org/10.1128/AAC.00097-18.

Lutkenhaus, J., and Du, S. (2017). *E. coli* cell cycle machinery. Subcell. Biochem. *84*, 27–65. https://doi.org/10.1007/978-3-319-53047-5_2.

Ma, S., Minch, K.J., Rustad, T.R., Hobbs, S., Zhou, S.-L., Sherman, D.R., and Price, N.D. (2015). Integrated modeling of gene regulatory and metabolic networks in *Mycobacterium tuberculosis*. PLOS Comp Biol *11*, e1004543. https://doi.org/10.1371/journal.pcbi.1004543.

Mackenzie, J.S., Lamprecht, D.A., Asmal, R., Adamson, J.H., Borah, K., Beste, D.J.V., Lee, B.S., Pethe, K., Rousseau, S., Krieger, I., et al. (2020). Bedaquiline reprograms central metabolism to reveal glycolytic vulnerability in *Mycobacterium tuberculosis*. Nat Commun *11*, 6092. https://doi.org/10.1038/s41467-020-19959-4.

Maczuga, N., Tran, E.N.H., Qin, J., and Morona, R. (2022). Interdependence of *Shigella flexneri* O-antigen and enterobacterial common antigen biosynthetic pathways. J Bacteriol *204*, e0054621. https://doi.org/10.1128/jb.00546-21.

Maeder, M.L., Linder, S.J., Cascio, V.M., Fu, Y., Ho, Q.H., and Joung, J.K. (2013). CRISPR RNA-guided activation of endogenous human genes. Nat Methods *10*, 977–979. https://doi.org/10.1038/nmeth.2598.

Mahenthiralingam, E., Coenye, T., Chung, J.W., Speert, D.P., Govan, J.R., Taylor, P., and Vandamme, P. (2000). Diagnostically and experimentally useful panel of strains from the *Burkholderia cepacia* complex. J Clin Microbiol *38*, 910–913. .

Mahenthiralingam, E., Vandamme, P., Campbell, M.E., Henry, D.A., Gravelle, A.M., Wong, L.T.K., Davidson, A.G.F., Wilcox, P.G., Nakielna, B., and Speert, D.P. (2001). Infection with *Burkholderia cepacia* complex genomovars in patients with cystic fibrosis: virulent transmissible strains of genomovar III can replace *Burkholderia multivorans*. Clin Infect Dis *33*, 1469–1475. https://doi.org/10.1086/322684.

Mahenthiralingam, E., Urban, T.A., and Goldberg, J.B. (2005). The multifarious, multireplicon *Burkholderia cepacia* complex. Nat Rev Microbiol *3*, 144–156. .

Mahmoud, S.A., and Chien, P. (2018). Regulated proteolysis in bacteria. Annu Rev Biochem *87*, 677–696. https://doi.org/10.1146/annurev-biochem-062917-012848.

Makarov, V., Manina, G., Mikusova, K., Mollmann, U., Ryabova, O., Saint-Joanis, B., Dhar, N., Pasca, M.R., Buroni, S., Lucarelli, A.P., et al. (2009). Benzothiazinones kill *Mycobacterium tuberculosis* by blocking arabinan synthesis. Science *324*, 801–804. https://doi.org/10.1126/science.1171583.

Malinverni, J.C., and Silhavy, T.J. (2009). An ABC transport system that maintains lipid asymmetry in the gram-negative outer membrane. Proc Natl Acad Sci U S A *106*, 8009–8014. https://doi.org/10.1073/pnas.0903229106.

Malott, R.J., Steen-Kinnaird, B.R., Lee, T.D., and Speert, D.P. (2012). Identification of hopanoid biosynthesis genes involved in polymyxin resistance in *Burkholderia multivorans*. Antimicrob Agents Chemother *56*, 464–471. https://doi.org/10.1128/AAC.00602-11.

Manat, G., Roure, S., Auger, R., Bouhss, A., Barreteau, H., Mengin-Lecreulx, D., and Touzé, T. (2014). Deciphering the metabolism of undecaprenyl-phosphate: the bacterial cell-wall unit carrier at the membrane frontier. Microb Drug Resist *20*, 199–214. https://doi.org/10.1089/mdr.2014.0035.

Manav, M.C., Sofos, N., Hove-Jensen, B., and Brodersen, D.E. (2018). The Abc of phosphonate breakdown: a mechanism for bacterial survival. BioEssays *40*, 1800091. https://doi.org/10.1002/bies.201800091.

Mangas, E.L., Rubio, A., Álvarez-Marín, R., Labrador-Herrera, G., Pachón, J., Pachón-Ibáñez, M.E., Divina, F., and Pérez-Pulido, A.J. (2019). Pangenome of *Acinetobacter baumannii* uncovers two groups of genomes, one of them with genes involved in CRISPR/Cas defence systems associated with the absence of plasmids and exclusive genes for biofilm formation. Microb Gen, *5*, e000309. https://doi.org/10.1099/mgen.0.000309.

Manno, G., Dalmastri, C., Tabacchioni, S., Vandamme, P., Lorini, R., Minicucci, L., Romano, L., Giannattasio, A., Chiarini, L., and Bevivino, A. (2004). Epidemiology and clinical course of *Burkholderia cepacia* complex infections, particularly those caused by different *Burkholderia cenocepacia* strains, among patients attending an Italian Cystic Fibrosis Center. J Clin Microbiol *42*, 1491–1497. .

Mao, D., Bushin, L.B., Moon, K., Wu, Y., and Seyedsayamdost, M.R. (2017). Discovery of scmR as a global regulator of secondary metabolism and virulence in *Burkholderia thailandensis*

E264. Proc. Natl. Acad. Sci. U.S.A. *114*, E2920–E2928. https://doi.org/10.1073/pnas.1619529114.

Marolda, C.L., Lahiry, P., Vinés, E., Saldías, S., and Valvano, M.A. (2006). Micromethods for the characterization of lipid A-core and O-antigen lipopolysaccharide. Methods Mol Biol *347*, 237–252. https://doi.org/10.1385/1-59745-167-3:237.

Martin, D.W., and Mohr, C.D. (2000). Invasion and intracellular survival of *Burkholderia cepacia*. Infect. Immun. *68*, 24–29. .

Martin, A., Takiff, H., Vandamme, P., Swings, J., Palomino, J.C., and Portaels, F. (2006). A new rapid and simple colorimetric method to detect pyrazinamide resistance in *Mycobacterium tuberculosis* using nicotinamide. J. Antimicrob. Chemother. *58*, 327–331. https://doi.org/10.1093/jac/dkl231.

Martin, J.K., Sheehan, J.P., Bratton, B.P., Moore, G.M., Mateus, A., Li, S.H.-J., Kim, H., Rabinowitz, J.D., Typas, A., Savitski, M.M., et al. (2020). A dual-mechanism antibiotic kills Gram-negative bacteria and avoids drug resistance. Cell *181*, 1518-1532.e14. https://doi.org/10.1016/j.cell.2020.05.005.

Martínez-Carranza, E., Barajas, H., Alcaraz, L.-D., Servín-González, L., Ponce-Soto, G.-Y., and Soberón-Chávez, G. (2018). Variability of bacterial essential genes among closely related bacteria: The case of *Escherichia coli*. Front. Microbiol. *9*. https://doi.org/10.3389/fmicb.2018.01059.

Masi, M., Réfregiers, M., Pos, K.M., and Pagès, J.-M. (2017). Mechanisms of envelope permeability and antibiotic influx and efflux in Gram-negative bacteria. Nat Microbiol *2*, 17001. https://doi.org/10.1038/nmicrobiol.2017.1.

Mathis, A.D., Otto, R.M., and Reynolds, K.A. (2021). A simplified strategy for titrating gene expression reveals new relationships between genotype, environment, and bacterial growth. Nucleic Acids Res *49*, e6–e6. https://doi.org/10.1093/nar/gkaa1073.

Matsuyama, S., Yokota, N., and Tokuda, H. (1997). A novel outer membrane lipoprotein, LolB (HemM), involved in the LolA (p20)-dependent localization of lipoproteins to the outer membrane of *Escherichia coli*. The EMBO Journal *16*, 6947–6955. https://doi.org/10.1093/emboj/16.23.6947.

Matthaiou, D.K., Chasou, E., Atmatzidis, S., and Tsolkas, P. (2011). A case of bacteremia due to *Burkholderia cepacia* in a patient without cystic fibrosis. Resp Med CME *4*, 144–145. https://doi.org/10.1016/j.rmedc.2010.11.002.

Matthews, D.A., Bolin, J.T., Burridge, J.M., Filman, D.J., Volz, K.W., Kaufman, B.T., Beddell, C.R., Champness, J.N., Stammers, D.K., and Kraut, J. (1985). Refined crystal structures of *Escherichia coli* and chicken liver dihydrofolate reductase containing bound trimethoprim. J Biol Chem *260*, 381–391. .

Mattingly, S.J., Dipersio, J.R., Higgins, M.L., and Shockman, G.D. (1976). Unbalanced growth and macromolecular synthesis in *Streptococcus mutans* FA-1. Infect Immun *13*, 941–948. .

Mazer, D.M., Young, C., Kalikin, L.M., Spilker, T., and LiPuma, J.J. (2017). In vitro activity of ceftolozane-tazobactam and other antimicrobial agents against *Burkholderia cepacia* complex and *Burkholderia gladioli*. Antimicrob. Agents Chemother. *61*. https://doi.org/10.1128/AAC.00766-17.

McNeil, M.B., Keighley, L.M., Cook, J.R., Cheung, C.-Y., and Cook, G.M. (2021). CRISPR interference identifies vulnerable cellular pathways with bactericidal phenotypes in *Mycobacterium tuberculosis*. Mol Microbiol. https://doi.org/10.1111/mmi.14790.

Mehla, J., Malloci, G., Mansbach, R., López, C.A., Tsivkovski, R., Haynes, K., Leus, I.V., Grindstaff, S.B., Cascella, R.H., D'Cunha, N., et al. (2021). Predictive rules of efflux inhibition and avoidance in *Pseudomonas aeruginosa*. MBio *12*, e02785-20, /mbio/12/1/mBio.02785-20.atom. https://doi.org/10.1128/mBio.02785-20.

Melander, R.J., Zurawski, D.V., and Melander, C. (2017). Narrow-spectrum antibacterial agents. Medchemcomm *9*, 12–21. https://doi.org/10.1039/c7md00528h.

Meng, J., Kanzaki, G., Meas, D., Lam, C.K., Crummer, H., Tain, J., and Xu, H.H. (2012). A genome-wide inducible phenotypic screen identifies antisense RNA constructs silencing *Escherichia coli* essential genes. FEMS Microbiology Letters *329*, 45–53. https://doi.org/10.1111/j.1574-6968.2012.02503.x; 10.1111/j.1574-6968.2012.02503.x.

Meselson, M., and Yuan, R. (1968). DNA restriction enzyme from E. coli. Nature *217*, 1110–1114. https://doi.org/10.1038/2171110a0.

Micek, S.T., Welch, E.C., Khan, J., Pervez, M., Doherty, J.A., Reichley, R.M., and Kollef, M.H. (2010). Empiric combination antibiotic therapy is associated with improved outcome against sepsis due to Gram-negative bacteria: a retrospective analysis. Antimicrob. Agents Chemother. *54*, 1742–1748. https://doi.org/10.1128/AAC.01365-09.

Michna, R.H., Commichau, F.M., Tödter, D., Zschiedrich, C.P., and Stülke, J. (2014). SubtiWiki-a database for the model organism *Bacillus subtilis* that links pathway, interaction and expression information. Nucleic Acids Res. *42*, D692-698. https://doi.org/10.1093/nar/gkt1002.

Miethke, M., Pieroni, M., Weber, T., Brönstrup, M., Hammann, P., Halby, L., Arimondo, P.B., Glaser, P., Aigle, B., Bode, H.B., et al. (2021). Towards the sustainable discovery and development of new antibiotics. Nat Rev Chem *5*, 726–749. https://doi.org/10.1038/s41570-021-00313-1.

Miller, D.P., and Scott, D.A. (2020). Inherently and conditionally essential protein catabolism genes of *Porphyromonas gingivalis*. Trend Microbiol *0*. https://doi.org/10.1016/j.tim.2020.09.002.

Miller, V.L., and Mekalanos, J.J. (1988). A novel suicide vector and its use in construction of insertion mutations: osmoregulation of outer membrane proteins and virulence determinants in *Vibrio cholerae* requires *toxR*. Journal of Bacteriology *170*, 2575–2583. .

Minato, Y., Gohl, D.M., Thiede, J.M., Chacón, J.M., Harcombe, W.R., Maruyama, F., and Baughn, A.D. (2019). Genome-wide assessment of *Mycobacterium tuberculosis* conditionally essential metabolic pathways. MSystems *4*, e00070-19. https://doi.org/10.1128/mSystems.00070-19.

Mingorance, J., Tamames, J., and Vicente, M. (2004). Genomic channeling in bacterial cell division. Journal of Molecular Recognition *17*, 481–487. https://doi.org/10.1002/jmr.718 [doi].

Mohr, S.E., Hu, Y., Ewen-Campen, B., Housden, B.E., Viswanatha, R., and Perrimon, N. (2016). CRISPR guide RNA design for research applications. FEBS J. *283*, 3232–3238. https://doi.org/10.1111/febs.13777.

Moore, R.A., and Hancock, R.E. (1986). Involvement of outer membrane of *Pseudomonas cepacia* in aminoglycoside and polymyxin resistance. Antimicrob Agents Chemother *30*, 923–926. .

Morin, M., Pierce, E.C., and Dutton, R.J. (2018). Changes in the genetic requirements for microbial interactions with increasing community complexity. ELife *7*, e37072. https://doi.org/10.7554/eLife.37072.

Moya, B., Dötsch, A., Juan, C., Blázquez, J., Zamorano, L., Haussler, S., and Oliver, A. (2009). β-lactam resistance response triggered by inactivation of a nonessential penicillin-binding protein. PLOS Pathogens *5*, e1000353. https://doi.org/10.1371/journal.ppat.1000353.

Mueller, E.A., Egan, A.J., Breukink, E., Vollmer, W., and Levin, P.A. (2019). Plasticity of *Escherichia coli* cell wall metabolism promotes fitness and antibiotic resistance across environmental conditions. ELife *8*, e40754. https://doi.org/10.7554/eLife.40754.

Muheim, C., Götzke, H., Eriksson, A.U., Lindberg, S., Lauritsen, I., Nørholm, M.H.H., and Daley, D.O. (2017). Increasing the permeability of *Escherichia coli* using MAC13243. Sci Rep *7*, 17629. https://doi.org/10.1038/s41598-017-17772-6.

Muir, A., Gurung, I., Cehovin, A., Bazin, A., Vallenet, D., and Pelicic, V. (2020). Construction of a complete set of *Neisseria meningitidis* mutants and its use for the phenotypic profiling of this human pathogen. Nat Commun *11*, 5541. https://doi.org/10.1038/s41467-020-19347-y.

Murray, C.J., Ikuta, K.S., Sharara, F., Swetschinski, L., Aguilar, G.R., Gray, A., Han, C., Bisignano, C., Rao, P., Wool, E., et al. (2022). Global burden of bacterial antimicrobial resistance in 2019: a systematic analysis. Lancet *399*, 629–655. https://doi.org/10.1016/S0140-6736(21)02724-0.

Nair, B.M., Jr, K.J.C., Griffith, A., and Burns, J.L. (2004). Salicylate induces an antibiotic efflux pump in *Burkholderia cepacia* complex genomovar III (*B. cenocepacia*). J Clin Invest *113*, 464–473. https://doi.org/10.1172/JCI19710.

Nakashima, N., and Tamura, T. (2009). Conditional gene silencing of multiple genes with antisense RNAs and generation of a mutator strain of *Escherichia coli*. Nucleic Acids Res *37*, e103. https://doi.org/10.1093/nar/gkp498.

Nally, E., Groah, S.L., Pérez-Losada, M., Caldovic, L., Ljungberg, I., Chandel, N.J., Sprague, B., Hsieh, M.H., and Pohl, H.G. (2018). Identification of *Burkholderia fungorum* in the urine of an individual with spinal cord injury and augmentation cystoplasty using 16S sequencing: copathogen or innocent bystander? Spinal Cord Ser Cases *4*, 85. https://doi.org/10.1038/s41394-018-0115-2.

Narayanan, A.M., Ramsey, M.M., Stacy, A., and Whiteley, M. (2017). Defining genetic fitness determinants and creating genomic resources for an oral pathogen. Appl Environ Microbiol *83*, AEM.00797-17. https://doi.org/10.1128/AEM.00797-17.

Ni, J., Zhang, G., Qin, L., Li, J., and Li, C. (2019). Simultaneously down-regulation of multiplex branch pathways using CRISPRi and fermentation optimization for enhancing β-amyrin production in *Saccharomyces cerevisiae*. Synth Syst Biotechnol *4*, 79–85. https://doi.org/10.1016/j.synbio.2019.02.002.

Nichols, R.J., Sen, S., Choo, Y.J., Beltrao, P., Zietek, M., Chaba, R., Lee, S., Kazmierczak, K.M., Lee, K.J., Wong, A., et al. (2011). Phenotypic landscape of a bacterial cell. Cell *144*, 143–156. https://doi.org/10.1016/j.cell.2010.11.052; 10.1016/j.cell.2010.11.052.

Nonejuie, P., Burkart, M., Pogliano, K., and Pogliano, J. (2013). Bacterial cytological profiling rapidly identifies the cellular pathways targeted by antibacterial molecules. Proc Natl Acad Sci *110*, 16169–16174. https://doi.org/10.1073/pnas.1311066110.

Nukaga, M., Yoon, M.J., Taracilia, M.A., Hoshino, T., Becka, S.A., Zeiser, E.T., Johnson, J.R., and Papp-Wallace, K.M. (2021). Assessing the potency of β-lactamase inhibitors with diverse inactivation mechanisms against the PenA1 carbapenemase from *Burkholderia multivorans*. ACS Infect Dis *7*, 826–837. https://doi.org/10.1021/acsinfecdis.0c00682.

Nunvar, J., Capek, V., Fiser, K., Fila, L., and Drevinek, P. (2017). What matters in chronic *Burkholderia cenocepacia* infection in cystic fibrosis: Insights from comparative genomics. PLoS Pathog. *13*, e1006762. https://doi.org/10.1371/journal.ppat.1006762.

Nunvar, J., Hogan, A.M., Buroni, S., Savina, S., Makarov, V., Cardona, S.T., and Drevinek, P. (2019). The effect of 2-thiocyanatopyridine derivative 11026103 on *Burkholderia cenocepacia*: Resistance mechanisms and systemic impact. Antibiotics *8*, 159. https://doi.org/10.3390/antibiotics8040159.

Nurjadi, D., Kocer, K., Chanthalangsy, Q., Klein, S., Heeg, K., and Boutin, S. (2021). New Delhi metallo-beta-lactamase facilitates the emergence of cefiderocol resistance in *Enterobacter cloacae*. Antimicrob Agents Chemother https://doi.org/10.1128/aac.02011-21.

O'Grady, E.P., Viteri, D.F., Malott, R.J., and Sokol, P.A. (2009). Reciprocal regulation by the CepIR and CciIR quorum sensing systems in *Burkholderia cenocepacia*. BMC Genomics *10*. https://doi.org/10.1186/1471-2164-10-441.

Okuda, S., and Tokuda, H. (2011). Lipoprotein sorting in bacteria. Annu Rev Microbiol *65*, 239–259. https://doi.org/10.1146/annurev-micro-090110-102859.

Okuda, S., Sherman, D.J., Silhavy, T.J., Ruiz, N., and Kahne, D. (2016). Lipopolysaccharide transport and assembly at the outer membrane: the PEZ model. Nat Rev Microbiol *14*, 337–345. https://doi.org/10.1038/nrmicro.2016.25.

O'Neill, J. (2014). Antimicrobial Resistance: Tackling a crisis for the health and wealth of nations (The Review on Antimicrobial Resistance).

Opijnen, T. van, Bodi, K.L., and Camilli, A. (2009). Tn-seq: high-throughput parallel sequencing for fitness and genetic interaction studies in microorganisms. Nat Methods *6*, 767–772. https://doi.org/10.1038/nmeth.1377.

Opperman, T.J., Kwasny, S.M., Li, J.B., Lewis, M.A., Aiello, D., Williams, J.D., Peet, N.P., Moir, D.T., Bowlin, T.L., and Long, E.C. (2016). DNA targeting as a likely mechanism underlying the antibacterial activity of synthetic bis-indole antibiotics. Antimicrob Agents Chemother *60*, 7067–7076. https://doi.org/10.1128/AAC.00309-16.

Ortega, X., Hunt, T.A., Loutet, S., Vinion-Dubiel, A.D., Datta, A., Choudhury, B., Goldberg, J.B., Carlson, R., and Valvano, M.A. (2005). Reconstitution of O-specific lipopolysaccharide expression in *Burkholderia cenocepacia* strain J2315, which is associated with transmissible infections in patients with cystic fibrosis. J Bacteriol*187*, 1324–1333. .

Ortega, X., Silipo, A., Saldías, M.S., Bates, C.C., Molinaro, A., and Valvano, M.A. (2009). Biosynthesis and structure of the *Burkholderia cenocepacia* K56-2 lipopolysaccharide core oligosaccharide: truncation of the core oligosaccharide leads to increased binding and sensitivity to polymyxin B. J. Biol. Chem. *284*, 21738–21751. https://doi.org/10.1074/jbc.M109.008532.

Ortega, X.P., Cardona, S.T., Brown, A.R., Loutet, S.A., Flannagan, R.S., Campopiano, D.J., Govan, J.R., and Valvano, M.A. (2007). A putative gene cluster for aminoarabinose biosynthesis is essential for *Burkholderia cenocepacia* viability. J Bacteriol *189*, 3639–3644. https://doi.org/JB.00153-07 [pii]; 10.1128/JB.00153-07 [doi].

Ortmayr, K., de la Cruz Moreno, R., and Zampieri, M. (2022). Expanding the search for small-molecule antibacterials by multidimensional profiling. Nat Chem Biol *18*, 584–595. https://doi.org/10.1038/s41589-022-01040-4.

Otoupal, P.B., Eller, K.A., Erickson, K.E., Campos, J., Aunins, T.R., and Chatterjee, A. (2021). Potentiating antibiotic efficacy via perturbation of non-essential gene expression. Commun Biol *4*, 1–15. https://doi.org/10.1038/s42003-021-02783-x.

Palleroni, N.J., Ballard, R.W., Ralston, E., and Doudoroff, M. (1972). Deoxyribonucleic acid homologies among some *Pseudomonas* species. J Bacteriol *110*, 1–11. https://doi.org/10.1128/jb.110.1.1-11.1972.

Palleroni, N.J., Kunisawa, R., Contopoulu, R., and Doudoroff, M.Y.R. (1973). Nucleic acid homologies in the genus *Pseudomonas*. Int J Syst Evol Microbiol *23*, 333–339. https://doi.org/10.1099/00207713-23-4-333.

Palmer, A.C., and Kishony, R. (2014). Opposing effects of target overexpression reveal drug mechanisms. Nature Communications *5*, 4296. https://doi.org/10.1038/ncomms5296.

Palmer, K.L., Aye, L.M., and Whiteley, M. (2007). Nutritional cues control *Pseudomonas aeruginosa* multi-cellular behavior in cystic fibrosis sputum. J Bacteriol *189*, 8079–8087. https://doi.org/10.1128/JB.01138-07.

Panta, P.R., Kumar, S., Stafford, C.F., Billiot, C.E., Douglass, M.V., Herrera, C.M., Trent, M.S., and Doerrler, W.T. (2019). A DedA family membrane protein is required for *Burkholderia thailandensis* colistin resistance. Front Microbiol *10*. .

Papaleo, M.C., Perrin, E., Maida, I., Fondi, M., Fani, R., and Vandamme, P. (2010). Identification of species of the *Burkholderia cepacia* complex by sequence analysis of the *hisA* gene. J. Med. Microbiol. *59*, 1163–1170. https://doi.org/10.1099/jmm.0.019844-0.

Papp-Wallace, K.M., Senkfor, B., Gatta, J., Chai, W., Taracila, M.A., Shanmugasundaram, V., Han, S., Zaniewski, R.P., Lacey, B.M., Tomaras, A.P., et al. (2012). Early insights into the interactions of different β-lactam antibiotics and β-lactamase inhibitors against soluble forms of <i>Acinetobacter baumannii<i> PBP1a and *Acinetobacter* sp. PBP3. Antimicrob Agents Chemother *56*, 5687–5692. https://doi.org/10.1128/AAC.01027-12.

Papp-Wallace, K.M., Taracila, M.A., Gatta, J.A., Ohuchi, N., Bonomo, R.A., and Nukaga, M. (2013). Insights into β-lactamases from *Burkholderia* species, two phylogenetically related yet distinct resistance determinants. J Biol Chem *288*, 19090–19102. https://doi.org/10.1074/jbc.M113.458315.

Papp-Wallace, K.M., Becka, S.A., Zeiser, E.T., Ohuchi, N., Mojica, M.F., Gatta, J.A., Falleni, M., Tosi, D., Borghi, E., Winkler, M.L., et al. (2017). Overcoming an extremely drug resistant (XDR) pathogen: avibactam restores susceptibility to ceftazidime for *Burkholderia cepacia* complex isolates from cystic fibrosis patients. ACS Infect Dis *3*, 502–511. https://doi.org/10.1021/acsinfecdis.7b00020.

Parr, J.T., Moore, R.A., Moore, L.V., and Hancock, R.E. (1987). Role of porins in intrinsic antibiotic resistance of *Pseudomonas cepacia*. Antimicrob Agents Chemother *31*, 121–123. https://doi.org/10.1128/AAC.31.1.121.

Pathania, R., Zlitni, S., Barker, C., Das, R., Gerritsma, D.A., Lebert, J., Awuah, E., Melacini, G., Capretta, F.A., and Brown, E.D. (2009). Chemical genomics in *Escherichia coli* identifies an inhibitor of bacterial lipoprotein targeting. Nat Chem Biol *5*, 849–856. .

Payne, D.J., Gwynn, M.N., Holmes, D.J., and Pompliano, D.L. (2007). Drugs for bad bugs: confronting the challenges of antibacterial discovery. Nat.Rev.Drug Discov. *6*, 29–40. https://doi.org/10.1038/nrd2201.

Pegues, D.A., Carson, L.A., Tablan, O.C., FitzSimmons, S.C., Roman, S.B., Miller, J.M., and Jarvis, W.R. (1994). Acquisition of Pseudomonas cepacia at summer camps for patients with cystic fibrosis. J Ped *124*, 694–702. https://doi.org/10.1016/S0022-3476(05)81357-5.

Pena Amaya, P., Haim, M.S., Fernández, S., Di Gregorio, S., Teper, A., Vázquez, M., Lubovich, S., Galanternik, L., and Mollerach, M. (2018). Molecular epidemiology of methicillin-resistant *Staphylococcus aureus* in cystic fibrosis patients from Argentina. Microb Drug Resist *24*, 613–620. https://doi.org/10.1089/mdr.2017.0162.

Peng, R., Wang, Y., Feng, W., Yue, X., Chen, J., Hu, X., Li, Z., Sheng, D., Zhang, Y., and Li, Y. (2018). CRISPR/dCas9-mediated transcriptional improvement of the biosynthetic gene cluster for the epothilone production in *Myxococcus xanthus*. Microb Cell Fact *17*. https://doi.org/10.1186/s12934-018-0867-1.

Peters, J.M., Colavin, A., Shi, H., Czarny, T.L., Larson, M.H., Wong, S., Hawkins, J.S., Lu, C.H., Koo, B.M., Marta, E., et al. (2016). A comprehensive, CRISPR-based functional analysis of essential genes in bacteria. Cell *165*, 1493–1506. https://doi.org/10.1016/j.cell.2016.05.003.

Peters, J.M., Koo, B.-M., Patino, R., Heussler, G.E., Hearne, C.C., Qu, J., Inclan, Y.F., Hawkins, J.S., Lu, C.H.S., Silvis, M.R., et al. (2019). Enabling genetic analysis of diverse bacteria with Mobile-CRISPRi. Nat Microbiol *4*, 244–250. https://doi.org/10.1038/s41564-018-0327-z.

Pierce, S.E., Davis, R.W., Nislow, C., and Giaever, G. (2007). Genome-wide analysis of barcoded *Saccharomyces cerevisiae* gene-deletion mutants in pooled cultures. Nat Protoc *2*, 2958–2974. https://doi.org/10.1038/nprot.2007.427.

Pittenger, R.C., Wolfe, R.N., Hoehn, M.M., Marks, P.N., Daily, W.A., and McGUIRE, J.M. (1953). Hygromycin. I. Preliminary studies on the production and biologic activity of a new antibiotic. Antibiot Chemother (Northfield) *3*, 1268–1278. .

Podnecky, N.L., Wuthiekanun, V., Peacock, S.J., and Schweizer, H.P. (2013). The BpeEF-OprC efflux pump Is responsible for widespread trimethoprim resistance in clinical and environmental *Burkholderia pseudomallei* isolates. Antimicrob Agents Chemother *57*, 4381–4386. https://doi.org/10.1128/AAC.00660-13.

Podnecky, N.L., Rhodes, K.A., and Schweizer, H.P. (2015). Efflux pump-mediated drug resistance in *Burkholderia*. Front. Microbiol. *6*, 305. https://doi.org/10.3389/fmicb.2015.00305.

Poirel, L., Rodriguez-Martinez, J.-M., Plésiat, P., and Nordmann, P. (2009). Naturally ccurring class A ß-lactamases from the *Burkholderia cepacia* complex. Antimicrob. Agents Chemother. *53*, 876–882. https://doi.org/10.1128/AAC.00946-08.

Porwollik, S., Santiviago, C.A., Cheng, P., Long, F., Desai, P., Fredlund, J., Srikumar, S., Silva, C.A., Chu, W., Chen, X., et al. (2014). Defined single-gene and multi-gene deletion mutant collections in *Salmonella enterica* sv Typhimurium. PLoS ONE *9*, e99820. https://doi.org/10.1371/journal.pone.0099820.

Poulsen, B.E., Yang, R., Clatworthy, A.E., White, T., Osmulski, S.J., Li, L., Penaranda, C., Lander, E.S., Shoresh, N., and Hung, D.T. (2019). Defining the core essential genome of *Pseudomonas aeruginosa*. Proc. Natl. Acad. Sci. U.S.A. *116*, 10072–10080. https://doi.org/10.1073/pnas.1900570116.

Powers, M.J., Simpson, B.W., and Trent, M.S. (2020). The Mla pathway in <i.>Acinetobacter baumannii</i> has no demonstrable role in anterograde lipid transport. ELife *9*, e56571. https://doi.org/10.7554/eLife.56571.

Poyatos, J.F. (2020). Genetic buffering and potentiation in metabolism. PLOS Comp Biol *16*, e1008185. https://doi.org/10.1371/journal.pcbi.1008185.

Pradenas, G.A., Ross, B.N., and Torres, A.G. (2016). *Burkholderia cepacia* complex vaccines: where do we go from here? Vaccines (Basel) *4*, 10. https://doi.org/10.3390/vaccines4020010.

Pribytkova, T., Lightly, T.J., Kumar, B., Bernier, S.P., Sorensen, J.L., Surette, M.G., and Cardona, S.T. (2014). The attenuated virulence of a *Burkholderia cenocepacia paaABCDE* mutant is due to inhibition of quorum sensing by release of phenylacetic acid. Mol. Microbiol. *94*, 522–536. https://doi.org/10.1111/mmi.12771.

Price, M.N., Wetmore, K.M., Waters, R.J., Callaghan, M., Ray, J., Liu, H., Kuehl, J.V., Melnyk, R.A., Lamson, J.S., Suh, Y., et al. (2018). Mutant phenotypes for thousands of bacterial genes of unknown function. Nature *557*, 503–509. https://doi.org/10.1038/s41586-018-0124-0.

Prinz, W.A., Åslund, F., Holmgren, A., and Beckwith, J. (1997). The role of the thioredoxin and glutaredoxin pathways in reducing protein disulfide bonds in the *Escherichia coli* cytoplasm. J. Biol. Chem. *272*, 15661–15667. https://doi.org/10.1074/jbc.272.25.15661.

Pristovsek, P., and Kidric, J. (1999). Solution structure of polymyxins B and E and effect of binding to lipopolysaccharide: an NMR and molecular modeling study. J Med Chem *42*, 4604–4613. https://doi.org/10.1021/jm991031b.

Pucci, M.J., Thanassi, J.A., Ho, H.T., Falk, P.J., and Dougherty, T.J. (1995). *Staphylococcus haemolyticus* contains two D-glutamic acid biosynthetic activities, a glutamate racemase and a D-amino acid transaminase. J Bacteriol *177*, 336–342. https://doi.org/10.1128/jb.177.2.336-342.1995.

Qi, L.S., Larson, M.H., Gilbert, L.A., Doudna, J.A., Weissman, J.S., Arkin, A.P., and Lim, W.A. (2013). Repurposing CRISPR as an RNA-guided platform for sequence-specific control of gene expression. Cell *152*, 1173–1183. https://doi.org/10.1016/j.cell.2013.02.022.

Raddaoui, A., Ben Tanfous, F., Chebbi, Y., Mabrouk, A., and Achour, W. (2022). An intermittent outbreak of *Burkholderia cepacia* contaminating hematopoietic stem cells resulting in infusate-related blood stream infections. J Infect Prev *23*, 75–78. https://doi.org/10.1177/17571774211066783.

Rajagopal, M., Martin, M.J., Santiago, M., Lee, W., Kos, V.N., Meredith, T., Gilmore, M.S., and Walker, S. (2016). Multidrug intrinsic resistance factors in *Staphylococcus aureus* identified by

profiling fitness within high-diversity transposon libraries. MBio *7*. https://doi.org/10.1128/mBio.00950-16.

Ranjan, R., Chowdhary, P., and Kamra, A. (2017). Community acquired *Burkholderia cepacia* bacteraemia presenting as MODS in an immunocompetent individual: an unusual case. J Clin Diagn Res *11*, DD01–DD02. https://doi.org/10.7860/JCDR/2017/16285.9435.

Rappleye, C.A., and Roth, J.R. (1997). A Tn10 derivative (T-POP) for isolation of insertions with conditional (tetracycline-dependent) phenotypes. J. Bacteriol. *179*, 5827–5834. https://doi.org/10.1128/jb.179.18.5827-5834.1997.

Rasmussen, B., Noller, H.F., Daubresse, G., Oliva, B., Misulovin, Z., Rothstein, D.M., Ellestad, G.A., Gluzman, Y., Tally, F.P., and Chopra, I. (1991). Molecular basis of tetracycline action: identification of analogs whose primary target is not the bacterial ribosome. Antimicrob Agents Chemother *35*, 2306–2311. .

Ratjen, F., Bell, S.C., Rowe, S.M., Goss, C.H., Quittner, A.L., and Bush, A. (2015). Cystic fibrosis. Nat Rev Dis Primers *1*, 1–19. https://doi.org/10.1038/nrdp.2015.10.

Reading, C., and Cole, M. (1977). Clavulanic acid: a beta-lactamase-inhibiting beta-lactam from *Streptomyces clavuligerus*. Antimicrob Agents Chemother *11*, 852–857. .

Regan, K.H., and Bhatt, J. (2019). Eradication therapy for *Burkholderia cepacia* complex in people with cystic fibrosis. Cochrane Database Syst Rev *4*, CD009876. https://doi.org/10.1002/14651858.CD009876.pub4.

Reis, A.C., Halper, S.M., Vezeau, G.E., Cetnar, D.P., Hossain, A., Clauer, P.R., and Salis, H.M. (2019). Simultaneous repression of multiple bacterial genes using nonrepetitive extra-long sgRNA arrays. Nat Biotechnol https://doi.org/10.1038/s41587-019-0286-9.

Rezzoagli, C., Archetti, M., Mignot, I., Baumgartner, M., and Kümmerli, R. (2020). Combining antibiotics with antivirulence compounds can have synergistic effects and reverse selection for antibiotic resistance in *Pseudomonas aeruginosa*. PLoS Biol *18*, e3000805. https://doi.org/10.1371/journal.pbio.3000805.

Rhodes, K.A., and Schweizer, H.P. (2016). Antibiotic resistance in *Burkholderia* species. Drug Resistance Updates *28*, 82–90. https://doi.org/10.1016/j.drup.2016.07.003.

Riber, L., Olsson, J.A., Jensen, R.B., Skovgaard, O., Dasgupta, S., Marinus, M.G., and Løbner-Olesen, A. (2006). Hda-mediated inactivation of the DnaA protein and dnaA gene autoregulation act in concert to ensure homeostatic maintenance of the *Escherichia coli* chromosome. Genes Dev *20*, 2121–2134. https://doi.org/10.1101/gad.379506.

Rice, S.A., Tan, C.H., Mikkelsen, P.J., Kung, V., Woo, J., Tay, M., Hauser, A., McDougald, D., Webb, J.S., and Kjelleberg, S. (2009). The biofilm life-cycle and virulence of *Pseudomonas aeruginosa* are dependent on a filamentous prophage. ISME J *3*, 271–282. https://doi.org/10.1038/ismej.2008.109.

Richards, S.M., Strandberg, K.L., Conroy, M., and Gunn, J.S. (2012). Cationic antimicrobial peptides serve as activation signals for the *Salmonella* Typhimurium PhoPQ and PmrAB regulons in vitro and in vivo. Front Cell Infect Microbiol *2*, 102. https://doi.org/10.3389/fcimb.2012.00102.

Rick, P.D., Barr, K., Sankaran, K., Kajimura, J., Rush, J.S., and Waechter, C.J. (2003). Evidence that the *wzxE* gene of *Escherichia coli* K-12 encodes a protein involved in the transbilayer movement of a trisaccharide-lipid intermediate in the assembly of enterobacterial common antigen. J Biol Chem *278*, 16534–16542. https://doi.org/10.1074/jbc.M301750200.

Riordan, J.R., Rommens, J.M., Kerem, B., Alon, N., Rozmahel, R., Grzelczak, Z., Zielenski, J., Lok, S., Plavsic, N., and Chou, J.L. (1989). Identification of the cystic fibrosis gene: cloning and characterization of complementary DNA. Science *245*, 1066–1073. .

Rock, J.M., Hopkins, F.F., Chavez, A., Diallo, M., Chase, M.R., Gerrick, E.R., Pritchard, J.R., Church, G.M., Rubin, E.J., Sassetti, C.M., et al. (2017). Programmable transcriptional repression in mycobacteria using an orthogonal CRISPR interference platform. Nat Microbiol *2*, 16274. https://doi.org/10.1038/nmicrobiol.2016.274.

Rodvold, K.A., George, J.M., and Yoo, L. (2011). Penetration of anti-infective agents into pulmonary epithelial lining fluid: focus on antibacterial agents. Clin Pharmacokinet *50*, 637–664. https://doi.org/10.2165/11594090-000000000-00000.

Roney, I.J., and Rudner, D.Z. (2022). Two broadly conserved families of polyprenyl-phosphate transporters. 2022.02.03.479048. https://doi.org/10.1101/2022.02.03.479048.

Roth, G.S., Shockman, G.D., and Daneo-Moore, L. (1971). Balanced macromolecular biosynthesis in “protoplasts” of *Streptococcus faecalis*. J Bacteriol *105*, 710–717. .

Rousset, F., Cui, L., Siouve, E., Becavin, C., Depardieu, F., and Bikard, D. (2018). Genome-wide CRISPR-dCas9 screens in *E. coli* identify essential genes and phage host factors. PLOS Genetics *14*, e1007749. https://doi.org/10.1371/journal.pgen.1007749.

Rousset, F., Cabezas-Caballero, J., Piastra-Facon, F., Fernández-Rodríguez, J., Clermont, O., Denamur, E., Rocha, E.P.C., and Bikard, D. (2021). The impact of genetic diversity on gene essentiality within the *Escherichia coli species*. Nature Microbiology *6*, 301–312. https://doi.org/10.1038/s41564-020-00839-y.

Roy, P.H., Tetu, S.G., Larouche, A., Elbourne, L., Tremblay, S., Ren, Q., Dodson, R., Harkins, D., Shay, R., Watkins, K., et al. (2010). Complete genome sequence of the multiresistant taxonomic outlier *Pseudomonas aeruginosa* PA7. PLOS ONE *5*, e8842. https://doi.org/10.1371/journal.pone.0008842.

Ruiz, N., Falcone, B., Kahne, D., and Silhavy, T.J. (2005). Chemical conditionality: a genetic strategy to probe organelle assembly. Cell *121*, 307–317. https://doi.org/10.1016/j.cell.2005.02.014.

Ruiz, N., Kahne, D., and Silhavy, T.J. (2006). Advances in understanding bacterial outer-membrane biogenesis. Nat Rev Microbiol *4*, 57–66. https://doi.org/10.1038/nrmicro1322.

Ruiz, N., Kahne, D., and Silhavy, T.J. (2009). Transport of lipopolysaccharide across the cell envelope: the long road of discovery. Nat Rev Microbiol *7*, 677–683. https://doi.org/10.1038/nrmicro2184.

Rusmini, R., Vecchietti, D., Macchi, R., Vidal-Aroca, F., and Bertoni, G. (2014). A shotgun antisense approach to the identification of novel essential genes in *Pseudomonas aeruginosa*. BMC Microbiology *14*, 24-2180-14–24. https://doi.org/10.1186/1471-2180-14-24; 10.1186/1471-2180-14-24.

Russel, M., and Holmgren, A. (1988). Construction and characterization of glutaredoxin-negative mutants of *Escherichia coli*. Proc Natl Acad Sci U S A *85*, 990–994. .

Saberi, F., Kamali, M., Najafi, A., Yazdanparast, A., and Moghaddam, M.M. (2016). Natural antisense RNAs as mRNA regulatory elements in bacteria: a review on function and applications. Cell Mol Biol Lett *21*, s11658-016-0007-z. https://doi.org/10.1186/s11658-016-0007-z.

Sabnis, A., Hagart, K.L., Klöckner, A., Becce, M., Evans, L.E., Furniss, R.C.D., Mavridou, D.A., Murphy, R., Stevens, M.M., Davies, J.C., et al. (2021). Colistin kills bacteria by targeting lipopolysaccharide in the cytoplasmic membrane. Elife *10*, e65836. https://doi.org/10.7554/eLife.65836.

Sanders, C.C., Bradford, P.A., Ehrhardt, A.F., Bush, K., Young, K.D., Henderson, T.A., and Sanders, W.E. (1997). Penicillin-binding proteins and induction of AmpC beta-lactamase. Antimicrob Agents Chemother *41*, 2013–2015. https://doi.org/10.1128/AAC.41.9.2013.

Sanderson, T., Bileschi, M.L., Belanger, D., and Colwell, L.J. (2021). ProteInfer: deep networks for protein functional inference. 2021.09.20.461077. https://doi.org/10.1101/2021.09.20.461077.

Santiago, M., Lee, W., Fayad, A.A., Coe, K.A., Rajagopal, M., Do, T., Hennessen, F., Srisuknimit, V., Müller, R., Meredith, T.C., et al. (2018a). Genome-wide mutant profiling predicts the mechanism of a Lipid II binding antibiotic. Nat Chem Biol *14*, 601–608. https://doi.org/10.1038/s41589-018-0041-4.

Santiago, M., Lee, W., Fayad, A.A., Coe, K.A., Rajagopal, M., Do, T., Hennessen, F., Srisuknimit, V., Müller, R., Meredith, T.C., et al. (2018b). Genome-wide mutant profiling predicts the mechanism of a Lipid II binding antibiotic. Nat. Chem. Biol. *14*, 601–608. https://doi.org/10.1038/s41589-018-0041-4.

Sarkar, P., Yarlagadda, V., Ghosh, C., and Haldar, J. (2017). A review on cell wall synthesis inhibitors with an emphasis on glycopeptide antibiotics. Medchemcomm *8*, 516–533. https://doi.org/10.1039/c6md00585c.

Sass, A., Everaert, A., Acker, H.V., Driessche, F.V. den, and Coenye, T. (2018). Targeting the nonmevalonate pathway in *Burkholderia cenocepacia* increases susceptibility to certain β-lactam

antibiotics. Antimicrob. Agents Chemother. *62*, e02607-17. https://doi.org/10.1128/AAC.02607-17.

Sass, A.M., Van Acker, H., Förstner, K.U., Van Nieuwerburgh, F., Deforce, D., Vogel, J., and Coenye, T. (2015). Genome-wide transcription start site profiling in biofilm-grown *Burkholderia cenocepacia* J2315. BMC Genomics *16*, 775. https://doi.org/10.1186/s12864-015-1993-3.

Sawana, A., Adeolu, M., and Gupta, R.S. (2014). Molecular signatures and phylogenomic analysis of the genus *Burkholderia*: proposal for division of this genus into the emended genus *Burkholderia* containing pathogenic organisms and a new genus *Paraburkholderia* gen. nov. harboring environmental species. Front. Genet. *5*. https://doi.org/10.3389/fgene.2014.00429.

Schimana, J., Gebhardt, K., Höltzel, A., Schmid, D.G., Süssmuth, R., Müller, J., Pukall, R., and Fiedler, H.-P. (2002). Arylomycins A and B, new biaryl-bridged lipopeptide antibiotics produced by *Streptomyces* sp. Tü 6075. I. Taxonomy, fermentation, isolation and biological activities. J Antibiot (Tokyo) *55*, 565–570. https://doi.org/10.7164/antibiotics.55.565.

Schmerk, C.L., and Valvano, M.A. (2013). *Burkholderia multivorans* survival and trafficking within macrophages. J Med Microbiol *62*, 173–184. https://doi.org/10.1099/jmm.0.051243-0.

Schmidt, H., and Hensel, M. (2004). Pathogenicity islands in bacterial pathogenesis. Clin. Microbiol. Rev. *17*, 14–56. .

Schmittgen, T.D., and Livak, K.J. (2008). Analyzing real-time PCR data by the comparative C(T) method. Nat Protoc *3*, 1101–1108. .

Schroth, M.N., Cho, J.J., Green, S.K., Kominos, S.D., and Microbiology Society Publishing (2018). Epidemiology of *Pseudomonas aeruginosa* in agricultural areas. Journal of Medical Microbiology *67*, 1191–1201. https://doi.org/10.1099/jmm.0.000758.

Schwab, U., Abdullah, L.H., Perlmutt, O.S., Albert, D., Davis, C.W., Arnold, R.R., Yankaskas, J.R., Gilligan, P., Neubauer, H., Randell, S.H., et al. (2014). Localization of *Burkholderia cepacia* complex bacteria in cystic fibrosis lungs and interactions with *Pseudomonas aeruginosa* in hypoxic mucus. Infection and Immunity *82*, 4729–4745. https://doi.org/10.1128/IAI.01876-14; 10.1128/IAI.01876-14.

Scoffone, V.C., Ryabova, O., Makarov, V., Iadarola, P., Fumagalli, M., Fondi, M., Fani, R., De Rossi, E., Riccardi, G., and Buroni, S. (2015). Efflux-mediated resistance to a benzothiadiazol derivative effective against *Burkholderia cenocepacia*. Front.Microbiol. *6*, 815. https://doi.org/10.3389/fmicb.2015.00815.

Scoffone, V.C., Chiarelli, L.R., Trespidi, G., Mentasti, M., Riccardi, G., and Buroni, S. (2017). *Burkholderia cenocepacia* infections in cystic fibrosis patients: drug resistance and therapeutic approaches. Front Microbiol *8*, 1592. https://doi.org/10.3389/fmicb.2017.01592.

Scoffone, V.C., Barbieri, G., Buroni, S., Scarselli, M., Pizza, M., Rappuoli, R., and Riccardi, G. (2020). Vaccines to overcome antibiotic resistance: the challenge of *Burkholderia cenocepacia*. Trends in Microbiology *28*, 315–326. https://doi.org/10.1016/j.tim.2019.12.005.

Scoffone, V.C., Trespidi, G., Barbieri, G., Irudal, S., Perrin, E., and Buroni, S. (2021). Role of RND efflux pumps in drug resistance of cystic fibrosis pathogens. Antibiotics *10*, 863. https://doi.org/10.3390/antibiotics10070863.

Scoffone V.C., Irudahl, S., AbuAlshaa, A., Aurora, P., Trespidi, G., Barbieri, G., Makarov, V., Migliavacca, R., De Rossi, E., Buroni, S. (2022). Bactericidal and anti-biofilm activity of the FtsZ inhibitor C109 against *Acinetobacter baumannii*. Antibiotics. *11* 1572.

Sekar, K., Gentile, A.M., Bostick, J.W., and Tyo, K.E.J. (2016). N-terminal-based targeted, inducible protein degradation in *Escherichia coli*. PLOS ONE *11*, e0149746. https://doi.org/10.1371/journal.pone.0149746.

Selin, C., Stietz, M.S., Blanchard, J.E., Gehrke, S.S., Bernard, S., Hall, D.G., Brown, E.D., and Cardona, S.T. (2015). A pipeline for screening small molecules with growth inhibitory activity against *Burkholderia cenocepacia*. PLoS ONE *10*, e0128587. https://doi.org/10.1371/journal.pone.0128587.

Sesto, N., Wurtzel, O., Archambaud, C., Sorek, R., and Cossart, P. (2013). The excludon: a new concept in bacterial antisense RNA-mediated gene regulation. Nat Rev Microbiol *11*, 75–82. https://doi.org/10.1038/nrmicro2934.

Shaw, D., Miravet-Verde, S., Piñero-Lambea, C., Serrano, L., and Lluch-Senar, M. (2020). LoxTnSeq: random transposon insertions combined with cre/lox recombination and counterselection to generate large random genome reductions. Microb Biotechnol https://doi.org/10.1111/1751-7915.13714.

Shelanski, M.L., Gaskin, F., and Cantor, C.R. (1973). Microtubule assembly in the absence of added nucleotides. Proc. Natl. Acad. Sci. USA *70*, 765–768. .

Shields, R.C., Walker, A.R., Maricic, N., Chakraborty, B., Underhill, S.A.M., and Burne, R.A. (2020). Repurposing the *Streptococcus mutans* CRISPR-Cas9 system to understand essential gene function. PLOS Pathogens *16*, e1008344. https://doi.org/10.1371/journal.ppat.1008344.

Shionogi Inc. (2019). Antimicrobial drugs advisory committee: Cefiderocol briefing document (Food and Drug Administration).

Siegele, D.A., and Hu, J.C. (1997). Gene expression from plasmids containing the araBAD promoter at subsaturating inducer concentrations represents mixed populations. Proc. Natl. Acad. Sci. U S A *94*, 8168–8172. .

Siewert, G., and Strominger, J.L. (1967). Bacitracin: An inhibitor of the dephosphorylation of lipid pyrophosphate, an intermediate in the biogenesis of the peptidoglycan of bacterial cell walls. Proc Natl Acad Sci U S A *57*, 767–773. .

Silvis, M.R., Rajendram, M., Shi, H., Osadnik, H., Gray, A.N., Cesar, S., Peters, J.M., Hearne, C.C., Kumar, P., Todor, H., et al. (2021). Morphological and transcriptional responses to CRISPRi knockdown of essential genes in *Escherichia coli*. MBio *12*, e02561-21. https://doi.org/10.1128/mBio.02561-21.

Simpkins, S.W., Deshpande, R., Nelson, J., Li, S.C., Piotrowski, J.S., Ward, H.N., Yashiroda, Y., Osada, H., Yoshida, M., Boone, C., et al. (2019). Using BEAN-counter to quantify genetic interactions from multiplexed barcode sequencing experiments. Nat Prot *14*, 415–440. https://doi.org/10.1038/s41596-018-0099-1.

Simpson, B.W., and Trent, M.S. (2019). Pushing the envelope: LPS modifications and their consequences. Nat Rev Microbiol *17*, 403–416. https://doi.org/10.1038/s41579-019-0201-x.

Singh, A.K., Carette, X., Potluri, L.P., Sharp, J.D., Xu, R., Prisic, S., and Husson, R.N. (2016). Investigating essential gene function in *Mycobacterium tuberculosis* using an efficient CRISPR interference system. Nucleic Acids Research https://doi.org/gkw625 [pii].

Singhal, T., Shah, S., and Naik, R. (2015). Outbreak of *Burkholderia cepacia* complex bacteremia in a chemotherapy day care unit due to intrinsic contamination of an antiemetic drug. Indian J Med Microbiol *33*, 117–119. https://doi.org/10.4103/0255-0857.148405.

Sit, B., Srisuknimit, V., Hullahalli, K., Bueno, E., Cava, F., and Waldor, M.K. (2022). Candidate undecaprenyl phosphate translocases enable conditional microbial fitness and pathogenesis. 2022.02.04.479082. https://doi.org/10.1101/2022.02.04.479082.

Smith, A.M., Heisler, L.E., Onge, R.P.S., Farias-Hesson, E., Wallace, I.M., Bodeau, J., Harris, A.N., Perry, K.M., Giaever, G., Pourmand, N., et al. (2010). Highly-multiplexed barcode sequencing: an efficient method for parallel analysis of pooled samples. Nucleic Acids Res *38*, e142. https://doi.org/10.1093/nar/gkq368.

Smith, A.M., Durbic, T., Kittanakom, S., Giaever, G., and Nislow, C. (2012). Barcode sequencing for understanding drug-gene interactions. Methods Mol. Biol. *910*, 55–69. https://doi.org/10.1007/978-1-61779-965-5_4.

Smith, P.A., Koehler, M.F.T., Girgis, H.S., Yan, D., Chen, Y., Chen, Y., Crawford, J.J., Durk, M.R., Higuchi, R.I., Kang, J., et al. (2018). Optimized arylomycins are a new class of Gram-negative antibiotics. Nature *561*, 189. https://doi.org/10.1038/s41586-018-0483-6.

Smith, T.C., Pullen, K.M., Olson, M.C., McNellis, M.E., Richardson, I., Hu, S., Larkins-Ford, J., Wang, X., Freundlich, J.S., Ando, D.M., et al. (2020). Morphological profiling of tubercle bacilli identifies drug pathways of action. Proc Natl Acad Sci *117*, 18744–18753. https://doi.org/10.1073/pnas.2002738117.

Snyder, D.S., and McIntosh, T.J. (2000). The lipopolysaccharide barrier: correlation of antibiotic susceptibility with antibiotic permeability and fluorescent probe binding kinetics. Biochemistry *39*, 11777–11787. https://doi.org/10.1021/bi000810n.

Somayaji, R., Stanojevic, S., Tullis, D.E., Stephenson, A.L., Ratjen, F., and Waters, V. (2017). Clinical outcomes associated with *Achromobacter* species infection in patients with cystic fibrosis. Annals ATS *14*, 1412–1418. https://doi.org/10.1513/AnnalsATS.201701-071OC.

Sønderholm, M., Bjarnsholt, T., Alhede, M., Kolpen, M., Jensen, P.Ø., Kühl, M., and Kragh, K.N. (2017). The consequences of being in an infectious biofilm: microenvironmental conditions governing antibiotic tolerance. Int J Mol Sci *18*, 2688. https://doi.org/10.3390/ijms18122688.

Sonnabend, M.S., Klein, K., Beier, S., Angelov, A., Kluj, R., Mayer, C., Groß, C., Hofmeister, K., Beuttner, A., Willmann, M., et al. (2020). Identification of drug resistance determinants in a clinical isolate of *Pseudomonas aeruginosa* by high-density transposon mutagenesis. Antimicrob Agents Chemother *64*, e01771-19. https://doi.org/10.1128/AAC.01771-19.

Speert, D.P., Bond, M., Woodman, R.C., and Curnutte, J.T. (1994). Infection with *Pseudomonas cepacia* in chronic granulomatous disease: role of nonoxidative killing by neutrophils in host defense. J Infect Dis *170*, 1524–1531. https://doi.org/10.1093/infdis/170.6.1524.

Speert, D.P., Henry, D., Vandamme, P., Corey, M., and Mahenthiralingam, E. (2002). Epidemiology of *Burkholderia cepacia* complex in patients with cystic fibrosis, Canada. Emerging Infectious Diseases *8*, 181–187. .

Spengler, G., Kincses, A., Gajdács, M., and Amaral, L. (2017). New roads leading to old destinations: efflux pumps as targets to reverse multidrug resistance in bacteria. Molecules *22*, E468. https://doi.org/10.3390/molecules22030468.

Sperandio, D., Rossignol, G., Guerillon, J., Connil, N., Orange, N., Feuilloley, M.G.J., and Merieau, A. (2010). Cell-associated hemolysis activity in the clinical strain of *Pseudomonas fluorescens* MFN1032. BMC Microbiol. *10*, 124. https://doi.org/10.1186/1471-2180-10-124.

Spoletini, G., Etherington, C., Shaw, N., Clifton, I.J., Denton, M., Whitaker, P., and Peckham, D.G. (2019). Use of ceftazidime/avibactam for the treatment of MDR *Pseudomonas aeruginosa* and *Burkholderia cepacia* complex infections in cystic fibrosis: a case series. J Antimicrob Chemother *74*, 1425–1429. https://doi.org/10.1093/jac/dky558.

Spoto, M., Guan, C., Fleming, E., and Oh, J. (2020). A Universal, Genome-wide GuideFinder for CRISPR/Cas9 targeting in microbial genomes. MSphere *5*. https://doi.org/10.1128/mSphere.00086-20.

Staerck, C., Gastebois, A., Vandeputte, P., Calenda, A., Larcher, G., Gillmann, L., Papon, N., Bouchara, J.-P., and Fleury, M.J.J. (2017). Microbial antioxidant defense enzymes. Microb Path *110*, 56–65. https://doi.org/10.1016/j.micpath.2017.06.015.

Stanojevic, S., Vukovojac, K., Sykes, J., Ratjen, F., Tullis, E., Stephenson, A.L. (2021). Projecting the impact of delayed access to elexacaftor/tezacaftor/ivacaftor for people with ystic fibrosis. J Cystic Fibrosis *20*, 243-9.

Stietz, M.S., Lopez, C., Osifo, O., Tolmasky, M.E., and Cardona, S.T. (2017). Evaluation of the electron transfer flavoprotein as an antibacterial target in *Burkholderia cenocepacia*. Can. J. Microbiol. *63*, 857–863. https://doi.org/10.1139/cjm-2017-0350.

Stone, V.N., Parikh, H.I., El-rami, F., Ge, X., Chen, W., Zhang, Y., Kellogg, G.E., and Xu, P. (2015). Identification of small-molecule inhibitors against meso-2, 6-diaminopimelate

dehydrogenase from *Porphyromonas gingivalis*. PLoS One *10*. https://doi.org/10.1371/journal.pone.0141126.

Strom, M.B., Haug, B.E., Skar, M.L., Stensen, W., Stiberg, T., and Svendsen, J.S. (2003). The pharmacophore of short cationic antibacterial peptides. J.Med.Chem. *46*, 1567–1570. https://doi.org/10.1021/jm0340039.

Sun, N., Lu, Y.-J., Chan, F.-Y., Du, R.-L., Zheng, Y.-Y., Zhang, K., So, L.-Y., Abagyan, R., Zhuo, C., Leung, Y.-C., et al. (2017a). A thiazole orange derivative targeting the bacterial protein FtsZ shows potent antibacterial activity. Front Microbiol *8*, 855. https://doi.org/10.3389/fmicb.2017.00855.

Sun, N., Du, R.-L., Zheng, Y.-Y., Huang, B.-H., Guo, Q., Zhang, R.-F., Wong, K.-Y., and Lu, Y.-J. (2017b). Antibacterial activity of N-methylbenzofuro[3,2-b]quinoline and N-methylbenzoindolo[3,2-b]-quinoline derivatives and study of their mode of action. European Journal of Medicinal Chemistry *135*, 1–11. https://doi.org/10.1016/j.ejmech.2017.04.018.

Sutaria, D.S., Moya, B., Green, K.B., Kim, T.H., Tao, X., Jiao, Y., Louie, A., Drusano, G.L., and Bulitta, J.B. (2018). First penicillin-binding protein occupancy patterns of β-lactams and β-lactamase inhibitors in *Klebsiella pneumoniae*. Antimicrob Agents Chemother *62*, e00282-18. https://doi.org/10.1128/AAC.00282-18.

Swick, M.C., Morgan-Linnell, S.K., Carlson, K.M., and Zechiedrich, L. (2011). Expression of multidrug efflux pump genes *acrAB-tolC, mdfA*, and *norE* in *Escherichia coli* clinical isolates as a function of fluoroquinolone and multidrug resistance. Antimicrob Agents Chemother *55*, 921–924. https://doi.org/10.1128/AAC.00996-10.

Swings, J., De Vos, P., van den Mooter, M., and Ley, J. (1983). Transfer of *Pseudomonas maltophilia* Hugh 1981 to the genus *Xanthomonas* as *Xanthomonas maltophilia*. International J Syst Bacteriol *33*, 409–413. .

Swoboda, J.G., Meredith, T.C., Campbell, J., Brown, S., Suzuki, T., Bollenbach, T., Malhowski, A.J., Kishony, R., Gilmore, M.S., and Walker, S. (2009). Discovery of a small molecule that blocks wall teichoic acid biosynthesis in *Staphylococcus aureus*. ACS Chem.Biol. *4*, 875–883. https://doi.org/10.1021/cb900151k.

Tablan, O.C., Chorba, T.L., Schidlow, D.V., White, J.W., Hardy, K.A., Gilligan, P.H., Morgan, W.M., Carson, L.A., Martone, W.J., and Jason, J.M. (1985). *Pseudomonas cepacia* colonization in patients with cystic fibrosis: risk factors and clinical outcome. J Pediatr *107*, 382–387. https://doi.org/10.1016/s0022-3476(85)80511-4.

Tacconelli, E., Carrara, E., Savoldi, A., Harbarth, S., Mendelson, M., Monnet, D.L., Pulcini, C., Kahlmeter, G., Kluytmans, J., Carmeli, Y., et al. (2018). Discovery, research, and development of new antibiotics: the WHO priority list of antibiotic-resistant bacteria and tuberculosis. The Lancet Infect Dis *18*, 318–327. https://doi.org/10.1016/S1473-3099(17)30753-3.

Takiff, H.E., Baker, T., Copeland, T., Chen, S.M., and Court, D.L. (1992). Locating essential *Escherichia coli* genes by using mini-Tn10 transposons: the *pdxJ* operon. J. Bacteriol. *174*, 1544–1553. https://doi.org/10.1128/jb.174.5.1544-1553.1992.

Tamae, C., Liu, A., Kim, K., Sitz, D., Hong, J., Becket, E., Bui, A., Solaimani, P., Tran, K.P., Yang, H., et al. (2008). Determination of antibiotic hypersensitivity among 4,000 single-gene-knockout mutants of *Escherichia coli*. J. Bacteriol. *190*, 5981–5988. https://doi.org/10.1128/JB.01982-07.

Tan, C.M., Therien, A.G., Lu, J., Lee, S.H., Caron, A., Gill, C.J., Lebeau-Jacob, C., Benton-Perdomo, L., Monteiro, J.M., Pereira, P.M., et al. (2012). Restoring methicillin-resistant *Staphylococcus aureus* susceptibility to β-lactam antibiotics. Sci Transl Med *4*, 126ra35. https://doi.org/10.1126/scitranslmed.3003592.

Tan, S.Z., Reisch, C.R., and Prather, K.L.J. (2018). A robust CRISPRi gene repression system in *Pseudomonas*. J. Bacteriol. *200*, e00575-17. https://doi.org/10.1128/JB.00575-17.

Tavares, M., Kozak, M., Balola, A., and Sá-Correia, I. (2020). *Burkholderia cepacia* complex bacteria: a feared contamination risk in water-based pharmaceutical products. Clin Microbiol Rev *33*, e00139-19. https://doi.org/10.1128/CMR.00139-19.

Tayler, A.E., Ayala, J.A., Niumsup, P., Westphal, K., Baker, J.A., Zhang, L., Walsh, T.R., Wiedemann, B., Bennett, P.M., and Avison, M.B. (2010). Induction of beta-lactamase production in *Aeromonas hydrophila* is responsive to beta-lactam-mediated changes in peptidoglycan composition. Microbiology (Reading) *156*, 2327–2335. https://doi.org/10.1099/mic.0.035220-0.

van Teeseling, M.C.F., de Pedro, M.A., and Cava, F. (2017). Determinants of bacterial morphology: from fundamentals to possibilities for antimicrobial targeting. Frontiers in Microbiology *8*. .

Telenti, A., Imboden, P., Marchesi, F., Lowrie, D., Cole, S., Colston, M.J., Matter, L., Schopfer, K., and Bodmer, T. (1993). Detection of rifampicin-resistance mutations in *Mycobacterium tuberculosis*. Lancet *341*, 647–650. https://doi.org/10.1016/0140-6736(93)90417-f.

Teufel, R., Mascaraque, V., Ismail, W., Voss, M., Perera, J., Eisenreich, W., Haehnel, W., and Fuchs, G. (2010). Bacterial phenylalanine and phenylacetate catabolic pathway revealed. Proc Natl Acad Sci *107*, 14390–14395. https://doi.org/10.1073/pnas.1005399107.

Therien, A.G., Huber, J.L., Wilson, K.E., Beaulieu, P., Caron, A., Claveau, D., Deschamps, K., Donald, R.G., Galgoci, A.M., Gallant, M., et al. (2012). Broadening the spectrum of beta-lactam antibiotics through inhibition of signal peptidase type I. Antimicrob.Agents Chemother. *56*, 4662–4670. https://doi.org/10.1128/AAC.00726-12;

Threlfall, E.J., Frost, J.A., Ward, L.R., and Rowe, B. (1994). Epidemic in cattle and humans of Salmonella typhimurium DT 104 with chromosomally integrated multiple drug resistance. Vet. Rec. *134*, 577. .

Tomich, M., Herfst, C.A., Golden, J.W., and Mohr, C.D. (2002). Role of flagella in host cell invasion by *Burkholderia cepacia*. Infect.Immun. *70*, 1799–1806. .

Tommasi, R., Brown, D.G., Walkup, G.K., Manchester, J.I., and Miller, A.A. (2015). ESKAPEing the labyrinth of antibacterial discovery. Nat Rev Drug Discov *14*, 529–542. https://doi.org/10.1038/nrd4572.

Tong, M., French, S., Zahed, S.S.E., Ong, W. kit, Karp, P.D., and Brown, E.D. (2020). Gene dispensability in *Escherichia coli* grown in thirty different carbon environments. MBio *11*. https://doi.org/10.1128/mBio.02259-20.

Tong, Y., Charusanti, P., Zhang, L., Weber, T., and Lee, S.Y. (2015). CRISPR-Cas9 based engineering of actinomycetal genomes. ACS Synth. Biol. *4*, 1020–1029. https://doi.org/10.1021/acssynbio.5b00038.

Tooke, C.L., Hinchliffe, P., Bragginton, E.C., Colenso, C.K., Hirvonen, V.H.A., Takebayashi, Y., and Spencer, J. (2019). β-lactamases and β-lactamase inhibitors in the 21st century. Journal of Molecular Biology *431*, 3472–3500. https://doi.org/10.1016/j.jmb.2019.04.002.

Trent, M.S., Ribeiro, A.A., Doerrler, W.T., Lin, S., Cotter, R.J., and Raetz, C.R. (2001a). Accumulation of a polyisoprene-linked amino sugar in polymyxin-resistant *Salmonella typhimurium* and *Escherichia coli*: Structural characterization and transfer to lipid A in the periplasm. J Biol Chem *276*, 43132–43144. https://doi.org/10.1074/jbc.M106962200.

Trent, M.S., Ribeiro, A.A., Lin, S., Cotter, R.J., and Raetz, C.R. (2001b). An inner membrane enzyme in *Salmonella* and *Escherichia coli* that transfers 4-amino-4-deoxy-L-arabinose to lipid A: Induction on polymyxin-resistant mutants and role of a novel lipid-linked donor. J Biol Chem *276*, 43122–43131. https://doi.org/10.1074/jbc.M106961200.

Trépanier, S., Prince, A., and Huletsky, A. (1997). Characterization of the penA and penR genes of Burkholderia cepacia 249 which encode the chromosomal class A penicillinase and its LysR-type transcriptional regulator. Antimicrob Agents Chemother *41*, 2399–2405.

Trespigi, G., Scoffone, V.C., Barbieri, G., Marchesini, F., AbuAlsaar, A., Coeyne, T., Ungaro, F., Makarov, V., Migliavacca, R., DeRossi, E., Buroni, S. (2021). Antistaphylococcal activity of the FtsZ inhibitor C109. Pathogens. *10*, 886.

Turner, K.H., Wessel, A.K., Palmer, G.C., Murray, J.L., and Whiteley, M. (2015). Essential genome of *Pseudomonas aeruginosa* in cystic fibrosis sputum. Proc Natl Acad Sci *112*, 4110–4115. https://doi.org/10.1073/pnas.1419677112.

Tyers, M., and Wright, G.D. (2019). Drug combinations: a strategy to extend the life of antibiotics in the 21st century. Nat Rev Microbiol *17*, 141. https://doi.org/10.1038/s41579-018-0141-x.

Umland, T.C., Schultz, L.W., MacDonald, U., Beanan, J.M., Olson, R., and Russo, T.A. (2012). *In vivo*-validated essential genes identified in *Acinetobacter baumannii* by using human ascites

overlap poorly with essential genes detected on laboratory media. MBio *3*, 10.1128/mBio.00113-12. Print 2012. https://doi.org/10.1128/mBio.00113-12; 10.1128/mBio.00113-12.

Valvano, M.A. (2015). Chapter 4 - Genetics and Biosynthesis of Lipopolysaccharide. In Molecular Medical Microbiology (Second Edition), Y.-W. Tang, M. Sussman, D. Liu, I. Poxton, and J. Schwartzman, eds. (Boston: Academic Press), pp. 55–89.

Van Acker, H., Gielis, J., Acke, M., Cools, F., Cos, P., and Coenye, T. (2016). The role of reactive oxygen species in antibiotic-induced cell death in *Burkholderia cepacia* complex bacteria. PLoS ONE *11*, e0159837. https://doi.org/10.1371/journal.pone.0159837.

Van den Driessche, F., Rigole, P., Brackman, G., and Coenye, T. (2014). Optimization of resazurin-based viability staining for quantification of microbial biofilms. Journal of Microbiological Methods *98*, 31–34. https://doi.org/10.1016/j.mimet.2013.12.011.

Venter, H., Mowla, R., Ohene-Agyei, T., and Ma, S. (2015). RND-type drug efflux pumps from Gram-negative bacteria: molecular mechanism and inhibition. Front. Microbiol. *6*. https://doi.org/10.3389/fmicb.2015.00377.

Vezina, B., Petit, G.A., Martin, J.L., and Halili, M.A. (2020). Prediction of *Burkholderia pseudomallei* DsbA substrates identifies potential virulence factors and vaccine targets. PLoS One *15*, e0241306. https://doi.org/10.1371/journal.pone.0241306.

Vincent, I.M., Ehmann, D.E., Mills, S.D., Perros, M., and Barrett, M.P. (2016). Untargeted metabolomics to ascertain antibiotic modes of action. Antimicrobial Agents and Chemotherapy *60*, 2281–2291. https://doi.org/10.1128/AAC.02109-15.

Voulhoux, R., Bos, M.P., Geurtsen, J., Mols, M., and Tommassen, J. (2003). Role of a highly conserved bacterial protein in outer membrane protein assembly. Science *299*, 262–265. https://doi.org/10.1126/science.1078973.

Wainwright, M., Canham, L.T., Al-Wajeeh, K., and Reeves, C.L. (1999). Morphological changes (including filamentation) in Escherichia coli grown under starvation conditions on silicon wafers and other surfaces. Lett Appl Microbiol *29*, 224–227. https://doi.org/10.1046/j.1365-2672.1999.00602.x.

Walsh, C.T. (1989). Enzymes in the D-alanine branch of bacterial cell wall peptidoglycan assembly. J Biol Chem *264*, 2393–2396. .

Walton, R.T., Christie, K.A., Whittaker, M.N., and Kleinstiver, B.P. (2020). Unconstrained genome targeting with near-PAMless engineered CRISPR-Cas9 variants. Science *368*, 290–296. https://doi.org/10.1126/science.aba8853.

Wang, B., and Kuramitsu, H.K. (2005). Inducible antisense RNA expression in the characterization of gene functions in *Streptococcus mutans*. Infect. Immun. *73*, 3568–3576. .

Wang, C., Lau, C.Y., Ma, F., and Zheng, C. (2021). Genome-wide screen identifies curli amyloid fibril as a bacterial component promoting host neurodegeneration. Proc Natl Acad Sci *118*. https://doi.org/10.1073/pnas.2106504118.

Wang, H., Claveau, D., Vaillancourt, J.P., Roemer, T., and Meredith, T.C. (2011). High-frequency transposition for determining antibacterial mode of action. Nat.Chem.Biol. *7*, 720–729. https://doi.org/10.1038/nchembio.643.

Wang, T., Guan, C., Guo, J., Liu, B., Wu, Y., Xie, Z., Zhang, C., and Xing, X.-H. (2018). Pooled CRISPR interference screening enables genome-scale functional genomics study in bacteria with superior performance. Nat Commun *9*, 2475. https://doi.org/10.1038/s41467-018-04899-x.

Wang, X., Possoz, C., and Sherratt, D.J. (2005). Dancing around the divisome: asymmetric chromosome segregation in *Escherichia coli*. Genes Dev. *19*, 2367–2377. https://doi.org/10.1101/gad.345305.

Wang, X., Ribeiro, A.A., Guan, Z., and Raetz, C.R.H. (2009). Identification of undecaprenyl phosphate-β-D-galactosamine in *Francisella novicida* and its function in lipid A modification. Biochemistry *48*, 1162–1172. https://doi.org/10.1021/bi802211k.

Wang, X., Quinn, P.J., and Yan, A. (2015). Kdo2-lipid A: structural diversity and impact on immunopharmacology. Biol Rev *90*, 408–427. https://doi.org/10.1111/brv.12114.

Wang, Y., Venter, H., and Ma, S. (2016). Efflux pump inhibitors: a novel approach to combat efflux-mediated drug resistance in bacteria. Curr Drug Targets *17*, 702–719. https://doi.org/10.2174/1389450116666151001103948.

Wang, Z., Soni, V., Marriner, G., Kaneko, T., Boshoff, H.I.M., Barry, C.E., and Rhee, K.Y. (2019). Mode-of-action profiling reveals glutamine synthetase as a collateral metabolic vulnerability of *M. tuberculosis* to bedaquiline. Proc Natl Acad Sci *116*, 19646–19651. https://doi.org/10.1073/pnas.1907946116.

Watkins, K., and Unnikrishnan, M. (2020). Chapter 9 - New strategies and targets for antibacterial discovery. In Drug Discovery Targeting Drug-Resistant Bacteria, P. Kesharwani, S. Chopra, and A. Dasgupta, eds. (Academic Press), pp. 249–272.

Weaver, A.I., Murphy, S.G., Umans, B.D., Tallavajhala, S., Onyekwere, I., Wittels, S., Shin, J.-H., VanNieuwenhze, M., Waldor, M.K., and Dörr, T. (2018). Genetic determinants of penicillin tolerance in *Vibrio cholerae*. Antimicrob. Agents Chemother. *62*. https://doi.org/10.1128/AAC.01326-18.

Weaver, A.I., Alvarez, L., Rosch, K.M., Ahmed, A., Wang, G.S., van Nieuwenhze, M.S., Cava, F., and Dörr, T. (2022). Lytic transglycosylases mitigate periplasmic crowding by degrading soluble cell wall turnover products. ELife *11*, e73178. https://doi.org/10.7554/eLife.73178.

Wei, J.R., Krishnamoorthy, V., Murphy, K., Kim, J.H., Schnappinger, D., Alber, T., Sassetti, C.M., Rhee, K.Y., and Rubin, E.J. (2011). Depletion of antibiotic targets has widely varying

effects on growth. Proc Natl Acad Sci *108*, 4176–4181. https://doi.org/10.1073/pnas.1018301108; 10.1073/pnas.1018301108.

Wenzler, E., Fraidenburg, D.R., Scardina, T., and Danziger, L.H. (2016). Inhaled antibiotics for Gram-negative respiratory infections. Clin. Microbiol. Rev. *29*, 581–632. https://doi.org/10.1128/CMR.00101-15.

de Wet, T.J., Winkler, K.R., Mhlanga, M., Mizrahi, V., and Warner, D.F. (2020). Arrayed CRISPRi and quantitative imaging describe the morphotypic landscape of essential mycobacterial genes. ELife *9*, e60083. https://doi.org/10.7554/eLife.60083.

Wetmore, K.M., Price, M.N., Waters, R.J., Lamson, J.S., He, J., Hoover, C.A., Blow, M.J., Bristow, J., Butland, G., Arkin, A.P., et al. (2015). Rapid quantification of mutant fitness in diverse bacteria by sequencing randomly bar-coded transposons. MBio *6*, e00306-00315. https://doi.org/10.1128/mBio.00306-15.

Wiersinga, W.J., Virk, H.S., Torres, A.G., Currie, B.J., Peacock, S.J., Dance, D.A.B., and Limmathurotsakul, D. (2018). Melioidosis. Nat Rev Dis Primers *4*, 17107. https://doi.org/10.1038/nrdp.2017.107.

Winzeler, E.A., Shoemaker, D.D., Astromoff, A., Liang, H., Anderson, K., Andre, B., Bangham, R., Benito, R., Boeke, J.D., Bussey, H., et al. (1999). Functional characterization of the *S. cerevisiae* genome by gene deletion and parallel analysis. Science *285*, 901–906. https://doi.org/10.1126/science.285.5429.901.

Woese, C.R., Weisburg, W.G., Paster, B.J., Hahn, C.M., Tanner, R.S., Krieg, N.R., Koops, H.-P., Harms, H., and Stackebrandt, E. (1984). The phylogeny of purple bacteria: The beta subdivision. Syst Appl Microbiol *5*, 327–336. https://doi.org/10.1016/S0723-2020(84)80035-1.

Wong, Y.-C., Abd El Ghany, M., Ghazzali, R.N.M., Yap, S.-J., Hoh, C.-C., Pain, A., and Nathan, S. (2018). Genetic determinants associated with *in vivo* survival of *Burkholderia cenocepacia* in the *Caenorhabditis elegans* model. Front Microbiol *9*, 1118. https://doi.org/10.3389/fmicb.2018.01118.

Woodford, N., and Ellington, M.J. (2007). The emergence of antibiotic resistance by mutation. Clinical Microbiology and Infection *13*, 5–18. https://doi.org/10.1111/j.1469-0691.2006.01492.x.

Wortinger, M.A., Quardokus, E.M., and Brun, Y.V. (1998). Morphological adaptation and inhibition of cell division during stationary phase in *Caulobacter crescentus*. Mol. Microbiol. *29*, 963–973. .

Wu, T., Malinverni, J., Ruiz, N., Kim, S., Silhavy, T.J., and Kahne, D. (2005). Identification of a multicomponent complex required for outer membrane biogenesis in *Escherichia coli*. Cell *121*, 235–245. https://doi.org/10.1016/j.cell.2005.02.015.

Xayarath, B., and Yother, J. (2007). Mutations blocking side chain assembly, polymerization, or transport of a Wzy-dependent *Streptococcus pneumoniae* capsule are lethal in the absence of

suppressor mutations and can affect polymer transfer to the cell wall. Journal of Bacteriology *189*. https://doi.org/10.1128/JB.01938-06.

Xiao, Y., Gerth, K., Muller, R., and Wall, D. (2012). Myxobacterium-produced antibiotic TA (myxovirescin) inhibits type II signal peptidase. Antimicrob.Agents Chemother. *56*, 2014–2021. https://doi.org/10.1128/AAC.06148-11;

Xu, H.H., Trawick, J.D., Haselbeck, R.J., Forsyth, R.A., Yamamoto, R.T., Archer, R., Patterson, J., Allen, M., Froelich, J.M., Taylor, I., et al. (2010). *Staphylococcus aureus* TargetArray: comprehensive differential essential gene expression as a mechanistic tool to profile antibacterials. Antimicrob.Agents Chemother. *54*, 3659–3670. https://doi.org/10.1128/AAC.00308-10.

Xu, P., Ge, X., Chen, L., Wang, X., Dou, Y., Xu, J.Z., Patel, J.R., Stone, V., Trinh, M., Evans, K., et al. (2011). Genome-wide essential gene identification in *Streptococcus sanguinis*. Scientific Reports *1*, 125. https://doi.org/10.1038/srep00125; 10.1038/srep00125.

Yabuuchi, E., Kosako, Y., Oyaizu, H., Yano, I., Hotta, H., Hashimoto, Y., Ezaki, T., and Arakawa, M. (1992). Proposal of *Burkholderia* gen. nov. and transfer of seven species of the genus *Pseudomonas* homology group II to the new genus, with the type species *Burkholderia cepacia* (Palleroni and Holmes 1981) comb. nov. Microbiol Immunol *36*, 1251–1275. https://doi.org/10.1111/j.1348-0421.1992.tb02129.x.

Yang, J.H., Wright, S.N., Hamblin, M., McCloskey, D., Alcantar, M.A., Schrübbers, L., Lopatkin, A.J., Satish, S., Nili, A., Palsson, B.O., et al. (2019). A white-box machine learning approach for revealing antibiotic mechanisms of action. Cell *177*, 1649-1661.e9. https://doi.org/10.1016/j.cell.2019.04.016.

Yang, P., Zhang, M., and Elsas, J.D. van (2017a). Role of flagella and type four pili in the co-migration of *Burkholderia terrae* BS001 with fungal hyphae through soil. Sci Rep *7*, 2997. https://doi.org/10.1038/s41598-017-02959-8.

Yang, X., Lyu, Z., Miguel, A., McQuillen, R., Huang, K.C., and Xiao, J. (2017b). GTPase activity–coupled treadmilling of the bacterial tubulin FtsZ organizes septal cell wall synthesis. Science *355*, 744–747. https://doi.org/10.1126/science.aak9995.

Yao, L., Cengic, I., Anfelt, J., and Hudson, E.P. (2016). Multiple gene repression in cyanobacteria using CRISPRi. ACS Synth Biol *5*, 207–212. https://doi.org/10.1021/acssynbio.5b00264.

Yapa, S.W.S., Li, J., Patel, K., Wilson, J.W., Dooley, M.J., George, J., Clark, D., Poole, S., Williams, E., Porter, C.J.H., et al. (2014). Pulmonary and systemic pharmacokinetics of inhaled and intravenous colistin methanesulfonate in cystic fibrosis patients: targeting advantage of inhalational administration. Antimicrob Agents Chemother *58*, 2570–2579. https://doi.org/10.1128/AAC.01705-13.

Yasir, M., Turner, A.K., Bastkowski, S., Baker, D., Page, A.J., Telatin, A., Phan, M.-D., Monahan, L., Savva, G.M., Darling, A., et al. (2020). TraDIS-Xpress: a high-resolution whole-

genome assay identifies novel mechanisms of triclosan action and resistance. Genome Res. *30*, 239–249. https://doi.org/10.1101/gr.254391.119.

Yocum, R.R., Waxman, D.J., Rasmussen, J.R., and Strominger, J.L. (1979). Mechanism of penicillin action: penicillin and substrate bind covalently to the same active site serine in two bacterial D-alanine carboxypeptidases. Proc Natl Acad Sci U S A *76*, 2730–2734. .

Yocum, R.R., Rasmussen, J.R., and Strominger, J.L. (1980). The mechanism of action of penicillin. Penicillin acylates the active site of *Bacillus stearothermophilus* D-alanine carboxypeptidase. J Biol Chem *255*, 3977–3986. https://doi.org/10.1016/S0021-9258(19)85621-1.

Yuan, J., Jin, F., Glatter, T., and Sourjik, V. (2017). Osmosensing by the bacterial PhoQ/PhoP two-component system. Proc Natl Acad Sci U S A *114*, E10792–E10798. https://doi.org/10.1073/pnas.1717272114.

Zaher, A., El Saygh, J., Elsori, D., El Saygh, H., Sanni, A. (2021). A review of Trikafta: triple cystic fibrosis transmembrane conductance regulator (CFTR) modulator therapy. Cureus *13*, e1644

Zampieri, M., Zimmermann, M., Claassen, M., and Sauer, U. (2017). Nontargeted metabolomics reveals the multilevel response to antibiotic perturbations. Cell Reports *19*, 1214–1228. https://doi.org/10.1016/j.celrep.2017.04.002.

Zampieri, M., Szappanos, B., Buchieri, M.V., Trauner, A., Piazza, I., Picotti, P., Gagneux, S., Borrell, S., Gicquel, B., Lelievre, J., et al. (2018). High-throughput metabolomic analysis predicts mode of action of uncharacterized antimicrobial compounds. Sci Transl Med *10*, eaal3973. https://doi.org/10.1126/scitranslmed.aal3973.

Zapun, A., Contreras-Martel, C., and Vernet, T. (2008). Penicillin-binding proteins and β-lactam resistance. FEMS Microbiology Reviews *32*, 361–385. https://doi.org/10.1111/j.1574-6976.2007.00095.x.

Zeiser, E.T., Becka, S.A., Wilson, B.M., Barnes, M.D., LiPuma, J.J., and Papp-Wallace, K.M. (2019a). “Switching partners”: piperacillin-avibactam is a highly potent combination against multidrug-resistant *Burkholderia cepacia* complex and *Burkholderia gladioli* cystic fibrosis isolates. J Clin Microbiol *57*, e00181-19. https://doi.org/10.1128/JCM.00181-19.

Zeiser, E.T., Becka, S.A., Barnes, M.D., Taracila, M.A., LiPuma, J.J., and Papp-Wallace, K.M. (2019b). Resurrecting old β-Lactams: potent inhibitory activity of temocillin against multidrug-resistant *Burkholderia* species isolates from the United States. Antimicrob Agents Chemother*63*, e02315-18. https://doi.org/10.1128/AAC.02315-18.

Zhanel, G.G., Zhanel, M.A., and Karlowsky, J.A. (2020). Oral and intravenous fosfomycin for the treatment of complicated urinary tract infections. Can J Infect Dis Med Microbiol *2020*, 8513405. https://doi.org/10.1155/2020/8513405.

Zhang, B., Liu, Z.-Q., Liu, C., and Zheng, Y.-G. (2016). Application of CRISPRi in Corynebacterium glutamicum for shikimic acid production. Biotechnol. Lett. *38*, 2153–2161. https://doi.org/10.1007/s10529-016-2207-z.

Zheng, S., Wang, W., Aldahdooh, J., Malyutina, A., Shadbahr, T., Tanoli, Z., Pessia, A., and Tang, J. (2022). SynergyFinder Plus: Toward better interpretation and annotation of drug combination screening datasets. Genom Proteom Bioinformat S1672-0229(22)00008-0. https://doi.org/10.1016/j.gpb.2022.01.004.

Zhou, J., Chen, Y., Tabibi, S., Alba, L., Garber, E., and Saiman, L. (2007). Antimicrobial susceptibility and synergy studies of *Burkholderia cepacia* complex isolated from patients with cystic fibrosis. Antimicrob Agents Chemother *51*, 1085–1088. https://doi.org/10.1128/AAC.00954-06.

Zhu, B., Green, S.P., Ge, X., Puccio, T.M., Nadhem, H., Ge, H., Bao, L., Kitten, T., and Xu, P. (2020). Genome-wide identification of *Streptococcus sanguinis* fitness genes in human serum and discovery of potential selective drug targets. Mol Microbiol https://doi.org/10.1111/mmi.14629.

Zimmerman, S.B., and Stapley, E.O. (1976). Relative morphological effects induced by cefoxitin and other beta-lactam antibiotics in vitro. Antimicrob Agents Chemother *9*, 318–326. https://doi.org/10.1128/AAC.9.2.318.

Zlitni, S., Ferruccio, L.F., and Brown, E.D. (2013). Metabolic suppression identifies new antibacterial inhibitors under nutrient limitation. Nat.Chem.Biol. *9*, 796–804. https://doi.org/10.1038/nchembio.1361.